NATIONAL COOPERATIVE HIGHWAY RESEARCH PROGRAM
REPORT 290

REINFORCEMENT OF EARTH SLOPES AND EMBANKMENTS

JAMES K. MITCHELL
Department of Civil Engineering
University of California
Berkeley, California

WILLEM C.B. VILLET
Dames & Moore
San Francisco, California

CONTRIBUTORS
Note: Affiliations of contributors are referenced to time of project initiation
JEROLD A. BISHOP, Dames & Moore
JAMES G. COLLIN, University of California, Berkeley
RICHARD R. DAVIDSON, Woodward-Clyde Consultants
JEAN-PIERRE GIROUD, Woodward-Clyde Consultants
RICHARD A. JEWELL, Binnie and Partners, United Kingdom
ILAN JURAN, Ecole Nationale des Ponts et Chaussees, France
FRANCOIS M. SCHLOSSER, Ecole Nationale des Ponts et Chaussees, France

RESEARCH SPONSORED BY THE AMERICAN ASSOCIATION OF STATE HIGHWAY AND TRANSPORTATION OFFICIALS IN COOPERATION WITH THE FEDERAL HIGHWAY ADMINISTRATION

AREAS OF INTEREST:

Structures Design and Performance
Construction
Maintenance
Soil and Rock Mechanics
(Highway Transportation, Public Transit, Rail Transportation)

TRANSPORTATION RESEARCH BOARD
NATIONAL RESEARCH COUNCIL
WASHINGTON, D.C.
JUNE 1987

NATIONAL COOPERATIVE HIGHWAY RESEARCH PROGRAM

Systematic, well-designed research provides the most effective approach to the solution of many problems facing highway administrators and engineers. Often, highway problems are of local interest and can best be studied by highway departments individually or in cooperation with their state universities and others. However, the accelerating growth of highway transportation develops increasingly complex problems of wide interest to highway authorities. These problems are best studied through a coordinated program of cooperative research.

In recognition of these needs, the highway administrators of the American Association of State Highway and Transportation Officials initiated in 1962 an objective national highway research program employing modern scientific techniques. This program is supported on a continuing basis by funds from participating member states of the Association and it receives the full cooperation and support of the Federal Highway Administration, United States Department of Transportation.

The Transportation Research Board of the National Research Council was requested by the Association to administer the research program because of the Board's recognized objectivity and understanding of modern research practices. The Board is uniquely suited for this purpose as: it maintains an extensive committee structure from which authorities on any highway transportation subject may be drawn; it possesses avenues of communications and cooperation with federal, state, and local governmental agencies, universities, and industry; its relationship to the National Research Council is an insurance of objectivity; it maintains a full-time research correlation staff of specialists in highway transportation matters to bring the findings of research directly to those who are in a position to use them.

The program is developed on the basis of research needs identified by chief administrators of the highway and transportation departments and by committees of AASHTO. Each year, specific areas of research needs to be included in the program are proposed to the National Research Council and the Board by the American Association of State Highway and Transportation Officials. Research projects to fulfill these needs are defined by the Board, and qualified research agencies are selected from those that have submitted proposals. Administration and surveillance of research contracts are the responsibilities of the National Research Council and the Transportation Research Board.

The needs for highway research are many, and the National Cooperative Highway Research Program can make significant contributions to the solution of highway transportation problems of mutual concern to many responsible groups. The program, however, is intended to complement rather than to substitute for or duplicate other highway research programs.

NCHRP REPORT 290

Project 24-2 FY '83

ISSN 0077-5614

ISBN 0-309-04024-8

L. C. Catalog Card No. 87-50559

Price $40.00

NOTICE

The project that is the subject of this report was a part of the National Cooperative Highway Research Program conducted by the Transportation Research Board with the approval of the Governing Board of the National Research Council. Such approval reflects the Governing Board's judgment that the program concerned is of national importance and appropriate with respect to both the purposes and resources of the National Research Council.

The members of the technical committee selected to monitor this project and to review this report were chosen for recognized scholarly competence and with due consideration for the balance of disciplines appropriate to the project. The opinions and conclusions expressed or implied are those of the research agency that performed the research, and, while they have been accepted as appropriate by the technical committee, they are not necessarily those of the Transportation Research Board, the National Research Council, the American Association of State Highway and Transportation officials, or the Federal Highway Administration, U.S. Department of Transportation.

Each report is reviewed and accepted for publication by the technical committee according to procedures established and monitored by the Transportation Research Board Executive Committee and the Governing Board of the National Research Council.

Special Notice

The Transportation Research Board, the National Research Council, the Federal Highway Administration, the American Association of State Highway and Transportation Officials, and the individual states participating in the National Cooperative Highway Research Program do not endorse products or manufacturers. Trade or manufacturers' names appear herein solely because they are considered essential to the object of this report.

Published reports of the

NATIONAL COOPERATIVE HIGHWAY RESEARCH PROGRAM

are available from:

Transportation Research Board
National Research Council
2101 Constitution Avenue, N.W.
Washington, D.C. 20418

Printed in the United States of America

FOREWORD

By Staff
Transportation
Research Board

This report provides a comprehensive compilation of information on various earth reinforcement systems used to construct embankments and stabilize existing slopes. Earth reinforcement systems are comprised of reinforcement material, backfill or in-place soil, and facing elements. The report includes an all-inclusive overview of earth reinforcement and details on specific earth reinforcement systems covering their mechanisms, behavior, applications, designs, and durability. The guiding objective in the preparation of this document has been to make it sufficiently complete to be a valuable handbook-type reference source for the researcher and the practicing engineer in considering applications of earth reinforcement.

The problem of economically constructing and maintaining stable slopes within limited right-of-way is a continuing concern. Where increasing traffic requires the addition of lanes within the same right-of-way, earth retaining structures are often necessary. Such structures are required also where existing or proposed slopes are unstable and flattening of the slope is not feasible.

In recent years, some of the most noteworthy advances in geotechnology have been in the area of earth reinforcement. Powerful, innovative techniques have been initiated and are being developed here and abroad that have the potential for improving stability at reasonable cost. Some techniques are proprietary, and information on many of the innovative methodologies is not widely distributed. Therefore, there was a need to collect, evaluate, and disseminate the current state of the art to realize the full potential of their use and determine their applicability.

With the assistance of a research team of noted international experts, the agency of Dames & Moore, San Francisco, California, developed a comprehensive resource document under NCHRP Project 24-2, "Reinforcement of Earth Slopes and Embankments." This report fills a void in the literature available to the researcher and the practicing engineer. Indeed, it provides in a convenient, single document a handbook-type reference for those individuals who wish to exploit the opportunities of these innovative techniques.

The format of the report is designed for time-saving reference work. The detailed table of contents provided at the beginning of each chapter in the main report and in the appendixes is intended to function as a reference device by which all divisions and subjects treated in the report can be easily located by page number. The alphanumeric system used in Chapter Five of the main text, Design Example section, to identify the primary and secondary section headings assists the reader in easily locating a cross-referenced section. The arabic numerals used throughout the appendixes fulfills the same purpose for which the numbering system was used in Chapter Five.

Acknowledgments

The research herein was conducted under NCHRP Project 24-2. Dr. Willem C.B. Villet, Associate and Senior Engineer, Dames & Moore, San Francisco, and Dr. James K. Mitchell, Professor and Chairman, Department of Civil Engineering, University of California, Berkeley, were the principal investigators. The main text of the report was prepared by the principal investigators. Initial drafts of the appendixes were first prepared by the different project team members, and then were reviewed and edited by the principal investigators. The team members who contributed substantially to the appendixes are as follows:

- Mr. Jerold A. Bishop, Dames & Moore, Salt Lake City (*Welded Wire Wall and Reinforced Soil Embankment,* Appendix B, Chapter One)
- Mr. James G. Collin, University of California, Berkeley (*Bar Mats,* Appendix B, Chapter Four)
- Mr. Richard R. Davidson, Woodward-Clyde Consultants, Denver (*Geotextiles and Plastic Strips,* Appendix A, Chapters Two and Three)
- Dr. Jean-Pierre Giroud, Woodward-Clyde Consultants, Chicago (*Geotextiles,* Appendix A, Chapter Two)
- Dr. Richard A. Jewell, Binnie and Partners, U.K. (*Anchored Earth* and *Geogrids,* Appendix B, Chapters Two and Three)
- Dr. Ilan Juran, Ecole Nationale des Ponts et Chaussees, France (*Reinforced Earth,* Appendix A, Chapter One; *Soil Nailing in Excavations* and in *Slope Stabilization,* Appendix C, Chapters One and Two)
- Prof. Francois M. Schlosser, Ecole Nationale des Ponts et Chaussees, France (*Reinforced Earth,* Appendix A, Chapter One; *Soil Nailing in Excavations* and in *Slope Stabilization,* Appendix C, Chapters One and Two)

Special recognition for their assistance with the critical review, rewriting, and editing of all appendixes is due Peter M. Vujaklia, Dames & Moore, and James G. Collin, University of California, Berkeley.

Contents

REINFORCEMENT OF EARTH SLOPES AND EMBANKMENTS

SUMMARY

The reinforcement of earth, which may be defined as the inclusion of resistant elements in a soil mass to improve its mechanical properties, has emerged over the last two decades as a technically attractive and cost-effective technique for extending the use of earth as a construction material. This is especially true on marginal sites with poor foundation soils that would otherwise require prohibitively expensive site improvement measures. Consequently, earth reinforcement techniques, and the resultant new composite materials, have been the subject of much interest and ongoing research both in the United States and abroad.

The use of earth reinforcement is so well suited to the needs of highway construction and reconstruction that many of the currently available techniques were specifically developed for highway applications. Steep slopes of reinforced soil reduce the required width of new rights-of-way and are specially suitable for the widening of existing traffic lanes in constricted rights-of-way. Reinforced soil is also extremely versatile in application. It may, for example, be used for the construction of new embankments, for the retention of excavations, and for the stabilization of slopes. Furthermore, because of the ease and speed of construction and the normally very limited site preparation requirements, reinforced soil construction results in less traffic disruption than conventional construction techniques.

In spite of the advantages of earth reinforcement, a comprehensive publication, providing both state-of-the-art knowledge and state-of-practice design guides regarding earth reinforcement techniques for engineers, has not previously existed. The lack of such a document inevitably posed a hindrance to the practicing engineer with regard to both the acceptance and efficient utilization of earth reinforcement. At worst, the practitioner was not aware of the concept and its inherent advantages; at best, it was necessary to sieve through a large body of often hard-to-come-by literature to design, or verify the design of, a single structure. Yet, many of the designs are relatively simple.

Accordingly, it is the purpose of this document to provide the practitioner with:

- A detailed introduction to the concept of earth reinforcement in general.
- Insight into the existing earth reinforcement methods and their inherent advantages and shortcomings.
- A description of the applicability of earth reinforcement to specific problems, especially those pertaining to highway engineering.
- A description of the internal mechanisms of reinforcement developed with various reinforcement types.
- A description of the engineering behavior of reinforced soil structures, and how the selection of a specific reinforcement type may influence that behavior.
- Clear guidance on the selection of reinforcement types appropriate to the solution of specific problems.
- Most importantly, a description of the design and construction methods, together with design examples, for each of the currently used reinforcement systems.

To meet the foregoing objectives, the report has been confined to a description of current design methods and technology as developed by various researchers and vendors. It was not the intent of this study either to provide new design methods or to develop improvements on the shortcomings inherent to some of the existing methods.

Organization of Report

The complete report is divided into two parts. The first part of the report, the main text, is concerned with the general concept of earth reinforcement and is divided into six chapters providing an introduction, as well as descriptions of the available systems, applications and costs, internal mechanisms and behavior, design methodology, and durability considerations. A seventh chapter identifies the areas in need of further research and development.

The second part is composed of five appendixes. Appendix A describes the systems designed on the basis of frictional reinforcement, i.e., Reinforced Earth, Geotextiles, and Plastics. Appendix B describes systems designed on the basis of passive resistance, i.e., Welded Wire Wall (including Reinforced Soil Embankment), Anchored Earth Geogrids, and Bar Mat Systems (including VSL Retained Earth, Mechanically Stabilized Embankments, and Georgia Stabilized Embankments). Appendix C describes soil nailing in excavations and slope stabilization. Each method-specific appendix provides an introduction and descriptions of applications, mechanisms and behavior, technology, durability and selection of backfill (or evaluation of in-situ ground in the case of soil nailing), construction, design methods, case histories, cost comparisons, future developments, and design examples. The final appendixes contain a comprehensive bibliography (Appendix D) and a glossary of terms and definitions of symbols (Appendix E).

The following discussion briefly brings together the fundamental concepts and current state of the art in earth reinforcement.

Summary of Topics Covered in the Report

Available Systems. An earth reinforcement system has three main components: reinforcements, backfill or in-situ ground, and facing elements. Both metallic and nonmetallic (geotextiles, plastics) materials are used for reinforcement. In strip reinforcement systems, a coherent, composite material is formed by placing the strips in horizontal planes between successive lifts of backfill. Grid reinforcement systems consist of metallic bar mats or polymeric tensile resisting elements arranged in rectangular grids placed in horizontal planes in the backfill. Wire mesh can be used in a similar manner, as can continuous sheets of geotextile laid between layers of backfill.

The facing elements currently used include precast concrete panels, prefabricated metal sheets and plates, gabions, welded wire mesh, shotcrete, seeded soil, masonry blocks, and geotextiles. Selection among these depends on type of reinforcement, function, and aesthetics.

In-situ reinforcement systems, or soil nailing, ordinarily utilize steel bars, metal tubes, or other metal rods that resist not only tensile stresses but also shear stresses and bending moments.

Presently used earth reinforcement systems are compared in Chapter Two, Table 1, in terms of soil geometry, soil type, stress transfer mechanism, and reinforcement material.

Applications. Earth reinforcement is presently used routinely for construction of retaining walls and abutment structures, for repair of slope failures, for retention of excavations, and for stabilization of slopes in-situ.

The inherent advantages of reinforced soil structures include the fact that the resulting systems are coherent and flexible, thus making them tolerant of large deformations; they are easy to construct; a range of backfill materials can be used; they are resistant to seismic loadings; they are often more economical than conventional structures; and the variety of available facing types and finishes makes possible visually pleasing structures. Furthermore, the keen competition among the developers and manufacturers of the different reinforcement systems has led to both innovation and economy.

In addition to the routine applications cited, other earth reinforcement applications have included foundation rafts, containment dikes, dams, seawalls, bulkheads, quays, and support for underground chambers.

Mechanisms and Behavior. Reinforcements, through their adherence to the surrounding soil, enable development of a coherent material that has the capacity both to stand unsupported and to resist externally applied loading. Most presently used reinforcements are inextensible in that they rupture at strains much less than those required to cause soil failure. Some geotextiles, which require large deformations to cause rupture, are an exception. Because these extensible reinforcements commonly have lower moduli of elasticity than the inextensible reinforcements,

larger soil strains are required to mobilize the reinforcement effect than with an inextensible reinforcement. High modulus reinforcements restrain soil deformation in a direction parallel to the reinforcements. The effect is as if there is an anisotropic cohesion or an increased confining pressure on the plane perpendicular to the reinforcements.

Transfer of stress between soil and reinforcements is by two basic mechanisms; namely, friction and passive soil resistance (or lateral bearing capacity). Both mechanisms are active in many reinforcement systems, and the relative contribution of each is indeterminate, at least on the basis of present knowledge.

Because the effective friction coefficient between soil and reinforcements is not amenable to estimation by analysis alone, pullout tests, model tests, and measurements on full-scale structures have been used to select appropriate values. Values of this coefficient ranging from 0.5 to greater than 1.0 are suitable for strip reinforcements. The lower values correspond to smooth reinforcements and large depths of burial, while the higher values are associated with rough or ribbed reinforcements and small overburden depths.

Passive soil resistance to reinforcement pullout develops against bearing surfaces normal to the direction of the force to be resisted. Relationships between vertical effective stress and lateral passive resistance (or bearing capacity) are commonly used to estimate the passive pullout resistance of a transverse earth reinforcement.

Many of the reinforcing elements used in soil nailing applications resist bending and shear stresses as well as tensile stresses. This introduces additional soil and reinforcement failure modes that must be considered.

For the case of soils reinforced with elements carrying only tensile stress, internal failure may occur if the reinforcements either pull out or rupture. The strength of the composite material is dependent on which of these failure modes develops first.

Knowledge or assumption of the earth pressures to be resisted by the reinforcements is essential for safe design of reinforced soil structures and slope stabilization by soil nailing. Values ranging from greater than the at-rest lateral pressure to the fully active earth pressure have been reported for different systems. Appropriate values for given reinforcement types are dependent on the degree of restraint which the reinforcement can impose on lateral soil deformations. This, in turn, depends on reinforcement stiffness and soil dilatancy. The fully active horizontal stress state is associated with those systems that are able to undergo relatively large lateral deformations, e.g., geotextiles. Higher lateral stress coefficients are appropriate for the less extensible reinforcements, e.g., steel strips, bar meshes, welded wire mesh, and relatively low confining pressures—in other words, at shallow depths in the backfill, where the soil dilatancy is most effective.

The mechanism of soil–reinforcement interaction is such that in a typical reinforced wall or embankment there is an active zone that tends to move out but which is retained by the reinforcements that transfer load to a resisting zone. Maximum tensile forces in the reinforcements occur between the active and resisting zones. Unfortunately, the locus of these maxima through a reinforced soil structure is not reliably known for all reinforcing systems or structure types.

Tensile reinforcement is most effective when oriented in the direction of maximum extension strain. This realization may be used to advantage in placement of reinforcements for soil nailing. However, construction considerations generally dictate that reinforcement be placed horizontally. Stiff reinforcements, which can resist both shear forces and bending moments, can sometimes be used effectively when aligned perpendicular to potential failure planes.

Most knowledge of reinforced soil structure behavior has been obtained for systems with cohesionless soil backfill. Further information is needed on the behavior of cohesive backfills. The use of soils with poorer strength, gradation, and plasticity characteristics will generally require more massive, more heavily reinforced, more deformable, and more costly structures. Creep and durability problems may be more severe in these soils as well. Nonetheless, use of lesser quality backfills may be possible in many cases.

The external stability of a reinforced soil system needs to be considered. Sliding of the reinforced mass on its base or at any level above its base, overturning, bearing capacity of the foundation soil, excessive settlement, and rotational or block sliding of the soil behind and beneath the structure must be considered. Usual methods of soil mechanics analysis may be used for this purpose.

Design. Reinforced soils and embankments must be designed for both internal and external stability. The external stability is evaluated following usual procedures of geotechnical engineering as just noted. The internal stability depends on there being neither pullout nor rupture of the reinforcement. For a given type of reinforcement this means that the length and spacings of the reinforcing members must be determined and that a suitable facing scheme must be selected.

The development of design methodology has been based on limit equilibrium analysis, working stress analysis based on measurements on full-scale and model structures, and the results of finite element analyses. Different assumptions have been made for the failure surface geometry for analyses of different types of reinforcement systems.

Pullout capacity determinations are made using the assumption that pullout resistance of a given reinforcement type is either primarily frictional, primarily by passive soil resistance, or a combination of the two. Most design methods which include both friction and passive resistance consider these independently and assume that they are simply additive. Because the strain produced by one mechanism may reduce the force or stress developed by the other mechanism, this simple addition may not be valid. The categorization of the systems described in this report and the equations used to calculate pullout resistance are presented in Chapter 5, Table 5. Knowledge or assumption of values for the horizontal earth pressure coefficient is also required, and the values used for the different earth reinforcement systems are given in Chapter 5, Table 6. A general design methodology is presented in Chapter 5.

Design of soil nailing involves the ensurance of an adequate global safety factor against combined soil and reinforcement failure. Four failure criteria—soil shear resistance, reinforcement pullout, passive failure of the soil loaded in bearing along the reinforcement, and the reinforcement strength—are used.

Durability. Reinforcement durability is a major consideration in reinforced soil systems. Possible damage during construction is always of concern, and deterioration due to chemical attack or the effects of prolonged stress application, temperature cycling, wetting and drying, and the like, during the life of the structure must be considered.

The corrosion of metallic reinforcements may be particularly rapid in soils containing a high content of dissolved salts, especially chloride and sulfate, and strongly acidic or alkaline pH. The relative corrosion resistances of different materials used as reinforcements are given in Chapter 6, Table 21.

Methods for estimation of corrosion rate are not precise; however, suitably conservative procedures for zinc galvanized steel reinforcement are given in Chapter 6. Highly resistant epoxy resin coating materials and methods for their application are now becoming available that may be both effective over long time periods and economical for use in particularly corrosive environments.

Special corrosion considerations may be required for soil nailing, because there is no choice of soil type and high strength steel may be used. Corrosion of high strength steel develops at crystal interfaces and is difficult to analyze. Often the soil nails are surrounded by grout; however, water may still reach the steel through microcracks. In some cases plastic or steel casings may be used around the grout for added protection, which can also be provided by prestressing of the grout to prevent water entry through the microcracks.

Nonmetallic reinforcements may be degraded because of mechanical damage, strength loss and elongation due to load, and deterioration due to exposure. Care during storage, handling, and construction can minimize mechanical damages. Strength loss and excessive elongation from loading are best minimized by limiting the stress levels in the reinforcements.

Most geotextiles and plastics are very resistant to chemical and biological attack, so degradation from these sources is not likely to be a problem. However, many of the synthetic materials are susceptible to rather rapid deterioration when exposed to ultraviolet radiation. Therefore, it is necessary that exposure to light be kept to a minimum. This means that geotextile wall facings must be covered with shotcrete, seeded, or otherwise protected after construction.

Concluding Comments

The research has amply confirmed that earth reinforcement can provide safe and economical solutions to many earthwork problems. Thousands of structures have been built, with very few failures, and it can be expected that many more applications will continue in number.

This report was designed to produce a single reference source of information on our present knowledge in earth reinforcement. It is important to recognize, however, that although much progress has been made in this field, our understanding of all aspects of earth reinforcement is not yet complete. There is no generally accepted universal design methodology. There are unanswered questions about durability, and the full potential of all systems has not yet been realized. Hopefully, the information documented in this report will serve as a guide to initiate technical advances that will lead to even more efficient reinforcement designs, more durable materials, and more improved construction techniques.

CHAPTER ONE

INTRODUCTION

Contents

CONCEPT OF EARTH REINFORCEMENT

Soil is the most abundant and least expensive construction material. Many soils when at a suitable density and water content can be strong enough to be structurally useful, particularly when loaded only in compression. Like portland cement concrete, soil is very weak in tension. This limits the use of soil for some applications, such as those requiring slopes steeper than the internal friction angle of the soil, about 30 deg in most cases. But also, as is the case for reinforced concrete, the inclusion of reinforcements that are strong in tension can produce a composite material that combines the best load carrying features of both components. The resultant composite material when earth and reinforcing elements are combined is referred to as reinforced soil in this report. An essential aspect in the success of any earth reinforcement system is that the two materials be compatible in terms of surface characteristics or geometry, or a combination of both, so that stress can be transferred from one to the other. The reinforced concrete analog is the bond between portland cement concrete and steel reinforcing bars.

The effect of tensile soil reinforcements on the stability of dry sand and, in fact, the concept of earth reinforcement are illustrated in Figures 1 and 2. Figure 1 shows a pile of sand with the steepest slope that can be maintained with the sand in its dry state. Figure 2 shows the same dry sand, only in this case strips of paper are incorporated as reinforcements. Note that in this case a vertical slope can be maintained. The paper used for the wall facing is needed to prevent running of the sand from the region between reinforcements; however, it does not assume a major structural or load carrying function. The horizontal strips of paper act as the reinforcements and provide the necessary apparent "cohesion" to the component material to allow the vertical slope.

Similarly, existing ground and embankments can be strengthened by the installation or inclusion of reinforcements. This offers a potential for increasing natural slope stability, for maintaining vertical slopes in embankments, and for enabling excavation of cuts with steep or vertical faces without internal excavation bracing.

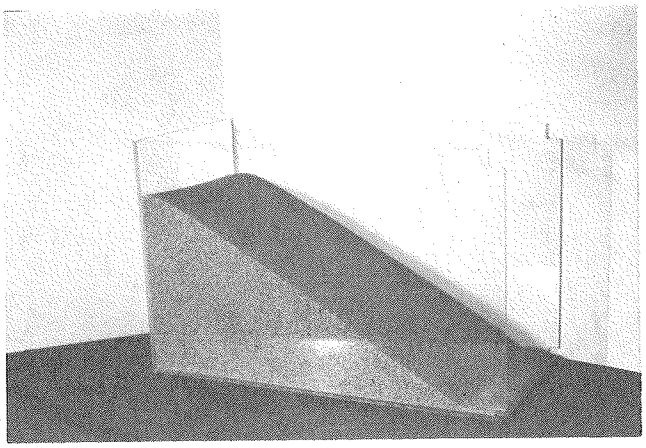

Figure 1. Dry sand with maximum stable slope.

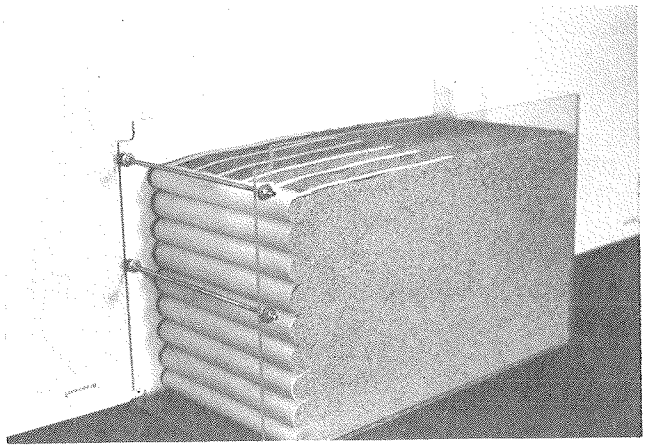

Figure 2. Dry sand reinforcement with strips of paper.

HISTORY OF DEVELOPMENT

Tensile inclusions have been used in soils for several thousand years. Large religious towers, called ziggurats, were built by the Babylonians between 5,000 and 2,500 years ago. These structures, of which an example is shown on Figure 3, had walls faced with clay bricks in an asphalt mortar with blocks of sun-dried brick behind. Layers of reed matting were laid as horizontal reinforcing sheets in the mud. Additional reinforcement was included in some ziggurats in the form of ropes about 2 in. (50 mm) in diameter placed perpendicular to the wall and regularly spaced in the horizontal and vertical directions [Mallowan (*1*)].

Many primitive peoples used sticks and branches for reinforcement of mud dwellings. Corduroy roads strengthened with logs placed transversely over soft subgrades were widely used for construction of roads across very weak ground in colonial America. In 1822, C. W. Pasley (*2*) reported tests on model walls, 4 ft 3 in. high, made of soil reinforced by horizontal layers of sacking material. The reinforcement was not connected to the wall face. The wall stability was reported to increase by 12 percent.

The French architect and inventor Henri Vidal (*3*) pioneered the development of modern earth reinforcement techniques; the system he developed, known as Reinforced Earth in the United States, was patented in 1966 as *Terre Armee* in France. The first highway use of a Vidal Reinforced Earth wall was near Nice, France (Fig. 4). Reinforced Earth walls of this type were first used in the United States in 1972 to provide support for California State Highway 39 along a steep slope in the San Gabriel Mountains north of Los Angeles (Fig. 5).

Since that time the use of earth reinforcement has greatly increased. Several types of reinforcement systems have been developed for applications in walls, embankments and strengthening of in-situ ground. Reinforcements made of steel, geotextile, and plastics are now readily available and commonly used. Wall facings of precast concrete, metal, geotextile, wire mesh, and shotcrete are common. Several thousand structures have been

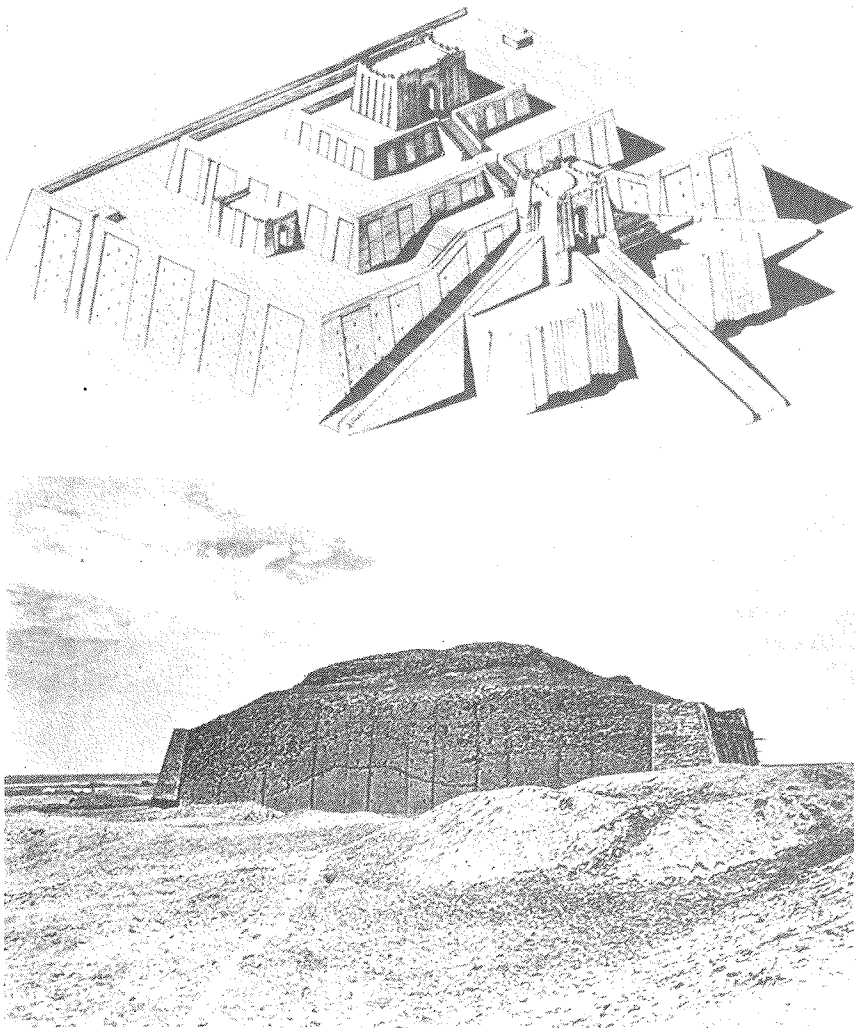

Figure 3. Ziggurat of Ur in Mesopotamia about 2500 B.C. Reinforcement is considered a major factor in its longevity. (Source: Ref. 1)

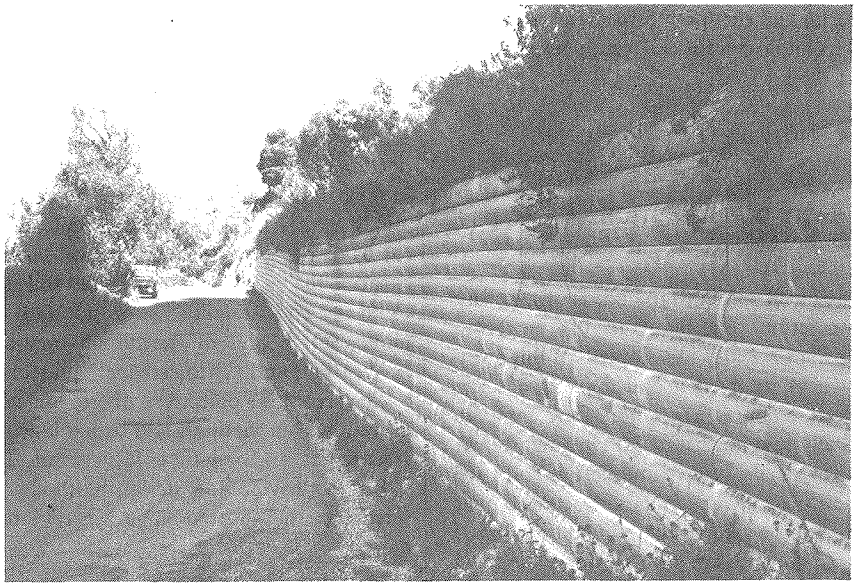

Figure 4. First highway use of modern Reinforced Earth wall, in France between Nice and the Italian border.

Figure 5. First Reinforced Earth wall constructed in the United States along Highway 39, in the San Gabriel Mountains of Southern California.

completed around the world, and earth reinforcement has taken a major place among the technologies for earth support systems.

APPLICATIONS TO HIGHWAY CONSTRUCTION, MAINTENANCE, AND IMPROVEMENT

Earth reinforcement is so well suited to the needs of highway construction and reconstruction that many of the currently available techniques were specifically developed for highway applications. Probably two of its most useful applications are for retaining walls and bridge abutments, where they compete favorably, both economically and aesthetically, with reinforced concrete. In some cases, especially when foundation soils are deformable, reinforced soil provides technical advantages over reinforced concrete because of the greater flexibility of reinforced soil structures. Any situation requiring an elevation change of more than a few feet over a relatively short distance is potentially suitable for earth reinforcement.

Steep slopes made possible by the use of reinforced soil reduce the required width of new rights-of-way. Slope steepening by construction of reinforced soil walls can facilitate the widening of existing traffic lanes in constricted rights-of-way. Reinforcement may be used for construction of new embankments, for the retention of excavations, and for the stabilization of slopes. Because of the ease and speed of construction and because site preparation requirements are usually minimal, reinforced soil construction normally results in less traffic disruption than conventional construction techniques.

Routine and special applications of earth reinforcement are described in more detail in the appendixes to this report, each of which is concerned with specific types of reinforcement. In addition to retaining walls and bridge abutments, reinforced soil has been used for construction of foundation rafts, sloping walls, containment dikes, dams, underground chambers, seawalls, bulkheads, and quays. Because reinforced soil structures are flexible, they are well suited for use on soft ground and can often be combined with other ground improvement methods to provide cost-effective remedies to problems posed by poor foundation soils.

OBJECTIVES OF THE REPORT

The basic concept of earth reinforcement is very simple. Because of the many applications to highway construction, maintenance, and improvement, and also to other earthwork construction, earth reinforcement has been implemented in many forms. Keen competition among the developers and manufacturers of different systems, combined with ongoing study and research by both the developers and manufacturers and independent researchers, has led to rapid technological development and continued cost reductions.

Thus, the use of some type of earth reinforcement may provide an effective and economical solution to many transportation corridor situations requiring retaining structures and slope stabilization. Unfortunately, while much specialized literature on the subject has appeared, there does not yet exist a comprehensive document that provides both state-of-the-art knowledge and state-of-practice design guidance for engineers. Accordingly, this report has been prepared for the purpose of providing such a document. In particular, the objectives are: (1) to provide insight into existing earth reinforcement methods and their advantages and limitations; (2) to describe applications to specific problems; (3) to explain the mechanisms of earth reinforcement; (4) to describe the behavior of reinforced soil structures; (5) to provide clear and concise guidance on selection of an appropriate technique; (6) to present the design methods and illustrate their application; and (7) to establish guidelines for estimating costs.

To meet these objectives, the report contains a description of current design methods and technology as developed by various researchers and vendors. It was not the intent of this study either to provide new design methods or to develop improvements on the shortcomings inherent to some of the existing methods.

REPORT ORGANIZATION

The main body of the report describes earth reinforcement in general, and it provides specific information about aspects important to all types of reinforcing systems, e.g., mechanisms, design approaches, durability considerations. Method-specific appendixes present details unique to particular systems and methods.

TERMINOLOGY

A glossary of terms commonly used in the description, analysis, and design of earth reinforcement systems is included at the end of the report (Appendix E). For internal consistency the geometrical and dimensioning scheme shown in Figure 6 has been adopted. Insofar as possible the same notation is used throughout the main report and all appendixes.

The terms earth reinforcement and reinforced soil are used generally throughout this report to refer to the composite material resulting when reinforcements are included in soil. Specific earth reinforcement methods developed by various companies, and which are often patented, are referred to by their specific trade names.

REFERENCES

1. MALLOWAN, M. E. L., *Early Mesopotamia and Iran.* London: Thames and Hudson (1963).
2. PASLEY, C. W., *Course of Elementary Fortification.* London: J. Murray (1822) Vol. 2, Ch. 26.
3. VIDAL, H., "The Principle of Reinforced Earth." *Highway Research Record 282,* Highway Research Board, National Research Council, Washington, D.C. (1969) pp. 1–16.

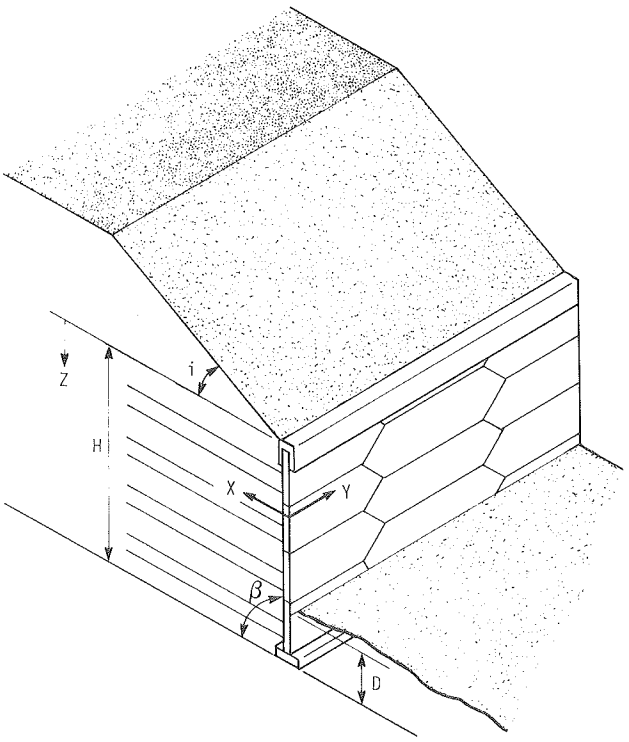

Notations:

X - Horizontal Distance Behind the Facing

Y - Horizontal Transverse Distance Along the Wall

Z - Depth Below Top of Wall

H - Height of Wall

D - Depth of Embedment at Toe of Wall

β - Facing Slope

i - Backfill Slope Angle

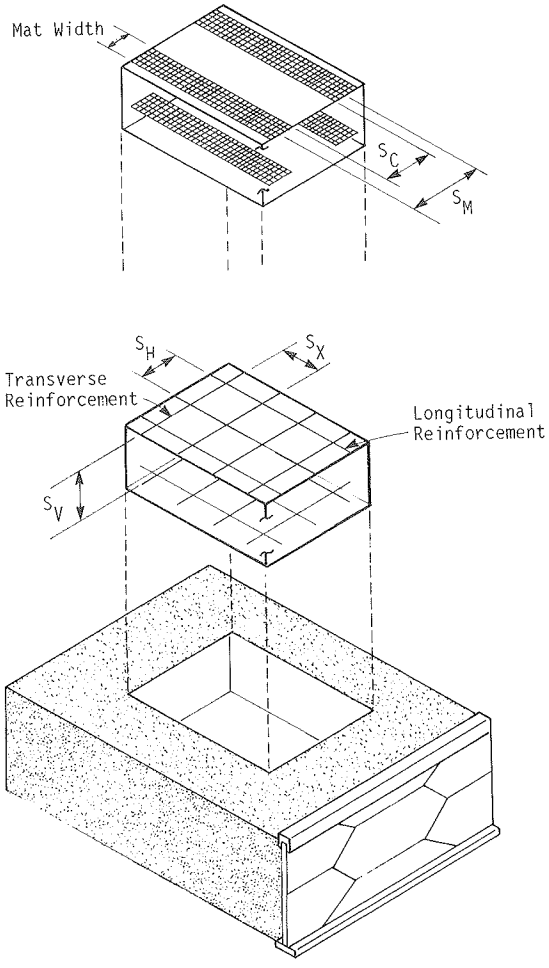

Notations:

S_V - Vertical Spacing Between Reinforcements

S_H - Center to Center Spacing Between Longitudinal Reinforcements

S_X - Center to Center Spacing Between Transverse Reinforcements

S_M - Mat Spacing, Center to Center

S_C - Clear Spacing

μ^* - Effective Friction Factor

Figure 6. Geometrical and dimensional notations used in this report.

CHAPTER TWO

AVAILABLE SYSTEMS

Contents

An earth reinforcement system has three major components: reinforcements, backfill or in-situ ground, and facing elements. The reinforcements may be described by the type of material used and the reinforcement geometry. The reinforcement materials can be broadly differentiated between metallic and nonmetallic materials, while the reinforcement geometries can be broadly categorized as strips, grids, sheets, rods, and fibers.

The type of backfill or in-situ ground is an important variable determining performance of the composite reinforced soil structure. Granular material is normally used for constructed embankment type applications to meet stress transfer, durability, and drainage requirements.

Facing elements are commonly provided to retain fill material at the face and to prevent slumping and erosion of steep faces. Available facing elements include precast concrete panels, prefabricated metal sheets and plates, gabions, welded wire mesh, shotcrete (reinforced or not), inclusion of intermediate reinforcements between main reinforcement layers at the face, seeding of the exposed soil, and looping of geotextile reinforcements at the face.

As discussed in detail in Chapter Four, the two main mechanisms of stress transfer between the reinforcement and soil are: (1) friction between plane surface areas of the reinforcement and soil; and (2) passive soil bearing resistance on reinforcement surfaces oriented normal to the direction of relative movement between soil and the reinforcement.

Strip, rod, and sheet reinforcements transfer stress to the soil predominantly by friction, while deformed rod and grid reinforcements transfer stress to the ground mainly through passive resistance, or both passive resistance and frictional stress transfer.

In this chapter brief descriptions of the available earth reinforcement systems are presented within the categories of constructed embankment and in-situ slope improvement applications. More detailed descriptions of several of the currently used systems are provided in the method-specific appendixes.

DESCRIPTION OF CONSTRUCTED EMBANKMENT-TYPE EARTH REINFORCEMENT SYSTEMS

Strip Reinforcement

With strip reinforcement methods, a coherent reinforced soil material is created by the interaction of longitudinal, linear reinforcing strips and the soil backfill. The strips, either metal or plastic, are normally placed in horizontal planes between successive lifts of soil backfill.

Reinforced Earth (see Fig. 7) is a strip reinforcement system which uses prefabricated galvanized steel strips, either ribbed or smooth. Facing panels fastened to the strips usually consist of either precast concrete panels or prefabricated metal elements. Backfill soil should meet specific geotechnical and durability criteria.

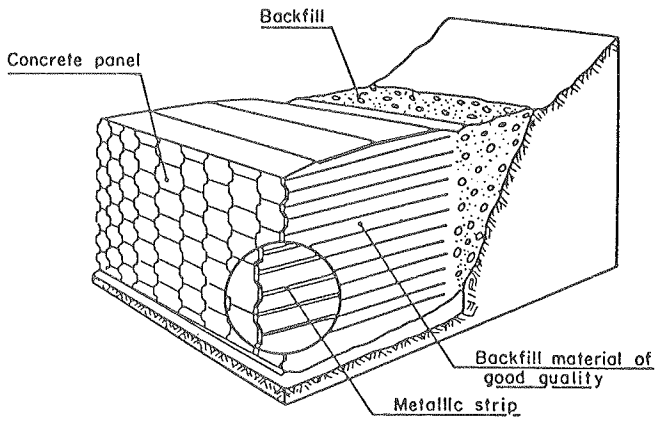

Figure 7. Schematic diagram of a Reinforced Earth wall.

Plastic strips have been introduced in an effort to avoid the problem of metal corrosion in adverse environments. However, all aspects of their durability are not yet fully known. Currently, the only commercially available nonmetallic strips are the Paraweb strip (see Fig. 8), in which the fibers are made of high tenacity polyester or polyaramid given added strength by extrusion through dies or by drawing and Fibretain. The strips are fastened to wall facings, typically consisting of precast concrete panels. Soil backfill is generally granular, ranging in size from sand to gravel.

Grid Reinforcement

Grid reinforcement systems consist of metallic or polymeric tensile resistant elements arranged in rectangular grids placed in horizontal planes in the backfill to resist outward movement of the reinforced soil mass. Grids transfer stress to the soil through passive soil resistance on transverse members of the grid and friction between the soil and horizontal surfaces of the grid.

The Mechanically Stabilized Embankment (MSE) system developed by the California Department of Transportation (see Fig. 9) employs prefabricated steel bar mat reinforcements positioned at standard horizontal and vertical spacings and uses standard rectangular precast facing panels. The backfill soil is usually on-site material with a drainage blanket but can be specified to be a granular material to maintain good drainage and to minimize creep movement. VSL Retained Earth (see Fig. 10) and Georgia Stabilized Embankments (GASE) use grid reinforcements similar to those of California Department of Transportation's design. Precast concrete facing panels for GASE are similar to those shown on Figure 9.

The Welded Wire Wall (Fig. 11) and Reinforced Soil Embankment (RSE) (Fig. 12) systems employ standard welded wire mesh grid reinforcements within the backfill to constitute a reinforced soil structure. The two systems differ, however, in the facing arrangements. In the Welded Wire Wall, the face end of each mesh layer is bent upwards to provide the facing and then attached to the mesh above. Backing meshes may also be added behind the outer facing to reduce the mesh opening size for retention of backfill soil. The Reinforced Soil Embankment couples the reinforcing mesh with precast concrete facing panels. The wire meshes used are the same type that have been used extensively for reinforcement of concrete slabs.

Grid reinforcements made of stable polymer materials may provide good resistance to deterioration in adverse soil and groundwater environments. Tensar Geogrids (Fig. 13) are high strength polymer grid reinforcements manufactured from high density polyethylene or polypropylene using a stretching proc-

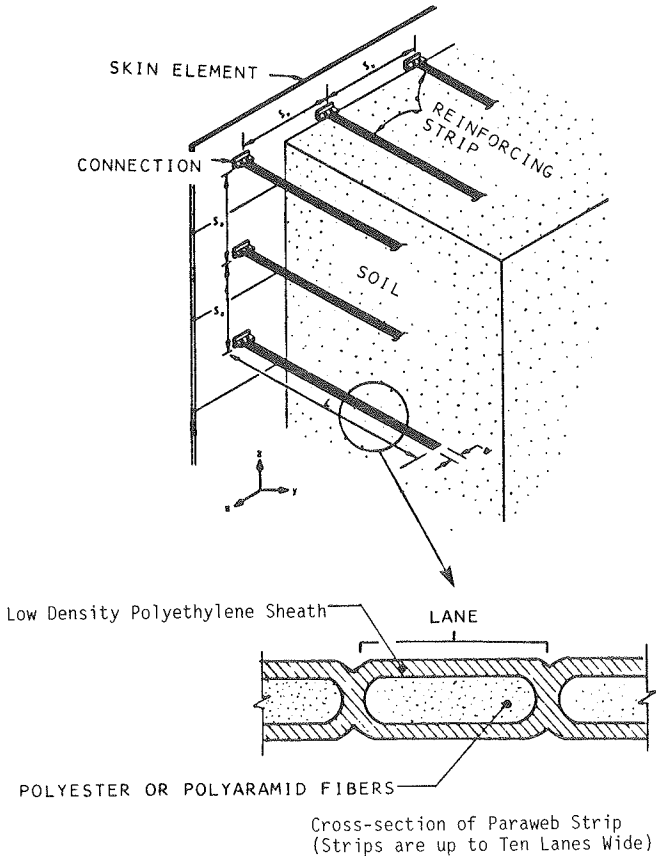

Figure 8. Schematic diagram of a nonmetallic strip reinforced wall.

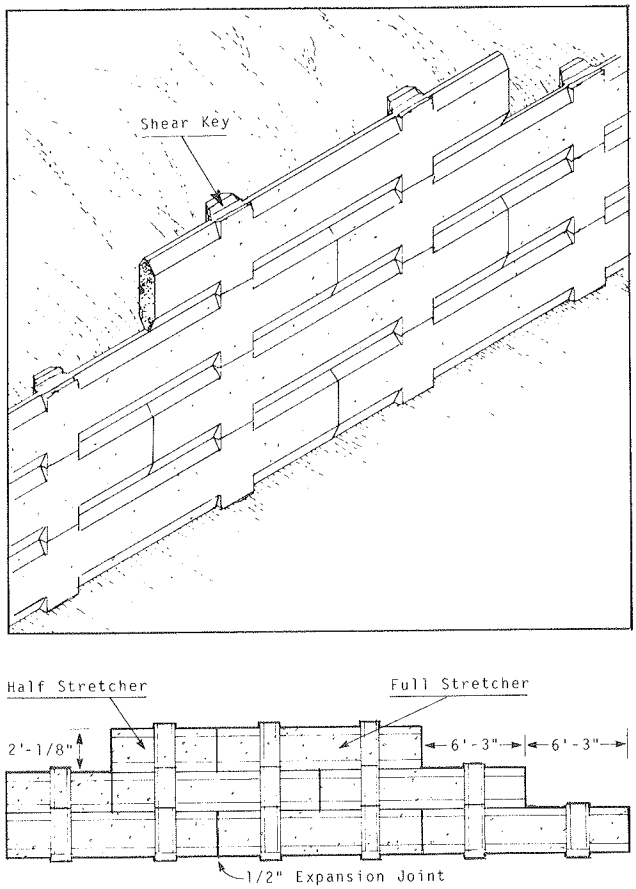

Figure 9. Mechanically Stabilized Embankment facing panel. (Source: Ref. 10)

ess. Facings can be formed for geogrids by looping reinforcements at the face or by attachment of the reinforcement grids to gabions or concrete panels.

Sheet Reinforcement

Continuous sheets of geotextiles laid down alternately with horizontal layers of soil form a composite reinforced soil material (see Fig. 14), with the mechanism of stress transfer between soil and sheet reinforcement being predominantly friction. The majority of geotextile fabrics used in soil reinforcement are made of either polyester or polypropylene fibers. Woven, nonwoven needle-punched, nonwoven heat-bonded, and resin-bonded fabrics are available as well as materials made by other processes. The backfill material typically consists of granular soil ranging from silty sand to gravel. Facing elements are commonly constructed by wrapping the geotextile around the exposed soil (see Fig. 14) at the face and covering the exposed fabric with gunite, asphalt emulsion, or concrete. Alternatively, structural elements such as concrete panels or gabions can be used. Connection between the geotextile sheet and structural wall elements can be provided by casting the geotextile into the concrete, friction, nailing, overlapping, or other bonding methods.

Rod Reinforcement

Anchored Earth, which is still in an early stage of development, employs slender steel rod reinforcements bent at one end to form anchors (see Fig. 15). Soil-to-reinforcement-stress transfer is assumed to be primarily through passive resistance, which implies that the system operates similarly to tied-back retaining

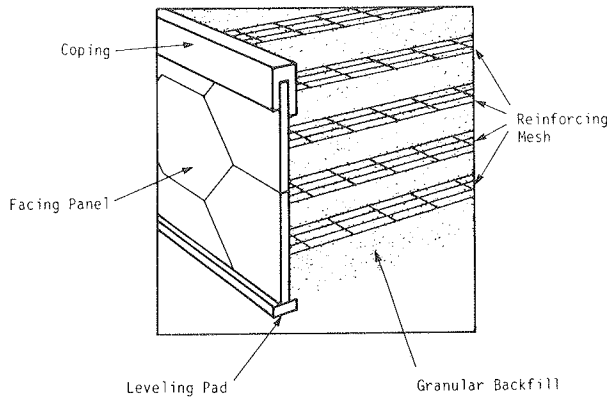

Figure 10. Schematic diagram of a VSL Retained Earth wall.

structures. As such, Anchored Earth is perhaps not truly a reinforced soil system. Nonetheless, friction should also be developed along the length of linear rod. Therefore, although this friction is not currently allowed for in design, the system may behave in some respects as a reinforced soil. As currently envisioned, the rods will be attached to concrete panel facings. Anchored Earth is undergoing continuing research and has not yet been extensively used.

Fiber Reinforcement

A composite construction material with improved mechanical

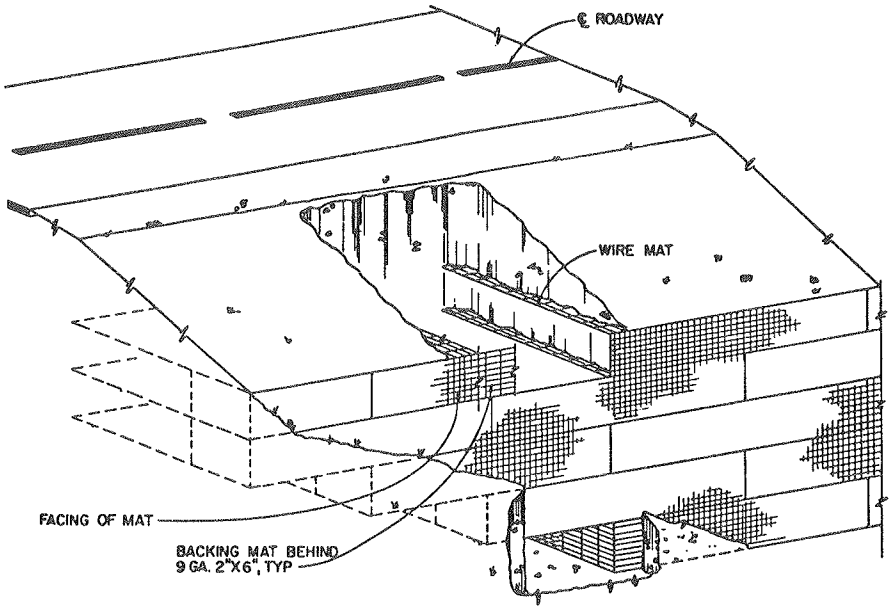

Figure 11. Schematic diagram of a Welded Wire Wall.

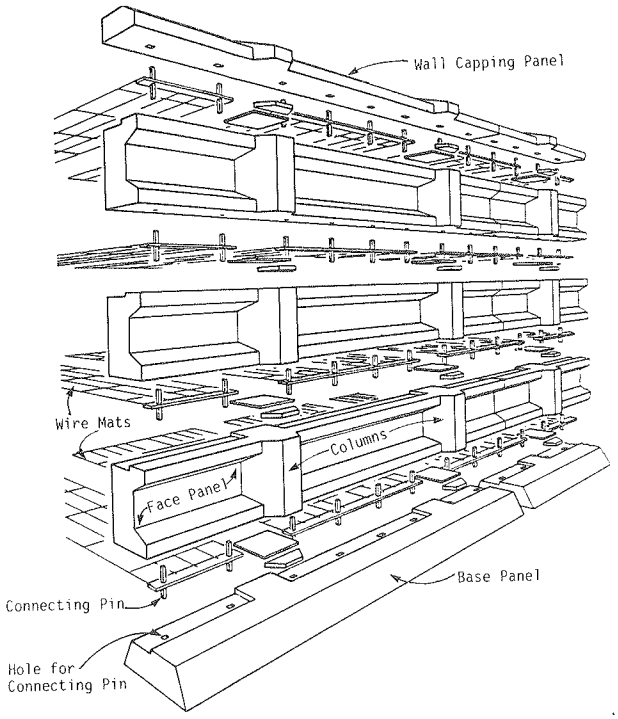

Figure 12. Schematic diagram of a Reinforced Soil Embankment (RSE).

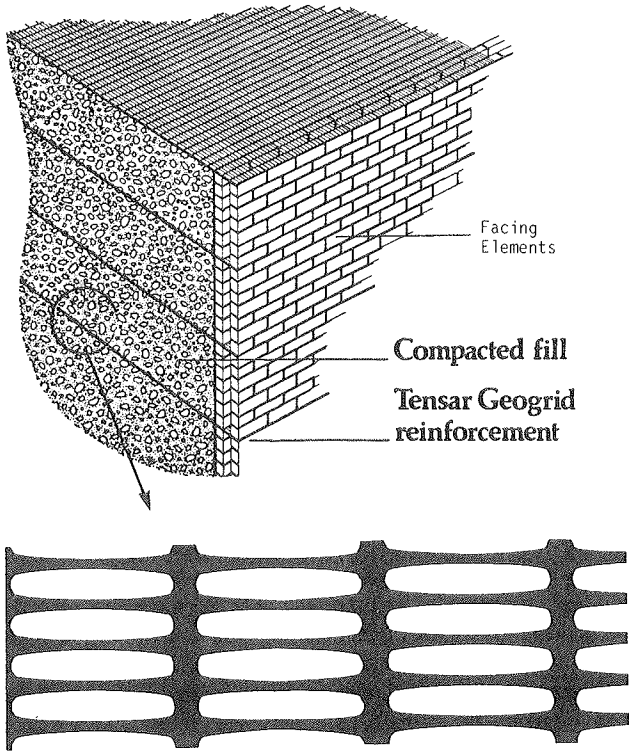

Figure 13. Schematic diagram of a reinforced soil wall using geogrid reinforcements.

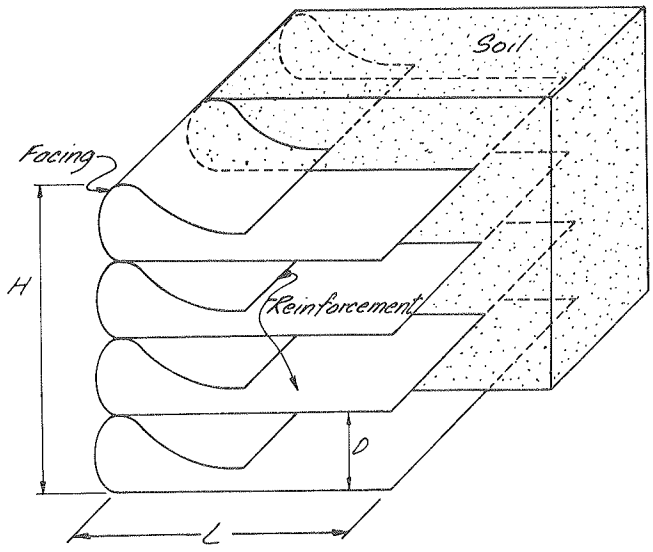

Figure 14. Schematic diagram of a reinforced soil wall using geotextile sheet reinforcements.

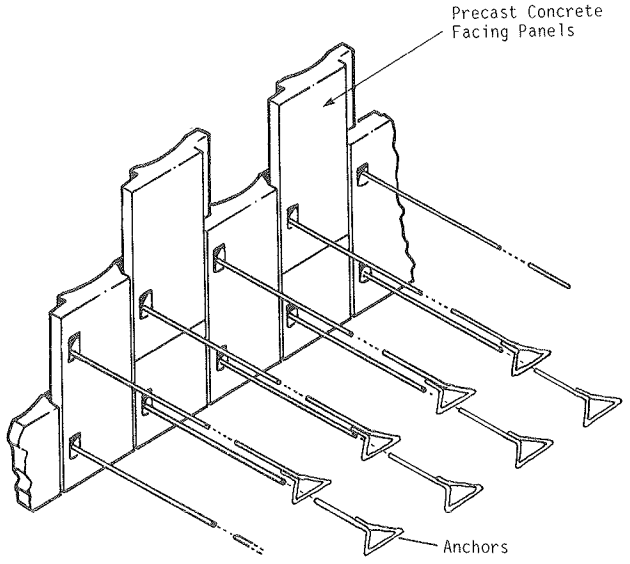

Figure 15. Schematic diagram of an Anchored Earth retaining wall. (Source: Ref. 6)

properties can be created by the inclusion of tensile resistant strands (fibers) within a soil mass. The engineering use of fiber reinforcements in soil, which is analogous to fiber reinforcement of concrete, is still in the early developmental stages. Materials being investigated for possible use include natural fibers (reeds and other plants), synthetic fibers (geotextile threads), and metallic fibers (small-diameter metal threads).

Unlike other reinforcements, fibers can potentially provide reinforcement in three directions. The major limitation to use of this method is the difficulties associated with efficiently and economically mixing the fibers uniformly into the backfill. In an experimental fiber reinforcement system described by Leflaive (*1*), continuous geotextile threads are incorporated into a sandy soil mass by a very complex mixing process. The limitations of

the mixing process currently still preclude full development of friction along the fibers. Thus far, the experimental system has demonstrated very high bearing capacity and also self-healing when subjected to erosion. However, the mixing process must be perfected before fiber inclusion can become an economically viable and routinely used reinforcement method. Retaining structures using this technology have already been constructed in France, demonstrating the technical viability of these methods.

Cellular Reinforcement Systems

Cellular reinforcements, as shown schematically in Figure 16, may be used at the base of embankments to significantly increase the bearing capacity of underlying weak soils and, hence, the stability of the embankments. Early laboratory investigations and theoretical analyses of such systems were performed at University of California, Berkeley, by Rea and Mitchell (*2*) and Mitchell et al. (*3*). Field tests of these "grid cells" were performed at the U.S. Army Engineer Waterways Experiment Station by, for example, Webster and Alford (*4*). More recently the systems have been further developed and are now commercially available under trade names such as GEOWEB.

Because this is a single reinforcing layer (analogous to a thick layer of geotextile at the base of an embankment), rather than a composite reinforced soil mass, these systems are not discussed further in this report.

DESCRIPTION OF IN-SITU SOIL, EARTH REINFORCEMENT SYSTEMS

Soil nailing, a method of reinforcement of in-situ soil by passive inclusions, can be used to retain excavations and to stabilize slopes by creating in-situ reinforced soil retaining structures. The main applications of soil nailing are shown schematically in Figure 17.

In nailed soil retained excavations (Fig. 17a), the reinforcements are generally steel bars, metal tubes, or other metal rods that can resist not only tensile stresses but also shear stresses and bending moments. The inclusions are mostly not prestressed and are relatively closely spaced. The nails can be installed in the excavated cut either by driving or grouting in predrilled boreholes. Stability of the ground surface between nails can be provided by a surface skin, often a thin layer of shotcrete reinforced with wire mesh, or by intermittent rigid elements analogous to large washers. Soil nailing in excavations has been used in both granular and cohesive in-situ soils and in relatively heterogeneous deposits. However, because of the difficulty of evaluating the corrosion rate of steel bars in the in-situ ground and of producing low cost, corrosion-resistant reinforcements, soil nailing has been limited primarily to temporary retaining structures.

The stabilization of unstable or creeping slopes by in-situ soil nailing consists of inserting rod reinforcements either vertically or perpendicularly to the failure surface. Reinforcements used for such applications have varied widely from large-diameter rigid piles to flexible steel rods grouted in boreholes (as also used for nailing of retained excavations). Typically, a single row of large-diameter rigid piles at the toe of an unstable slope would be used to stabilize the slope of providing passive resistance to the soil tending to slide downslope (see Fig. 17b). When small-diameter flexible rods are used, the unstable or creeping zone is generally uniformly reinforced by relatively closely spaced reinforcements (see Fig. 17c).

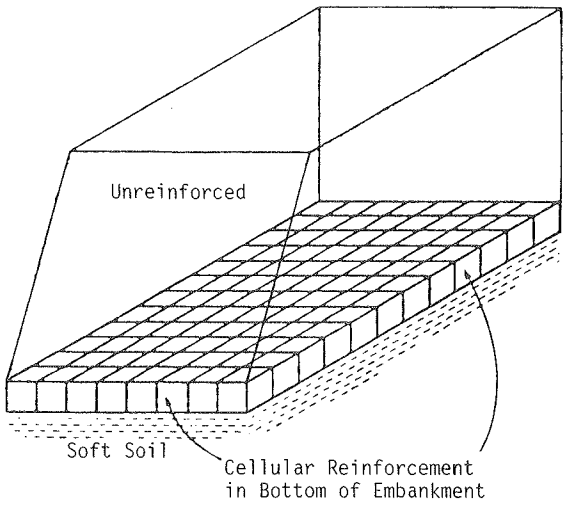

Figure 16. Embankment reinforcement using grid cells. (Source: Ref. 7)

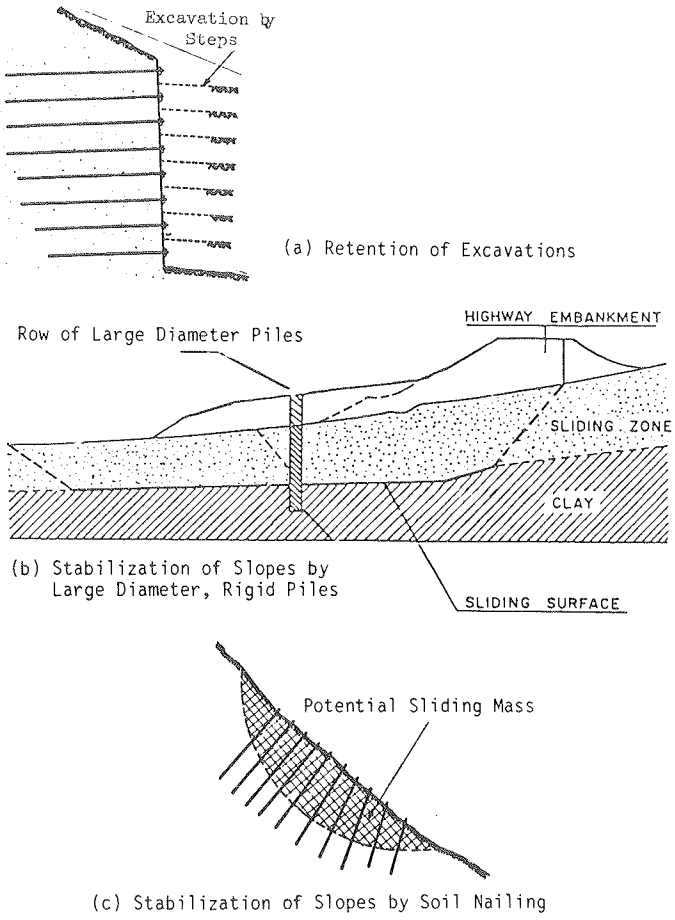

Figure 17. Main applications of soil nailing.

Element walls or prestressed multianchor walls employ prestressing of metallic rod reinforcements installed into in-situ ground, with the prestressing limiting the deflection required to mobilize the reinforcing pullout resistance. The concept is different from conventional prestressed anchored retaining walls in that the soil mass and anchors themselves form a coherent material and act as the retaining wall or retained face of an excavation. To accomplish this, the spacing of anchors is typically much less than in a conventional anchored wall and most of the components of a conventional anchored wall system (e.g., soldier piles, wales, lagging) are not required. Section and elevation views of an element wall retained excavation are shown in Figure 18.

Similar prestressing of reinforcements installed into existing ground can be employed with a recent Anchored Earth development; the anchor rods have a tip (at the end away from the retained face) that will expand when the rod is prestressed [*Engineering News Record* (*5*)].

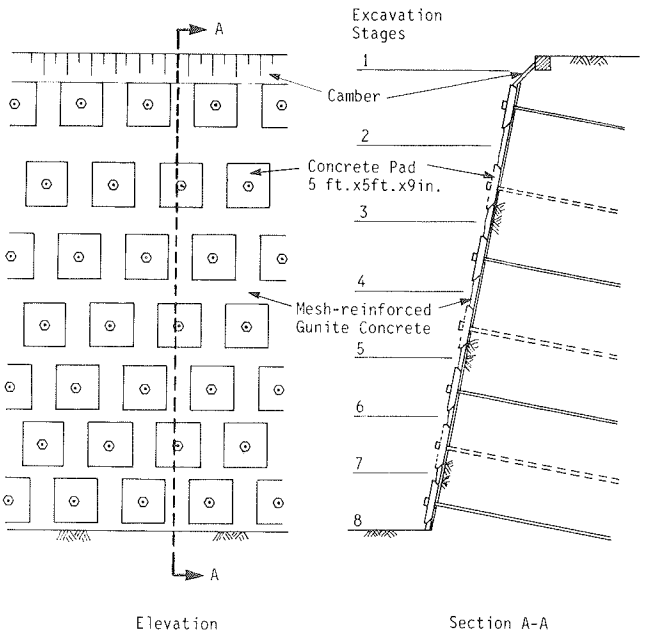

Figure 18. Section and elevation views of a typical element wall retained excavation. (Source: Ref. 8)

COMPARISON OF EARTH REINFORCEMENT SYSTEMS

The commonly used earth reinforcement systems are compared in Table 1 in terms of soil geometry, soil type, stress transfer mechanism, and reinforcement material. This table can be used as a preliminary guide to select possible earth reinforcement techniques appropriate to a specific application.

Table 1. Comparison of earth reinforcement systems. Note: Soil Type is based on stress transfer between soil reinforcement. Other criteria may preclude use of some soils for specific applications. (Adapted from Jewell, R.A. (1984), "Material Requirements for Geotextiles and Geogrids in Reinforced Slope Applications." *Proc.* 23rd International Man-Made Fibres Congress, Dornbirn, Austria)

	REINFORCEMENT TYPE		SOIL GEOMETRY (Slope 30 60 90 — Wall)	SOIL TYPE (Clay .002 — Silt .02 — Sand .2 — Gravel 2mm)	STRESS TRANSFER MECHANISM (Surface Friction — Passive Resistance)	REINFORCEMENT MATERIAL: Metal	REINFORCEMENT MATERIAL: Non-Metal	PROPRIETY SYSTEMS/PRODUCT NAMES
IMPORTED EMBANKMENT TYPE APPLICATION	STRIP	Smooth	●	●	●	●		Reinforced Earth
							●	
		Ribbed	●	●	●	●		Reinforced Earth
							●	Paraweb
	GRID		●	●	●	●		VSL, MSE, GAS, RSE, and Welded Wire Wall
							●	Tensar Geogrids
	SHEET		●	●	●		●	Geotextiles
	BENT ROD		●	●	●	●		Anchored Earth
	FIBER		●	●	●	●	●	
IN SITU GROUND IMPROVEMENT APPLICATIONS	FLEXABLE, SMALL DIAMETER NAILS		●	IN SITU SOILS	●	●		
	RIGID, LARGE DIAMETER PILES		●	IN SITU SOILS	●	●	●	

REFERENCES

1. LEFLAIVE, E., "The Reinforcement of Granular Materials with Continuous Fibers." *Proc. 2nd International Conference on Geotextiles,* Las Vegas, Nevada (Aug. 1982) Vol. III, pp. 721–726.
2. REA, C., and MITCHELL, J. K., "Sand Reinforcement Using Paper Grid Cells." *ASCE Proc. Symposium on Earth Reinforcement,* Pittsburgh, Penn. (1978) pp. 644–663.
3. MITCHELL, J. K., KAO, T. C., and KAVAZANJIAN, E., "Analysis of Grid Cell Reinforced Bases." *Technical Report*

GL-79-8, Geotechnical Engineering Laboratory, U.S. Army Engineer Waterways Experiment Station, Vicksburg, Miss. (1979).
4. WEBSTER, S. L., and ALFORD, "Investigation of Construction Concepts for Pavements Across Soft Ground." *Technical Report S-78-6,* U.S. Army Engineer Waterways Experiment Station, Vicksburg, Miss. (1978).
5. *Engineering News Record,* "Earth Reinforcing Progresses." Vol. 210, No. 15 (Apr. 14, 1983) pp. 26–27.
6. MURRAY, R. T., and IRWIN, M. J., "A Preliminary Study of TRRL Anchored Earth." *TRRL Supplementary Report 674* (1981).
7. MITCHELL, J. K., VILLET, W. C. B., and DIMILLIO, A. F., "Soil Reinforcement for Stabilization of Earth Slopes and Embankments." *Public Roads,* Vol. 48, No. 3, Federal Highway Administration (Dec. 1984) pp. 88–95.
8. *Ground Engineering,* "Germany's First Element Wall Installed in Stuttgart." Vol. 9, No. 2 (Mar. 1976) pp. 14–18.
9. JEWELL, R. A., "Material Requirements for Geotextiles and Geogrids in Reinforced Slope Applications." *Proc. 23rd International Man-Made Fibres Congress,* Dornbirn, Austria (Sept. 1984).
10. CHANG, J. C., HANNON, J. B., FORSYTH, R. A., "Field Performance of Earthwork Reinforcement." *CA/TL-81/06,* California Department of Transportation, Sacramento, California (Nov. 1981).

CHAPTER THREE

APPLICATIONS AND COSTS

Contents

Earth reinforcement is presently used routinely for construction of retaining walls and abutment structures, for repair of slope failures, for retention of excavations, and for stabilization of slopes in-situ. The principle has taken hold in practice because it offers specific technical, economic, and aesthetic advantages compared to more conventional methods.

This chapter looks at the general advantages, applications, and economics of earth reinforcement. The considerations presented here are common to all earth reinforcement systems. For an extensive discussion of the advantages and applications specific to individual systems, the reader is directed to the appendixes.

ADVANTAGES

Technical Advantages

Composite Construction Material. The stress transfer between soil and reinforcement creates a composite material with improved structural properties compared to nonreinforced soil. In fact, the use of abundant and relatively inexpensive soil as a construction material can be greatly extended as shown by some of the special applications discussed later in this chapter.

Flexibility. The deformation response characteristics of reinforced soil structures often provide technically attractive solu-

tions on sites with poor foundation soils. In comparison with conventional retaining walls, reinforced soil structures are extremely tolerant of large deformations, both laterally and vertically.

The performance of a 33-ft-high Reinforced Earth wall built in Roseburg, Oregon, demonstrates the flexibility and coherence of reinforced soil structures [McKittrick (*1*)]. The earth wall was built on an existing slope with weak foundation soils. A slide occurred in the poor foundation soils when the wall construction was near completion, and the wall consequently moved 18 ft laterally and 12 ft vertically. The cross section of the in-situ slope and the wall before and after the slide is shown in Figure 19. As can be seen from the figure, the Reinforced Earth wall remained a coherent mass despite the large movement.

The flexibility of reinforced soil structures also allows the use of lower factors of safety for bearing capacity design than conventional more rigid structures. The latter are normally designed to have bearing capacity factors of safety equal to 3 to restrict settlements to tolerable values, while reinforced soil structures are routinely designed with bearing capacity factors of safety as low as 1.5 to 2.0.

Construction. In general, placement of successive layers of backfill material, reinforcements, and facing elements does not require specialized contractors, skilled labor, or specialized equipment, and can be carried out with the same equipment and at a rate comparable to ordinary highway embankment construction. Many of the components of the available earth reinforcement systems are prefabricated, thus providing ease of forming and handling and allowing relatively quick construction. Often, only minimal working space is required in front of the earth structure, which is especially advantageous when working along existing highways or in restricted areas.

The use of in-situ earth reinforcement to retain excavations offers construction advantages over classical excavation bracing schemes, in that it avoids both obstructions within the excavation, such as cross-lot braces, and the excessive noise associated with driving of sheet piles or soldier piles. Also, although not yet used on a large scale, corrosion-resistant reinforcement could provide permanent soil restraint, thus reducing the design loads on buried structures.

Backfill Material. A fairly wide range of backfill materials has been used for reinforced soil structures. Suitable quality backfill material can frequently be found near the construction site and thus need not be imported. Typically, predominantly granular materials, such as clean sands and gravels, or silty sands and gravels have been used for backfill soils. Clayey and silty soils have been used successfully in a few applications. As performance experience is gained, use of these soil types may become more frequent.

Although not yet fully investigated, the use of admixture stabilizers, such as cement and lime, to improve plastic soils may further enhance the range of materials that can satisfactorily be used for reinforced soil.

Resistance to Seismic Loading. As a coherent yet flexible gravity mass, reinforced soil structures seem to be particularly well suited for construction in seismically active regions. The structures provide the high degree of structural damping needed to absorb large energy releases associated with earthquakes.

Economic Advantages

Reinforced soil can often provide the most economic retaining wall for embankments constructed under the constraints of limited access or right-of-way. The materials used are often less expensive than those required for a conventional wall; the soil, which comprises by far the largest percentage of volume, is relatively inexpensive, and cost effectiveness may hinge on cost of reinforcements and facing elements. The ease and speed of construction generally associated with the earth reinforcement methods is another source of cost savings relative to conventional walls.

Especially where the construction of rigid retaining walls would require deep foundations (e.g., mountainous areas with unstable slopes and sites underlain by compressible soils), the use of reinforced soil can result in significant cost savings. Because of inherent flexibility, a reinforced soil structure can tolerate large differential settlement and lateral movement. Hence, expensive deep foundations are not required provided overall stability requirements can still be satisfied.

More details on costs are provided later in this chapter.

Architectural Advantages

Because the facing elements play only a secondary structural role, a greater flexibility in choice of facing is available to meet aesthetic requirements than is the case for normal retaining walls. A wide variety of architectural finishes are available for the facing elements of reinforced soil structures. Available facing arrangements range from concrete panels of various geometric shapes, textures, and colors to provision of vegetation at the exposed face of the soil. For example, a VSL Retained Earth wall was constructed in an historic area of Hot Springs, South Dakota, with precast concrete panels textured and colored to complement the surrounding native sandstone in accordance with specifications of the local government and historical society. Another example of the potential for aesthetically pleasing architectural finishes is the Vail Pass tiered wall (see Fig. 20). The tiered embankment, required for construction of Interstate Route 70 through a highly scenic area in the Colorado Rockies, employed Reinforced Earth with special curved facing panels.

GENERAL APPLICATIONS

Probably the most frequent uses of earth reinforcement techniques have been for retaining walls and bridge abutments. Other applications have included repair of slope failures, foundation rafts, containment dikes, dams, seawalls, bulkheads, and quays. In addition to the built embankment applications, soil reinforcement has also been used for the improvement of ground in-situ; specific applications include stabilization of unstable or sliding slopes, retained excavations, and underground chambers.

SPECIAL APPLICATIONS

At the present state of soil reinforcement practice, most applications can be categorized as routine; however, as earth reinforcement methods become more widely used, more specialized uses will undoubtedly be developed.

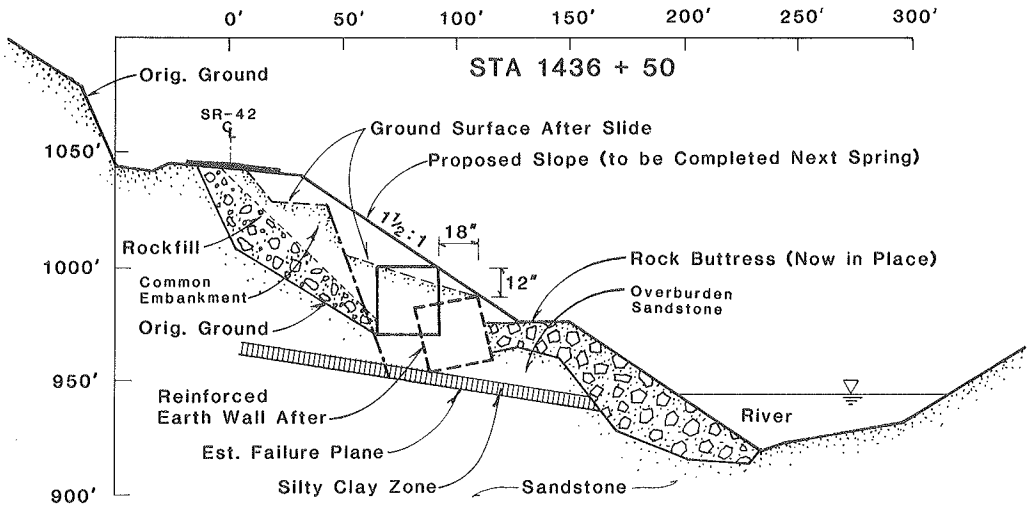

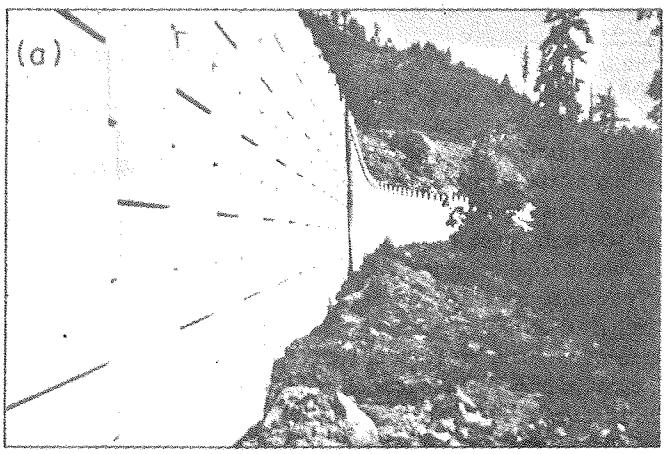

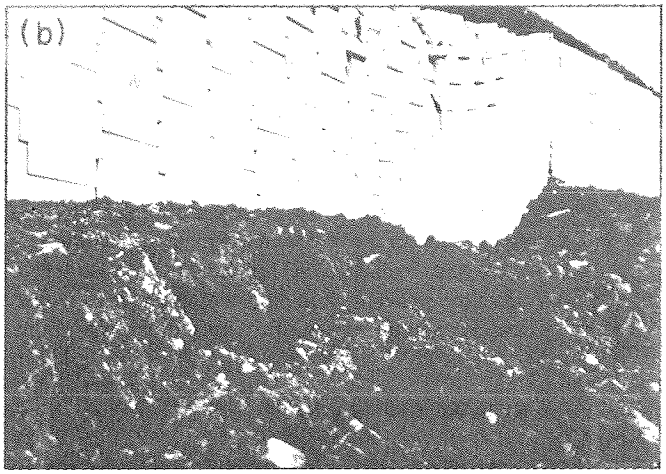

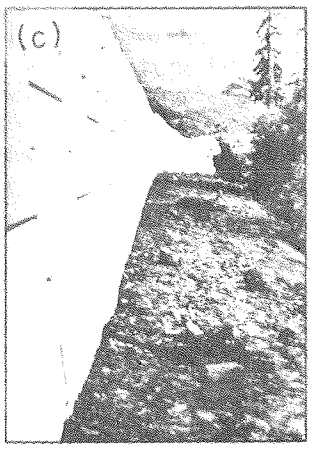

Figure 19. Roseburg-Coos Bay Highway, Oregon Route 42: (a) photograph of wall before the slide, (b) and (c) photographs of wall after the slide. (Source: Ref. 1)

Some special applications of built-embankment-type earth reinforcement systems are as follows:

- *Marine structures.* Reinforced soil structures have been used for seawalls, bulkheads, quays, and dams. Figure 21 shows a cross section of a typical seawall built with Reinforced Earth, and Figure 22 is a photograph of construction of a Reinforced Earth seawall in Petersburg, Alaska.
- *Storage slots.* A sloped wall form of Reinforced Earth has been developed and used for construction of roof-covered bulk storage facilities, as shown in Figure 23.
- *Foundation rafts.* Figure 24 is a schematic diagram of a Reinforced Earth slab constructed for support of a highway embankment of Pennsylvania Route 202. The slab was required to distribute embankment loads and span over sinkhole cavities at the site. An adapted form of Reinforced Earth with both longitudinal and transverse strips was used. A similar Reinforced Earth slab was constructed in Mercer County, West Virginia, to span over sinkhole cavities (see Fig. 25).

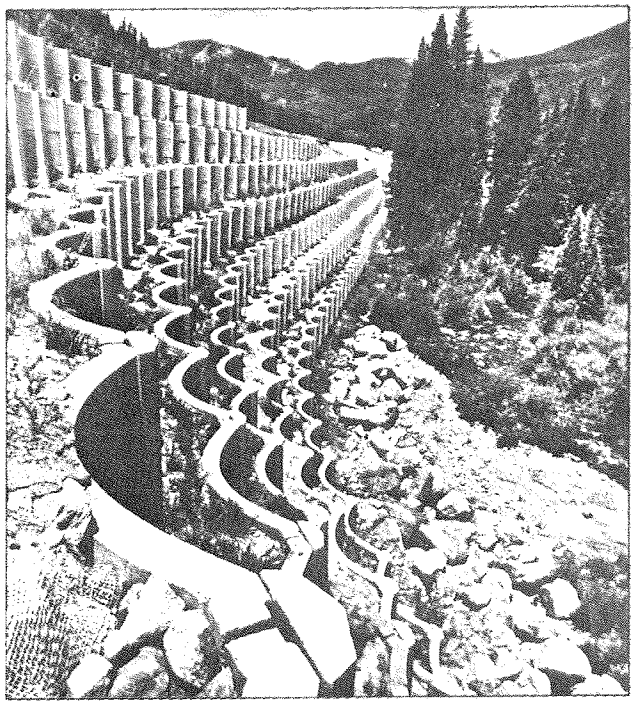

Figure 20. Vail Pass tiered Reinforced Earth wall. (Source: Ref. 1)

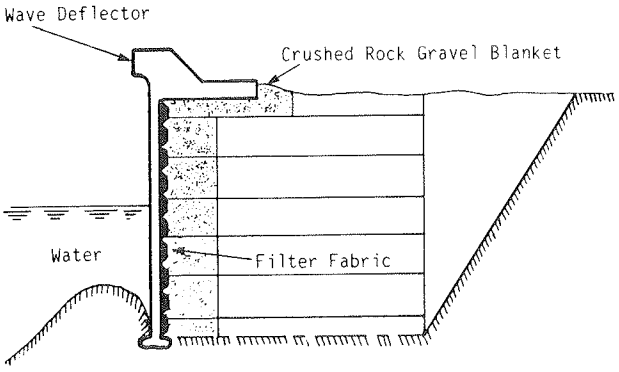

Figure 21. Cross section of a typical Reinforced Earth seawall.

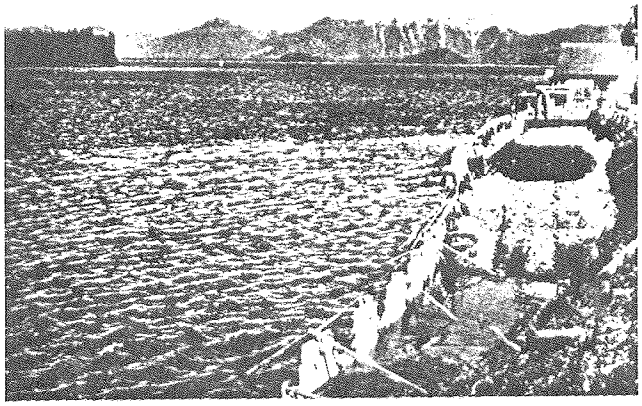

Figure 22. Reinforced Earth seawall under construction, Petersburg, Alaska. (Source: Ref. 2)

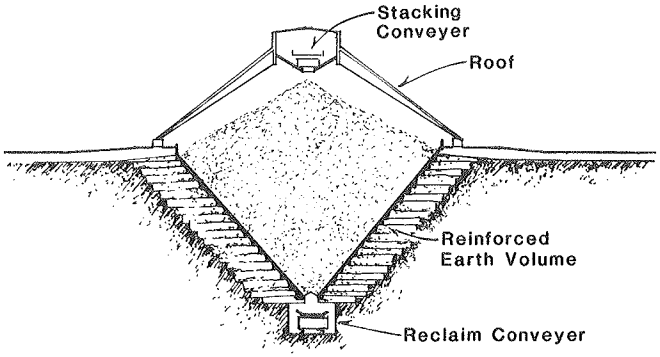

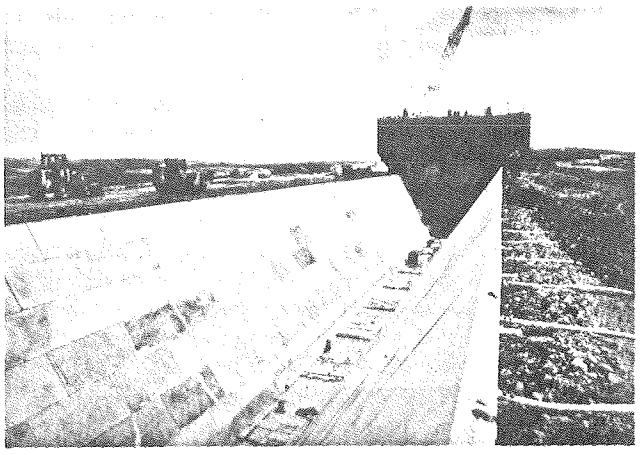

Figure 23. Bulk storage slot using Reinforced Earth.

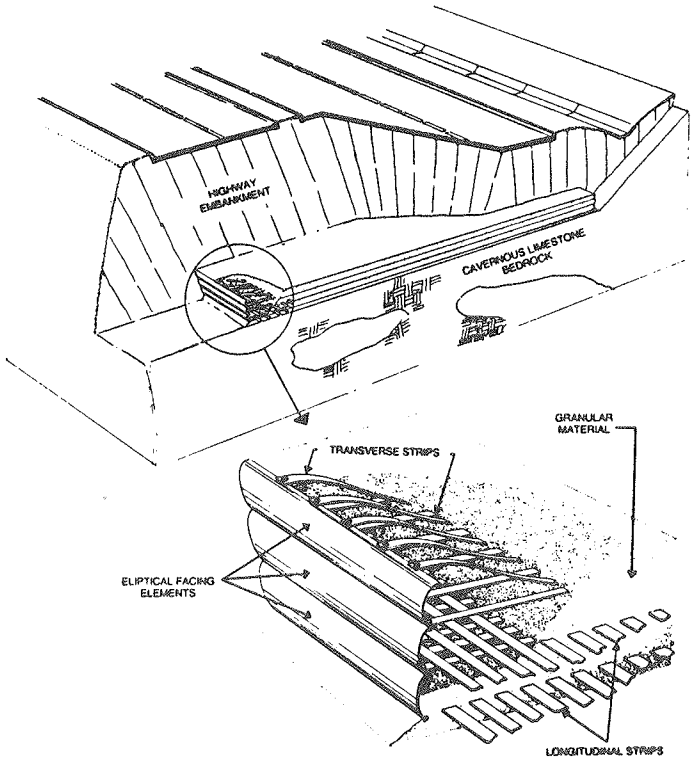

Figure 24. Reinforced Earth foundation raft, Pennsylvania Route 202. (Source: Ref. 2)

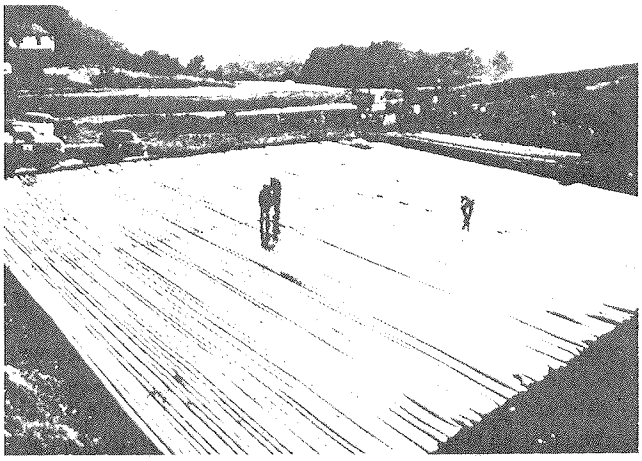

Figure 25. Reinforced Earth foundation raft, Mercer County, West Virginia. (Source: Ref. 2)

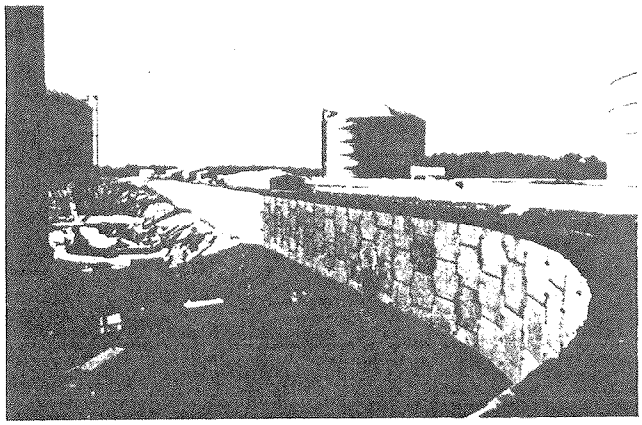

Figure 26. Reinforced Earth containment dike, Cove Point LNG Terminal, Maryland. (Source: Ref. 2)

- *Containment dikes.* Reinforced soil dikes have been used for secondary containment of hazardous liquids (LNG, crude oil) in tank storage areas. Reinforced Earth containment dikes built for the Cove Point LNG Terminal in Maryland are shown in Figure 26.
- *Embankments for high-speed railways.* Reinforced soil structures are effective in supporting high-speed railway lines because of their mass, flexibility, and high degree of structural damping. Reinforced soil structures would likewise be suitable for other applications where cyclical and dynamic loads are important (e.g., for blast protection at military installations and munitions plants).
- *Cantilevered wall.* At Sequoia Park Zoo in Eureka, California, a cantilevered Welded Wire Wall was constructed. The upper portion of the 12-ft-high wall was cantilevered out 18 in. in a 3-ft vertical section to keep the animals in.

To date, most of the special applications of imported embankment type reinforcement have employed Reinforced Earth; this is because it is the oldest available system and the one that has been most widely used. More specialized uses of other available earth reinforcement systems will no doubt be developed in the years to come.

Special applications of in-situ ground reinforcement by soil nailing are still rather limited. Soil nailing has been used for many tunneling applications, for example, the Marseilles subway tunnels constructed in 1978 (see Fig. 27). A potential special application of soil nailing is support of circular shafts, as shown in Figure 28.

COMBINATION OF EARTH REINFORCEMENT SYSTEMS

There are many possible applications of combinations of different earth reinforcement methods that have not been fully explored, or explored at all. For example, a reinforced soil embankment structure can be combined with soil nailing to enable high embankments on very weak soils. Where the width of an existing fill is restricted by right-of-way limitations, traffic lanes can be widened without disruption of traffic using element walls or prestressed multianchors near the bottom of the fill and a reinforced soil embankment near the top. Two or more

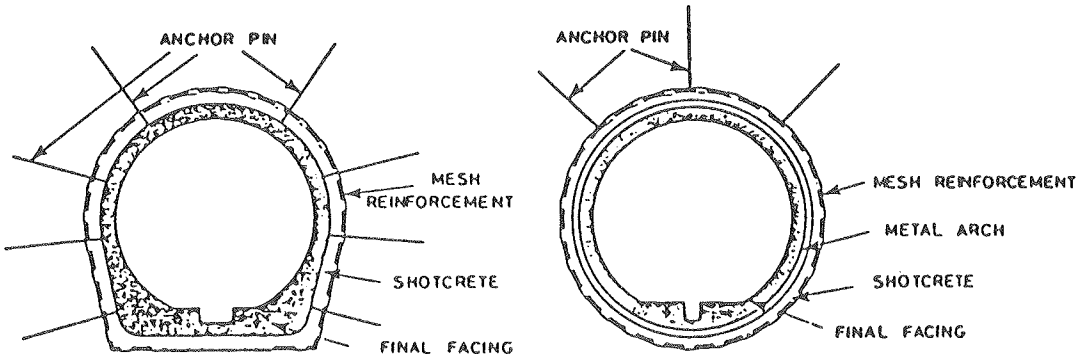

Figure 27. Typical cross sections of the tunnels of the Marseilles underground constructed by soil nailing in 1978.

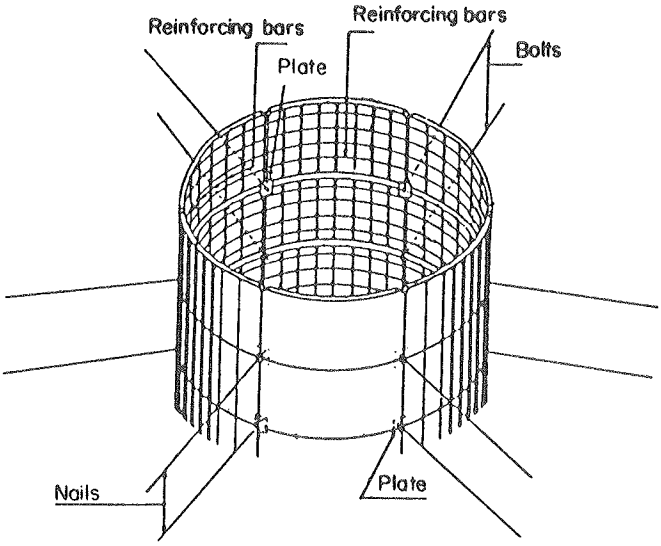

Figure 28. Schematic diagram of support of circular shafts using soil nailing.

reinforcement systems can be combined to take advantage of both frictional and passive resistance stress transfer mechanisms. The Websol frictional anchor system (Appendix A), as an example, is a combination of plastic strip reinforcements, geotextile sheets, and anchor bars.

Such combinations of systems are likely to be most useful when site conditions are especially demanding, for example, severe right-of-way limitations or extremely poor foundation soils.

COST CONSIDERATIONS

The cost of several reinforced soil projects constructed in California in the past 15 years is given in Table 2. The total cost of any reinforcement system is composed of materials, construction and backfill soil costs, and any special project features. Backfill soil costs depend highly on the suitability of on-site soil. Special project features might include a special wall facing treatment or restricted site access.

The cost of soil reinforcement in constant dollars is less today than it was 8 to 10 years ago because the technology is maturing and emergence of different reinforcing systems makes the market competitive. The 1984 cost of materials for Reinforced Earth walls 10 to 15 ft high was about $15 per sq ft, and about $17 to $18 per sq ft for walls 15 to 30 ft in height. In areas where construction equipment is readily available, reinforced concrete may be more economical than reinforced soil for walls up to 10 ft high. The two materials are competitive for the 10 to 30 ft height range, and the reinforced soil wall is likely to be less expensive for heights greater than 30 ft. Figures 29 and 30 indicate the comparative cost of reinforced soil and conventional reinforced concrete walls. A significant advantage of reinforced soil construction is the reduced cost of wall materials and erection. This is shown on Figure 31, which compares wall material and erection costs for six different wall types.

Cost comparisons are more difficult for slope and embankment reinforcement because each situation is likely to be unique, and there may be several options for each situation.

REFERENCES

1. McKittrick, D. P., "Reinforced Earth: Application of Theory and Research to Practice." *Proc. Symposium on Reinforcing and Stabilizing Techniques,* sponsored by the New South Wales Institute of Technology (Oct. 1978) (Also available from the Reinforced Earth Company).
2. Elias, V., and McKittrick, D. P., "Special Uses of Reinforced Earth in the United States." *Proc. International Conference on Soil Reinforcement: Reinforced Earth and Other Techniques,* Paris (Mar. 1979) Vol. I, pp. 255–259.
3. Transportation and Roads Research Laboratory "Reinforced Earth and Other Composite Techniques." Supplementary Report No. 457 (1979).

Table 2. Construction costs of reinforced soil projects in California. (Provided by California Department of Transportation)

Completion Year	Type of Wall	Type of Wall Facing	Unit Cost* w/perm. material	Unit Cost* w.o./perm. material	Remarks or Maximum Height
1972	RE	Steel	34.97	29.50	55'
1976	MSE	Pre-Cast Concrete 13,300 ft^2	34.34	27.34	20'
1976	RE	Pre-Cast Concrete 13,000 ft^2	28.14	21.14	20'
1977	RE	Pre-Cast Concrete 4,375 ft^2	-----	34.95	22'
1978	MSE	Wood 793 ft^2	-----	34.11	Small Job
1979	RE	Pre-Cast Concrete 21,000 ft^2	33.18	29.78	Built by Cost Incentive Proposal
1979	MSE	Pre-Cast Concrete 3,518 ft^2	37.10	33.40	24'
1979	MSE	Wood 22,000 ft^2	-----	8.00	Temporary Wall
1981	RE	Pre-Cast Concrete 11,080 ft^2	40.68	37.41	14'
1983	MSE	Pre-Cast Concrete 17,626 ft^2	28.27	25.00	16'(Used low quality backfill materials)

*Unit cost per square foot of wall face, in $/square foot.

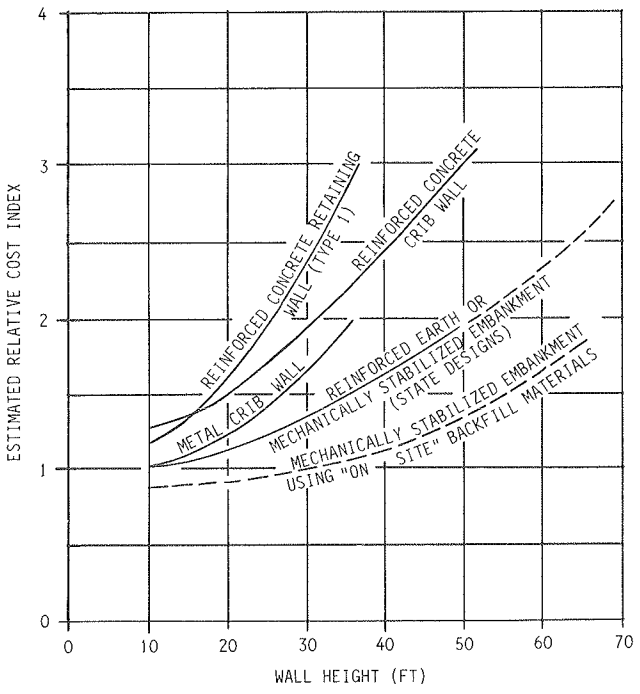

Figure 29. Relative cost comparison of various retaining walls, based on 1974 cost data. (Provided by California Department of Transportation)

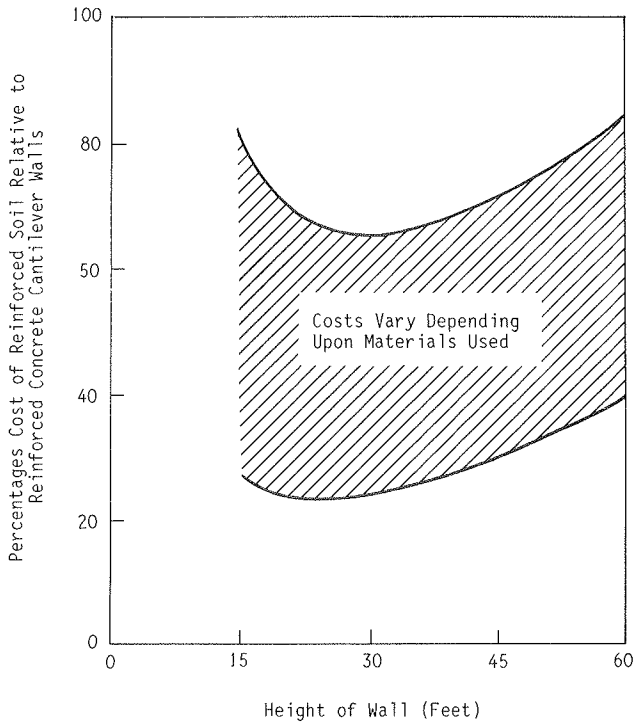

Figure 30. Comparative cost of reinforced soil and conventional reinforced concrete walls. (Source: Ref. 3)

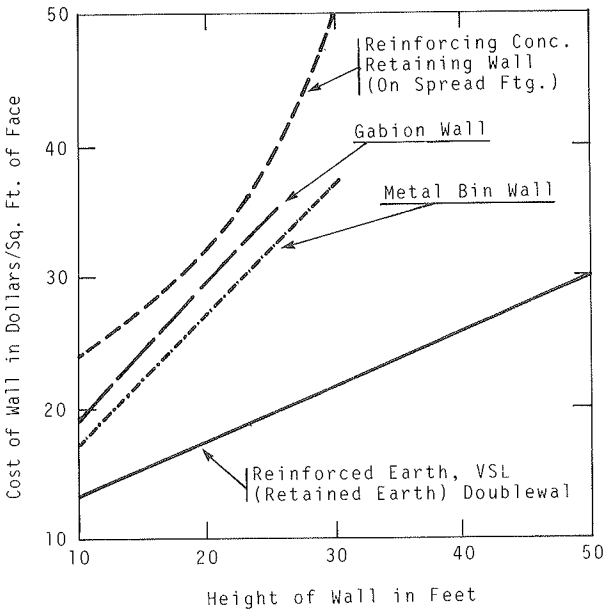

NOTES

(1) Costs shown are for wall materials and erection.

(2) Backfill and structural excavation costs are not included, except for Gabion and metal bin walls, where the costs include the cost of backfill placed inside the Gabion baskets and metal bins.

(3) For each individual project, backfill, structure and architectural treatment costs should be added to costs from the chart to make an overall cost comparison of wall types.

(4) Cost variations between RE, VSL Reinforced Earth, and Doublewal do not appear sufficient to justify separate cost curves for estimating purpose.

(5) Costs shown are intended for preliminary estimating and cost comparison purpose only.

(6) Costs shown are based on a combination of recent bid experience in FHWA Region 10.

(7) Chart was compiled by Ron Chassie, FHWA Region 10 Geotechnical Engineer, Portland, OR.

Figure 31. Cost comparison of six wall types, 1981. (Provided by California Department of Transportation)

CHAPTER FOUR

MECHANISMS AND BEHAVIOR

Contents

Success in earth reinforcement requires that the combination of soil and reinforcements be such that the interactions between the two materials produce a composite structural material that combines their best characteristics. The low cost soil, which

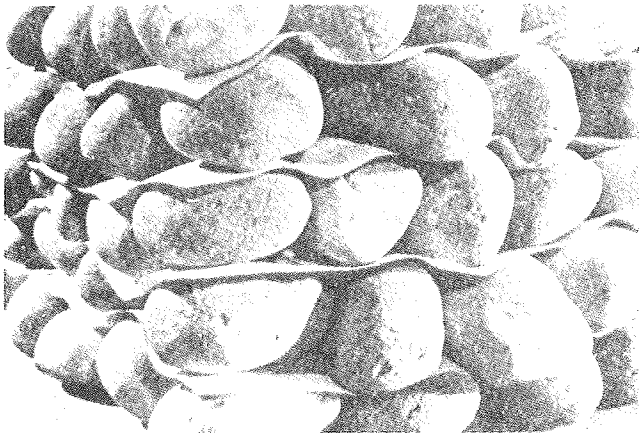

Figure 32. Idealized reinforced mass. (Source: Ref. 2)

contributes mass, good resistance to compression, and significant resistance to shear, represents by far the greatest volume of material. The much higher cost reinforcements contribute tensile strength and, through adherence to the surrounding soil, enable the development of a coherent material that seems to "hold itself up by its bootstraps."

A simple example of this is shown in Figure 32. The friction between the sheets of paper and the gravel particles prevents the lateral translation of the gravel. The result is that the system is self-supporting and can stand with vertical slopes. Of course, in an actual construction it would not be possible to have each soil grain in contact with a reinforcement. Thus, it is necessary that there be internal stress transfer between grains and also that there be a wall facing to prevent soil at the face from flowing outwards.

A broad division of reinforcement types can be made in terms of their extensibility. In Table 3 the general characteristics of ideally inextensible and ideally extensible reinforcements are described. With the exception of some of the geotextiles, the reinforcement systems described in this report are essentially inextensible.

The presence of high modulus (as compared to the soil) reinforcements serves to restrain the deformation of the soil in a direction parallel to the reinforcements. This can be viewed as imparting an anisotropic soil cohesion or increased confining pressure on the plane perpendicular to the reinforcements, thus restraining deformations in the direction of the reinforcements. In most currently available systems this is done in a way that the system retains its ability to deform without distress, thus producing a composite material that can adapt to movements of the surrounding ground.

The basic soil and reinforcement interaction mechanisms and the behavior of the resulting composite material are presented in this chapter.

MECHANISMS

Transfer of stress between soil and reinforcements of high strength and tensile stiffness involves two basic mechanisms; namely, friction and passive soil resistance. In many systems both mechanisms are active, and the relative contribution of each is indeterminate. Together they determine the bond strength that controls the maximum rate of change of axial force in the reinforcement along its length.

Frictional Load Transfer

Frictional stress transfer between soil and reinforcements is illustrated schematically in Figure 33. The load that can be

Table 3. Comparative behavior of earth reinforcement.

Type of Reinforcement	Stress-Deformation Behavior of Reinforcement	Role and Function of Reinforcement
Ideally inextensible inclusions (metal and plastic strips, bars, grids, etc.)	Inclusions have rupture strains less than the maximum tensile strains in the soil w/o inclusions, under the same stress conditions Depending on the ultimate strength of the inclusions in relation to the imposed loads, these inclusions may or may not rupture.	Strengthens soil (increases apparent shear resistance) and inhibits both internal and boundary deformations. Catastrophic failure and collapse of soil can occur if reinforcement breaks.
Ideally extensible inclusions (natural and synthetic fibers, roots, fabrics, geotextiles)	Inclusions have rupture strains larger than the maximum tensile strains in the soil w/o inclusions These inclusions cannot rupture no matter their ultimate strength nor the imposed load.	Some strengthening . . . but more importantly provides greater extensibility (ductility) and smaller loss of post peak strength compared to soil alone.

transferred per unit area of reinforcement depends on the interface characteristics of the soil and reinforcing materials and on the normal stress between them. The latter depends on the stress-deformation behavior of the soil, which is itself stress-dependent. Consequently, the effective friction coefficient is not readily amenable to estimation by analysis alone. The results of experiments, e.g., pullout tests, direct shear tests between soil and reinforcement, instrumented models and full-scale structures, are often used as a basis for selection of appropriate values [Mitchell and Schlosser (*1*)].

Analysis of the local equilibrium of a section of reinforcement within the soil gives the stress transfer condition shown in Figure 34.

$$dT = T_2 - T_1 = 2b\tau(d\ell) \tag{1}$$

where b = reinforcement width; ℓ = length along reinforcement; T = tensile force; and τ = shear stress along soil-reinforcement interface.

If τ is generated only by interface friction, then

$$\tau = \mu\sigma_v \tag{2}$$

where σ_v = the normal stress exerted on the reinforcement; μ = the coefficient of friction between the soil and reinforcement material.

The interface friction coefficient between sands and silts and different construction material surfaces in direct shear is known to be in the range of about 0.5 to 0.8 times the direct shearing resistance that can be mobilized within the soil. That is

$$\mu = \tan\delta = (0.5 \text{ to } 0.8)\tan\phi \tag{3}$$

where δ = friction angle between soil and smooth surface; and ϕ = angle of internal friction of the soil. Values of μ of the same order can be expected to hold for smooth reinforcement elements.

Thus, if the value of σ_v is known, it should be a simple matter to calculate the limiting value of reinforcement pullout resistance in any case. Unfortunately, such a simple calculation cannot reliably be made because the effective normal stress is altered by the soil-to-reinforcement interaction. More specifically, as shear strain is imposed on a dense granular soil, the soil tends to dilate. If this tendency to dilate is partially restrained (i.e., if volume increase is partially prohibited) by boundary conditions, local confining stresses can increase significantly. For a soil of given density, the tendency to dilate decreases with increasing confining stress. Hence, the influence of dilatancy on friction coefficients computed from pullout tests can be expected to decrease with depth. Furthermore, with the possible exception of geotextiles, none of the reinforcements in current use have smooth, plane surfaces along their full lengths. Accordingly, the most reliable values of friction coefficient are obtained by direct measurement. The value so determined is commonly referred to as the apparent or effective friction coefficient μ^*, and it is usually taken as the average mobilized shear stress along the reinforcement divided by the normal stress as given by the overburden pressure.

Values of μ^* ranging from 0.5 to considerably greater than 1.0 have been reported, with the lower values corresponding to smooth reinforcements and large depths of burial, and the higher values associated with rough or ribbed reinforcements and small depths of overburden. In dense highly dilatant granular backfill material, the presence of ribs results in not only a larger value of μ^*, but also a significant increase in the relative soil displacement required to fully mobilize pullout resistance. This is illustrated in Figure 35 for the case of smooth metallic strips and for the ribbed strips used in Reinforced Earth construction. Construction methods may influence μ^* in reinforced soil construction, and installation method will affect μ^* in soil nailing. Recommended values of μ^* for use in the design of different earth reinforcement systems are given in Chapter Five and in the method-specific appendixes to this report.

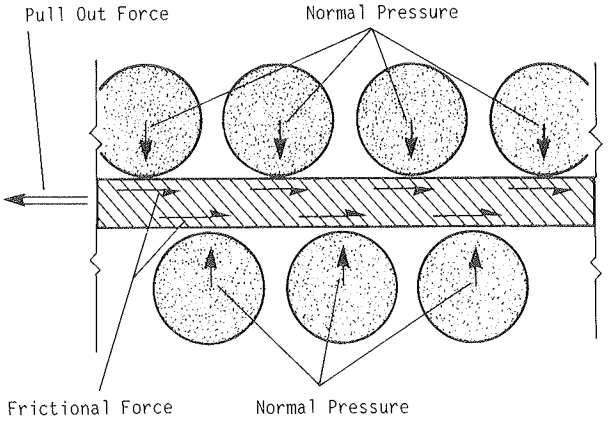

Figure 33. Frictional transfer between soil and reinforcement.

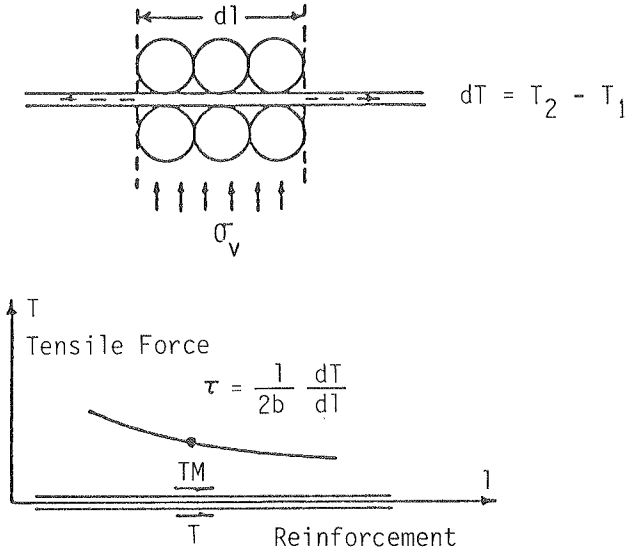

Figure 34. Variation of the tensile force along a reinforcement.

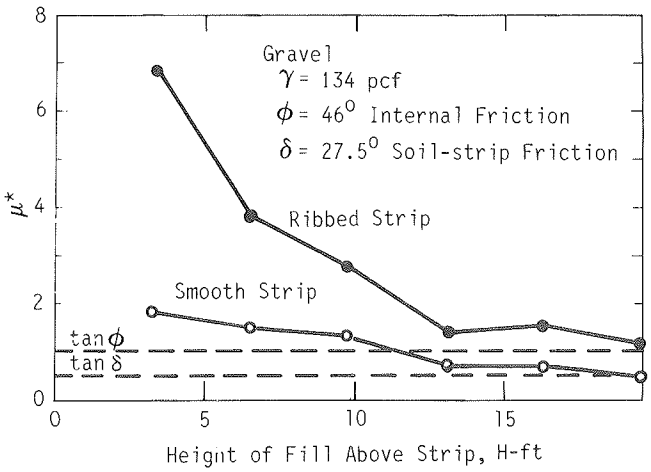

Figure 35. Influence of reinforcement type and overburden stress on apparent friction coefficient. (Source: Ref. 3)

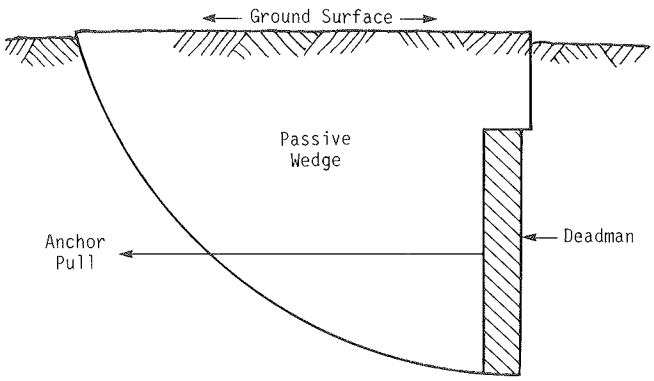

Figure 36. Load transfer by passive soil resistance.

Passive Earth Resistance

Load transfer by passive soil resistance is shown schematically in Figure 36. In this case a bearing surface normal to the direction of the force to be resisted is pulled into the soil. The classic example of the use of passive resistance in an earth retaining structure is a deadman anchor. It is important to note, however, that a system of tendons and anchors is not at all the same as earth reinforcement. Anchored wall systems consist of facing elements and ties or tendons of high tensile strength extending to some distance into the soil where they are connected to vertical plates or other anchor types which provide the resisting force needed for stability of the wall face.

In a reinforced soil system that relies in whole or in part on passive soil resistance there are a number of elements oriented transverse to the pullout force direction, each of which develops passive resistance along its front face. A reinforced soil system can be subdivided to give elements having properties representative of the whole. In contrast, a true anchor system does not behave as a composite material and therefore can not be considered a reinforced soil.

The maximum pullout resistance that can be developed by a reinforcement element oriented transverse to the direction of loading (e.g., the transverse bars which serve as the bearing members of a grid) is related to the bearing capacity of a deep foundation. The bearing members can be considered similar to a line of anchors at a spacing S_x (Fig. 37). As the reinforcement thickness is usually small in comparison to the depth of burial, i.e., Z/t is large, the bearing members can be considered deeply embedded. The vertical effective stress at the level of the reinforcement σ_v' can be estimated from the depth and density of the overlying soil, i.e.,

$$\sigma_v' = \gamma' Z \tag{4}$$

where γ' is the effective unit weight of the soil, with due consideration of submergence if appropriate.

It is convenient to express the passive resistance or effective bearing resistance which can be developed on the transverse members, σ_b', as a function of the vertical effective stress in the form

$$\sigma_b' = F\gamma' \sigma_v' \tag{5}$$

where $F\gamma'$ is a bearing factor primarily dependent on soil strength and soil dilatancy and to a lesser extent on reinforcement roughness and initial stress state in the soil. As the effects of roughness and initial stress state are small for large depths, they can be neglected with little loss in accuracy.

Values of $F\gamma'$ have been obtained as a function of soil friction angle using several analysis procedures, with the results shown in Figure 38. Rowe and Davis's (*5*) curves were obtained by analysis of vertical surfaces loaded horizontally using the finite element method. The curve labeled constant volume is for the assumption of no dilatancy. If a punching mode of failure is assumed, the lower curve in Figure 38 is obtained from the slip line solution derived by Jewell et al. (*4*). The curve marked Prandtl is the classical Prandtl bearing capacity solution applied with the assumption made by Jewell et al. that $\sigma'_h = \sigma'_v = \sigma'_n$ to give:

$$\sigma'_b = \sigma'_v(\exp(\pi \tan\phi))\tan^2(45 + \phi/2) \tag{6}$$

The results of several investigations to determine the bearing resistance of anchors and grids have been summarized by Jewell et al. (*4*), and they are compared with the theoretical values in Figure 39. Hueckel and Kwasniewski (*6*) did pullout tests on short grids embedded in sand. Chang et al. (*7*) and Peterson (*8*) did relatively large-scale pullout tests on grids. Large direct shear tests with a reinforcement grid inclined across the central plane were done by Jewell (*9*).

Although there is some spread and variability in the test results, they are bounded by the upper and lower theoretical predictions, with average values defined reasonably well by Rowe and Davis's curves. It would seem, therefore, that Figure 39 can be used for reasonable estimation of the passive pullout resistance of a transverse earth reinforcement.

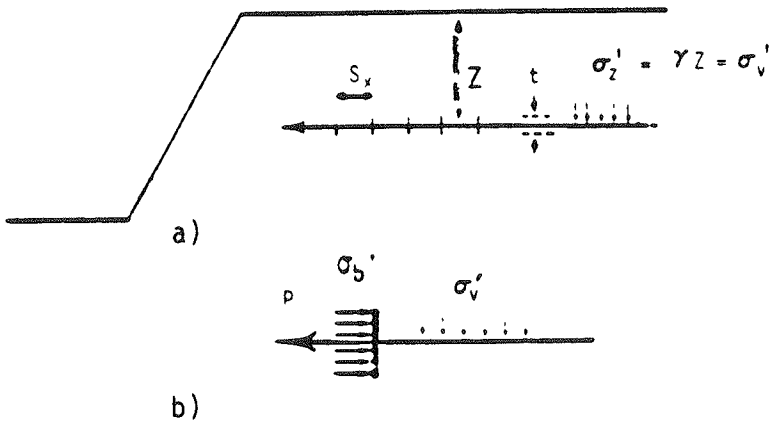

Figure 37. Definitions for bearing stresses on a reinforcement grid. (Source: Ref. 4)

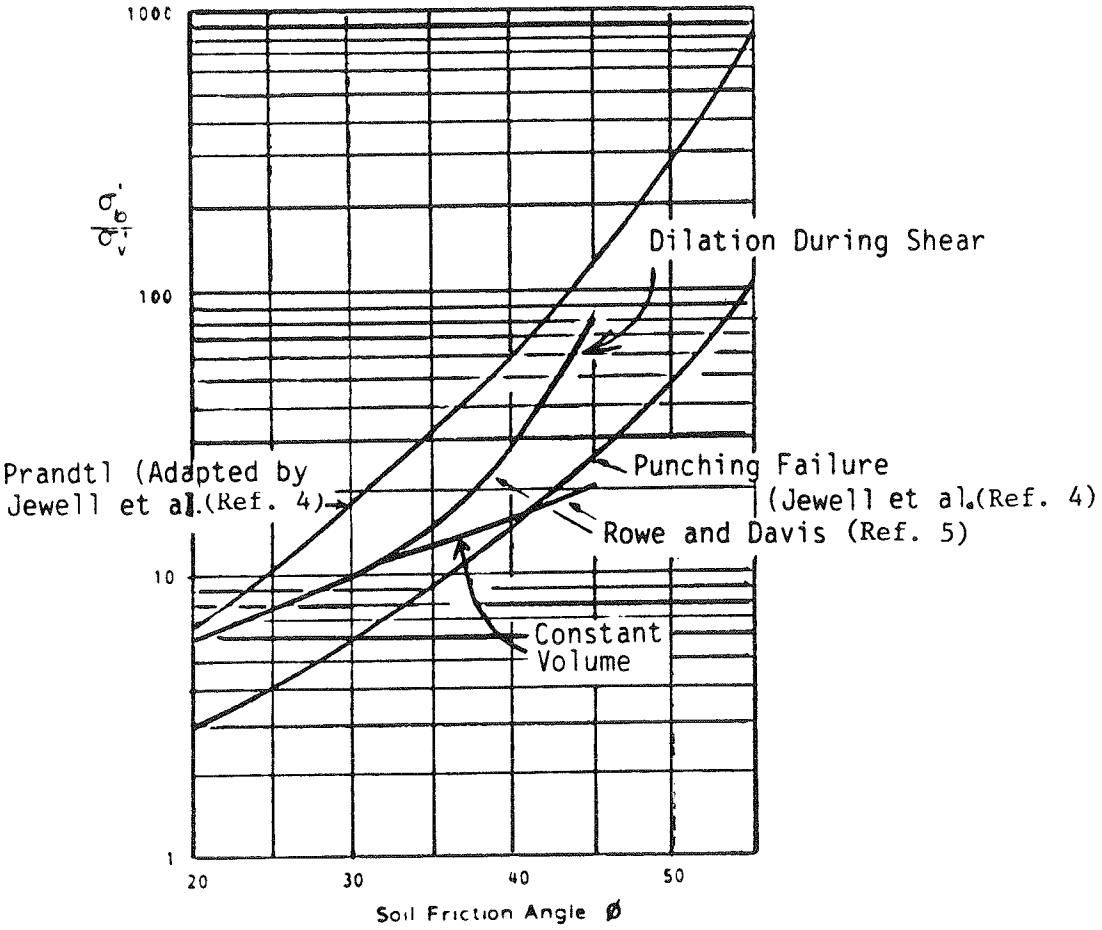

Figure 38. Theoretical relationships between bearing stress and soil friction angle. (Source: Ref. 4)

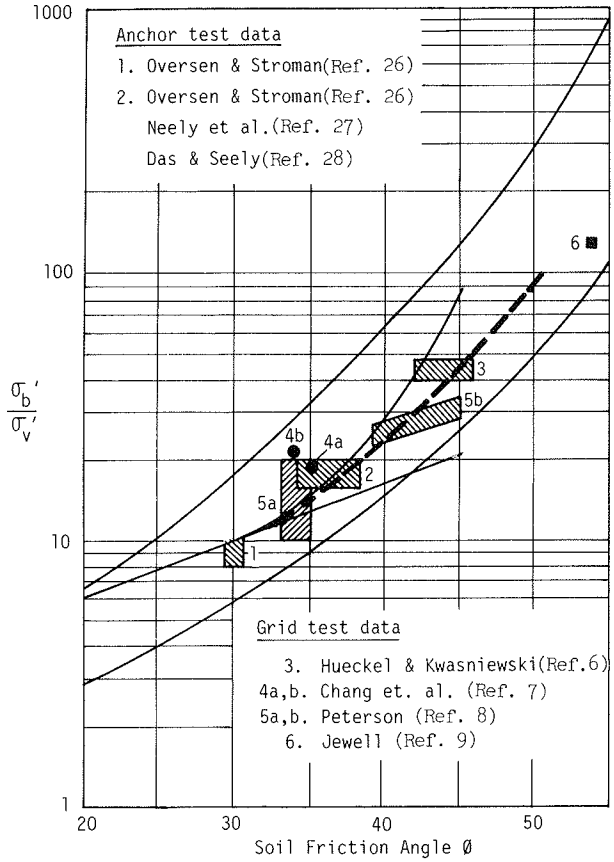

Figure 39. Comparison of test results with predicted values of bearing stress. (Source: Ref. 4)

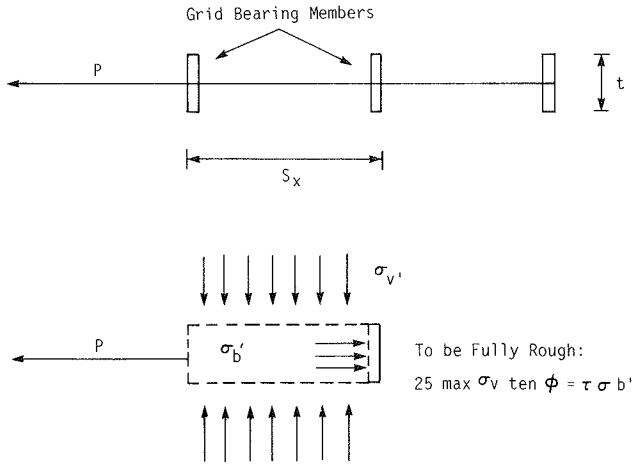

Figure 40. Analysis of maximum passive resistance developed by a grid system. (Source: Ref. 4)

There should be a limiting maximum value of pullout resistance that can be mobilized by the transverse members of a grid reinforcement system. Consider a system with grid bearing members at a longitudinal spacing S_x as shown in Figure 40. The vertical dimension of each bearing member is t, and the proportion of the transverse member area on which bearing can be fully developed is α_b. For bar mesh systems in which the transverse and longitudinal members are in different horizontal planes $\alpha_b = 1$. For grid systems, such as Tensar, in which all members are in the same plane, α_b is less than 1.

The maximum pullout resistance, P_{max}, that could be developed in a frictional soil would be for the case where the transverse bearing members are close enough together so that the grid and its contained soil act as a rough sheet of thickness t being pulled through the soil. For this case

$$P_{max} = 2bS_{max}n\sigma'_v\tan\phi \tag{7}$$

where n is the number of transverse bearing members.

The same resistance developed by bearing would be

$$P_{max} = \alpha_b bt\sigma'_b n \tag{8}$$

Combining Eqs. 7 and 8, Jewell et al. (*4*) derived an expression for the value of S_{max}:

$$S_{max} = t\frac{\sigma'_b\alpha_b}{\sigma'_v 2\tan\phi} \tag{9}$$

Estimates of (S_{max}/t) for development of P_{max} can now be made with the aid of Figure 39 which gives values of σ'_b/σ'_v as a function of soil friction angle ϕ. The dashed line in Figure 39 drawn through the experimental data was used for the case of $\alpha_b = 1$ and taking mean values of σ'_b/σ'_v to yield the values of S_{max}/t in Table 4.

There would be no increase in pullout resistance for values of S/t less than those indicated in Table 4. Thus, use of smaller transverse member spacings than provided by the tabulated values might be uneconomical. Spacings greater than those indicated will result in a system that is not capable of developing the full passive bearing resistance that could be mobilized within the area of reinforcement. The available data summarized by Jewell et al. (*4*) support these findings.

Combined Frictional Load Transfer and Passive Soil Resistance

With the exception of geotextiles used as sheet reinforcement and smooth strip or rod reinforcements, each reinforcing system affects stress transfer between the soil and reinforcements by a combination of sliding friction between the reinforcement sur-

face and soil and the passive soil resistance generated by the soil in bearing against the transverse reinforcement elements. The relative proportions of the total pullout resistance that are contributed by each mechanism depend on the reinforcing material, including its surface characteristics and geometry, on the soil characteristics, and on the in-situ stress conditions.

Proven theoretical means for computing the relative contributions are not available, and actual data are very limited. In one study [Chang et al. (*7*)], it was found that for a bar mesh in sandy gravel, the transverse bars contributed about 90 percent of the total pullout resistance.

The relative contributions of friction and passive resistance to the pullout resistance of a given earth reinforcement system depend not only on the maximum values of frictional force and passive resistance force that can be mobilized, but also on the relative soil-to-reinforcement deflections to fully mobilize them.

Based on the results of pullout tests performed on different types of reinforcements [Alimi et al. (*3*); Schlosser and Elias (*10*)], two phenomena which influence load transfer versus relative displacement can be clearly identified: (1) friction between the soil and a smooth reinforcement, requiring only a small displacement of about 0.05 in.; and (2) bearing or passive soil resistance against surfaces normal to the direction of displacement, requiring displacements as large as 4 in. for complete mobilization. However, a significant portion (more than 50 percent) of the maximum value is mobilized at deflections of about ¼ in., as shown in Figure 41.

Table 4. Longitudinal spacing of transverse bearing members for development of maximum pullout resistance. (Source: Ref. 4)

Soil Friction Angle ($\delta°$)	$\tan\delta = \mu^*$	σ_b'/σ_v' (Fig. 39)	S_{max}/t
30	0.577	10	8.7
35	0.700	15	10.7
40	0.839	25	14.9
45	1.000	45	22.5

Measurements by VSL Corporation have indicated relative soil-to-reinforcement displacements of 0.2 and 0.5 to more than 2 in., respectively, for mobilization of friction and passive resistance.

The effect of ribs on the pullout resistance of strip reinforcements is to significantly increase the apparent coefficient of friction, μ^*, at low confining stresses (see Fig. 35). A third soil-to-reinforcement interaction phenomenon has been postulated [Schlosser et al. (*25*)] to explain this increase. According to Schlosser, it is largely caused by the soil restraint against di-

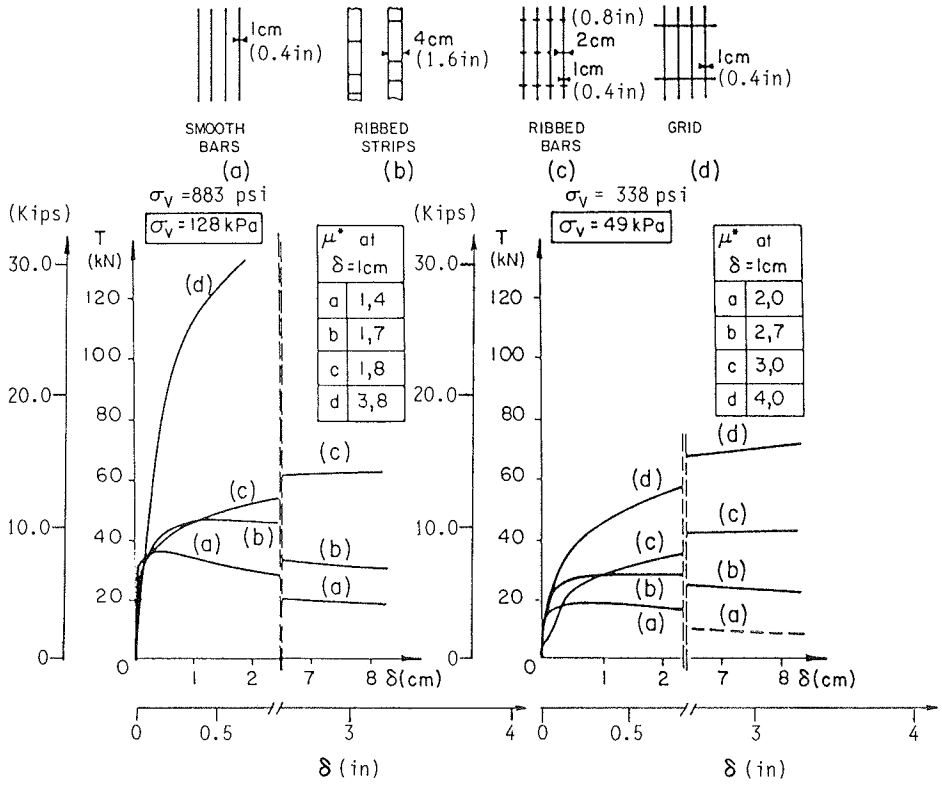

Figure 41. Influence of reinforcement shape on pullout resistance. (Source: Ref. 25)

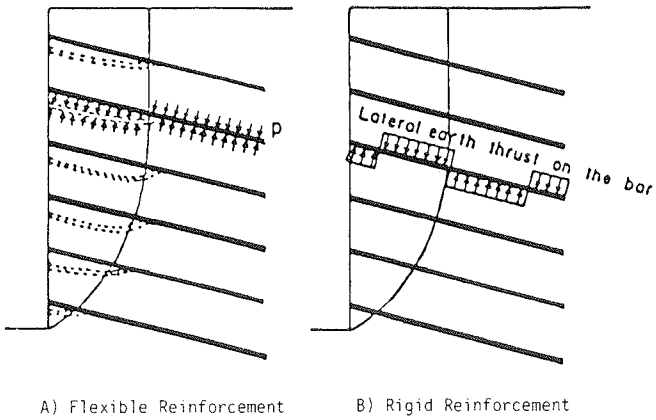

Figure 42. Effect of reinforcement rigidity on stress and deformation patterns.

latancy which locally increases confining stress. However, it is not certain that the increase is not simply the result of bearing or passive soil resistance on the ribs.

Friction and passive resistance are not necessarily completely additive. Some relative reinforcement-to-soil deflection or strain has to occur for either friction or passive resistance to mobilize. In some cases, the strain associated with the development of one mechanism may prohibit the full development of the other. For example, imagine a flat plate attached to a rod so that the plane of the plate is perpendicular to the rod. If the plate is embedded in soil and is pulled through the soil by a force exerted on the rod, the soil immediately ahead of the plate would move with the plate. Although full soil-to-rod friction would be developed at some distance from the plate, the movement of the soil with the plate would preclude the full development of soil-to-rod friction immediately in front of the plate. Similar interaction can occur with ribbed reinforcement strips and with grid reinforcements.

This is seldom an important factor because the methods used to measure coefficients of friction for ribbed reinforcing strips, or to establish the pullout resistance of grids, already include the same degree of interaction. The interaction does, however, mean that caution is appropriate when extrapolating test results obtained with a reinforcement of one given geometry to another.

Reinforcements with Shear and Bending Resistance

Many of the reinforcing elements that are used for soil nailing are of sufficient diameter and stiffness that they resist shearing and bending stresses. The results of recent studies of soil nailing mechanisms, summarized in Appendix C, show that the total shearing resistance mobilized along a potential failure surface is the sum of three components: (1) an apparent cohesion due to shear forces mobilized in the reinforcement, (2) the shear stress mobilized in the soil in the absence of the bars, and (3) the modification of shear stresses in the soil caused by the effect of the reinforcements on the stress and displacement fields.

Variations in normal stress along a soil nail or micropile are responsible for the generation of bending stress. The behavior is in many ways analogous to that of a laterally loaded pile. The effect of rigidity on the normal stresses acting on the reinforcements and on their deformation patterns is shown schematically in Figure 42.

When considering the interaction between stresses and displacements as schematically illustrated in Figure 42, it is clear that a complete analysis and design of rigid reinforcements must consider, in addition to pullout and tensile strength, failure of the reinforcement in bending, soil failure due to the lateral thrust of the bar (analogous to p-y behavior of a laterally loaded pile), and movement of soil between bars.

The relative soil-to-nail displacement required to mobilize shearing and bending resistance of the nail is greater than that necessary to mobilize its tensile resistance.

BEHAVIOR OF REINFORCED SOIL MATERIAL

The mechanisms by which stresses are transferred between soil and reinforcements were delineated in the preceding section. These interactions result in stress and strain fields within the reinforced soil that are considerably different from that in an unreinforced soil mass. Consequently, the earth pressures and failure modes are not necessarily the same as in unreinforced ground. Nonetheless, it is necessary that the internal stress distributions and locations of potential failure surfaces be known if safe, economical designs are to be possible.

Shear Strength

The mechanism by which tensile reinforcements are responsible for the increased shear strength of the soil and reinforcement composite material has been explained in two ways. In one [Schlosser and Vidal (*11*)] the tensile strength of the reinforcements and the stress transfer between the soil and reinforcements are considered to give the material an apparent cohesion. The second concept [Bassett and Last (*12*)] considers that the reinforcements provide an anisotropic restraint to soil deformation in the direction of the reinforcements. This leads to a rotation of the principal strain and stress directions.

Under low confining stresses a given reinforcement system will fail by slippage (pullout) between soil and reinforcements. Under high confining pressures this same system will fail by breakage of the reinforcements. This behavior is illustrated by the results of triaxial compression tests by Schlosser and Long (*13*) on unreinforced sand and sand reinforced by thin aluminum sheets placed horizontally, as shown in Figure 43. Zones showing failure by reinforcement breakage and failure by slippage are indicated.

In the region where failure is by reinforcement breakage, the strength increase according to the apparent anisotropic cohesion concept is explained by the Mohr diagram shown in Figure 44. C'_R is the apparent cohesion generated by the reinforcement, and σ_{1R} is the increase in major principal stress at failure. The friction angle of the reinforced sand is taken as the same as that for the unreinforced sand, which is a reasonable assumption according to Figure 43.

For reinforcements having a tensile breaking resistance R_T, and a vertical spacing between horizontal layers of reinforcements S_v, the geometry of Figure 44 leads to:

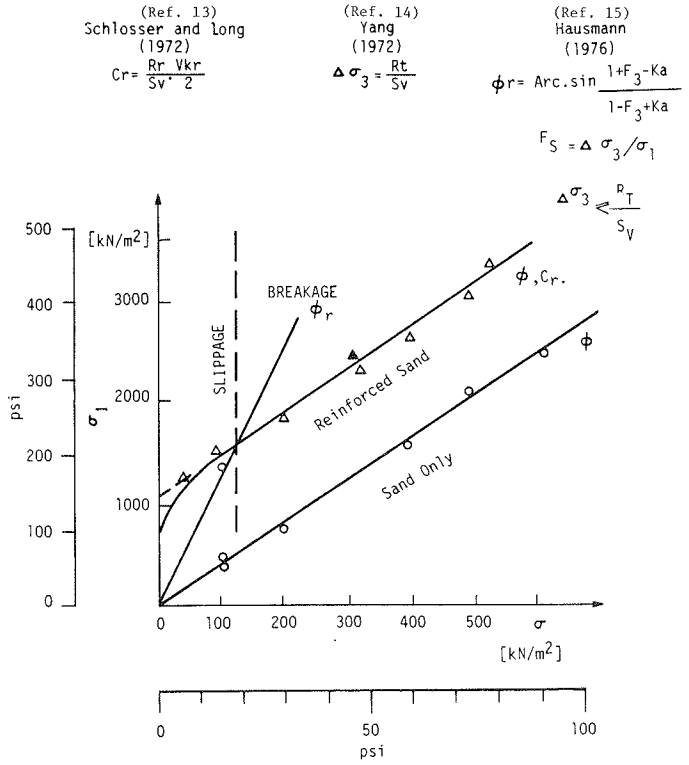

Figure 43. Strength envelopes for sand and reinforced sand.

$$C'_R = \frac{R_T\sqrt{K_p}}{2S_v} \tag{10}$$

where

$$K_p = \tan^2(45 + \phi/2) \tag{11}$$

The alternative approach of increased effective confinement was analyzed by Yang (*14*) and is shown in Figure 45. The apparent increase $\Delta\sigma_{3R}$ in minor effective confining pressure at failure is given by

$$\Delta\sigma_{3R} = \frac{R_T}{S_v} \tag{12}$$

The equation of the failure envelope is then

$$\sigma_{1R} = \left(\sigma_{3C} + \frac{R_T}{S_v}\right) K_p \tag{13}$$

Both analyses give the same resulting strength for the composite material provided failure is by rupture of reinforcements.

Horizontal Stresses in a Reinforced Soil Mass

Knowledge or assumption of the earth pressures to be resisted by the reinforcements is essential to the safe design of reinforced

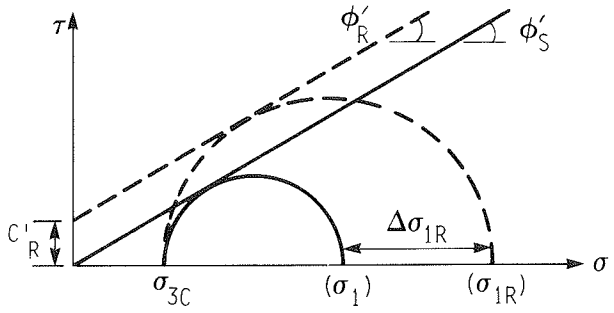

Figure 44. Apparent cohesion interpretation of strength increase due to reinforcements. (Source: Ref. 13)

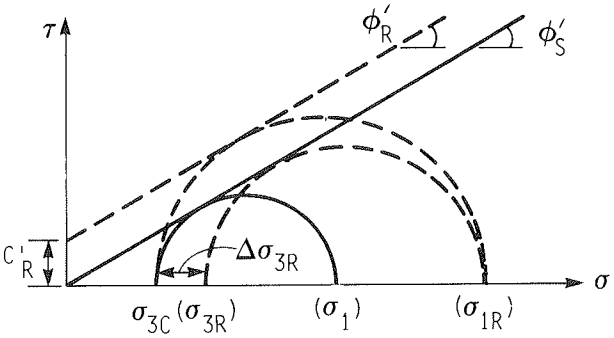

Figure 45. Increased confinement concept of soil reinforcement. (Source: Ref. 14)

soil structures and slope stabilization by soil nailing. In the absence of data from model tests and instrumented structures it has often been assumed that the effective horizontal earth pressure σ_h behind the wall face can be approximated by the Rankine active value; i.e.,

$$\sigma'_h = K_a\sigma'_v \tag{14}$$

where

$$K_a = \tan^2(45 - \phi/2) \tag{15}$$

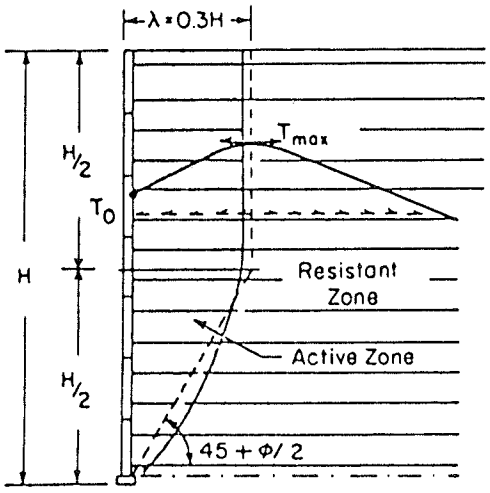

A) Full Scale Experiments

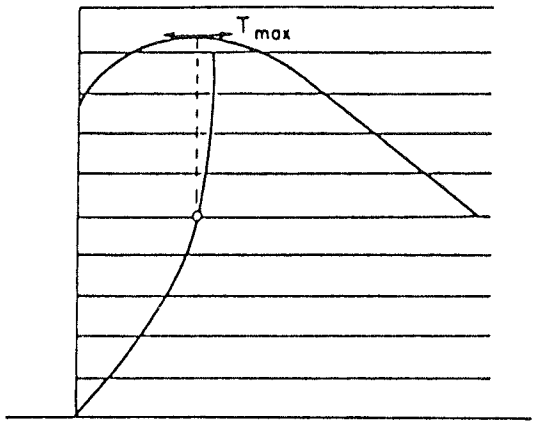

B) F.E.M. (Purely Elastic Materials)

Figure 46. Tensile force distributions along reinforcements. (Source: Ref. 10)

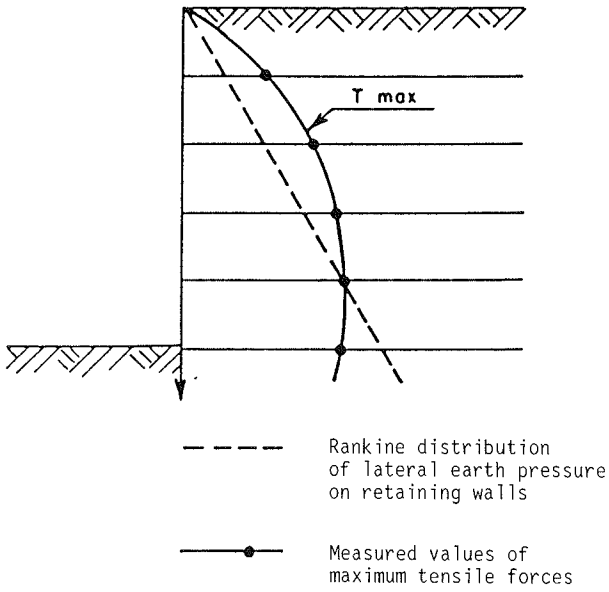

Figure 47. Distribution of maximum tensile forces with depth in a Reinforced Earth wall. (Source: Ref. 10)

Such an assumption would appear quite reasonable for systems which undergo significant lateral deformations. This would be the case both when more extensible reinforcements, such as geotextiles, are used, or when reinforcement is by inclusions relying mainly on passive resistance for their effectiveness. On the other hand, in systems using stiffer, essentially nonextensible reinforcements lateral deformations are restrained. In this case it could be argued that use of an at-rest earth pressure coefficient would be more appropriate. Unfortunately, only very limited earth pressure data are available for systems other than Reinforced Earth.

Measurements on Reinforced Earth structures [Schlosser and Elias (*10*)] indicate that the tensile forces mobilized in the reinforcements are relatively small at the wall face but increase to a maximum at some distance behind the face, as shown in Figure 46. Also shown in Figure 46 is the distribution of forces determined from finite element analyses. The reasonably good qualitative agreement between the field measurements and theoretical analysis indicates that earth reinforcement systems can be modeled using existing analytical methods.

The distribution of maximum tensile forces with depth in a Reinforced Earth wall is compared with the Rankine active earth pressure diagram in Figure 47. If the horizontal earth pressures in the soil are calculated from the measured tensile forces, it is found that the lateral pressure coefficient decreases from a value approximately equal to K_o, the at-rest coefficient, at the top of the wall to a value of K_a for depths greater than about 20 ft (6 m).

The distribution of lateral earth pressure within reinforced soil is depending on a number of factors, including the extensibility of the reinforcements, the construction methods used, and the type of reinforced soil structure.

The lateral earth pressures measured in a Paraweb plastic strip structure are shown on Figure 48. The structure is very similar to a Reinforced Earth structure, except that the Paraweb reinforcements are more extensible. Comparison with Figure 47 shows that lateral earth pressure in the Paraweb structure relative to active earth pressures is significantly lower than in the Reinforced Earth wall.

The effects of construction methods on lateral earth pressures are believed to be dependent on the type of compaction used for built embankments. The complex interaction among locked-in compaction stresses and the extensibility of reinforcements is not yet fully understood, although theoretical analyses in which compaction and gravity stresses are separated have shown reasonable agreement with field measurements [Collin (*16*)].

The lateral stress distribution is also dependent on whether the reinforced soil is a built embankment, a preexisting slope, or a reinforced excavation. Typically, lateral earth pressures

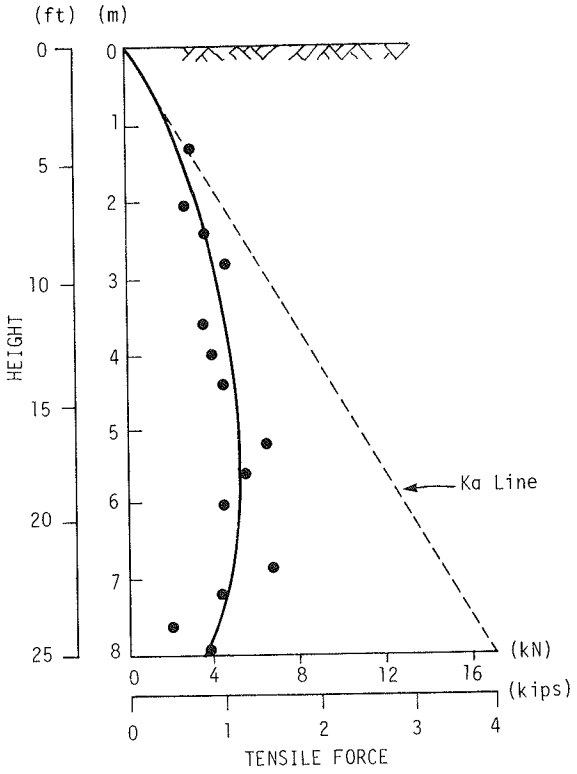

Figure 48. Tensile forces in a Reinforced Earth wall with Paraweb strips.

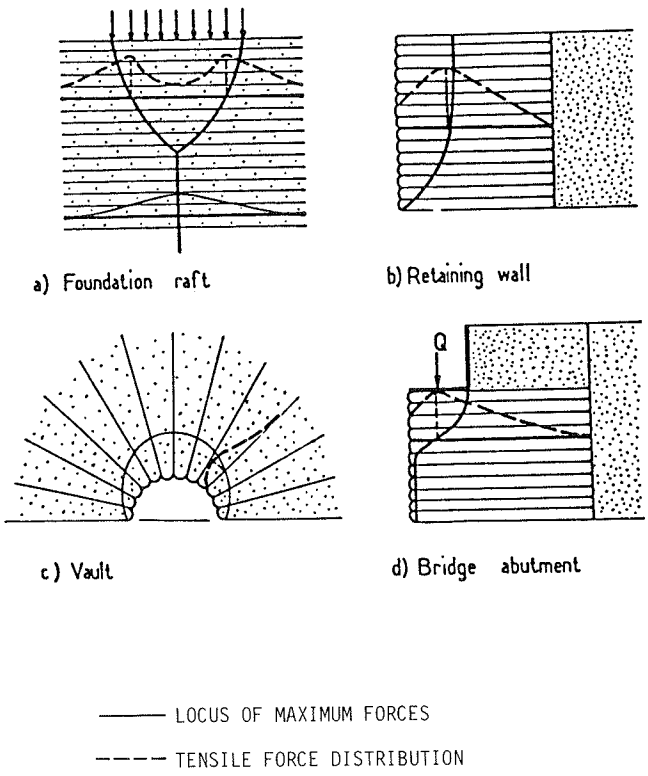

Figure 49. Locus of maximum tensile force lines in different Reinforced Earth structures.

appear to be higher near the upper portions of nailed excavations than in reinforced embankments.

Active and Resistant Zones and Failure Surfaces

The results of experiments and measurements on full-scale structures have shown that the locus of maximum tensile stresses defines a surface that coincides closely with the failure surface in reinforced soil structures that are loaded to failure. For Reinforced Earth walls with vertical faces this surface has the shape shown in Figure 46(a).

The soil in the active zone is restrained by shear stresses directed as shown along the reinforcements. The load thus transferred to the reinforcements is distributed into the resistant zone soil by shear stresses directed in the opposite direction.

Unfortunately, the locus of maximum tensile forces is not reliably known for all reinforcement systems and types of structures. The locus of maximum tensile force lines for some different types of Reinforced Earth structures as found through both model and field tests on instrumented structures and by various analyses is as shown in Figure 49. The locus of maximum tensile forces and shape of the potential failure surface for vertical VSL Retained Earth walls is assumed to be the same as for Reinforced Earth walls.

The internal failure surface for geotextile-reinforced walls is commonly assumed to coincide with the Rankine failure surface. That is, failure occurs along a plane inclined at $(45 + \phi/2)$ to the horizontal. The results of laboratory model tests reported by Bell et al. (*17*) conformed well to this pattern except for a slight curvature near the top.

When geotextile-reinforced walls are constructed using cohesive soil backfills, failure may be initiated by cracking if the length of reinforcement is insufficient or the height of wall is excessive. The failure surface has been approximated by Giroud (*18*) as a plane (Fig. 50) for determination of the spacing and length of reinforcement. For an uncracked soil mass, however, Giroud recommends using the assumption of a circular failure surface as shown in Figure 51.

Some analyses of reinforced slopes are based on the assumption of failure wedges, as shown schematically in Figure 52. Full-scale experiments on nailed soil slopes and embankments [e.g., Stocker et al. (*19*); Gassler and Gudehus (*20*); Shen et al. (*21*); Cartier and Gigan, (*22*); Schlosser, (*23*); Guilloux et al. (*24*)] have shown that the distribution of tensile forces along the reinforcements for steep slopes is very similar to that in Reinforced Earth walls.

Orientation of Reinforcements

Tensile reinforcement is most effective when oriented in the direction of maximum extension strain [Bassett and Last (*12*)]. By restraining the soil dilation, the effective stress and, hence, the strength of the soil are increased. When a high modulus

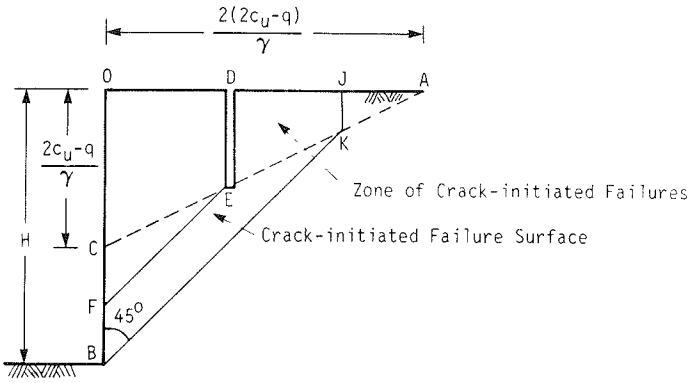

Figure 50. Crack-initiated failure surface in a geotextile Reinforced Earth wall with cohesive backfill. (Source: Ref. 18)

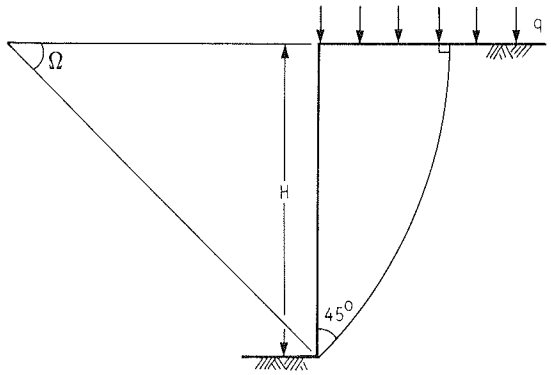

Figure 51. Failure surface in a geotextile-reinforced wall with an uncracked cohesive soil backfill. (Source: Ref. 18)

reinforcement constitutes a zero extension line, the failure plane becomes perpendicular to the reinforcements.

The development of tensile forces in reinforcements during direct shearing of a reinforced soil mass depends strongly on the orientation of the reinforcements with respect to the failure surface. The maximum increase in shear strength of a sand reinforced by bars or grids is obtained when the reinforcement is oriented in the same direction as the principal tensile strain increment which would have occurred in the unreinforced sand at failure. Orientation of reinforcements in a compressive strain direction can result in a decrease in shear strength of the soil because of a reduction of the average normal stress in the soil on the failure surface.

An analysis of the effects of reinforcement orientation was made by Jewell (*9*) which led to the conclusion that the two main effects of the reinforcement are to reduce the average shear stress supported by the soil and to increase the normal stress on the failure surface for a given externally applied loading condition. An apparent friction angle ϕ^* for the soil can be defined by

$$\tan\phi^* = \tan\phi' + \frac{T_{max}}{A_{CR}\sigma}(\cos\theta\tan\phi' + \sin\theta) \quad (16)$$

or

$$\tan\phi^* = \tan\phi + \frac{\Delta\tau_{reinf}}{\sigma} \quad (17)$$

where T_{max} = lesser of the pullout resistance or tensile strength of the reinforcement; ϕ' = internal friction angle of the unreinforced sand; A_{CR} = cross-sectional area of the failure surface; σ = applied normal stress; and θ = reinforcement orientation angle, shown in Figure 53.

The quantity $\Delta\tau_{reinf}$ represents the contribution to soil shear strength due to the additional normal stress generated by the component of the reinforcement force that acts across the failure surface.

For values of T_{max} less than the rupture strength of the reinforcement, i.e., failure by pullout, T_{max} would be proportional

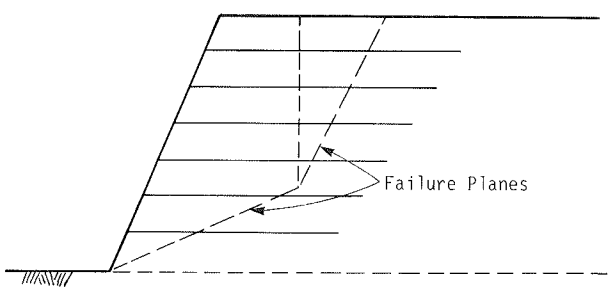

Figure 52. Failure wedges in a reinforced slope.

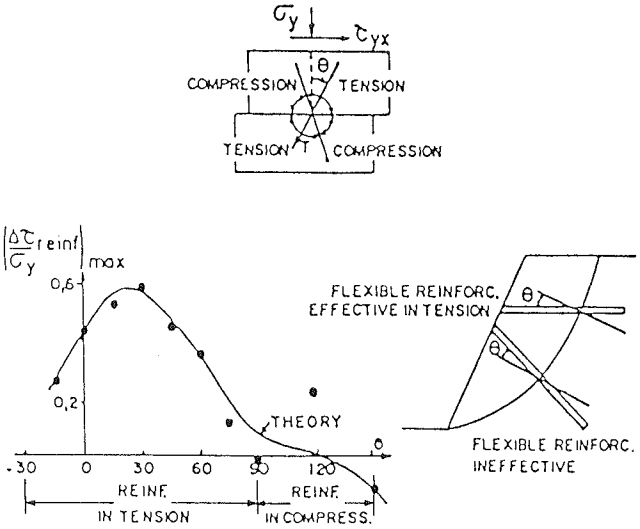

Figure 53. Effect of reinforcement orientation on shear strength of sand. (Source: Ref. 9)

to σ. Hence, the ratio $T_{max}/A_{CR}\sigma$ in Eq. 16 would be a constant and the value of ϕ^* would depend only on θ. For practical orientations of the reinforcements, Eq. 16 implies that ϕ^* would exceed ϕ if the rupture strength of the reinforcement is not exceeded.

When, however, T_{max} is determined by the tensile strength of the reinforcement, the ratio $T_{max}/A_{CR}\sigma$ decreases for increasing σ and will approach zero at large confining stresses. Hence, at large confining stresses ϕ^* would be nearly equal to ϕ'. This behavior is consistent with the failure envelopes shown for reinforced and nonreinforced soil in Figure 43.

The results of experiments by Jewell (*9*) (Fig. 53) showed good agreement between values of $\Delta\tau_{reinf}$ predicted by Eqs. 16 and 17 and values measured in direct shear tests. It seems clear, therefore, that the effectiveness of tensile reinforcements could be optimized in any case through analysis of their orientation relative to the in-situ stress conditions and potential failure surface. To do this in practice, however, is complicated by the fact that in slopes and embankments and within earth walls the principal stress directions and the failure plane orientation are not the same at all points. Thus the optimum reinforcement orientation would be variable throughout the system, which would complicate the construction process. Backfill placement and compaction in earth walls would not be possible for reinforcements placed with a large inclination to the horizontal. Therefore, the optimization of reinforcement inclination would have its greatest applicability to soil nailing and root pile systems. In such systems it may also be necessary to allow for the effects of bending and shearing resistance of the reinforcements, which was not done in the analysis above.

Strain Compatibility

The reinforcement of soil can only be successful if the magnitude of soil strain required to mobilize the reinforcing mechanism is acceptable. With high modulus reinforcements, such as metals, this is nearly certain. However, with lower modulus reinforcements, such as geotextiles and geogrids, several percent of strain may be required before sufficient force in the reinforcement is developed to mobilize the necessary restraint. Consequently, when low modulus materials are used, the acceptable magnitude of strain and the associated reinforcement forces mobilized may be a design criterion rather than rupture stress. In cases where high strains are tolerable in design, it would be appropriate to use soil strength properties also measured at large strains, i.e., residual values.

SOIL-TYPE CONSIDERATIONS

Most earth wall construction using reinforcements is done with cohesionless soil backfill. Proprietary systems such as Reinforced Earth and VSL Retained Earth specify certain minimum backfill soil properties, usually in terms of a maximum allowable amount of fines and plasticity and a minimum effective friction angle. Much of our present knowledge about internal stress distribution, effective friction coefficient, transverse bar bearing values, and geometry and location of failure surface has been obtained using soils satisfying these criteria.

Although there is no evidence to show that backfill of lesser quality will lead to significant differences in the internal stress distributions and potential failure modes, it is not yet certain that this will be so, and further data are needed. It is, however, well established, that the use of soils with poorer strength, gradation, and plasticity characteristics will generally lead to more massive, more heavily reinforced, more deformable, and possibly more costly structures for the following reasons:

- The lower the soil friction angle, the higher will be the internal horizontal earth pressure to be restrained by the reinforcements.
- The lower the soil friction angle, the lower will be the apparent friction coefficient for frictional reinforcing systems, and the lower the bearing value for passive reinforcement systems.
- The higher the plasticity of the backfill, the greater will be the possibility of creep deformations, especially when the backfill is wet.
- The greater the percentage of fines in the backfill, the poorer will be the drainage and the more severe will be potential problems from high water pressures.
- The more fine grained and plastic the backfill, the more potential there is for corrosion of metallic reinforcement.

Thus, when high quality backfill is readily available, it should be used. When it is not, the cost of importing good quality backfill must be weighed against the higher cost and potentially poorer performance of a larger, more heavily reinforced structure constructed using the lower quality but available soil.

It is important also to distinguish the soil used in the reinforced structure and that to be retained or supported by the reinforced structure. The latter soil, in conjunction with the site geometry (especially the ground surface slope) determines the magnitude of the external forces to be resisted by the reinforced earth.

FAILURE MODES

Internal Failure Modes

The discussion and analyses in this chapter have concentrated on the nature of soil-reinforcement interaction and the resulting behavior of the composite reinforced soil material. It is clear that for a reinforced soil structure to be internally stable, the reinforcements must be able to carry the tensile stresses (and also the bending and shear stresses in the case of stiff reinforcements) transferred to them by the soil without rupture. In addition, there must be sufficient bond between the reinforcements and the soil in the resisting zone that reinforcements do not pull out under the load that they are required to carry. The basis for the internal design is to evaluate the required spacing and lengths of reinforcements so as to satisfy these conditions.

A very important additional internal design consideration concerns loss of reinforcement durability over time. Reinforcement deterioration can result from corrosion, creep, and chemical and biological attack of the different reinforcement materials. Durability aspects of soil reinforcement are treated in some detail in Chapter Six and in the appendixes specific to each reinforcement type. Current practices in design to prevent failure as a result of reinforcement deterioration include use of additional reinforcement cross section to allow for corrosion loss, epoxy coating of metallic reinforcements, protection of

geotextiles from exposure to ultraviolet light, and design at reduced stress levels to minimize creep in plastic grids and geotextiles.

External Failure Modes

A properly designed volume of reinforced soil forms a coherent mass that can be expected to behave as a unit. This internal stability, of course, does not ensure overall stability of a given structure. External stability must also be evaluated to assure that failure would not occur because of one or more of the following mechanisms: sliding of the reinforced volume on its base; overturning of the earth wall; bearing capacity failure or loss of serviceability because of excessive settlement of the foundation soil; and rotational or block sliding failure of the soil behind and beneath an earth wall (i.e., an overall slope failure).

The usual methods of soil mechanics and foundation engineering are used to evaluate the factors of safety against these failure modes. Commonly used approaches are summarized briefly in Chapter Five; however, standard geotechnical references should be consulted for more explicit details.

Sliding Along Reinforcement Layers

In earth walls reinforced by strips (e.g., Reinforced Earth), by wire mesh (e.g., Welded Wire Wall), and by bar meshes and grids (e.g., VSL Retained Earth and Mechanically Stabilized Embankments), the plan area of the reinforcement at any level is very small relative to the plan area of the soil at that level. Thus, the total sliding resistance of the soil at that level will be essentially equal to the weight of the overlying soil times the effective coefficient of soil friction. Unless there are large horizontal forces applied at the top of the wall, adequate resistance to sliding is likely to be available at all levels provided there is an adequate factor of safety against base sliding.

On the other hand, when sheet geotextiles are used, the possibility exists for sliding along the soil-to-reinforcement interface at any level, as shown in Figure 54. Such a failure could result if the coefficient of friction between soil and geotextile, $\tan\delta$, is less than that for direct sliding of soil on soil, $\tan\phi'$.

A similar possibility exists when geogrids, such as Tensar, are used because the relatively smooth plastic grids cover a significant proportion of the total plan area at any reinforcement level. Mechanisms of direct sliding in this case have been examined in some detail by Jewell et al. (*4*). These possibilities are shown in Figure 55. The two mechanisms of soil shearing over plane reinforcement surfaces (Case a) and soil shearing over soil through the grid apertures (Case c) are likely to govern direct sliding resistance, as indicated by the following equations [Jewell et al. (*4*)]:

$$f_{ds} \tan\phi' = \alpha_{ds} \tan\delta + (1 - \alpha_{ds}) \tan\phi' \qquad (18)$$

where f_{ds} = coefficient of resistance to direct sliding; ϕ' = angle of friction for soil in direct shear; δ = angle of skin friction for soil on plane reinforcement surfaces; and α_{ds} = ratio of grid plan area that resists direct shear with soil to total plan area at the level of reinforcement.

Rearrangement of Eq. 18 gives

$$f_{ds} = 1 - \alpha_{ds}\left(1 - \frac{\tan\delta}{\tan\phi'}\right) \qquad (19)$$

In most cases $\alpha_{ds} = \alpha_s$ where α_s is the fraction of solid surface area in a grid. This corresponds to Case a in Figure 53. On the basis of available data a conservative value for direct sliding resistance of a grid is obtained using Eq. 19 when the ratio of maximum aperture dimension to average soil particle size is greater than 3 and α_{ds} is taken as α_s.

Few values of δ are available; however, it was found that

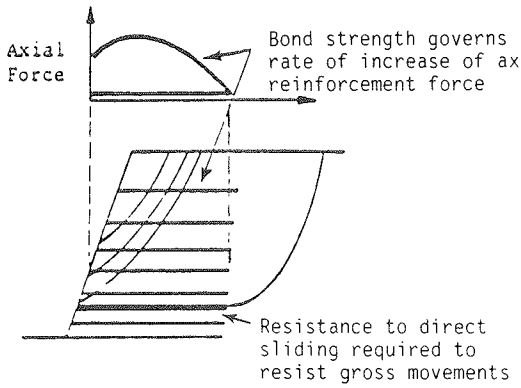

Figure 54. Failure by direct sliding along reinforcements. (Source: Ref. 4)

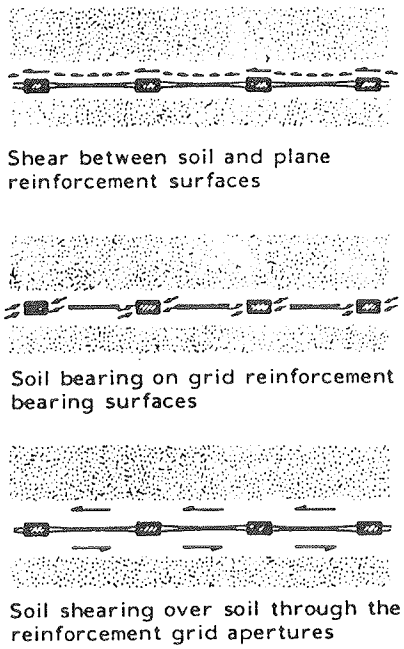

Figure 55. Three mechanisms resisting direct sliding of a soil mass over a layer of reinforcement. (Source: Ref. 4)

$$\frac{\tan\delta}{\tan\phi'} = 0.63 \qquad (20)$$

for crushed limestone on a high density polyethylene. Values of this magnitude are probably reasonable for other granular materials sliding against plastic grids.

REFERENCES

1. MITCHELL, J. K., and SCHLOSSER, F., "General Report, Session Number 1." *Proc. International Conference on Soil Reinforcement: Reinforced Earth and Other Techniques,* Paris (Mar. 1979).
2. Vidal, H., "La Terre Armee." *Annales de l'Institut Technique du Batiment et des Travaux Publics,* No. 259–260 (1969) pp. 1–59.
3. ALIMI, I., BACOT, J., LAREAL, P., LONG, N. T., and SCHLOSSER, F., "Etude de l'Adherence Sols-armatures." *Proc. 9th International Conference on Soil Mechanics and Foundation Engineering,* Tokyo (1977) Vol. I, pp. 11–14.
4. JEWELL, R. A., MILLILGAN, G. W. E., SARSBY, R. W., and DUBOIS, D., "Interaction Between Soil and Geogrids." *Proc. Symposium on Polymer Grid Reinforcement in Civil Engineering,* Science and Engineering Research Council and Netlon Limited (Mar. 22–23, 1984).
5. ROWE, R. K., and DAVIS, E. H., "The Behavior of Anchor Plates in Sand." *Geotechnique 32,* No. 1 (1982) pp. 25–41.
6. HUECKEL, S. M., and KWASNIEWSKI, J., "Scale Model Tests on the Anchorage Values of Various Elements Buried in Sand." *Proc. 5th International Conference on Soil Mechanics and Foundation Engineering,* Paris (1961) Vol. II, pp. 431–434.
7. CHANG, J. C., HANNON, J. B., and FORSYTH, R. A., "Pull Resistance and Interaction of Earthwork Reinforcement and Soil." *Transportation Research Board Record 640,* TRB, National Research Council, Washington, D.C. (1977).
8. PETERSON, L. M., "Pullout Resistance of Welded Wire Mesh Embedded in Soil." M.S. Thesis, Utah State University, Logan, Utah (1980).
9. JEWELL, R. A. "Some Effects of Reinforcement on the Mechanical Behavior of Soils." Ph.D. Thesis, University of Cambridge (1980).
10. SCHLOSSER, F., and ELIAS, V., "Friction in Reinforced Earth." *Proc. ASCE Symposium on Earth Reinforcement,* Pittsburgh, Penn. (1978) pp. 735–763.
11. SCHLOSSER, F., and VIDAL, H., "Reinforced Earth." *Bull. de Liaison des Laboratoires Routiers—Ponts et Chaussees,* No. 41 (Nov. 1969).
12. BASSETT, R. H., and LAST, N. C., "Reinforcing Earth Below Footings and Embankments." *Proc. ASCE Symposium on Earth Reinforcement,* Pittsburgh, Penn. (1978) pp. 202–231.
13. SCHLOSSER, F., and LONG, N. C., "La Terre Armee dans L'Echageur de Sete." *Revue Generale des Rates et des Aerodromes,* No. 480 (Oct. 1972).
14. YANG, Z., "Strength and Deformation Characteristics of Reinforced Sand." Ph.D. Dissertation, University of California at Los Angeles (1972).
15. HAUSMANN, M. R., "Strength of Reinforced Earth." *ARRB Proc.,* (1976) Vol. 8.
16. COLLIN, J. G. "Earth Wall Design," Submitted as partial fulfillment for the Degree of Doctor of Philosophy, Department of Civil Engineering, University of California, Berkeley (Feb. 24, 1986).
17. BELL, J. R., STILLEY, A. N., and VANDRE, B., "Fabric Retained Earth Walls." *Proc. 13th Annual Engineering Geology and Soils Engineering Symposium,* Moscow, Idaho (Apr. 1975).
18. GIROUD, J. P., "Geotextile Reinforced Cohesive Soil Mass." Woodward-Clyde Consultants, Chicago (1982).
19. STOCKER, M. F., KORBER, G. W., GASSLER, G., and GUDEHUS, G., "Soil Nailing." *Proc. International Conference on Soil Reinforcement: Reinforced Earth and Other Techniques,* Paris (1979) Vol. II, pp. 469–474.
20. GASSLER, G., and GUDEHUS, G., "Soil Nailing—Some Aspects of a New Technique." *Proc. 10th International Conference on Soil Mechanics and Foundation Engineering,* Stockholm (1981) Vol. III, pp. 665–670.
21. SHEN, C. K., HERRMANN, L. R., ROMSTAD, K. M., BANG, S., KIM, Y. S., and DENATALE, J. S., "An In-situ Earth Reinforcement Lateral Support System." *Report No. 81-03,* University of California, Davis, Calif. (Mar. 1981).
22. CARTIER, G., GIGAN, J. P., "Experiments and Observations on Soil Nailing Structures." *Proc. 8th European Conference on Soil Mechanics and Foundation Engineering,* Helsinki (1983).
23. SCHLOSSER, F., "Analogies et differences dans le comportement et le calcul des ouvrages de soutenement en Terre Armee et par clouage du sol." *Annales de l'Institut Technique du Batiment et des Travaux Publics,* No. 418 (1983).
24. GUILLOUX, A., and NOTTE, G., "Experience on a Retaining Structure by Nailing." *Proc. 8th European Conference on Soil Mechanics and Foundation Engineering,* Helsinki (1983).
25. SCHLOSSER, F., MAGNAN, J. P., and HOLTZ, R. D., "Construction Geotechnique." *Proc. 11th International Conference on Soil Mechanics and Foundation Engineering,* San Francisco (1985) Vol. 1, pp. 211–254.
26. OVERSEN, N. K., and STROMAN, H., "Design Methods for Vertical Anchor Plates in Sand." *Proc. ASCE Speciality Conference on Performance of Earth and Earth Support Structures* (1972) pp. 1481–1500.
27. NEELY, W. J., STUART, J. G., and GRAHAM, J., "Failure Loads of Vertical Anchor Plates in Sand." *J. Soil Mechanics and Foundations Division,* ASCE (Sept. 1973) Vol. 99, No. SM9, pp. 669–685.
28. DAS, V. M., and SEELY, G. R., "Pullout Resistance of Vertical Anchors." *J. Geotechnical Division,* ASCE (1975) Vol. 101, No. GT1, pp. 87–91.

CHAPTER FIVE

DESIGN METHODOLOGY

Contents

Reinforced embankments and reinforced soil walls must be designed so that they are stable both internally and externally. Internal stability requires that the reinforced soil structure be coherent and self-supporting under the action of its own weight and any externally applied forces. This is accomplished through stress transfer from the soil to the reinforcement as discussed in Chapter Four.

The reinforcements must be sized and spaced so that they (1) do not rupture under the stresses that they are required to carry, and (2) do not pull out of the soil mass.

Reinforced soil walls are subject to the same external design criteria as conventional retaining walls, independently of which reinforcing system is chosen. The wall must be stable against sliding because of the lateral pressure of the soil retained by the wall, it must resist overturning about its toe, it must be safe against foundation failure, and there must be overall slope stability. Classical methods of soil mechanics have been found satisfactory for analysis of the external stability of reinforced soil structures.

DIFFERENT DESIGN APPROACHES

Many numerical analyses, laboratory modeling, and full-scale field tests have been done to better understand the mechanisms and behavior of reinforced soil walls and embankments. Several different design approaches have evolved. Some are based on analysis under failure conditions, while others use a working stress approach.

Design Based on At-Failure Conditions

Limit equilibrium analysis has been used extensively for the design of reinforced soil walls under failure conditions. In a limit equilibrium analysis the potential failure surfaces throughout the soil mass are examined. Calculations are made to determine if the forces tending to cause movement along the failure surface can be resisted and held in equilibrium by the available shear strength of the reinforced soil mass. Surfaces with almost any shape can be analyzed, including planes, wedges, circles, logarithmic spirals, and noncircular shapes.

Limit equilibrium analysis deals with the stability of a structure at incipient failure. Model tests have been widely used as a basis for determination of failure surface location and geometry. Two types of limit analysis have been developed.

The first of these is based on failure mechanisms observed in laboratory models, which demonstrated clearly that the behavior of reinforced soil walls is quite different from that of classical, more rigid retaining walls. The local equilibrium of each layer containing a reinforcement at its center and limited by the failure surface is considered. The shape of the failure surface, as indicated by the results of both models and full-scale structures, has conformed closely to a logarithmic spiral, and it coincides with the locus of maximum tensile forces in the reinforcements. Failure is assumed to be caused by progressive rupture of reinforcing strips. Full shear resistance of the soil is assumed to be mobilized along the failure surface.

Limit analysis of local equilibrium conditions of the active zone gives the locus and maximum tensile forces in each reinforcement. This approach was developed by Juran (*1*) and forms the current basis for design of Reinforced Earth [Schlosser and Segrestin (*2*)]. More recently this limit analysis approach was generalized to allow for design of nailed soil structures in cohesionless soils as well [Juran et al. (*3*)].

The second type of limit analysis is similar to that used for classical slope stability studies. The available shearing, tensile, and pullout resistances of the reinforcements are considered when they cross a potential sliding surface. Any shape of potential sliding surface may be analyzed (e.g., planes, wedges, circles, logarithmic spirals, and noncircular shapes).

Single-Plane Failure Surfaces. Analyses were presented by the U.K. Department of Transport (1978), in which the normal, N, and tangential, T, components of the reinforcement force are added to the fully mobilized soil shear strength (Fig. 56). Different slip plane angles were examined, and the reinforcement force required to provide equilibrium was calculated for each. The slip plane angle giving the largest required reinforcement force for equilibrium to be maintained is determined. This force is compared with the lesser of the reinforcement strength or the mobilized bond force to determine the factor of safety of the system.

Infinite Slope Failure Surfaces. An infinite slope calculation procedure for analysis of the stability of long shallow slopes reinforced with tensile members is presented by Ingold (*4*) and

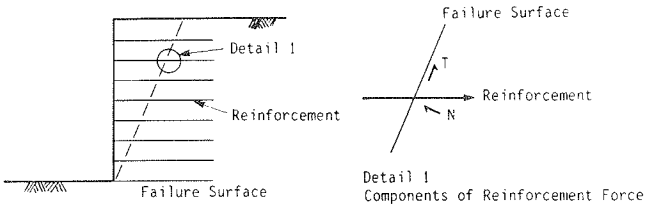

Figure 56. Limited equilibrium analysis—single-plane failure surface.

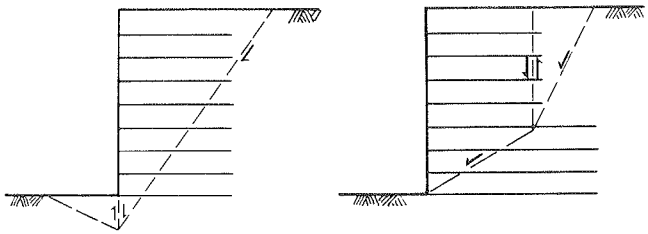

Figure 57. Two-part wedge failure surface.

in Appendix A of this report. The tangential component of the reinforcement force is ignored. The normal component N (see Fig. 56, Detail 1) is added to the available resisting force contributed by the shear strength of the soil to determine the factor of safety of the reinforced slope. The factor of safety is given by the ratio:

$$F.S. = \frac{\Sigma \text{ available resisting forces}}{\Sigma \text{ disturbing forces}} \qquad (21)$$

Two-Part Wedge Failure Surface. A two-part wedge failure surface (Fig. 57) may be the most critical failure mechanisms for steep reinforced slopes. Stocker et al. (*5*) and Romstad et al. (*6*) calculate the reinforcement force required for equilibrium assuming mobilization of full soil shear strength and compare it to the maximum available reinforcement force to obtain a factor of safety.

Circular Failure Surfaces. A number of design methods based on slip circles have been presented. The methods differ in the use of factors of safety. Phan et al. (*7*) use the soil strength and a factored reinforcement force to find the equilibrium safety factor for the embankment. Christie and El Hadi (*8A*) assess the reinforcement force based on the strength of the reinforcement, which is reduced by a safety factor. A bilinear failure surface, as shown in Figure 58, is used for design of some systems (e.g., Reinforced Earth and VSL Retained Earth).

The main differences between the various limit equilibrium analyses are concerned with the location and shape of the failure surface and the magnitude of the reinforcement force incorporated into the analysis. For example, the breaking force or the maximum pullout resistance is often used for calculations without allowing for the possibility of lower values being mobilized.

The reinforcement force may be incorporated into the equations of equilibrium differently for the various methods. In some methods, both the forces tangential and normal to the failure surface are included; in others, only the tangential component is considered (Fig. 56).

Finally, the definition of safety factor seems to vary considerably among the different limit equilibrium design methods and is probably their most significant difference. The reinforcement force required to support the structure, assuming full mobilization of soil strength, is often calculated. The factor of safety is then defined as the maximum reinforcement force available (working strength of the reinforcement) divided by the force required to provide stability.

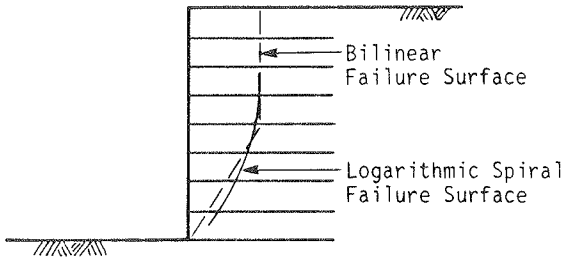

Figure 58. Logarithmic spiral failure surface.

Design Based on Working Stress Considerations

In the true sense, working stress analyses would be based on the stress-deformation behavior of the reinforced soil mass and the internal strain response of the coherent reinforced mass to externally imposed and internally developed stresses.

To date, design assumptions about the magnitudes and distributions of internal stresses that are used in working stress analyses are based on field measurements in full-scale structures. These measurements have resulted in the assumption that lateral earth pressures are at rest, rather than active, for the design of the upper portions of Reinforced Earth and VSL Retained Earth. As this assumption results in stresses larger than those of the limit state active condition, it implicitly satisfies the limit state analysis.

Finite Element Analysis

Different types of finite element analyses are available today for reinforced soil structures. All involve the subdivision of the soil into discrete elements, with properties specified for each. In some methods the reinforced soil mass is considered as a composite material [Romstad et al. (*8B*)] with each element in the soil reinforcement matrix having properties representative of the composite soil and reinforcement. Another approach is to model the soil and reinforcements separately as discrete materials [Al-Hussaini and Johnson, (*9*); Herrmann and Al-Yassin, (*10*); Al-Yassin and Herrmann, (*11*)]. Al-Hussaini and Johnson used a two dimensional finite element code, developed by Clough and Duncan (*12*), for the analysis of an instrumented test wall built at the U.S. Army Engineer Waterways Experiment Station.

The wall was 12 ft high with reinforcing strips 10 ft long and spaced 2 ft on center vertically. In order to perform a two dimensional analysis on a three dimensional problem it was assumed that the stresses induced into the soil by the reinforcing strips were constant along the plan length of the wall. Plane strain conditions were assumed to prevail.

The soil-reinforcement interaction was modeled using interface elements as developed by Goodman et al. (*13*) and hyperbolic soil behavior was assumed to model the stress-strain characteristics of the soil [Duncan and Wong, (*14*)]. The calculated stress in the reinforcements using this finite element method compared very well with the measured values from the field wall.

Other discrete finite element methods are very similar to the one outlined above. There are two problems associated with discrete models. First, in two-dimensional analysis discontinuous reinforcements (strips, rods, meshes) are modeled as continuous (sheet) reinforcements, because a plane strain condition is assumed to prevail. Secondly, this method quickly becomes cost-prohibitive when analyzing large complicated structures because of the large number of elements that must be used.

Finite element analysis can be used to analyze working stresses and displacements in an earth wall. This method of analysis is being used presently, mainly to verify existing semiempirical design methods and for the design of unusual and or complicated structures. Because of the complexity of finite element analyses, they are not yet well-suited for routine design purposes.

DESIGN METHODS CURRENTLY USED IN PRACTICE TO DETERMINE THE PULLOUT CAPACITY OF THE REINFORCEMENT

The ability of the reinforcement to withstand tensile stresses without pulling out of the reinforced soil mass is essential for the successful performance of a reinforced soil structure. There are three general approaches used today for determining pullout capacity: analyses that consider only friction; analyses that consider only passive resistance; and analyses that consider both.

The various reinforcement systems described in this report and the design equations used to determine the pullout capacity of the reinforcement in each case are given in Table 5. Each system is categorized as either frictional, passive, or a combination of the two for design purposes.

Analyses Considering Friction

The reinforcements in several earth wall systems derive most of their pullout resistance from friction. The bond between the soil and reinforcement can be estimated empirically using an apparent or effective coefficient of friction between the materials, the normal pressure on the reinforcement, and the surface area of the reinforcement. A general equation for the pullout capacity of frictional reinforcement is:

$$P_f = \mu^* \gamma Z A_s \tag{22}$$

where P_f = pullout capacity due to friction; μ^* = apparent coefficient of friction between soil and reinforcement; γ = unit weight of soil; Z = depth to reinforcement; and A_s = surface area of reinforcement.

The reinforcement soil systems that currently consider the soil reinforcement interaction as primarily frictional for design purposes are those employing strips (Reinforced Earth and plastics), sheet (geotextile), and rod (soil nailing) reinforcements. More detailed design procedures for these systems are provided in the method-specific appendixes.

Analyses Considering Passive Resistance

The soil reinforcement mechanism has been approximated for some reinforced soil systems as a passive resistance that is developed between transverse members of the reinforcement system and the soil. Grid reinforcement systems (like VSL Retained Earth, MSE, and GASE) and rod reinforcement systems (Anchored Earth) consider the bond mechanism between the soil and the tensile reinforcement as a passive resistance, because only a small proportion of the resistance is developed through friction.

A generalized equation for the pullout capacity of a reinforcement system characterized by passive resistance is:

$$P_p = N_p Z \gamma n A_b \tag{23}$$

where P_p = pullout capacity developed by passive resistance; N_p = passive resistance anchorage factor (or "bearing capacity factor") (this factor has been defined for different systems using field pullout tests); n = number of transverse bearing members behind the failure surface; and A_b = surface area of reinforcement in bearing.

The design methods for the systems that rely predominantly on passive resistance (i.e., VSL Retained Earth and Anchored Earth) are described in detail in the method-specific appendixes.

Analyses Considering Both Frictional and Passive Resistance

Nearly all types of soil reinforcement generate both frictional and passive soil resistance. Systems that rely predominantly on friction or on passive resistance are designed accordingly, as described above. However, those reinforcement systems which develop a significant proportion of their pullout resistance from each of these mechanisms should take both into account for design.

As an example, Tensar Geogrids have a relatively large percentage of surface area that develops a frictional resistance to pullout. Accordingly, their design is based on ultimate pullout capacity equal to the sum of pullout capacity due to friction plus that due to passive resistance. A generalized equation for the total pullout capacity is

$$P_T = P_p + P_f = \gamma Z(A_s \mu^* + N_p n A_b) \tag{24}$$

Because of the possible interaction between the development of friction and passive resistance, it is preferable that the coefficients μ^* and N_p be measured for these systems in a manner which takes the interaction into account.

Table 5. Pullout capacity design equations (for definition of terms, see list of symbols in Appendix E).

Reinforcement Type	Trade Name	Semi Empirical Equation for Pullout Capacity		
		Frictional	Passive	Frictional + Passive
Strip Reinforcement	Reinforced Earth	$P = \mu^* \gamma z L_e 2b$ $0.5 \leq \mu^* \leq 1.5$		
Sheet Reinforcement	Geotextiles	$P = \tan(2\phi/3)\gamma z L_e 2$		
Rod Reinforcement	Soil Nailing	$P = \pi d l_e (c + \gamma z \tan\phi)$		
	Anchored Earth		$P = \frac{K_p \gamma z \theta t}{\cos\alpha_1} e^{(2(3/4\pi - \alpha_1)\tan\phi')}$	
Grid Reinforcement	VSL Retained Earth		$P = A_c \gamma z d b n$ $15 \leq A_c \leq 40$	
	Welded Wire Wall			$P = (633 + \gamma z d[\pi L_e M \tan\delta + 36.8n])$ for clean sands $11° \leq \delta \leq 22°$
	Tensar Geogrid			$P = L_e b \gamma z[(2\alpha_s \tan\delta) + (\frac{b'}{\sigma_z} \frac{t}{S_x} \alpha_b)]$ $5 \leq \frac{\sigma_b}{\sigma_z} \leq 100$

SOIL NAILING

The design of nailed excavations and slopes is based on a limit equilibrium analysis where the failure surface is unknown and may pass through both the reinforced and unreinforced earth. There are three design approaches that are currently being used for soil nailing analysis. Schlosser and Juran (see Appendix C, Chapters One and Two, of this report) consider the shear resistance and bending moment in addition to the tensile resistance of the reinforcement in the analysis. Shen et al. (*15*) and Gassler and Gudehus (*16*) used only the tensile resistance of the reinforcement for design. Gassler and Gudehus's design approach is based on a kinematical method where force polygons and displacement vectors are used to determine the minimum factor of safety of the earth structure.

Iterative processes are used by Shen et al. (*15*) and Schlosser et al. (*17*); however, the failure criteria considered are different. Shen et al. consider reinforcement failure by either pullout or breakage, as well as soil failure along a potential sliding surface. In Schlosser's method (see Appendix C, Chapter One) account is taken of failure of reinforcements due to a combination of shearing, tension, and bending developed in rigid reinforcements; failure by pullout; soil failure by sliding along a potential failure surface; and soil creep between reinforcements.

DESIGN PARAMETERS

The internal stability of any reinforced soil wall system requires that the reinforcements neither rupture nor pull out. The design parameters required for analysis of these failure modes can be classified into five main groups: (1) mechanical properties of the backfill material or in-situ ground, particularly the internal friction angle and the unit weight; (2) mechanical properties of the reinforcements, including the modulus of deformation, tensile strength, and bending stiffness; (3) parameters relating to the soil-to-reinforcement interaction density of the soil, geometric configuration (vertical and horizontal spacing) of the reinforcement, normal pressure, surface characteristics of the reinforcement, angularity of the soil grains, frictional characteristics of the soil, portion of fine material, and the effects of water; (4) the geometric properties of the reinforcements (thickness, width, length); and (5) parameters related to construction, such as compaction stress and reinforcement orientation.

Once the type of reinforcement system has been chosen the design becomes limited by practical considerations concerning the standardization of the prefabricated reinforcements and facing elements. The final design parameters for an earth wall include the density of reinforcements (vertical and horizontal spacing), the length of the reinforcement, the size of reinforcement (e.g., bar diameter, strip width), and the service life of the structure.

DESIGN PROCEDURE

Site Conditions and General Considerations

The local soil that is available for backfill must be evaluated to determine if its properties meet the specifications. If not, a suitable imported material must be located and used. Settlement analyses should be performed to determine anticipated wall settlements using measured or estimated soil properties. Reinforced soil structures are generally very flexible retaining systems which can tolerate large differential settlements. Nonetheless, settlement analysis is still required to assure that the top of the wall will be at the desired elevation after settling.

The foundation soil must be able to support the weight of the wall and any surcharge loading without a bearing capacity failure. The external stability conditions of the wall must be satisfied before a site can be deemed acceptable for an earth wall.

Engineering Properties of Embankment Material or In-Situ Ground

The backfill material must meet certain minimum requirements to ensure adequate soil-to-reinforcement stress transfer. The grain size distribution, plasticity index, friction angle, and cohesion of the soil are often used to assess the pullout resistance of the reinforcement.

The durability of the reinforcing system depends directly on the compositional properties of the backfill. Knowledge of the soil pH, resistivity, and chloride and sulfate concentrations is required before the rate of degradation of the reinforcement can be estimated. Thus, the properties that are generally required for the internal stability of an earth wall include pH, resistivity, chlorides, sulfates, grain size distribution, plasticity index, friction angle, cohesion, unit weight, and an assessment or judgment as to how these properties may change during the planned life of the structure.

The external stability of an earth wall depends on the engineering properties of the in-situ soils and the geometry of the system. A conventional site investigation and laboratory testing program are required to provide the parameters needed for the geotechnical analysis and design. The analysis should include assessment for stability at various times during the life of a structure (i.e., during construction, at the end of construction, and during periods of extreme loading). Both the drained and undrained shear strength of the soil may, therefore, be required for analysis.

Water Conditions

The groundwater table should be located prior to design, and appropriate steps should be taken to ensure a stable structure under the worst anticipated hydrostatic loading conditions.

The backfill material used for most earth walls and reinforced embankments is a granular soil that is assumed to be free draining. The original groundwater table at a site may be altered by the construction of the wall, but usually no hydrostatic load is applied to the wall face. If fine-grained soils are used as the backfill and the water table is above the base of the wall, hydrostatic pressures must be allowed for when checking the stability of the wall. A drainage system may also be required behind the reinforced soil mass to assure that the fine-grained backfill does not become saturated (Fig. 59). Accumulation of water in the backfill could cause a reduction in the effective vertical stress between soil and reinforcement which would lower the pullout capacity of the reinforcement, resulting in significant horizontal wall movements.

Assumptions for Preliminary Design

The preliminary design is concerned with determining the feasibility of a reinforced soil wall for a particular site. The height, H, of the proposed wall is normally determined by external factors. It is measured from the top of the concrete leveling pad at the bottom of the wall face to the top of the facing elements.

The preliminary design of a reinforced soil system leads to selection of reinforcement length. The type of reinforcement (strip, sheet, rod, or grid) used for the reinforced embankment is not of primary importance in the preliminary design.

A preliminary estimate of the length of the reinforcements can be made by determining the width of the wall necessary to prevent the wall from sliding along its base or along any plane above the base due to the earth pressure exerted by the soil retained by the wall. The length of reinforcement required to prevent this sliding failure often governs the design.

External Stability Evaluation

The external stability of an earth wall depends on the ability of the reinforced soil mass to withstand the external loads, including the horizontal earth pressure from the soil being retained behind the wall and loads applied to the top of the wall, without failure by one of the following mechanisms: sliding along the base of the wall or along any plane above the base, overturning about the toe of the wall, bearing capacity failure of the foundation soil, and general slope stability failure. Figure 60 shows the external loading of a typical earth wall.

Failure Due to Sliding Along the Base of the Wall. The shear strength of the backfill material and foundation soil must be large enough to withstand the horizontal stresses applied to the reinforced soil mass from the retained soil and any additional live loads. The factor of safety of an earth wall against sliding has typically been taken as 1.5 by most earth wall designers. Using this value, the length of reinforcement required for stability against sliding for a vertically faced wall with surcharge loading is determined by the following equation, for granular backfills:

$$L = \frac{1.5K_a\,(q + (\gamma H/2))}{\gamma \tan \phi} \tag{25}$$

where L = length of reinforcement; K_a = active earth pressure coefficient, which is equal to $\tan^2(45 - \phi_1/2)$; H = height of wall; q = surcharge load; γ = unit weight of soil; ϕ_1 = internal friction angle of the soil retained by the wall; and ϕ = the internal friction angle of foundation soil or backfill, whichever is smaller. Note that for cohesive foundation soils the effective cohesion of the soil could be added to the denominator of Eq. 25, provided it can be relied on over sustained time periods.

Live loads, such as traffic loads, are treated as uniform surcharge loads, with the assumption that the load acts behind the reinforced soil mass for stability calculations and on top of the reinforced soil mass for maximum horizontal stress calculations (Fig. 60). This is a conservative approach which gives the most severe loading conditions for both cases.

Failure Due to Overturning About the Toe of the Wall. It has generally been accepted by design engineers that reinforced soil walls should have a factor of safety of at least 2.0 with respect to overturning. The sum of the resisting moments divided by the sum of the driving moments should be greater than or equal to the factor of safety.

$$F.S. \leq \frac{\Sigma M_R}{\Sigma M_D} \tag{26}$$

where $F.S.$ = factor of safety with respect to overturning; ΣM_R = sum of the resisting moments; and ΣM_D = sum of the driving moments. For the case shown in Figure 60,

$$\Sigma M_R = \frac{WL}{2} = \frac{\gamma HL^2}{2} \tag{27}$$

$$\Sigma M_D = \frac{P_q H}{2} + \frac{P_E H}{3} \tag{28}$$

where P_q = resultant horizontal earth force from surcharge loading; P_E = resultant horizontal earth force from soil retained by earth wall; and W = weight of reinforced soil mass. Note that this approach assumes the reinforced soil mass to behave as a block or monolith. Because of its flexibility there is some question about whether a reinforced soil wall could ever fail by overturning. Although lower factors of safety may thus be acceptable, their potential use has not yet been investigated.

Bearing Capacity Failure. The bearing capacity of the foundation soil must be checked to ensure that the vertical load exerted from the weight of the wall and surcharge is not excessive. The generally accepted minimum factor of safety against this type of failure for reinforced soil walls is 2.0. This is lower than that used for conventional reinforced concrete retaining walls because of the flexible nature of reinforced soil walls and their ability to function satisfactorily even after experiencing large differential settlements.

The distribution of stress under a reinforced soil wall has been represented several different ways; e.g., as a uniform stress across the full width of the wall, as a trapezoidal stress distribution, and according to Meyerhof's (*18*) stress distribution assumption for eccentrically loaded footings (Fig. 61). The Meyerhof method is used for many earth wall designs.

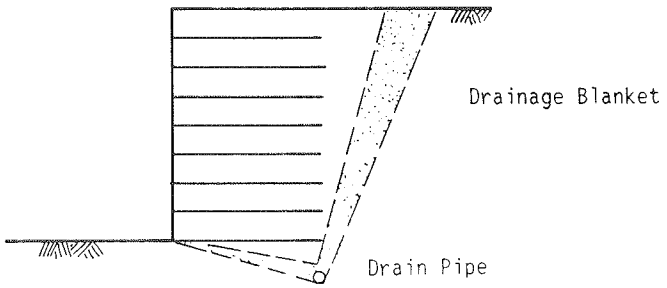

Figure 59. Earth wall with drainage blanket.

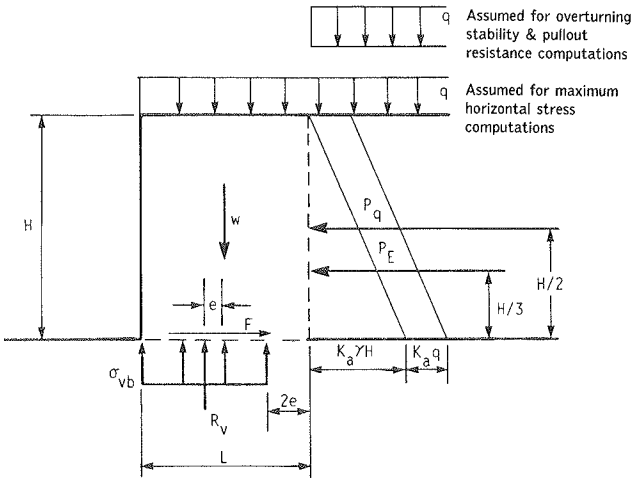

Using Meyerhof's Eccentrically Loaded Footing Analysis to Determine e (eccentricity)

$$e = \frac{\sum M_o}{R_v} = \frac{P_q(H/2) + P_E(H/3)}{R_v}$$

$$vb = \frac{W + qL}{L - 2e}$$

$$Pq = K_a qH$$

$$P_E = \frac{K_a \gamma H^2}{2}$$

R_v = Vertical Reaction

= W + qL

External Stability Criteria

F.S. = 1.5 Against Sliding $\quad 1.5 \leq \frac{eW \tan}{P_a - P_e}$

F.S. = 2.0 Against Bearing $\quad 2.0 \leq \frac{q_{ult}}{\sigma_{vb}}$

F.S. = 2.0 Against Overturning $\quad 2.0 \leq \frac{M_{toe}}{M_{toe}}$

F.S. = 1.5 General Stability

Figure 60. External stability of an earth wall.

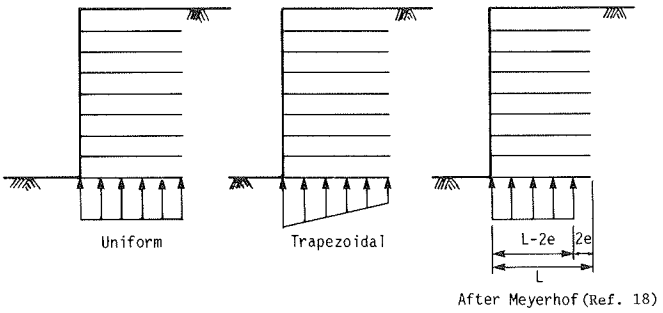

Figure 61. Stress distribution under an earth wall.

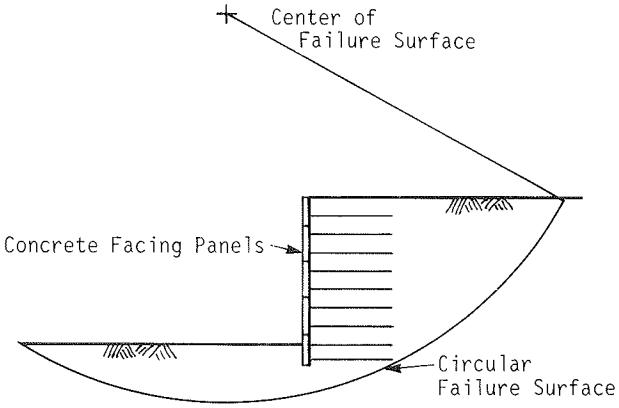

Figure 62. General slope stability of an earth wall.

The eccentricity, e, is found by setting the sum of the moments about the centerline of the reinforced soil mass equal to zero. For the loading conditions presented in Figure 60, e is given by:

$$e = \frac{\Sigma M_D}{R_V} = \frac{P_q(H/2) + P_E(H/3)}{R_V} \tag{29}$$

where R_V = vertical reaction = $W + qL$.

The eccentricity, e, should be less than $\frac{1}{6}$ the length of the reinforcement, L, when using Meyerhof's stress distribution. For greater eccentricities the bearing stress rapidly increases with the smaller effective contact area ($L - 2e$), making Meyerhof's assumption of a uniform stress distribution less reasonable.

The vertical stress at the bottom of the wall then is assumed to act over a length of $L - 2e$. The magnitude of foundation bearing stress is found by dividing the vertical reaction by the reduced wall length:

$$\sigma_{vb} = \frac{W + qL}{L - 2e} \tag{30}$$

The factor of safety against bearing capacity failure is defined by

$$F.S._{bearing} = \frac{q_{ult}}{\sigma_{vb}} \tag{31}$$

where q_{ult} = ultimate bearing capacity.

The ultimate bearing capacity of the foundation soil is evaluated using classical soil mechanics methods.

Sliding, overturning, and bearing capacity analyses must be made for imported embankment earth walls, but are not required for in-situ reinforced slopes.

General Slope Stability. Both in-situ reinforced slopes and imported embankment earth walls must satisfy general slope stability. The reinforced soil mass is treated as a gravity retaining structure. Any appropriate slope stability analysis method can be used to determine the minimum overall factor of safety for general slope stability (Fig. 62).

Internal Stability Evaluation

Failure Surface. As discussed in Chapter Four, the reinforced soil mass in both imported embankment earth walls (vertical or sloping face) and in-situ reinforced slopes can be divided into two regions, the active and resistant zones. The active zone is located immediately behind the face of the wall. In this region the soil is trying to move away from the soil behind. The stresses produced by this movement are directed outward, and must be resisted by the reinforcements. These forces in the reinforcements are transferred to the resistant zone where the soil shear stresses are mobilized in the opposite direction to prevent the pullout of the reinforcements. Figure 63 shows these two different regions. The reinforcement holds these two zones together making a coherent soil mass.

The demarcation between these two zones is important, because it determines the points of maximum tensile force in the reinforcements and it corresponds to the potential failure surface within the reinforced soil mass. The location of this failure surface is not well defined for all the different reinforcing systems used today. Some designers use a Rankine failure surface that extends from the base of the wall to the ground surface at an angle of $45 + \phi/2$ from the horizontal. Other reinforcement systems are designed using a bilinear failure surface to approximate a curved surface. Figure 64 shows these potential failure surfaces, and the shear assumed for design of the different presently available wall types is given in Table 6.

A single failure surface can be defined by designers of imported embankment type reinforced soil wall systems, because

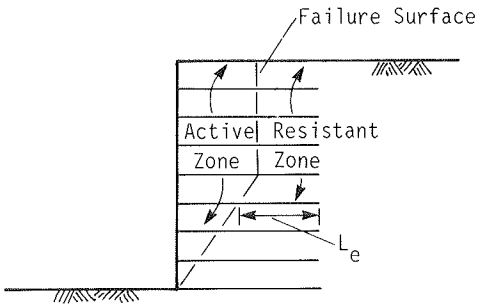

Figure 63. Active and resistant zones of an earth wall.

the backfill material is relatively homogeneous and the reinforcement spacing is uniform. In contrast, in-situ slope reinforcement is often done in heterogeneous ground. Hence, the geometry of the reinforcement system (vertical and horizontal spacing) at each site can vary considerably, and the actual shape of the potential failure surface becomes difficult to predetermine.

For these reasons the current design of in-situ reinforced slopes is based on a general stability analysis approach considering potential failure surfaces which cross the reinforcements (Fig. 64). Numerous failure surfaces are analyzed, with the potential failure surface defined as that surface which gives the lowest factor of safety.

Earth Pressure Coefficient. Internal stability analysis requires knowledge or the assumption of values for the coefficient of horizontal earth pressure within the reinforced soil mass. Designers of reinforcement systems that do not have a large data base of field instrumented walls have used the active earth pressure coefficient for determining horizontal stresses. In some systems (Reinforced Earth and VSL Retained Earth) a linear variation in earth pressure coefficient from K_o (the coefficient of earth pressure at rest) at the top of the wall to K_a (active earth pressure coefficient) at some depth (e.g., 20 ft) below the top of the wall is assumed. One grid reinforcement system (Welded Wire Wall) uses a value of $K = 0.65$, which is larger than the at-rest earth pressure coefficient for the soils generally used in earth wall construction (Fig. 65). The earth pressure coefficient assumptions for design of the various reinforcing systems are given in Table 6. The results of field measurements on full-scale structures under working stress conditions form the bases for most of these assumptions.

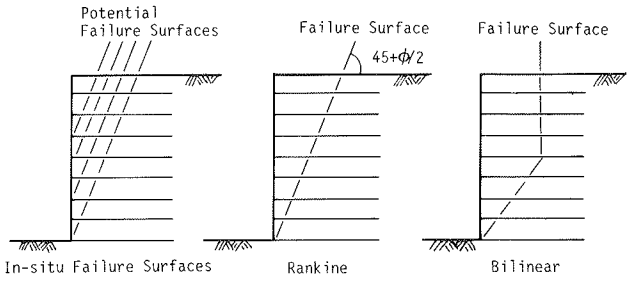

Figure 64. In-situ reinforced slope potential failure surface versus Rankine and bilinear.

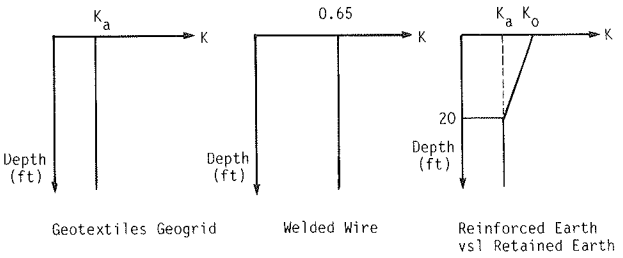

Figure 65. Assumed variation in earth pressure coefficient with depth for different wall types.

Table 6. Internal design characteristics of earth walls.

Reinforcement Type	Trade Name	Failure Surface			Earth Pressure Coefficient				Durability	
		Rankine	Bilinear	Wedge with varying angles from horizontal	K_a	K_o	$>K_o$	varying from K_o at top of wall to K_a 20 ft below top	Reinforcement susceptible to corrosion	Degradation by Ultra Violet Light Radiation
Strip Reinforcement	Reinforced Earth		X					X	X	
	Plastics		X					X	X	
Sheet Reinforcement	Geotextiles	X				X				X
Rod Reinforcement	Soil Nailing			X	X					
	Anchored Earth			X	X				X	
Grid Reinforcement	VSL Retained Earth		X					X	X	
	MSE, GASE	X	X		X					
	Welded Wire Wall	X					X (0.65)		X	
	Geogrid	X			X					X

Reinforcement Rupture. The reinforcement system must be able to withstand the stresses transferred to it from the soil without breaking. The horizontal stress, σ_h, at any depth within a wall is determined as follows:

$$\sigma_h = K \sigma_v \tag{32}$$

where K = coefficient of horizontal earth pressure, and σ_v = vertical stress at any depth. The vertical stress at any depth can be determined by finding the eccentricity, e, of the reactive force at that depth and then determining the vertical stress according to Meyerhof's stress distribution (see section under "External Stability Evaluation").

If the vertical spacing between reinforcements is S_v and the horizontal spacing center-to-center between reinforcements is S_H, the total horizontal load, FH, to be resisted by a given layer of reinforcement is:

$$FH = \sigma_h \times S_H \times S_v \tag{33}$$

The stress induced in the reinforcement from the horizontal load, FH, must be less than the allowable working stress of the tensile member to assure adequate safety against rupture.

Pullout Capacity. The pullout capacity of any reinforcement system can be determined from semiempirical equations, as discussed under "Analyses Considering Friction," "Analyses Considering Passive Resistance," and "Analyses Considering Both Frictional and Passive Resistance." The embedment length of the reinforcement, L_e—i.e., the length of the reinforcement behind the potential failure surface (Fig. 63)—must be great enough to assure the transfer of stress from the reinforcement to the soil without reinforcement pullout. Pullout equations used in design of various reinforcing systems are given in Table 5.

Durability. The reinforcements must be able to withstand degradation for the life of the structure. The most critical forms of degradation for earth structures result from corrosion and exposure to ultraviolet light radiation. Reinforcements that are made from metal (Reinforced Earth, Anchored Earth, VSL Retained Earth, MSE, GASE, Welded Wire Walls, and Soil Nailing) are susceptible to corrosion. The service life of these reinforcement systems can be extended by adding additional "sacrificial" steel to the reinforcement members. Zinc galvanizing or epoxy coatings are also used to extend the life of these materials.

Geotextiles are susceptible to degradation from ultraviolet light radiation. Hence, if they are left exposed to the sun, they will lose strength. It is therefore necessary to protect geotextile reinforcement from prolonged exposure. Asphalt and shotcrete are currently being used as a protective coating for the face of geotextile reinforced walls and embankments. The long-term resistance of geotextiles to chemical and biological attack is not known. Durability considerations pertinent to each type of reinforcement system are given in Table 6. Durability is covered in detail in Chapter Six of this report.

Special Loading Conditions

The special loading conditions to which a reinforced soil wall or reinforced embankment might be subjected, can be separated into two categories, static and dynamic.

Some typical types of static loads are: vertical and horizontal concentrated loads (e.g., from bridge abutments), cyclic vehicular traffic loads that are often represented by an equivalent uniformly distributed surcharge, earth slopes and embankments above the top of the wall, and hydraulic loads (i.e., quay walls).

Concentrated line loads and strip loads can be incorporated into design by using a Boussinesq stress distribution to determine the vertical and horizontal components of stress at any depth within the reinforced soil mass. Some designers have simplified this procedure by assuming the horizontal stress at any level can be determined as follows:

$$\sigma_{HT} = \sigma_{Vsoil} K + \sigma_{Vline} K_o + \sigma_{Hsup} \tag{34}$$

where σ_{HT} = total horizontal pressure at any depth; σ_{Vsoil} = vertical pressure from the soil; σ_{Vline} = vertical pressure from the vertical component of the line load; σ_{Hsup} = horizontal pressure from the horizontal component of the line load; K = coefficient of earth pressure within reinforced soil mass; and K_o = coefficient of earth pressure at rest.

The horizontal pressure distribution from a horizontal concentrated load has been assumed to be triangular as shown in Figure 66. Once the stresses within the reinforced soil mass have been determined, the internal stability analysis can follow the procedures outlined in the previous sections of this chapter.

Uniformly distributed surcharge loads from slopes and embankments above the top of the wall can be represented by adding an equivalent weight of soil above the wall. The general internal and external design approach can then be used for analysis.

Hydrostatic loads on earth walls should be handled the same way as for conventional reinforced concrete retaining walls. The hydrostatic pressure should be added to the back of the wall and the effective unit weight of the soil below the water table should be used for stability calculations.

The dynamic loads that a reinforced soil wall or reinforced embankment might be subjected to are vertical and horizontal vibrations from traffic, and seismic events. The design of reinforced soil walls and embankments with respect to dynamic loading was initially based on the results of laboratory model tests. Relatively few instrumented full-scale walls have experienced seismic loading.

One currently used seismic design method is based on the pseudostatic Mononobe-Okabe analysis [Mononobe (*19*); Okabe (*20*)]. This analysis is based on the following assumptions. The

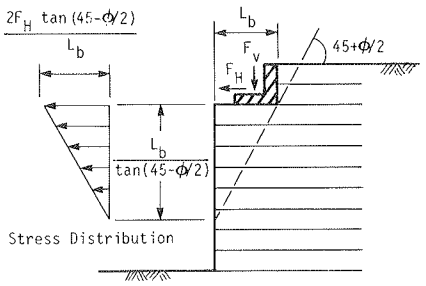

Figure 66. Distribution of stress from concentrated horizontal load.

dynamic load does not modify the location of the maximum tensile force in the reinforcement. The active zone in the reinforced soil mass behaves as a rigid mass. The dynamic active force due to the seismic event is equal to the horizontal inertia force of the active zone. The total active force is equal to the sum of the dynamic active force and the static active force. A triangular dynamic pressure distribution is used. The resultant dynamic force is therefore assumed to act at a distance of $\frac{2}{3}$ H from the bottom of the wall (Fig. 67).

There are several other seismic design procedures that have been proposed for earth wall design. Seed and Whitman (*21*) developed a simplified procedure for the design of earth retaining structures for dynamic loads that can be adapted for earth walls. Richardson and Lee (*22*) and Richardson (*23*) also developed an empirical design procedure for estimating dynamic forces in an earth wall. This method is based on a complex dynamic analysis and extrapolations of small-scale model test data.

Richardson et al. (*24*) performed a series of forced vibration tests and explosive vibration tests on a test wall constructed at the University of California, Los Angeles, that support the results found on the small-scale tests performed by Richardson and Lee.

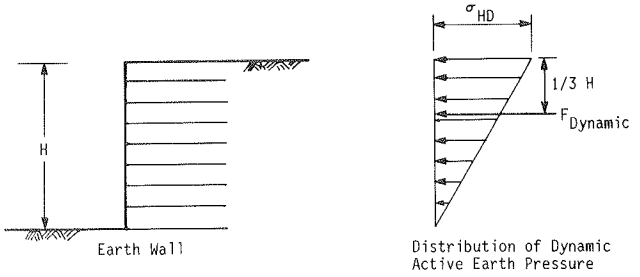

Figure 67. Mononobe-Okabe pseudo-static pressure diagram.

Soil Nailing—Special Considerations

The design approach used for soil nailing is based on classical stability analysis (e.g., Fellenius or Bishop methods) in which the normal and shear forces in each reinforcement crossing the potential failure surface can be added to the other resisting forces to determine the factor of safety.

This general stability analysis, unlike the internal analysis used for imported embankment-type earth walls, does not provide an evaluation of the locus and values of the maximum tensile and shear forces in the reinforcements. The method is therefore limited to the evaluation of a global safety factor with respect to an overall failure of the structure.

Four failure criteria can be considered in this general stability analysis approach: (1) shear resistance of the soil; (2) soil-to-reinforcement friction—the mobilized tensile force must be balanced by the effective friction mobilized at the soil reinforcement interface; (3) normal interaction between the soil and the inclusion—the normal interaction between the soil and the relatively rigid reinforcement results in a progressive mobilization of passive earth pressure along the reinforcement; and (4) strength of the reinforcement—the tensile and shearing resistance of the reinforcements must not be exceeded. Appendix C on "Soil Nailing in Excavations" describes this type of general stability analysis and design methodology in greater detail.

CURRENT DESIGN CAPABILITIES

There are several limitations that should be recognized when designing a reinforced soil structure. The semiempirical design approach is based on a relatively small data base. More full-scale reinforced soil walls need to be instrumented to provide designers with a better understanding of the mechanisms that govern their behavior.

The design procedures currently used are for granular backfills. More study of fine-grained soils is required to develop suitable design approaches for cases where their use as backfill materials is necessary.

The satisfactory performance of the thousands of reinforced soil walls and reinforced embankments constructed to date suggests that the current design procedures are conservative. However, with more information from instrumented walls and embankments, the design methods can perhaps be refined to give even more economical solutions to reinforced soil wall and slope problems.

DESIGN EXAMPLES

A flow diagram for the design of reinforced walls and embankments is illustrated in Figure 68. The general sequence shown in this chart can be used for design of any of the reinforced structure types described in this report, although there may be some differences in specific details as noted in the method-specific appendixes.

The general design methodology for earth walls developed in this chapter and summarized in Figure 68 has been used to prepare illustrative designs for a number of types of earth wall using several different reinforcement systems. The overall dimensions have been determined for each case to ensure external stability against overturning or sliding. The required bearing capacity of the foundation soil at the toe has been evaluated. The overall stability of the reinforced soil structure and the foundation against sliding or rotational failure has not been analyzed because the risk of failure by these mechanisms is specific to each particular site.

A slip circle method for analysis of reinforced soil embankments is discussed in Appendix A, Chapter One, Section 7.4. Design methods for embankments are also discussed in Appendix B, Chapter Three, Section 7.2, with design examples provided in Section 11.

Internal designs have been completed for each system and each case to include size, length, and spacings of reinforcements; factors of safety against reinforcement rupture and pullout; and the determination of safety against failure by corrosion or loss of durability. The corrosion and durability analyses are based on the considerations contained in Chapter Six and method-specific appendixes of this report. Complete computations are presented for the first case, namely, a 15-ft high vertical wall retaining a level backfill with no surcharge. The reinforcement systems for which internal designs have been prepared are: (1) strip reinforcement—Reinforced Earth; (2) grid (bar mat) reinforcement—VSL Retained Earth; (3) grid reinforcement—Welded Wire Wall; (4) grid reinforcement—Geogrids; and (5) sheet reinforcement—Geotextile.

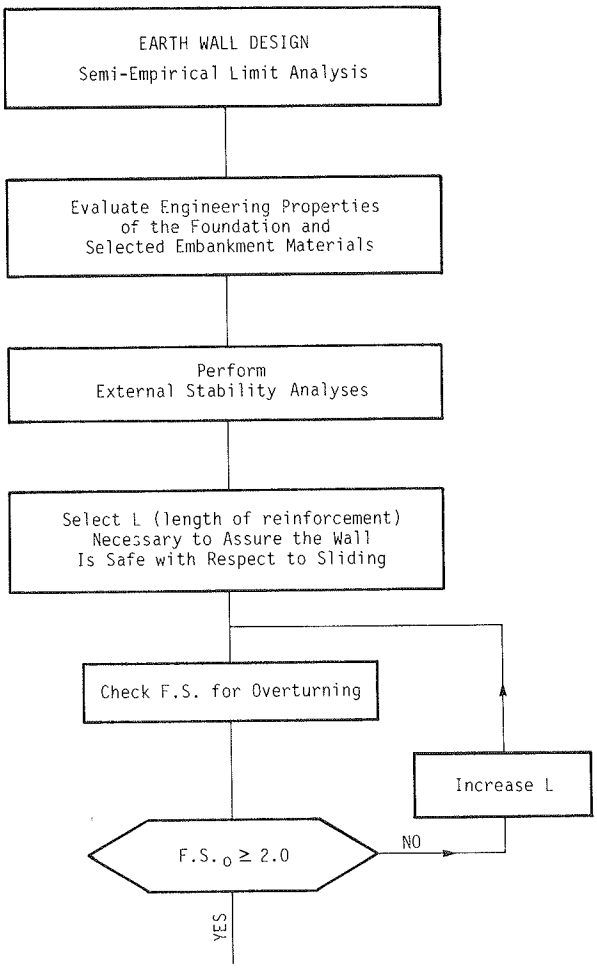

Figure 68. Design flow chart.

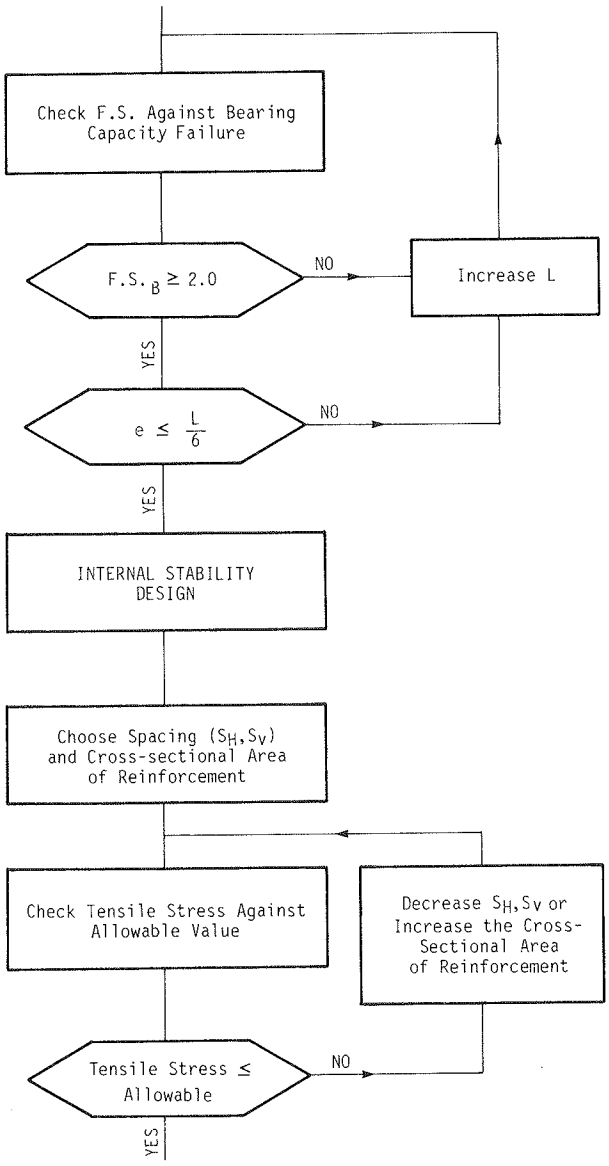

Subsequent cases are presented in considerably less detail, but any significant differences from the first case and the final results are indicated.

DESIGN EXAMPLE I—LOW WALL WITH HORIZONTAL BACKFILL

A. Given Conditions

The given conditions for the design of a reinforced soil wall are shown in Diagram 1. The foundation soil is assumed to have the same properties as the soil behind the reinforced zone.

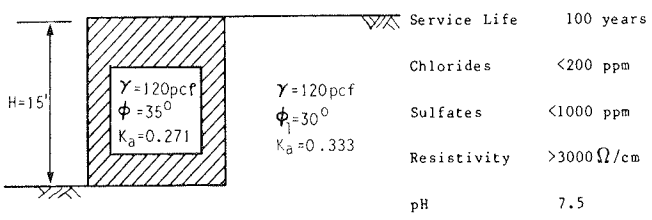

Diagram 1

B. External Stability

The external stability computations are identical for all wall types and follow the procedures presented earlier in this chapter under "External Stability Evaluation." Diagram 2 shows the

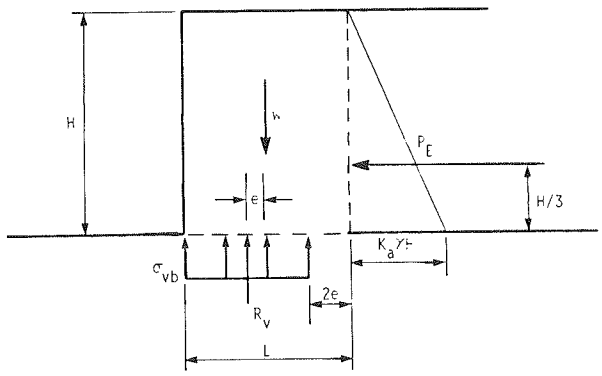

Diagram 2

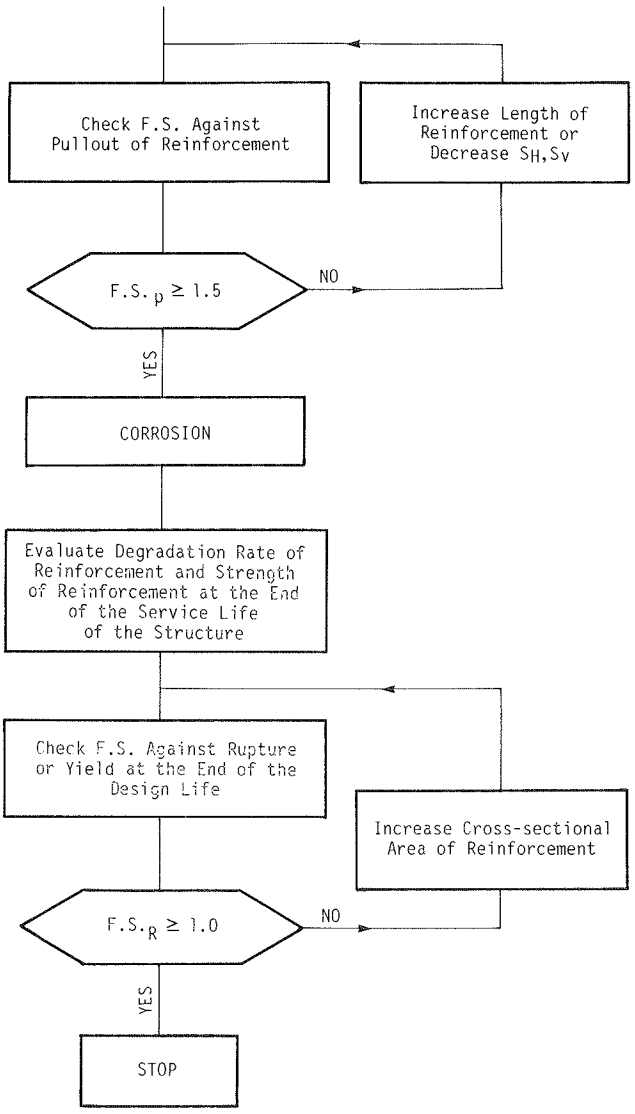

Figure 68. Continued

forces and variables that must be considered. Computations must be performed to assure adequate safety against (1) sliding, (2) overturning, and (3) bearing capacity failure.

B1. Computations To Assure Safety

B1.1. Sliding on base

- A factor of safety exceeding 1.5 is required.
- Resistance to sliding is computed based on the lesser of the shear strengths of the backfill used in the reinforced zone, or the foundation soil at the base of the structure. For the case analyzed here, since the retained soil and the foundation soil are the same material, the internal friction angle ϕ of the foundation soil is equal to the internal friction angle of the retained soil, ϕ_1. Therefore, the foundation soil with an internal friction angle equal to ϕ_1 of 30 deg controls. For a frictional foundation soil with an internal friction angle, in this case ϕ_1, the available resistance can be computed as $\gamma LH \tan \phi_1$.
- The driving force is given by the total horizontal active earth force acting on the back of the wall. In the absence of external loads, its value can be computed as $P_E = \frac{1}{2}K_a\gamma H^2$, where $K_a = \tan^2\left(45° - \frac{\phi 1}{2}\right) = 0.333$.
- The factor of safety, *F.S.*, is obtained by dividing the available resisting force by the driving force, $F.S. = \frac{\phi LH \tan \phi_1}{\frac{1}{2} K_a \phi H^2}$.
- For a minimum factor of safety of 1.5, the minimum length of reinforcement, L, can be computed as $L = \frac{1.5\, K_a H}{2 \tan \phi_1}$. In the absence of a surcharge, Eq. 25 would also simplify to this solution, but it should be borne in mind that Eq. 25 represents the more general case.
- $L = \frac{1.5(0.333)15}{2 \tan 30°} = 6.5$ ft.

B1.2. Overturning about toe

- The factor of safety against overturning is given by $F.S. = \frac{\overrightarrow{\Sigma M}_{Toe}}{\overleftarrow{\Sigma M}_{Toe}}$ (where clockwise rotation indicates resisting moment and anticlockwise rotation indicates overturning moment) and its value must be greater than 2.0 (Section under "External Stability Evaluation).
- $\overrightarrow{\Sigma M}_{Toe} = W\frac{L}{2}$ = Resisting moment (Diagram 2).
- $\overleftarrow{\Sigma M}_{Toe} = P_E\frac{H}{3}$ = Overturning moment (Diagram 2).
- Based on the above definitions of resisting and overturning moments, the factor of safety can be computed as $F.S. = \frac{3\gamma HL^2}{K_a\gamma H^2 H} = \frac{3L^2}{K_a H^2}$.
- Accordingly, the minimum base width of the wall (or the minimum length of reinforcement), L, to yield a factor of safety of 2 can be computed from $L^2 = \frac{F.S.\ K_a H^2}{3}$; $L = \sqrt{2\,\frac{(0.333)(15)^2}{3}} = 7.07 \simeq 7.0$ ft.

B1.3. Bearing capacity failure

- As noted in the section under "External Stability Evaluation," the minimum factor of safety against bearing capacity failure should be 2.0. Meyerhof's stress distribution (see Fig. 61) for eccentrically loaded footings is used to compute bearing pressure. Thus, eccentricity must be computed first.
- For the case of $L = 7.0$ ft, eccentricity, e, can be computed as $e = \frac{\overleftarrow{\Sigma M}_{centerline}}{R_v} = \frac{P_E(H/3)}{R_V}$, where R_V is the total vertical reaction across the base.
- $e = \frac{\frac{1}{2}K_a\gamma H^2\left(\frac{H}{3}\right)}{\gamma LH} = \frac{K_a H^2}{6L} = \frac{(0.333)(15)^2}{(6)(7)} = 1.78$ ft.
- This eccentricity (1.78) is greater than the allowable value, $L/6(1.17)$, which could maintain the reaction in the middle third.
- Therefore, compute eccentricity with a larger assumed value of L, say 9 ft.

- Thus, $e = \frac{(0.333)(15)^2}{2(3)(9)} = 1.39 \leq \frac{L}{6} = 1.5$, which is satisfactory.
- Determine the required soil bearing capacity to ensure a factor of safety above 2.0. the maximum bearing pressure, σ_{vb}, can first be computed as $\sigma_{vb} = \frac{W}{L - 2e}$ (Meyerhof distribution).

$$\sigma_{vb} = \frac{\gamma LH}{L - 2e} = \frac{(120)(0)(15)}{9 - 2(1.39)} = 2{,}604 \text{ lb/ft}^2.$$

- To assure a factor of safety larger than 2.0, the ultimate bearing capacity of the foundation soil must exceed 5,200 lb/ft^2.
- The final result of the external stability calculation is that $L = 9$ ft is required, and the foundation soil must have an ultimate bearing capacity greater than 5,200 lb/ft^2.

C. Internal Stability

The procedures used for internal design follow the general methodology given under "Internal Stability Evaluation" and in Figure 68. Because details vary for each reinforcement system, examples for several wall types are provided below.

C1. Strip Reinforcement System—Reinforced Earth

- The reinforcement spacing both vertically and horizontally is predetermined by the connector tab spacings on the precast facing elements. Usual minimum values for these spacings are $S_v = 30$ in. and $S_H = 40$ in.
- The vertical spacing of the reinforcements and the reinforcement layer numbering are shown below. Upper most reinforcement is at a depth below grade that is equal to half the distance between other reinforcement layers. The assumed boundary between the active and resistant zones (see Fig. A-34 in Appendix A) is indicated by the dashed line in Diagram 3.

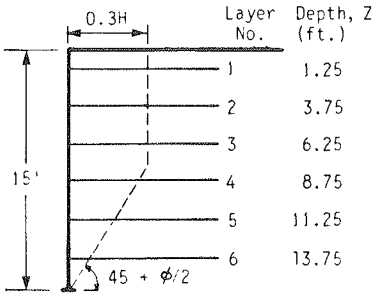

Diagram 3

- The assumed variations with depth of horizontal earth pressure coefficient, K, and apparent soil to reinforcement friction coefficient, μ^* (see Fig. A-34), are shown on Diagram 4, with K_o being equal to $1 - \sin \phi = 0.426$ and K_a being equal to $\tan^2 (45 - \phi/2) = 0.271$.
- The values of K and μ^* are used to calculate the horizontal earth forces to be resisted by the reinforcements and the reinforcement pullout resistance, respectively. If standard cruciform facing panels are used, each reinforcement supports 6.05 ft^2 of facing panel surface area (4 strips per panel; 24.2 ft^2 panel area—see Appendix A, Chapter One).
- Standard reinforcement strips are available in two sizes: 40 mm × 5 mm or 60 mm × 5 mm. Calculations of the type shown below for reinforcement layer 4 at a depth of 8.75 ft (Diagram 3) are required for each level of reinforcement:

C1.1. Tensile forces to be resisted by reinforcement

- Horizontal earth pressure at depth $Z = 8.75$ ft is computed by multiplying K for that depth (Diagram 4) by the vertical pressure, σ_{vb}, at that depth. This vertical pressure is somewhat greater than the overburden pressure owing to eccentricity caused by the external lateral earth pressures.
- Vertical load $R_V = \gamma ZL = (120)(8.75)(9) = 9{,}450$ lb per foot of wall.
- The external horizontal force acting on the wall above depth Z can be computed as $P_E = \gamma K_a \frac{Z^2}{2} = 120\ (0.333)\ \frac{(8.75)^2}{2} = 1{,}530$ lb.
- Eccentricity at depth Z can be computed as $e = \frac{P_E\,(Z/3)}{R_V} = 1{,}530\ \frac{(8.75)}{3(9{,}450)} = 0.47$ ft.
- Bearing pressure on the reduced bearing area can be computed as $\sigma_{vb} = \frac{\gamma LZ}{L - 2e} = \frac{120\ (9)\ (8.75)}{(9 - 2(0.47))} = 1{,}172$ lb/ft.
- Compute K (Diagram 4) at depth of 8.75 ft based on $K = K_o = 1 - \sin \phi = 0.426$ at top of wall and $K = K_a = 0.271$ at a depth of 20 ft.
- $K = 0.426 - \frac{8.75}{20}\ (0.426 - 0.271) = 0.358.$
- Compute the horizontal stress to be resisted by the reinforcement $\sigma_h = K\ \sigma_{vb} = 0.358\ (1{,}172) = 420$ lb/ft^2.
- Compute the horizontal force supported by a single reinforcement, $FH = \sigma_h A_R = 420\ (6.05) = 2{,}541$ lb, where $A_R =$ contributing area per reinforcement.

C1.2. Tensile stress in reinforcement

- Assume that the smaller, i.e., 40 mm × 5 mm reinforcing strips will be used.
- Compute the cross-sectional area, $A_{CR} = \frac{40\ (5)\ \text{mm}^2}{\left(\frac{25.4\ \text{mm}}{\text{in.}}\right)^2} = 0.310$ in^2.

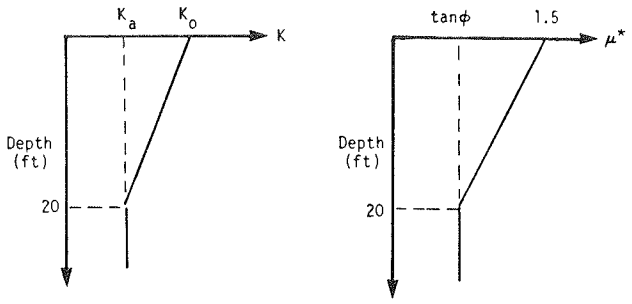

Diagram 4

- Compute tensile stress in each strip, $F_T = \frac{FH}{A_{CR}} = \frac{2{,}541}{0.310} =$ 8,197 psi. Allowable tensile stress in reinforcement = 40,000 psi; thus, use of this strip would be satisfactory.

C1.3. Tensile stress at connection

- In design of Reinforced Earth, it is assumed that the horizontal stress in the soil near the connection is equal to 85 percent of the maximum horizontal stress, or $\sigma_{h\,(CONN)} = \sigma_h$ (0.85) = 420 (0.85) = 357 lb/ft^2.
- Compute the reduced cross-sectional area due to a bolthole of $\frac{9}{16}$ in. (14.29 mm) diameter; $A_{Reduced} = \frac{5\ (40 - 14.29)\ \text{mm}^2}{\left(\frac{25.4\ \text{mm}}{\text{in.}}\right)^2} = 0.199\ \text{in.}^2$
- Compute the tensile stress at the connection; $F_{T(CONN)} = \frac{\sigma_{hCONN} A_R}{A_{Reduced}} = \frac{357 \times 6.05}{0.199} = 10{,}853$ psi, which is less than the allowable working stress of 20,000 psi.

C1.4. Pullout of reinforcement

- The pullout resistance at depth Z can be computed as $P = 2b\ \gamma\ Z\ \mu^*\ L_e$ where L_e is the depth of embedment into the resisting zone and b is the width of reinforcement.
- The apparent coefficient of friction between the soil and the reinforcement, μ^*, is selected from Diagram 4 for a depth of embedment of 8.75 ft, based on a linear variation from 1.5 at $Z = 0$ to tan ϕ at $Z = 20$ ft.
- $\mu^* = 1.5 - \left[\frac{(1.5 - \tan\phi)}{20} Z\right]$; $\mu^* = 1.5 - \left[\frac{(1.5 - \tan 35^\circ}{20} 8.75\right] = 1.15$.
- From the boundary between the active and resistant zones (Fig. A-34 in Appendix A), L_e, can be computed as: for $Z \leq \frac{H}{2}$, $L_e = L - 0.3H$; for $Z > \frac{H}{2}$, $L_e = L - \left[\frac{(H - Z)}{\tan\left(45 + \frac{\phi}{2}\right)}\right]$.
- Thus, for $Z = 8.75$ ft, $L_e = 9 - \left[\frac{15 - 8.75}{\tan 62.5^\circ}\right] = 5.746$ ft.
- Compute $P = 2\left(\frac{40}{25.4 \times 12}\right)$ (120)8.75(1.15)5.746 lb = 1,821 lb.
- $F.S._{pullout} = \frac{P}{FH} = \frac{1{,}821}{2{,}541} = 0.71 \leq 1.5$, which is unsatisfactory.
- To increase the factor of safety to above 1.5, either the length or the width of the reinforcement can be increased. First, try increasing the width of the reinforcement to 60 mm, and recompute pullout resistance.
- $P = 2\left(\frac{60}{25.4 \times 12}\right)$ (120)8.75(1.15)5.746 = 2,732 lb. $F.S._{pullout} = \frac{P}{FH} = \frac{2{,}732}{2.541} = 1.075$, which is still unsatisfactory.
- Thus, it is necessary to extend the length of reinforcements. Try $L = 11$ ft with reinforcement strips of 60 mm width. The value of L_e will now be 7.746 ft.
- $P = 2\left(\frac{60}{25.4 \times 12}\right)$ (120)8.75(1.15)7.746 = 3,682 lb, which would yield $F.S._{pullout}$ of 1.45.
- It is also necessary to recalculate the horizontal force FH, because the increased strip length results in slightly decreased values of eccentricity and σ_{vb}. Following the same procedures as described above yields: $R_V = \gamma ZL = 11{,}550$ lb; $e = 0.386$ ft; $\sigma_{vb} = 1{,}129$ lb/ft^2 and $\sigma_h = K\ \sigma_{vb} = 404$ lb/ft^2; and $FH = \sigma_h A_R = 2{,}444$ lb.
- Consequently, $F.S._{pullout} = \frac{P}{FH} = \frac{3{,}682}{2{,}444} = 1.51$, which is O.K.
- Calculations are carried out in a similar manner for each level of reinforcement, with the results being summarized in Table 7 for reinforcing strip lengths of 11 ft. It may be seen that the factor of safety against pullout is slightly less than 1.5 for the upper three levels of reinforcement. Use of 12-ft long reinforcement strips would ensure that the safety factor was greater than 1.5 throughout.

C1.5. Corrosion

- According to the data provided in Chapter Six under "Estimation of Corrosion Rate," corrosion rates for the materials in galvanized strips would be: zinc—6 μm/year for the first 2 years, 2 μm/year thereafter; carbon steel—45 μm/year for the first 2 years, 9 μm/year thereafter.
- The zinc coating thickness on Welded Wire is 87 μm. Thus, the service life of zinc can be computed as follows: zinc loss for first 2 years = 2 years (6 μm/year) = 12 μm, zinc thickness after 2 years = 87 − 12 = 75 μm. At the reduced corrosion rate after 2 years, remaining life would be: (75 μm)/(2 μm/yr) = 37.5 years. Thus, total life of zinc = 37.5 + 2 = 39.5 years.
- Cross-sectional area of reinforcement after 100 years: Initial thickness of reinforcement without the galvanizing is 5 mm = 5,000 μm. Thickness after 100 years of corrosion = t_{100}. Thus, t_{100} = 5,000 − [(2) 9 μm/yr (100 − 39.5) years] = 3,911 μm.
- Cross-sectional area after 100 years is 60 mm × 3.91 mm = 0.3637 in.^{2}
- The tensile stress in reinforcement layer 6, which supports the maximum tensile load, can be computed (Table 7) as (3,857 lb)/(0.3637 in.^{2}) = 10,606 psi (which is less than the allowable working stress of 20,000 psi).
- The foregoing steps complete the design of the wall.

C2. Grid (Bar Mat) Reinforcement—VSL Retained Earth

- The design conditions are as shown on Diagram 1. For VSL Retained Earth the vertical spacing of reinforcements and the horizontal spacing of reinforcing mats center-to-center will be 2.5 ft and 4.33 ft, respectively. The vertical spacing between

Table 7. Design summary—Reinforced Earth wall (height = 15 ft, level backfill, no surcharge, reinforcement length = 11 ft).

Reinf. Layer No.	Z (ft.)	e (ft.)	σ_{vb} (psf)	K	σ_h (psf)	FH (lbs.)	F_T(1) (psi)	F_{TCONN} (psi)	F.S. Rupture	μ^*	L_e (ft.)	P (lbs.)	F.S. Pullout
1	1.25	0.0	150	0.42	63	378	813	908	44.0	1.45	6.5	555	1.47
2	3.75	0.07	456	0.40	181	1095	2355	2630	15.2	1.35	6.5	1554	1.42
3	6.25	0.20	778	0.38	294	1778	3825	4270	9.4	1.25	6.5	2399	1.35
4	8.75	0.38	1129	0.36	404	2444	5258	5869	6.8	1.15	7.7	3682	1.51
5	11.25	0.63	1526	0.34	517	3129	6829	7506	5.3	1.05	9.0	5021	1.60
6	13.75	0.95	1993	0.32	638	3857	8295	9252	4.3	0.95	10.3	6355	1.65

(1) For 60mm x 5mm strips.

reinforcements is shown on Diagram 5. The assumed boundary between the active and resistant zone (see Fig. B-110) is also shown.

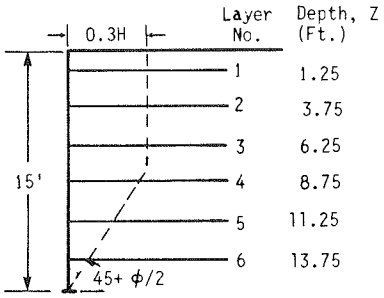

Diagram 5

- The variations of earth pressure coefficient and anchorage factor with depth used for design of VSL Retained Earth Walls (see Appendix B, Chapter Four) are shown in Diagram 6.

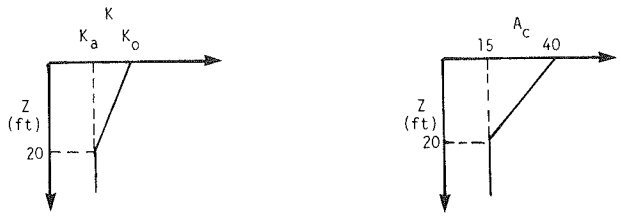

Diagram 6

- The values of K and A_c are used to calculate the horizontal earth forces to be resisted by the reinforcements and the reinforcement pullout resistance, respectively. A single mat supports a facing area 2.50 ft by 4.33 ft, i.e., 10.83 ft^2.
- The calculations required for the analysis of layer 4 at a depth of 8.75 ft below the top of the wall are presented below. The results for all layers of reinforcement are given in Table 8 for a length of reinforcement mats, L, of 11 ft.

C2.1. Tensile forces to be resisted by reinforcement

- Horizontal earth pressure at depth Z = 8.75 ft.
- Vertical load $R_V = \gamma ZL$ = (120)(8.75)(11) = 11,550 lb per foot of wall.
- Horizontal force $P_E = \gamma \frac{K_a}{2} H^2 = 120\ (0.333)\ \frac{(8.75)^2}{2} =$ 1,530 lb.
- Eccentricity $e = \frac{P_E(H/3)}{R_V} = \frac{1{,}530\ (8.75/3)}{11{,}550} = 0.386$ ft.
- $\sigma_{vb} = \frac{\gamma LZ}{L - 2e} = \frac{120\ (11)\ (8.75)}{(11 - 2(0.38))} = 1{,}128$ psf.
- $\sigma_h = K\sigma_{vb} = 0.358\ (1{,}128) = 404$ lb/ft^2.
- Horizontal force, FH, can be computed by multiplying σ_h by the facing area supported by each mat (10.83 ft^2).
- $FH = 404 \times 10.83 = 4{,}376$ lb.

C2.2. Tensile stress in longitudinal bars

- W11 or W20 bars are typically used as longitudinal members. These have the following dimensions and stress parameters:
  - W11, diameter 0.375 in.; cross-sectional area = 0.110 in^2.
  - W20, diameter 0.500 in.; cross-sectional area = 0.196 in^2.
  - Yield stress = 65 ksi.
  - Allowable stress = 35.75 ksi.

Table 8. Design summary—VSL Retained Earth wall (height = 15 ft, level backfill, no surcharge, reinforcement length = 11 ft).

Reinforcement Layer No.	z (ft)	e (ft)	σ_{vb} (psf)	K	σ_h (psf)	FH (lbs)	Bar Size	Tensile Stress in Bar (psi)	F.S. Rupture	N	A_c	P (lbs)	F.S. Pullout
1	1.25	0.01	150	.42	63	678	4w11	1541	23.2	4	38.4	1080	1.59
2	3.75	0.07	456	.40	181	1960	4w11	4455	8.0	4	35.3	2978	1.52
3	6.25	0.20	778	.38	294	3183	4w11	7234	4.9	4	32.2	4528	1.42
4	8.75	0.38	1128	.36	404	4376	4w11	9944	3.6	4	29.1	5729	1.31
5	11.25	0.63	1526	.34	517	5601	4w11	12730	2.8	5	25.9	8195	1.46
6	13.75	0.95	1993	.32	638	6905	4w11	15694	2.3	6	22.8	10580	1.53

- Assume W11 bars are used as longitudinal reinforcement members and 4 bars are used per mesh.
- $F_T = \frac{FH}{4A_{CR}} = \frac{4{,}376 \text{ lb}}{4(0.11) \text{ in.}^2} = 9{,}945$ psi. $F.S._{rupture} = \frac{F_a}{F_T} = 35{,}750/9{,}945 = 3.6$, which is adequate.

C2.3. Tensile stress at connection

VSL Retained Earth does not have a reduced cross-sectional area of reinforcement at the facing panel. Thus, the tensile stress check computations of Section C2.2 are adequate for design.

C2.4. Pullout of reinforcement

- As described in Appendix B, Chapter Four, the pullout resistance of a mat is computed from $P = A_c \gamma Z d b N$, where A_c = anchorage factor (an empirically derived factor) from Diagram 6; Z = depth to reinforcement; d = diameter of reinforcement bars; b = width of reinforcement mesh (as discussed in Appendix B, Chapter Four, the longitudinal bars are 6 in. apart and thus, b would be 1.5 ft); and N = number of transverse bars behind assumed failure surface. Assuming a bar spacing of 2.0 ft, this number can be computed as $N = \frac{(L - 0.3H)}{2.0}$ (rounded to the next highest integer) for $Z < \frac{H}{2}$; $N = \frac{(L - (H - Z) \tan (45 - \phi/2)}{2.0}$ (rounded to the next highest integer) for $Z \geq \frac{H}{2}$.
- Since $Z = 8.75$ which is $> \frac{H}{2} = 7.5$, $N = \frac{[11 - (15 - 8.75) \tan (27.5)]}{2.0} \dashrightarrow 4 = 4$.
- A_c at $Z = 8.75$ ft, as shown on Diagram 6, can be computed as $A_c = 40 - \left(\frac{40 - 15}{20}\right)(8.75) = 29.1$.
- Thus pullout resistance for the mat at 8.75 ft depth can be computed as $P = A_c \gamma Z d b N$. $P = (29.1)(120)(8.75)\frac{(0.375)}{12}(1.5)(4) = 5{,}729$ lb.
- $F.S._{pullout} = (P/FH) = (5{,}729/4{,}376) = 1.31$. This is somewhat less than the desirable factor of safety of 1.5 against pullout. Values at other levels, Table 8, are somewhat higher, and the design is probably safe. Pullout safety factor can be increased at any level by incorporation of additional transverse bars (increased N) or by adding a longitudinal bar to increase the width of the mesh, b.

C2.5. Corrosion

- The same corrosion rates as in the Reinforced Earth example (section under "C1.5. Corrosion") are used. As shown in this example, a zinc coating of 87 μm thickness would have a service life of 39.5 years. The remaining cross-sectional area of steel after 100 years of service can be computed as follows.
- $d_{100 \text{ yrs}} = 9{,}525$ μm − [9 μm/yr (2) (100 − 39.5) yrs)] = 8,436 μm = 0.332 in.
- $A_{CR} = \pi (d^2/4) = 0.0865$ in^2.
- The reinforcement in layer 6 must resist the largest tensile force. Stress in steel with reduced cross-sectional area for layer 6 (depth of 13.75 ft) is: $F_{T\,100 \text{ yrs}} = \frac{6{,}905 \text{ lb}}{4 \times 0.0865 \text{ in}^2.} =$ 19,957 psi < 35,750 psi, which is O.K.

C3. Grid Reinforcement—Welded Wire Wall

- The design conditions are shown on Diagram 1. Using standard spacings, the vertical spacing between reinforcements would be 1.5 ft. Two feet of fill are typically used above the top reinforcement. This makes the design height of the wall

15.5 ft. The design cross section is shown in Diagram 7.

- The calculations required for the analysis of layer 6 at a depth of 9.5 ft below the top of the wall are presented below. The results for all layers of reinforcement are summarized in Table 9 for a reinforcement length of 11 ft.

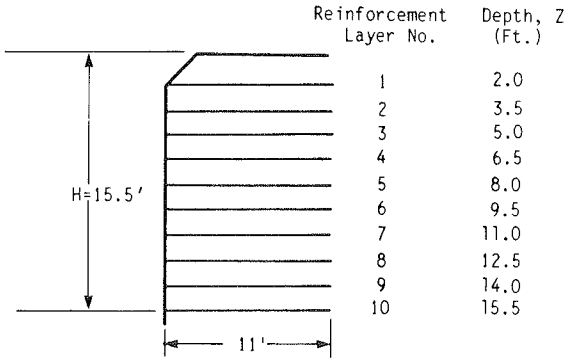

Diagram 7

C3.1. Tensile forces to be resisted by reinforcement

- Horizontal earth pressure at depth $Z = 9.5$ ft can be computed as: $\sigma_h = K \gamma Z$.
- Welded Wire design is currently based on the assumption that K is 0.65. Although this may be changed in the near future (see Appendix B, Chapter One), the 0.65 value is used for this example. Thus, $\sigma_h = 0.65\ (120)\ 9.5 = 741$ lb/ft^2.
- The horizontal force acting on each longitudinal wire of continuous reinforcement can be computed based on the spacings between wires in the standard meshes. These are 2 in. and 6 in., respectively, between longitudinal and transverse wires.
- $FH = (741)(2/12)(1.5\text{ ft}) = 185.3$ lb.

C3.2. Tensile stress in reinforcement

- With the force acting on each longitudinal wire known, the tensile stress developed can be computed. It is necessary to assume a nominal wire size. Meshes frequently used include:
  - W1.7; 0.148-in. diameter; 0.0172-in.^{2} area
  - W2.5; 0.178-in. diameter; 0.0249-in.^{2} area
  - W3.4; 0.207-in. diameter; 0.0337-in.^{2} area
- Try W1.7 wire and compute tensile stress: $F_T = \dfrac{FH}{A_{CR}} = \dfrac{185.3}{0.0172} = 10{,}773$ psi.
- With an allowable tensile stress of 35,750 psi, the factor of safety against rupture can be computed as: $F.S._{rupture} = \dfrac{F_a}{F_T} = \dfrac{35{,}750}{10{,}773} = 3.32$.

C3.3. Tensile stress at connection

- In the case of welded wire walls, there is not a reduced reinforcement area at the wall face. Hence, this computation is not applicable.

Table 9. Design summary—Welded Wire Wall (height = 15 ft, level backfill, no surcharge, reinforcement length = 11 ft).

Reinforcement Layer No.	Depth z (ft)	σ_h (psf)	FH (lbs)/wire	Wire Size	Stress in Longitudinal Wire (psi)	FH/ft of wall (lbs/lf)	M	L_e (ft)	N	P (lbs/lf)	F.S. Pullout	F.S. Rupture
1	2.0	156	39.0	w 1.7	2267	234	6	4.0	8	941	4.0	15.8
2	3.5	273	68.3	w 1.7	3971	410	6	4.8	10	2053	5.0	9.0
3	5.0	390	97.5	w 1.7	5669	585	6	5.5	12	3509	6.0	6.3
4	6.5	507	126.8	w 1.7	7372	761	6	6.3	13	4764	6.2	4.8
5	8.0	624	156.0	w 1.7	9070	936	6	7.1	15	5824	6.2	3.9
6	9.5	741	185.3	w 1.7	10773	1112	6	7.9	16	6834	6.1	3.3
7	11.0	854	213.5	w 1.7	12413	1281	6	8.7	18	8261	6.5	2.8
8	12.5	975	243.8	w 1.7	14174	1463	6	9.4	19	9484	6.5	2.5
9	14.0	1092	273.0	w 1.7	15872	1638	6	10.2	21	11201	6.8	2.2
10	15.5	1209	302.3	w 1.7	17576	1814	6	11	23	13098	7.2	2.0

C3.4. Pullout of reinforcement

- As discussed in Section 3.3.3 of Appendix B, Chapter One, empirical equations have been developed to predict pullout resistance. For silty sand backfill, these equations are: $P = 2{,}143 + \sigma_v d\,[0.75\,\pi L_e M \tan\delta + 17.61\,N]$, for $N\,\sigma_v d > 113.6$; $P = \sigma_v d\,[0.75\,\pi L_e M \tan\delta + 36.47\,N]$, for $N\,\sigma_v d \leq 113.6$. The symbols are defined as: σ_v = vertical stress; d = wire diameter, in feet; L_e = embedment length of reinforcement behind potential failure surface; M = number of longitudinal wires; δ = friction angle between soil and reinforcement; and N = number of transverse bars behind potential failure surface.
- Assume δ is equal to $\tan^{-1}(2/3 \tan\phi)$, which yields 25°. (The expression δ is equal to $2\phi/3$ is also sometimes used. Either is satisfactory.)
- Compute the number of transverse wires in the resistant zone. The potential failure surface dividing the active and resistant zones is assumed inclined at $45 + \phi/2$ to the horizontal and passes through the toe of the wall. Thus, the length of reinforcement in the resistant zone is: $L_e = L - (H - Z)\tan(45 - \phi/2) = 11 - (15.5 - 9.5)\tan 27.5° = 7.88$ ft.
- With a 6-in. spacing between transverse wires, the number of transverse wires in the resistant zone is: $N = (7.88/0.5)$ --> 16 for a transverse wire spacing of 6 in.
- Determine P per linear foot of wall. Compute $M = (12/2) = 6$. Compute $N\,\sigma_v d = 16(120)(9.5)\,(0.148/12) = 225 > 113.6$.
- Thus, $P = 2{,}143 + (120)(9.5)\,(0.148/12)\,[\pi\ 0.75\ (7.88)(6)\,(\tan 25°) + (17.61)(16)] = 6{,}834$ lb/linear ft.
- Compute the factor of safety by dividing the pullout resistance per linear foot by the force acting on the reinforcements per linear foot (M times FH): $F.S._{pullout} = P/(M(FH)) = 6{,}834/(6(185.3)) \approx 6.1$.

Table 10. Safety factors for determining characteristic strength of geogrids in service. (Source: Ref. 25)

Basic Soil Type	Particle Size (mm)	Suggested partial factors of safety m
BOULDERS	200	Limited to 75 mm max. size. Sand carpet or alternative protection to be used with this type of fill material.
COBBLES	75 60	
GRAVELS	coarse 20	1.5-1.6
	medium 6	1.3-1.5
	fine 2	1.25-1.4
SANDS	coarse 0.6	
	medium 0.2	1.1-1.25
	fine 0.06	
SILTS	coarse 0.02	Not normally used in construction
	medium 0.006	
	fine 0.002	
CLAYS		1.1-1.3
Pulverized Fuel Ash		1.1-1.25

C3.5. Corrosion

- Assume a 100-year service life and a nonsaturated backfill.
- Zinc coating on wire mesh, as discussed in Section 4.3 of Appendix B, Chapter One, is 0.4 oz/sf, which is equivalent to an 0.685-mil thick coating. As discussed in Appendix B, the zinc coating is assumed to be lost at a rate of 0.24 mil per year for the first 2 years and 0.08 mil per year thereafter until it is depleted. Thus, time until loss of zinc is complete, t, is given by $2(0.24) + (t - 2)(0.08) = 0.685$; $t = 4.6$ years.
- Steel loss is at a rate of 0.36 mil per year for $(100 - 4.6)$ years for a total loss of 34.3 mils.
- The final wire diameter is $[0.148 - 2(.0343)] = 0.0794$ in. Remaining area = 0.00495 in^2.
- The reinforcement in layer 10 must withstand the highest tensile force (Table 9). The tensile stress at the end of the design life can be computed as $F_T = \dfrac{FH}{A_{CR}} = \dfrac{302.3\text{ lb}}{0.00495\text{ in}^2.} =$ 61,070 psi.
- At the end of the service life of the structure, the tensile stress in the reinforcement should not exceed the yield strength of the steel, which is 65,000 psi. A factor of safety of 1.0 is used for this part of the design. Thus, the resistance to corrosion is satisfactory. The results in Table 9 indicate an unnecessarily high factor of safety against pullout. A more economical design could be achieved by reducing the reinforcement mesh length.

C4. Grid Reinforcement—Geogrid-Reinforced Wall

- Design procedures for geogrid-reinforced walls are described in detail in Appendix B, Chapter Three and are not repeated here. The design example shown below is based on the conditions shown in Diagram 1. A tieback wedge analysis is used.
- The characteristic strength of SR2 grids for a design life of 100 years is 29 kN/m $\approx$ 2,000 lb/ft (see Sec. 4.4.3, Appendix B, Chapter Three). A partial safety factor of 1.25 (Table 10) for medium-to-fine sands is used to determine: Characteristic strength in service $= \dfrac{\text{Characteristic strength}}{F.S.}$. This partial factor of safety is applied to account for the effects of different soil types on the grid strength.
- The in-service characteristic strength is divided by an appropriate $F.S.$ to yield a safety design value as follows: Safe design strength $= \dfrac{\text{Characteristic strength in service}}{\text{Factor of safety}}$.
- The foregoing two equations yield: Characteristic strength in service $= \dfrac{2{,}000}{1.25} = 1{,}600$ lb/ft. Safe design strength =

$$\frac{1{,}600}{1.35} = 1{,}185 \text{ lb/ft}$$

C4.1. Vertical spacing between geogrids

- The vertical spacing between geogrids must be determined. The horizontal stress, σ_h, at any depth below the top of the wall is given by $\sigma_h = K_a \sigma_{vb}$.
- The vertical bearing stress acting on the reduced bearing width is computed exactly as shown for Reinforced Earth in Section C1.1. Computed values for Reinforced Earth are given in Table 11 (the σ_{vb} values are reproduced from Table 7). The horizontal stresses given in Table 11 are computed by multiplying with a K_a value of 0.271 (see Diagram 1) corresponding to the friction angle of 35 deg for the soil in the reinforced zone.
- The maximum vertical spacing, S_v, between reinforcement layers is determined by $S_v = \dfrac{\text{Safe design strength}}{\sigma_h}$.
- The calculated values of S_v are also given in Table 11. These indicate that a spacing of 3 ft can be used to a depth of about 9 ft, with a reduced spacing of 2 ft thereafter. The resultant design cross section is shown on Diagram 8.

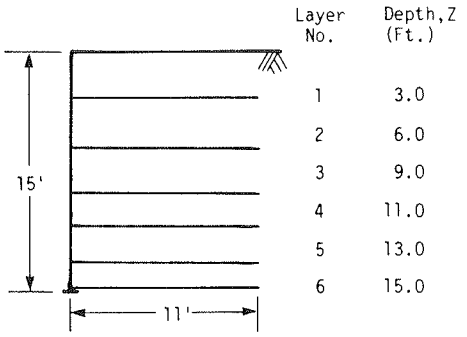

Diagram 8

C4.2 Rupture of reinforcement

- The tension in each reinforcement layer must be checked. Calculations to assure internal stability against rupture and pullout are presented for layer 3 at a depth of 9 ft below the top of the wall, with the results for the remaining reinforcement layers being summarized in Table 12.
- The tensile force, *FH*, per linear foot of wall in the grid, at any depth *Z*, can be calculated as: $F_H = K_a \sigma_{vb} S_v$.
- Thus, at a depth of 9 ft $\sigma_{vb} = \dfrac{\gamma L Z_b}{L - 2e}$, in which $e = \dfrac{P_E(H/3)}{R_V} = \dfrac{\gamma K_a \frac{Z^2}{2}\frac{Z}{3}}{\gamma Z L} = \dfrac{k_a Z^2}{6L} = \dfrac{(0.333)(9)^2}{(6)(11)} = 0.41$ ft. Thus, $\sigma_{vb} = \dfrac{120(11)(9)}{11 - 2(0.41)} = 1{,}167$ lb/ft^2. $FH = K_a \sigma_{vb} S_v = 0.271\ (1{,}167)\left(\dfrac{3+2}{2}\right) = 791$ lb/linear ft (vertical spacing, S_v, has been determined by taking the spacing dimensions between the layers directly above and below the one under consideration and dividing by 2 for an average spacing).

Table 11. Maximum vertical spacing of geogrids.

Depth (ft)	σ_{vb} (lb/ft^2)	σ_h (lb/ft^2)	S_v (ft)
1.25	150	41	28.9
3.75	456	124	9.6
6.25	778	211	5.6
8.75	1129	306	3.9
11.25	1526	414	2.9
13.75	1993	540	2.2

- The factor of safety against rupture can then be computed as: $F.S._{rupture} = \dfrac{\text{Safe design strength}}{FH} = \dfrac{1{,}185 \text{ lb/linear ft}}{791 \text{ lb/linear ft}} = 1.5$.

C4.3. Pullout of the Reinforcement

- The general equation for pullout resistance (Eq. 24) for a grid is $P_t = \gamma Z(A_s \mu^* + N_p\, n\, A_b)$, where: A_s is the surface area of the grid in frictional contact with the backfill in the resistant zone; A_b is the bearing area of each transverse member in the resistant zone; n is the number of transverse members in the resistant zone; N_p is a bearing capacity coefficient, or the ratio of ultimate bearing pressure, σ_b, to vertical stress, σ_v; and μ^* is the apparent friction coefficient.
- By defining the following symbols (see Appendix B, Chapter Three, Sec. 3.1.3), the foregoing equation can be rewritten, as shown, and is referred to as the Jewell's method. Accordingly, α_s = fraction of grid that is solid, α_b = fraction of grid which has a bearing surface, σ_b = horizontal stress on transverse member, σ_v = vertical stress, b = width of mat, t = thickness of transverse member, S_x = spacing between transverse members, and δ = friction angle between soil and polymer = $2\phi/3$. Then, $P_t = \gamma Z\left[2\ \alpha_s L_e\ b \tan\delta + \dfrac{\sigma_b}{\sigma_v}\dfrac{L_e}{S_x}\alpha_b - b\right]$, which simplifies to $P_t = L_e b \gamma Z\left[2\alpha_s \tan\delta + \dfrac{\sigma_b}{\sigma_v}\dfrac{t}{S_x}\alpha_b\right]$.
- Geogrid design is based on the assumption of a Rankine failure surface. Thus, $L_e = [L - (H - Z)\tan(45 - \phi/2)]$.

Table 12. Design summary—geogrid wall (height = 15 ft, level backfill, no surcharge, reinforcement length = 11 ft).

Reinforcement Layer No.	z_t (ft)	e (ft)	σ_{vb} lb/ft^2	FH lb/LF	F.S. Rupture	L_e ft	P* lb/lf	F.S. Pullout	P** lb/lf	F.S. Pullout
1	3.0	0.05	363	443	2.7	4.7	1531	3.5	2133	4.8
2	6.0	0.18	745	605	1.9	6.3	4069	6.7	5717	9.5
3	9.0	0.41	1167	791	1.5	7.9	7630	9.6	10754	13.6
4	11.0	0.61	1485	805	1.5	8.9	10534	13.1	14807	18.4
5	13.0	0.85	1847	1000	1.2	10.0	13902	13.9	19662	19.7
6	15.0	1.14	2269	615	1.9	11.0	17718	28.8	24955	40.6

*Determined with Jewell Method.
**Determined with Tensar Method.

- For SR-2 Geogrid (see Appendix B, Chapter Three), α_s = 0.46; α_b = 0.9 (assumed); t = 4.1 mm = 0.161 in.; and S_x = 111 mm = 4.37 in.
- The bearing ratio coefficient σ_b/σ_v, can be approximated from Figure 39 or Table 4 as: $\sigma_b/\sigma_v = 15$.
- For the case under consideration (Z = 9 ft), $L_e = 11 - (15 - 9) \tan 27.5° = 7.9$ ft.
- $P_t = L_e b \gamma Z \left[2\alpha_s \tan \delta + \frac{\sigma_b t}{\sigma_v S_x} \alpha_b\right]$.
- $P_t = 7.9\ (1)(120)(9) \left[2\ (0.46) \tan (2\phi/3) + 15 \left(\frac{0.161}{4.37}\right) 0.9\right]$ (b is set equal to 1 to provide a measurement per linear foot of wall) = 7,630 lb/linear ft.
- The pullout capacity for geogrids has also been approximated (Tensar Brochure) by the following equation: $P = L_e 2\alpha_b (\tan \phi)\gamma Z$, where α_b is the coefficient of soil reinforcement interaction is assumed to be 0.9, and P_t = 7.9 (2)(0.9) tan 35° (120)(9) = 10,754 lb/linear ft.
- The above results, together with those for reinforcements at other depths, are given in Table 12. As indicated in this table, the reinforcement subjected to the highest stress is at a depth of 13.0 ft, with a horizontal force of 1,000 lb/ft. Data presented in Appendix B, Chapter Three (Fig. B-70) indicate that this force could result in creep strain of the reinforcement, after 120 years at 20°C, of about 5 percent. As discussed in Section 3.2 of Appendix B, Chapter Three, this should be acceptable from a performance viewpoint, but deformation serviceability requirements could result in a design change.
- The data in Table 12 indicate that the safety factors against pullout are, in general, excessive. A more economic design could be obtained by shortening the grids.

C5. Sheet Reinforcement—Geotextiles

- As discussed in Appendix A, Chapter Two, there is currently more than one design method for geotextile-reinforced soil structures. The example below follows the U.S. Forest Service method. Design conditions are shown on Diagram 1.
- The geotextile used for design is assumed to be Fibretex 300, which has an ultimate tensile strength, T_u, of 2,520 lb/ft. To obtain an allowable long-term tensile stress value, T_u has to be divided by 3, i.e., $T_a = T_u/3$, which yields 840 lb/ft.

C5.1. Vertical spacing

- The vertical spacing between fabric layers is determined as follows: $S = \frac{T_a}{\sigma_{hc}\ F.S.}$, where T_a = allowable long-term sension in fabric ($T_u/3$); σ_{hc} = lateral pressure in middle of the layer; and F.S. = factor of safety ($F.S.$ = 1.5).
- Check vertical spacing at bottom of the wall.
- $\sigma_{hc} = K_o \gamma Z$. Assume 1-ft spacing between layers and that stress acting on lower layer is an average stress for the lowest step increment ($K_o = 1 - \sin \phi$). $Z = 15 - 1/2 = 14.5$ ft; σ_{hc} = (1 − sin 35°)(120)(14.5) = 742 psf. Hence, vertical spacing = $S_v = \frac{(2{,}520/3)}{(742)(1.5)} = 0.75$ ft.
- The vertical spacing of the geotextile reinforcement can be varied with the wall height. This may be particularly economical for high walls or walls that have a large wall face area. In this example, it is assumed that a constant vertical spacing of 0.75 ft will be used in the lower section of wall and 1.5 ft in the upper section of wall. The computation below indicates that a spacing of 1.5 ft would be satisfactory to a

depth of 7.5 ft. The resultant design cross section is shown on Diagram 9.

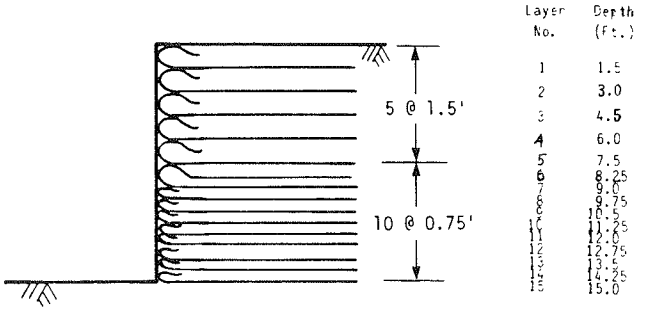

Geogrid Reinforced Wall Reinforcement Layout

Diagram 9

- At a depth of 7.5 ft, vertical spacing should be $S_v = \frac{(2{,}520/3)}{(1 - \sin 35°)(120)(6.75)(1.5)} = 1.6$ ft. This value is near enough 1.5 that the 1.5-ft spacing can be considered satisfactory.

C5.2 Pullout of reinforcement

- The horizontal force per linear foot of wall acting on a reinforcement can be calculated from $FH = S_v K_o Z_m \gamma$, where S_v = vertical spacing and Z_m = depth to middle of layer.
- Calculations are presented below for reinforcement layer 5 at a depth of 7.5 ft below the top of the wall. The results for the remainder of the wall are presented in Table 13.
- At depth 7.5 ft, $FH = S_v K_o Z_m \gamma = 1.5\,(1 - \sin 35°)(6.75)120 = 518$ lb/linear ft.
- Pullout resistance can be computed with $P = L_e\, 2\, Z_b\, \gamma \tan 2\phi/3$, where Z_b is the depth to the bottom of the layer under consideration.
- The design method assumes a Rankine failure plane between the active and the resistant zones. Thus, $L_e = L - [\tan (45 - \phi/2)(H - Z_b)] = 11 - [\tan (27.5°)(15 - 7.5)] = 7.1$ ft; and $P = (7.1)(2)(7.5)(120) \tan 23.3° = 5{,}504$ lb/linear ft.
- The factor of safety against pullout can be computed as $F.S._{pullout} = \frac{P}{FH} = \frac{5{,}504}{518} = 10.6$.
- As in the case of the geogrid and welded wire walls, the safety factor against pullout resistance is excessive when an 11-ft reinforcement length is used, while the safety factor against rupture is reasonable. Thus, a safe wall could be designed and constructed using shorter fabric layers.

C5.3. Wraparound length

- As shown by Eq. A-17 (Appendix A, Chapter Two), the length of wrapped fabric embedment is computed as $L_o = \frac{\sigma_{hc} S_v (F.S.)}{2 Z_f \gamma \tan (2\phi/3)}$, where Z_f is the depth to top of layer (i.e., depth to where wraparound extends into reinforced soil).
- For the layer at 7.5-ft depth, σ_{hc} is computed at 6.75-ft depth [$\sigma_{hc} = (1 - \sin 35)(120)(6.75) = 345.4$ psf], and the depth to the wraparound, Z_f, is 6.0 ft (see Diagram 9). Thus, $L_o = \frac{345.4\,(1.5)1.5}{2(6.0)120 \tan 23.3°} = 1.25$ ft. It is recommended that a value of 3 ft be used when the computed value is lower.

DESIGN EXAMPLE II—HIGH WALL WITH HORIZONTAL BACKFILL

A. Given Conditions

The given conditions for the second design example are shown on Diagram 10. Note that conditions are identical to those for Design Example I, except that wall height has increased to 35 feet. It is assumed that the reader has studied the first design example prior to examining the examples shown in this section.

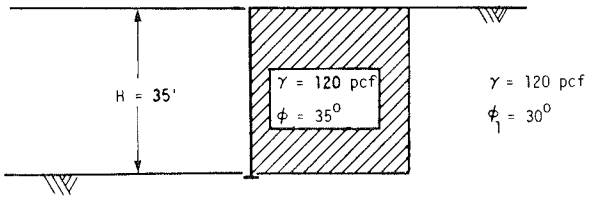

Service Life	100 years
Chlorides	<200 ppm
Sulfates	<1000 ppm
Resistivity	>3000 /cm
pH	7.5

Diagram 10

B. External Stability

As noted previously under Design Example I, the external stability computations follow the procedures presented earlier in this chapter under the heading "External Stability Evaluation." The forces to be taken into account in the computations for this case are shown on Diagram 11. These are identical in nature, but not in magnitude, to those shown for the 15-ft high wall in Diagram 2.

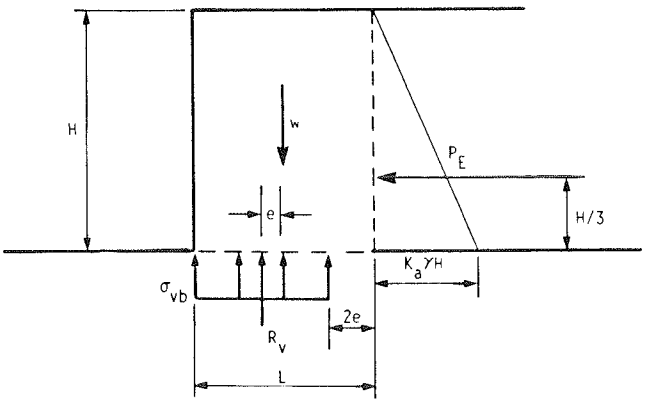

Diagram 11

Table 13. Design summary—geotextile reinforced wall (height = 15 ft, level backfill, no surcharge, reinforcement length = 11 ft).

Reinforcement Layer No.	Depth to Bottom of Layer Z_b (ft)	Depth to Middle of Layer Z_m (ft)	FH (lb/lf)	L_e (ft)	P (lb/lf)	F.S. Pullout	F.S. Rupture
1	1.50	0.75	58	4.0	621	10.7	14.7
2	3.00	2.25	173	4.7	1457	8.4	4.9
3	4.50	3.75	288	5.5	2558	8.9	2.9
4	6.00	5.25	403	6.3	3907	9.7	2.1
5	7.50	6.75	518	7.1	5504	10.6	1.6
6	8.25	7.88	302	7.5	6395	21.2	2.8
7	9.00	8.63	331	7.9	7349	22.2	2.5
8	9.75	9.38	360	8.3	8364	23.2	2.3
9	10.50	10.12	388	8.7	9441	24.3	2.2
10	11.25	10.88	418	9.0	10465	25.0	2.0
11	12.00	11.63	446	9.4	11659	26.1	1.9
12	12.75	12.38	475	9.8	12914	27.2	1.8
13	13.50	13.13	504	10.2	14232	28.2	1.7
14	14.25	13.88	533	10.6	15612	29.3	1.6
15	15.00	14.63	561	11.0	17054	30.4	1.5

B1. Computations to Assure Safety

B1.1. Sliding on base

- As shown under Design Example I, Section B, the minimum wall width to yield a given factor of safety against sliding can be computed as $L = \dfrac{R_a\, H\ (F.S.)}{2 \tan \phi_1}$.
- For a friction angle of 30 deg under the structure, the required length for a factor of safety of 1.5 is 15.2 ft.

B1.2. Overturning about toe

- The minimum length of reinforcement (or width of wall) to yield a given factor of safety can be computed as $L^2 = \dfrac{F.S.\ K_a\, H^2}{3}$ or $L = \sqrt{\dfrac{F.S.\ K_a\, H^2}{3}}$.
- *The above equation yields* $L = 16.5$ ft for a factor of safety of 2.

B1.3. Bearing capacity failure

- Compute eccentricity for an assumed reinforcement length of 17 ft: $e = \dfrac{K_a\, H^2}{6L} = 4$ ft.
- This exceeds $L/6$., i.e., the reaction is outside the middle third. Try a length of 21 ft, which yields 3.24, a value less than $L/6$.
- Bearing pressure on reduced area is: $\sigma_{vb} = \dfrac{W}{L - 2_e} = \dfrac{(120)(21)(35)}{21 - 2(3.24)} = 6{,}074$ psi.
- To yield a factor of safety of 2.0, an ultimate bearing capacity of about 12,000 psf would thus be required of the foundation soil.

C. Internal Stability

C1. Strip Reinforcement System—Reinforced Earth

- Assuming that standard facing panels are used, the vertical spacing between reinforcements and the reinforcement layer numbering are shown on Diagram 12.
- The variation of earth pressure coefficient with depth and the variation of apparent coefficient of soil to reinforcement friction with depth are as shown on Diagram 4.
- Calculations for the internal stability of each layer are made in the same way as for the preceding design example. The results are shown in Table 14. The tensile stress in the reinforcements will increase to a maximum of 28,500 psi at the connections by the end of the 100-year design life as a result of corrosion.

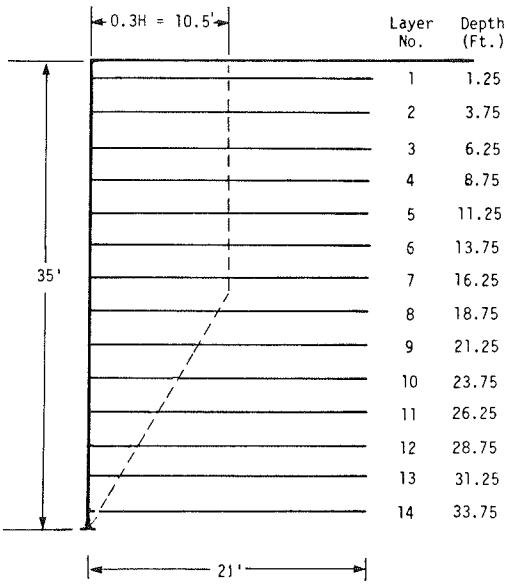

Diagram 12

Table 14. Design summary—Reinforced Earth wall (height = 35 ft, level backfill, no surcharge, reinforcement length = 21 ft).

Reinforcement Layer No.	Depth (ft)	e (ft)	σ_{vb} (psf)	K	σ_h (psf)	FH (lbs)	Strip Size mm	Tensile Stress in Strip (psi)	Tensile Stress in Strip at Connection (psi)	F.S. Rupture	μ^*	L_e (ft)	P (lbs)	F.S. Pullout
1	1.25	0.01	150	0.417	63	379	60 x 5	814	909	43.9	1.45	10.5	899	2.37
2	3.75	0.04	452	0.397	179	1085	60 x 5	2333	2605	15.3	1.35	10.5	2511	2.31
3	6.25	0.10	757	0.378	286	1732	60 x 5	3725	4159	9.6	1.25	10.5	3874	2.24
4	8.75	0.20	1070	0.358	383	2318	60 x 5	4986	5567	7.2	1.15	10.5	4990	2.15
5	11.25	0.33	1394	0.339	473	2859	60 x 5	6148	6865	5.8	1.05	10.5	5858	2.05
6	13.75	0.50	1733	0.320	554	3352	60 x 5	7210	8050	5.0	0.95	10.5	6478	1.93
7	16.25	0.70	2089	0.300	626	3789	60 x 5	8148	9097	4.4	0.85	10.5	6850	1.81
8	18.75	0.93	2469	0.281	693	4193	60 x 5	9017	10067	4.0	0.75	10.5	6974	1.66
9	21.25	1.19	2876	0.271	779	4711	60 x 5	10132	11313	3.5	0.70	13.8	9677	2.05
10	23.75	1.49	3321	0.271	900	5445	60 x 5	11710	13065	3.1	0.70	15.1	11891	2.19
11	26.25	1.82	3810	0.271	1033	6250	60 x 5	13441	14996	2.7	0.70	16.4	14233	2.28
12	28.75	2.18	4354	0.271	1180	7139	60 x 5	15353	17129	2.3	0.70	17.7	16825	2.36
13	31.25	2.58	4972	0.271	1347	8149	60 x 5	17525	19553	2.0	0.70	19.0	19631	2.42
14	33.75	3.01	5678	0.271	1539	9311	60 x 5	20024	22341	1.8	0.70	20.3	22652	2.43

Horizontal Strip Spacing = 40 in.

C2. Grid (Bar Mat) Reinforcement—VSL Reinforced Earth

- The vertical spacings between reinforcement layers are the same as for the Reinforced Earth design (Diagram 12). The assumed variations in lateral earth pressure coefficient and anchorage factor with depth are the same as shown for the 15-ft high wall on Diagram 6. Calculations for the internal stability of each layer in terms of tensile stress in the reinforcements and reinforcement pullout are made in the same manner as for the 15-ft high wall. The results are presented in Table 15. The corrosion analysis leads to a factor of safety, relative to the 65,000-psi yield stress, of 1.68 at the end of a 100-year period.

C3. Grid Reinforcement—Welded Wire Wall

- Assuming the standard 1.5-ft vertical spacing, the numbering and depth to each of the reinforcement layers would be as shown on Diagram 13.

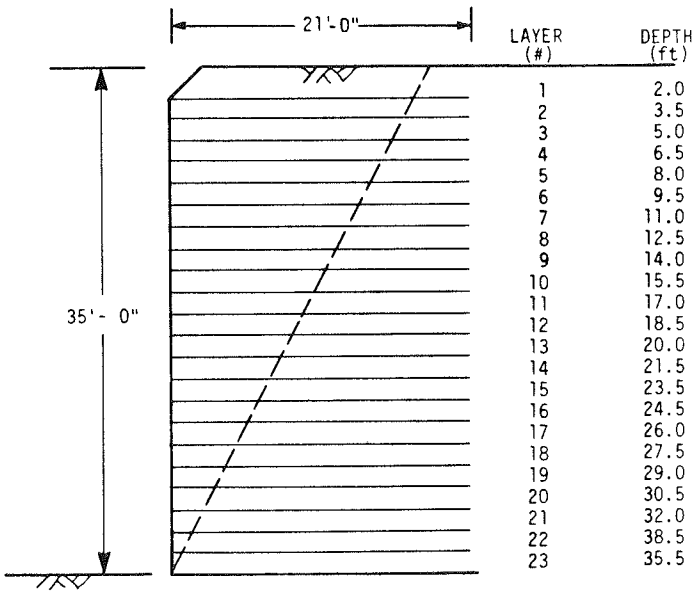

Diagram 13

Table 15. Design summary—VSL Retained Earth wall (height = 35 ft, level backfill, no surcharge, reinforcement length = 21 ft).

Reinforcement Layer No.	Depth (ft)	e (ft)	σ_{vb} (psf)	K	σ_h (psf)	FH (lbs)	Bar Size	# of Longitudinal Bars	Tensile Stress in Bars psi	F.S. Rupture	N	A_c	P (lbs)	F.S. Pullout
1	1.25	0.01	150	0.417	63	678	w 11	5	1232	29.0	6	38.4	2160	3.19
2	3.75	0.04	451	0.397	179	1942	w 11	5	3530	10.1	6	35.3	5957	3.07
3	6.25	0.10	757	0.378	286	3100	w 11	5	5637	6.34	6	32.2	9056	2.92
4	8.75	0.20	1070	0.358	383	4150	w 11	5	7545	4.74	6	29.1	11458	2.76
5	11.25	0.33	1394	0.339	473	5118	w 11	5	9305	3.84	6	25.9	13112	2.56
6	13.75	0.50	1733	0.320	554	6000	w 11	5	10910	3.28	6	22.8	14108	2.35
7	16.25	0.70	2089	0.300	626	6782	w 11	5	12330	2.90	6	19.7	14406	2.12
8	18.75	0.93	2469	0.281	693	7505	w 11	5	13645	2.62	6	16.6	14006	1.87
9	21.25	1.19	2876	0.271	779	8436	w 11	5	15338	2.33	7	15.0	16745	1.98
10	23.75	1.49	3321	0.271	900	9747	w 11	5	17722	2.02	8	15.0	21375	2.20
11	26.23	1.82	3810	0.271	1033	11165	w 11	5	20300	1.76	9	15.0	26578	2.38
12	28.75	2.18	4354	0.271	1180	12779	w 11	5	23235	1.54	9	15.0	29109	2.28
13	31.25	2.58	4972	0.271	1347	14588	w 11	5	26524	1.35	10	15.0	35156	2.41
14	33.75	3.01	5678	0.271	1539	16667	w 11	5	30304	1.18	11	15.0	41766	2.51

Longitudinal bar spacing = 6 in.
Width of reinforcement mesh = 2 ft.

Table 16. Design summary—Welded Wire Wall (height = 35 ft, level backfill, no surcharge, reinforcement length = 21 ft).

Reinforcement Layer No.	Depth (ft.)	σ_h (psf)	FH (lbs)	Wire Size	Stress in Longitudinal Wire (psi)	FH/ft of wall lb/lf	M	L_e (ft)	M	P (lb/lf)	F.S. Pullout	F.S. Rupture
1	2.0	156	39	W1.7	2267	234	6	3.8	8	938	4.0	15.8
2	3.5	273	68	W1.7	3971	410	6	4.6	10	2046	5.0	9.0
3	5.0	390	98	W1.7	5669	585	6	5.4	11	3232	5.5	6.3
4	6.5	507	127	W1.7	7372	761	6	6.2	13	4738	6.2	4.8
5	8.0	624	156	W1.7	9070	936	6	6.9	14	5600	6.0	3.9
6	9.5	741	186	W1.7	10773	1112	6	7.7	16	6818	6.1	3.3
7	11.0	854	215	W1.7	12413	1281	6	8.5	18	8216	6.4	2.8
8	12.5	975	244	W1.7	14174	1463	6	9.8	19	9528	6.5	2.5
9	14.0	1092	273	W1.7	15872	1638	6	10.1	21	11185	6.8	2.2
10	15.5	1209	303	W1.7	17576	1814	6	10.3	22	12588	6.9	2.0
11	17.0	1326	332	W1.7	19302	1989	6	11.6	24	14700	7.4	1.8
12	18.5	1443	362	W1.7	21047	2165	6	12.4	25	16435	7.6	1.7
13	20.0	1560	391	W1.7	22733	2340	6	13.2	27	18793	8.0	1.6
14	21.5	1677	419	W1.7	24375	2516	6	14.0	29	21330	8.5	1.5
15	23.0	1794	449	W2.5	18032	2691	6	14.7	30	27739	10.3	2.0
16	24.5	1911	478	W2.5	19197	2867	6	15.5	32	31174	10.9	1.9
17	26.0	2028	508	W2.5	20402	3042	6	16.3	33	34010	11.2	1.8
18	27.5	2145	537	W2.5	21566	3218	6	17.1	35	37831	11.7	1.7
19	29.0	2262	566	W2.5	22731	3393	6	17.9	36	40959	12.1	1.6
20	30.5	2379	596	W2.5	23936	3569	6	18.6	38	45129	12.6	1.5
21	32.0	2496	625	W2.5	25100	3744	6	19.4	39	48547	12.9	1.4
22	33.5	2613	655	W2.5	26305	3920	6	20.2	41	53137	13.5	1.4
23	35.0	2730	684	W2.5	27469	4095	6	21.0	43	57943	14.1	1.3

Note: Corrosion considerations (see text) require that the above design be modified so as to have W1.7 wire for reinforcement layers 1-10, W2.5 wire for layers 11-20, and W3.4 wire for layers 21-23.

- The calculations required for the analysis of each layer are done in the same manner as for the 15-ft high Welded Wire Wall design example. The results for all layers of reinforcement are shown in Table 16.
- The corrosion loss during a 100-year service life will be 34.3 mils (see Design Example I, Section C3). From Table 16 it may be seen that a W1.7 wire must resist a maximum tensile force of 419 lb (level 14). The wire diameter at the end of the service life will be [0.148 − 2(0.0343)] = 0.0794 in., giving an area of 0.00495 in^2. The tensile stress will be $F_T = \frac{419}{0.00495} = 84,646$ psi, which exceeds the yield stress of 65,000. Thus, a larger wire size must be used.
- The maximum load per wire to ensure that the tensile stress will be below yield at the end of the service life will be $FH = 65,000 \times 0.00495 = 322$ lb. From Table 16 it is seen that this load is reached below level 10 ($Z = 15.5$ ft).
- The next larger wire size is W2.5 with a diameter of 0.178 in. At the end of the 100-year design life its diameter will be [0.178 − 2(0.0343)] = 0.1094 in., giving an area of 0.00940 in^2. The maximum allowable load in this wire size at the end of the design life will be $FH = 65,000 \times 0.00940 = 611$ lb. This load is exceeded for reinforcement layers below layer 20 ($Z = 30.5$ ft). Thus, W3.4 wire will be required for the lower three levels.

C4. Grid Reinforcement—Geogrid-Reinforced Wall

- The safe design strength of SR2 grids as determined for the low wall case in Design Example I is 1,185 lb/linear ft (see Design Example I, Section C4).
- As done for the 15-ft high-wall design example, the ratio of the safe design strength to the horizontal stress at any level is used to obtain the vertical grid spacings, which are shown on Diagram 14. The factors of safety against reinforcement rupture and grid pullout are computed in the same manner as for the 15 ft high wall example (Design Example I, Section C4). The results are presented in Table 17.
- The results in Table 17 show that the design is controlled by

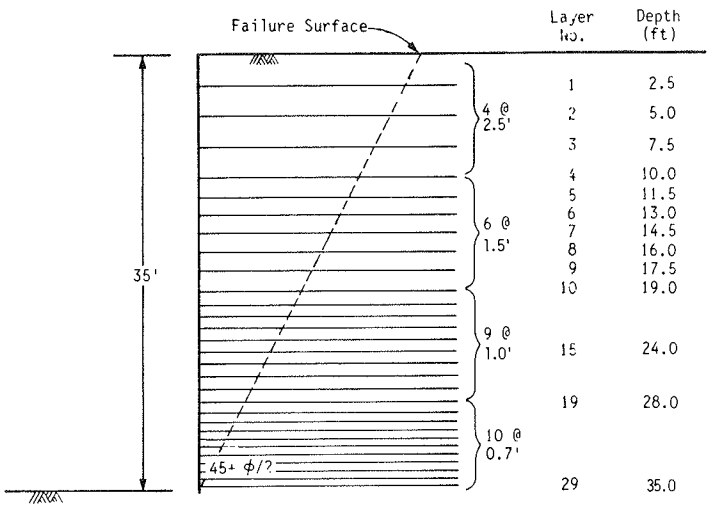

Diagram 14

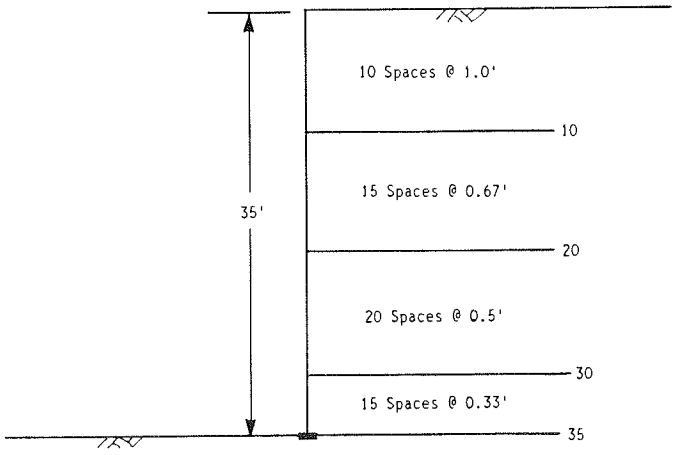

Diagram 15

the rupture strength of grids and by the length of reinforcements (21 ft) to ensure safety against sliding and bearing failure. The safety factor against pullout is very high on the basis of both the Tensar equation and Jewell's equation (see Design Example I, Section C4.3) for pullout resistance.

C5. Sheet Reinforcement—Geotextile-Reinforced Wall

- The example in this section follows the U.S. Forest Service Method. The geotextile used for this wall is assumed to be Fibretex-400 with an ultimate tensile strength, T_u, of 3,120 lb/linear ft.
- The vertical spacing, S_v, of the fabric layers is computed using $S_v = \dfrac{T_a}{\sigma_{hc}\,(F.S.)}$, where T_a = allowable long-term tension in fabric ($T_u/3$); σ_{hc} = lateral pressure in middle of the layer; $F.S.$ = factor of safety (usually 1.5); and $\sigma_{hc} = K_o\,\gamma\,Z$.
- Values of σ_{hc} and the required corresponding vertical spacings of geotextile reinforcement are given in Table 18 as a function of depth.
- It may be seen that the reinforcement layers would need to be spaced at 4 in. vertically for the bottom 5 ft and then at 6 in. for the next 10 ft. As shown on Diagram 15, this would require more than 30 layers of reinforcement for the bottom half of the wall alone, and 61 layers of reinforcement for the entire wall. It is not likely, therefore, that reinforcement of a 35-ft high wall could be justified using this geotextile either from an economic standpoint or because of the difficulty of such thin layer construction. Some of the newer geotextiles are reported to have tensile strengths in excess of 10,000 lb per foot. These materials could be used to construct a wall of the height considered in this example using more practical layer spacings. The design would proceed in the same manner as for the 15-ft high-wall design example.

DESIGN EXAMPLE III—LOW WALL WITH SLOPING BACKFILL

A. Given Conditions

As shown on Diagram 16, the conditions are the same as for Design Example I, except that the reinforced soil wall retains a sloping backfill with a slope of 2 horizontal to 1 vertical. It is assumed that the reader is familiar with the details presented in Design Example I.

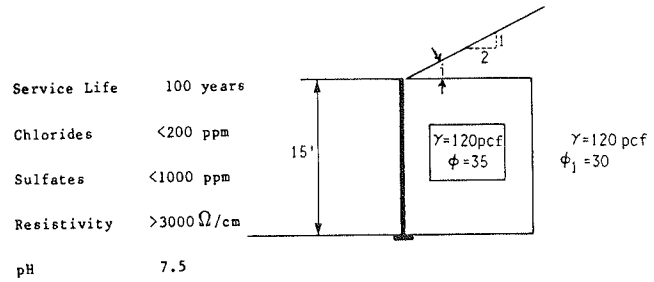

Diagram 16

B. External Stability

The forces that must be considered in design are shown on Diagram 17. By comparison with the forces for a level backfill (Diagram 2), it can be seen that force W_2 has been added. In this case the earth pressure coefficient, K_{aH}, is the horizontal component of the active earth pressure coefficient for a slope.

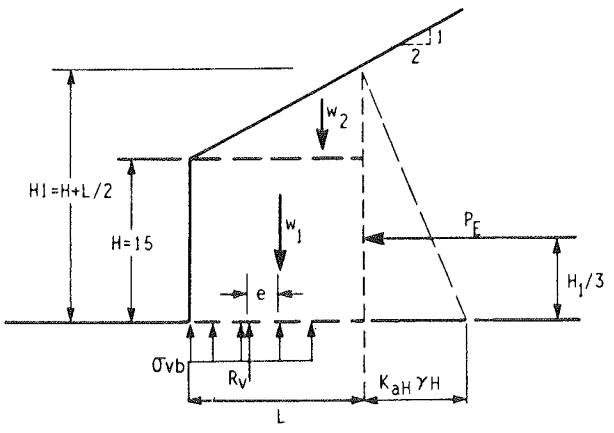

Diagram 17

Table 17. Design summary—geogrid wall (height = 35 ft, level backfill, no surcharge, reinforcement length = 21 ft).

Reinforcement Layer No.	Depth (ft)	e (ft)	σ_{vb} (psf)	FH (lb/lf)	F.S. Rupture	L_e (ft)	P* (lb/lf)	F.S. Pullout*	P† (lb/lf)	F.S. Pullout†
1	2.5	0.01	300	203	5.79	4.1	1010	5.4	1550	7.6
2	5.0	0.05	603	409	2.88	5.4	2897	7.1	4084	9.9
3	7.5	0.12	910	617	1.91	6.7	5392	8.7	7600	12.3
4	10.0	0.22	1225	664	1.77	8.0	8584	12.9	12099	18.2
5	11.5	0.28	1418	576	2.04	8.8	10859	18.9	15306	26.5
6	13.0	0.36	1616	657	1.79	9.5	13252	20.1	18679	28.4
7	14.5	0.45	1818	739	1.59	10.3	16026	21.7	22588	30.6
8	16.0	0.55	2026	824	1.43	11.1	19058	23.1	26861	32.6
9	17.5	0.66	2241	911	1.29	11.9	22346	24.5	31497	34.6
10	19.0	0.78	2462	834	1.41	12.7	25893	31.0	36495	43.7
11	20.0	0.86	2614	708	1.66	13.2	28329	40.0	39929	56.4
12	21.0	0.95	2770	751	1.57	13.7	30872	41.1	43513	58.0
13	22.0	1.04	2930	794	1.48	14.2	33522	42.2	47249	59.5
14	23.0	1.14	3095	839	1.40	14.7	36280	43.2	51136	60.9
15	24.0	1.24	3265	885	1.33	15.3	39403	44.5	55537	62.8
16	25.0	1.34	3440	932	1.26	15.8	42386	45.5	59742	64.0
17	26.0	1.45	3621	981	1.20	16.3	45476	46.4	64098	65.3
18	27.0	1.57	3809	1032	1.14	16.8	48674	47.2	68605	66.5
19	28.0	1.68	4002	922	1.28	17.4	52280	56.7	73686	79.9
20	28.7	1.77	4143	786	1.50	17.7	54510	69.4	76831	97.7
21	29.4	1.86	4287	813	1.45	18.1	57102	70.2	80483	98.9
22	30.1	1.95	4435	841	1.40	18.4	59430	70.7	83765	99.6
23	30.8	2.03	4580	869	1.36	18.8	62135	71.5	87577	100.8
24	31.5	2.13	4744	900	1.31	19.2	64899	72.1	91473	101.6
25	32.2	2.23	4906	931	1.27	19.5	67378	72.4	94966	102.0
26	32.9	2.33	5073	962	1.22	19.9	70254	73.0	99022	102.9
27	33.6	2.43	5245	995	1.18	20.3	73191	73.6	103161	103.7
28	34.3	2.53	5422	1029	1.14	20.6	75820	73.7	106867	103.9
29	35.0	2.63	5607	531	2.21	21.0	78870	148.5	111165	209.0

*Pullout determined from Jewell's pullout equation.

†Pullout determined from Tensar's pullout equation.

The slope angle, i, can be computed as $\tan^{-1}(\frac{1}{2}) = 26.6$ deg. For the remainder of this example, it is assumed to be 26 deg.

From standard soil mechanics theory, the horizontal component of the active earth pressure coefficient for a slope can be computed as:

$$K_{aH} = K_a \cos i = \cos^2 i \left[\frac{\cos i - \sqrt{\cos^2 i - \cos^2 \phi_1}}{\cos i + \sqrt{\cos^2 i - \cos^2 \phi_1}}\right]$$

$$= \cos^2 (26°) \left[\frac{\cos (26°) - \sqrt{\cos^2 (26°) - \cos^2 (30°)}}{\cos (26°) + \sqrt{\cos^2 (26°) - \cos^2 (30°)}}\right]$$

$$= 0.47$$

Because the active earth pressure acts parallel to the slope, there is also a downwards component of the force exerted by the soil behind the reinforced mass on the reinforced mass. It is conservative to ignore this component.

B1. Computations To Assure Safety

B1.1. Sliding on base

- A factor of safety greater than 1.5 is required. Thus, $\frac{(W_1 + W_2) \tan \phi_1}{P_E} \geq 1.5$, where $P_E = \frac{K_{aH} \gamma H_1^2}{2}$; $W_1 = LH\gamma$; and $W_2 = \frac{L(H_1 - H)}{2}\gamma$.
- Substitution for P_E, W_1, and W_2 gives: $\left(LH\gamma + L\frac{(H_1 - H)}{2}\gamma\right)\tan \phi_1 \geq 1.5 \frac{K_{aH} \gamma H_1^2}{2}$.
- Since $H_1 = (L/2) + H$, $L\gamma\left(H + \frac{L}{4}\right)\tan \phi_1 \geq \frac{1.5 K_{aH} \gamma}{2}\left(\frac{L}{2} + H\right)^2$.
- Solving for L gives $L \geq 18.0$ ft.

B1.2. Overturning about toe

- A factor of safety greater than 2.0 is required. Thus, $F.S. = \frac{\Sigma \overset{\frown}{M}_{Toe}}{\Sigma \overset{\frown}{M}_{Toe}} \geq 2.0$.
- $\Sigma \overset{\frown}{M}_{Toe} = W_1\left(\frac{L}{2}\right) + W_2\left(\frac{2L}{3}\right)$. $\Sigma \overset{\frown}{M}_{Toe} = P_E \frac{H_1}{3}$.
- $F.S. = \dfrac{\frac{L^2 H \gamma}{2} + L^2 \frac{(H_1 - H)\gamma}{3}}{\frac{K_{aH} \gamma H_1^3}{6}} =$

$$\frac{\frac{18.0^2 (15)\ 120}{2} + \frac{18.0^2 (9.0)\ 120}{3}}{\frac{0.47(120)}{6}(24.0)^3}$$

- $F.S. = 3.1$, which is satisfactory.

Table 18. Maximum vertical spacing of geotextile layers.

Depth (ft)	σ_{hc} (psf)	S_v (ft)
5	255.8	2.70
10	511.7	1.35
15	767.6	0.90
20	1023.4	0.67
25	1279.3	0.54
30	1535.1	0.45
35	1790.9	0.39

B1.3. Bearing capacity failure

- Use Meyerhof's stress distribution for eccentrically loaded footings and $L = 18.0$ ft and compute eccentricity. $e = \frac{\Sigma \overset{\frown}{M}_{centerline}}{R_V}$.
- First compute the moment around the centerline at the base. $\Sigma \overset{\frown}{M}_{centerline} = P_E \frac{H_1}{3} - W_2\left(\frac{L}{2} - \frac{L}{3}\right) = \frac{K_{aH} \gamma H_1^3}{6} - \left(\frac{L(H_1 - H)\gamma}{2}\right)\left(\frac{L}{2} - \frac{L}{3}\right)$. $\Sigma \overset{\frown}{M}_{centerline} = \frac{0.47(120)(24)^3}{6} - \left[\left(\frac{18(24 - 15)(120)}{2}\right)\left(\frac{18}{2} - \frac{18}{3}\right)\right] = \frac{0.47(120)(24.0)^3}{2(3)} - \frac{(18.0)(9.0)(120)(3.0)}{2} = 100{,}785$ ft-lb.
- Compute vertical reaction. $R_V = W_1 + W_2 = (18.0)(15)(120) + \frac{(18.0)(9.0)(120)}{2} = 42{,}120$ lb.
- Compute eccentricity. $e = (100{,}785/42{,}120) = 2.39$.
- Verify that eccentricity is acceptable, i.e., within middle third. For $e < (L/6)$, $e < (18.0/6) = 3.0$. Hence, $L = 18$ ft is sufficient to maintain the resultant within the middle third.
- Thus, external stability is controlled by sliding, and it will be satisfied for $L = 18.0$ ft. Since the downward vertical component of the retained earth lateral force was neglected, the sliding resistance was underestimated. Had it been included, a somewhat lower value of L would have been obtained. Accordingly, the internal designs that follow have been based on a reinforcement length of 17.5 ft. Nonetheless, the increase in L required by the sloping backfill relative to Design Example I is substantial.
- Designs have been completed based on these parameters. The same procedures were used as for Design Examples I and II, and the results are similar in form. The results may be summarized briefly as follows.

C. Internal Stability

C1. Strip Reinforcement System—Reinforced Earth

- Six levels of reinforcement are used as for Design Example

I. Because of the reinforcement length required to ensure external stability (17.5 ft vs. 11 ft), the effective length, L_e, is substantially increased relative to Case I. As a consequence, the pullout resistance increased, and the use of 5 mm × 40 mm ribbed strips gives a safety factor greater than 1.5. Tensile stresses in the reinforcement are well below the allowable 40,000 psi, even after allowance for corrosion.

- The vertical spacing of the reinforcements and the reinforcement layer numbering are as shown on Diagram 18.
- The locus of the maximum tensile force (the failure surface shown on Diagram 18) is determined from the average of the height of the wall face and the height of a vertical section at the back of the reinforced soil mass.
- The variation of earth pressure coefficient with depth and the variation of apparent coefficient of friction with depth are as shown on Diagram 4. The depth is taken as Z_2, with Z_2 being defined as on Diagram 18.
- The calculations for the internal stability of layer 4 at a depth below the top of wall face of 8.75 ft are presented below, while the results for all layers of reinforcement are given in Table 19.

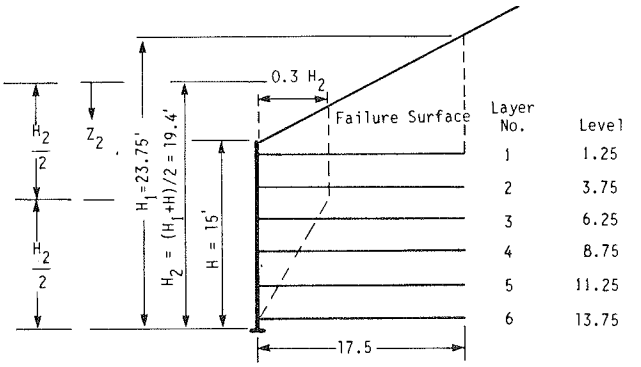

H_1 = Vertical dimension from top of slope to bottom of wall measured at back of reinforcements.

H_2 = Average of H and H_1, called equivalent wall length.

Z_2 = Equivalent depth used in respect to equivalent wall length (H_2).

Diagram 18

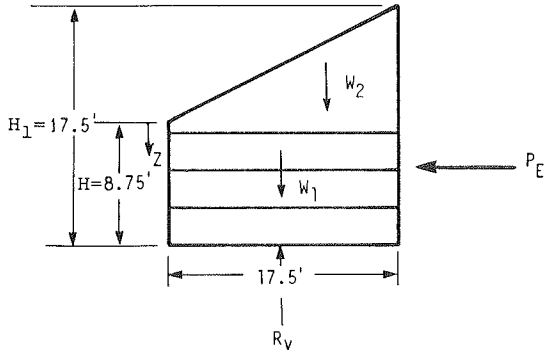

H_1 = Vertical dimension from top of slope to bottom of wall measured at back of reinforcements.

Diagram 19

C1.1. Rupture of reinforcement

- Compute the horizontal earth pressure at $Z = 8.75$ ft. The forces shown on Diagram 19 must be taken into account.
- Vertical load $R_V = W_1 + W_2 = L\ H\ \gamma + \left(\frac{L(H_1 - H)\ \gamma}{2}\right) = \left(\frac{H_1 + H}{2}\right) L\ \gamma = \frac{(8.75 + 17.5)}{2}(17.5)\ 120 = 27{,}562$ lb.
- Horizontal force $P_E = \frac{K_{aH}\ \gamma\ H^2}{2} = \frac{0.47(120)17.5^2}{2} = 8{,}636$ lb.
- For eccentricity: $e = \frac{P_E \frac{H}{3} - W_2\left(\frac{L}{2} - \frac{L}{3}\right)}{R_V} = \frac{(8{,}636)\left(\frac{17.5}{3}\right) - 9{,}188\ (2.9)}{27{,}562} = 0.9$ ft.
- $\sigma_{vb} = \frac{R_V}{L - 2e} = \frac{27{,}562}{17.5 - (2(0.9))} = 1{,}755$ psf.
- *NOTE:* Because of the negative moment from W_2, the eccentricity in the upper layers may be negative, meaning that R_v is located to the right of the centerline of the reinforced mass. For those layers, it is conservative to take $e = 0$ and $\sigma_{vb} = R_v/L$.
- The lateral earth pressure in the reinforced mass can be computed from the equation $\sigma_h = K\ \sigma_{vb}$.
- The applicable earth pressure coefficient K can be determined from Diagram 4, provided depth is taken as Z_2 shown on Diagram 18. The boundary K values are: $K_a = 0.271$ and $K_o = 0.426$.
- Z_2 at $Z = 8.75$ ft is $8.75 + 8.75/2 = 13.13$ ft.
- By proportion, K can be computed as: $K = (0.426 - 13.1)((0.426 - 0.271)/(20)) = 0.32$.
- Compute $\sigma_h = 0.32\ (1{,}755) = 562$ psf.
- Contributing area per reinforcement $A_R = 6.05$ ft^2.
- Horizontal force per reinforcement, FH, at $Z = 8.75$ ft.
- Thus, $FH = A_R\ \sigma_h = 6.05\ (562) = 3{,}400$ lb.

C1.2. Tensile stress in reinforcement

- Assume 60 mm × 5 mm reinforcing strip (2.362 in. × 0.197 in.).
- Cross-sectional area $A_{CR} = 0.465$ in^2.
- Thus, tensile stress $F_T = FH/A_{CR} = 3{,}400/0.465 = 7{,}312$ psi.
- Allowable tensile stress is known as 40,000 psi. Therefore, the strip is of adequate size.

C1.3. Tensile stress at connection

- Horizontal force at connection is equal to 85 percent of maximum horizontal force. Thus $FH_{CONN} = 0.85\ FH = 3{,}400\ (0.85) = 2{,}890$ psi.
- Reduced cross-sectional area due to $^9/_{16}$ in. diameter bolt hole, $A_{reduced} = 0.354$ in^2. Thus $F_{T(CONN)} = \frac{FH_{CONN}}{A_{reduced}} = \frac{2{,}890}{0.354} = 8{,}164$ psi.

Table 19. Design summary—Reinforced Earth wall (height = 15 ft, sloping backfill.

Reinforcement Layer No.	Depth (ft)	e (ft)	σ_{vb} (psf)	K	σ_h (psf)	FH (lbs)	Strip Size (mm)	Tensile Stress in Strip (psi)	Tensile Stress in Strip at Conn (psi)	F.S. Rupture	μ^*	L_e (ft)	P (lbs)	F.S. Pullout
* 1	1.25	-	675	.38	257	1552	60 x 5	3337	3727	10.7	1.28	11.7	3979	2.6
* 2	3.75	-	975	.36	351	2124	60 x 5	4567	5100	7.8	1.18	11.7	5298	2.5
3	6.25	0.2	1305	.34	444	2686	60 x 5	5777	6450	6.2	1.08	12.9	6992	2.6
4	8.75	0.9	1755	.32	562	3400	60 x 5	7312	8164	4.9	0.98	14.2	8630	2.5
5	11.25	1.3	2202	.30	660	3993	60 x 5	8587	9588	4.2	0.88	15.5	10066	2.5
6	13.75	1.8	2360	.28	660	3993	60 x 5	8587	9588	4.2	0.78	16.8	11220	2.8

*Note: Minus value for e means R_v is located to the right of the centerline for the reinforced soil mass.

C1.4. Pullout of reinforcement

- The pullout capacity of a reinforcement strip, P, is computed as $P = 2b\ \gamma\ Z\ L_e\ \mu^*$.
- The apparent coefficient of friction between the soil and reinforcement μ^* is computed using the average height of overburden. As shown on Diagram 4, it is assumed that μ^* decreases linearly from 1.5 at the surface to tan ϕ at a depth of 20 ft and remains constant at tan ϕ for greater depths.
- At $Z = 8.75$ ft, $Z_2 = 8.75 + 8.75/2 = 13.13$ ft.
- With tan ϕ = tan 35° = 0.7, μ^* can be computed by proportion: $\frac{1.5 - 0.7}{20} = \frac{1.5 - \mu^*}{13.13}$, hence, $\mu^* = 0.98$.
- The effective embedment length behind the failure surface, L_e, can be assessed from Diagram 18. For $Z_2 \leq \frac{H_2}{2}$, $L_e = L - 0.3H_2$. For $Z_2 > \frac{H_2}{2}$, $L_e = L - \left[\frac{H_2 - Z_2}{\tan(45 + \phi/2)}\right]$.
- Since $Z_2 = 13.13$ ft $> \frac{H_2}{2} = \frac{19.4}{2} = 9.7$ ft, $L_e = 17.5 - \left[\frac{19.4 - 13.13}{\tan 62.5°}\right] = 14.2$ ft.
- The pullout resistance is given by $P = 2b\ \gamma\ ZL_e\ \mu^*$ as for Example I. Thus, P = 2 (0.06 m) 3.28 ft/m (120 lb/ft^3) 13.13 ft (14.2 ft) 0.98 = 8,630 lb.
- The factor of safety against pullout can be computed as $F.S._{pullout} = \frac{P}{FH} = \frac{8,630}{3,400} = 2.5$.

C1.5. Corrosion

- Cross-sectional area of reinforcement after 100 years = 0.3637 in^2. (see Design Example I for details of calculation).
- Stress in reinforcement layer 6 after 100 years ($F_{T(100)}$) is $F_{T(100)} = \frac{FH}{A_{100}} = \frac{3,993}{0.3637} = 10,979$ psi, < 40,000 psi.
- Stress in reinforcement layer 6 at the connection after 100 years ($F_{T(CONN)100}$) is $F_{T(CONN)100} = \frac{0.85 \times FH}{A_{CONN(100)}} = \frac{3,394}{0.2769} =$ 12,257 psi, < 40,000 psi.

C2. Grid (Bar Mat) Reinforcement—VSL Retained Earth

- The use of four W11 bars with four longitudinal bars per mesh and six levels of reinforcement, as for Design I, yields a safe design because of the increased lengths needed for external stability. Minimum factor of safety against pullout is 2.0 and occurs at level 5. The overall safety factor against pullout is 2.2. Minimum factor of safety against rupture of reinforcements is 2.2 and occurs at level 6. The maximum steel stress after allowances for corrosion is about 21,000 psi.

C3. Grid Reinforcement—Welded Wire Wall

- Because of the sloping backfill, the first mesh can be located at the top of the wall. Vertical spacings of 1.5 ft between meshes are chosen as for Design Example I. Horizontal earth pressures are again determined using an earth pressure coefficient, K_o, of 0.65. Analysis of tensile and pullout forces shows that the initial factors of safety are more than adequate if W1.7 wire is used. For a design life of 100 years, corrosion requirements dictate that W2.5 wire be used for level 10, which is located a vertical distance of 13.5 ft below the top of the wall face.

C4. Grid Reinforcement—Geogrid-Reinforced Wall

- On the basis of the safe design strength for SR2 grid of 1,185

lb/linear ft as determined in Design Example I, the vertical spacing between geogrids was computed using the same procedure as shown in that example. The result is the arrangement shown on Diagram 20.

- Analysis of the tensile stresses in the reinforcements shows that the safe design value is reached in layers 7 and 8, but mobilized stress values are lower than the safe design value in the other layers. Because of the length of reinforcement required for external stability, factors of safety against pullout are quite high (19 to 30).

C5. Sheet Reinforcement—Geotextile-Reinforced Wall (U.S. Forest Service Method)

- Design procedures are similar to those in Design Example I, with the modifications for sloping backfill already shown for Reinforced Earth. Computed vertical spacings for geotextile sheets with a tensile strength of 2,520 ft are shown on Diagram 21. The higher horizontal stresses caused by the sloping backfill result in the requirement for more reinforcement layers than for Design Example I. For this arrangement, the factors of safety against tensile failure of the reinforcement range from a minimum of 1.5 at layer 11 (depth of 10.5 ft below top of wall face) to 2.7 in layer 1. Pullout resistance is much greater than required owing to the larger wall width.

DESIGN EXAMPLE IV—LOW WALL WITH SURCHARGE

A. Given Conditions

This example is the same as Design Example I, except that there is uniform vertical surcharge loading of $q = 600$ psf on the ground surface at the top of the wall, producing the conditions shown on Diagram 22. It is assumed that the reader is thoroughly familiar with Design Example I.

B. External Stability

The external horizontal force can be computed as: $P_E = \frac{K_a \gamma H^2}{2} = \frac{0.333 \times 120 \times (15)^2}{2} = 4{,}495$ lb/ft.

The resultant horizontal force from surcharge loading can be computed as follows: $P_q = qK_aH = 600 \times 0.333 \times 15 = 2{,}997$ lb/ft.

B1. Computations to Assure Safety

B1.1. Sliding on base

- The factor of safety against sliding should exceed 1.5. Thus, $F.S. = \frac{(W_1 + qL)\tan\phi_1}{P_E + P_q} = \frac{[(15)L(120) + 600L]\tan 30°}{4{,}495 + 2{,}997}$, ≥ 1.5.
- Solving for L gives $L \geq 8.1$ ft. Try $L = 8.5$ ft.

B1.2. Overturning about toe

- The factor of safety should exceed 2.0.

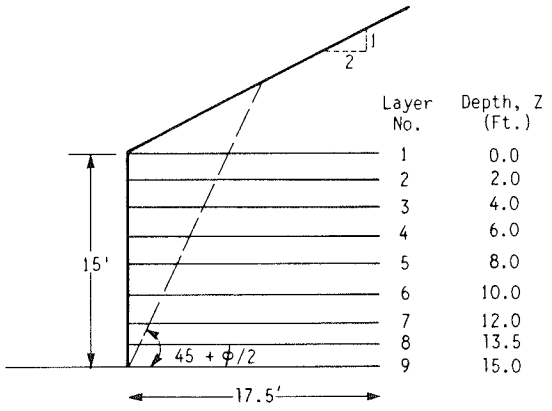

Diagram 20

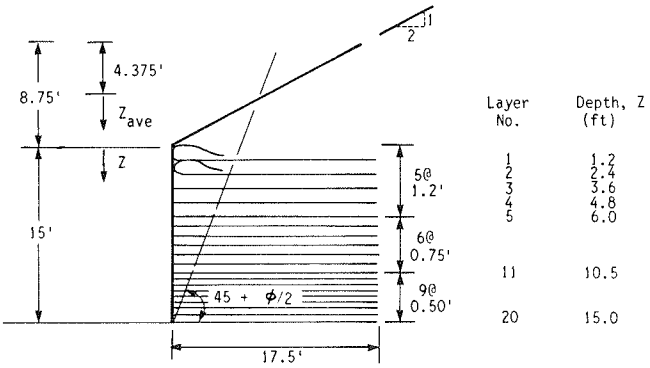

Diagram 21

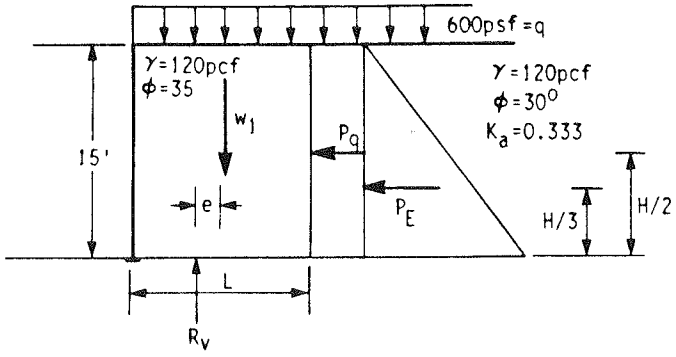

Diagram 22

- For $L = 8.5$ ft, the factor of safety can be computed as $F.S. = \frac{(q + (\gamma H))(L)(L/2)}{P_E(H/3) + P_q(H/2)}$. Thus, $F.S. = \frac{(600 + (120 \times 15))(8.5)(8.5/2)}{4{,}495(15/3) + 2{,}997(15/2)} = 1.93 < 2.0$.
- Try a base width of 10 ft.
- $F.S. = \frac{(600 + (120 \times 15))(10)5}{44{,}952} = \frac{120{,}000}{44{,}952} = 2.7$, which is O.K.

B1.3. Bearing capacity failure

- Compute vertical reaction as $R_v = qL + HL\gamma$.
- Take moments about center of base to compute eccentricity.
- $e = \dfrac{P_q \dfrac{H}{2} + P_E \dfrac{H}{3}}{R_V} = \dfrac{2{,}997(7.5) + 4{,}495(5)}{600(10) + 15(10)120} = 1.87$ ft. $\dfrac{L}{6} = \dfrac{10}{6} = 1.66$ ft. Hence, the resultant is outside middle third.
- Try $L = 11$ ft.
- $R_V = 600(11) + 15(11)120 = 26{,}400$ lb. $e = \dfrac{44{,}952}{26{,}400} = 1.7$. $\dfrac{L}{6} = 1.83$, which is satisfactory.
- Compute vertical stress on reduced bearing area: $\sigma_{vb} = \dfrac{R_V}{L - 2e} = \dfrac{26{,}400}{11 - 2(1.7)} = 3{,}474$ psf.
- Thus, external stability would be satisfactory if $L = 11$ ft and the ultimate bearing capacity of the foundation exceeds $2 \times 3{,}474$ or about 7,000 psf.

C. Internal Stability

C1. Strip Reinforcement System—Reinforced Earth

- The vertical spacing of the reinforcements and the reinforcement layer numbering are shown on Diagram 23.
- The calculations for the internal stability of layer 3 at a depth of 6.25 ft are presented as follows.

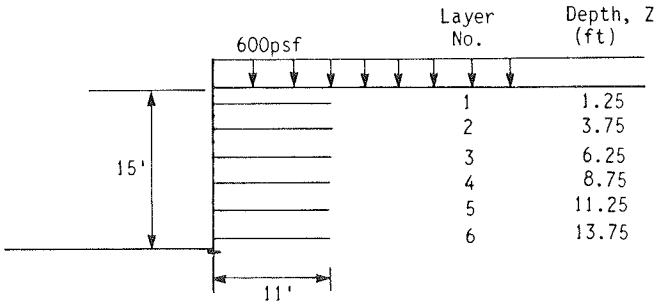

Diagram 23

C1.1. Tensile forces to be resisted by reinforcement

- The forces to be taken into account for the layer of reinforcement at $Z = 6.25$ ft are shown on Diagram 24.

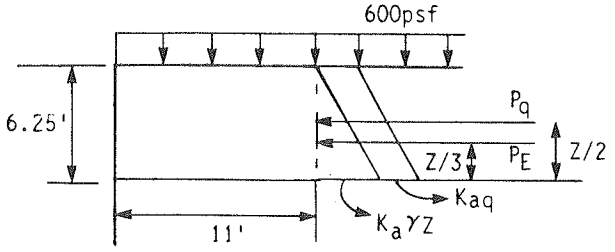

Diagram 24

- Compute eccentricity for $Z = 6.25$ ft.
- $e = \dfrac{P_E \dfrac{Z}{3} + P_q \dfrac{Z}{2}}{R_V}$, wherein P_E, P_q, and R_v are determined for Z = 6.25 ft. Thus, $e = \dfrac{(0.333)(120)(6.25)^3/6 + (0.333)(600)(6.25)^2/2}{(11)(120)(6.25) + 600(11)} = 0.372$ ft.
- Compute bearing pressure on reduced area: $\sigma_{vb} = \dfrac{R_V}{L - 2e} = \dfrac{14{,}850}{11 - 2(0.372)} = 1{,}448$ psf.
- Compute horizontal stress in reinforced mass with $\sigma_h = K\sigma_{vb}$, where K can be interpreted from Diagram 4 as $K = 0.426 - \left(\dfrac{0.426 - 0.271}{20}\right)(6.25) = 0.378$; $\sigma_h = (0.378)(1448) = 547$ psf.
- Compute the horizontal tensile force, FH, acting on the reinforcement: $FH = \sigma_h A_R = (547)(6.05) = 3{,}309$ lb.

C1.2. Tensile stress in reinforcement

- Using 60 mm $\times$ 5 mm reinforcing strip, $A_{CR} = 0.465$ in^2; $F_T = \dfrac{FH}{A_{CR}} = \dfrac{3{,}309}{0.465} = 7{,}116$ psi; $F.S._{rupture} = \dfrac{40{,}000}{7{,}116} = 5.6$.

C1.3. Tensile stress at connection

- $FH_{CONN} = 0.85\ FH = 0.85(3{,}309) = 2{,}813$ lb.
- $A_{reduced} = 0.354$ in^2 (see Design Example III).
- $F_{T(CONN)} = \dfrac{2813}{0.354} = 7{,}946$ psi.
- $F.S._{rupture} = \dfrac{40{,}000}{7{,}946} = 5.0$.

C1.4. Pullout of reinforcement

- The surcharge pressure above the reinforced zone is ignored in calculations of the pullout resistance in Reinforced Earth design. As shown later, this is conservative. The design distribution is shown on Diagram 25.
- Pullout resistance is computed with the equation $P = 2b\ \gamma\ Z\ L_e \mu^*$.
- μ^* is computed from Diagram 4 as: $\mu^* = 1.5 - [(1.50 - \tan 35°)/(20)] \times 6.25 = 1.25$.
- Because Z is less than $H/2$ (see Diagram 3), the effective embedment length can be computed as $L_e = L - 0.3H$ ft $= 11 - 0.3 \times 15 = 6.5$ ft.

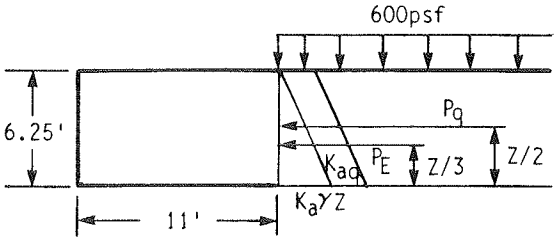

Diagram 25

- P = (2)(0.06 m)(3.28 ft/m)(120 lb/ft^3)(6.25 ft)(6.5 ft)(1.25) = 2,399 lb.
- Because the surcharge directly above the reinforced mass is being ignored (Diagram 25), the eccentricity is different from when the surcharge is taken into account. Accordingly, $e = \frac{P_E \frac{H}{3} + P_q \frac{H}{2}}{R_V} = \frac{5{,}528}{(11)(120)(6.25)} = 0.67$ ft.
- Vertical stress on the reduced bearing area can be computed as $\sigma_{vb} = \frac{R_V}{L - 2e} = \frac{8{,}250}{11 - 2 \times 0.67} = 854$ psf.
- Horizontal stress can then be computed as σ_h = (0.378)(854) = 323 psf, which provides the tensile force on the reinforcement, FH = (323)(6.05) = 1953 lb. Hence $F.S._{pullout} = \frac{2{,}399}{1{,}953} = 1.2$, which is not satisfactory. Thus, the length of the reinforcement has to be increased. Use of 12-ft long reinforcements would yield the values given in Table 20, which would be satisfactory for design.
- To demonstrate that it is conservative to ignore the surcharge immediately above the reinforced mass, the same computations can be repeated taking the surcharge into account. These would yield: L_e = 7.5 ft, for L = 12 ft. P = 2(0.06)(3.28)[(120)(6.25) + 600](7.5)(1.25) = 4,982 lb/ft. $e = \frac{5{,}528}{11(120)6.25 + 11(600)} = 0.37$. $\sigma_{vb} = \frac{11(120)6.25 + 11(600)}{12 - 2\,(0.37)} = 1{,}319$ psf. σ_h = (0.378)(1,319) = 499 psf. FH = (499)(605) = 3,019 lb.
- Therefore, $F.S._{pullout} = \frac{4{,}982}{3{,}019} = 1.65$, which is higher than the value of 1.4 (Table 20) computed when the surcharge was ignored.

C1.5. Corrosion

- For reinforcement layer 6 after 100 years and following the same procedure as for previous design examples: $F_{T(100)} = \frac{5{,}609}{0.3637} = 15{,}422$ psi < 40,000 psi, which is O.K. $F_{T(CONN)100} = \frac{0.85 \times FH}{A_{CR(CONN)100}} = \frac{0.85 \times 5{,}609}{0.2769} = 17{,}218$, which is O.K.

C2. Grid (Bar Mat) Reinforcement—VSL Retained Earth

- The vertical spacings between reinforcement layers are the same as for the Reinforced Earth design. The assumed variations in lateral earth pressure coefficient and anchorage factor with depth are the same as for the VSL design shown on Diagram 6.
- Calculations for the internal stability of each layer, for a reinforcement length of 11 ft, are made in the same manner as in Design Example I, but using the same surcharge arrangement for rupture and pullout calculations as for the Reinforced Earth Design above. Five W11 longitudinal bars per grid are used.
- The minimum factor of safety against pullout is 1.5 and occurs at level 4. The tensile stress in the bars is well below the allowable tensile strength (35,750 psi), even after allowance for corrosion.

C3. Grid Reinforcement—Welded Wire Wall

- The same reinforcement configuration used for Design Example I and shown on Diagram 7 can be used.
- If W1.7 wire is used, the factor of safety against pullout varies between 4.7 at level 2 and 6.8 at level 10. At level 1 the factor of safety is somewhat lower, but still satisfactory. The stress in the wire is less than the allowable value (0.55 F_y = 35,750 psi). However, corrosion considerations necessitate the use of W2.5 wire for levels 8, 9, and 10.

C4. Grid Reinforcement—Geogrid-Reinforced Wall

- On the basis of the safe design strength for SR2 grid of 1,185 lb/linear ft as determined in Design Example I, the vertical spacing between geogrids was computed by the same procedure as for that example, and taking the surcharge into account. The result is the arrangement shown on Diagram 26.
- A reinforcement length of 11 ft, the minimum length required for external stability, has been used for this wall. The minimum factor of safety against pullout is 3.3 and occurs at layer 1. The minimum factor of safety against exceeding the safe design strength of SR2 grids (1,185 lb/linear ft) is 1.1 and occurs at level 6. Inclusion of an additional layer of rein-

Table 20. Design summary—Reinforced Earth (15-ft high wall, length of reinforcement 12 ft, 600-psf surcharge).

	FOR RUPTURE									FOR PULLOUT							
Reinf. Layer #	z (ft)	e (ft)	σ_{vb} (psf)	K	σ_H (psf)	F_H (lbs)	F_T (psi)	$F_{T_{conn.}}$ (psi)	F.S. rupture	e (ft)	σ_{vb} (psf)	σ_H (psf)	FH (lbs)	μ^*	L_e (ft)	P (lbs)	F.S. pullout
1	1.25	0.02	753	0.417	314	1898	4083	4558	8.8	0.09	152	64	384	1.45	7.5	642	1.7
2	3.75	0.14	1075	0.397	427	2582	5553	6200	6.5	0.33	476	189	1144	1.35	7.5	1793	1.6
3	6.25	0.34	1431	0.378	541	3272	7038	7858	5.1	0.61	836	316	1910	1.25	7.5	2768	1.4
4	8.75	0.61	1837	0.358	658	3978	8555	9552	4.2	0.96	1250	448	2712	1.15	8.7	4157	1.5
5	11.25	0.95	2317	0.339	785	4751	10219	11409	3.5	1.37	1748	593	3586	1.05	10.0	5607	1.6
6	13.75	1.34	2897	0.320	927	5609	12061	13467	3.0	1.83	2374	759	4590	0.95	11.3	7003	1.5

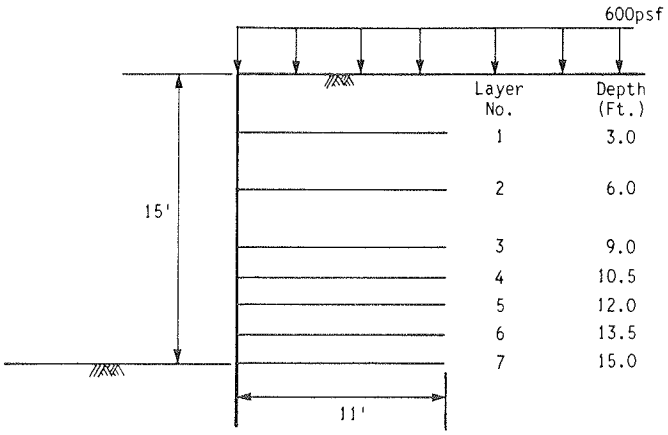

Diagram 26

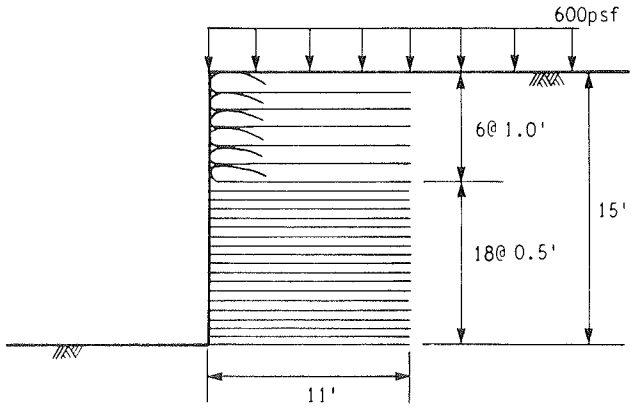

Diagram 27

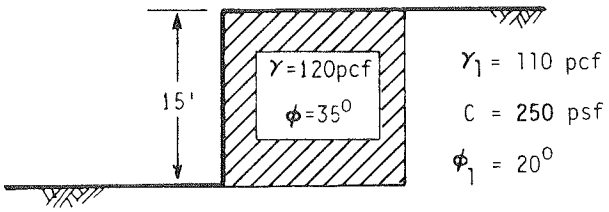

Diagram 28

forcement between layers 4 and 7 would provide an adequate increase in the factor of safety against rupture.

C5. Sheet Reinforcement—Geotextiles

- Stresses caused by the additional surcharge result in the requirement for more reinforcement layers than for Design Example I. However, the sheets are not required to be longer. This is because the factor of safety against pullout is the same as in Design Example I if pullout calculations are carried out assuming no surcharge above the reinforced mass, and the factor of safety is even higher if the surcharge is included. Computed vertical spacings of geotextile sheets having a tensile strength of 2,520 lb/ft are shown on Diagram 27.

DESIGN EXAMPLE V—LOW WALL WITH COHESIVE RETAINED SOIL AND FOUNDATION SOIL

A. Given Conditions

This example is the same as Design Example I, except that the retained soil and the foundation soil are cohesive with the properties shown on Diagram 28.

The short-term effect of the cohesion component of the retained soil is to decrease the horizontal pressure on the reinforced mass and therefore to decrease the tension in the reinforcing material.

However, cohesive soils are known to exhibit creep under sustained shear stress as would be the case in the retained soil or in the foundation. Thus, the lateral forces on the retaining structure are likely to increase with time.

Because of the limited experience with the use of reinforced soil structures to retain cohesive material, it appears prudent to ignore the cohesion component of both the retained and the foundation soils, although this is probably a very conservative assumption.

The calculations for both internal and external stability of the wall are therefore done using the following properties for the retained soil and the foundation: $\gamma_1 = 110$ pcf, C = 0 psf, $\phi_1 = 20°$, $K_a = \tan^2 [45° - (20°/2)] = 0.49$.

B. External Stability

The forces to be taken into account are shown on Diagram 29. The external horizontal force can be computed as $P_E = \frac{K_a \gamma H^2}{2} = \frac{0.490 \times 110 \times (15)^2}{2} = 6{,}067$ lb/ft.

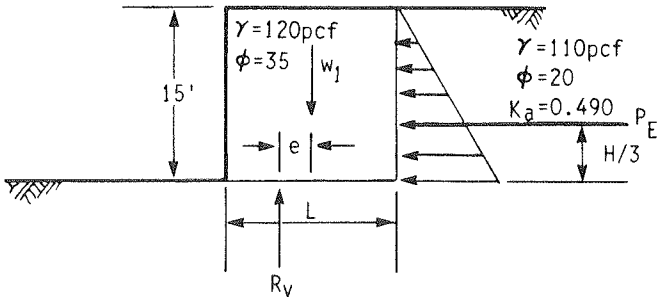

Diagram 29

B1. Computations To Assure Safety

B1.1. Sliding on base

- The factor of safety against sliding can be computed as $F.S. = \frac{\gamma LH \tan \phi_1}{P_E}$.
- Thus, the minimum length of reinforcement can be computed as $L \geq \frac{1.5\, P_E}{H \gamma \tan \phi_1} = \frac{1.5 \times 6{,}067}{15 \times 120 \times \tan 20°}$; $L \geq 13.9$ ft $\Rightarrow$ 14 ft.

B1.2. Overturning about toe

- The factor of safety against overturning about the toe can be computed as $F.S. = \frac{\Sigma \overbrace{M}^{\curvearrowright}_{toe}}{\Sigma \overbrace{M}^{\curvearrowleft}_{toe}}$.
- For a reinforcement length of 14 ft, the factor of safety would be $F.S. = \frac{\gamma_b HL \times L/2}{P_E (H/3)} = \frac{3\gamma_b L^2}{2 P_E} = \frac{3 \times 120 \times (14)^2}{2 \times 6{,}067} = 5.8 > 2.0$, which is satisfactory.

B1.3. Bearing capacity failure

- Compute eccentricity as $e = \frac{P_E H/3}{R_V} = \frac{6{,}067 \times 15/3}{120 \times 15 \times 14} = 1.2 \text{ ft} \leq \frac{L}{6} = 2.3$ ft. Hence, resultant is inside middle third, which is satisfactory. $\sigma_{vb} = \frac{R_v}{L - 2e} = \frac{120 \times 15 \times 14}{14 - (2 \times 1.2)} = 2{,}172$ psf.
- Thus, for external stability, $L = 14$ ft, and the ultimate bearing capacity of the foundation should be at least $2 \times 2{,}172$ psf. The increase in required length of reinforcement relative to Design Example I because of the weak foundation soil is substantial. (In Design Example I a reinforcement length of 9 ft was required.)

C. Internal Stability

Internal designs for the different wall types and $L = 14$ ft can be prepared using the same procedures as for Design Examples I and II, and the results are similar in form. Results obtained in this manner can be summarized as follows.

C1. Strip Reinforcement System—Reinforced Earth

Six levels of reinforcement are used as for Design Example I. Because of the reinforcement length required to ensure external stability, the effective length, L_e, is increased relative to Design Example I. As a consequence, pullout resistance increases and the factor of safety against pullout of 60 mm $\times$ 5 mm reinforcement strips varies between 2.0 and 2.2. Tensile stresses in the reinforcement are well below the allowable 40,000 psi, even after allowance for corrosion.

C2. Grid (Bar Mat) Reinforcement—VSL Retained Earth

The use of four W11 bars with four longitidinal bars per mesh and six levels of reinforcement, as for Design Example I, yields a safe design because of the increased lengths needed for external stability. Minimum factor of safety against pullout is 1.8 and occurs at level 3. Minimum factor of safety against rupture is 2.4 and occurs at level 6. The maximum steel stress after allowance for corrosion is about 20,000 psi.

C3. Grid Reinforcement—Welded Wire Wall

The horizontal pressure used for internal stability calculations of Welded Wire Walls does not depend on the properties of the retained soil: $\sigma_h = K_o \sigma_v$, where $K_o = 0.65$ and $\sigma_v = \gamma_b Z$.

The wall used in Design Example I can, therefore, also be computed to be safe for this Design Example. It has the same factor of safety against rupture, and a higher factor of safety against pullout because of the increased reinforcement length required to satisfy external stability criteria.

C4. Grid Reinforcement—Geogrid-Reinforced Wall

The same wall used in Design Example I can be used for this example. However the reinforcement length is 14 ft to satisfy external stability requirements. Six layers of SR2 grid are used, at depths of 3.0, 6.0, 9.0, 11.0, 13.0, and 15.0 ft. The minimum factor of safety against rupture is 1.2 and occurs at level 5. The factor of safety against pullout is very high because of the 14-ft lengths of the reinforcements.

C5. Sheet Reinforcement—Geotextile-Reinforced Wall

The horizontal pressures used for internal stability calculations of geotextile-reinforced walls according to the U.S. Forest Service Method are a function of the properties of the backfill material of the wall itself and do not depend on the retained soil properties.

The wall used in Design Example I can, therefore, also be computed to be safe for this Design Example. It has the same factor of safety against rupture, and a higher factor of safety against pullout because of the increased reinforcement required length to satisfy external stability criteria.

REFERENCES

1. JURAN, I., "Dimensionnement interne des ouvrages en terre armee." Thesis for Doctorate of Engineering, Laboratoire Central des Ponts et Chaussees, Paris (1977).
2. SCHLOSSER, F., and SEGRESTIN, P., "Dimensionnement des ouvrages en Terre Armee par la methode de l'equilibre local." *Proc. International Conference on Soil Reinforcement: Reinforced Earth and Other Techniques,* Paris (1979) Vol. I.
3. JURAN, I., BEECH, J., and DE LAURE, E., "Experimental Study of the Behavior of Nailed Soil-Retaining Structures on Reduced Scale Models." *International Symposium on In Situ Soil and Rock Reinforcement,* Paris (1984).
4. INGOLD, T. S., "An Analytical Study of Geotextile Reinforced Embankments." *Proc. 2nd International Conference on Geotextiles,* Las Vegas (1982).
5. STOCKER, M. F., KORBER, G. W., GASSLER, G., and GUDEHUS, G., "Soil Nailing." *Proc. International Conference on Soil Reinforcement: Reinforced Earth and Other Techniques,* Paris, Vol. I (Mar. 1979) pp. 469–474.

6. ROMSTAD, K. M., AL-YASSIN, Z., HERRMANN, L. R., and SHEN, C. K., "Stability Analysis of Reinforced Earth Retaining Structures." *Proc. ASCE Symposium on Earth Reinforcement,* Pittsburgh, Penn. (1978) pp. 685–713.
7. PHAN, T. L., SEGRESTIN, P., SCHLOSSER, F., and LONG, N. T., "Stability Analysis of Reinforced Earth Walls by Two Slip Circle Methods." *Proc. International Conference Soil Reinforcement,* Paris (1979) pp. 119–123.

8A. CHRISTIE, I. F., and EL HADI, K. M., "Some Aspects of the Design of Earth Dams Reinforced with Fabric." *Proc. 1st International Conference on Geotextiles,* Paris (1979) Vol. II, pp. 99–103.

8B. ROMSTAD, K. M., HERRMANN, L. R., and SHEN, C. K., "Integrated Study of Reinforced Earth—1: Theoretical Formulation." *ASCE J. Geotech. Eng. Div.,* Vol. 102, No. GT5 (May 1976) pp. 457–471.

9. AL-HAUSSAINI, and JOHNSON, L. D., "Finite Element Analysis of a Reinforced Earth Wall." *Technical Report S-77,* Soils and Pavements Design Laboratory, U.S. Army Engineer Waterways Station, Vicksburg, Miss. (May 1977).
10. HERRMANN, L. R., and AL-YASSIN, Z., "Numerical Analysis of Reinforced Earth Systems." *Proc. ASCE Symposium on Reinforced Earth,* Pittsburgh, Penn. (Apr. 1978) preprint 3125, pp. 428–457.
11. AL-YASSIN, Z., and HERRMANN, L. R., "Finite Element Analysis of Reinforced Earth Walls." *Proc. International Conference on Soil Reinforcement: Reinforced Earth and Other Techniques,* Paris (Mar. 1979) Vol. I, pp. 3–9.
12. CLOUGH, G. W., and DUNCAN, J. M., "Finite Element Analyses of Port Allen and Old River Locks." *Contract Report S-69-6,* U.S. Army Engineer Waterways Experiment Station, Vicksburg, Miss. (Sept. 1969).
13. GOODMAN, R. E., TAYLOR, R. L., and BREKKE, T. L., "A Model of the Mechanics of Jointed Rock." *ASCE J. Soil Mechanics and Foundation Division,* Vol. 94, No. SM3 (May 1968) pp. 637–659.
14. DUNCAN, J. M., and WONG, K. S., "Hyperbolic Stress-Strain Parameters for Nonlinear Finite Element Analyses of Stresses and Movements in Soil Masses." *Report E-74-3,* College of Engineering, University of California, Berkeley (July 1976).
15. SHEN, C. K., HERMANN, L. R., ROMSTAD, K. M., BANG, S., KIM, Y. S., and DENATALE, J. S., "An In-Situ Earth Reinforced Lateral Support System." *Report 81-03,* University of California, Davis, Calif. (Mar. 1981).
16. GASSLER, G., and GUDEHUS, G., "Soil Nailing—Some Aspects of a New Technique." *Proc. 10th International Conference on Soil Mechanics and Foundation Engineering,* Stockholm (1981) Vol. III, pp. 665–670.
17. SCHLOSSER, F., JURAN, I., and JACOBSEN, H. M., "Soil Reinforcement." General Report, *8th European Conference on Soil Mechanics and Foundation Engineering,* Helsinki (1983).
18. MEYERHOF, G. G., "The Bearing Capacity of Foundations under Eccentric and Inclined Loads." *Proc. 3rd International Conference on Soil Mechanics and Foundation Engineering,* Zurich, Switzerland (1953) Vol. I, pp. 440–445.
19. MONONOBE, N., "Earthquake-Proof Construction of Masonry Dams." *Proc. World Engineering Conference,* Vol. 9 (1929).
20. OKABE, S., "General Theory of Earth Pressure." *J. Japanese Society of Civil Engineers,* Vol. 12, No. 1 (1926).
21. SEED, H. B., and WHITMAN, R. V., "Design of Earth Retaining Structures for Dynamic Loads." *Proc. ASCE Specialty Conference on Lateral Stresses in the Ground and Design of Earth Retaining Structures,* Cornell University (1970) pp. 103–147.
22. RICHARDSON, G. N., and LEE, K. L., "Response of Model Reinforced Earth Walls to Seismic Loading Conditions." *Report GI 38983, UCLA-ENG-7412* (Feb. 1974).
23. RICHARDSON, G. N., "Earthquake Resistant Reinforced Earth Walls." *Proc. ASCE Symposium on Earth Reinforcement,* Pittsburgh, Penn. (Apr. 1979) pp. 664–684.
24. RICHARDSON, G. N., FEGER, D., FONG, A., and LEE, K. L., "Seismic Testing of Reinforced Earth Walls." ASCE, *J. Geotech. Eng. Div.,* Vol. 103, No. GT1 (Jan. 1977) pp. 1–17.
25. NETLON LIMITED, "Test Methods and Physical Properties of Tensor Geogrids." *Technical Guidelines* (1984).

CHAPTER SIX

DURABILITY CONSIDERATIONS

Contents

One of the most important considerations in earth reinforcement is to ensure that the reinforcements will survive for the full design life of the structure without impairment of their load-carrying ability as a result of degradation. Hence, knowledge of the durability of the materials used to reinforce soils and the potential changes in properties that may occur with time of exposure in a moist soil environment are of paramount importance.

An assessment of reinforcement durability must take two types of degradation into account: damage and deterioration due to physical factors such as abrasion during construction, sustained loading, cyclic loading, and temperature cycles; and deterioration due to chemical attack brought about by exposure to air, water, chemicals in the ground, and sunlight. Unfortunately, the complexities of corrosion, which is the major process leading to deterioration of metallic reinforcements, and the relatively short experience record for the nonmetallic reinforcement materials, mean that considerable uncertainty surrounds the incorporation of durability aspects into design of reinforced soil structures. This explains both some of the conservatism used by designers in the selection of reinforcement quantities and the extensive ongoing research on the durability of reinforcing materials.

The corrosion of metallic reinforcements, the degradation of nonmetallic reinforcements, the means for assessing durability in reinforcement applications, and the approaches to incorporating corrosion and durability into design are considered in this chapter. Emphasis is on the reinforcing elements that are buried or inserted in the soil. The durability of concrete facing elements is not discussed, because in almost all cases conventional reinforced concrete design and construction practices will ensure that it is adequate.

CORROSION OF METALLIC REINFORCEMENTS

Definition and Description

Corrosion is primarily an electrochemical process. For it to occur there must be a potential difference between two points that are electrically connected in the presence of an electrolyte. In the case of buried metals, the electrolyte solution consists of soil pore water containing oxygen and dissolved salts.

In the initial or anodic step of the corrosion process metal cations go into solution. Continuation of the process requires neutralization of the residual electronegativity, which forms the cathodic reaction step, and involves oxygen reduction and hydrogen evolution. Oxygen availability is a major factor controlling corrosion rate.

Different types of corrosion are associated with different types of metals. Galvanized steel and black steel corrode relatively uniformly, which means that strip reinforcements of these materials lose thickness more or less uniformly as corrosion proceeds. Metals such as stainless steel and aluminum alloys are protected by a film of oxides. If this protective layer is locally damaged, pitting and rapid corrosion can ensue [Weatherby (*1*)]. Corrosion rates in these materials are more difficult to evaluate.

Factors Controlling Corrosion Rate

The most important factors influencing the corrosion rate of buried metals are: content of dissolved salts, pH, porosity, and degree of saturation.

The most comprehensive data available on the corrosion of buried metals were obtained in field tests done by the National Bureau of Standards and reported by Romanoff (*2*). Extensive field testing of plain and galvanized metal culverts was done from 1910 to 1955, as well as testing of many types of ferrous and other metals, with and without protection, which were buried in many different soils at different locations. A full range of soil types from clean, granular materials to clay, muds, and peat were included, only some of which are typical of those used in reinforced soil structures.

From these and other studies [Juran (*3*)], it has been established that a high content of total dissolved salts, a high chloride concentration, a high sulfate content, and acidic or alkaline pH conditions produce the highest corrosion rates. Chloride concentration up to 200 ppm and sulfate contents up to 1,000 ppm have no significant effect, however. The electrical resistivity of the soil is an excellent measure of the dissolved salt concentration, so it is a commonly used index of potential corrosiveness. The resistance to corrosion of a number of materials that have application as ground reinforcements have been compared by King (*4*) and are shown in Table 21.

Table 21. Corrosion resistance of reinforcement materials. (Source: Ref. 4).

Soil Property \ Material		Mild Steel	Galvanised Steel	Aluminum Coated (Calorised) Steel	Lead-coated Steel	Low-Alloy Steel	High Alloy Steel	Aluminum and Alloys	Glass Reinforced Plastic (GRP)	Copper	Copper Steels
Resistivity Ω cm	< 700	xx	x	x	✓	xP	✓	xx	✓✓	✓	x
	700-4000	x	x	✓	✓	✓P	✓✓	x	✓✓	✓	✓
	> 4000	✓✓	✓✓	✓✓	✓✓	✓✓	✓✓	✓✓	✓✓	✓✓	✓✓
Redox Potential mV NHE	> 400	✓✓	✓✓	✓✓	✓✓	✓✓	✓✓	✓✓	✓✓	✓✓	✓✓
	200-400	✓	✓	x	✓	✓	✓✓	x	?	✓	✓
	< 200	xx	xx	xx	x	xxP	x?	xx	?	x	x
Moisture Content %	> 80%	✓	✓	✓	✓	✓	✓	✓	✓	✓	✓
	10-80%	x	x	x	✓	✓	✓	x	✓	✓	x
	< 10%	✓✓	✓✓	✓✓	✓✓	✓✓	✓✓	✓✓	✓✓	✓✓	✓✓
Dissolved salts		x	x	x	✓	✓	✓	xx	✓	x	x
chloride		x	x	xx	✓	xx	x	xx	✓	x	x
pH acidic	< 6	x	xx	xx	✓	x	✓	xx	✓✓	x	xx
neutral	6-8	✓✓	✓✓	✓✓	✓✓	✓✓	✓✓	✓✓	✓✓	✓✓	✓✓
alkaline	> 8	✓	x	xx	x	✓✓	✓✓	xx	✓✓	✓	✓✓
Organic acids		x	x	x	xx	✓	✓	xx	?	xx	xx
		← coating intact →									

✓✓ generally unaffected in this environment
✓ affected only slightly
x affected
xx markedly affected
P pitting attack pronounced
? behavior unknown

Estimation of Corrosion Rate

The results of the NBS studies confirmed that the rate of corrosion decreases with time, at least in a quiet environment. Romanoff (*2*) proposed that the average loss of thickness for plain steel as a function of time can be expressed, as shown in Figure 69, by

$$x_1 = S_c\, t^n \qquad (35)$$

where t is time in years, S_c is a site characteristic, and m depends on the site, but is always less than 1.0.

The damping rate, expressed by m, is more significant than the initial speed of corrosion, determined by S_c.

The NBS also showed that for galvanized steel, the steel is not attacked as long as zinc is available. Initially zinc corrosion is damped, but once the zinc is entirely oxidized the rate becomes constant. Tests have not been conducted for a sufficient time beyond this point to indicate subsequent behavior. A conservative prediction might be made by assuming that after some particular time, for example 10 years, the corrosion rate of galvanized steel will equal the rate of nongalvanized steel at the same time. This leads to a thickness loss vs. time relationship similar to that shown in Figure 70. Galvanizing has the added

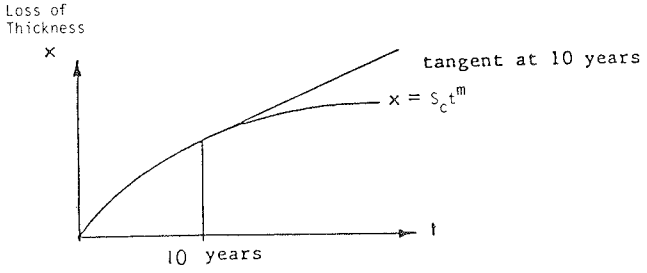

Figure 69. Development of corrosion with time.

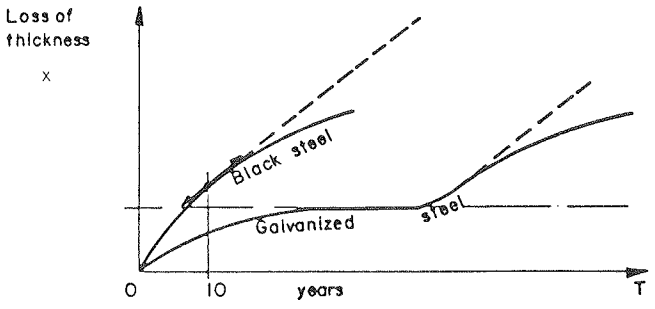

Figure 70. Comparison between galvanized steel and unprotected steel corrosion rates.

advantage of preventing formation of pits in the base metal during the highly aggressive period.

Applicable data from the NBS study (*2*) are replotted in Figure 71 to examine the influence of resistivity and pH on metal loss rate. No clearly defined relationship exists; however, there is a trend of smaller metal losses with increased resistivity, especially for resistivity values greater than 10,000 ohm-cm. On the basis of pH alone the plot in Figure 72 is obtained. Again, a well-defined relationship does not exist; however, there is a greater metal loss rate for pH values less than about 4.5. From the data in Figures 71 and 72 it appears that in the pH range of 4.5 to 9.5, the average metal loss will be of the order of 0.15 oz/sq ft/yr, with a maximum of 0.25 oz/sq ft/yr, without regard to the grain size characteristics of the soil and assuming that metal loss on galvanized steel can be extrapolated linearly from the 10-year values.

Further analysis of the NBS data relative to the internal drainage characteristics of the test soils indicates significantly smaller losses in well-drained, aerated soils, as may be seen in Figure 73. Soils of this type are more typical of those used in permanent reinforced soil structures. The metal loss rates, which average 0.08 oz/sq ft/yr with a maximum of 0.15 oz/sq ft/yr are about one-half those in poorly drained soils.

A synthesis of available data on corrosion rates from the NBS study, from in-situ observations of buried plain steel pipe [Electricite de France (*5*)], from studies of galvanized steel culverts [Haviland et al. (*6*)], from observations of steel piles [Romanoff (*7*)], from observations of Reinforced Earth structures built since 1968, and from laboratory tests [Darbin et al. (*8*)] show that corrosion loss rates for both zinc and steel can be represented as shown in Figure 74. There is a rather rapid loss in the first 2 or 3 years for both galvanized and bare steel followed by a progressive decrease in rate of corrosion.

A conservative approach for prediction of corrosion loss for use in design has been developed by the Reinforced Earth Company and the same procedure is used for design of VSL Retained Earth. It is based on the assumption that the continuing loss rate of bare steel, V_2 in Figure 74, would occur after all the zinc coating on a reinforcement is used in a sacrificial manner. Thus, estimates of the longevity of the zinc coating and of the

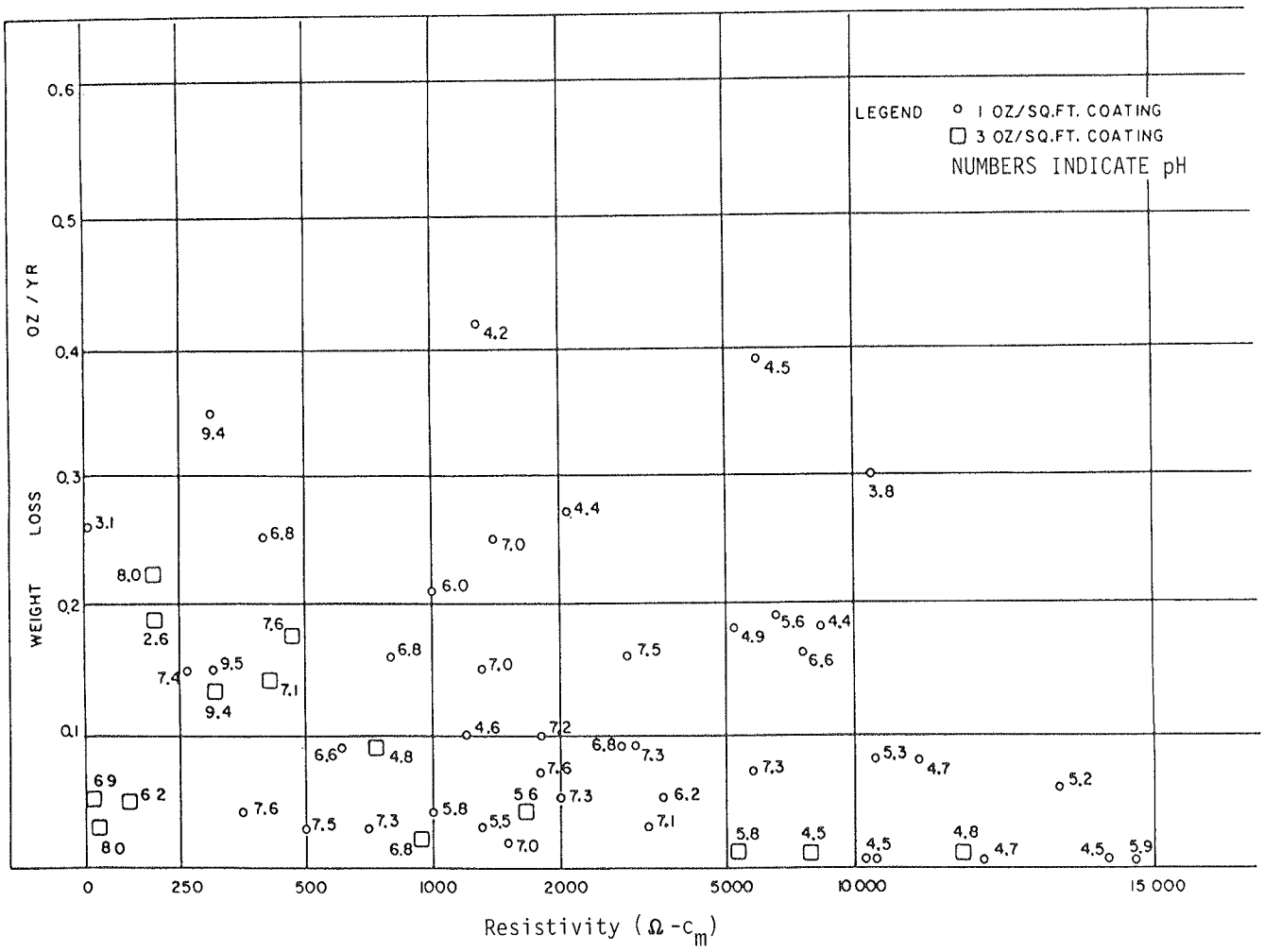

Figure 71. Corrosion rate as a function of resistivity and pH. (Source of Data: Ref. 2)

loss rate of the bare steel are required. Values of V_1 and V_2 are as follows.

Normal Backfill Soils. Soils in this category have corrosion index parameters in the following ranges:

pH in range 4.5 to 9.5
Resistivity > 1,000 ohm-cm
Chlorides < 200 ppm
Sulfates < 1,000 ppm

For these conditions:

Zinc: $V_1 = 6$ μm/year (0.24 mil/year) (first 2 years)

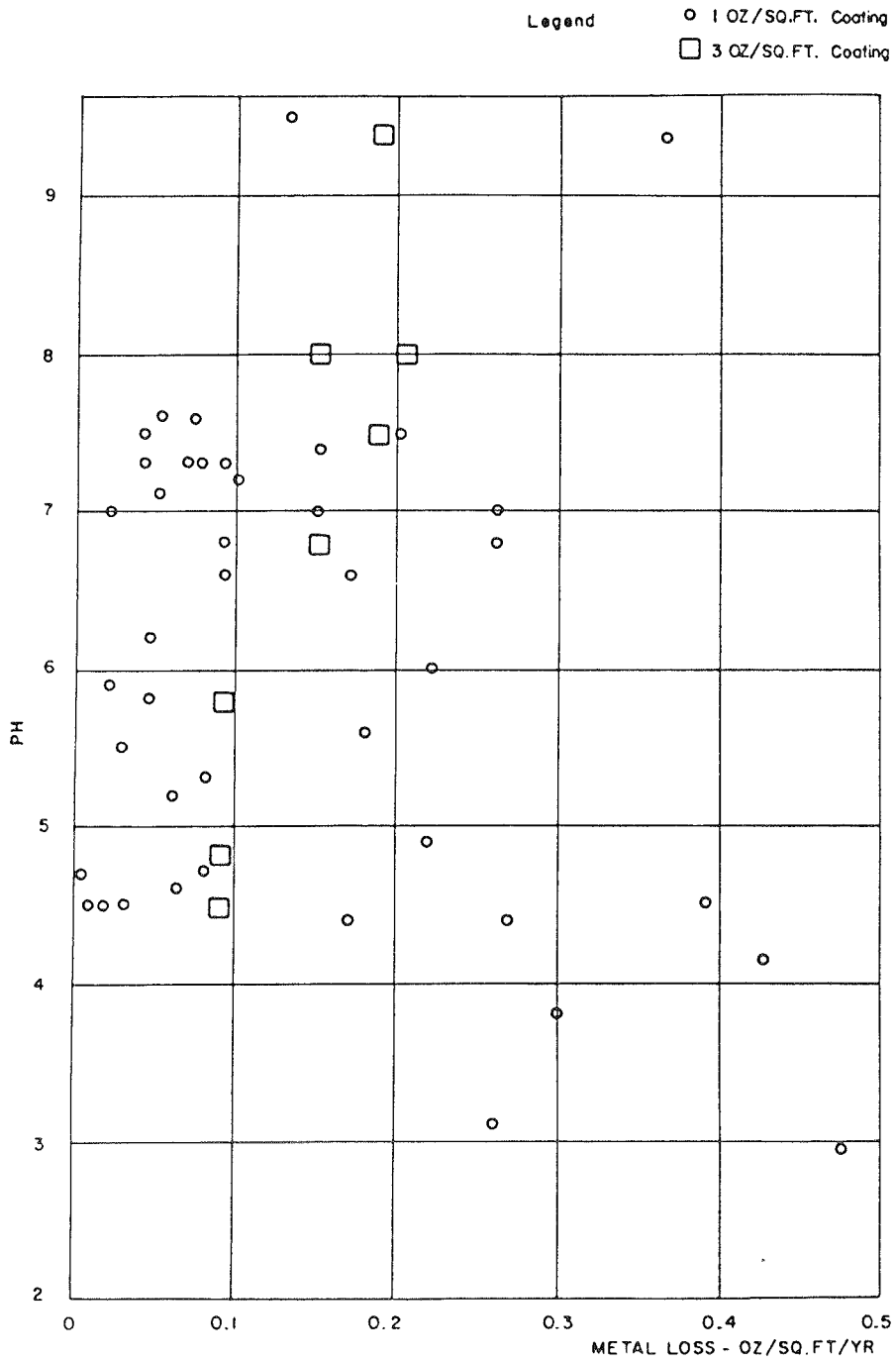

Figure 72. Corrosion rate as a function of pH. (Source of Data: Ref. 2)

V_2 = 2 μm/year (0.08 mil/year)

Carbon Steel: V_1 = 45 μm/year (1.77 mil/year) (first 2 years)
V_2 = 9 μm/year (0.35 mil/year) (for resistivity range of 1,000 to 10,000 ohm-cm)
V_2 = 6 μm/year (0.24 mil/year) (for resistivity > 10,000 ohm-cm)

Saline Soils and Sea-Water Saturated Soils. When the chloride concentration exceeds 200 ppm:

Zinc: V_1 = 17 μm/year (0.67 mil/year) (first 3 years)
V_2 = 2 μm/year (0.08 mil/year)

Carbon Steel: V_1 = 80 μm/year (3.15 mil/year) (first 2 years)
V_2 = 12 μm/year (0.4 mil/year)

Using these curves, a corrosion loss allowance can be made in the selection of a reinforcement cross section so that a sufficient area of steel will remain at the end of the required serviceability period to resist the applied tensile stresses.

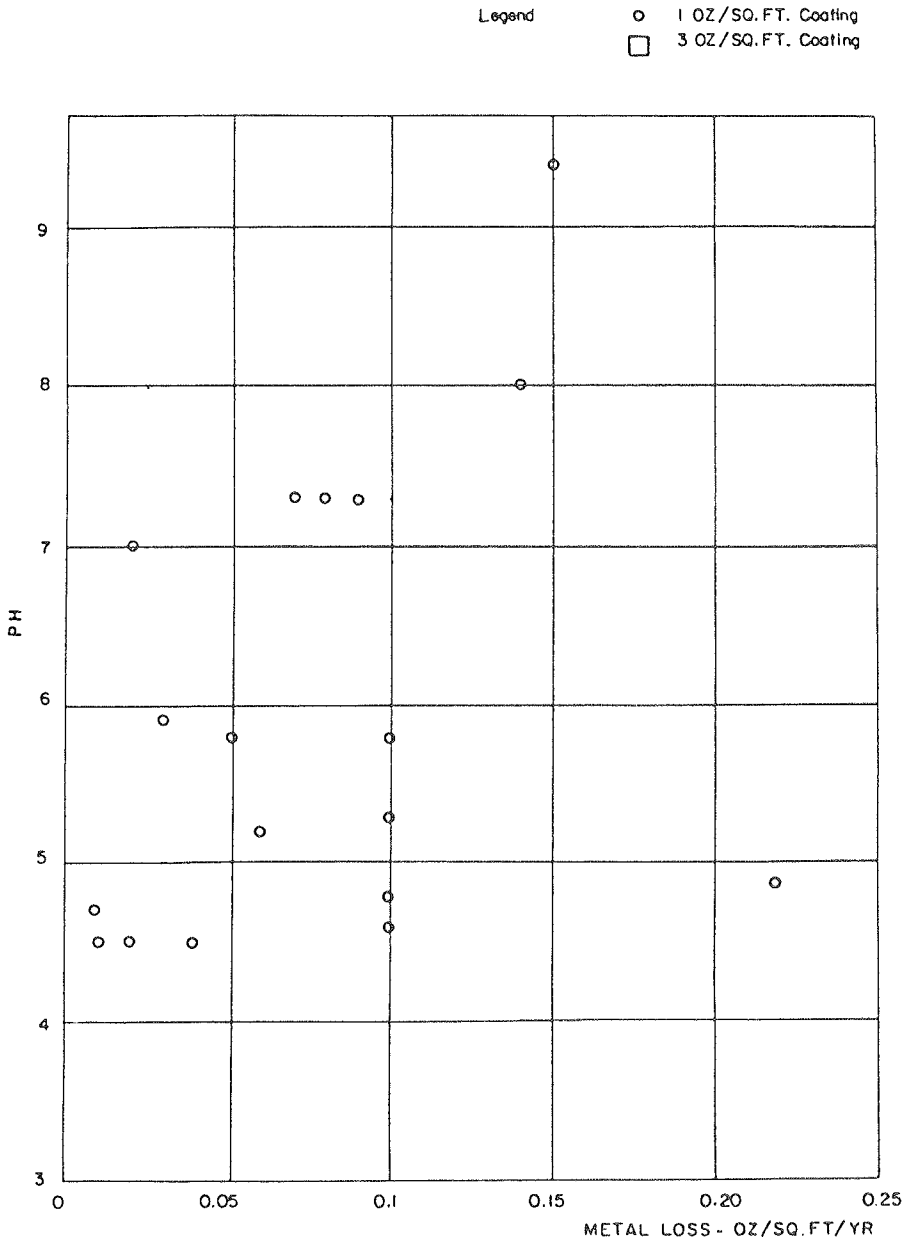

Figure 73. Corrosion rates in well-drained soils. (Source of Data: Ref. 2)

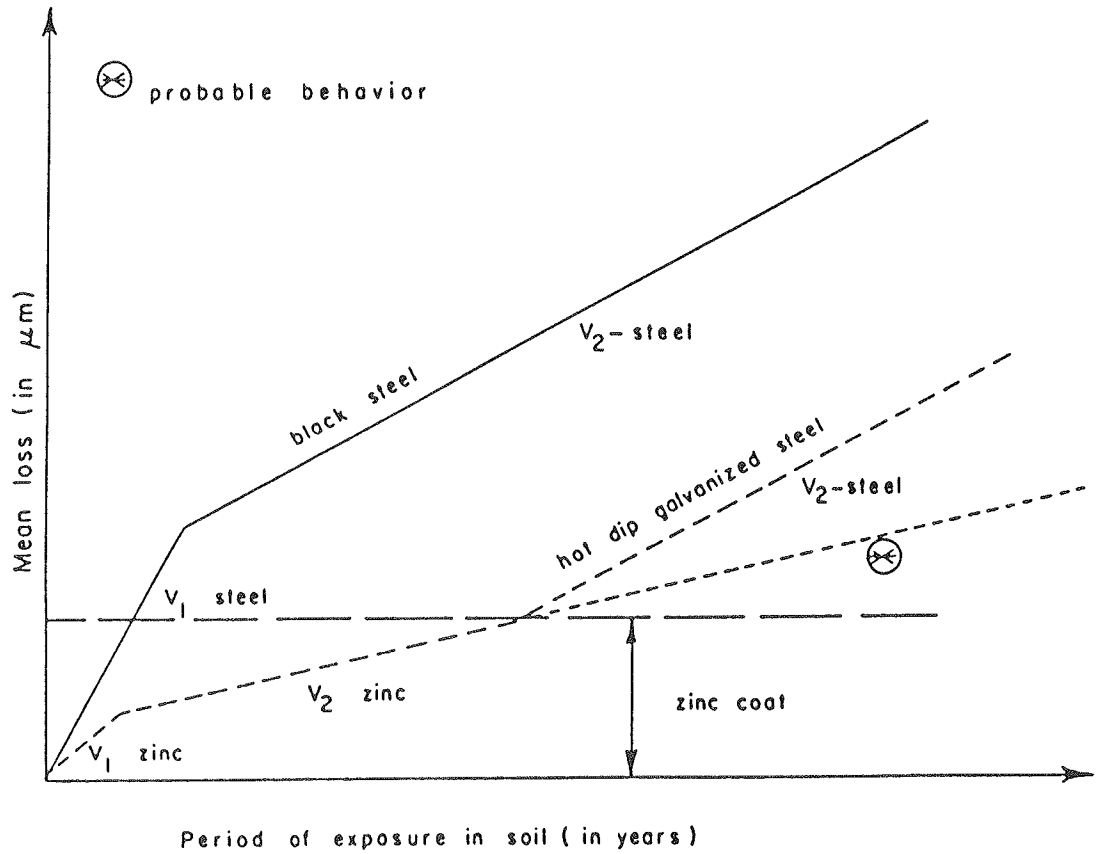

Figure 74. Schematic relation between corrosion loss and time derived from available field observations and laboratory test data.

An alternative approach for estimating corrosion rates is illustrated by the method used by the State of California Department of Transportation (*9*). The cross-sectional area remaining on steel reinforcing elements after corrosion loss is determined using the following algorithms:

Round Rod Types:

$$A = \frac{[D - 2K(Y - C)]^2}{D^2} \times 100 \text{ Percent} \qquad (36a)$$

Flat Strap Types:

$$A = \frac{[W - 2K(Y - C)]\,[T - 2K(Y - C)]}{(W)\,(T)} \times 100 \text{ Percent} \qquad (36b)$$

where A = percent of original cross-sectional area remaining (round calculated values of A to the nearest 5 percent); D = original diameter, in.; W = original strap width, in.; T = original strap thickness, in.; Y = time of exposure in soils, years; K = general corrosion rate factor; and C = useful life of coating, years (for bare steel, $C = 0$).

The general corrosion rate factor, K, is dependent on the type of backfill, and the total dissolved salt content, chloride and sulfide concentration and pH, and can be determined from Table 22. The useful life of coating, C, is then obtained from Table 23.

Table 22. General corrosion rate factors for Caltrans design criteria.

Chemical Environment	pH	R (ohm-cm)	Cl^- (mg/kg)	SO_4^- (mg/kg)	General Corrosion Rate Factor, K	
					Normal Backfill	Select* Granular
Neutral & Alkaline	≥7	≥1000	<500	<2000	.0011	.0005
Acidic	<7	≥1000	<500	<2000	.0013	.0005
Corrosive		<1000	<500	<2000	.0028	.0010
Very ** Corrosive		<1000	≥500	≥2000		

*Select granular backfill is that conforming to the following criteria:

Sieve Size	Grading Limits Percent Passing
6 inches	100
3 inches	100-75
No. 4	25-0
No. 200	5

** Not recommended

Tests to Determine Corrosion Rate

The methods described in the preceding section are based on knowledge of certain soil parameters and correlations between

Table 23. Assumed useful life of coatings for Caltrans design criteria.

Soil Type* and Chemical Environment	Useful Life of Coating, C, years		
	Paint	Galvanized 2 oz./ft^2	Galvanized 3 oz./ft^2
Normal			
Neutral & Alkaline	5	10	15
Acidic	5	10	15
Corrosive	5	6	9
Select Granular**			
Neutral & Alkaline	5	20	30
Acidic	5	20	30
Corrosive	5	12	20

*See Table 22

**Specifically selected well-draining backfill as defined by Table 22

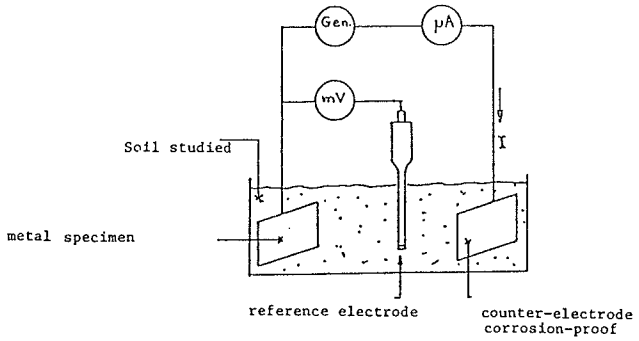

A) Principle of Measurement Method Center

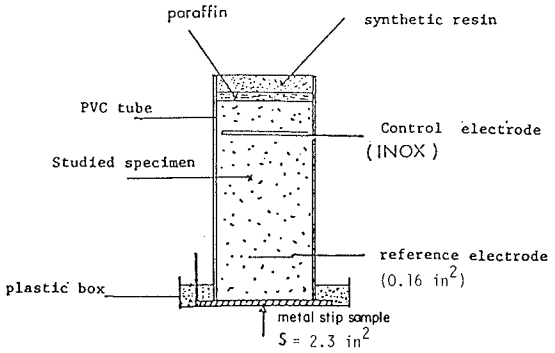

B) Corrosion Cell

Figure 75. Corrosion test in electrochemical cells. (Source: Ref. 8)

these parameters and rate of corrosion. Four types of tests have also been used for assessment of the corrosion rate of buried reinforcements: (1) tests in boxes, (2) tests in electrochemical cells, (3) measurement on reinforcements in actual structures, and (4) full-scale experiments on actual structures that are caused to fail by accelerated induced corrosion.

Tests in Boxes. In box tests, specimens are placed into wet soils of well-established properties, and weight loss is measured as a function of time. Because of the limited volumes of material and short test durations, the suitability of such tests for yielding results representative of actual field conditions is questionable.

Tests in Electrochemical Cells. The principle of this test is that the current generated during the corrosion process is related to the amount of metal dissolved per unit time according to Faraday's Law. The principle of the measurement is shown in Figure 75(A) [Darbin et al. (*8*)]. Two electrodes are placed in the cell as shown. In the absence of an electrolytic current flow, an electrochemical potential is generated at the electrode by conversion of metal atoms into ions. This potential can be measured using a reversible reference electrode.

In addition, application of a potential difference between the test metal and the inert electrode causes a current to flow through the soil, and this current can be measured as a function of the potential. From the analysis of the data from the two measurements the corrosion current can be determined.

A schematic diagram for the corrosion cell used for such measurements is shown in Figure 75(B). Electrochemical cell tests can be useful for determination of the influences of dissolved salt concentrations on corrosion rates and for study of the influences of different substances as corrosion inhibitors.

Measurements on Actual Structures. Observations were made on 46 different full-sized Reinforced Earth structures that were built after 1968 and in service for up to 10 years. All contained galvanized steel reinforcements, and the original zinc coatings were 0.98 to 1.18 mil thick. The results of these determinations are compared in Figure 76 with predictions based on the NBS test results and with the results of box tests using several soil types as indicated [Darbin et al. (*8*)]. It is evident that the actual field losses were less than would have been predicted by either Eq. 35 or box tests.

Failure Test of a Full-Scale Wall. A full-scale Reinforced Earth wall, 20 ft high, was designed to fail by accelerated corrosion of its nongalvanized steel strips [Guilloux and Jailloux (*10*)]. The initial strip thickness was 2.36 mil. Corrosion was induced by spraying salty water on the backfill surface. After several days of salt-water treatment the salt concentration in the backfill rose to 1,500 ppm, and the resistivity dropped to 500 to 1,000 ohm-cm.

Weight and thickness losses as a function of time were determined and the results are shown in Figure 77(a). Agreement between the measured values and Eq. 35 using $S_c = 23$ and $m = 0.55$ is excellent. Decreases in the tensile strength and elastic limit of the steel were also measured, as shown in Figure 77(b). At failure, the tensile resistance and the elastic limit were equal.

Methods for Delaying and Minimizing Corrosion

The most widely used means, thus far, for controlling the corrosion of metallic reinforcements in reinforced soil structures has been zinc galvanizing. Economic, structural, and durability factors have limited the use of other metals (e.g., stainless steel, aluminum, alloys).

Nonaggressive backfills should be used whenever available, and designs should allow for good drainage and minimize the risk of influx of aggressive chemicals.

Highly resistant epoxy resin coating materials and methods for their application are now becoming available that may prove effective and economical for routine application in earth reinforcement. Epoxy-coated welded-wire mats and strip reinforce-

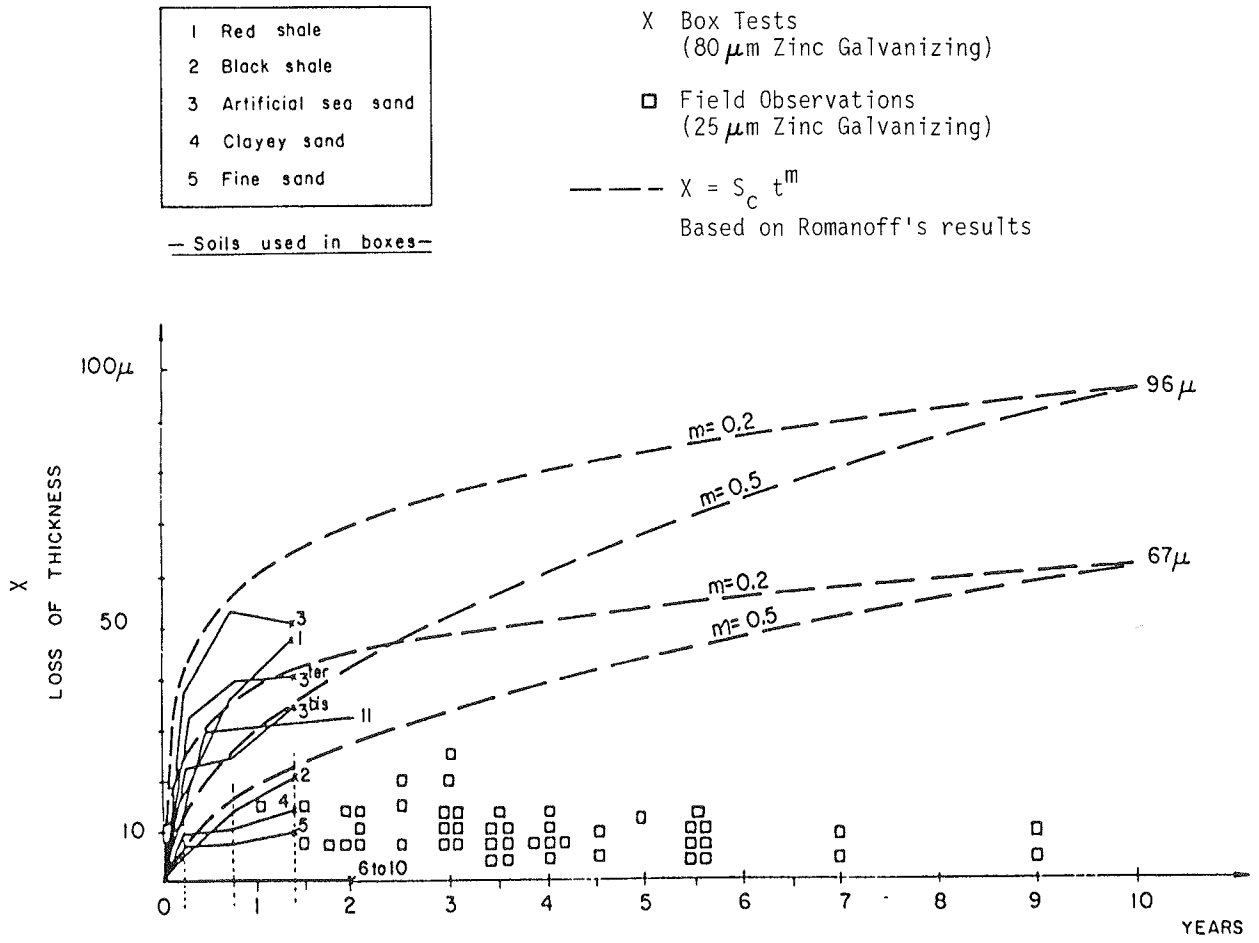

Figure 76. Comparison of predicted and observed corrosion losses for galvanized reinforcement strips.

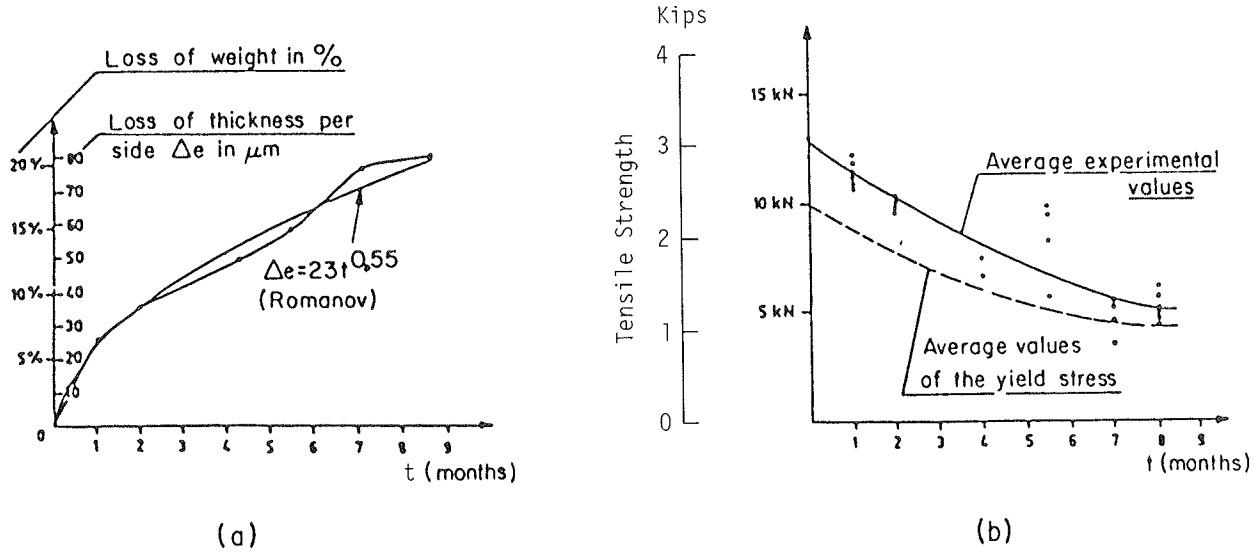

Figure 77. Full-scale failure test by accelerated corrosion. (Source: Ref. 10)

ments are now available for use in earth walls in corrosive regimes. This coating appears to be sufficiently hard and durable to withstand abrasion under normal construction conditions.

Importance of Quality Control

When coated reinforcing materials are used, care must be exercised to prevent abrasion or anything else that could produce local exposure of corrodable base metal during handling, placement, and backfill compaction. Such spots could serve as the initiators of local electrolytic cell formation and the subsequent pitting of the reinforcement. Ideally, coatings should be applied after the reinforcements are either welded or bent to the desired shapes.

Coating and galvanizing processes must be monitored to ensure that the specified thickness is obtained uniformly over the reinforcement. Imperfections will lead to local corrosion, and this will be difficult or impossible to detect after the structure is completed. These local failures could compromise the stability of the whole structure. It is, therefore, clear that close material inspection is required at the outset.

Corrosion Monitoring

Because the reinforcements are hidden from view in reinforced soil structures, direct observation of corrosion rate cannot be made without incorporation of special features at the outset. Periodic sampling and testing of the backfill can provide an indication of changed conditions that could lead to increased corrosion rates. The pH and electrical resistivity measurements are particularly useful.

If a more positive means for monitoring corrosion rate is desired, dummy reinforcements can be placed in the backfill that can be retrieved periodically by pulling them out through the wall or slope facing. There is some uncertainty even with this method, however, because the response of reinforcements under load to corrosion is different from the response of the same material in a stress-free state [Weatherby (*1*)]. Nonetheless, this is probably the most reliable method presently available.

Corrosion Considerations in Reinforcement of In-Situ Soils

When steel bars are used for reinforcement of the existing ground as, for example, in the case of soil nailing, there are additional factors that must be considered. In these applications there is no choice of soil type; thus, if aggressive soils are encountered, the reinforcements must be designed accordingly or a conventional slope stabilization technique must be used.

High strength steel may be used for soil nailing. Corrosion of high strength steel under tension develops at crystal interfaces. It is called "intergranular corrosion" and proceeds from the surface of the steel inwards. This type of corrosion is difficult to analyze. At present, the decrease in tensile strength because of intergranular corrosion cannot be predicted.

Often the steel bar is surrounded with grout, so there is no direct contact between the soil and the steel. Only if there is microcracking of the grout can water and oxygen come into contact with the steel and initiate corrosion processes. There is no rational basis for predicting the rate of corrosion under such conditions. A very conservative approach is to assume that the grout has no effect and the corrosion rate is the same as for the steel buried directly in the ground.

The increasing use of soil nailing in permanent structures means that special measures must be taken to minimize or prevent corrosion. One such measure [Appendix C and Weatherby (*1*)] is to surround a high strength steel bar with grout, which is, in turn, surrounded by a steel or plastic casing. Prestressing of the steel bars may also be done so as to keep the grout always in compression, thus preventing water entry through microcracks.

DURABILITY OF NONMETALLIC REINFORCEMENTS

The durability of the nonmetallic materials that are used for earth reinforcement (geotextiles and plastics) may be impaired by the effects of three categories of influences: (1) degradation due to mechanical damage, (2) loss of strength and elongation due to loading, and (3) deterioration as a result of exposure.

Some general considerations relative to each of these are presented in this section. More specific information and details are given in Appendixes A and B.

Factors Controlling Degradation Rate

Mechanical Damage. Mechanical damage to geotextiles and plasic reinforcements, such as geogrids, most commonly occurs during construction. Types of damage may include abrasion and wear, punching and tearing failures, and scratching, notching, and cracking of the harder, more brittle materials. Avoidance of this type of damage can only be achieved by care during storage, handling and placement of the material, and during backfill placement and compaction. It is particularly important that construction equipment does not traffic directly on the material. If angular stone and gravel are present in the backfill, tests should be done to determine whether they puncture geotextiles when dumped and compacted. When geotextiles are exposed, as has been the case for some fabric wall facings, vandalism has been a source of mechanical damage. For this reason, and also to protect the material from degradation due to ultraviolet light exposure, a protective covering (usually shotcrete) is often used.

Strength Loss Due to Loading. The geotextiles and plastics used in earth reinforcement are subject to more or less constant confining stresses due to overburden and tensile stresses resulting from the lateral earth pressure. The polymer materials used to fabricate these reinforcing materials are susceptible to creep elongations under sustained stresses, and there may be internal structural changes that cause a loss of strength with time [Finnigan (*11*); Van Leeuwen (*12*)].

A typical relationship between fabric strain under a constant tensile load and time is shown in Figure 78. Primary creep is defined as the initial period during which strain increases at a decreasing rate. Secondary creep follows, characterized by a more or less constant rate of strain. Tertiary creep, at an increasing rate of strain, may develop if the stress level is greater than some threshold value. For stresses above this value the time to onset of tertiary creep decreases with increasing stress.

The behavior of a geotextile during the primary creep phase is significantly influenced by fabrication method (e.g., needle-punched, bonded, woven) because of fiber reorientation. The behavior during secondary creep is generally dependent on filament characteristics [Koerner et al. (*13*); Shrestha and Bell (*14*); Bell and Green (*15*)].

In both phases of creep, polyester fabrics tend to creep less than polypropylene fabrics. Primary creep strains are greatest for needle-punched fabrics and least for the bonded and woven materials.

Deterioration Due to Exposure. Nonmetallic earth reinforcing materials may be adversely affected by prolonged exposure to water and chemicals in the ground, to sunlight, and as a result of temperature changes.

Although temperature variations within the normal ranges encountered in the ground may result in some variations in the stress-strain and strength properties, these variations are generally not of sufficient magnitude to significantly affect performance. Continuous exposure to temperatures above 60°C (140°F) can result in thermal embrittlement of some materials, such as low density polyethylene. Allen et al. (*16*) found that the strength of geotextiles was not adversely affected by long exposure to subfreezing temperatures, and geotextiles are now routinely used in the arctic.

Polypropylene filaments do not absorb moisture, so geotextiles made of this material are not influenced by exposure to water. Polyester filaments do absorb some moisture which leads to hydrolysis [McMahon et al. (*17*); Fuzek (*18*)]. Some increase in creep deformations and loss of strength may occur in the long term.

Most of the geotextiles are very resistant to chemicals, so degradation due to chemical attack will not normally be a problem, unless the material is used in connection with a chemical storage facility or there is a chemical spill. Organic solvents can cause some swelling at low temperatures; however, high temperatures (e.g., 200°F) are required for damage to become excessive [Sotton and Leclercq (*19*); Rhone Poulenc Industries (*20*)]. Acids, bases, and seawater have been shown not to have any significant effect.

Significant decreases in tensile strength and elongation to failure can result from exposure to sunlight. The short wavelength ultraviolet (UV) radiation in sunlight breaks chemical links of the polymer fibers. Although all geotextiles degrade with exposure to UV light, some have higher resistances which allow temporary exposures for construction purposes. These differences are illustrated by Raumann (*21*) in Figure 79, where 11 different geotextiles were exposed over a year and then tested mechanically. These tests indicated that polyester fibers generally had a higher resistance to outdoor exposure degradation than polypropylene geotextiles, except when the polypropylene is treated with a significant amount of carbon black. Some of the untreated unwoven polypropylene fabrics lost over 50 percent of their strength after 8 weeks and disintegrated after 16 weeks. Thicker fabrics of the same polymer (B2 vs. B1) apparently had better resistance to UV light because of shielding action. The size of individual fibers also influences their resistance to UV light degradation. The same duration of exposure produces the same depth of influence on the fibers and thereby produces a higher proportion of degradation of the cross-sectional area of a small-diameter fiber than a large-diameter fiber.

Provided that care is taken to prevent extended exposure to sunlight during stockpiling and construction, UV degradation is unlikely to be important for buried reinforcements. Adequate protection should, however, be provided for exposed sections through use of asphalt, shotcrete, or earth covers.

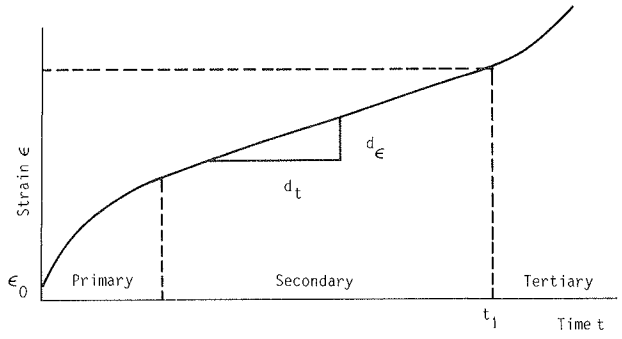

Figure 78. Creep of fabric under constant stresses.

Evaluation of Durability

There are a number of ASTM test methods for evaluation of geotextile mechanical properties that can be applied to geotextiles used as reinforcements in soil. Thus, properties of interest can be measured on samples before and after exposure, and the effects of degradation can be assessed. Unfortunately, data for geotextiles that have been used in actual reinforcement applications for long time periods are not yet available, and there is no assurance that laboratory tests on isolated samples give a relevant simulation of the actual field conditions.

Several laboratory test methods [Sotton and Leclercq (*19*)] have been proposed to study the degradation of geotextiles due to UV light exposure or chemical attack. None realistically model the complexity of outdoor exposure conditions or provide a completely reliable basis for extrapolation of short-term test results to long-term behavior. Thus considerable uncertainty remains concerning means for evaluating the durability of nonmetallic reinforcements.

Nonetheless, it may be sufficient in many cases to know if a proposed material is susceptible to degradation and, if so, the extent of deterioration that could develop under extreme conditions. Some of the test methods that are commonly used are given in Table 24.

Quality Control and Monitoring

In most applications monitoring of internal conditions is not crucial, because geotextiles and plastics are highly resistant to chemical attack. On the other hand, exposed portions of these materials are susceptible to UV degradation; any potential problem areas should be readily visible and protective covering can be applied during and after construction.

In any case, where there is concern for the long-term durability of buried reinforcements, dummy sections can be buried at the time of construction and recovered at a later date for assessment of their condition and, hence, their degree of deterioration.

Damage due to abrasion, tearing, and puncture is likely to be the major concern in most cases. To avoid problems from

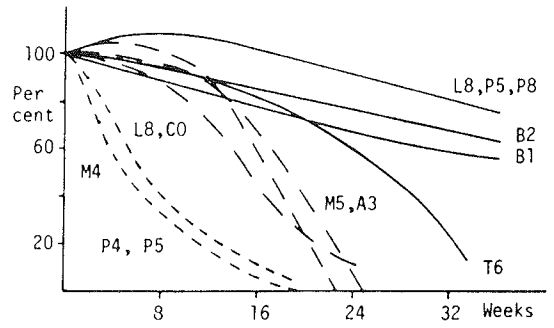

A) Strength Retained

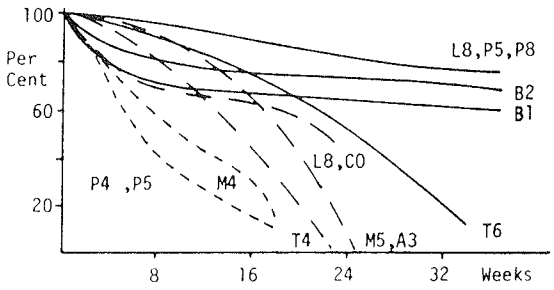

B) Elongation Retained

Fabric Code	μ* kg/m²	Polymer,Construction Color †		Grab F_G, kN MD	Grab F_G, kN TD	Grab ϵ_G, % MD	Grab ϵ_G, % TD
B1	.150	PE,C,N,NW	Grey	.658	.560	74	83
B2	.270	PE,C,N,NW	Grey	1.041	1.133	64	67
B6	.160	PE,C,N,NW	White	.534	.455	72	89
C0	.270	PP,C,N,NW	Buff	1.170	.791	110	158
F2	.360	PP,S,N,NW	White	.734	1.205	129	112
M4	.150	PP,C,B,NW	White	.525	.511	127	124
T4	.135	PP,C,B,NW	Grey	.609	.484	60	69
T6	.200	PP,C,B,NW	Grey	1.112	1.023	58	69
S4	.125	PP,S,B,N,NW	Grey	.436	.502	51	52
S5	.170	PP,S,B,N,NW	Grey	.498	.703	60	67
M5	.140	PP,C,W,SF	Buff	.823	.925	21	18
A3	.105	PP,C,W,SF	Buff	.609	.418	21	16
P8	.260	PP,C,W,MF	Black	2.063	1.325	26	32
L8	.235	PP,C,W,MF	Black	1.965	1.125	27	32
P5	.175	PP,C,W,MF	Black	.712	.832	22	25

† Key: B = heat bonded, C = continuous filament, MF = monofilament, N = needled, NW = nonwoven, PE = polyester, PP = polypropylene, S = staple fibers, SF = slit film, W = woven

* Mass per unit area

C) Fabric Description and Grab Test Results

Figure 79. Effects of outdoor exposure on geotextile strength and elongation at failure. (Source: Ref. 21)

these causes care in handling of the materials and during construction is needed. Construction crews and inspectors must understand the causes of mechanical damage and adopt procedures to avoid them.

INCORPORATING DURABILITY INTO DESIGN

Durability considerations play a major role in the design and economics of earth reinforcement systems. Modes of degradation of metallic and nonmetallic reinforcement materials, methods for evaluating durability, methods for predicting degradation rates, and considerations in construction to minimize deterioration of materials have been discussed in this chapter. It is clear that present knowledge is not complete. Consequently, conservatism in design is mandated to ensure safe performance for the full design life.

Current practice for incorporating corrosion of metallic reinforcements into design is to estimate the metal loss that will occur during the design life and to use sufficient metal cross section that enough will remain at the end of the period to retain the desired factor of safety against reinforcement rupture. Two approaches are used to evaluate the required cross sections. Both are normally used for design of galvanized steel reinforcements. However, they could also be applied to plain steel alone.

One approach assumes a relationship between corrosion loss and time of the form shown in Figure 74. Values for the coefficients V_1 and V_2 for steel and zinc are used as indicated under "Estimation of Corrosion Rate." In the other approach, the zinc coating is assumed to last for some specific time period and then loss of the underlying steel is assumed to occur at a constant rate. The remaining cross-sectional area can be determined from Eqs. 36a and 36b.

There is no generally accepted procedure for incorporating degradation of nonmetallic reinforcements into design. If the manufacturer's data or other sources of information indicate values for strength loss under sustained stresses, this information can be taken into account by the designer by designing for suitably low working stresses. Similarly, for specific geotextiles there may be data available about the influences of different types of exposure on strength and elongation properties that can be used.

In conclusion, rational methods exist to provide a given design life for metallic reinforcing elements in a given chemical environment. While this is not yet the case for plastics and geotextiles, these reinforcements are manufactured from some of the most resistant and durable materials known. Thus, the hesitancy of some engineers not yet familiar with earth reinforcement to make use of the techniques may reflect unnecessary conservatism.

REFERENCES

1. Weatherby, D. E., "Tiebacks." Federal Highway Administration, *FHWA/RD-82/047* (July 1982).
2. Romanoff, J., "Underground Corrosion." *National Bureau of Standards Circular 579* (Apr. 1957).
3. Juran, I., "Design of Reinforced Earth Structures." Notes from the Louisiana State University Short Course on Reinforced Earth, *Report GE-82/02* (1982).
4. King, R. A., "Corrosion in Reinforced Earth, Reinforced Earth and Other Composite Techniques." *TRRL Supplementary Report 457,* Transport and Road Research Laboratory, Crowthorne, Berkshire, England (1977).
5. Electricite de France, EDF-SPH, "Conduites Forcées." Enquête du 14/2/1957 (1957).
6. Haviland, J. E., Bellair, P. J., and Morrell, V. D.,

Table 24. Degradation tests.

Test	Reference	Resistance Tested				
		Abrasion	Radiation	Chemical	Thermal	Other
Trapezoidal Tear (outdated)	ASTM D2263	x				
Tongue Tear, Burst Strength	ASTM D751	x				
Impact Strength (Elemendorf Tear)	ASTM D1424	x				
Burt Tearing (Mullen Burst)	ASTM D774	x				
Cone Penetration Impact						
Abrasion Resistance, Trapezoidal Tear, Mullen Burst, Ball Burst						
Fatigue	ASTM D1682					
Resistance to Chemical Reagents	ASTM D543			x		
Resistance to Light and Weather	ASTM D1435		x			
Resistance to Temperature	ASTM D794, D746				x	
Burial Deterioration	National Research Council of Canada AATCC 30-1974 Federal Standard #121, method 5762 ASTM D774					x x x x
Tearing Resistance		x				
Geotextile-Ballast Impact Abrasion Test	Van Dine et al. (Ref. 22)	x				
Geotextile-Aggregate Repeated Loading Test	Van Dine et al. (Ref. 22)	x				
Simulated Vibrating Road	Gray (Ref. 23)	x				
Vibrating Steel Cones	Gray (Ref. 23)	x				
Modified Martindale Abrasion Tester	Gray (Ref. 23)	x				
Puncture	ASTM D3787	x				
UV Stability	FEDTM CCC-T191, #5804		x			
Accelerated Weathering						
Puncture Strength	U.S. Army Corps of Engineers CW-02215	x				

"Durability of Corrugated Metal Culverts." *Highway Research Record 242,* HRB, National Research Council, Washington, D.C. (1968).

7. ROMANOFF, M., "Corrosion of Steel Pilings in Soils." *National Bureau of Standards Monograph 127,* NBS Papers on Corrosion of Steel Pilings (1962–1971), (1972).
8. DARBIN, M., JAILLOUX, J. M., and MONTEUELLE, J., "Performance and Research on the Durability of Reinforced Earth Reinforcing Strips." ASCE Symposium on Earth Reinforcement, Pittsburgh, Penn. (1978) pp. 305–333.
9. CALIFORNIA DEPARTMENT OF TRANSPORTATION, "Corrosion of Earth Retaining Systems, Interim Design Criteria—1984." Corrosion Unit, Transportation Laboratory (1984).
10. GUILLOUX, A., JAILLOUX, J. M., "Comportement d'un mur experimental en terre armee vis-a-vis de la corrosion." *Proc. International Conference on Soil Reinforcement: Reinforced Earth and Other Techniques,* Paris (1979) Vol. II, pp. 503–508.
11. FINNIGAN, J. A., "The Creep Behavior of High Tenacity Yarns and Fabrics Used in Civil Engineering Applications." *Proc. International Conference on the Use of Fabrics in Geotechnics,* Paris (1977) Vol. II, p. 305.
12. VAN LEEUWEN, J. H., "New Methods of Determining the Stress-Strain Behavior of Woven and Nonwoven Fabrics in the Laboratory and in Practice." *Proc. International Conference on the Use of Fabrics and Geotechnics,* Paris (1977) Vol. 2.
13. KOERNER, R. M., ROSENFARB, J. L., DOUGHERTY, W. W., and MCELROY, J. J., "Stress-Strain-Time Behavior of Geotextiles." *Proc. ASCE Symposium on the Use of Geotextiles for Soil Improvements,* Portland (1980) p. 31.
14. SHRESTHA, S. C., and BELL, J. R., "Creep Behavior of Geotextiles Under Sustained Loads. *Proc. 2nd International Conference on Geotextiles,* Las Vegas (1982) Vol. III.
15. BELL, A. L., and GREEN, H. M., "Factors Influencing the Selection of Woven Polypropylene Geotextiles for Earth Reinforcement." *Proc. 2nd International Conference on Geotextiles,* Las Vegas (1982) Vol. III.
16. ALLEN, T., VINSON, T. S., and BELL, J. R., "Tensile

Strength and Creep Behavior of Geotextiles, in Cold Regions Applications." *Proc. 2nd International Conference on Geotextiles,* Las Vegas (1982) Vol. III, p. 775.
17. McMahon W., Birdsall, H. A., Johnson, C. R., and Camilli, C. T., "Degradation Studies of Polyethylene Terephthalate." *J. Chem. Eng. Data* (1959) Vol. 4.
18. Fuzek, J. F., "Glass Transition Temperature of Wet Fibers, Its Measurement and Significance." *ACS Symposium Series No. 127,* Paper 31 (1980).
19. Sotton, M., and Leclercq, B., "Geotextiles and Aging Tests." *Proc. 2nd International Conference on Geotextiles,* Las Vegas (1982) Vol. II, p. 559.
20. Rhone Poulenc Industries, "Reaction of Filaments and Monofilament Polyesters in an Alkaline Solution." Report included in *Terre Armee Internationale Information, Report No. 1* (1970).
21. Raumann, G., "Outdoor Exposure Tests of Geotextiles." *Proc. 2nd International Conference on Geotextiles,* Las Vegas (1982) Vol. II, p. 541.
22. Van Dine, D., Raymond, G., and Williams, S. E. "An Evaluation of Abrasion Tests for Geotextiles." *79th International Conference on Geotextiles,* Las Vegas (1982) pp. 811–816.
23. Gray, C. G., Abrasion Resistance of Geotextile Fabrics." *2nd International Conference on Geotextiles,* Las Vegas (1982) pp. 817–821.

CHAPTER SEVEN

FUTURE RESEARCH AND DEVELOPMENT

Contents

RESEARCH NEEDS

Modern earth reinforcement technology has developed very rapidly during the past 15 years. Thousands of structures have been built, and there have been but a very few failures of any type. Nonetheless, understanding of all aspects of earth reinforcement mechanisms is not yet complete, no generally accepted universal design methodology is available, some of the design methods may be overly conservative, some may incorporate unconservative assumptions for unusual wall geometries, there are unanswered questions about durability, and the full potential of all the systems has not yet been realized. Accordingly, several areas can be identified in which further research and development are needed.

- The load transfer and stress distribution between reinforcements and soil needs more careful definition for most earth reinforcement systems. Much of the data so far available pertain to Reinforced Earth and granular soil backfills. Interaction data for other reinforcement and soil types are needed, especially for systems which develop their resistance by bearing of transverse elements and by combined friction and bearing.
- A better understanding of the relationships between reinforced extensibility and horizontal earth pressures is needed. Consideration must be given in these studies to the influences of backfill type and construction procedures.
- Further determination of the locus of maximum tensile forces in reinforcements and the boundary between active and resistant zones is needed for reinforced structures of various types. The effects of structure geometry, backfill types, reinforcement types, applied loadings, and foundation soil conditions need to be studied. Model tests, centrifuge model tests, finite element studies, and instrumented full-scale structures can all provide useful information.
- Shear box tests, laboratory model tests, and numerical analyses have indicated that reinforcement orientation influences their effectiveness. Field verification is needed, and if the predictions are substantiated, new designs and construction techniques should be developed to take advantage of orientation where possible.
- Most available design methods do not consider the relative reinforcement-to-soil displacement required to mobilize the full reinforcement effect. Design methods are needed that not only consider this displacement, but can also predict the consequent displacement of the entire structure or excavation.
- The extent to which reinforcement can be used for construction of safe and cost-effective earth structures when only poor backfill soils are available needs further definition.
- The possibility for upgrading poor or marginal backfill soils by use of admixture stabilizers such as cement and lime should

be investigated. If suitable, the cost of the stabilization could be offset by savings in required reinforcement.

- Development and acceptance of a general methodology for design that can be readily understood and applied by engineers responsible for selection among alternative structure types for a given situation could be expected to broaden the appeal of earth reinforcement systems.
- Continued accumulation of field data on durability of reinforcements of various types under different exposure conditions in different soils is essential. The history of modern earth reinforcement is still short relative to the desired service life of most structures. Thus there has been no alternative but to rely on predictions based on short-term tests and on observations of buried materials used for other purposes. With time, the durability behavior of actual reinforcements can be better understood if suitable field monitoring observations are made. The long-term performance of the newly developed epoxy coatings for metallic reinforcements must also be evaluated.
- The design of soil reinforcement for seismic or other dynamic loading conditions has not been addressed in this report. Although there has not yet been any evidence of seismic damage to a reinforced soil structure, experience is limited and observations are still few. Further research is needed to ensure safety while maintaining economy.

FUTURE DEVELOPMENTS

It is now well established that soil reinforcement can provide safe and economical solutions to many earthwork problems. There is no doubt that soil will remain the least expensive and most abundant construction material. Current interest in the existing and new methods is high, and competition between developers and manufacturers is keen.

It is reasonable to expect that applications will increase in number and that technical advances will continue. This should lead to even more efficient reinforcement designs, more durable materials, and improved construction techniques.

APPENDIX A

FRICTIONAL REINFORCEMENT SYSTEMS

CHAPTER ONE—REINFORCED EARTH

Contents

1. INTRODUCTION

1.1 Physical Description

Reinforced Earth is a construction material consisting of a frictional backfill material and linear reinforcing strips, usually placed horizontally. The reinforcements, which are capable of withstanding high tensile forces, restrain the lateral deformation of the reinforced mass. Reinforced Earth retaining structures have three components: the backfill material, the linear reinforcing strips which, combined with the backfill, constitute the reinforced soil mass, and the facing, which has only a local role preventing the backfill material from sloughing away from the wall face. These components are shown in a schematic view of a Reinforced Earth wall on Figure A-1.

Except for the backfill material, Reinforced Earth is constructed using entirely prefabricated elements. This enables easy and rapid construction without the need for specialized workmanship, and also allows standardization and quality control. The prefabricated elements are the reinforcements, which are linear strips made of steel, galvanized to protect against corrosion; and the facing, which is made either of semielliptical metal elements or of prefabricated cruciform concrete panels.

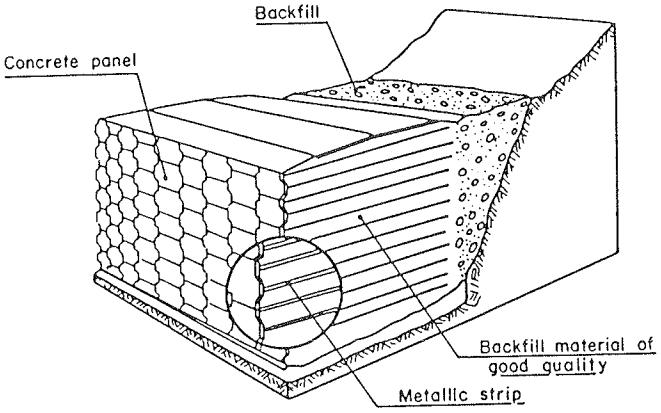

Figure A-1. Schematic view of a Reinforced Earth wall.

1.2 History and Development

The development of Reinforced Earth, since its introduction in 1963 by the French architect and engineer H. Vidal, was marked by the following milestones: (1) The first retaining wall was built in Pragneres, France, in 1965. (2) The first group of structures was constructed on the Roquebrune-Menton highway in the south of France during 1968 and 1969. Ten retaining walls with a total facing area of 6,600 sq yd were built on unstable slopes. (3) The first highway bridge abutment (46 ft high) was built in Thionville in 1972. (4) The first wall was built in the United States in 1972 on California State Highway 39 northeast of Los Angeles. It offered significant cost savings as compared with more conventional alternates for difficult hillside foundation conditions.

In late 1974, after a 4-year demonstration program, the Federal Highway Administration released Reinforced Earth from its "experimental category" and approved it as an economical and safe alternate to other earth retaining techniques.

Technological development was highlighted by two significant advances: (1) the introduction of concrete facing panels in 1971 (most Reinforced Earth structures are now built with this type of facing); and (2) the development in 1975 of ribbed reinforcement strips (these strips, made of ordinary mild galvanized steel, enable a large increase in the stress transfer capacity between the soil and reinforcemens, compared to smooth strips).

In the last 15 years more than 5,000 Reinforced Earth structures, representing over 27,000,000 sq ft of wall facing, have been completed in 37 different countries. Reinforced Earth is now in service as retaining walls, marine structures, retention dikes, bridge abutments, foundation slabs, slide buttresses, and other earth retention and load-supporting structures.

Substantial and continuous research and testing efforts have contributed to this rapid development. The research focused on: (1) fundamental mechanism of soil-reinforcement interaction as a function of the different types of soils and reinforcing strips; (2) failure mechanisms of Reinforced Earth structures; (3) study of structure behavior under working conditions; (4) development of appropriate design methods; (5) aging and durability of metallic reinforcements buried in the soil; (6) dynamic behavior characteristics of Reinforced Earth structures and resistance to seismic loading; (7) construction and aesthetic improvements; and (8) new fields of application.

1.3 Proprietary Restrictions

Reinforced Earth™ is a civil engineering material invented by Henri Vidal and subject to patents owned by him. The Reinforced Earth Company of Arlington, Virginia, is the exclusive licensee in the United States under Patents 3,421,326; 3,686,326; 3,981,038, and others covering the design, engineering, and construction of Reinforced Earth Structures for retaining walls and special applications of the Reinforced Earth method, such as bridge abutments and bulk storage facilities.

2. APPLICATIONS

2.1 Inherent Advantages

Reinforced Earth structures possess several features that are attractive in many situations requiring retaining structures. These advantages are common to most reinforcement systems and are described in Chapter Three of the main report in Part I.

2.2 Site Conditions Appropriate for Use

The choice of a Reinforced Earth structure for a specific site should take into consideration both environmental and geotechnical conditions.

As Reinforced Earth can withstand relatively high differential settlement, it has been successfully used in areas where unstable slopes have been encountered. As noted previously, the Roquebrune-Menton Highway structures, shown in Figure A-2, were built on unstable slopes of calcareous debris. The classical solution would have been rigid retaining walls based on deep piles, as shown. In some cases the use of Reinforced Earth has enabled a cost saving of 50 to 60 percent, as well as elimination of the risk of pile shearing which could be caused by an eventual movement of the unstable slope.

On the other hand, the construction of large Reinforced Earth structures on slopes often requires wide excavations, which can be critical with respect to the overall stability of the slope. Therefore, special precautions may be necessary during construction.

The behavior of a Reinforced Earth structure on a compressible foundation soil is comparable to that of an embankment. This consideration justified the choice of this technique rather than the use of deep piles for the construction of the first Reinforced Earth bridge abutment which was built at Thionville, France, in 1972. The 46-ft high abutment was built on heterogeneous compressible soil as shown in Figure A-3. The choice of Reinforced Earth for this particular case resulted in a cost saving of 60 percent.

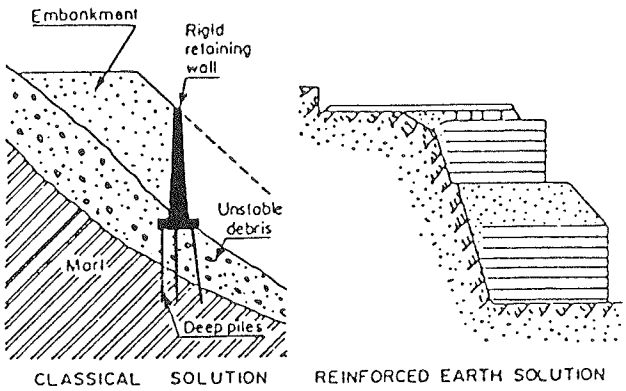

Figure A-2. Application of Reinforced Earth in mountainous areas. Comparison with a classical solution. [Roquebrune-Menton Highway, 1968]

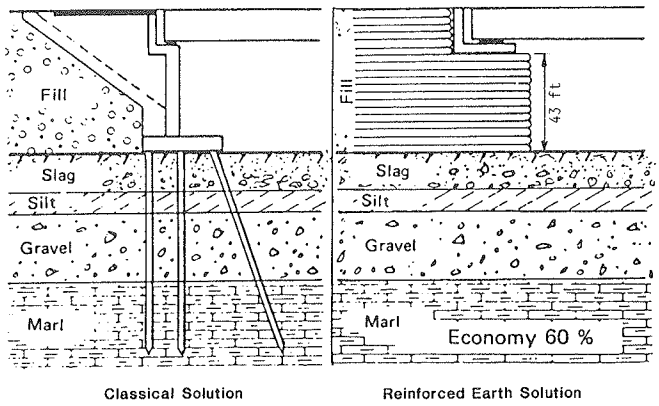

Figure A-3. The Reinforced Earth bridge abutment in Thionville, France. Comparison with a classical solution.

In urban areas, where environmental considerations can have significant design influence (such as restricted sites and difficult scheduling), Reinforced Earth can provide innovative solutions to both architectural demands and space limitations. Since construction requires no forming, pouring, or curing, it is not only rapid but takes place behind the wall face, with no scaffolding or form work to interrupt traffic. Structures can be built very close to property lines without incurring additional cost and can easily follow curving alignments. Prefabricated architectural finishes can be provided at relatively low cost to better integrate structures into urban surroundings.

The main limitation of the Reinforced Earth technique concerns the choice of the backfill material. This technique cannot be used unless a suitable frictional backfill material is available to ensure the necessary stress transfer and pullout resistance between the soil and the reinforcements. Furthermore, the back-

fill material should not be corrosive to the metallic reinforcing strips.

The present state of technological development does not yet enable reliable Reinforced Earth construction under water.

2.3 Routine and Special Applications

2.3.1 General Considerations

The main application of Reinforced Earth has been for retaining structures, walls, and bridge abutments. However, some other structure types, such as foundation rafts, sloping walls, containment dikes, underground chambers, and dams, have also been built.

2.3.2 Special Applications

Reinforced Earth has been used for seawalls, bulkheads, quays, and dams. These structures, because of their flexibility and mass, are capable of withstanding the severe forces imposed by storm wave action and currents, tides and floods, driven pack ice, and even the impact of boats and barges. A typical seawall cross section is shown in Figure A-4. The speed of Reinforced Earth construction, along with its capacity to stage construction in small sections if necessary, reduces the risk of storm or flood damage during construction.

As a coherent yet flexible gravity mass, Reinforced Earth is particularly well suited for construction in seismically active regions. The structures provide the high degree of structural damping needed to absorb large energy releases associated with earthquakes.

For these same reasons, Reinforced Earth has proven effective in supporting high-speed railway lines, the heavy and shifting loads of haul vehicles at mines and crushing or sampling plants, and as blast protection structures at military installations and munitions plants.

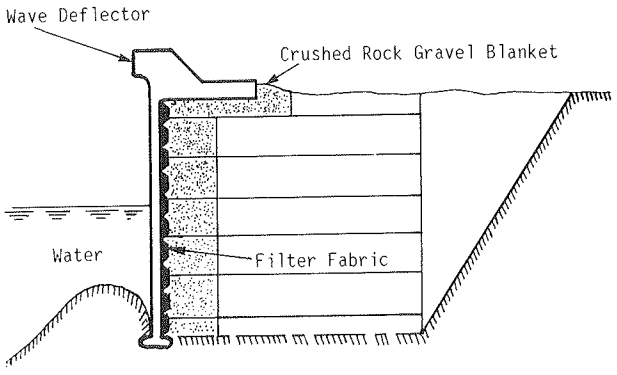

Figure A-4. Typical section of Reinforced Earth seawall with wave deflector.

3. MECHANISMS AND BEHAVIOR

3.1 Principle of Soil-Reinforcement Interaction

3.1.1 General Considerations

In Reinforced Earth, the mechanism of soil-to-reinforcement stress transfer is friction between the soil and reinforcement surfaces. Knowledge of the stress transfer in Reinforced Earth has been gained from many pullout tests on reinforcements located either in actual structures or in scale models. Although this type of test is not entirely representative of true conditions, it does give results that are sufficiently precise for deduction of factors influencing soil-reinforcement stress transfer.

In pullout tests, the reinforcements are extracted from the reinforced soil mass, and the pullout force-displacement curve is recorded. Because of soil dilatancy which develops in the vicinity of the reinforcements, the normal stresses exerted on the reinforcement surface are actually unknown. The pullout tests give only an apparent friction coefficient, μ^*, which is defined by the ratio:

$$\mu^* = \frac{\tau}{\sigma_v} = \frac{T}{2bL\sigma_v} \qquad \text{(A-1)}$$

where τ = the average shear stress along the reinforcement, σ_v = the overburden stress, T = the applied pullout force, b = the width of the reinforcement, and L = the length of the reinforcement.

In dense granular soils, the values of μ^* are usually significantly greater than the values obtained from direct shear tests. This is mainly because dense granular soil in the vicinity of the reinforcements tends to increase its volume, i.e., dilate, during shear. As illustrated in Figure A-5, this positive volume change is restrained by the surrounding soil. When ribbed strips are used, the ribs cause the shearing zone of soil to increase in size. Both the increase of the shearing volume, and the increase in

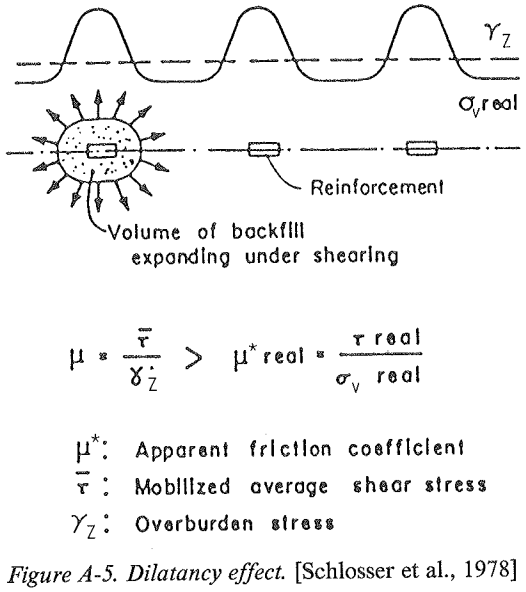

Figure A-5. Dilatancy effect. [Schlosser et al., 1978]

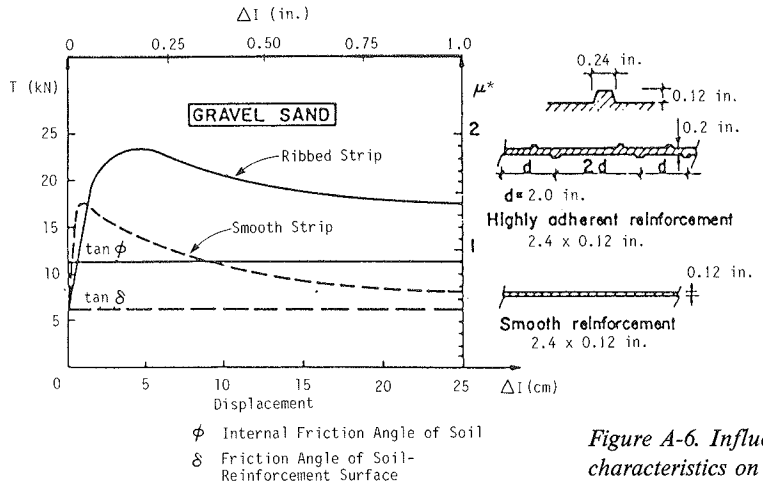

Figure A-6. Influence of the reinforcement surface characteristics on the apparent friction coefficient.

local stress because of soil dilatancy, result in an increase in the apparent coefficient of friction, μ^*, as shown on Figure A-6.

Available information on the factors affecting the value of the apparent friction coefficient μ^* has been reviewed and summarized by Schlosser and Elias [1978], McKittrick [1978], and Mitchell and Schlosser [1979]. The data provide a clear indication that peak and residual values of μ^* are functions of the nature of the soil (grading and angularity of the grains), the friction characteristics of the soil, the soil density, the effective overburden stress, the geometrical factors and surface roughness of the reinforcements, the rigidity of the reinforcements, and the amount of fines in the backfill—this factor being a most critical one.

3.1.2 Influence of Reinforcement Surface Characteristics

All the pullout tests performed on smooth reinforcements and on ribbed reinforcements (also referred to as highly adherent, or H.A.) have shown that the curves of μ^* as a function of displacement are of the form illustrated in Figure A-6.

In the case of a smooth reinforcement, the curve has a very noticeable peak which is obtained at a small displacement, and the residual value of μ^* is approximately half of the peak value. In the case of ribbed reinforcements, the values of μ^* at the maximum of the curve and at the residual value are only slightly different, and the maximum is obtained at comparatively large displacements.

3.1.3 Influence of Overburden Stress

Pullout tests on reinforcements located in actual structures, as well as laboratory studies using dense sands, have shown that the value of the apparent friction coefficient decreases when the vertical overburden stress increases (see Fig. A-7a). This phenomenon is more pronounced in the case of ribbed reinforcements than in the case of smooth reinforcements. This decrease in μ^* is because dilatancy decreases when mean confining stress increases. Under high overburden stress the coefficient μ^* approaches the value of tan ϕ, where ϕ is the internal friction

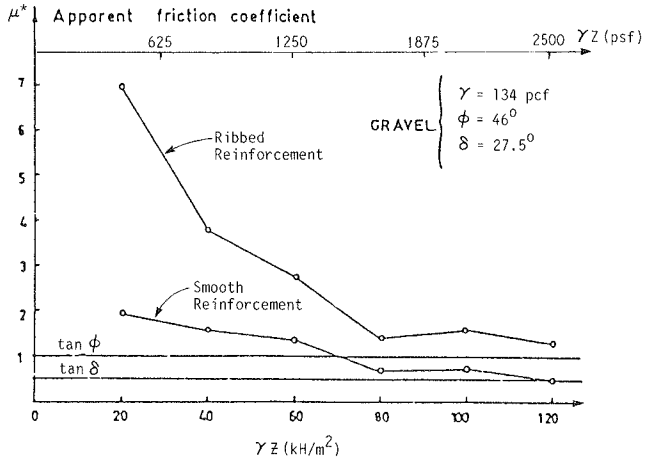

Figure A-7a. Influence of the overburden stress on the apparent friction coefficient. [Guilloux and Schlosser, 1979]

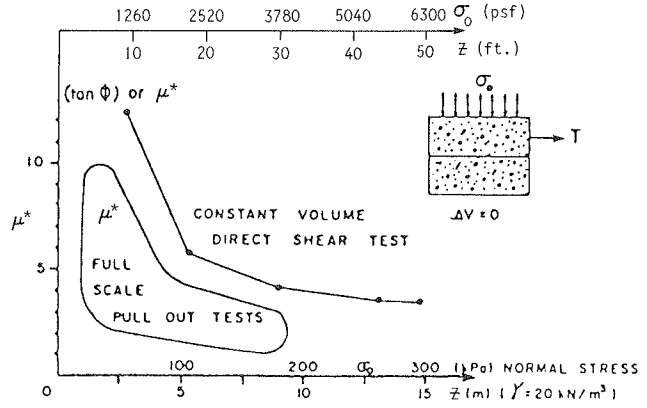

Figure A-7b. Variation of the apparent friction coefficient with the initial normal stress. [Guilloux and Schlosser, 1979]

angle of the soil, for the ribbed reinforcements which also mobilize soil-to-soil shearing; and the value of tan δ, where δ is the soil to reinforcement surface friction angle, for smooth reinforcements.

The dilatancy effect that develops in dense granular soil is a very important contribution to the pullout resistance of ribbed reinforcements. To demonstrate this, shear tests were done under constant volume conditions in densely compacted sand [Guilloux and Schlosser, 1979]. These tests represented an extreme case and are expected to give the maximum increase of the normal stress that can be obtained when dilatancy is prevented. The results showed a very large increase of the normal stress, and the corresponding values of the apparent friction coefficient, μ^*, calculated as the ratio between the average applied shear stress and the initially applied normal stress, were very high. As illustrated in Figure A-7b, the values of μ^* obtained in the constant volume tests exceeded those measured in laboratory models and in full-scale embankments, where some volume increases could develop by a significant margin.

3.2 Behavior and Failure Modes

The general behavior and failure modes of the Reinforced Earth composite material are similar to those of other reinforcing systems and are presented in detail in Chapter Four of the main report.

3.3 Behavior of Reinforced Earth Walls

In Reinforced Earth structures, the tensile forces mobilized in the reinforcements are a maximum at some distance from the facing. Figure A-8 shows the theoretical locus of maximum tensile forces obtained by finite element analysis [Corte and Payen, 1974] and the experimental one deduced from observations on actual Reinforced Earth walls. Figure A-9 shows that the locus of maximum tensile forces depends on the type of structure and on the loading conditions. In a Reinforced Earth structure this locus delineates two zones: (1) an "active zone," behind the facing, where the shear stresses are directed outwards, giving rise to an increase of the tensile forces in the reinforcements; and (2) a "resistant zone," where the shear stresses mobilized to prevent the pullout of the reinforcements are directed inwards, towards the free ends of the reinforcements.

These two zones are "held together" by the reinforcements. However, the mechanism, i.e., apparent cohesion, is different from that in systems of anchors and tiebacks where the soil is held in place because of stress transfer between the facing and the embedded anchors.

Observations on both laboratory models and full-scale structures have demonstated that when failure is caused by the breakage of the reinforcements, the maximum tensile forces line coincides with a potential failure surface relatively closer to the facing and quite different from the classical Coulomb failure plane.

Bolton et al. [1978] demonstrated by a centrifugal model study that the locus of the maximum tensile forces in the strips remains vertical during the construction of the wall (Fig. A-10a). In these tests, the construction of the wall to greater height was simulated by increasing centrifugal acceleration. The results of

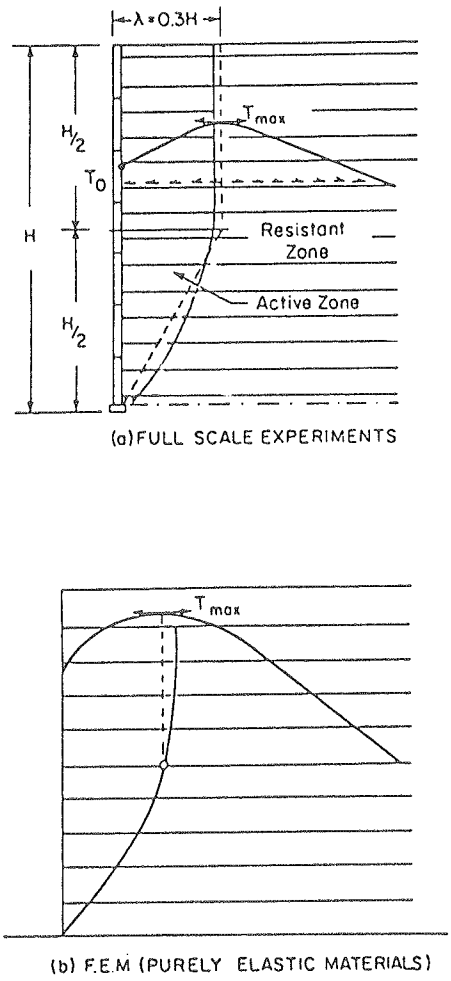

Figure A-8. Tensile force distributions along reinforcements. [Schlosser, 1978]

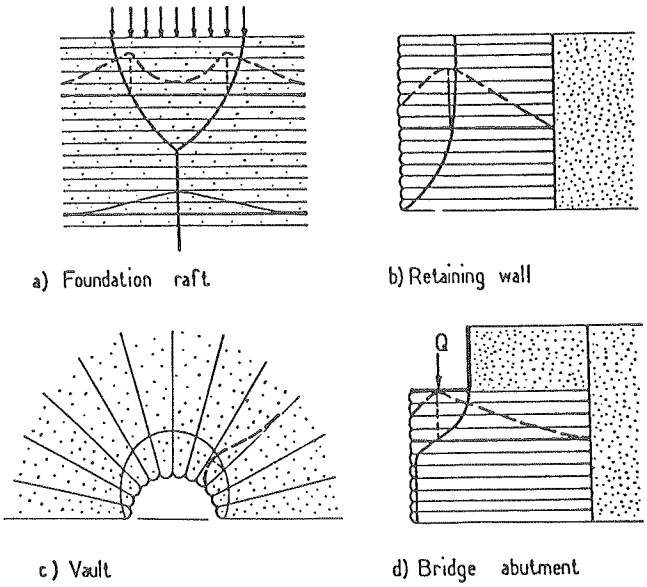

Figure A-9. Locus of maximum tensile force lines in different Reinforced Earth structures.

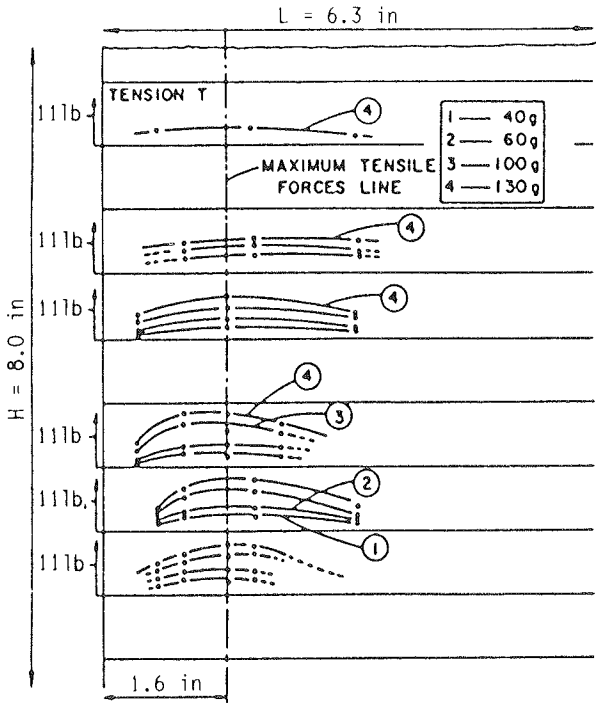

Figure A-10a. Tension distribution along strips under different accelerations in centrifugal model tests. [Bolton et al., 1978]

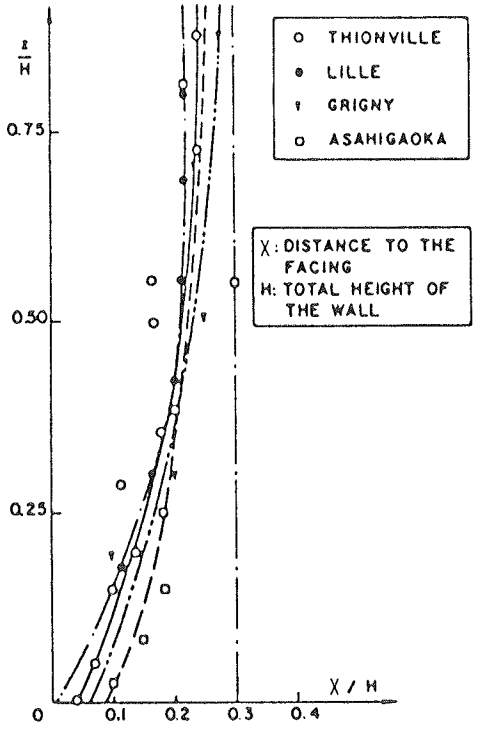

Figure A-10b. T_{max} *Lines in full-scale experiments.* [Schlosser and Segrestin, 1979]

these studies were consistent with measurements on actual structures reported by Schlosser and Elias [1978], Figure A-10b, which illustrates the locus of the maximum tensile forces in the strips of four Reinforced Earth walls of different heights. These experimental observations support the theoretical considerations outlined by Bassett and Last [1978].

The effect of inextensible reinforcements on the displacement pattern which develops in the Reinforced Earth mass results in a state of stresses which is close to the K_o condition. Consequently, as shown in Figure A-11, the variation of maximum tensile stress with depth observed in Reinforced Earth walls is quite different from that predicted by the classical plasticity approach using Rankine's theory. It is close to the lateral earth thrust of the soil at rest in the upper part of the wall and at greater depth it attains values that can be less than the lateral active earth pressure determined using Rankine's theory [Bassett and Last, 1978].

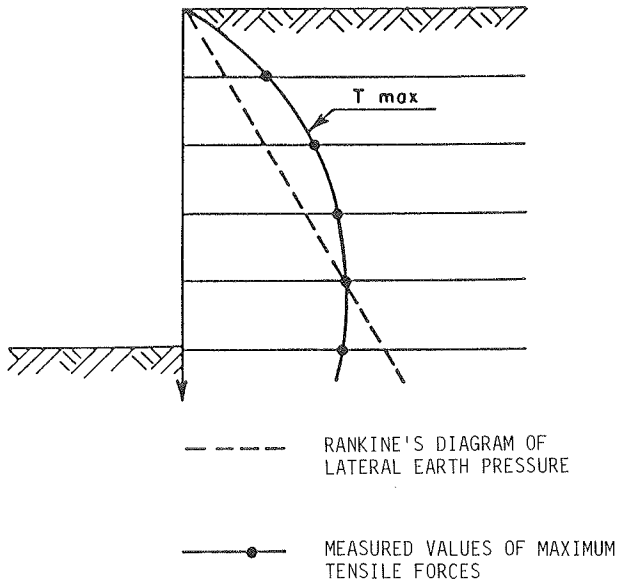

Figure A-11. Distribution of the maximum tensile forces with depth.

4. TECHNOLOGY

4.1 Description and Fabrication of Components

4.1.1 Facing Panels

In early Reinforced Earth walls, the basic facing elements were metallic half-cylinders of a semielliptic section, which were flexible and stable with respect to the thrust exerted by the backfill soil. Since 1971, plane cross-shaped concrete panels have been used more often than the metallic facing. This second type of facing enables the building of walls that can easily be curved in plan, and are well adapted to retaining structures in urban sites. The metallic facings are still used in structures where difficult access or difficult handling requires light facing elements.

Metallic facing elements are fabricated in lengths varying from 6.6 to 33 ft (2 to 10 m). The thickness varies from 0.08 to 0.12 in. (2 to 3 mm), depending on the application and height of a structure. An element has an effective height of 13.1 in. (33.3 cm) (a distance corresponding to the spacing between the levels of reinforcement). The maximum weight of an element is 253 lb (115 kg), which allows it to be placed by hand. The connection between two elements is made with the help of an overlapping-joint, Figure A-12, which is simply adjusted on the internal face. It prevents the soil from sloughing away and ensures, in the transverse direction, the deformability of the facing by the sliding of the elements on the overlapping-joint.

Facing with concrete panels requires the standard precast element (Fig. A-13) that is cross-shaped, with overall dimensions of 4.9 ft by 4.9 ft (1.50 m by 1.50 m) and is made of either unreinforced or reinforced concrete. According to the French specification for Reinforced Earth structures, the concrete panels do not include an internal reinforcement and their thickness varies from 7.1 to 10.2 in. (18 to 26 cm).

Between 1976 and 1982, several types of testing programs (field tests, photoelastic model tests, theoretical analyses) were conducted to evaluate variables thought to have an effect on the structural capacity of precast concrete facing panels [Terre Armee Internationale, 1982a, 1982b].

The results of the tests and theoretical analyses have shown that the use of a 14-cm thick (about 6 in.) concrete panel is justified in the following ranges: unreinforced concrete panels, up to a mean value of horizontal stress $\sigma_H = 33$ kPa (680 psf); and reinforced concrete panels, up to a mean value of horizontal stress $\sigma_H = 71$ kPa (1,1480 psf). For higher values of mean horizontal stress, it is necessary to use 18- or 22-cm thick (7 to 9 in.) concrete panels.

The 14-cm thick concrete panels, used for values of horizontal stress less than 33 kPa (680 psf) need only include light steel reinforcement. The 14-cm thick reinforced concrete panels, used when horizontal stress exceeds 33 kPa but is less than 71 kPa, should include standard reinforcing bars. In the United States, where unreinforced concrete is not commonly used, reinforced concrete panels as thin as 5.5 in. are available. Each panel normally provides connections for four or more reinforcing strips. The connections are made by tie-strips that are embedded in the concrete and made of the same metal as the reinforcing strips.

Vertical assembly-alignment pins provide correct alignment between the panels but are designed to allow some horizontal deformation. Compressible material is placed in horizontal joints between panels and allows some vertical deformation. Each panel contains lifting anchors to facilitate handling and placing using a small crane.

The panels are generally prefabricated in molds, thus enabling good uniformity and quality control. In addition to the standard panels, there are special panels that can be used to obtain desired overall geometry. These special panels include half-panels, 2.5 ft (0.75 m) high, that are used at the base and at the top of the wall; special panels, of which height varies by steps of 8 in. (20 cm), and which are used to give the upper line of the facing the desired shape; and angle elements that enable changes in the direction of the facing.

4.1.2 Reinforcing Strips

Ideally, reinforcements should have the following characteristics: (1) They should have a high tensile strength, a failure

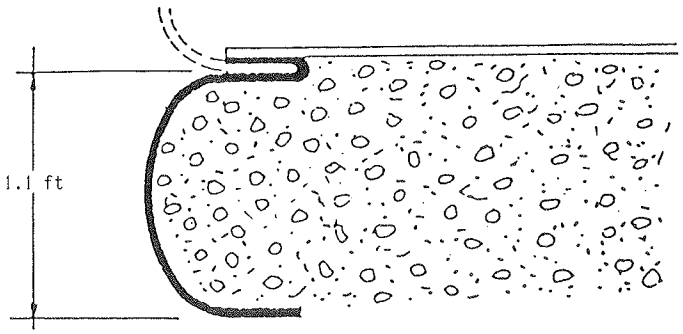

Figure A-12. Sketch of a metallic facing element.

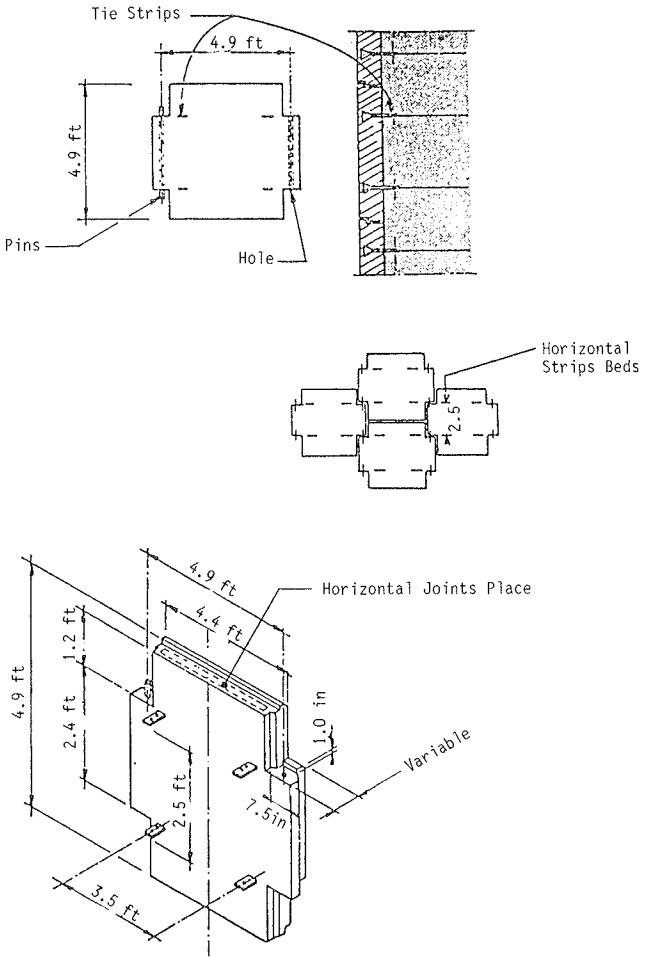

Figure A-13. Characteristics of a concrete facing panel.

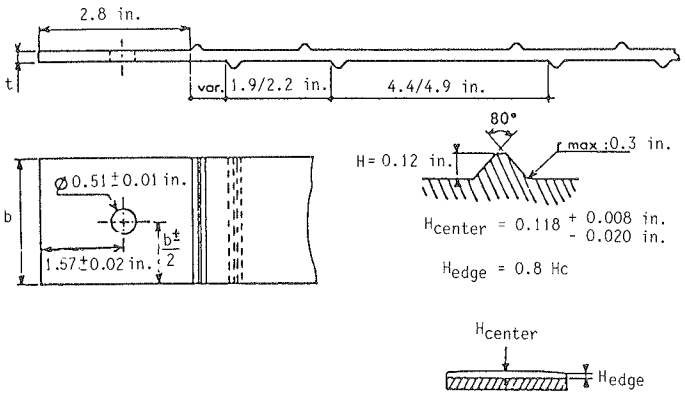

Figure A-14. Geometric characteristics of ribbed strips.

mode which is not brittle, and a very limited susceptibility to creep. (2) They should provide a high apparent friction coefficient with the backfill material. (3) They should exhibit low deformability under working loads. (4) They should be flexible enough to conform with the deformability of the Reinforced Earth material in order to enable easy construction. (5) They should have a high durability. (6) They should be economical.

At present, ordinary mild galvanized steel is the most frequently used. The reinforcement strips are generally linear bands, a few millimeters thick and a few centimeters wide.

The general reinforcement characteristics for the two most common types of Reinforced Earth walls are as follows: (1) For metallic facings, the reinforcement strips are cut of the same sheet that is used for the fabrication of the facing elements. They are made of mild galvanized steel and are generally 0.1 in. (3 mm) thick. They have a width of 2.0, 2.4 or 3.5 in. (50, 60 or 90 mm). (2) For concrete panel facings, the reinforcement strips are made of mild galvanized steel, with a cross section of 1.6 by 0.2 in. or 2.4 by 0.2 in. (40 by 5 mm, or 60 by 5 mm) or of high strength steel with a cross section of 2.0 by 0.16 in. (50 by 4 mm). Their surface is ribbed in order to improve the apparent soil-reinforcement friction. These ribbed strips are called *highly adherent reinforcements.* The dimensions and the spacings of the ribs were designed in order to maximize the apparent friction coefficient (Fig. A-14).

4.2 Tolerances and Fabrication Quality Control

Specifications for tolerances and fabrication quality control for Reinforced Earth components have been issued by the Federal Highway Administration (Sec. 613, "Mechanically Stabilized Embankments," in *Standard Specifications for Construction of Roads and Bridges on Federal Highway Projects, FP-85,* 1985). The most important specifications are described below.

4.2.1 Concrete Facing Panels

Cement normally conforms to AASHTO M-85, and concrete is expected to have a minimum compressive strength of 4,000 psi at 28 days. Air entraining, retarding or accelerating agents, or any additive containing chloride is not ordinarily used.

Tie-strip connectors, PVC tubes, as well as lifting and handling devices are placed to dimensions and tolerances shown on the plans prior to casting.

The units are manufactured within the following tolerances: dimensions within $\frac{3}{16}$ in., and angular distortion, with regard to the height of the panel, should not exceed 0.2 in. in 5 ft.

Acceptance of the concrete face panels with respect to compressive strength is normally determined on a lot basis. The lot consists of all production units (batches of concrete or panels) produced within a week's or 7-day production operation. Production units are randomly selected in accordance with the production day sample sizes listed in Table A-1 and are tested for compressive strength. Compression tests are performed on standard 6-in. diameter 12-in. long test specimens prepared in accordance with AASHTO T-23 or cores obtained and prepared in accordance with AASHTO T-24. Compressive Strength testing is conducted in accordance with AASHTO T-22.

Table A-1. Sample quantities as a function of production rate.

Production Day Quantities	Sample Quantities
0-35 cu yds (0-50 Panels)	1 set of four cylinders
36-70 cu yds (51-100 Panels)	2 sets of three cylinders
71-106 cu yds (101-150 Panels)	3 sets of three cylinders
Over 106 cu yds (+151 Panels)	5 sets of three cylinders

When standard 6-in. by 12-inch. test specimens are used, a minimum of four cylinders are cast for each production unit sampled. Two of these specimens are cured in the same manner as the panels and tested at 7 days. The remaining two cylinders are cured in accordance with AASHTO T-23 and tested at 28 days. The average compressive strength of each two cylinder group is considered their test value. A lot is accepted when all acceptance tests in a lot are greater than 4,500 psi or provided no individual 28-day compressive strength test result falls below 4,000 psi, and the average 28-day compressive strength of all test results for the lot equals or exceeds the acceptance limits delineated in Table A-2. The same specifications also apply to compressive strength tests performed on cores.

Table A-2. Lot acceptance criteria.

Number of Lot Acceptance Tests	Average of All Lot Acceptance Tests Must Equal or Exceed These Limits
3-7	4500 + 0.33 R*
8-16	4500 + 0.44 R*
16	4500 + 0.46 R*

*(Range) The difference between the largest and smallest acceptance test result.

The early strength determination procedures of FHWA Rapid Test Procedure RT-6 can sometimes be used in lieu of the standard 28-day compressive strength test procedures.

4.2.2 Steel Facing Panels

Steel facing panels are fabricated of cold rolled galvanized steel conforming to the minimum requirements of ASTM A-446, Grade C, or other approved metal. The panels are galvanized to conform to the minimum requirements of ASTM A-525, coating class G 90.

4.2.3 Reinforcements and Tie-Strips

Tie-strips, i.e., the brackets protruding from facing panels that are used for connection of the reinforcement strips, are shop fabricated of hot rolled steel conforming to the minimum requirements of ASTM A-123. Reinforcing strips are hot rolled from bars to the required shape and dimensions, with their physical and mechanical properties conforming to ASTM A-36. They are hot-dipped galvanized to conform to the minimum requirements of ASTM A-123, and cut to plan length and tolerances. Holes for bolts are punched in the end of the strips. All reinforcements and tie-strips are inspected to ensure they are true to size and free from defects.

5. DURABILITY AND SELECTION OF BACKFILL

5.1 Members Susceptible to Degradation

Of the different Reinforced Earth elements, the metallic reinforcing strips that are buried in the backfill material are most sensitive to degradation. This degradation results from the electrochemical corrosion of the metal in contact with the soil. Chapter Six of the main report presents a detailed description of the process.

5.2 Parameters Governing the Rate of Corrosion

A discussion of the parameters controlling the rate of corrosion of metallic reinforcements, including details of the U.S. National Bureau of Standards (NBS), Study of Metallic Corrosion, is presented in Chapter Six of the main report.

In general, the most corrosive soils contain large concentrations of soluble salts, especially in the form of sulfates, chlorides, and bicarbonates, and they may have very acidic or highly alkaline pH values. Clayey and silty soils (characterized by fine texture, high water holding capacity and, consequently, by poor aeration and poor drainage) are also prone—because of their poor aeration—to being potentially more corrosive than soils of a coarse nature such as sand and gravels, where there is free circulation of air and where corrosion approaches the atmospheric type. Additionally, buried metals can corrode significantly by differential aeration or bacterial action. Corrosion by differential aeration may result from substantial local differences in type and compaction of soil or the resultant variations in the oxygen or moisture content. However, such behavior is mostly associated with fine-grained soils.

The Reinforced Earth Company [Darbin and Montuelle, 1979] has conducted extensive laboratory testing to determine the effect of chlorides and sulfates on the corrosion rate of buried galvanized strips. The results indicate that chlorides in concentrations up to 200 ppm and sulfates up to 1,000 ppm have no significant effect.

5.3 Methods to Predict Rate of Corrosion

The methods used to predict the corrosion rate of galvanized steel reinforcing strips in Reinforced Earth are presented in detail in Chapter Six of the main report.

Briefly, the calculation of corrosion loss according to the Reinforced Earth Company procedure is made assuming corrosion loss behavior for the zinc and steel as shown schematically in Figure A.15. A relatively rapid corrosion rate, V_1, for the first few years is followed by a continuing, but reduced, corrosion rate, V_2. It is conservatively assumed that the continuing loss rate of bare steel, V_2, occurs after all the zinc coating is used in a sacrificial manner. Specific corrosion loss rates estimated from NBS and other data (see Chapter Six of the main report) are used to calculate the loss in cross-sectional area of the reinforcing strips over the structure's life.

Continuing research undertaken by the Reinforced Earth Company focused on the actual performance of reinforcing strips in in-service environments on the oldest structures available for examination [Terre Armee Internationale, 1982c]. To date, samples from many of these nonmarine structures have been removed for examination. Statistically the environment in which the tested structures have been constructed can be characterized as follows: (1) resistivity—97.9 percent of sites have resistivities greater than 1,000 ohms-cm; (2) pH—98 percent of the sites fall in a pH range of 5 to 9.5; (3) chlorides—97.6 percent of the sites have chloride concentrations less than 200 ppm; and (4) sulfates—96.6 percent of the sites have sulfate concentrations less than 1,000 ppm.

The measured loss of metal has been plotted on Figure A-16 as a function of time, together with loss rates presently used in Reinforced Earth design (see Chapter Six of the main report).

It seems that the design method presently used provides a reasonable upper-bound approach.

5.4 Tests to Predict Rate of Corrosion

Four types of tests have been used to assess the rate of corrosion of buried reinforcements: tests in boxes; tests in electrochemical cells; measurements on reinforcements of actual structures; and full-scale experiments on actual structures that failed by an accelerated induced corrosion. Details of these tests and specific test results for Reinforced Earth structures are presented in Chapter Six of the main report.

5.5 Selection of Backfill Material

Backfill material for a Reinforced Earth structure is selected to satisfy the following requirements: (1) frictional strength, i.e., friction angle, should be high enough to ensure the necessary soil-reinforcement interaction. (2) Susceptibility to creep should be sufficiently low to prevent excessive deformation of the structure under the expected service loads. (3) Maximum grain size should not be so large as to adversely affect placement of reinforcements or compaction. (4) Moisture content may have to be limited to avoid difficulties during compaction. (5) Corrosiveness should not be excessive.

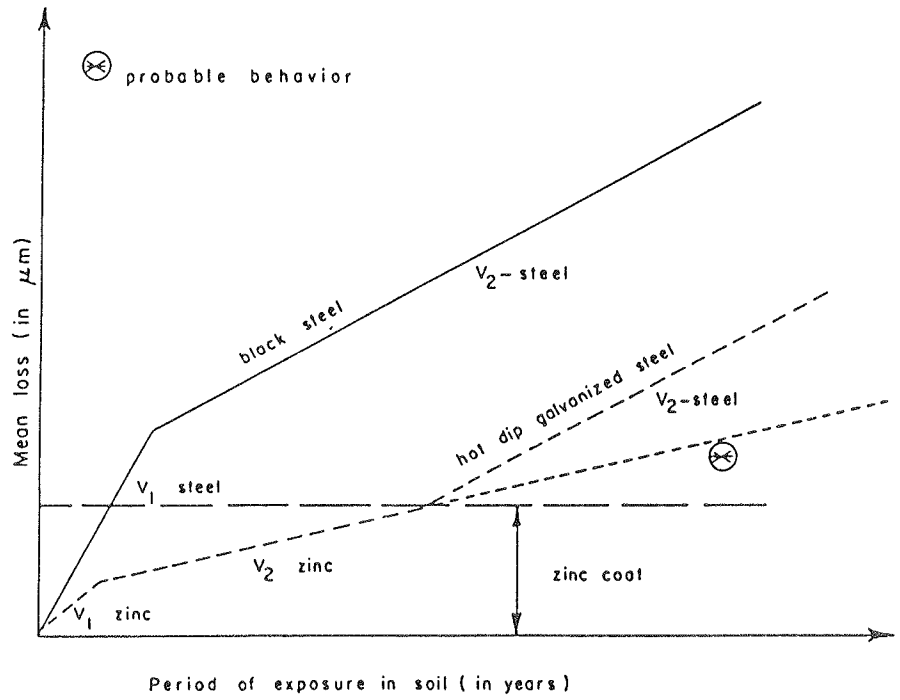

Figure A-15. Schematized mean corrosion loss relationship.

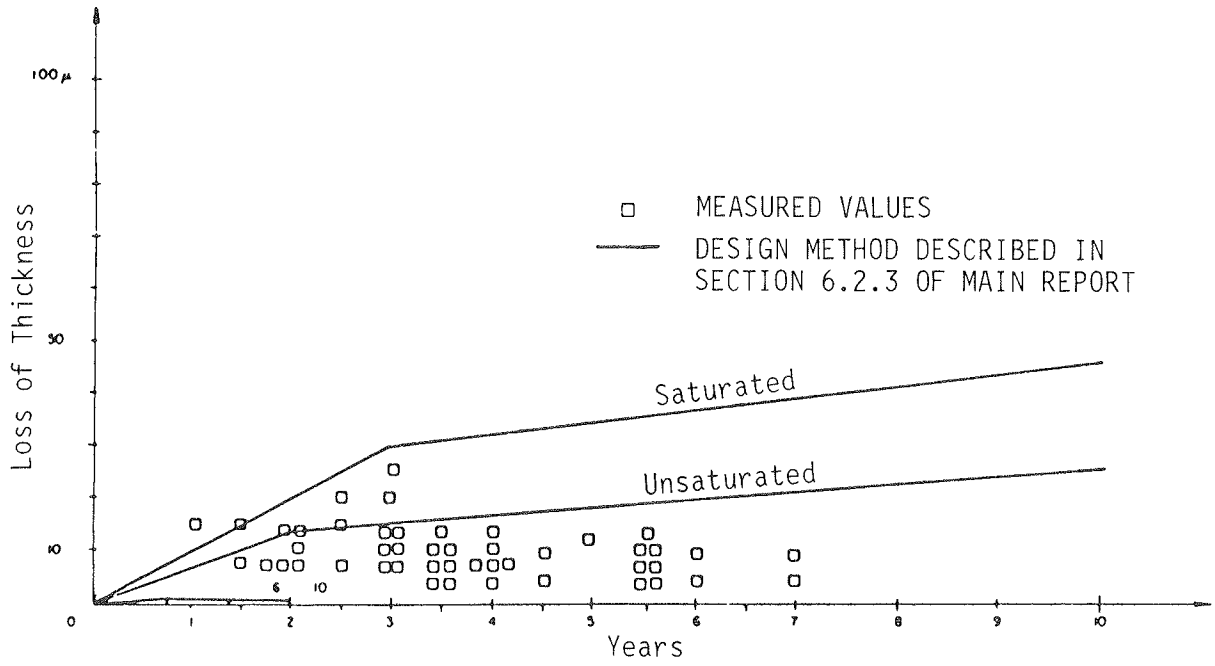

Figure A-16. Reinforced Earth Company design method of corrosion rate.

5.5.1 Durability Criteria

Table A-3 shows the present Federal Highway Administration (FHWA) specifications for suitable backfill material to satisfy durability criteria. The measurement of the resistivity is a spe-

Table A-3. Specifications for the selection of backfill material—durability criteria.

ENVIRONMENTAL	RESISTIVITY	ACIDITY (pH)	CONTENT OF SOLUBLE SALTS	
			CHLORINE	SULFATE
Out of water	>1000 ohm-cm		≤200 mg/kg	≤1000 mg/kg
In fresh water	>3000 ohm-cm	5 to 10	≤100 mg/kg	≤ 500 mg/kg

cific test described in various standards; e.g., California Department of Transportation, California Test Method 643 [1978].

In addition, all backfill material should be free from organic and other deleterious materials. The organic content as expressed in organic carbon weight ratio (ratio of total carbon content to mineral carbon content) should not exceed 100 ppm.

5.5.2 Geotechnical Criteria

According to FHWA specifications, the backfill material used in Reinforced Earth structures should conform to the gradation limits as determined by AASHTO T-27 (Table A-4).

If the fraction finer than the 200 mesh sieve is between 15 and 25 percent, the backfill should also conform to the following additional requirements: (1) The Plasticity Index (P.I.) as determined by AASHTO T-90 shall not exceed 6. (2) The fraction finer than 15 microns (0.015 mm) as determined by AASHTO T-88 shall not exceed 15 percent. (3) The material shall have an angle of internal friction of not less than 34 deg, as determined by the standard Direct Shear Test—AASHTO T-236, utilizing a sample of the material compacted to 95 percent of AASHTO T-99, Methods C or D (with oversize correction as outlined in Note 7) at Optimum Moisture Content.

Some states have additional criteria concerning backfill quality. For example, New York State Department of Transportation requires that the amount of material passing the No. 40 sieve be less than 70 percent in order to prevent excessive movement of facing panels during construction.

Table A-4. Grain size specifications.

Sieve Size	Percent Passing
6 inches	100
3 inches	100 - 75
No. 200	0 - 25

5.6 General Creep Considerations

Creep can occur in Reinforced Earth retaining structures either in the backfill material itself or at the soil-reinforcement interfaces. In either case, the creep can result in an excessive deformation of the facing.

The major factors governing creep behavior of the reinforced soil are the nature and quantity of the fine-grained portion of the backfill material and the excess of moisture content above the optimum moisture content.

A few attempts have been made in the past to build Reinforced Earth structures using backfill materials with a relatively high content of silty and clayey soils. Case histories have been reported by Hashimoto [1979] and Battelino [1983].

Hashimoto [1979] described the behavior of a Reinforced Earth wall 26 ft high, constructed using a clayey backfill material (80 percent < 74 μm, $I_p \approx 40$ percent) at a water content greater than 50 percent. The lateral displacement measured during a period of 40 days after the end of construction only reached 1.6 in. (4 cm), even though the maximum vertical displacement of the top of the wall was equal to 28 in. (71 cm).

Batellino [1983] reported observations on an 11.5-ft high Reinforced Earth wall with polyester strips and with a clayey silt backfill material (80 percent < 80 μm), at a water content of about 20 percent. The creep of the backfill material resulted in a lateral displacement of the facing which reached 1.4 in. 152 days after the end of construction. The rate of creep decreased rapidly and was negligible at the end of this period. In the two cases mentioned above the water content was approximately constant during and after construction. Other unpublished case histories have shown that the increase of water content because of heavy rains during construction can be critical when the backfill material has a content of fines approaching the limits of specifications.

To investigate creep in a Reinforced Earth structure under normal working conditions of optimum moisture content and in the range of 95 percent of the maximum density, creep pullout tests were carried out in a large direct shear box on strips buried in a wide variety of soils [Elias, 1979]. The tested soils included Virginia silt, Georgia silt, French silt, Kaolin clay, and aeolian sand. During conventional pullout tests, strips were subjected to creep testing by a constant pullout force acting for 175 hours. The applied pullout force was approximately 50 to 60 percent of the ultimate pullout load, a stress level which corresponds to service load conditions.

The test results indicated low or no tendency to creep at the load level tested under the specific test conditions for any of the typical soils involved in this program. Surprisingly, even the Kaolin clay did not exhibit creep. Typical results are shown in Figure A-17. However, no pullout creep tests have yet been done under conditions of full saturation, which may significantly affect the creep behavior.

Present specifications for Reinforced Earth structures do not require specific tests to evaluate the susceptibility of the backfill material to creep. However, the geotechnical backfill selection criteria provide the necessary protection by limiting the nature and the content of the fines. Furthermore, when the backfill material contains a relatively high portion of fines, it is generally required to ensure appropriate drainage in order to prevent eventual saturation of the backfill material.

It is suggested, when backfill materials with a fines content larger than that allowed by the specifications are used, that creep tests be done in a direct shear box on saturated samples. The tested soil should be compacted at 95 percent of AASHTO

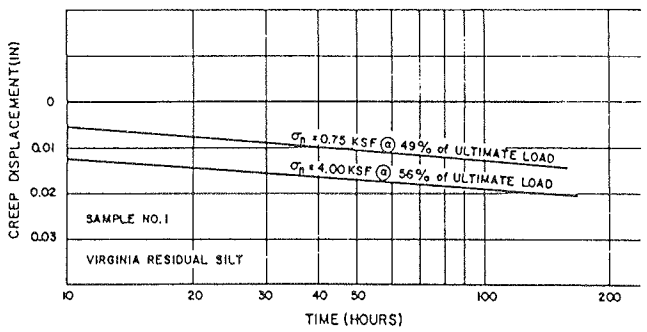

Figure A-17. Typical creep test results.

T-99, Methods C or D, at optimum moisture content, then saturated and subjected to a constant shear stress at different stress levels in order to provide a reasonable assessment of the tendency of the backfill material to creep under the extreme conditions of full saturation.

5.7 Other Existing Specifications

Specifications for Reinforced Earth have also been developed in France [Laboratoire Central des Ponts et Chaussées, SETRA, 1979]; the main difference between these and the American specifications with regard to geotechnical criteria pertain to classification of suitable soils according to the type of reinforcements (smooth or ribbed) and the shear testing procedure adopted to evaluate the mechanical properties of the backfill material. The French specifications require shear tests on saturated samples consolidated under a normal stress of 200 kPa (about 4,000 psf). The American specifications require shear tests on samples compacted to 95 percent of AASHTO T-99 at optimum moisture content in order to evaluate the soil properties at the actual site conditions.

U.S. and French specifications concerning rate of corrosion are also based on two different concepts. The French specifications consider the concept of a sacrificed thickness to allow for the corrosion propagation, taking into account a minimum life service period which is a function of the environmental conditions and the type of metal used. At the end of the design life, the available remaining thickness of the strips should be sufficient to still satisfy the factors of safety considered in the design. The American specifications pertain to the time required for increasing stresses (because of decreasing section) to reach yield conditions and this time is compared with design life. If this condition is satisfied, no additional reinforcement section is required.

6. CONSTRUCTION

The construction of a Reinforced Earth structure must be managed in the same manner as any other earthwork.

6.1 Site Preparation

During construction, it is necessary to verify: (1) agreement between actual and specified base elevation; (2) conformance of the soil actually encountered and used during construction with the engineering properties considered during design; (3) the absence of unexpected hard or soft spots in the foundation soil under the leveling strip; and (4) protection of the foundation soil against inclement weather and provision of adequate drainage during construction.

6.2 Phases of Construction and Placement of Different Components

6.2.1 Setting Leveling Pads

The footing located beneath the facing panels is an ordinary leveling pad of reinforced or nonreinforced concrete, intended to serve as elevation control, not as a structural footing. It must be correctly leveled in order to ensure an appropriate alignment for the first row of panels and to facilitate the setting up of the whole facing. The longitudinal location must be carefully controlled whenever the facing is connected to an existing structure, particularly in the case of a bridge abutment.

6.2.2 Setting Facing Elements

It is important that facing panels are not damaged during handling. In the event that damage does occur, a decision to reject the considered element must be made rapidly. The replacement of a panel behind which backfill has already been placed is a time-consuming operation which requires a complete dismantling of a part of the structure.

The stability of the facing during the backfilling operation is ensured for the first row of panels by temporary struts placed on the external side of the wall, and for successive levels by temporarily securing facing panels by wooden wedges and screw clamps. The wooden wedges are extracted regularly (leaving three rows in place) to maintain flexibility in the facing.

Concrete facing panels are joined as shown on Figure A-13. In structures where there is a risk of fine materials migrating through the joints between facing panels under the action of water, the vertical joints are sealed by a filter fabric applied against the inside of the concrete. Horizontal joints are sealed because of cork placed between layers of panels.

If the facing panels start tilting to unacceptable tolerances or batter, corrective measures need to be taken. It may be necessary to correct the upper row of panels if the inclination is less than the specified tolerances, or to dismantle the inclined part if the inclination exceeds the tolerances.

The tolerance between three successive panels measured using a 15-ft long straight edge, placed in any direction against at least 2 panels, should not exceed 1 in. according to Reinforced Earth Company specifications.

6.2.3 Placement of Reinforcements

The reinforcements should be laid flat on the compacted embankment and fixed to the tie-strips protruding from the panels. Before backfilling, all the reinforcements must be bolted to the tie-strips, and corrosive protection should be applied to the bolts.

It may be necessary to lower the reinforcements in order to provide either the necessary space for a road base, or to provide enough overburden to develop the required pullout resistance (see Fig. A-18). In this case the thickened part of the upper embankment layer, layer 4 in Figure A-18, must be placed before placing the last reinforcements.

6.2.4 Placement and Compaction of Backfill Soil

The placement of the backfill material on a layer of reinforcement should begin at the center of the first reinforcement reached by the equipment. Equipment should not cross directly over exposed reinforcements. Care should be taken to ensure that the reinforcing strips are properly aligned after dumping the backfill. Backfill layer thickness should average 12 in. in

the case of metallic facing and 15 in. in the case of concrete facing.

Proper compaction of the backfill soil is required to minimize subsequent settlements and to ensure good soil-reinforcement stress transfer.

Each fill layer must be leveled after compaction to ensure that all the reinforcements are in contact with the soil over their entire bottom surface. This may require some manual filling and tamping, particularly near the connection of the reinforcements to the facing and in zones of difficult access.

If backfilling is done with materials sensitive to water, the contractor must take measures to prevent any ponding of rainwater or flow through or over the facing. It is sometimes necessary to scarify or disc the backfill to aerate it following rain.

Backfilling in front of the embedded part of the lower row of facing panels is usually done before the structure reaches a height of 10 ft.

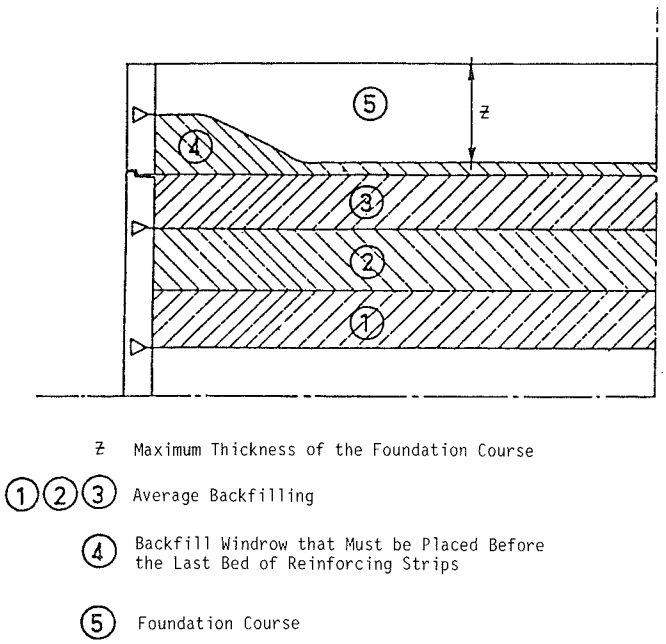

Figure A-18. Construction under a foundation course.

6.3 Construction Equipment

Construction of Reinforced Earth structures requires, in addition to earthwork equipment, small vibrating compactor to compact the zone to a distance of 3 ft to 5 ft from the facing (to avoid damage to facing panels by heavy compaction equipment); lifting equipment, about 2 tons capacity, for transport of the panels from the storage area and for their set up; and hand tools.

6.4 Work Organization

6.4.1 Personnel

The setting up of the facing panels and the placing of the reinforcements is done by a team generally consisting of one foreman and five workers, or at least three workers, amongst whom one should be a qualified mason.

6.4.2 Storage of Prefabricated Elements

A storage area should be provided for the prefabricated elements. It is important to provide a sufficient on-site stock of prefabricated elements for construction periods of at least 48 hours for the concrete facing panels, and for one week for the reinforcements or metallic facings in order to avoid delays at the site between deliveries.

Metallic facing elements are delivered in stacks that are to be untied only when needed for construction. The stacks must be laid flat. Facing elements improperly stored, i.e., laid down either on one point or on two extreme points, can undergo deformations that can cause difficulties during construction.

Concrete facing requires the panels to be delivered on pallets where they are placed horizontally, tie-strips upwards. This orientation should also be maintained during unloading and storage. They can be handled by using four connection links to the tie-strips or cast-in easy-lift pins. Storage is generally by stacking a maximum of 6 panels placed horizontally. The panels are isolated by timber to avoid deformation of the tie-strips.

Reinforcements are delivered in bundles of 50 units of a weight ranging from 1 to 2 tons. Reinforcements longer than 20 ft must be unloaded by a swing (lifting) bar. The reinforcements are stored on pieces of timber.

6.5 Quality Control

6.5.1 Prefabricated Elements

The Reinforced Earth Company guarantees conformance of the prefabricated materials (facings, reinforcements, bolts, joints) with the specifications. On site, it is necessary to ensure that these materials conform with the measurements provided by the construction drawings, that the components have not been damaged, and that they are properly stored.

It must be ensured that the reinforcements have not been damaged and particularly that galvanization or other coatings have not been scarred.

The panels (concrete facings) must be clear from cracks and splinterings, and they must have a relatively uniform color. The tie-strips must not be bent.

The elements of metallic facing should be clear from dents or other defects, and galvanization should not have been damaged.

6.5.2 Backfilling

The principles for control of backfilling in Reinforced Earth structures are the same as those used for the control of ordinary road embankments. As for any earth structure, this includes quality control of the type of backfill material and control of the placing and compaction.

7. DESIGN METHODS

7.1 Internal and External Stability Analyses

The current design procedures for Reinforced Earth retaining structures consider the internal and external stability analyses separately.

For internal stability, two failure mechanisms are considered: (1) failure by breakage of the reinforcing strips—designed for by assuring that reinforcement cross section is adequate; and (2) failure by pullout of the reinforcing strips—designed for by assuring that reinforcement surface area and length are adequate.

For external stability, the Reinforced Earth structure is considered to behave as a gravity structure, and three classical failure mechanisms are analyzed: (1) sliding of the structure on its base; (2) bearing capacity failure of the foundation soil; and (3) general failure of a zone including the Reinforced Earth structure, i.e., a slope failure.

This separation between internal and external failure mechanisms is in some cases quite arbitrary, since the failure surfaces may cross the reinforced soil mass as shown in Figure A-19. In these cases the stability analysis should consider mixed internal-external failure modes.

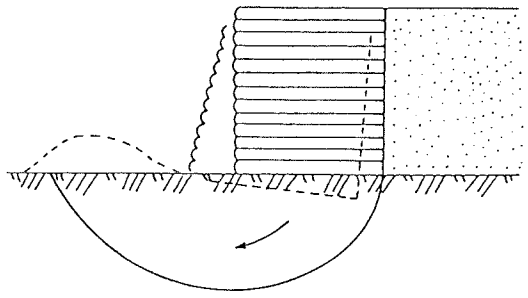

A) Foundation Failure in the Case of a Wall Whose Ratio $\frac{L}{H}$ Is Low

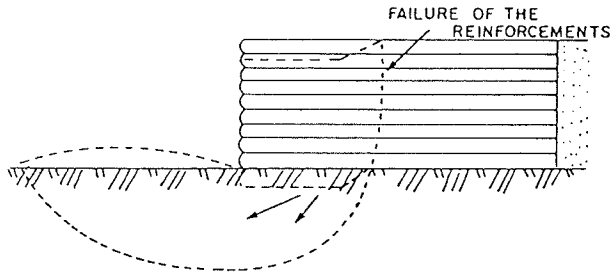

B) Foundation Failure in the Case of a Wall Whose Ratio $\frac{L}{H}$ Is High

Figure A-19. Modes of foundation failure under Reinforced Earth walls.

7.2 Influence of Soil Conditions and Topography on Retaining Structures

7.2.1 Unstable Slopes

Reinforced Earth has in numerous cases been found to be one of the few possible techniques for construction of retaining walls on unstable slopes. The design of these structures must satisfy requirements that are sometimes contradictory, for example: minimization of the volume of the excavation and ensurance of its short-term stability either by reducing the depth of embedment or by shortening the length of the reinforcements at the lower part of the structure; and improvement of the external stability of the structure and deepening of the potential failure surfaces by increasing the depth of embedment and the width of the wall.

To satisfy these two different requirements, it is necessary to study at an early stage of the project the external stability of the structure as a whole in its surroundings, and the construction methods and excavation support required for construction of the Reinforced Earth structure (bracing, anchoring, nailing).

The safety factor with respect to the long-term internal stability of the Reinforced Earth structure should be at least as great as that of the natural slope. To limit the disturbance created by the construction of the wall, the following procedures can be used: (1) construction in steps (see Fig. A-20) such as for the walls on the Roquebrune-Menton Road—1968); and (2) construction by phases (Fig. A-21).

To avoid irregularities in the facing that can result from the movement of marginally stable ground, it is necessary to increase the flexibility of the facing by placing special vertical joints uniformly spaced. In the case of walls in excavations where the backfill material is poorly draining, it is necessary to collect and to remove the accumulated infiltration on water by providing a drainage blanket at the back and beneath the Reinforced Earth structure (Fig. A-22).

In all cases, the hydrologic conditions in the wall or in the ground around it must be evaluated because saturation of the backfill material can increase the tensile forces in the reinforcements, and seepage in the embankment may have to be prevented or limited, especially if the soil water is believed to contain aggressive chemicals with respect to the reinforcement durability.

7.2.2 Compressible Foundation Soils

As the deformability of Reinforced Earth is relatively high, the allowable settlements are limited only by the longitudinal deformability of the facing and by the serviceability requirements of the structure. However, longitudinal differential settlements exceeding 5 percent can cause cracks and breakages of concrete facing panels or cracks in the metallic elements detrimental to the structure and eventually harmful to its long-term behavior and stability. Therefore, in the case of structures on highly compressible soils, a specific investigation of stability and potential settlements should be performed.

The allowable differential settlement for the standard facing is a function of the height of the wall. Structures up to a height of 50 ft can sustain without damage longitudinal differential settlements of 1 percent for a facing with concrete panels and 2 percent for a metallic facing.

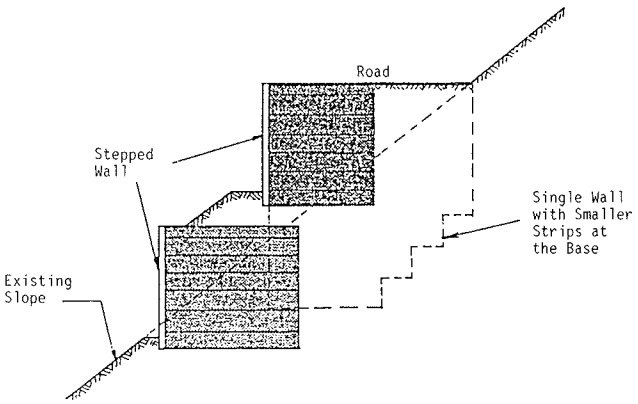

Figure A-20. Construction of a stepped Reinforced Earth wall on an unstable slope.

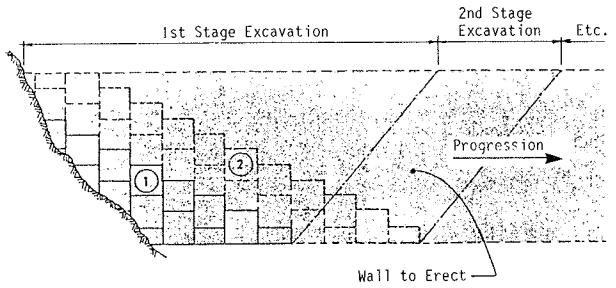

Figure A-21. Phased construction of a Reinforced Earth wall on an unstable slope.

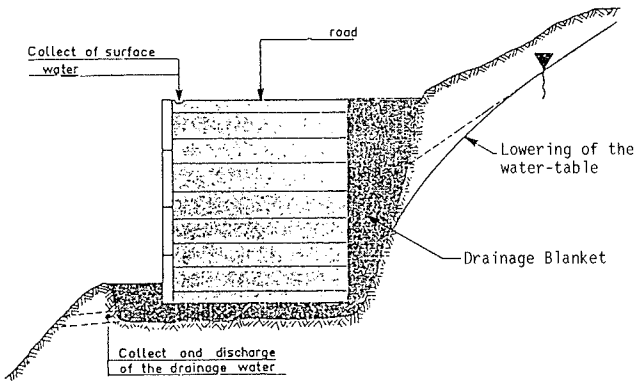

Figure A-22. Drainage of Reinforced Earth walls.

7.2.3 Marine Walls

The design of marine structures should allow for variations of water level inside the wall because of fluctuations of the water level outside the wall.

If exterior water level can lower rapidly or if the decrease is of large amplitude, it is desirable that the backfill material be highly permeable to quickly reduce the water pressures within the Reinforced Earth mass. This precaution minimizes the rapid drawdown-induced increase in reinforcement tensile forces and also minimizes the decrease in pullout resistance associated with the high hydraulic gradients resulting if the precaution is not taken. Some layers of a freely draining material are placed in the embankment and a drainage layer of the same nature is placed behind the facing (Fig. A-23). Dependent on material availability, it may be more economical to use closer reinforcement spacings combined with backfill material of lower quality or lower permeability.

Retaining walls along river banks must be well protected from erosion. The embedment of these structures must therefore be deep enough, and in some cases they must also be protected by rock or by cribs to prevent damage by scour.

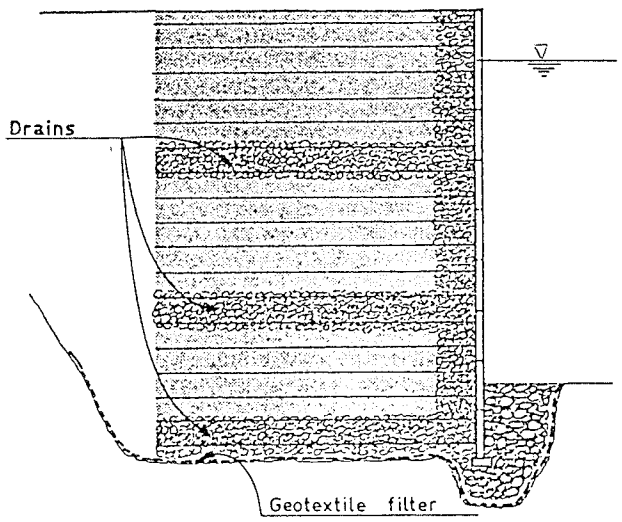

Figure A-23. Example of a drainage system for a submerged Reinforced Earth wall.

7.3 Loading and Boundary Conditions

Reinforced Earth structures can be designed to support different types of boundary loadings. The most common conditions, as shown in Figure A-24, include: (1) static loads (earth thrust, vertical and horizontal concentrated line (or point) loads on bridge abutments, cyclic traffic loads that are represented by an equivalent uniformly distributed surcharge, earth slopes and highway embankments on walls, and water pressure on Reinforced Earth dams); (2) dynamic load (vertical and horizontal vibrations induced by railway traffic, and seismic loadings).

7.4 Assumptions for Preliminary Design

Except for special cases of walls either founded on slopes or those having sloped faces, Reinforced Earth retaining structures normally have rectangular cross sections, i.e., reinforcement strips are of the same length for the full height of the wall, and the wall face is vertical.

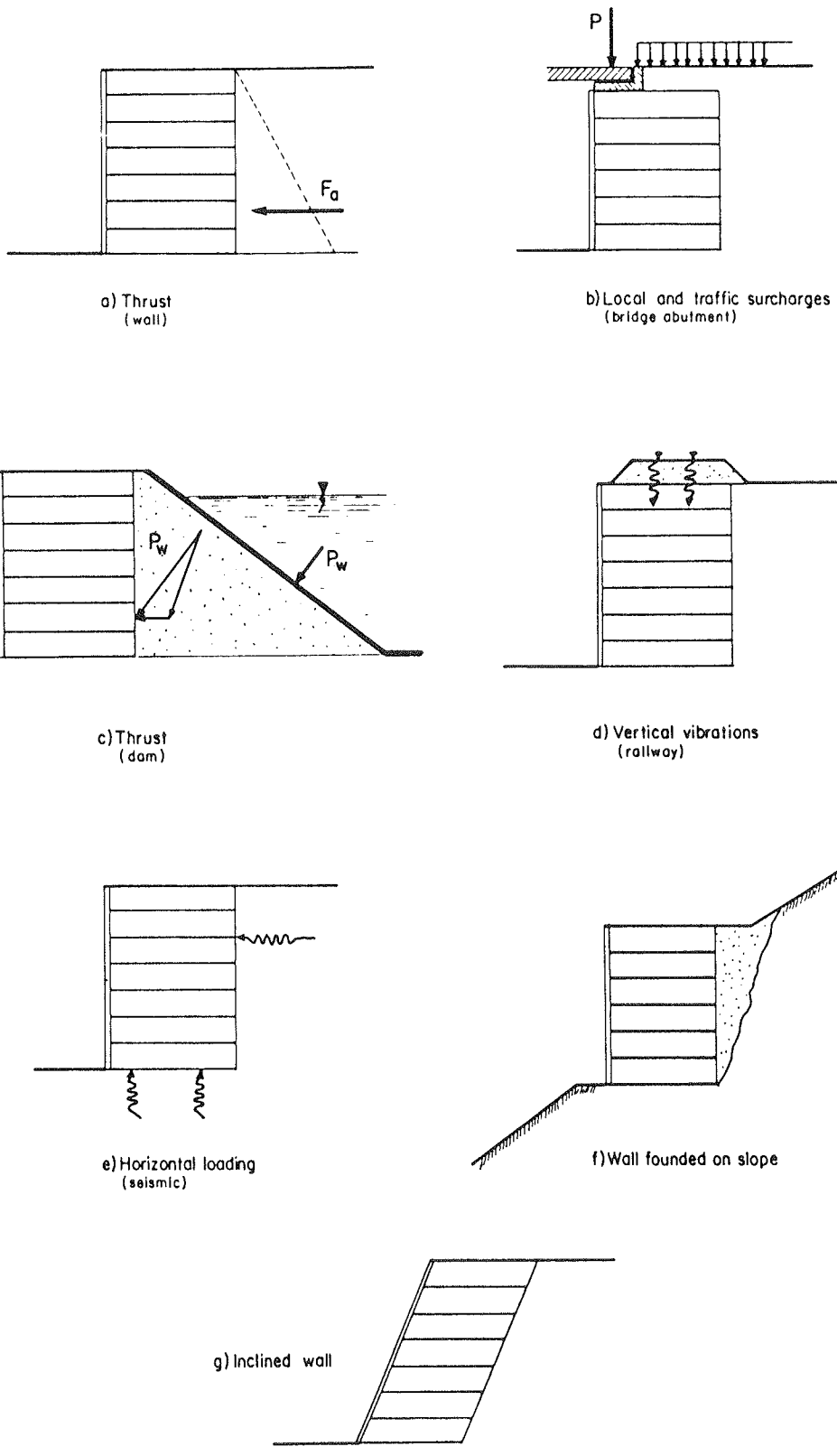

Figure A-24. Different loading and boundary conditions.

The preliminary design of a wall of height H requires determination of the following geometrical parameters: embedment depth D of the structure (Fig. A-25); and cross-section ratio L/H, where L is the reinforcement length.

7.4.1 Structure Height

Figure A-25 shows typical geometry. H_1 is the total height of the facing, including the embedment depth; H is the height used in the computations; and L is the reinforcement length. For a horizontal backfill and no surcharge, H is equal to H_1.

7.4.2 Embedment Depth

An embedment depth, D, is usually required for Reinforced Earth structures to avoid bearing failure of the foundation soil. Embedment is also required because of risk of local failure in the vicinity of the facing, depth of frost, and risk of scour or erosion-induced local damage.

In any case, an embedment depth of 0.1 H is usually used, with a minimum of 1.3 ft, unless the structure is founded on a compact soil that is not sensitive to frost.

Preliminary estimates of the required embedment to prevent the stress underneath the facing from exceeding the bearing capacity of the foundation soil are given as a function of the structure height in Table A-5, according to French practice.

7.4.3 Cross-Section Ratio

Reinforced Earth masses that are used as retaining structures, bridge abutments, and dams generally have a reinforcement length L which is equal to 0.7 H, and this value may be used for preliminary design.

Considerations of general stability, soil-reinforcement adherence, and the fact that reinforcements are manufactured in standard lengths can result in a value of L which is greater than 0.7 H.

Table A-5. Embedment depth as a function of structure height H—estimates for preliminary design.

Ground Slope in Front of the Wall		Embedment Depth D
$\beta_1 = 0$	Walls	H/20
	Abutments	H/10
$\beta_1 = 18°$ ($\cot\beta = 3/1$)	Walls	H/10
$\beta_1 = 27°$ ($\cot\beta = 2/1$)	Walls	H/7
$\beta_1 = 34°$ ($\cot\beta = 3/2$)	Walls	H/5

7.5 Internal Stability Evaluation and Design Parameters

For a rectangular Reinforced Earth wall it is necessary to verify the two following design criteria at each level of reinforcements (see Fig. A-26).

1. Failure by rupture of reinforcements:

$$T_{max} \leq \frac{R_T}{FS_R} tb \qquad \text{(A-2)}$$

where T_{max} = the maximum developed tensile force in the reinforcement; R_T = the maximum allowable tensile stress, or elastic limit, of the reinforcing material; FS_R = the required safety factor with respect to the tensile resistance of the reinforcing material; and t and b = respectively, the thickness and width of the reinforcing strips.

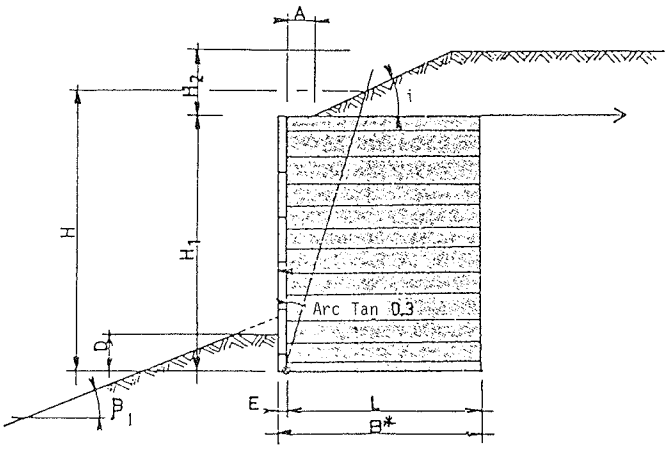

Figure A-25. Illustration of geometric parameters used for design.

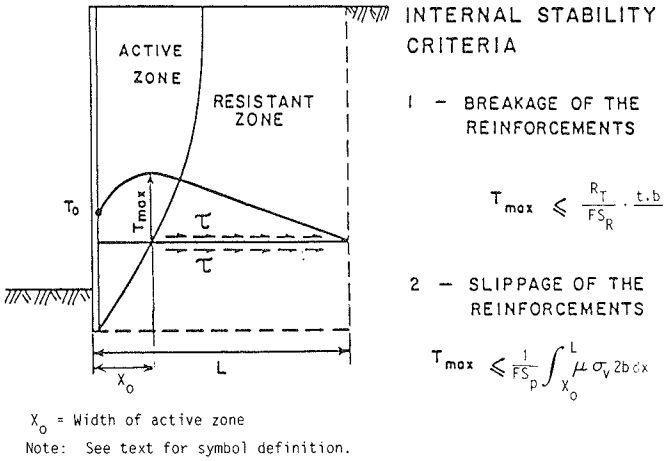

Figure A-26. Principles of internal design of Reinforced Earth walls.

2. Failure by pullout of reinforcements:

$$T_{max} \leq \frac{1}{FS_p} 2b \int_{x_o}^{L} \tau(x).\, dx \text{ with: } (x) = \mu^* \sigma_v(x) \quad \text{(A-3)}$$

in the case of vertical rectangular Reinforced Earth wall without exterior loads:

$$T_{max} \leq \frac{1}{FS_p} \cdot b(L - x_o) \cdot 2\mu^* \gamma\, ZH = \frac{F_p}{FS_p} \quad \text{(A-4)}$$

where FS_p = the required safety factor with respect to the pullout resistance of the reinforcement; x_o = the width of the active zone at the considered level; L = the total length of the reinforcement; Z = depth below the top of the wall; $\tau(x)$ = the mobilized shear stress at the soil-reinforcement interfaces at a point x; μ^* = the apparent friction coefficient defined in Section 3.3; $\sigma_v(x)$ = the vertical effective stress on the soil-reinforcement interfaces at the point (x); and F_p = the available pullout resistance.

As indicated in Section 3.3, the soil-reinforcement interaction results in vertical stress concentrations and, therefore, the vertical stress at the soil-reinforcement interfaces is actually unknown. The value of $\sigma_v(x)$ considered in the design corresponds to the initial vertical stress, which in the case of a vertical Reinforced Earth wall without external loads is equal to the effective overburden pressure.

According to these two failure criteria, the main design parameters of a Reinforced Earth system can be classified in five main groups: (1) mechanical properties of the backfill material, particularly internal friction angle and density; (2) mechanical properties of the reinforcements including allowable tensile stress and elastic limit; (3) parameters related to the soil-reinforcement interaction, particularly the apparent friction coefficient μ^*; (4) the geometric properties of the reinforcements: thickness, width, length as well as vertical and horizontal spacings between the reinforcements; and (5) parameters related to the functioning of the structure under the expected site conditions, the required service life, and the corresponding extra thickness for durability considerations.

In practice, for a given type of backfill material, the choice of some design parameters is limited by practical considerations concerning the standardization of the prefabricated reinforcements and facing panels. The geometric and mechanical properties of the reinforcements generally used are presented in Section 4.1. Considering these properties, the main design parameters which can be selected are: (1) the horizontal spacing of reinforcements, subject to the limitations of standard spacing increments in prefabricated facing elements; (2) the length of the reinforcements; (3) the type of the reinforcement (currently available reinforcements have a standard thickness of 0.2 in. (5 mm) and widths of 1.6 or 2.4 in. (40 or 60 mm) or a thickness of 0.16 in. (4 mm) and a width of 2.0 in. (50 mm) in high strength steel; they can be either ribbed or smooth); and (4) the service life of the structure for the specific site conditions.

7.6 Analytical Approaches

Generally speaking two analytical approaches have been developed. The first considers local internal stability of the active zone in the Reinforced Earth wall with respect to the two failure modes: failure by pullout of the reinforcements and failure by rupture of the reinforcements. The analysis of the local equilibrium conditions of the active zone provides a solution for the locus and values of maximum tensile forces in each reinforcement.

The second considers the general stability of the Reinforced Earth wall and its surroundings. Classical slope stability analysis methods, such as Fellenius's or Bishop's methods of slices, have been adapted to evaluate the safety factor with respect to failure along circular potential sliding surfaces, taking into account the available tensile and pullout resistances of the reinforcements crossing the potential sliding surfaces.

These approaches are discussed in more detail below.

7.6.1 Internal Stability of Reinforced Earth Structures

At failure considerations. The analysis of the failure mechanisms observed in scale-model walls provided the basis for a limit analysis method [Juran, 1977] to predict the locus and values of maximum tensile forces at failure and the corresponding critical height of the wall. The method is based on the analysis of the equilibrium conditions of the active zone defined by the failure surface which is developed in the soil along the maximum tensile forces line. It considers both the static and kinematic boundary conditions corresponding to the effect of the reinforcements on the strain field in the Reinforced Earth mass.

The model studies [Juran and Schlosser, 1978] showed that in the case of a failure by rupture of the reinforcements, the failure mechanism involves essentially a rotation of the active zone, which can be considered as a quasi-rigid and incompressible block bounded by a thin layer of soil at a limit state of stresses. Observations of failed models suggest that the failure surface is perpendicular to the ground surface at the top of the wall. This failure surface was assumed to be a logarithmic spiral.

Furthermore, it is assumed that the failure is caused by a progressive breakage of the reinforcing strips, and that as the first breakage occurs the soil resistance to shearing is entirely mobilized all along the failure surface.

The method proposed to analyze the stability of the active zone enables determination of a unique logarithmic spiral which satisfies all the static equilibrium conditions (Fig. A-27). The maximum tensile force per unit length of wall facing in a given strip layer, T_{max}, is calculated from the local horizontal equilibrium of horizontal slices of the active zone of thickness S_v, each slice containing a single strip layer at its center. It is reasonably assumed that no horizontal shear stresses act along the horizontal planes bounding these slices and, consequently:

$$T_{max} = \frac{\left[1 + \frac{S_v}{2\cos\alpha}\right]}{\left[1 - \frac{S_v}{2\cos\alpha}\right]} \left[\frac{\sigma(\alpha)}{\cos\alpha} \cos(\alpha + \phi) d\ell\right] \quad \text{(A-5a)}$$

where α = angle of the tangent of the spiral with the vertical; ϕ = internal friction angle of the soil; $\sigma(\alpha)$ = the normal stress acting on the failure surface, which is calculated using Koter's equation:

$$\frac{\partial \sigma}{\partial \ell} + 2\,\sigma \tan \frac{\partial \alpha}{\partial \ell} = \gamma \cos(\alpha + \phi) \cos\phi \qquad \text{(A-5b)}$$

Solution of these equations [Juran, 1977] gives the values of the maximum tensile force T_{max} and the distance X of the loci of this maximum tensile force from the facing, as two nondimensional factors:

$$K^* = \frac{T_{max}}{\gamma H_f S_v} \text{ and } X_H = \frac{X}{H_f} \qquad \text{(A-6)}$$

where H_f is the failure height of the model wall.

The variations of the nondimensional factors K^* and X_H with the nondimensional height Z/H_f is a function of the structure geometry (inclination of the facing and eventually of the reinforcement) and of the internal friction angle of the soil, ϕ.

Assuming for design purposes that failure is caused by breakage of the reinforcement, the maximum tensile force in the reinforcement must be equal to its tensile strength, R_T. The value of K^* at this level is known from the theoretical solution outlined above and is equal to the critical value K_c which is only a function of the internal friction angle ϕ. The failure height can be calculated from:

$$H_f = \frac{R_T}{K_c\,\gamma\,S_v} \qquad \text{(A-7)}$$

Figure A-28 shows that the predicted log spiral failure surface agrees fairly well with the experimental one [Juran et al., 1978]. It also illustrates that the theoretical distribution of K corresponds closely to the lateral pressure of a soil at a K_o state of stress in the upper part of the wall. Also, the coefficient of earth pressure reduces with depth and reaches a value below K_a. In fact, below a given depth, lateral earth pressure appears to remain constant.

Test results shown in Figure A-29 indicate that the proposed limit analysis based on a log spiral failure surface provides a reasonably good prediction of the failure heights of model walls which failed by breakage of their reinforcement strips [Juran, 1977; Juran and Schlosser, 1978].

This limit analysis approach has been generalized to allow for the at-failure design of bridge abutments taking into consideration the static and kinematic boundary conditions at the upper loaded surface of the wall [Juran et al., 1978].

Working stress conditions and empirical approaches. The limit analysis approach has provided significant and valuable information concerning the locus and distribution of maximum tensile forces at failure. However, the assumptions involved in such an analysis cannot be expected to apply to the behavior of Reinforced Earth walls failure under typical working stress conditions. In particular, there is no basis to assess the mobilization of the shear strength of the backfill material before failure.

The development of an appropriate design method for estimating the stress distributions in the reinforcements and in the soil under expected service loads requires a formulation of a constitutive model capable of representing the response of the anisotropic, composite Reinforced Earth material to different types of loads. The difficulties involved in the formulation of such a model have led to the development of semiempirical approaches integrating observations and experimental measurements on full-scale instrumented structures [Schlosser and Segrestin, 1979]. These approaches are presently used in the design of Reinforced Earth walls and bridge abutments (see Sec. 7.7 of this chapter).

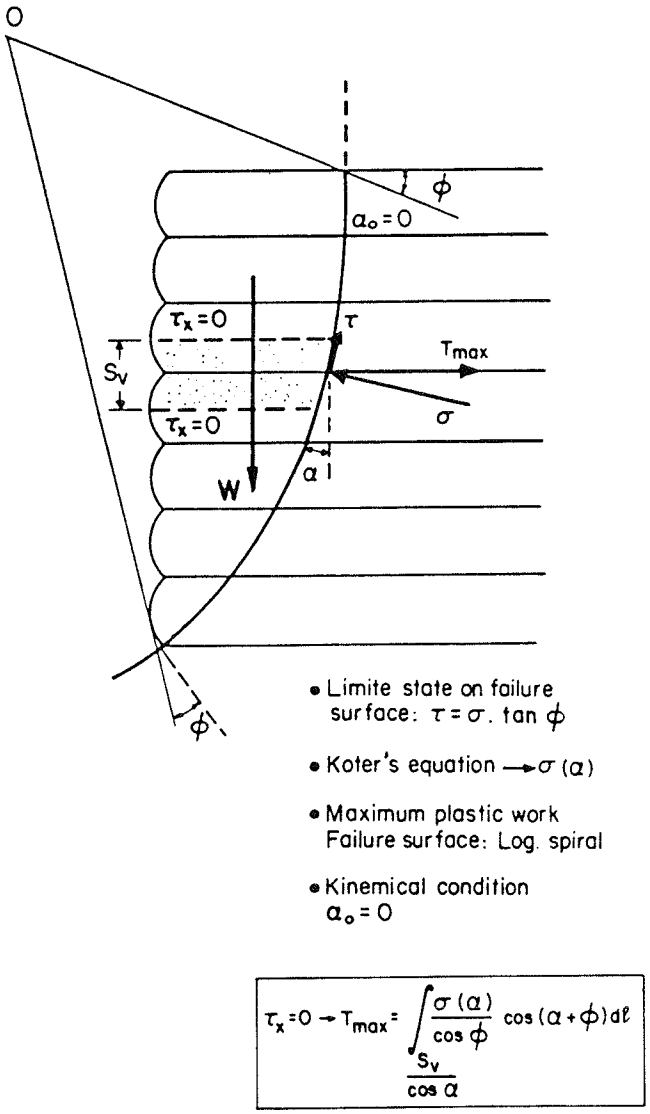

Figure A-27. Internal design of Reinforced Earth walls using a log spiral failure surface. [Juran, 1977]

Numerical analyses and finite element studies have been carried out to analyze the behavior of both laboratory models and prototype instrumented walls. Both equivalent composite body and discrete material approaches have been used. In a discrete representation [Corte, 1977; Al-Hussaini and Johnson, 1978], the reinforced system is treated as a heterogeneous body. The soil and each reinforcing member are separately represented, and their interaction is simulated either by using different types of joint elements or simply by assuming a perfect adherence between the soil and reinforcements. In an equivalent composite body representation [Herrmann and Al-Yassin, 1978] the reinforced system is modeled as a locally homogeneous orthotropic material. The composite material properties assigned to the con-

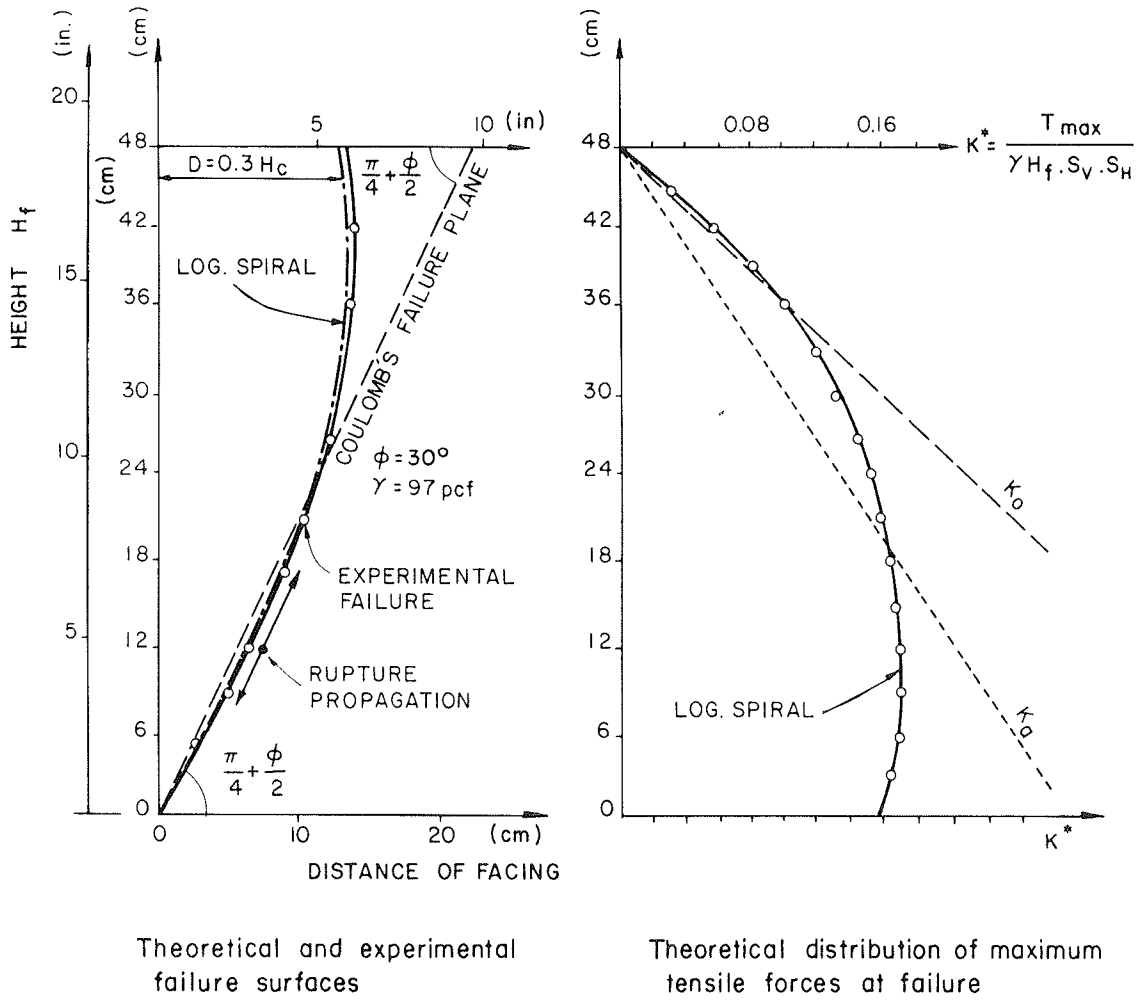

Theoretical and experimental failure surfaces

Theoretical distribution of maximum tensile forces at failure

Figure A-28. Analysis of the failure of model walls by breakage of the reinforcements. [Juran et al., 1978].

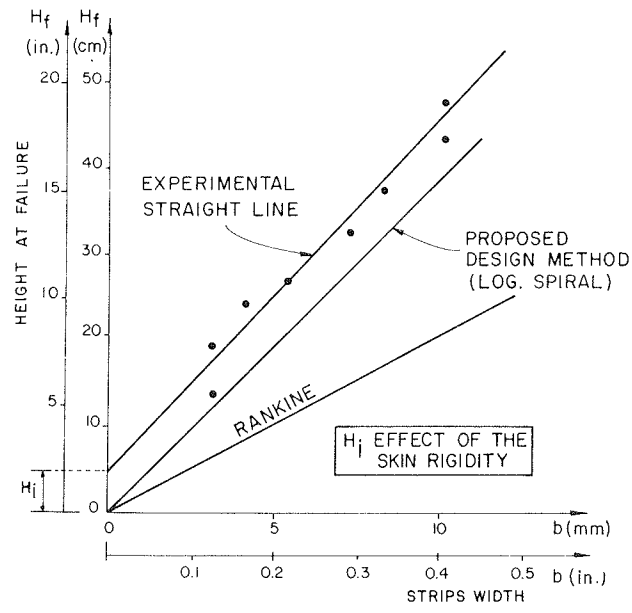

Figure A-29. Experimental and theoretical critical heights of model walls. [Juran et al., 1978]

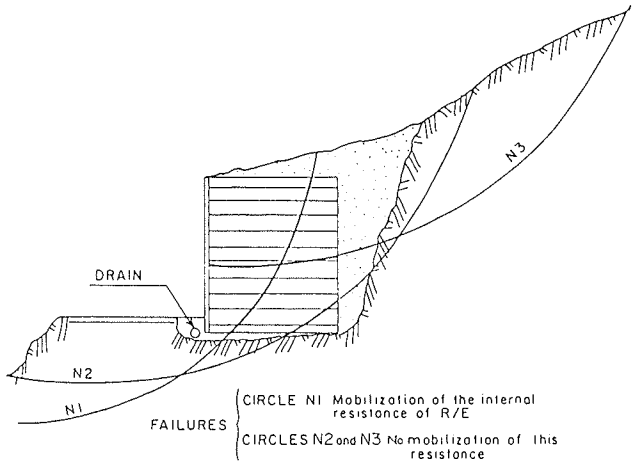

Figure A-30. Special circles of failure.

tinuum elements reflect the properties of the matrix material, the reinforcing members, and their composite interaction.

Both elasticity theory and finite element methods have been used to analyze the effect of concentrated line (or point) loads applied at the surface of Reinforced Earth walls on the tensile forces in the reinforcements.

Harrison and Gerrard [1972] considered Reinforced Earth essentially as a homogeneous, orthotropic linearly elastic composite material in which the soil is reinforced by closely spaced parallel layers of thin and stiff material. Their elastic model yields analytical solutions for the stresses developed in the "weightless" earth and in the reinforcements due to different types of surface loadings. Harrison and Gerrard's model has been successfully used to analyze the effect of concentrated loads on the stresses in the soil and reinforcements of a 39-ft high Reinforced Earth wall supporting traveling gantry cranes [Juran et al., 1979]; the solutions and their practical applications are discussed in Section 7.7.2.

7.6.2 External Stability of Reinforced Earth Structures

As discussed in Chapter Five of the main report, the external stability of reinforced soil structures can be analyzed by assuming the earth structure behaves as a coherent gravity mass and employing classical soil mechanics methods of analysis. This approach is typically used for Reinforced Earth structures.

As noted earlier, the explicit separation of internal and external failure modes in this approach is arbitrary in some cases, because the failure surfaces which develop may cross both the Reinforced Earth mass and the surrounding in-situ soil. The possibility of sliding surfaces which intersect parts of the wall means that tensile forces in the reinforcements should also be considered for these cases. However, in order to mobilize the internal strength of the Reinforced Earth, the surfaces of failure must be inclined with respect to the reinforcements and at some distance from their free extremities. For example, in Figure A-30, circles N2 and N3 hardly mobilize any tensile strength in the reinforcements (because they intersect few reinforcements), while circle N1 involves significant internal stability evaluation (because it crosses many reinforcements).

The consideration of circular sliding surfaces passing through the Reinforced Earth mass led to the development of a design method [Phan et al., 1979] which enables a simultaneous investigation of both the internal stability and the external stability. This method, based on Bishop's method, is particularly useful in the cases of Reinforced Earth retaining structures on steep slopes, or Reinforced Earth dams and for structures of special geometry.

The principles of the method are shown in Figure A-31. The considered circular sliding surface is divided into slices of width b and the base of each slice cuts a reinforcement at the base's center. Failure can result either from breakage of the reinforcements or from pullout. Consequently, the maximum tensile force which can be mobilized in each reinforcement is equal either to the maximum pullout resistance F_p or to the limit tensile force T_R.

The investigation of the equilibrium of the cylindrical zone enables the determination of the safety factors with respect to the soil shearing resistance and with respect to both the pullout resistance and the tensile resistance of the reinforcement. The equation for the composite factor of safety is shown on Figure A-31.

7.7 Current Design Practice—Walls and Bridge Abutments

7.7.1 Internal Design—Retaining Walls

The data shown on Figure A-32 indicate that the locus of maximum tensile forces in full-scale structures is quite similar to the loci observed in model walls. It is practically vertical in the upper portions of the wall and is closer to the facing than the breakout point of a Coulomb failure plane.

Full-scale experiments also showed that the coefficient K characterizing the state of stresses (ratio between the horizontal and the vertical normal stresses) within the backfill material varies with depth from K_o at the top of the wall to a value that can be less than the value of the active earth pressure coefficient K_a at the lower part of the wall. The high values of K at the top of the wall are mainly due to the effects of compaction and to the reinforcements which restrain the lateral deformations and maintain the equivalent K_o state of stresses.

Figure A-33 shows the variation of the ratio K/K_a as a function of the height of the embankment above the considered reinforcement strips in seven experimental structures [Schlosser, 1978]. The heavy full line indicates the variation of the ratio K/K_a adopted by the French specifications for the design of Reinforced Earth walls

The simplified design method currently used is shown on Figure A-34. The maximum tensile forces line is vertical in the top half of the wall and its distance from the facing is 0.3 H. The maximum tensile force in the reinforcement is calculated from the horizontal equilibrium of the corresponding soil layer, considering the local horizontal stress σ_H at the locus of the maximum tensile forces, and introducing an empirically determined coefficient K to characterize the state of stresses within the backfill material. It is assumed that the K-value varies linearly with depth from K_o at the top of the wall to K_a at a depth of 20 ft and that it remains constant at K_a for larger depths.

As shown on Figure A-35, the vertical stress σ_v is calculated using Meyerhof's method based on the equilibrium of the portion of the Reinforced Earth mass above the considered reinforcement under the effect of its weight and of the active earth pressure exerted by the embankment on the wall. The maximum tensile force in a reinforcement is equal to:

$$T_{max} = \sigma_H S_v S_H = K \sigma_v S_v S_H \qquad \text{(A-8)}$$

The required length of the reinforcement is determined considering the locus of the maximum tensile forces and the available effective adherence length in the resistant zone. The values of the apparent friction coefficient μ^* are deduced from the considerations of soil-reinforcement interaction presented earlier.

When ribbed reinforcements are used it is generally assumed that dilatancy causes the values of μ^* to vary with depth from high values at the top of the wall to a value of $\mu^* = \tan \phi$ at a depth of 20 ft. The variation of μ^* with depth is assumed to be linear, as shown on Figure A-34. From experience it has been found that μ_o^*, i.e., the value of μ^* at the top of the wall,

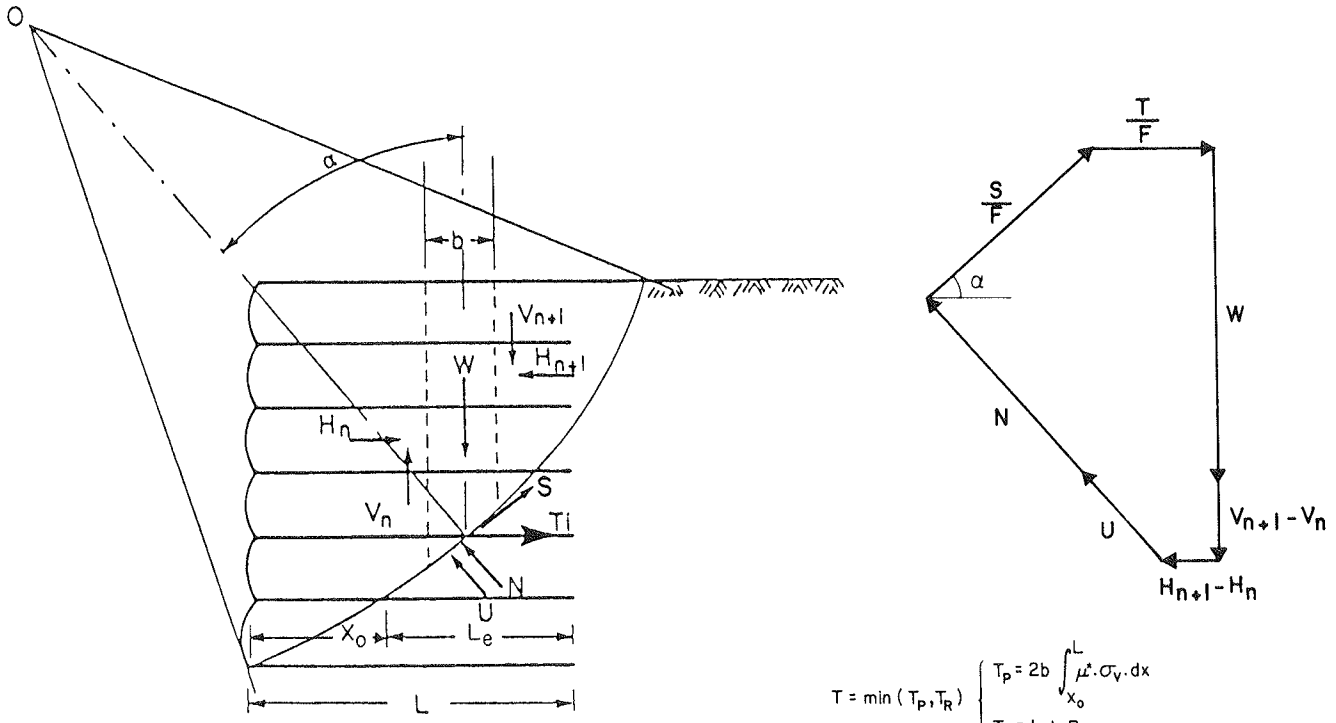

$$F = \frac{\sum_n \left[cb + (W_n - ub)\tan\phi\right] \dfrac{1}{\cos\alpha_n \left(1 + \tan\alpha_n \dfrac{\tan\phi}{F}\right)} + \sum T_n \cos\alpha_n}{\sum_n W_n \sin\alpha_n}$$

Figure A-31. Stability analysis of Reinforced Earth walls by slip circle method. [Phan et al., 1979]

depends on the grain-size distribution; in the FHWA specifications μ_o^* is taken as 1.2 for all acceptable backfills, while the French specifications give μ_o^* as

$$\mu_o^* = 1.2 + \log C_u \qquad \text{(A-9a)}$$

where $C_u = D_{60}/D_{10}$ is the coefficient of uniformity. However, if a uniform fine sand with a uniformity coefficient of 2.5 or less is used for backfill, μ_o^* is reduced to 1.2 in French practice. If special backfills, such as lightweight fill and bottom ash, or backfills with a relatively high fines content, are used, the design values of μ_o^* provided above cannot be considered applicable, and appropriate design criteria should be developed from the results of full-scale or laboratory pullout tests.

When smooth reinforcements are used, it is generally assumed that dilatancy is negligible, and that:

$$\mu^* = \tan\delta \qquad \text{(A-9b)}$$

where δ is the soil-to-reinforcement friction angle measured in direct shear tests (see Sec. 3.4 of this chapter).

7.7.2 External Vertical Loads

Full-scale experiments on bridge abutments have shown that the reinforced mass behaves elastically. Hence, elastic methods that consider the reinforced soil as an equivalent composite medium of soil layers reinforced by closely spaced parallel layers of thin and stiff material [Harrison and Gerrard, 1972] can provide a reasonable approach to the determination of load effects on the tensile forces in the reinforcements.

Figure A-36 shows the results of a full-scale experiment on a double-faced Reinforced Earth wall, 39 ft high, constructed in the port of Dunkirk to support traveling gantry cranes. The experimental distributions of the tensile forces due to the loads are compared with the theoretical ones derived with Harrison and Gerrard's methods. The reasonable agreement between theoretical and actual values indicates that elastic methods can provide a reasonable approach to the determination of boundary load effects on the tensile forces in the reinforcements. However, this approach entails sophisticated modeling. In practice, a simplified empirical approach has therefore been adapted to approximate the additional tensile forces caused by vertical loads. The additional maximum tensile force is computed with the equation:

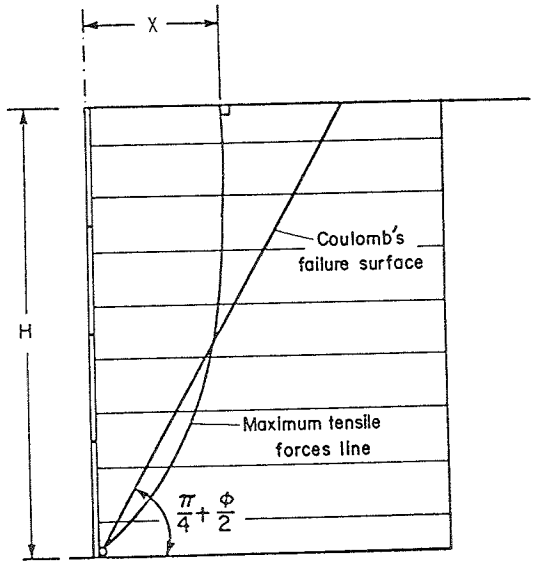

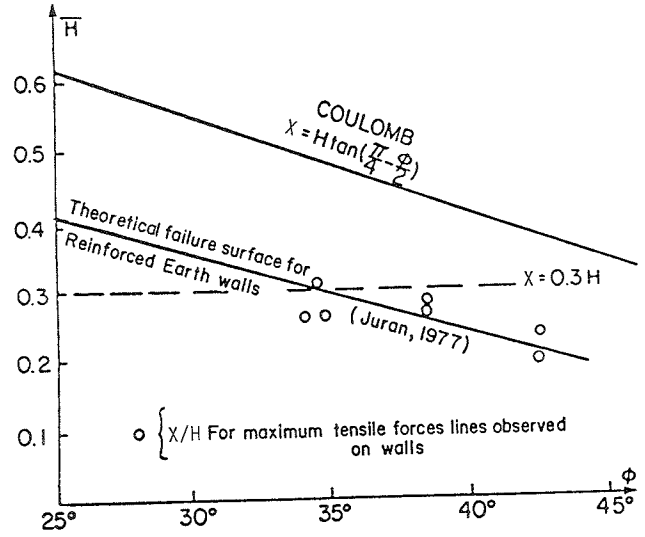

Figure A-32. Theoretical determination of maximum tensile force lines. [Juran and Schlosser, 1978]

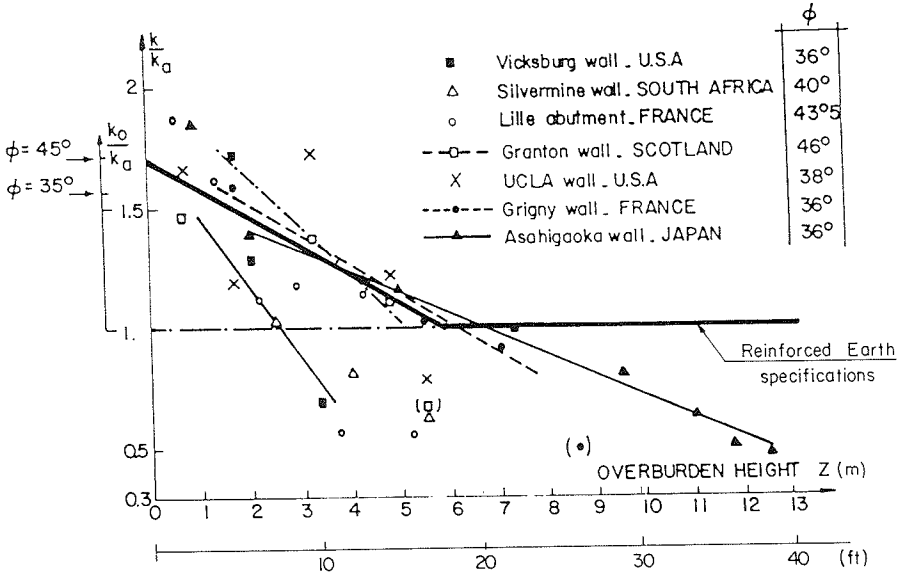

Figure A-33. Variation of K *for several instrumented walls.* [Schlosser, 1978]

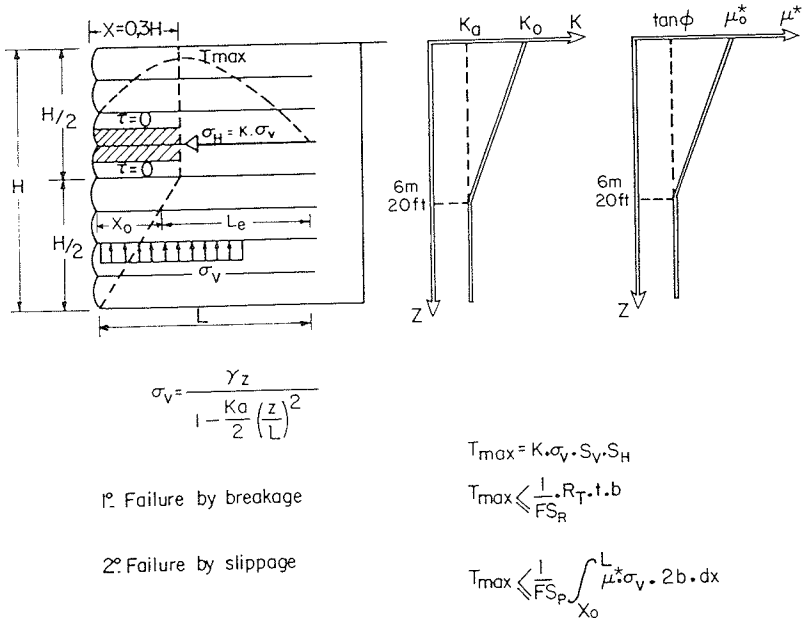

Figure A-34. Internal design of Reinforced Earth walls.

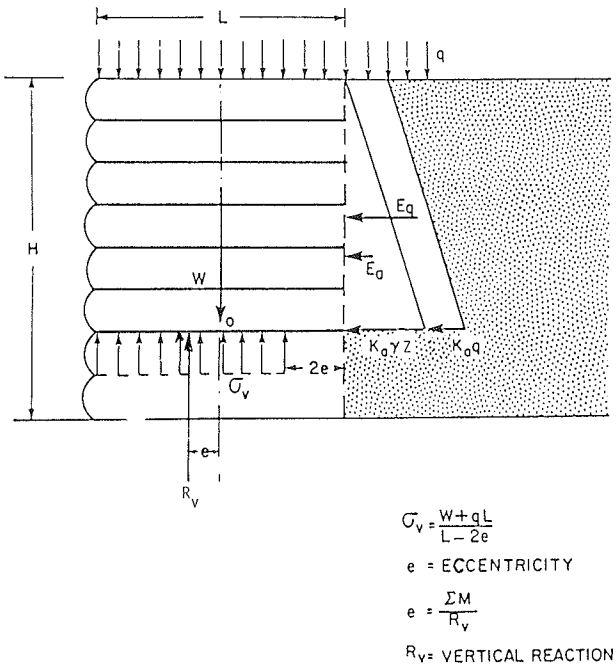

Figure A-35 Calculation of vertical stress by the Meyerhof method.

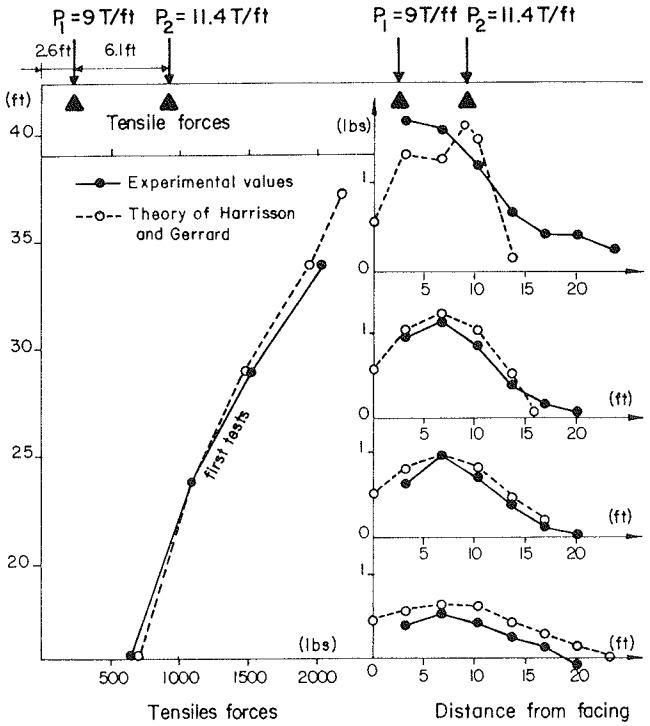

Figure A-36. Theoretical and experimental distributions of tensile forces due to surface loads on the Dunkirk wall. [Juran, 1977]

$$\Delta T_{max} = K \Delta \sigma_v S_v S_H \qquad \text{(A-10)}$$

where $\Delta \sigma_v$ is the increase in vertical stress due to the load at a point coinciding with the locus of maximum tensile forces.

The vertical stress is calculated assuming a uniform surface stress distribution and a load diffusion of two vertical to one horizontal (Fig. A-37). The empirical coefficient K, characterizing the state of stresses within the backfill material, varies with depth from K_o at the upper surface of the structure to K_a at a depth of 20 ft.

7.7.3 Bridge Abutments

Figures A-38 and A-39 show the principles of the design of Reinforced Earth bridge abutments under normal working loads.

The tensile forces in the reinforcements are calculated from the equation:

$$T_{max} = K \sigma_v S_v S_H \qquad \text{(A-11)}$$

where σ_v is the vertical stress at the point of the maximum tensile force in the considered reinforcement.

The vertical stress is calculated by superimposing the effects of all the forces exerted on the portion of the Reinforced Earth mass above the considered reinforcement.

First, the vertical stress is computed as if the bridge abutment is a retaining wall (see Sec. 7.7.1 of this chapter and Fig. A-35) with the following contributions to vertical stress at a given depth: (1) the unit weight of the reinforced soil; (2) the weight of the pavement layer, $\gamma_R H_R$, and the uniformly distributed traffic load, q (as shown on Fig. A-39b, it is assumed that these are both uniformly distributed up to the facing); (3) the vertical stress caused at a given depth by the active earth pressure behind the embankment (Sec. 7.7.1 and Fig. 1.A-35).

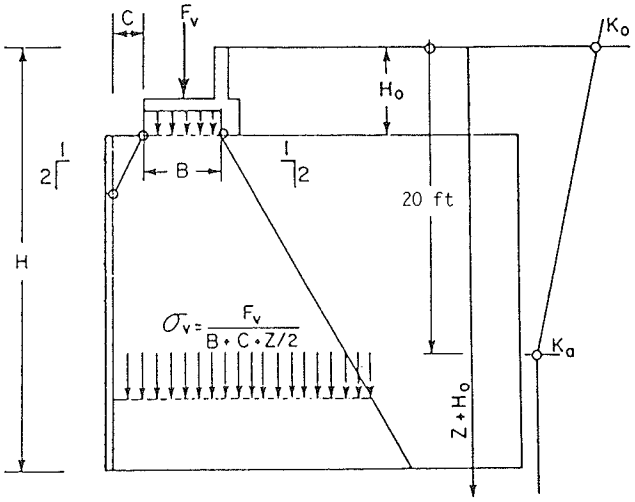

Figure A-37. Load diffusion and earth pressure coefficient in a bridge abutment.

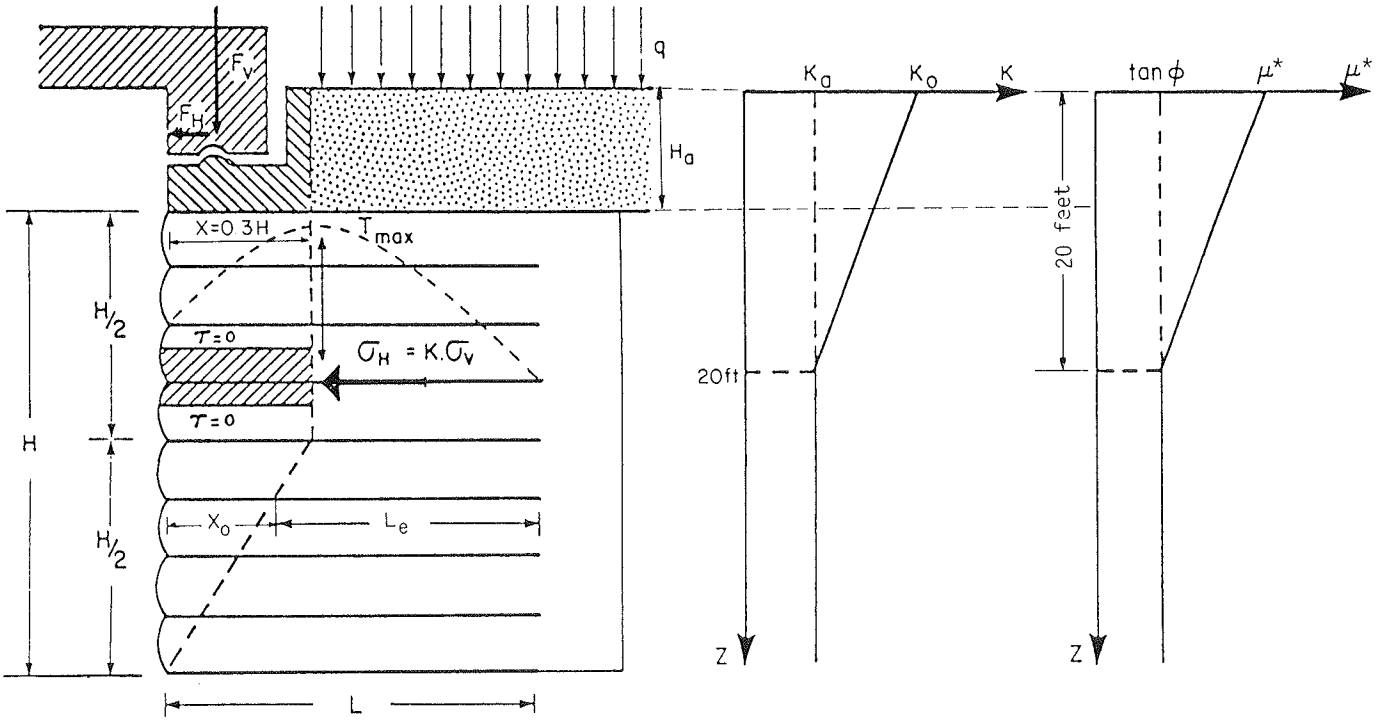

$T_{max} = K.\sigma_v.S_v.S_H$

1°- FAILURE BY BREAKAGE ..... $T_{max} \leq \frac{1}{FS_R}.R_T.t.b$

2°- FAILURE BY SLIPPAGE ..... $T_{max} \leq \frac{1}{FS_S}\int_{X_0}^{L} 2.b\,\sigma_v.\mu^*.dx$

Figure A-38. Internal design of Reinforced Earth bridge abutment.

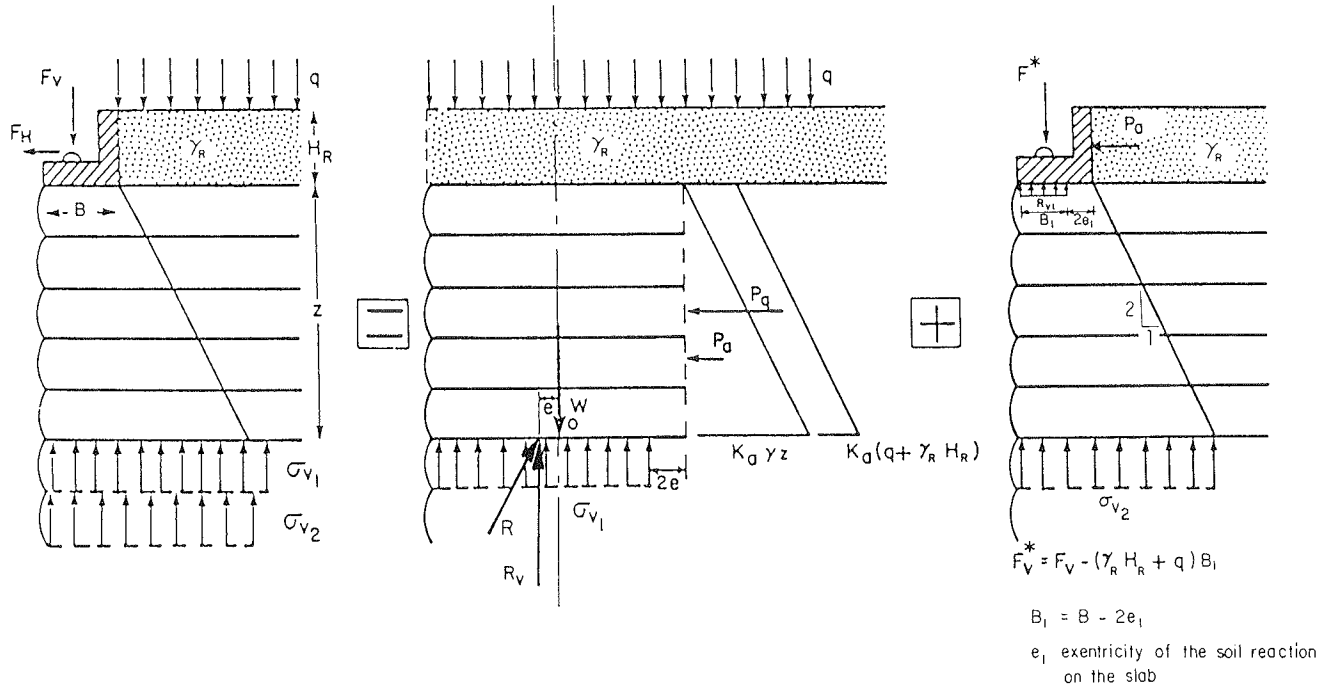

Figure A-39. Calculation of vertical stress.

The vertical stress confinement due to the bridge abutment line load, F_v (Fig. A-39a), is computed as follows. The width of the slab foundation on the Reinforced Earth, B, is reduced to an equivalent width B_1 as shown on Figure A-39c in accordance with the Meyerhof method. Because the traffic and pavement loads were assumed to be uniformly distributed up to the facing, an equivalent bridge slab line load, F_v^*, is computed as:

$$F_v^* = F_v - (q + \gamma_R H_R) \cdot B_1 \qquad \text{(A-12)}$$

The footing load is assumed to be uniformly distributed over the reduced width B_1 at the base of the footing (Fig. A-39c) and is dispersed with depth using a slope of 2 vertical to 1 horizontal (Fig. A-39d).

The horizontal forces exerted by the slab on the Reinforced Earth are assumed to mobilize tensile stresses which decrease linearly with depth to a zero value at $Z = 2B_1$. The magnitude of the tensile stress at the base of the slab foundation is completed by dividing the horizontal force by the reduced width of the slab.

The application of a vertical load on a Reinforced Earth structure modifies the locus of the maximum tensile forces. Figure A-40a illustrates the effect of the position of a vertical line load on the locus of maximum tensile forces as obtained by numerical studies using the finite element method. Figure A.40b shows the different maximum tensile forces lines which have been adopted for the design of Reinforced Earth bridge abutments as a function of the structure geometry.

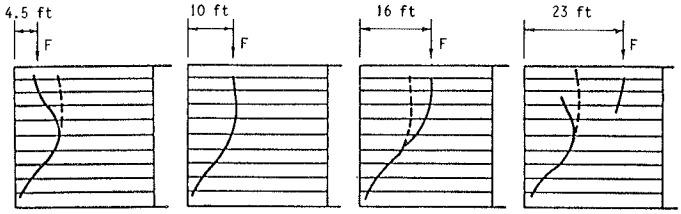

Figure A-40a. Effect of location of vertical surface loads on the locus of tensile forces as determined by finite element analysis of a 30-ft high wall. [Schlosser and Segrestin, 1979]

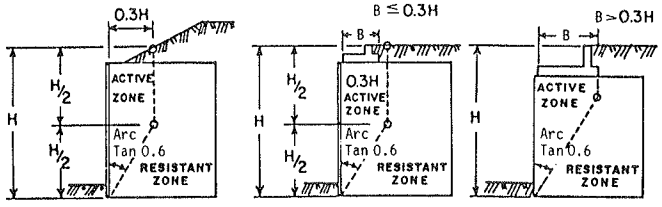

Figure A-40b. Maximum tensile force lines in a bridge abutment. [Schlosser and Segrestin, 1979]

7.8 Practical Considerations

7.8.1 Design Loads

The external design loads for Reinforced Earth structures are usually established according to the current practice of highway and bridge design in different countries. Generally the following conditions are assumed for design.

7.8.2 Soil Properties

Soil properties need not be measured for all walls. For small routine projects, provided the backfill criteria described in Section 5.5.2 of this chapter are satisfied, the following soil properties can be assumed:

Internal friction angle of backfill material—34 deg
Internal friction angle of random fill—30 deg
Unit weight of backfill material—125 lb/ft^3
Coefficient of earth pressure:
active—$K_a = 0.28$
at rest—$K_o = 0.44$

7.8.3 Properties of Prefabricated Elements

For prefabricated elements supplied in the United States, the minimum yield and allowable stresses listed in Table A-6 can be safely assumed. Higher strength steels may also be used.

It is assumed that the tensile force at the facing connection is equal to 85 percent of the maximum tensile force in the reinforcing strip. The required safety factor with respect to pullout resistance in the reinforcement is generally $F = 1.5$, and it should be verified that this factor of safety exists at the connecting end of a reinforcement, i.e., where the bolt hole is located.

7.9 Applications under Special Loading Conditions

7.9.1 Complex Boundary Conditions

The design methods outlined above are used for the design of Reinforced Earth walls and bridge abutments under the most

Table A-6. Yield and allowable stresses for reinforcements and tie-strips.

Component	Yield Stress	Allowable Working Stress
Reinforcing elements:		
reinforcing strips (A.36)	f_y = 36.0 ksi	f_t = 20.0 ksi
tie-strips (A.5.70.grade C)	f_y = 33.0 ksi	f_t = 18.0 ksi
Concrete	f_c = 4000 psi	

common types of static loading, i.e., the weight of the Reinforced Earth mass, the active earth thrust of a supported embankment, and the external loads applied on a bridge abutment. In cases of Reinforced Earth structures of unusual geometry, under more complicated boundary conditions or under special types of static loading, a general stability analysis approach can be used to evaluate an overall safety factor.

7.9.2 Dynamic Loading

The design of Reinforced Earth structures to resist dynamic loading (vibrations, impact, seismic effect) was initially based on the results of a research program carried out at the University of California at Los Angeles under the direction of Prof. K. Lee from 1974 to 1977; reduced scale laboratory models were used to evaluate the effects of horizontal and vertical harmonic and irregular accelerations [Richardson, 1978; Wolfe et al., 1978]. In addition, the effects of explosive-induced motion were studied on a full-scale prototype wall [Richardson et al., 1977].

An important concept which resulted from this research was that the total dynamic force, the distribution of dynamic forces, and the dynamic strain are influenced by the density and geometry of the reinforcing strips and by the magnitude of the horizontal acceleration. Empirical relationships based on this stiffness concept were used to establish the first design procedures [McKittrick and Wojciechowski, 1979]. Subsequent analysis of available experimental results has shown that for ordinary Reinforced Earth walls a triangular or trapezoidal distribution of dynamic forces can be used.

The current seismic design method for Reinforced Earth structures is based on the pseudostatic Mononobe-Okabe analysis approach [Mononobe and Matsuo, 1929; Okabe, 1926]. The principles of this design method are illustrated in Figure A-41.

The method is based on the following assumptions: (1) The dynamic load does not change the location of the maximum tensile forces in the reinforcements. (2) The active zone in the Reinforced Earth wall behaves as a rigid body. (3) The dynamic active force resulting from the seismic event is equal to the horizontal (and/or vertical) inertia force of the active zone, which is given by:

$$F_{ad} = W \cdot \frac{a_h}{g} \qquad \text{(A-13)}$$

where W = the weight of the active zone; a_h = the horizontal component of earthquake acceleration; and g = the acceleration due to gravity. (4) The total active force is equal to the sum of the dynamic active force and the static active force; consequently, at each level the maximum tensile force in the reinforcement is given by:

$$(T_{max})_n = (\sigma_{HD} + \sigma_{HS})\, S_v S_H \qquad \text{(A-14)}$$

where σ_{HD} = the horizontal dynamic active earth pressure at the considered level, and σ_{HS} = the horizontal static active earth pressure at the considered level, calculated according to the current static design methods outlined above. (5) A triangular dynamic pressure distribution, based on the results of both laboratory studies and finite element analysis, is assumed. The resultant dynamic force is therefore assumed to act at a distance of ⅔ of the wall height from the wall base. A detailed design example is given in Section 10 of this chapter.

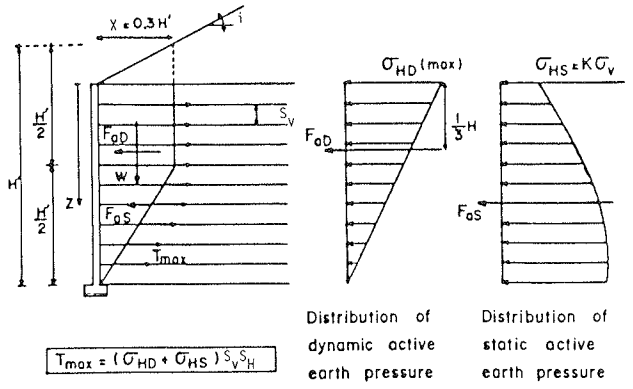

Figure A-41. Seismic design of Reinforced Earth wall.

Although this method provides a simple solution that is often used, the assumptions have not been verified.

Because of the difficulties associated with modeling the dynamic behavior of Reinforced Earth walls, the results obtained on small models cannot necessarily be extrapolated for the design of full-scale structures. In particular, the first and second assumptions of the five listed above require verification or modification. Consequently, further research on the dynamic response of Reinforced Earth structures is required to provide a fully rational basis for the development of appropriate seismic design methods.

8. CASE HISTORIES

8.1 Observations on Full-Scale Structures

Since 1968, a large number of Reinforced Earth structures have been instrumented. The first of these were in France, where a research program on Reinforced Earth was performed by the Laboratoire Central des Ponts et Chaussées from 1966 to 1976. As indicated on Table A-7 [Baguelin, 1978], 13 structures were instrumented by the French Highway Administration, including retaining walls and bridge abutments.

In 1968, measurements in the Incarville wall indicated that the tensile forces in the reinforcements were not a maximum at the facing but at some distance inside the wall. The full-scale experiment performed on the Dunkirk Wall (1970) confirmed the existence of active and resistant zones separated by the maximum tensile forces line. As shown in Figure A-42, these observations, which were followed by others on more recent structures in different countries, have led to the schematic maximum tensile forces line presently used in the design methods.

In the United States, the first instrumented Reinforced Earth wall was built in 1974 to reopen a section of Highway 39 in the San Gabriel Mountains north of Los Angeles. The wall has a metal facing and was 56 ft high and 525 ft long.

Measurements of tensile forces in the strips were made at three levels and were characterized by a continuous change of readings for many months after completion of the structure. This wall has been followed by many other full-scale experiments, e.g., Vicksburg [Al-Hussaini and Perry, 1978], Pennsyl-

Table A-7. Characteristics of walls observed or instrumented in France. [Baguelin, 1978]

YEAR	NAME	TYPE	FACING	LENGTH OF WALL	HEIGHT (H)	LENGTH OF STRIPS (L)
1968	INCARVILLE	Retaining Wall	Metal	165 ft	33 ft	33 ft
1968-69	LE PEYRONNET	Retaining wall with sloping backfill	"	165 ft	72 ft	131 ft
	MENIERI	Retaining wall and road platform	"	225 ft	16 ft	26 ft
	VIGNA II	Double retaining wall-highway platform	"	580 ft and 750 ft	and 29 ft	33 ft and 49 ft
1970	DUNKIRK	Retaining wall with moving cranes at the edge	"	2100 ft	33 ft	49 ft (joining two facings)
1971	SETE	Retaining wall - road platform	Concrete	600 ft	30 ft	30 ft
1971	FREJUS	Retaining wall	Metal	260 ft	43 ft	33 ft
1972	BRIMBORION	Urban expressway platform	Concrete	490 ft	26 ft	39 ft
1972	THIONVILLE	Abutment	Metal	60 ft and 320 ft	46 ft	36 ft
1973	LA DOUFINE	Retaining wall with sloping backfill	Concrete	260 ft	26 ft	26 ft
1974	CHAMBERY	Retaining wall on sheet piling quay	"	1300 ft	26 ft	26 ft
1974	LILLE	Abutment	"	50 ft	18 ft	23 ft and 33 ft
1976	ANGERS	Abutment	"	55 ft	20 ft	25 ft and 36 ft

vania Route 28 [Dash, 1978], UCLA [Richardson et al., 1977]. Full-scale experiments have also been performed in the United Kingdom [Murray and Baden, 1979] and in Japan [Hashimoto, 1979] since 1973. An interesting full-scale experiment in Japan has been described by Chida [1979]. An experimental Reinforced Earth wall 20 ft (6 m) high was built and failed with measurement of internal stresses.

Most of the observations of full-scale structures have focused on the measurement of tensile forces developed in the reinforcing strips. The tensile forces are measured by means of strain gauges. For the displacements of the facing, benchmarks located on the panels are generally used. Sometimes an inclinometer is attached to the facing and embedded in the foundation soil in order to obtain horizontal deformations directly. Pullout tests are performed in order to determine the value of the apparent friction coefficient μ^* and its variation with depth. Short reinforcing strips have to be placed during the construction of the backfill behind a special panel with holes (Fig. A-43). These strips must be short in order to prevent their breakage during the pullout.

Figure A-44 shows the instrumentation placed in a Reinforced Earth wall built at Krugersdorp, South Africa, in 1979 [Jones and Smith, 1979]. Stresses and deformations within the earth mass, as well as overall deformations of the structure, were measured.

To maximize information gained from an instrumented wall, the following measurements should be performed: tensile forces in the reinforcing strips, at least near the locus of maximum tensile force and near the facing panels; horizontal and vertical displacements of the facing; soil pressures on the facing or on a vertical plane close to the facing, on the base of the Reinforced Earth wall, and on perpendicular planes (one horizontal, one vertical) near the maximum tensile force line, if possible; and pullout tests on short reinforcing strips (3 ft to 6 ft long).

8.2 Comparison of Observations and Predictions

8.2.1 Reinforced Earth Walls

Reinforced Earth structures are currently designed mainly on the basis of limit state analysis, i.e., for failure conditions. However, most of the design assumptions are based on measurements in structures at working stress, rather than failure stress, conditions. Thus, it is of particular interest to obtain information on structures at failure conditions. However, only one full-scale experiment has been conducted on a wall that has failed under controlled conditions. This experiment was performed by the Reinforced Earth Company in Spain [Guilloux and Jailloux, 1979] to investigate a failure induced by accelerated corrosion of the strips. A cross section of the wall is shown in Figure A-45.

The wall was 20 ft (6 m) high, and the strips were very thin, 0.02 in. (0.6 mm) thick. Salty water was poured on the top of the wall in order to accelerate the corrosion of the strips. Failure, which was expected 6.5 months after construction, occurred after 9 months.

The instrumentation of the wall consisted of the following: measurements of the rate of corrosion on small pieces of strips located inside the Reinforced Earth backfill; measurements of the water and salt contents of the backfill by means of resistivity cells; and measurements of the displacements of the facing.

The displacements of the facing at failure were relatively low, as indicated on Figure A-46a. The total displacement at failure was about 0.8 in. The failure occurred by sliding along a surface (Fig. A-46b) which is very close to the maximum tensile force line and failure shape assumed in the design method.

Figure A-46c shows the variation of the safety factor with time, calculated according to the then current French method. It shows that the design method is slightly conservative, because it leads to a service life of 6.5 months as opposed to the 9 months actually required for failure.

8.2.2 Bridge Abutments

As discussed in Section 7.7.3, the design method for the case of external vertical loads at the top of a Reinforced Earth wall is based on assumption of a load dispersion angle of 2 vertical to 1 horizontal with depth. As for walls, the empirical coefficient K characterizing the state of stresses within the backfill material is assumed to vary with depth from K_o at the upper surface of the structure to K_a at a depth of 20 ft.

Very few full-scale experiments have been performed on Reinforced Earth structures loaded externally. Figure A-47 shows the theoretical and experimental variations with depth of the maximum tensile forces due to external vertical loads in two Reinforced Earth structures: a bridge abutment in Lille [Juran et al., 1978] and the wall of Dunkirk [Juran et al., 1979], which is a double-faced Reinforced Earth wall, 40 ft high, constructed to support traveling gantry cranes. These results indicate that the assumed load dispersion angle of 2 vertical to 1 horizontal leads to conservative results and that a dispersion angle of 1 to 1 may be more reasonable.

8.3 Shortcomings in Prediction Methods

8.3.1 General

The recommended static design method for Reinforced Earth walls and bridge abutments is safe and relatively conservative. However, there are some remaining uncertainties because it has not yet been possible to perform observations and full-scale experiments on all types of structures over a sufficiently large range of heights to check the validity of all aspects of the semi-empirical design methods. This is particularly true in the case of seismic design, for which only the results of small-scale model tests are available.

8.3.2 Unusually High Reinforced Earth Walls

The present design method has been checked for rectangular walls with vertical facing over a range of heights from 13 ft to 46 ft. Extrapolation of the design procedures to very high walls or to walls with a very different geometry, e.g., very narrow walls or sloping walls, cannot yet be fully justified and requires further investigation. Of the two failure modes possible for a Reinforced Earth wall, i.e., failure by pullout and failure by

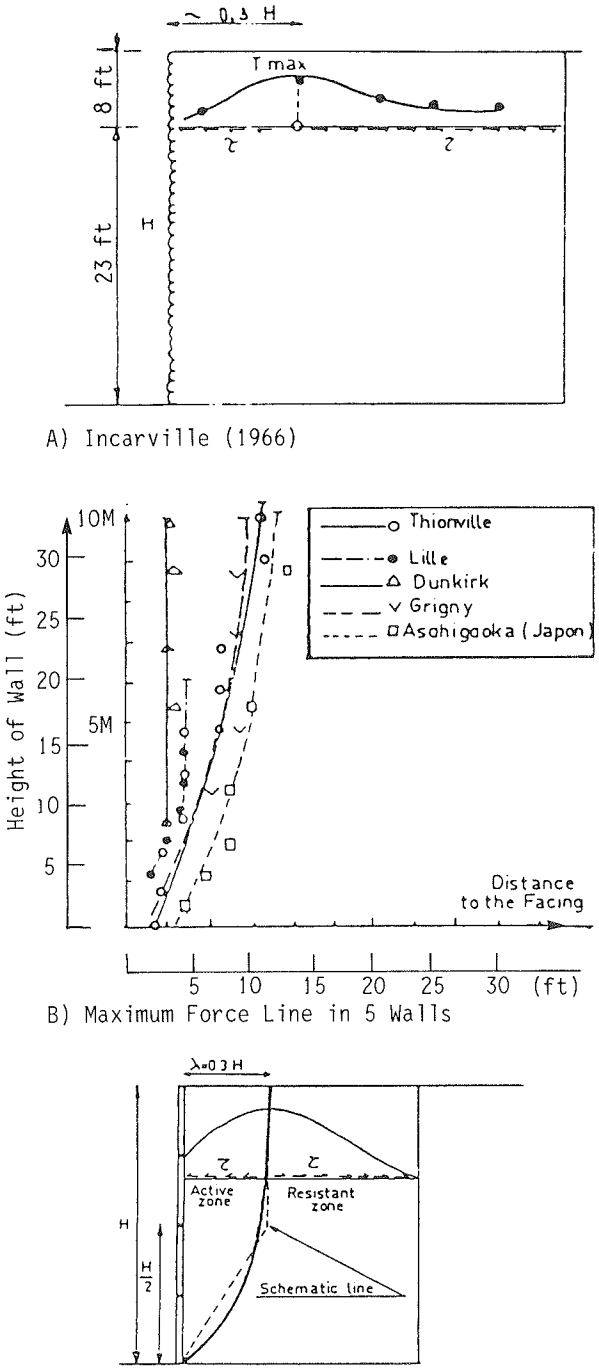

Figure A-42. Observations on location of the maximum tensile force line.

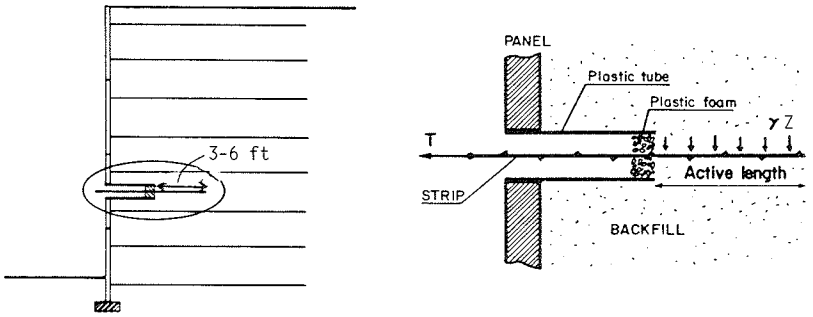

Figure A-43. Location of a short strip for a pullout test.

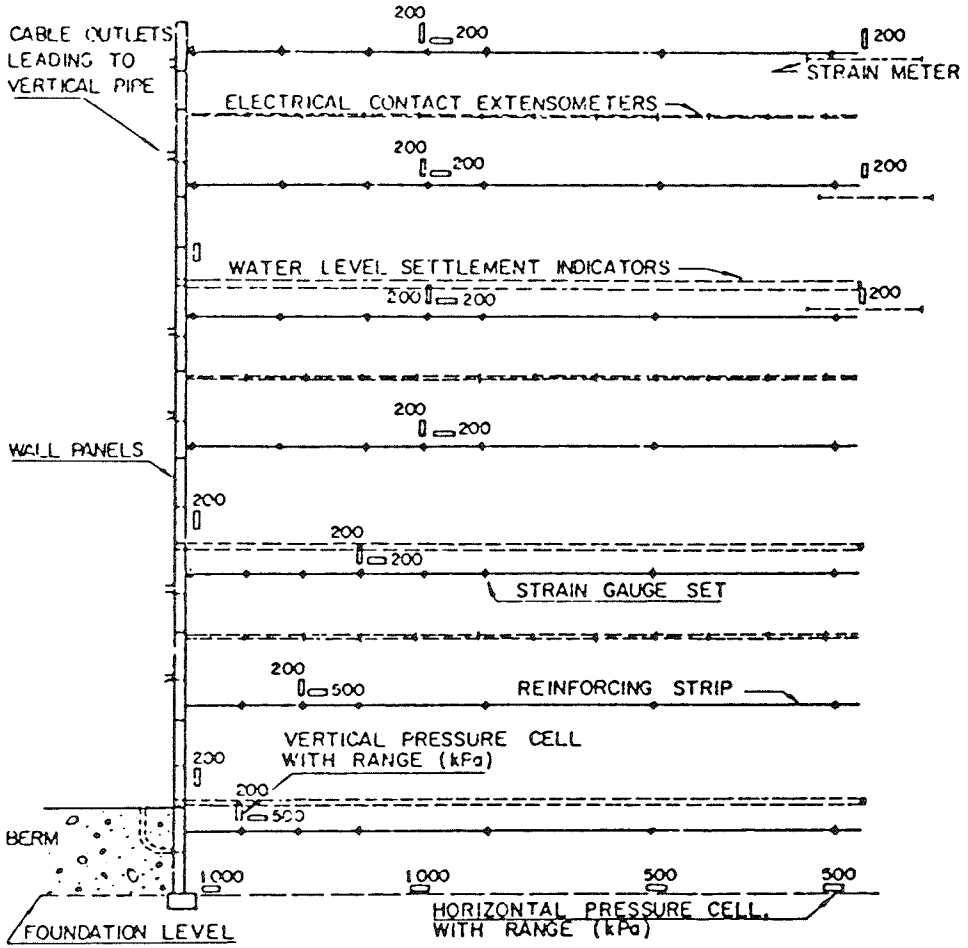

Figure A-44. Instrumentation of the Krugersdorp's wall. [Jones and Smith, 1979]

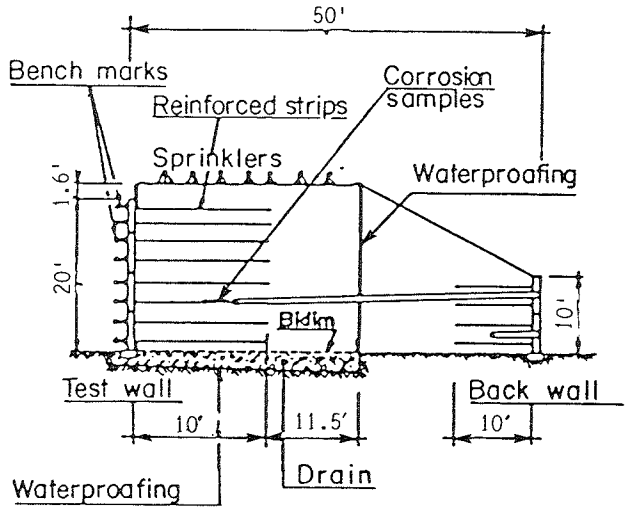

Figure A-45. Experiment on failure by corrosion. [Guilloux and Jailloux, 1979]

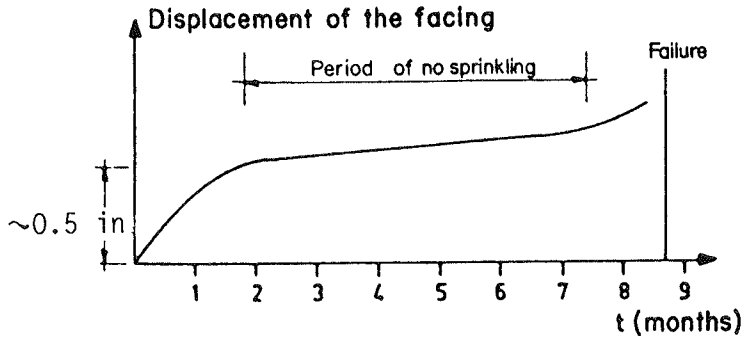

a) Horizontal displacement of the facing

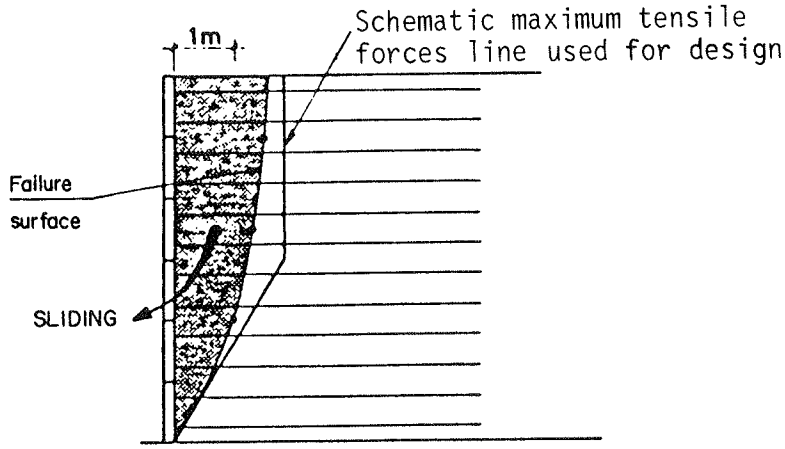

b) Location of the sliding surface

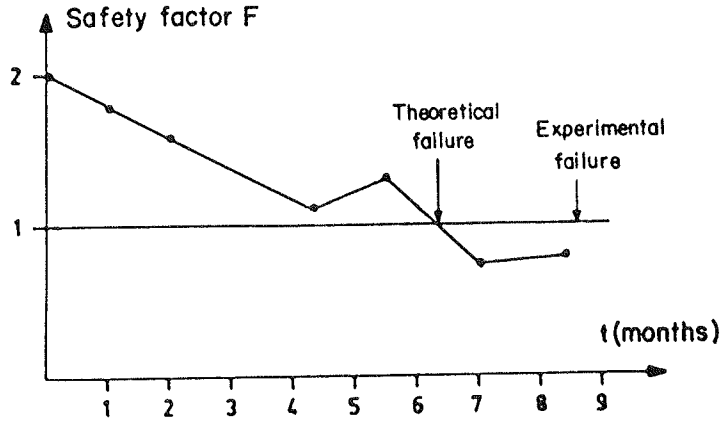

c) Variation with time of the safety factor with respect to the tensile resistance of the reinforcements

Figure A-46. Full-scale experimentation failure induced by accelerated corrosion. [Guilloux and Jailloux, 1979]

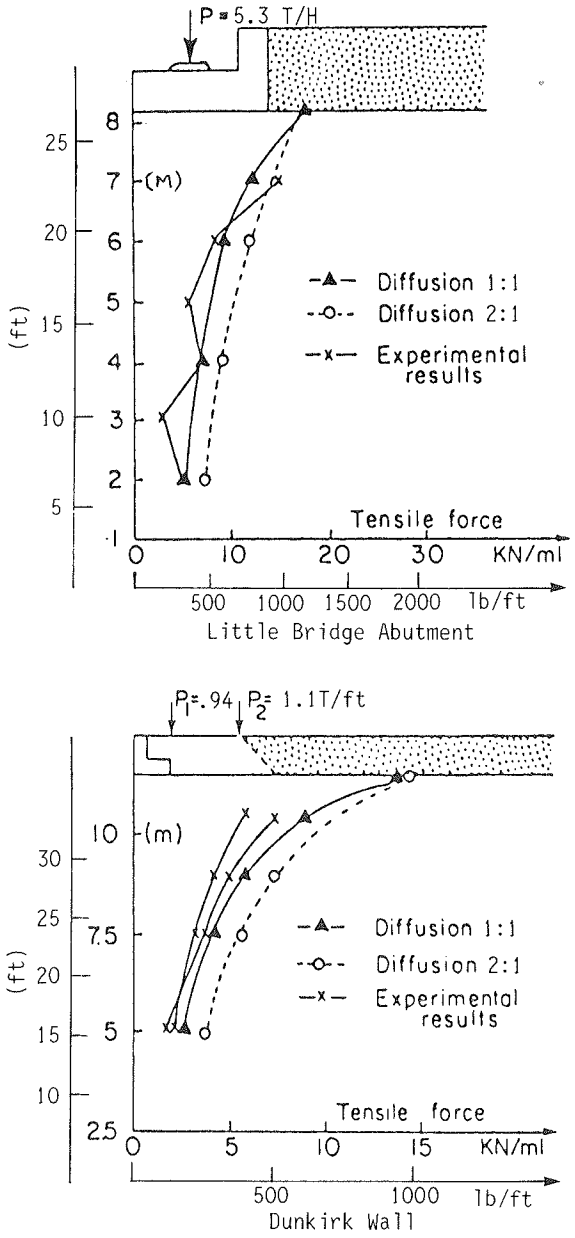

Figure A-47. Tensile forces due to external vertical loads

breakage of reinforcements, research has been focused mainly on the latter mode. It now appears [Schlosser and Juran, 1983] that some anomalies in the results of reduced scale model tests on Reinforced Earth walls may be explained by slippage of reinforcements that resulted in a failure line closer to Rankine conditions than assumed in the design. Although the Rankine conditions result in lower overall lateral stresses, the loci of the maximum tensile stresses in the reinforcements may thus be further behind the wall face than assumed in design.

8.3.3 Bridge Abutments and Walls with Exterior Loads

Only a small number of full-scale experiments have been performed on Reinforced Earth bridge abutments. However, the satisfactory performance of about one thousand such structures indicates that the design is certainly adequate to conservative. It seems that at the top of a Reinforced Earth abutment the length of the reinforcements could be reduced or the spacing between reinforcements may be increased considering the safety factor with regard to failure by slippage.

Very little experimental and theoretical work has been done on the effect of horizontal concentrated loads at the top of a Reinforced Earth wall. The present design method for such loads is essentially based on the behavior of classical retaining structures and may be conservative for a Reinforced Earth wall because of its inherent flexibility.

8.3.4 Seismic Loading and Vibrations

Reinforced Earth structures are well adapted to withstand seismic loadings because of their flexibility and high inherent damping. Progressively more and more Reinforced Earth structures around the world have been subjected to earthquakes, and observations on these structures can contribute to a better understanding of their dynamic behavior. However, the experimental and theoretical background for design is still limited. Experiments have been performed mainly on reduced scale models on shaking tables. There have been limited full-scale experiments using vibrations imposed near or at wall tops and explosions near wall bottoms. The results of reduced scale model tests on shaking tables cannot readily be extrapolated to actual structures because of the laws of similitude, and the vibratory and explosive loads are not representative of seismic loading.

Shortcomings in present dynamic design of Reinforced Earth structures can be summarized by the following three questions: Is the geometry of the active zone modified significantly when vibrations are applied to a Reinforced Earth structure? Is the apparent coefficient of friction between the soil and reinforcements under dynamic load different from that under static loads? Are the calculated stress increases in the strips due to dynamic loads in good agreement with the actual ones?

9. FUTURE DEVELOPMENTS OF REINFORCED EARTH

At the present time, Reinforced Earth is a well-developed, patented technique, with much experience from a large number of structures in different countries. Although retaining walls with vertical facings constitute the most common type of structure, new applications have been or are being developed (for example, bridge abutments, quay walls, and sloping walls for slot storage facilities). Other applications proposed by the inventor, Henri Vidal, have had very limited development to date. These include foundation rafts above cavities or on compressible soil and underground chambers or vaults.

9.1 Required and Present Research

Fundamental and theoretical research was initially performed by universities and research centers, while technological research was performed by the various Reinforced Earth companies. Presently, university research interests are more focused on other types of soil reinforcement, and current theoretical, ex-

perimental, and technological research is being conducted mainly by the Reinforced Earth companies. The main thrust of this research is related to material durability, use of fine-grained soil backfill, dynamic behavior of structures and seismic design, design methods for new applications of Reinforced Earth, and technological studies of prefabricated elements.

The purpose of the research on fine-grained soil backfill and on durability is to enlarge the range of backfill materials suitable for Reinforced Earth and to provide better understanding of the corrosion process and its rate.

Research on dynamic behavior and seismic design includes finite element analyses and a synthesis of observed results from all Reinforced Earth structures which have been subjected to earthquakes.

New applications of Reinforced Earth for which design methods are needed include sloping walls, trapezoidal walls, and narrow walls.

9.2 Anticipated Future Trends

As Reinforced Earth is a well-developed technique, it appears that only limited additional development of the system will occur in the future. Some improvements in the prefabricated elements can be expected as a consequence of current research, but no fundamental changes are anticipated.

New applications of Reinforced Earth are likely, but they are difficult to anticipate because of the uncertainty of various factors, such as comparative cost with classical solutions, market opportunities, and technical requirements.

10. DESIGN EXAMPLES

Several design examples for walls of different heights and geometries are presented in Chapter Five of the main report.

11. REFERENCES

AL-HUSSAINI, M. M., and JOHNSON, L. D. [1978]. "Numerical Analysis of a Reinforced Earth Wall," *Proc. ASCE Symposium on Earth Reinforcement,* Pittsburgh, Apr. 27, 1978, pp. 98–126.

AL-HUSSAINI, M. M., and PERRY, E. B. [1978]. "Field Experiment of Reinforced Earth Wall," *ASCE Symposium on Earth Reinforcement,* Pittsburgh, Apr. 1978, pp. 127–156.

BAGUELIN, F. [1978]. "Construction and Instrumentation of Reinforced Earth Walls in French Highway Administration," *ASCE Symposium on Earth Reinforcement,* Pittsburgh.

BASSETT, R. H., and LAST, M. C. [1978]. Reinforcing Earth Below Footings and Embankments," *Proc. ASCE Symposium on Earth Reinforcement,* Pittsburgh, Apr. 27, 1978, pp. 202–231.

BATTELINO, D. [1983]. "Some Experience in Reinforced Earth Wall," *Proc. 8th European Conference on Soil Mechanics and Foundation Engineering,* Helsinki, Vol. 2, pp. 463–468.

BOLTON, M. D., CHOUDHURY, S. P. and PANG, P. L. [1977]. "Modelling Reinforced Earth," *Proc. Symposium on Reinforced Earth and Other Composite Soil Techniques,* Edinburgh.

BOLTON, M. D., CHOUDHURY, S. P. and PANG, P. L. [1978]. "Reinforced Earth Walls, a Centrifugal Model Study," *Proc. ASCE Symposium on Earth Reinforcement,* Pittsburgh, Apr. 27, 1978, pp. 252–282.

CHIDA, S. [1979]. "Experimental Studies Regarding Reinforced Earth for Road Embankments," *International Conference on Soil Reinforcement: Reinforced Earth and Other Techniques,* Paris, Mar. 1979, Vol. II.

CORTE, J. F., and PAYEN, G. [1974]. "Etude d'un Mur en Terre Armee par la Methode des Elements Finis," Rapport Interne, Laboratoire Central des Ponts et Chaussées.

DARBIN, M., and MONTUELLE, J. [1979]. "Durabilite des Armatures de Terre Armee. Observation sur les Ouvrages," *International Conference on Soil Reinforcement: Reinforced Earth and Other Techniques,* Paris, March, Vol. II.

DASH, U. [1978]. "Design and Field Testing of a Reinforced Earth Wall," *Proc. ASCE Symposium on Earth Reinforcement,* Pittsburgh, April, pp. 334–347.

ELIAS, V. [1979]. "Friction in Reinforced Earth Utilizing Fine Grained Backfills," *International Conference on Soil Reinforcement: Reinforced Earth and Other Techniques,* Paris, March, Vol. II.

GUILLOUX, A., and JAILLOUX, J. M. [1979]. "Comportement d'un Mur Experimental en Terre Armee vis-a-vis de la Corrosion," *International Conference on Soil Reinforcement: Reinforced Earth and Other Techniques,* Paris, March, Vol. II.

GUILLOUX, A., and SCHLOSSER, F. [1979]. "Etude du Frottement Sol-Armature en Laboratoire," *International Conference on Soil Reinforcement: Reinforced Earth and Other Techniques,* Paris, March, Vol. I.

HARRISON, W. J., and GERRARD, C. M. [1972]. "Elastic Theory Applied to Reinforced Earth," *J. Soil Mechanics and Foundation Division,* S.M. 12, pp. 1325–1344, 1972.

HASHIMOTO, Y. (1979). "Comportement du Procede de 'Terre Armee' lors de l'Utilisation du Limon de Kanto Comme Materiau de Remblai," *International Conference on Soil Reinforcement: Reinforced Earth and Other Techniques,* Paris, March, Vol. II.

HERRMAN, L. R., and AL-YASSIN, Z. [1978]. "Numerical Analysis of Reinforced Soil Systems," *Proc. ASCE Symposium on Earth Reinforcement,* Pittsburgh, Apr. 27, 1978, pp. 428–457.

JONES, G. A., and SMITH A. C. S. [1979]. "Design, Construction and Monitoring of a Reinforced Earth Wall for Reconstruction of a Highway Slope Failure," *International Conference on Soil Reinforcement: Reinforced Earth and Other Techniques,* Paris, Mar. 1979, Vol. II.

JURAN, I. [1977]. "Dimensionnement Interne des Ouvrages en Terre Armee," Thesis for Doctorate of Engineering, Laboratoire Central des Ponts et Chaussées, July.

JURAN, I., and SCHLOSSER, F. [1978]. "Theoretical Analysis of Failure in Reinforced Earth Structures," *Proc. ASCE Symposium on Earth Reinforcement,* Pittsburgh, April 27, 1978, pp. 528–555.

JURAN, I., SCHLOSSER, F., LONG, N. T., and LEGEAY, G. [1978]. "Full Scale Experiment on a Reinforced Earth Bridge Abutment in Lille," Proc. *ASCE Symposium on Earth Reinforcement,* Pittsburgh, Apr. 27, 1978, pp. 556–584.

JURAN, I., SCHLOSSER, F., LEGEAY, G., and LONG, N. T. [1979]. "Experimentation en Vraie Grandeur sur un Mur Soumis

a des Surcharges en Tete a Dunkerque," *International Conference on Soil Reinforcement: Reinforced Earth and Other Techniques,* Paris, Mar. 1979, Vol. II.

LABORATOIRE CENTRAL DES PONTS ET CHAUSSÉES SETRA [1979]. Les Ouvrages en Terre Armee, Recommendations et Regles de l'Art, Direction des Routes et de la Circulation Routiere, September.

LONG, N. T., GUEGAN, Y. and LEGEAY, G. [1972]. "Etude de la Terre Armee a l'Appareil Triaxial," Laboratoire des Ponts et Chaussées, *Rapport de Recherche 17.*

MCKITTRICK, D. P. [1978]. "Reinforced Earth: Applications of Theory and Research to Practice," *Symposium on Soil Reinforcing and Stabilizing Techniques,* University of New South Wales, Sydney, Australia, Oct. 16, 1978 (also available as *Reinforced Earth Technical Series Report 79-1,* Reinforced Earth Co., Washington, D.C.).

MCKITTRICK, D. P., and WOJCIECHOWSKI, L. J. [1979]. "Design and Construction of Seismically Resistant Reinforced Earth Structures," *International Conference on Soil Reinforcement: Reinforced Earth and Other Techniques,* Paris, March, Vol. I.

MITCHELL, J. K., and SCHLOSSER, F. [1979]. General Report Session No. 1, *Proc. International Conference on Soil Reinforcement: Reinforced Earth and Other Techniques,* Paris, March.

MONONOBE, M., and MATSUO, H. [1929]. "On the Determination of Earth Pressures During Earthquakes," *Proc. World Engineering Conference 9,* 176–182.

MURRAY, R. T., BODEN, J. B. [1979]. "Reinforced Earth Wall Constructed with Cohesive Soils," *International Conference on Soil Reinforcement: Reinforced Earth and Other Techniques,* Paris, Vol. 2, pp. 569–577.

OKABE, S. [1926]. "General Theory of Earth Pressure," *J. Japanese Society of Civil Engineers,* Tokyo, 12, (1).

PHAN, T., SEGRESTIN, P., SCHLOSSER, F., and LONG, N. T. [1979]. "Etude de la Stabilite Interne et Externe des Ouvrages en Terre Armee par Deux Methodes de Cercles de Rupture," *International Conference on Soil Reinforcement: Reinforced Earth and Other Techniques,* Paris, March, Vol. I.

RICHARDSON, G. N. [1978]. "Earthquake Resistant Reinforced Earth Walls," *ASCE Symposium on Earth Reinforcement,* Pittsburgh.

RICHARDSON, G. N., FEGER, D., FONG, A. and LEE, K. L. [1977]. "Seismic Testing of Reinforced Earth Walls," *ASCE, J. Geotech. Eng. Div.,* Vol. 103, No. GT1.

SCHLOSSER, F. [1978]. "History, Current and Future Developments of Reinforced Earth," *Symposium on Soil Reinforcing and Stabilizing Techniques,* sponsored by New South Wales Institute of Technology and the University of New South Wales, Sydney, Australia, Oct. 1978.

SCHLOSSER, F., and ELIAS, V. [1978]. "Friction in Reinforced Earth," *ASCE Symposium on Earth Reinforcement,* Pittsburgh.

SCHLOSSER, F., and GUILLOUX, A. [1979]. "Etude du Frottement Sable-Armature en Modele Reduit," *International Conference on Soil Reinforcement: Reinforced Earth and Other Techniques,* Paris, March, Vol. I.

SCHLOSSER, F., and JURAN, I. [1983]. "Behavior of Reinforced Earth Retaining Walls from Models Studies," Chapter 6, Developments in Soil Mechanics and Foundation Engineering I, edited by R. K. Banerjee and R. Butterfield, Applied Science Publishers, Ltd.

SCHLOSSER, F., and SEGRESTIN, P. [1979]. "Dimensionnement des Ouvrages en Terre Armee par la Methode de l'Equilibre Local," *International Conference on Soil Reinforcement: Reinforced Earth and Other Techniques,* Paris, March, Vol. I.

TERRE ARMEE INTERNATIONALE [1982a]. "Essais sue les Ecailles Cruciformes. Campagnes de 1978 a 1982," *Rapport R23,* June.

TERRE ARMEE INTERNATIONALE [1982b]. Comportement Mecanique des Ecailles Cruciformes," *Rapport R24,* June.

TERRE ARMEE INTERNATIONALE [1982c]. "Durabilite de L'Acier Galvanise Enterre," *Rapport R25,* December.

WOLFE, W. E., LEE, L. K., LEE, D., and YOURMAN, A. M. [1978]. "The Effect of Vertical Motions on the Seismic Stability of Reinforced Earth Walls," *ASCE Symposium on Earth Reinforcement,* Pittsburgh.

CHAPTER TWO—GEOTEXTILES

Contents

1. INTRODUCTION

1.1 Physical Description

Geotextile-reinforced soil walls having vertical or sloping faces derive their support from multiple layers of continuous geotextile sheet embedded in the soil backfill behind the face of the wall. The wall facing is typically constructed by wrapping each geotextile sheet around its overlying layer of backfill and then reembedding the free end into the backfill, as shown schematically on Figure A-48. The wrapped geotextile wall facing retains the soil immediately behind the wall face, and the embedded portion of the sheet transmits the lateral earth pressure loading to the soil behind the active wedge by friction between the geotextile and the soil. The geotextile face is usually covered with asphalt emulsion, gunite, concrete, masonry, gabions, or soil and vegetation for long-term protection from exposure to ultraviolet light. Alternately, structural elements can be used as the wall facing, including precast concrete panels, steel soldier piles and wood lagging, masonry, gabions, or cast-in-place concrete. Different types of geotextile-reinforced soil walls are shown in Figure A-49. Connection between the geotextile sheet and the structural wall element can be provided by casting the geotextile into the concrete element, friction, nailing, overlapping, or other bonding methods.

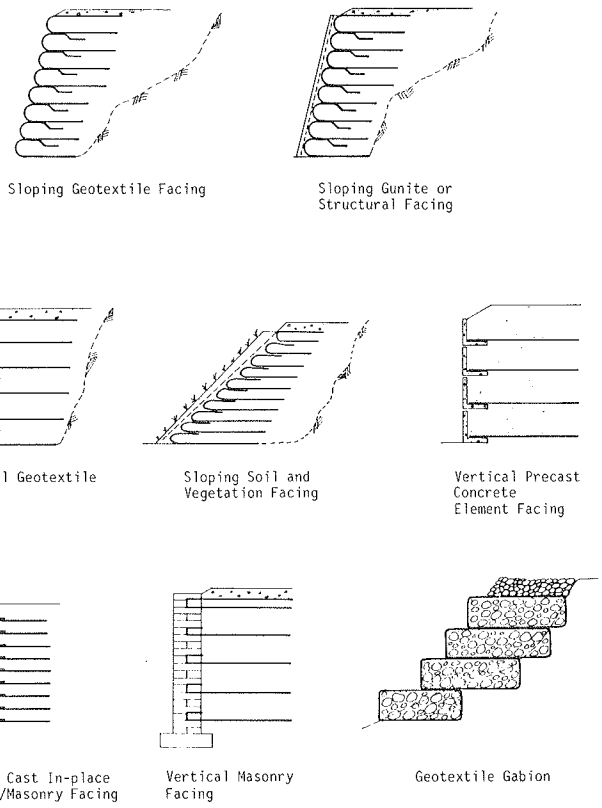

Figure A-49. Types of geotextile reinforced walls.

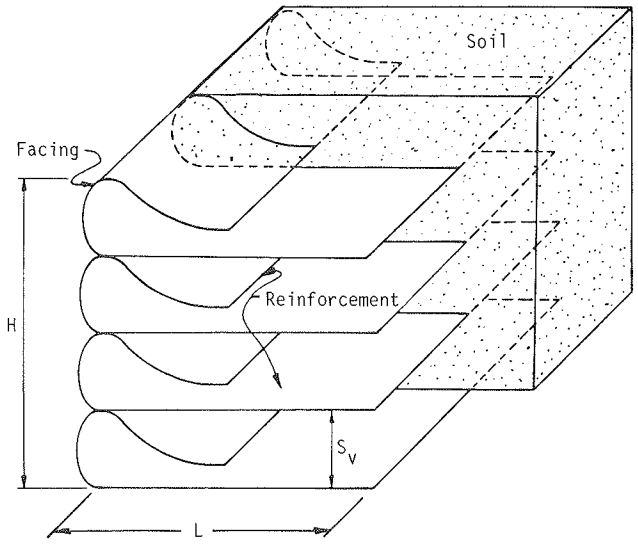

Figure A-48. Concept of the geotextile reinforced soil wall.

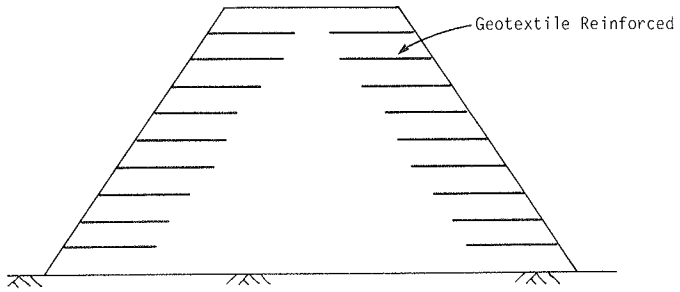

Figure A-50. Schematic of fabric reinforced embankment.

The backfill typically consists of granular fill ranging from silty sand to coarse gravel that is compacted in lifts with the geotextile. Compacted cohesive backfill has also been used. A wide variety of geotextiles with a wide range of mechanical properties and environmental resistances have been used, including nonwoven, needle-punched or heat-bonded polyester and polypropylene, and woven polypropylene and polyester. Geotextile-reinforced walls have in the past typically been located in remote areas or were used for temporary purposes; however, they are now being used for permanent urban installations, as well. The walls generally range in height from 3 ft to 30 ft, with one sloping wall having been constructed in France to a height of 66 ft.

Geotextiles are also used for reinforcement of embankments, as shown in Figure A-50. When used in this way, the reinforcements enable construction of embankments with steeper, more stable slopes than would be feasible without the reinforcements.

This report and its appendixes are specifically concerned with the reinforcement of soils to enable the construction of steeper slopes than would otherwise be possible with the nonreinforced soil, and also to enable slope stabilization in in-situ ground. Hence, many of the other applications of geotextiles in highway engineering, such as their use as filter fabrics, separations between road courses, and for initial filling over soft ground, are not discussed.

1.2 History and Development

The results of tests on model walls 4 ft 3 in. high, made of soil reinforced by horizontal layers of sacking material, were reported by Pasley in 1822. An increased stability of 12 percent was observed, even though the reinforcements were not connected to the wall face. More recently, geotextile-reinforced walls were introduced to avoid the corrosion problems associated with steel reinforcements. Research in Sweden and France with geotextile-reinforced highway embankments was extended to a highway embankment wall for Autoroute A.15 in Rouen, France, in 1971 [Puig et al., 1977]. This 13-ft high, 66-ft long vertical wall was the first installation of geotextile sheet reinforcement with a wrapped fabric face construction.

In 1974, the U.S. Forest Service initiated model tests at Oregon State University on geotextile-reinforced walls to be used for remote mountain roads. The small-scale model tests [Bell et al., 1975] were carried out to verify that the analytical design techniques developed for a Reinforced Earth wall [Lee et al., 1973] could be adapted for geotextile-reinforced walls. Based on these model tests, geotextile-reinforced walls were constucted in Siskiyou National Forest in Oregon in 1974 and Olympic National Forest in Shelton, Washington, in 1975 [Steward and Mohney, 1982]. The wrapped fabric face was covered with gunite at Siskiyou and asphalt emulsion at Olympic National Forest. The Forest Service developed construction and design guidelines for geotextile-reinforced walls in 1977 [Steward et al., 1977; revised 1983], based on this experience.

The excellent performance and low cost of these two U.S. Forest Service walls provided impetus for other geotextile-reinforced walls to be constructed in Gifford Pinchot National Forest, Mt. Baker National Forest and Willamette National Forest in 1980–1981 [Chassie, 1983]. Under FHWA sponsorship, highway departments in New York [Douglas, 1981], Colorado [Bell et al., 1983], and Oregon [Hart, 1984] installed geotextile-reinforced walls in 1980, 1982, and 1983, respectively. Along Interstate Highway 70 at Glenwood Canyon, Colorado, a geotextile-reinforced test wall was constructed in ten 30-ft (9 m) long segments with a different fabric or fabric strength combination in segments 1 through 8. Segments 9 and 10 were identical to 1 and 2 except the lower fabric layers were shortened to initiate failure. The geotextile walls were compared with other proprietary reinforced wall types including: Reinforced Earth, Welded Wire Wall, and VSL Retained Earth. All of the geotextile-reinforced walls performed well.

In Europe in 1975, model studies of geotextile-reinforced walls were initiated by a fabric manufacturer at the Swedish Geotechnical Institute as an extension of work on reinforced embankments started in 1971 [Holm and Bergdahl, 1979]. This work was continued in 1976 at the Royal Institute of Technology in Stockholm [Holtz and Broms, 1977] on a model geotextile-reinforced wall designed to simulate precast concrete face elements. This work resulted in a geotextile-reinforced wall design method proposed by Broms [1978].

At St. Ferreol, in the French Alps, a road was stabilized over a landslide using a geotextile-reinforced sloping wall in 1975. In 1976, at Pierrefeu, France, a geotextile-reinforced wall was used in construction of a dam spillway weir [Kern, 1977]. A temporary construction road was made for a 1,800-MW power plant at Allemand, France, in 1981, using a 66-ft high geotextile-reinforced sloping wall. Other geotextile-reinforced walls 26 ft to 33 ft high have been constructed for roads in Grenoble and Romans, France. In Canton Aargau, Switzerland, a permanent sound absorbing highway wall was constructed using geotextile reinforcement.

In England, masonry faced wall systems have been reinforced with geotextiles in urban environments. Rockfilled gabions were used as facing for one wall constructed to stabilize a small slip in a minor road. Information on these case histories is presented in Section 8 of this chapter and summarized in Table A-8.

Recent developments have included use of prefabricated structural facing elements, improved connections between geotextile reinforcement and these facing elements, and bonding of geotextile sheets with stiff geotextile reinforcing strips to form an easy-to-install, stiff geotextile reinforcement (discussed in Chapter Three of this appendix).

1.3 Proprietary Restrictions

There are no current proprietary restrictions associated with geotextile-reinforced walls.

2. APPLICATIONS

2.1 Inherent Advantages

Geotextile-reinforced walls have numerous advantages over conventional gravity retaining walls, and to a lesser degree over other types of reinforced soil walls; for example: (1) ease of transportation of construction materials; (2) construction by unskilled labor; (3) limited heavy equipment required, in fact, in some cases no heavy equipment is required; (4) flexible wall; (5) limited foundation preparation required; (6) no corrosion problem; (7) drainage of backfill through geotextile reinforcing layers; (8) low costs; and (9) speedy construction.

Table A-8. Geotextile reinforced wall case histories.

	Name	Location	Date	Structure	Height (ft)	Length (ft)	Fabric	Backfill	Facing	Construction	Cost	Comments	Reference
(1)	Autoroute A15	Rouen, France	1971	Highway embankment wall	13	66	Bidim U34-1.6 foot layer spacing	Weathered chalk silt and fire stone	Wrapped vertical	Berm on passive side partly removed after construction	-	Unprotected facing fabric	Puig et al., (1977)
(2)	Illinois River Road	Siskiyou National Forest, Oregon	1974	Road	11	33	Fibertex 400 0.75-1.0 feet layer spacing	Silty sand & gravel	Wrapped 1:8 slope gunite	Sand berm and sand bags placed in a row in front of facing	-	First fabric reinforced wall built in U.S.	Bell and Steward, (1977)
(3)	Olympic National Forest Road	Shelton, Washington	1975	Timber haul road wall	3-20	164	Bidim and Fibretex 0.75-1.0 feet layer spacing	Crushed basalt	Wrapped vertical asphalt emulsion	Temporary wood form system	11.56 ft^2 of wall	Coupons of treated and untreated fabric left on site for durability evaluation	Steward and Mahney, (1977)
(4)	Barrage de Maraval	Pierrefeu, France	1976	Dam spillway weir	21	52	Tri X 2.0 foot layer	Rounded gravel near facing, otherwise compacted clay & schist colluvium	Wrapped resin coated	-	-	Withstood three overtoppings before end of construction without damage	Kern, (1977)
(5)	NY 22	Columbia County	1980	Slide corrections in hill embankment	16	110 and 150	Bidim C34	Crushed stone	Wrapped 1:3 slope 3 inch thick wire mesh reinforced concrete	Temporary wood form system	42.00/ft^2 of wall	Stepping lifts to follow road grade	Douglas (1981)
(6)	Camp Hill Road	Willamette National Forest, Oregon	1981	Road widening across slide area	28		Supac 5W	Sawdust	Asphalt emulsion	-	18.90/ft^2	Sawdust used to provide lightweight backfill across slide area	Chassie, (1983)
(7)	Allemond Road	Allemond, France	1981	Mountain road for Electricite de France 1800 MW power plant	66	492	Stabilenka 200 26 foot layer spacing	Gravel and sand	Wrapped 1:2 slope bituminous with sand	-	-	-	CII, (1982)
(8)	Yorkshire Test	West Yorkshire, England	1981	Urban environment test	7	30	Terram 100 0.5 foot layer spacing	Granular fill Crusher run	4.4 inch brick 8.8 inch brick 4.4 inch brick unreinforced	Fabric wrapped around regular shaped backing blocks		Limited distortions of facing	Jones, (1982)
(9)	I-70	Glenwood Canyon, Colorado	1982	Highway embankment wall founded on highly compressible silts and clays	15	300	Fibretex 200, 400, Supac 4, 6, Trevira 1115, 1127, Typar 3401, 3601, 0.75-1.3 foot layer spacing	Clean sandy gravel	Wrapped 1:5 slope, 2 inch gunite	Temporary wood form system lifts to place backfill over the first 0.5-7.5 feet	11.00-12.50/ft^2 of wall	Settlements of about 30 cm recorded after 6 months	Bell et al., (1983)

2.2 Disadvantages

Geotextile-reinforced walls also have several limitations: (1) reduction in geotextile strength on exposure to ultraviolet light; (2) susceptibility to damage during construction and vandalism; (3) less desirable aesthetic appearance than some other wall types; (4) uncertain long-term durability; (5) large deformations developing under working loads; (6) lack of proven theories and tests for analysis and design (current designs are very conservative); and (7) height limitations compared with metallic reinforcement systems, because of the comparatively low tensile resistance of geotextile fabrics.

The first three disadvantages can be minimized by use of appropriate wall facing material such as gunite, soil and vegetation, precast concrete, or asphalt emulsion.

2.3 Site Conditions Appropriate for Use

Geotextile-reinforced walls can be constructed at most sites where other types of reinforced soil walls are constructed. Geotextile-reinforced walls can be used on very steep slopes because of the limited requirements for heavy equipment and modest slope excavation required for embedment of reinforcement. These walls can be constructed in difficult to reach terrain because the materials are light and easily transported.

2.4 Routine Applications

Typical applications include slide stabilization on remote mountain roads, highway retaining walls on steep mountain slopes, temporary or permanent road widening or diversion embankment walls, and road embankment walls over compressible foundation soils. Geotextiles also have wide application for subgrade reinforcement and for soft foundation reinforcement.

2.5 Special Applications

In Europe there have been several unique applications of geotextile-reinforced walls including a dam spillway weir, sound absorbing or noise barrier embankment walls for highways or airports, masonry or concrete gravity wall stabilization and repair, and an embankment wall for a car parking facility (see Sec. 8 and Table A-8). Other potential applications include small slope stabilization projects for small commercial or residential properties; various urban retaining wall projects; temporary military facilities requiring rapid, low-cost construction in remote areas; and small, narrow dams.

3. MECHANISMS AND BEHAVIOR

3.1 General Behavior and Mechanism of Failure of Geotextile-Reinforced Wall

The soil mass in a geotextile-reinforced wall is retained by the reinforcing action of the geotextile sheet, and erosion of soil at the face is prevented by wrapping the end of the geotextile sheet over the overlying layer of soil and embedding it into the backfill. As with other types of reinforced soil walls, the reinforced soil backfill is both the load-carrying and load-applying medium in the wall system. As the wall deforms, the earth pressure in the soil is transmitted through the geotextile sheet to the soil backfill behind the zone of active deformation through friction between the soil and geotextile. Of the currently used soil reinforcement systems, geotextiles are most clearly a purely frictional system, i.e., there is no development of passive soil resistance.

3.2 Soil–Geotextile Reinforcement Interaction

Geotextile-reinforced soil is a composite material and, as such, the mechanical properties of each component must be understood in order to establish the interaction between soil and geotextile. The mechanical and physical properties of the soil and conditions that affect interaction with geotextile sheet reinforcement include particle size distribution, particle angularity, effective unit weight, location of groundwater table, elastic modulus, and angle of internal friction (cohesion for clays must also be considered). The particle angularity and size distribution influence how the soil interlocks with the fabric structure. The stress-deformation properties control how much the soil deforms under applied stresses. The friction mobilized between the soil and geotextile is controlled by the angle of internal friction of the soil and the effective unit weight and location of the groundwater table. These latter parameters, in turn, determine the vertical soil stress applied normal to the geotextile sheet.

The important mechanical properties of the geotextile under tensile stresses include elastic modulus, elongation to failure, and rupture strength. These properties should be determined using a sufficiently large sample with wide end clamping. Ideally, the effect of confining stress should be reflected in the testing procedure. Geotextiles confined in soil generally have higher strengths than unconfined geotextiles because of soil particles interlocking with the fabric openings. Weaknesses in the geotextile caused during placement or compaction may lead to stress concentrations that can result in rupture at stresses below their apparent strength.

The geotextile carries tensile stress that is transmitted to the soil by friction between the geotextile and soil surfaces. The stress-deformation response of the geotextile and soil is generically different and thus stress-level dependent. Hence, to characterize the shear behavior of the composite material, the movement of the geotextile in a confined soil mass must be understood.

Geotextile–soil interaction can be studied by reinforcing a cylindrical reconstituted sample of soil with one or more parallel geotextile discs [Broms, 1977; Holtz et al., 1982; Gray et al., 1982; and Ingold and Miller, 1982a]. Axial loading of the specimen models a shear plane crossing the axis of the geotextile at an angle of approximately $45° + \phi/2$, as shown in Figure A-51, a condition which is not valid for an entire geotextile-reinforced wall.

Tests performed in a shear box may provide a better representation of the shear conditions that develop between geotextile and soil in a geotextile-reinforced wall. Tests can be performed to model both shear and pullout resistances, as shown in Figure A-52. Collios et al. [1980] discuss these types of tests in detail. Tests have been performed with the same soil in both the upper and lower halves [Holtz, 1977; Salomone et al., 1980; Schwab et al., 1977; Collios et al., 1980; and Delmas et al., 1979]. Different soils have been used in the two halves, for example,

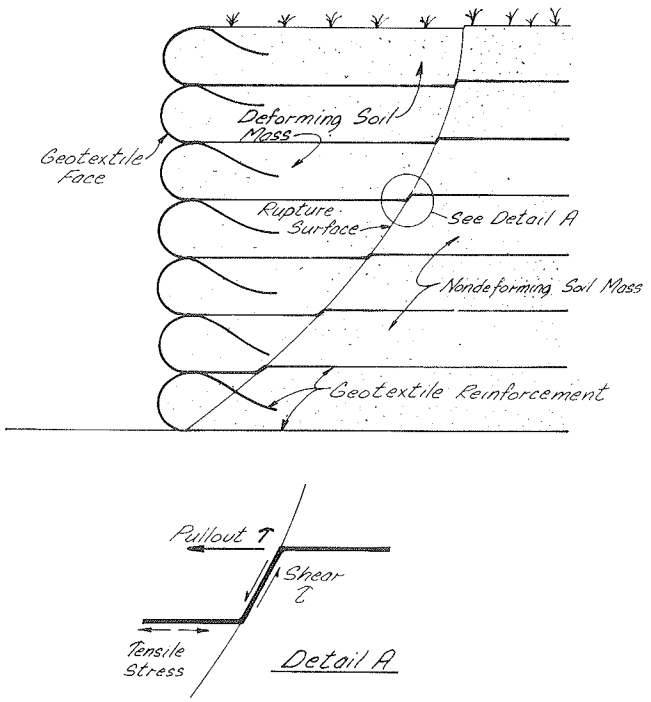

Figure A-51. Failure mechanism of geotextile reinforced wall.

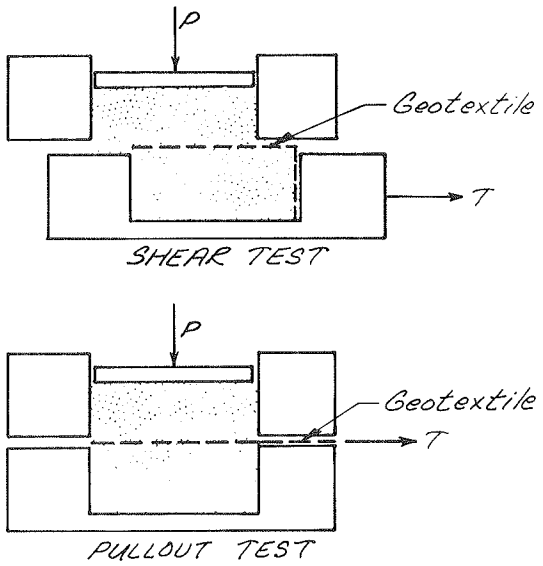

Figure A-52. Types of shear box tests. [After Collios et al., 1980]

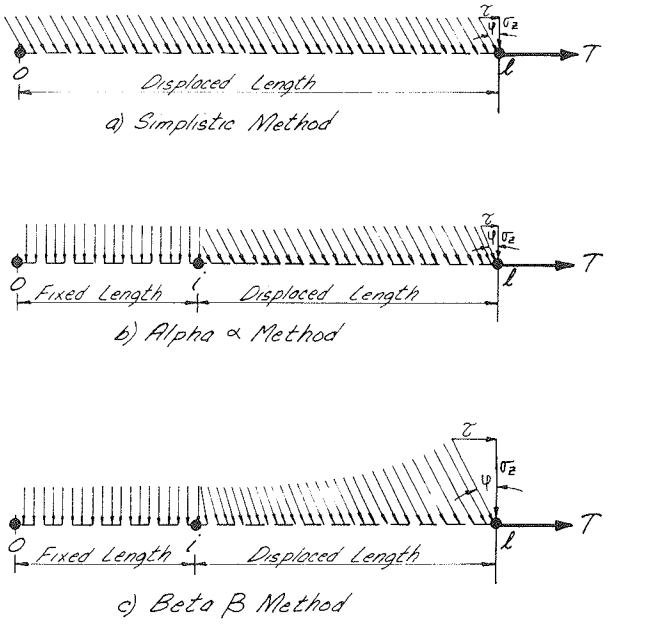

Figure A-53. Interpretation of soil-geotextile interaction—shear box pullout tests.

sand on top, and gravel on bottom [Collios et al., 1980; Delmas et al., 1979]. Also, granular soil has been used in the upper half and geotextile glued or free on a smooth or rough plate [Myles, 1982; Collios et al., 1980; Delmas et al., 1979; and Schwab et al., 1977].

Collios et al. [1980] showed that shear tests with the geotextile on a rigid plate gave results close to pullout test results, especially if the soil particles are coarse and rounded. This is because the geotextile is flat in both cases. Pullout tests and shear tests with rigid plates give values of soil-to-geotextile friction angle, δ, smaller than those obtained from the results of shear tests with soil on both sides of the fabric.

For most geotextile-reinforced wall applications, tests using the same soil in both halves of the shear box are appropriate. Interpretation of the shear tests is straightforward: the horizontal force T divided by the normal force P equals the tangent of the apparent angle of friction, δ, between the geotextile and the soil.

Interpretation of pullout tests is more difficult because of elongation of the geotextile and because the applied stress σ_v is not uniformly distributed on the geotextile–soil surface. Three methods can be used to interpret pullout tests, as shown in Figure A-53, and described below.

The method used by Collios et al. [1980] assumes that the applied stress, σ_v, is uniform over the uniformly displacing geotextile. The assumption is valid if the geotextile has a high modulus and if the normal stress is small. The interpretation is the same as for the shear test, i.e., $\tan \delta = T/P$.

The alpha method [Delmas et al., 1979; Holtz, 1977] assumes that the normal stress is uniformly distributed, but that the geotextile can elongate within the shear box. As the tensile load is applied, the geotextile displaces relative to the soil along a portion of its length (Fig. A-53b). The remainder of the geotextile remains fixed to the soil until the displacement front reaches this point as the tensile load is increased. The displacement of the geotextile must be measured at numerous locations using strain rods [Delmas et al., 1979], magnets [Holtz, 1977], or x-ray diffraction [Schwab et al., 1977]. The strain in the fabric is derived from the displacement measurements. Then, knowing the fabric modulus, the force used to elongate the fabric is determined. The remaining portion of the applied force rep-

Table A-9. Geotextile soil friction angles, δ, determined from shear box tests.

Type of Soil	Type of Reinforcement							Type of Test	Reference
	None	Nonwovens		Wovens			SS*		
		NP*	HB*	Multi*	Mono*	Slit*			
Rigid Plate Used As A Cover	36			32.5				Shear	Schwab (1977)
Unknown	38	35.5	34	38		32	29	Shear	Myles (1982)
	43	42	40		42			Shear	Myles (1982)
	45	44	39		40			Shear	Myles (1982)
Same Material In Support And Cover	35		35					Pullout	Holtz (1977)
	45		45					Pullout	Holtz (1977)
Sand	38		37-40					Pullout	Salamone et al. (1980)
	39	35		35				Shear	Collios et al. (1980)
	39	35						Pullout	Collios et al. (1980)
Rounded gravel	49	37		35				Shear	Collios et al. (1980)
Crushed gravel	53	48		48	52			Shear	Collios et al. (1980)
Ballast	63	53			50			Shear	Collios et al. (1980)

*Notes:

NP = Needlepunched
HB = Heatbonded
Multi = Multifilament
Mono = Monofilament
Slit = Slit film
SS = Smooth steel

Angles are in degrees.

resents the mobilized geotextile-soil friction, from which the apparent coefficient of friction, tan δ, is calculated by dividing by the normal force.

The beta method assumes nonuniform normal stress, which therefore creates nonuniform geotextile displacement. The beta method was developed because the alpha method determines values of pullout load that are not in agreement with experimental data. Delmas et al. [1979] present a theory in which the value of normal stress on the fabric is determined. This value of normal stress is qualitatively realistic since it is likely that there will be more stress near the front wall of the box, towards which the soil is displacing (Fig. A-53c). The beta method produces a theoretical curve for the horizontal force, which is in good agreement with experiment results.

The range of geotextile–soil interface friction angles for various soil and fabric combinations is significant and is summarized in Table A-9. For some geotextiles the friction angle is the same as the soil friction angle, while for others it is less. Site-specific laboratory testing may be required for major projects if reliable information is not available.

3.3 Behavior of Reinforced Soil Structures

Laboratory studies [Bell et al., 1975] on small-scale models of geotextile-reinforced walls with rigid facings (Fig. A-54), loaded to failure, have shown the following mechanisms of failure: failure of the reinforced soil mass by general sliding in the vicinity of the wall (overall instability), and failure of the reinforced soil material by rupture or pullout of the geotextile reinforcement layers.

In these small-scale model tests it was observed that the failure surface in the reinforced soil mass was a plane oriented at an angle very close to $45° + \phi/2$ above the horizontal at the bottom of the wall, with a slight upward curve near the top. Failure in the reinforced soil occurred either by rupture of the reinforcement layer, when the load in the reinforcement layer

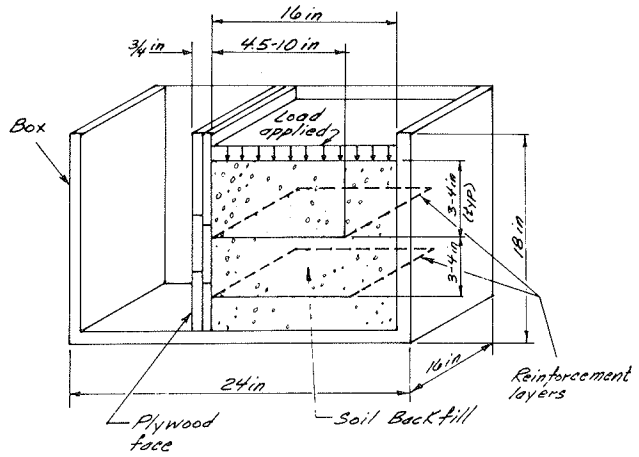

Figure A-54. Small-scale geotextile reinforced wall model. [Bell et al., 1975].

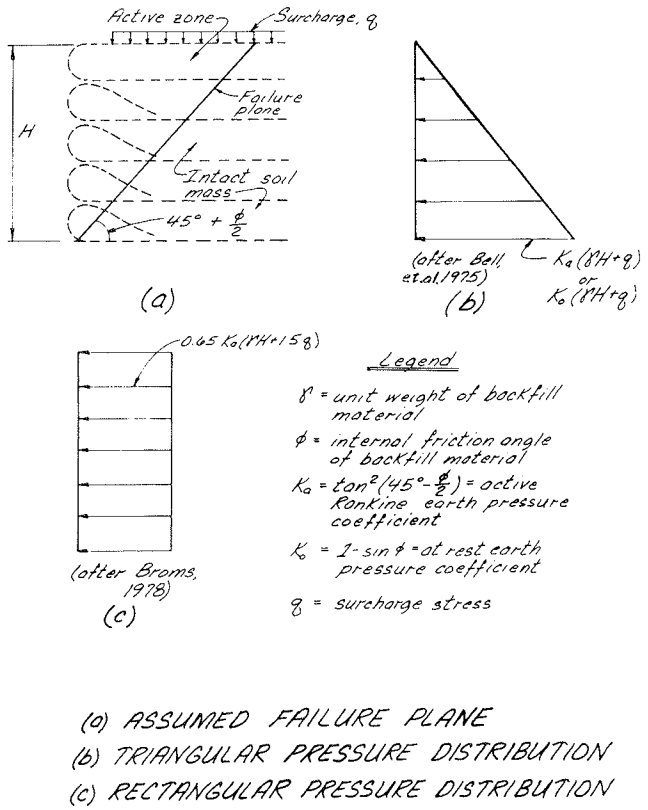

Figure A-55. Assumptions for analysis of geotextile reinforced soil structures.

exceeded the tensile strength of the geotextile, or by pullout of the reinforcement, when its anchor length was not sufficient to overcome the tensile load due to earth pressure. The models that failed by rupture of the reinforcement did not fail suddenly; rupture was evident in the bottom two or three layers, generally parallel to the wall face, at the intersection of the reinforcement layer and the failure surface.

The analysis of geotextile-reinforced walls by Bell et al. [1975] employs concepts developed by Lee et al. [1973] for reinforced soil walls using steel strips. As shown in Figure A-55a, the failure surface is assumed to be a plane oriented at an angle $45° + \phi/2$ above the horizontal, extending from the bottom to the top of the wall. The failure plane separates the active zone immediately behind the wall face and the resistant zone. Inside the active zone, the soil is assumed in an active state of plastic equilibrium, and the Rankine earth pressure theory thus applies. The lateral earth pressure against the wall face follows a triangular distribution, and its value at any depth may be obtained using the Rankine earth pressure coefficient, $K_a = \tan^2(45° - \phi/2)$, as shown in Figure A-55b. In order for the soil mass behind the wall face to reach active conditions, the wall must deform laterally by an amount equal to approximately 1 percent of the wall height [Holtz and Broms, 1977]. A deformation of this order of magnitude is much greater than the typical value of 0.1 percent of wall height used for more rigid walls. This is because the flexible geotextile reinforcement layers are relatively highly extensible in plane, and significant deformations are, consequently, needed to develop shearing resistance along the soil–reinforcement interface.

The use of the at-rest earth pressure coefficient, $K_o = 1 - \sin\phi$, instead of the active Rankine earth pressure coefficient, K_a, was proposed by Lee et al. [1975] for the design of Reinforced Earth structures. This approach was adopted by the U.S. Forest Service [Steward et al. 1977] for the design of geotextile-reinforced walls. As shown in Chapter One of this appendix, the coefficient K_o is applicable at the ground surface for Reinforced Earth structures—i.e., where relatively small lateral deformations would develop—because of wall facing rigidity and the small amount of deformation needed to mobilize shearing resistance along the reinforcing steel strip–soil interface. However, in low-modulus geotextile-reinforced walls, this may be a conservative approach because of the relatively large deformations which occur. The conservatism of the K_o method has been verified by a series of full-scale tests conducted by the Colorado Highway Department [Bell et al., 1983], where two of the test sections designed using a K_o analysis were expected to fail, but neither experienced excessive deformations. It is possible that the method may be more realistic for woven geotextiles with a high modulus.

Observations made during small-scale model tests [Bell et al., 1975] have shown that even the use of K_a may be conservative, because the failure loads for the models were at least 1.3 times higher than the loads predicted by theory. It should be pointed out that by computing loads in the reinforcement layers equal to lateral earth pressure at a given reinforcement depth multiplied by the area bounded by the middistances between the reinforcement layers above and below, it is implicitly assumed that there is no interaction between adjacent layers. This may not be the actual behavior in a reinforced soil structure using extensible geotextiles, because the more highly stressed reinforcement layers may transfer part of their loads to adjacent layers after significant strain has developed. Actual loads in the reinforced soil structure are thus expected to be more uniform with depth, as evidenced by field measurements [John et al., 1982].

The results of strain–stress interaction tests in a geotextile-reinforced wall have been approached differently by Broms [1978]. He considered the equilibrium of a column element of soil extending between two adjacent reinforcement layers and assumed that the column element resists the lateral earth pres-

sure imposed on it by friction developed at its contact areas with both layers of reinforcement (see Fig. A-66). In effect, as discussed later, this would transfer stress from the lower to the upper reinforcement as long as the element does not rotate. Broms indicated that the lateral earth pressure against the wall facing could be as much as 10 times less than the earth pressure at a distance behind the wall equal to the reinforcement layer spacing because of this redistribution. For design of the spacing between fabric layers, Broms proposes to use a uniform rectangular pressure distribution similar to the distribution for anchored walls developed by Terzaghi and Peck [1967], shown in Figure A-55c. Under this assumption, the loads in the reinforcement layers will remain reasonably equal, regardless of the depth considered, which is in agreement with the uniform load distribution with depth observed in the field [John et al., 1982].

As discussed previously, failure of reinforcement layers by rupture occurred in the small-scale model tests at the intersection with the Rankine failure surface, which corresponds approximately to the location of the maximum tensile stress in the reinforcement layer [Bell et al., 1975]. Figure A-56 illustrates the distribution of tensile stresses in the reinforcement layer for a wall with a rigid facing according to Broms [1978]. In a reinforced soil mass, lateral displacement of the active wedge has a tendency to pull the remainder of the reinforcement out of the resisting soil mass. As a result, the directions of the shearing stresses reverse at the location of intersection with the failure surface, as indicated in Figure A-56a. This location for the maximum tensile stresses in the reinforcement layer is compatible with the concept of increased lateral earth pressure with increased distance from wall facing. However, in the case of flexible, geotextile-wrapped facings, higher tensile stresses may exist in the reinforcement layers near the wall facing and the tensile stress distribution may be as represented in Figure A-56b.

As a coherent structure, a geotextile-reinforced wall behaves like a conventional retaining wall, and, as such, should be checked against other possible modes of failure including overturning about the toe, bearing capacity failure, excessive differential settlement of the foundation soil, lateral sliding of the wall on its base, and rotational sliding along a failure surface behind the reinforced zone. The first three modes of failure, i.e., overturning, bearing capacity, and settlement, can be evaluated using classical geotechnical engineering methods, and are not described herein.

For a wall with reinforcements of equal length, lateral sliding can be analyzed by considering the wall as a rigid block resisting lateral earth pressure through friction along the lower face of the bottom reinforcement layer only (Fig. A-57a). For the case of variable reinforcement length, resistance to lateral sliding is provided by friction along the lower face of the bottom reinforcement layer and friction along the lower faces of that portion of each reinforcement layer extending beyond a failure plane having the embedded end of the reinforcement layer immediately below as its terminus (Fig. A-57b).

Stability of a geotextile-reinforced wall against rotational failure can be evaluated by considering the wall as a rigid block bounded by a failure surface, passing beyond the reinforcement layers, which is assumed to consist of a logarithmic spiral and a plane tangent to the spiral at an angle of $45° + \phi/2$ above the horizontal [Broms, 1978], as shown in Figure A-57c. This rigid block is acted on by its own weight and the active earth

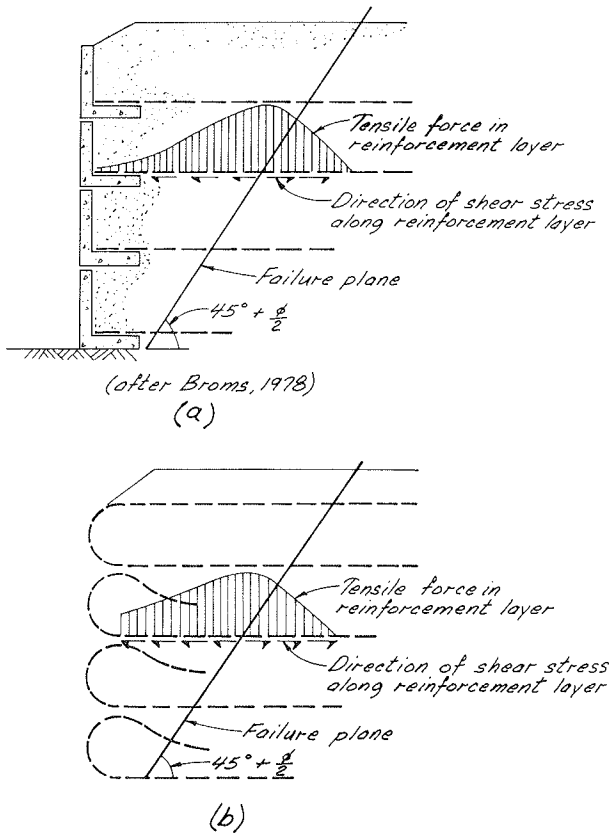

Figure A-56. Stress distribution in reinforcement layer.

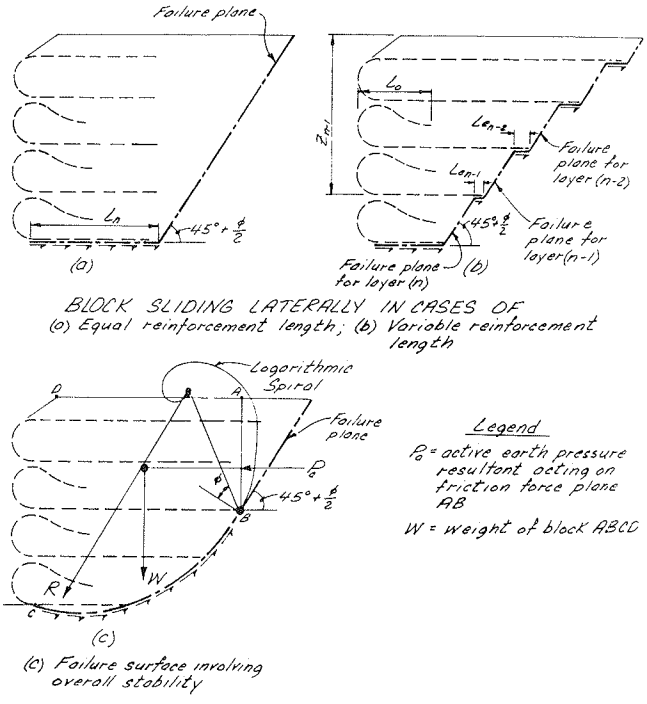

Figure A-57. Failure surfaces for external modes of failure.

pressure resultant with respect to the straight part of the failure surface, calculated by a triangular pressure distribution.

4. TECHNOLOGY

4.1 Description and Fabrication of Components

A geotextile-reinforced wall generally consists of three components: geotextile reinforcement, wall facing, and soil backfill. Many types of geotextile reinforcement have been used, including nonwoven needle-punched fabrics made of spun-bonded continuous polyester or polypropylene filaments; nonwoven needle-punched and heat-bonded fabric made of short (staple) polypropylene fibers; woven heat-bonded monofilament polypropylene fabric; and woven multifilament polyester fabric. The mass per unit area has ranged from approximately 140 g/m^2 (4 oz/yd^2) to 550 g/m^2 (16 oz/yd^2), with corresponding ranges of strength and deformability. Geotextile resistance to chemical attack also varies. Some geotextiles are treated with carbon black to increase resistance to ultraviolet light. The properties of some geotextiles used for wall reinforcement are summarized in Table A-10.

Many types of wall facings have been used, e.g., uncoated or uncovered geotextile, asphalt emulsion, gunite, resin spray precast concrete element, cast-in-place concrete, soil and vegetation, masonry and gabions (see Fig. A-49). There are also many types of precast concrete elements similar to those used with other soil reinforcement methods that can be used for geotextile-reinforced wall facings. Concrete elements may be L-shaped beams, hexagonal-shaped interlocking plates, or rectangular plates, all of which require precast fabrication at a concrete plant. The major problem associated with precast concrete elements is the connection between the geotextile and the face element. To circumvent this difficulty, prefabricated concrete panels have been developed which have one end of an alkaline resistant geotextile sheet embedded into the concrete.

Other types of facings also require preconstruction fabrication. For example, gabions made with wire mesh require fabrication of the boxes separately from the geotextile-reinforced walls; gunite requires fabrication of wire mesh reinforcement on the face of the wall; cast-in-place concrete requires fabrication of concrete forms along the face of the slope; and even vegetation on a sloping geotextile-reinforced wall has to be started. This can be accomplished by fabricating a wire mesh onto the slope and then hydroseeding with a colloidal spray. One manufacturer [Myles, 1984] has developed a geotextile which has a 4-in. diameter pocket sewn into the fabric at the intersection of each layer interface with the wall face, to be filled with peat. Vegetation is then cascaded down the slope. This system, although appearing simple and elegant, was not easily constructed because of problems associated with filling the geotextile pocket with peat.

For some walls where the geotextile forms the wall facing, with some external protection, there is no preconstruction fabrication required outside of manufacture of the geotextile sheet. The geotextile sheet width may be increased at the factory to a maximum width of 23 ft using a special seam which gives a high percentage (90 percent) of the fabric tensile strength [Myles, 1984]. In many cases, fabric seams are not sewn, but adjacent sheets are simply overlapped. However, on the Prapoutel Les Sept Laux road widening near Grenoble, France, transverse spreading of the geotextile sheets opened a gap in the fabric facing allowing exit of the granular backfill. Geotextile sheets can be sewn in the field.

Soil backfill is generally granular, ranging in size from silty sand to coarse gravel. In several cases, cohesive soil has also been used. Sawdust was used for two walls in national forests in Washington and Oregon. The backfill is compacted in lifts after placement of each level of geotextile.

4.2 Fabrication Quality Control

Fabrication of the various components of geotextile-reinforced walls is subject to quality control requirements used in other types of civil engineering structures. For example, fabrication of precast concrete wall elements is subject to ASTM and ACI testing requirements for precast reinforced concrete structural elements. The properties of the geotextile sheets and seams are tested in accordance with ASTM specifications (see Table A-11).

5. DURABILITY AND SELECTION OF BACKFILL

5.1 Members Susceptible to Degradation

5.1.1 Geotextiles—Outdoor Exposure

Geotextile sheets are susceptible to degradation due to outdoor exposure. This degradation leads to a decrease in tensile strength and elongation to failure with increasing exposure time. Outdoor exposure includes the effects of sunlight, humidity and precipitation, wind, air pollutants, and vandalism. The short wavelength ultraviolet (UV) radiation in sunlight breaks chemical links of the polymer fibers. UV light intensity is quite variable depending on latitude, longitude and altitude, on daily and seasonal variations, and on variations from one year to another. For example, the degradation of geotextiles exposed to sunlight in Florida, Arizona, and North Carolina occurred at quite different rates [Raumann, 1982]. This is because the latitude and altitude influence the angle of incidence of the sunlight and therefore the amount of sunlight filtering through the atmosphere.

Although all geotextiles degrade with exposure to UV light, some have higher resistances, which allow temporary exposures for construction purposes. These differences were illustrated by Raumann [1982], as shown in Figure A-58. Eleven different geotextiles were exposed for more than a year and then tested mechanically. These tests indicated that polyester fibers generally had a higher resistance to outdoor exposure degradation than polypropylene geotextiles, except when the polypropylene was treated with a significant amount of carbon black. Some of the untreated nonwoven polypropylene fabrics lost over 50 percent of their strength after 8 weeks and disintegrated after 16 weeks. Thicker fabrics of the same polymer (B2 vs. B1) apparently had better resistance to UV light due to shielding action. The size of individual fibers also influences their resistance to UV light degradation, because the same duration of exposure has the same depth of influence on the fibers and thereby produces a higher proportion of degradation of the cross-sectional area of a small-diameter fiber than a large-diameter fiber.

Table A-10. Properties of geotextile reinforcement.

Manufacturer	Name-Grade	Type	Polymer	Mass per Unit Area oz/yd^2 (g/m^2)	E.O.S. m (US Sieve)	Thickness Mils (mm)	Grab Strength lb (N)	Grab Elongation (%)	Tear Strength lb (N)	Burst Strength psi (kN/m^2)	Puncture Strength lb (N)	Permeability cm/s	1984 Cost $/yds^2 ($/m^2$)
Rhone Poulenc	Bidim U34	Needlepunched Nonwoven	Polyester	8 (270)	(55-90)	90 (2.3)	225 (1150)	75	125 (556)	400 (2757)	-	0.30	-
Rhone Poulenc	Bidim U64	Needlepunched Nonwoven	Polyester	16.2 (550)	(55-85)	190 (4.8)	610 (2711)	60	250 (1012)	850 (5860)	-	0.30	-
Dupont	Typar 3401	Heatbonded Nonwoven	Polypropylene	5.9 (200)	70-110 (150-210)	15 (0.4)	130 (578)	62	75 (334)	200 (1378)	-	0.03	0.81 (0.97)
Dupont	Typar 3601	Heatbonded Nonwoven	Polypropylene	4 (136)	140-170 (88-105)	18 (0.5)	207 (921)	-	103 (458)	263 (1813)	-	0.03	0.71 (0.86)
Crown Zellerbach	Fibertex 200	Needlepunched Nonwoven	Polypropylene	6 (200)	70-110 (150-210)	60 (1.5)	140 (623)	125	60 (267)	250 (1724)	-	0.30	0.89 (1.07)
Crown Zellerbach	Fibertex 400	Needlepunched Nonwoven	Polypropylene	12 (400)	80-100 (150-177)	110 (2.8)	260 (1156)	160	100 (445)	450 (3102)	150 (667)	0.30	1.61 (1.93)
Hoechst	Trevira S1115	Needlepunched Nonwoven	Polyester	4.5 (153)	70+ (210+)	85 (2.2)	130 (578)	90	50 (222)	220 (1517)	60 (267)	0.30	0.54 (0.65)
Hoechst	Trevira S1127	Needlepunched Nonwoven	Polyester	8 (272)	70-100 (150-210)	125 (3.2)	260 (1156)	90	100 (445)	380 (2620)	125 (558)	0.30	1.08 (1.29)
Phillips	Supac 4NP	Needlepunched Nonwoven	Polypropylene	4.1 (139)	80-120 (125-177)	40 (1)	115 (512)	65	-	260 (1792)	75 (334)	0.10	0.54 (0.65)
Mirafi	Mirafi 600X	Slit-Film Woven	Polypropylene	6 (204)	50-80 (177-297)	33 (0.8)	300 (1334)	35	120 (534)	600+ (4136+)	135-(600)	0.01	0.94 (1.13)
Enka	Stabilenka 200	Multifilament Woven	Polyester	13.3 (120)	120 (130)	28 (0.7)	1143 (5080)	10	-	-	-	-	2.26 (2.70)
ICI Fibres	Terram RF/12	Knitted	Polyester	8.8 (300)	-	40 (1)	680 (3000)	17	-	-	-	-	1.67 (2.00)
Low Brothers	Loktrak 16/15	Slit-Film Woven	Polypropylene	3.5 (120)	100 (150)	12 (0.3)	85.7 (381)	15	-	-	-	-	-

Table A-11. Geotextile property test summary.

Property Tested/Test Name	Reference	Description	Comments
Weight	ASTM D-3776	Measured as mass per unit area	
Thickness	ASTM D-1777	Thickness measured under a specified pressure	
Compressibility	ASTM D-1777	Thickness response measured with varying pressure	
Strip Tensile Test	ASTM D-1682, D-751	Specimen gripped in clamps for full width, tested to failure	Poisson's ratio effects may cause up to 50% decrease in width.
Grab Tensile Test	ASTM D-1682, D-751	Part of specimen width gripped in clamps, tested to failure	Nonloaded part provides some transverse stiffness.
Resistance to Chemical Reagents	ASTM D-543	50 standard reagents named	Measures changes in weight, dimensions, appearance, strength.
Resistance to Light and Weather	ASTM D-1435	Samples mounted on racks and exposed	Indicates long-term in-situ behavior
Resistance to Temperature	ASTM D-794 ASTM D-746	Test for heat exposure (continuous and cyclic) of plastics Test for cold effects (brittleness, impact strength)	Care required in placing hot materials on fabric. Many samples required brittleness definition is statistical.
Impact Strength (Elmendorf Tear)	ASTM D-1424	Tongue-type tear initiated with cut, forced to continue	Questionable validity for nonwoven fabrics.
Burst Tearing, Out of Plane Loading (Mullen Burst)	ASTM D-774	Fabric distored in hemispherical shape	Measures fracture and deformation.
Cone Penetration Impact Test	Alfheim & Sorlie (1977)	Cone dropped onto restrained specimen, size of hole measured	Attempts to simulate dropping of stone on fabric.
Abrasion Resistance	ASTM D-4157, D-4158	Oscillatory cylinder, uniform abrasion	Results in % weight loss

External treatment of geotextiles can influence their resistance to UV light. Steward and Mohney [1982] report that in 1977, 3 years after the geotextile-reinforced wall in Olympic National Forest in Washington was constructed, samples of untreated fabric and fabric treated with emulsified asphalt were exposed and tested after various durations of exposure to measure strength change. The untreated, non-UV-stabilized, nonwoven, needle-punched polypropylene deteriorated very rapidly, and the lightly UV-stabilized polyester deteriorated more slowly. The asphalt-treated geotextiles retained their strength, and the treated wall has performed well for 10 years, with only one asphalt recoating in 1979.

Geotextile faced walls are susceptible to damage by vandals, who may cut holes in the fabric, causing loss of backfill. This problem occurred during construction of the geotextile-reinforced wall in Siskiyou National Forest, Oregon [Bell and Steward, 1977]. The U.S. Forest Service then sprayed gunite on the wrapped geotextile face to provide protection from vandals and UV light exposure, and no further problems developed.

Sunlight may also influence geotextiles by raising the temperature of the geotextile to higher than the air temperature. Although the temperature would not be high enough to induce thermal degradation in the geotextile, it could generate hydrolitic oxidizing and secondary photochemical degradation, or could increase creep. Polyester is generally more thermally stable than polypropylene. Embedment in soil has an insulating effect, and thus lessens thermal effects.

Outdoor exposure can influence the geotextile through the effects of humidity and precipitation. Allen et al. [1983] found that load-strain behavior of geotextiles was not adversely affected by the presence of moisture, and that strength, modulus, and failure strain were not significantly affected by freeze-thaw cycles. Precipitation may also carry pollutants that may aid hydrolysis and catalysis. Air pollutants including SO_2, SO_3, H_2S and O_3, and organic compounds may chemically degrade the exposed geotextile. However, most geotextiles are very resistant to chemical attack. The mechanical action of wind, which may carry granular particles, can damage the geotextile through impact. Martin [1982] points out that these actions during outdoor exposure may influence each other and their effects combine to increase the rate of degradation.

5.1.2 Geotextiles—Burial and Chemical Attack

Geotextile sheets may be damaged during placement and compaction of backfill over them. Use of angular crushed rock and heavy compaction equipment can cause rupture of fibers and puncture of fabric sheets.

Giroud et al. [1977] compared nonwoven, needle-punched

polyester geotextiles exposed to sunlight for 2 years and buried in a soil-riprap embankment for 6 years. The exposed geotextile lost 50 percent of its strength; in contrast, the buried geotextile lost only 10 percent of its strength and much of this loss was considered to be because of mechanical stresses resulting from applied loads and from the riprap being moved by wave action.

Sotton et al. [1982] documented a study made by the French Committee on Geotextiles in which samples of geotextiles buried in 20 different locations, varying in age from 2 to 10 years, some with light exposure, were mechanically tested. They concluded that the geotextiles selected considering the proper plastic and fabrication method for the intended application were still performing their intended design function after 10 years and would continue to do so for at least 100 years under normal conditions. For needle-punched nonwoven geotextiles, most of the samples tested did not lose more than 30 percent of their strength. These losses were due to mechanical stresses from installation and creep and from environmental effects. Geotextiles with a mechanical function, such as supporting loads, suffered the largest losses in strength. Some slit film and monofilament woven fabrics were severely punctured by backfill or other means, and strength losses exceeded 30 percent. Geotextiles exposed to sunlight for a long time also suffered losses in strength exceeding 30 percent. The results did not indicate any significant degradation of the geotextile from chemical or biological attack.

Both polypropylene and polyester are very resistant to chemical or biological degradation. Sotton and Leclercq [1982] conducted a study of accelerated aging of treated polypropylene and polyester geotextiles using laboratory chemical immersion and UV light exposure, and a combination of outdoor exposure and laboratory chemical immersion or outdoor exposure and burial. The results of these tests indicated that immersion in moderate concentrations of acids, bases, or seawater over a 19-month period after 3 months of outdoor exposure had no significant effect on the geotextile. Burial in vegetated soil following outdoor exposure does not lead to significant degradation of mechanical properties beyond that caused by exposure (less than 25 percent), except for that caused by installation problems.

5.1.3 Geotextiles—Abrasion and Damage during Construction

Abrasion most commonly occurs during the construction process. Handling and driving equipment over unrolled fabric will cause it to wear and possibly tear. Damage may also occur if fabric rolled on paper core tubes is poorly stacked, and then subjected to alternate wetting and drying. The paper cores may then collapse, and the fabric may become damaged. If angular stones or gravel is included in the backfill material, dropping such on the geotextile can tear or puncture the fabric.

Abrasion may also occur when an embankment reinforced with fabric is subject to live loads, such as traffic. The dynamic nature of the loading may cause abrasion of the fabric included in the soil.

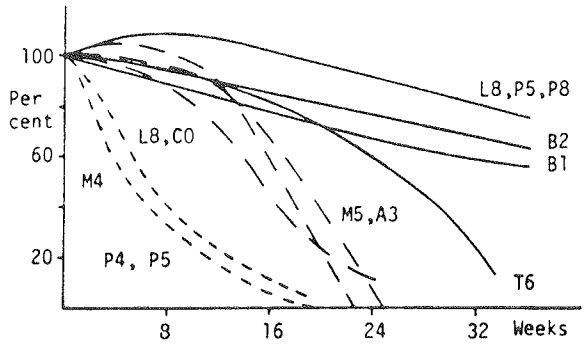

A) Strength Retained

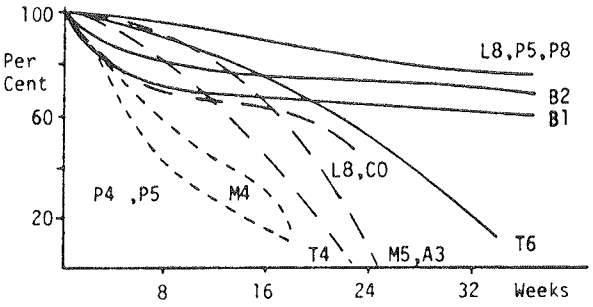

B) Elongation Retained

Fabric Code	μ* kg/m^2	Polymer, Construction + Color		Grab F_G, kN MD	Grab F_G, kN TD	Grab ϵ_G, % MD	Grab ϵ_G, % TD
B1	.150	PE,C,N,NW	Grey	.658	.560	74	83
B2	.270	PE,C,N,NW	Grey	1.041	1.133	64	67
B6	.160	PE,C,N,NW	White	.534	.455	72	89
C0	.270	PP,C,N,NW	Buff	1.170	.791	110	158
F2	.360	PP,S,N,NW	White	.734	1.205	129	112
M4	.150	PP,C,B,NW	White	.525	.511	127	124
T4	.135	PP,C,B,NW	Grey	.609	.484	60	69
T6	.200	PP,C,B,NW	Grey	1.112	1.023	58	69
S4	.125	PP,S,B,N,NW	Grey	.436	.502	51	52
S5	.170	PP,S,B,N,NW	Grey	.498	.703	60	67
M5	.140	PP,C,W,SF	Buff	.823	.925	21	18
A3	.105	PP,C,W,SF	Buff	.609	.418	21	16
P8	.260	PP,C,W,MF	Black	2.063	1.325	26	32
L8	.235	PP,C,W,MF	Black	1.965	1.125	27	32
P5	.175	PP,C,W,MF	Black	.712	.832	22	25

+ Key: B = heat bonded, C = continuous filament, MF = monofilament, N = needled, NW = nonwoven, PE = polyester, PP = polypropylene, S = staple fibers, SF = slit film, W = woven

* Mass per unit area

C) Fabric Description and Grab Test Results

Figure A-58. Effects of outdoor exposure on geotextile strength and elongation at failure. [After Raumann, 1982]

5.2 Tests and Methods to Predict Rate of Degradation

Several laboratory methods have been proposed to study the degradation of geotextiles due to UV light exposure or chemical attack, but none has been found to realistically model actual in-situ conditions because of practical limits on their duration, inability to model the complexity of outdoor exposure conditions, the random combinations of outdoor conditions at dif-

ferent locations, or inappropriate acceleration of long-term processes. For example, short-term exposure and photochemical tests (even with increased intensity) do not give a reliable measure of degradation due to outdoor exposure. Outdoor exposure produces more severe degradation and includes exposure over a long period of time to UV light and many other factors of varying intensities including temperature, wind, and precipitation, which cannot be practically duplicated in the laboratory. Identical long-term outdoor exposure tests with the same geotextile in two different locations will give very different rates of degradation, and extrapolation to other locations is not necessarily reasonable [Martin, 1982]. Sotton et al. [1982] point out that laboratory immersion in high concentrations of chemicals at elevated temperatures produces more severe deterioration of geotextiles than observed under actual long-term field exposure to more moderate chemical concentrations and temperatures.

Simple laboratory tests for studying degradation of geotextiles are generally not representative of field durability. Precise site conditions, including UV light conditions, weather and groundwater chemistry, over a long exposure time, must be strictly modeled. This is typically impractical and too complex for the laboratory. Outdoor exposure testing at the project site is preferable, but the long times required usually prohibit such testing within normal project schedule constraints. Simple laboratory tests under various combinations of environmental conditions can provide useful indices to the selection of geotextiles with the most appropriate level of durability under site conditions. However, no methods exist at present to make reliable quantitative predictions of the rate of degradation of the geotextile in the field.

5.3 Selection of Backfill

5.3.1 Durability Criteria

Backfill interacts with the geotextile sheets to provide support that must last for the full design life of the structure. The deformation of the wall must also be maintained at a tolerable level over the life of the structure. Reductions in wall support and excessive deformation may be caused by degradation of the backfill. For example, a significant groundwater gradient through a gypsum-rich backfill could dissolve the gypsum, leaving solutioned openings around the pervious geotextile sheets. Similar problems can occur with dispersive clay backfills [see Sherard and Decker, 1976]. Other types of chemical attack may reduce the geotextile–soil backfill friction. Some types of backfill may decompose with time, e.g., municipal refuse. The backfill must be stable in the chemical environment of the site. Special considerations must be given to hazardous waste storage sites where toxic chemicals may be in the groundwater system.

5.3.2 Geotechnical Criteria

Generally, free draining granular backfill is used in geotextile-reinforced walls, if available, because of its high frictional characteristics, high permeability, ease of transport and placement, and limited compaction requirements. However, in some cases, granular backfill was not available, and cohesive backfill was used successfully. The major criterion for selection of backfill is that it must be able to mobilize friction or adhesion between the geotextile sheets and the soil. In the case of granular soil, the higher the friction angle, the higher the geotextile-to-soil friction angle, and in the case of cohesive soil, the greater the compacted density the higher the geotextile-soil adhesion. In addition, the lateral pressures to be resisted in high-density backfills are ordinarily less because of their high strength.

5.3.3 Specific Tests

The properties of the backfill as a geotechnical material can be evaluated using standard (ASTM) laboratory and field soil mechanics tests including grain size, water content, density, compaction, unconfined compression, direct shear, triaxial compression, pinhole and permeability tests. The properties of the soil-geotextile interaction can be determined using geotextile shear box pullout and shear tests, as discussed in Section 3 of this chapter and by Collios et al. [1980], Delmas et al. [1979], Holtz [1977], and Myles [1982].

5.4 General Creep Considerations

The time-dependent stress-deformation behavior of a geotextile-reinforced wall is of concern because the wall may undergo excessive deformation due to creep of the geotextile reinforcement, even though adequate factors of safety are provided against geotextile rupture or pullout. The tensile creep behavior of polyamide (nylon) and polyester geotextiles in unconfined tests was first studied by Finnigan [1977] and Van Leeuwen [1977]. They found that geotextiles exhibit instantaneous recoverable primary creep, long-term nonrecoverable secondary creep and tertiary creep to rupture (Fig. A-59) similar to that observed in soil by Singh and Mitchell [1968]. Additional laboratory studies have been conducted on other geotextiles including nonwoven polyester, nonwoven polypropylene heat-bonded and needle-punched, and woven polypropylene monofilament and slit film [Koerner et al., 1980; Shrestha and Bell, 1982; and Bell et al., 1982]. These studies indicated that nonwoven needle-punched polypropylene exhibited more creep than nonwoven heat-bonded or woven polypropylene and substan-

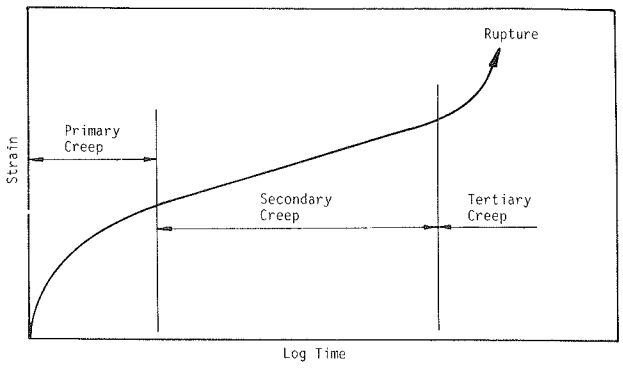

Figure A-59. Phases of creep for a typical geotextile tested without soil confinement at constant load and temperature.

tially more than nonwoven polyester. Apparently, fastening or interlocking of the geotextile fibers by heat or resin bonding or by a woven structure can also reduce creep deformations. Secondly, unconfined samples of polyester undergo smaller creep deformation than polypropylene. Laboratory tests by Allen et al. [1982] indicated that the creep behavior of geotextiles is not adversely affected by subfreezing temperatures.

Koerner et al. [1980] suggest that for a geotextile-reinforced wall, the creep characteristics of the geotextile (determined experimentally) should be matched empirically with the creep characteristics of the soil, based on the type of performance desired. They suggest that the Singh and Mitchell [1968] three-parameter equation be used for creep behavior of the geotextile. Shrestha and Bell [1982] present a four-element rheological model based on rate process theory which, in some cases, provides a closer representation of the experimental creep curves than the Singh-Mitchell model. Measurements of the behavior of actual geotextile-reinforced walls have shown that creep deformations of the magnitude predicted by models based on laboratory tests of geotextiles without soil confinement have not occurred. For example, at Glenwood Canyon in Colorado, several portions of the geotextile-reinforced wall were expected to experience substantial creep deformations. Bell et al. [1983] report that even though many of the wall segments had factors of safety with respect to creep rupture much less than 1.0, no significant creep deformations were measured.

Creep tests by McGown et al. [1982] have also shown that geotextiles confined in soil undergo substantially reduced creep deformations compared to those not confined in soil. As shown in Figure A-60, nonwoven, needle-punched polypropylene Terram 1000 under soil confinement had creep deformation similar to that of nonwoven polyester Bidim U24, whereas unconfined, the Terram experienced creep rupture while the Bidim experienced only moderate secondary creep. Apparently, creep testing of geotextiles without soil confinement can grossly overestimate long-term deformations. Similar, relatively stable creep deformations were measured in triaxial creep tests performed by Holtz et al. [1982] on dense sand samples reinforced with woven and nonwoven polypropylene geotextile discs.

6. CONSTRUCTION

6.1 Site Preparation

Site preparation consists of excavating the area where construction is to take place to the limits shown in the plans. The excavation width at any depth should be equal to or exceed the length of the reinforcement layer planned for that elevation. Foundation preparation includes removal of unsuitable materials or regrading the bottom of the excavation. Unsuitable foundation material may need to be replaced with compacted backfill prior to construction of the geotextile wall.

6.2 Phases of Construction

A typical geotextile-reinforced wall is constructed by placing horizontal layers of geotextile in an earth fill (backfill), with the front edge of each geotextile layer wrapped around the overlying layer of backfill to form the wall face. Reinforcement layers and backfill are placed alternately as the wall height increases. Walls using facing panels instead of goetextile-wrapped facings require placement of the panels prior to the alternating geotextile and backfill layers at any level.

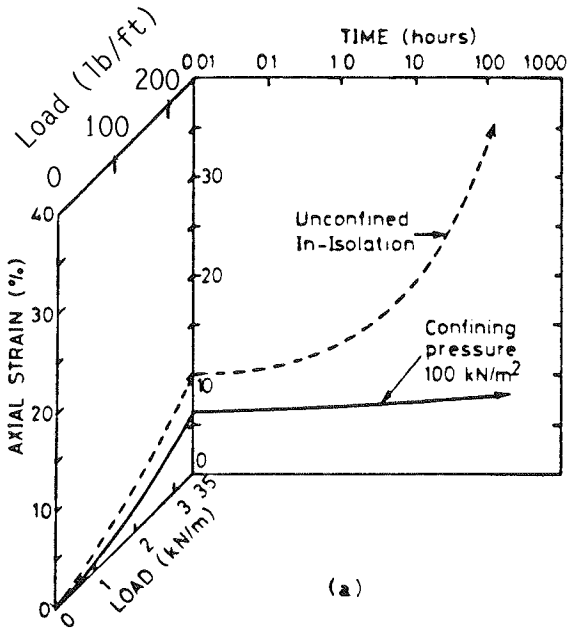

A) Terram 1000

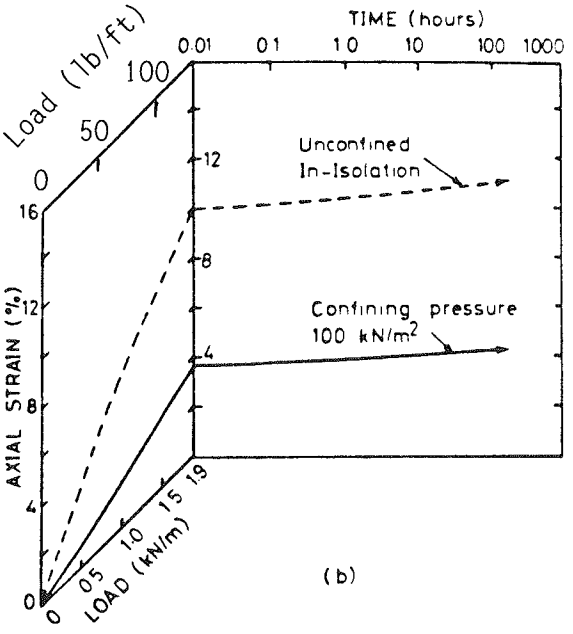

B) Bidim U24

Figure A-60. Creep test data. [After McGown et al., 1982]

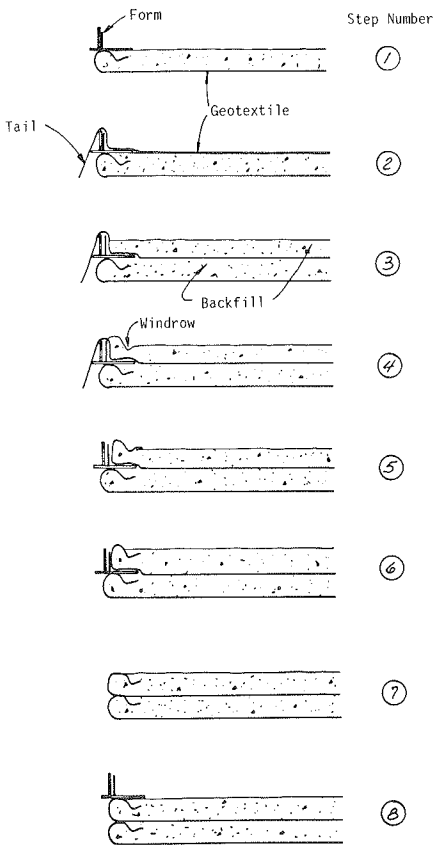

Figure A-61. Geotextile reinforced wall, U.S. Forest Service construction procedure. [After Bell et al., 1983]

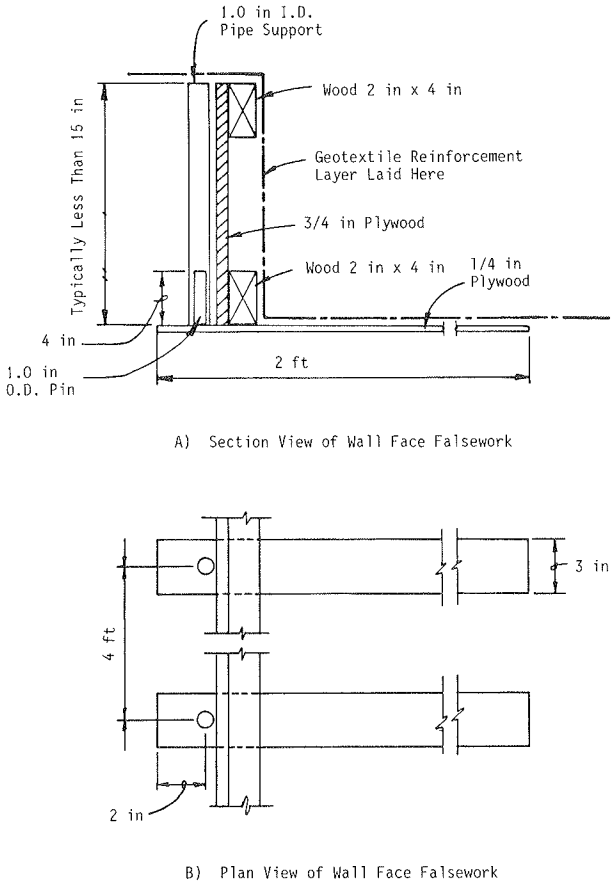

Figure A-62. Details of typical form system used to form fabric wall face.

Two methods currently in use for the construction of geotextile-reinforced walls with geotextile-wrapped facings are described in this section. The first method, developed by the U.S. Forest Service, has been widely used for walls built in the United States. The second method, which differs by the inclusion of a different type of backfill material near the facing, has been used in Europe.

6.2.1 U.S. Forest Service Method

The steps involved in the Forest Service construction procedure for the completion of one lift are illustrated in Figure A-61. This sequence has also been used successfully by the Colorado Division of Highways [Bell et al., 1983] and the New York State Department of Transportation [Douglas, 1981] on recent projects. The construction sequence is as follows:

- *Step 1.* A temporary wood form system, such as the one shown in Figure A-62, is needed in order to achieve both a uniform face and good control of the wall batter. This form should be as high as the loose height of fill lift. Prior to unrolling the geotextile, the form, which can be handled manually should be positioned over the foundation soil or the underlying compacted layer of backfill.
- *Step 2.* The geotextile is unrolled in the direction specified in the design (machine or cross-machine direction) and positioned so that a 3 ft long "tail" drapes over the form.
- *Step 3.* The backfill is placed in such quantity that the thickness after compactions is about half the total lift height.
- *Step 4.* A windrow is placed so that the backfill height against the form is slightly greater than full life height. This windrow does not need to be compacted.
- *Step 5.* The hanging tail is folded back over the window and held in place with additional backfill.
- *Step 6.* The layer is backfilled and compacted to its full design thickness.
- *Step 7.* The form is removed and the uncompacted backfill near the facing is allowed to deform.
- *Step 8.* The form is reset over the lift that has just been completed, ready to start another lift.

6.2.2 European Method

The steps involved in the European construction procedure for the completion of one lift are similar to the Forest Service procedure in many respects. However, as shown in Figure A-63, it is different in that after setting the form and unrolling the geotextile (Step 1), placement of the lower half of the total lift is not continued up to the form in order to allow for placement of rounded gravel near the facing. The hanging tail of the reinforcement layer is wrapped around this gravel, which is placed thicker than the final compacted lift thickness, and the upper half of the lift is placed in a loose state to the same height

as the gravel (Step 2). Eventually, the form is removed and the upper half of the lift is compacted (Step 3).

The use of rounded gravel near the facing has the advantage of providing better drainage at the wall face. The gravel is not compacted because: (1) compaction near the wall face is difficult to achieve, (2) compaction near the wall face is dangerous for the workers' safety if no scaffolding is installed, and (3) deformation of the noncompacted gravel initiates beneficial prestressing of the reinforcement layers upon removal of the form.

6.3 Placement of Different Components

6.3.1 Geotextile

The geotextile should be unrolled in the direction specified in the design (machine or cross-machine direction). When the geotextile is unrolled parallel to the wall face, transverse joining of adjacent geotextile layers is done by overlapping the layers a minimum of 4 in. and sewing them together. When the geotextile is unrolled perpendicular to the wall face, lontitudinal joining is performed either by: (1) overlapping the layers a minimum of 3 ft, installing the overlaps in such a way that backfill placements will not push the two geotextiles apart, or (2) overlapping the layers a minimum of 4 in. and sewing them together.

6.3.2 Backfill

Backfill is progressively dumped and spread toward the wall face. During backfilling operations, no construction equipment should be permitted to roll directly over the installed geotextile, and a minimum backfill thickness of 6 in. should be maintained at any time between the geotextile and moderate size construction equipment (e.g., Caterpillar D6 or 955). Each lift should not exceed 12 in. in loose thickness and should be compacted to achieve a minimum of 95 percent of the maximum dry density according to ASTM D698.

6.3.3 Wall Face

Materials used in the construction of a geotextile-wrapped wall face may be asphalt, gunite, structural material, or soil. Placement of either asphalt or gunite is usually by spraying in one or several coats directly onto the geotextile-wrapped face. A wire mesh may be necessary to keep the asphalt, gunite, or topsoil attached to a veritcal or steeply battered wall face.

6.4 Construction Labor and Equipment

Geotextile-reinforced walls can be built in a timely fashion with less labor and equipment than that normally required for other types of structural retaining walls. In walls constructed to date in the United States, construction crew size has typically ranged from 4 to 6 workers [Chassie, 1983], and construction equipment has included a track-mounted front end loader or a track-mounted dozer. With this crew size and equipment, typical production rates have ranged from 250 to 500 sq ft (25 sq m to 50 sq m) of wall face per day.

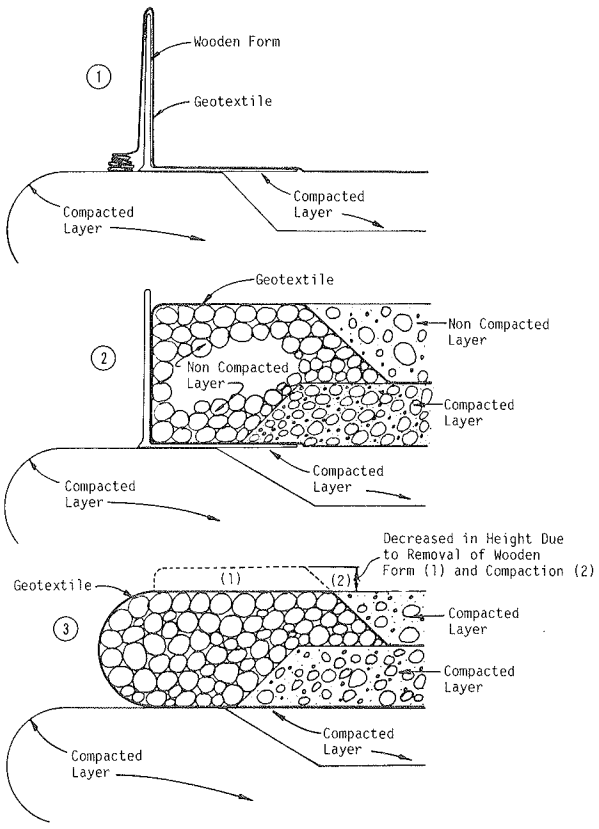

Figure A-63. Geotextile reinforced wall construction procedure used in Europe.

6.5 Work Organization

Work organization on such projects as geotextile-reinforced walls, where construction consists of a repetitive sequence of activities, is a major consideration in completing the project in an efficient and timely manner. In order to allow for an inexperienced construction crew to become familiar with the construction technique, it is prudent to specify thin lifts (6 to 9 in.) for the first 2 to 3 ft of wall, because it takes a new crew three to four lifts to develop the technique for obtaining a uniform face [Bell et al., 1983].

To minimize cutting of the geotextile rolls and for greater economy, the geotextile reinforcement may be unrolled parallel to the wall face. If the geotextile reinforcement is to be unrolled perpendicular to the wall face, adjacent geotextile layers can be sewn in the manufacturing plant to form blankets prior to transporting them to the site.

Geotextiles are sensitive to environmental exposure, as explained in Section 5, Chapter three of this appendix. The part of the wall most prone to deterioration by ultraviolet light is the wall face because the remainder of each reinforcement layer is buried in the backfill. Consequently, each new lift face must be temporarily protected shortly after placement, unless the geotextile is treated polypropylene or polyester which does not need such immediate protection.

6.6 Quality Control

6.6.1 Geotextile Materials

The contractor should furnish the engineer a mill certification of affidavit signed by a legally authorized official from the company manufacturing the geotextile. The certificate should attest that the geotextile has been tested and meets chemical, physical, manufacturing, and testing requirements. A sample of the geotextile should be furnished to the engineer from each geotextile roll for verification testing. The fabric samples should be labeled to identify the roll, shipment, brand, mass per unit area (oz/yd^2 or g/m^2), machine and cross-machine directions and wrapped in dark plastic to protect them from sunlight.

Each mill run or manufacturing lot of geotextile material shipped to the site should be tested for its mass per unit area (g/m^2) according to ASTM D-1910, and tensile strength and elongation at failure in both machine and cross-machine directions according to ASTM D-1682, The tensile test should be performed by either the strip or grab test method.

6.6.2 Backfill

The backfill material ordinarily should be clean (less than 5 percent fines), free-draining and should not contain stones larger than 6 in. (150 mm). Use of finer grained materials may require special design and construction considerations. The compacted material should be sampled and tested for moisture content and dry density. A minimum of 95 percent of the maximum dry density according to ASTM D-698 should be achieved.

Thickness measurements of each layer of backfill should be made at various locations to verify that the compacted thickness is not over or under the design thickness by more than 2 in.

7. DESIGN METHODS

7.1 Internal vs. External Stability

The design of geotextile-reinforced soil walls, like any other type of wall system, must consider both internal and external stability. The internal stability of the wall is controlled by the ability of the reinforced soil mass to act as a cohesive unit, which is accomplished through a transfer of stress from the soil to the reinforcement. Like other reinforcing systems, two criteria are evaluated: the tension developed in the reinforcement and the resistance of the reinforcing elements to pullout.

External stability refers to failures outside the reinforced zone; bearing capacity, sliding of the reinforced earth mass as a unit and over-turning. Classical methods of soil mechanics have been used quite successfully for this design evaluation.

7.2 General Design Considerations

Two general design methods for geotextile-reinforced soil walls are presented in the following sections: Broms [1978] and the U.S. Forest Service [Steward et al., 1977, revised 1983]. A method for the design of geotextile-reinforced embankments, Ingold [1979], is also described. The Broms method is generally used in Europe, and the U.S. Forest Service method is used in the United States. Both geotextile-reinforced wall design methods have been used successfully for different types of geotextile walls. Performance of actual geotextile walls, especially the I-70 Glenwood Canyon walls, indicates that both methods are conservative.

7.3 Wall Design

The Broms and U.S. Forest Service design methods address internal stability, including vertical spacing of the fabric layers and fabric length, external wall stability, and exposure protection. The Broms method provides for the design of structural, L-shaped wall elements that are not included in the Forest Service method. Both methods have been used by various wall designers either directly or with minor conservative variations. Critical to both methods is a determination of the allowable tensile strength of the geotextile and the geotextile-to-soil coefficient of friction. The design approaches are primarily empirical using experimentally determined design parameters.

7.3.1 U.S. Forest Service Method

The U.S. Forest Service design method for geotextile-reinforced walls [Steward et al., 1977, revised 1983] was developed for remote roadway retaining walls in national forests in Oregon and Washington. The method is based on the design method developed by Lee et al. [1973, 1975] for Reinforced Earth walls and was adapted for geotextile-reinforced walls by Bell et al. [1975] and Bell and Steward [1977]. This method is appropriate for a vertical or sloping wall with wrapped geotextile construction and nonrigid element facing.

7.3.1.1 Internal stability.

Vertical spacing of fabric layers. The U.S. Forest Service method assumes that a failure plane develops an angle of $45° + \phi/2$ above the horizontal, as shown in Figure A-64a. Lateral earth pressure σ_h within this wedge is assumed to have a triangular distribution (Fig. A-64b) equal to at-rest earth pressure conditions:

$$\sigma_h = K_o \gamma Z \qquad \text{(A-14)}$$

where K_o = coefficient of earth pressure at rest ($= 1 - \sin\phi$); γ = unit weight of backfill material; and Z = depth below the top of wall.

The use of at-rest earth pressure, especially at depth, is probably conservative. If the wall undergoes a small deformation, the horizontal pressures probably reduce to values corresponding to the active state.

Incremental horizontal stress components developed by a surficial live load must be added to the at-rest design earth pressure. This method considers the loading from vehicles as live-loading. Dead and live surcharge loads at the surface are resolved into their horizontal stress components, acting on the wall, commonly by using a Boussinesq stress distribution or other reasonable methods for computing stress distribution such as presented in NAVFAC DM7.2, Figure 11, reproduced here as Figure A-64C. From the at-rest lateral earth pressure and the horizontal stress components imposed by surcharged loads, a

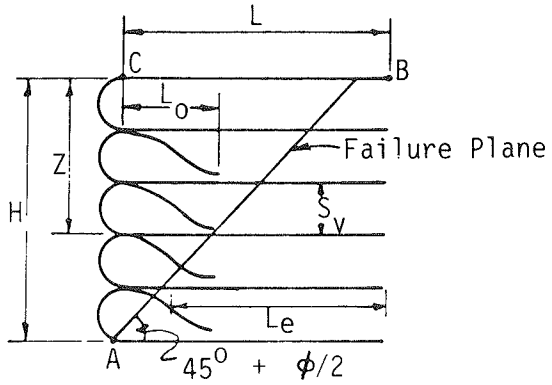

A) Sketch of Section Through Fabric Retained Earth Wall

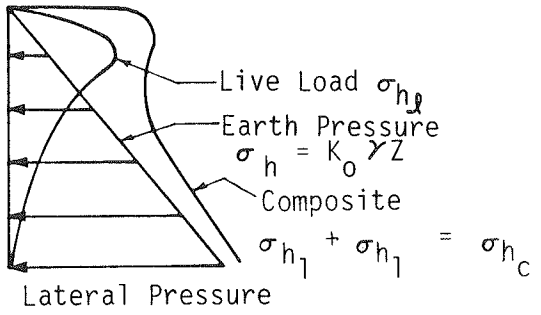

B) Assumed Earth Pressure Distribution

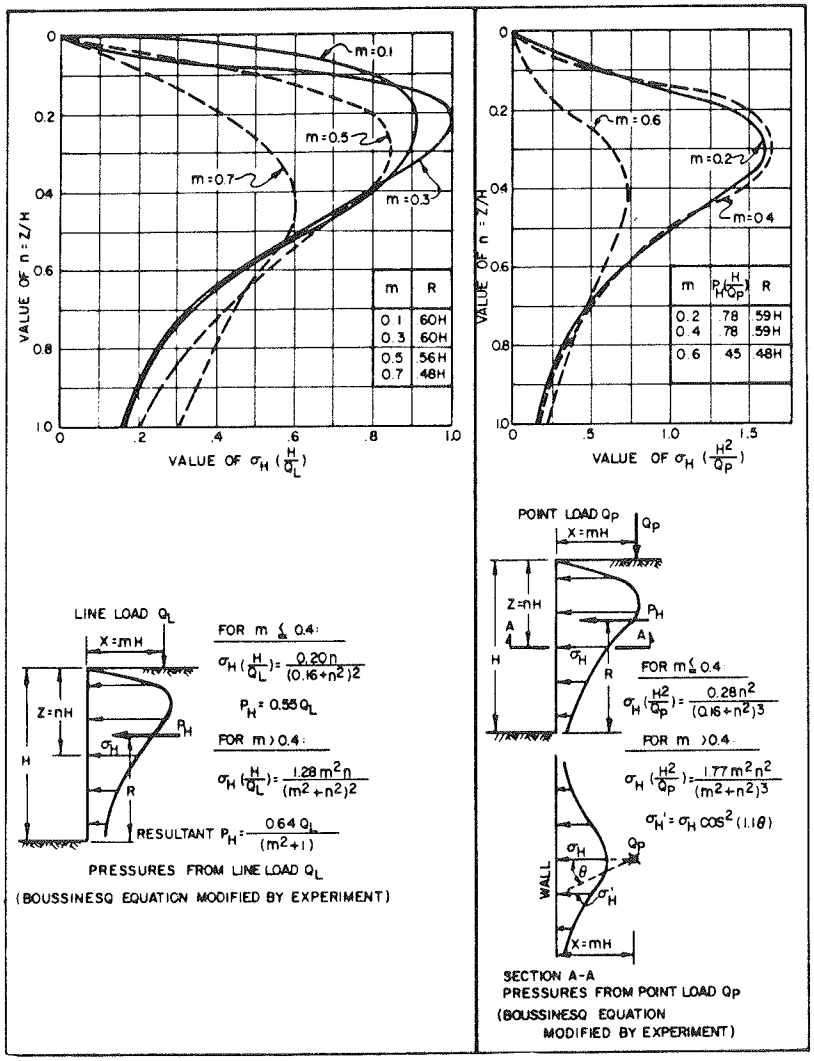

C) Horizontal Earth Pressures from a Surface Load (Figure 11 from NAVFAC DM7.2, 1982)

Figure A-64. U.S. Forest Service design method.

Table A-12. Long-term creep criteria by fabric type—strip tensile test.

Polymer Type & Style	Percent of Strip Tensile Strength
Polyester needled	70
Polypropylene needled	55
Polypropylene bonded	40
Polypropylene woven	25

Table A-13. Long-term creep criteria by fabric type—grab and 1-in. strip tensile test.

Polymer Type & Style	Factor
Polyester needled	1.0
Polypropylene needled	0.8
Polypropylene bonded	0.6
Polypropylene woven	0.4

composite lateral pressure diagram, σ_{hc} is constructed (see Fig. A-64b).

The vertical spacing of fabric layers (S_v) is calculated from:

$$S_v = \frac{T_a}{\sigma_{hc}\,(FS)} \tag{A-15}$$

where T_a = allowable fabric long-term tensile force per unit width; FS = factor of safety (equal to 1.2 to 1.5 depending on confidence level in strength and load parameters); and σ_{hc} = average composite lateral pressure for the layer.

The allowable long-term tension can be calculated using one of the following two methods:

1. *Method A.* Strip Tensile Test ASTM D-1682, D-75—Same direction as installed. The strengths measured in accordance with the ASTM procedures are reduced as tabulated in Table A-12 for various fabric types. The following conditions should be provided for in the test procedure:
   a. Maintain minimum width-to-gauge length ratio of 2:1 and minimum spacing between test grips of 0.1 m (0.33 ft).
   b. Test at constant strain rate of 10 percent per minute.
   c. Test at standard laboratory conditions of 54 + 2 percent relative humidity and temperature of 21 + 1°C (70 + 1.8°F).
   d. Condition specimens by soaking for minimum of 12 hours and test surface damp.
   e. Use grips that do not weaken the specimen (disallow tests which fail at the grips) and which hold the geotextile without slippage. If slippage cannot be sufficiently limited, elongation must be measured between points on the specimen rather than between grips.
   f. Results should present the total unit load (applied force per unit width of specimen) vs. strain curve as well as failure unit load and strain.
2. *Method B.* Grab and 1-in. Cut Strip Tensile Tests—Use the lesser value of the following two strengths as the fabric strength, S: (a) 90 percent of the 1-in. cut strip strength; and (b) 33 percent of the grab tensile strength. To account for long-term creep potential, multiply the lesser of these two values by the factors shown in Table A-13.

Required fabric embedment length. The fabric embedment length, L_e, required to resist the lateral pressure on the wall is calculated from the lateral pressure on the wall, σ_{hc}, the allowable long-term tension in the fabric, T_a, and the friction generated by the vertical stress normal to the geotextile sheet and the apparent coefficient of friction between soil and geotextile.

In this method the apparent soil-to-geotextile friction angle, δ, is conservatively assumed to be equal to $\frac{2}{3}$ of the soil friction angle, ϕ. The required fabric embedment length, L_e, is calculated from:

$$L_e = \frac{K_o S_v (FS)}{2\tan(2\phi/3)} \geq 3 \text{ ft} \tag{A-16}$$

where FS = factor of safety (1.5 to 1.75).

The required fabric embedment length is measured from the failure plane as indicated in Figure A-64a. A minimum fabric embedment length, L_e, of 3 ft should be used.

The length of fabric-wrapped embedment, L_o, is calculated by dividing the lateral pressure-induced tension in the fabric by the friction mobilized between the soil and fabric over its overlap length:

$$L_o = \frac{\sigma_{hc} S_v\,(FS)}{2 Z_f \gamma \tan(2\phi/3)} \tag{A-17}$$

where σ_{hc} = average composite lateral stress for the layer; FS = factor of safety (equals 1.2 to 1.5); and Z_f = depth to top layer.

A minimum fabric overlap length, L_o, of 3 ft is recommended.

7.3.1.2 External wall safety. The overall stability of the wall system can be evaluated by checking three potential failure modes: overturning, sliding on base, and bearing capacity at the toe. Classical methods of soil mechanics can be used to check the external stability of these walls.

7.3.2 Broms Method

The Broms method [Broms, 1978] is appropriate for vertical or sloping walls with structural facing elements (Fig. A-65). This method is based on the results of model tests conducted at the Royal Institute of Technology in Stockholm [Holtz and Broms, 1977] and, to date, has primarily been used in Europe.

Lateral earth pressures acting on the wall, and the long-term creep strength of the fabric, are the primary factors determining reinforcement spacing and length. It is also important that the fabric be ductile enough for redistribution of lateral earth pressure to occur should part of the wall be overloaded. The effect of the reinforcement is to move the actual failure surface away from the wall.

The lateral earth pressure on the face elements is small, because the major portion of the lateral earth thrust is resisted by

friction between the fabric layers and soil. Broms [1978] calculated the lateral restraint provided by the fabric reinforcement and the associated reduction in lateral earth pressure relative to the at-rest value by considering the force equilibrium of a soil element cut between two adjacent fabric layers (see Fig. A-66). The friction resistance along the fabric, f, is calculated as $f = \sigma_v' \tan \delta$ where $\delta = \phi$ for a woven fabric (rough-surfaced in comparison with steel or aluminum) and cohesionless soil. Broms suggests that the fabric-to-soil friction angle, δ, should be reduced to a value less than the soil friction angle if the silt or clay content of the soil is greater than 10 percent. The stresses, σ_v' and σ_h', are not principal stresses, due to the presence of frictional component f, and the corresponding lateral earth pressure coefficient, K_b, is thus larger than the Rankine coefficient. The coefficient can be computed as $K_b = 1/(1 + 2 \tan^2\phi)$ for cohesionless soil, provided the soil-to-fabric friction angle equals the soil friction angle.

Earth pressures, σ_v' and σ_h', were found to increase with distance from the wall face, as shown in Figure A-67. This means that wall elements may be designed for lateral earth pressures smaller than the Rankine active earth pressure.

A check of the horizontal stresses on a wall face element for a given reinforced layer is made as follows: Figure A-67 is used to determine σ'/σ_o' at x = width of L-shaped facing element. If the facing element is designed for σ'_{ho}, the soil can carry $\sigma'_h = (\sigma'/\sigma_o')\sigma'_{ho}$ at that x distance. The soil bearing capacity is then $\sigma_v' = \sigma'_h/K_b$, and the maximum height of soil permissible above that level $= \sigma'_v/\gamma$.

The required reinforcement spacing and embedment length are determined by the maximum tension in the reinforcement. To compute this tension Broms suggests using a value of σ'_h determined as in the Terzaghi and Peck method for anchored sheet pile walls, i.e.,

$$\sigma'_h = 0.65\, K_a(1.5\, q + \gamma H) \qquad \text{(A-18)}$$

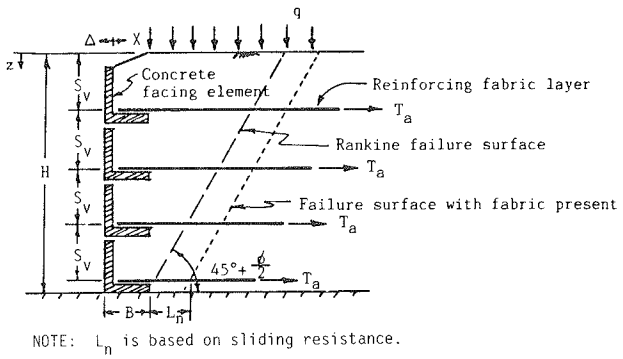

Figure A-65. Design configuration for Broms method.

where K_a = coefficient of active earth pressure, and q = surcharge.

By using this value of σ'_h, which provides an overall active force larger than computed from Rankine active earth pressure, natural variations in σ'_h and ϕ are supposed to be taken into account.

Spacing of fabric layers is then given by:

$$S_v = T_a/(\sigma'_h - B\gamma \tan\delta) \qquad \text{(A-19)}$$

where T_a = allowable long-term tension in the fabric = ⅓ ultimate to account for creep and degradation losses, and B = length of horizontal facing element protruding into reinforced soil volume (see Fig. A-65).

The required length of fabric reinforcement (beyond the failure zone) is determined by considering sliding of a soil wedge lying above each fabric layer (refer to Fig. A-68):

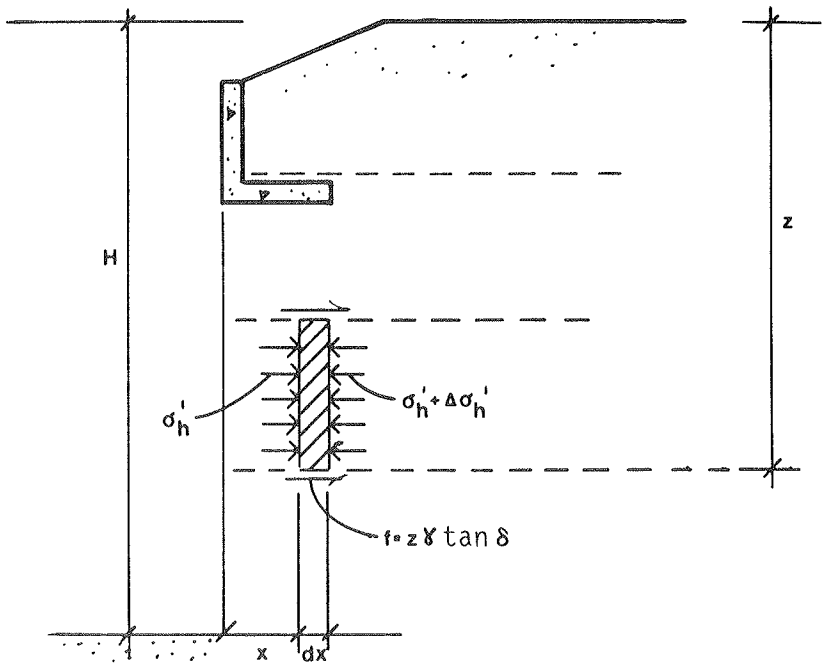

Figure A-66. Stress distribution in the backfill.
[Broms, 1978]

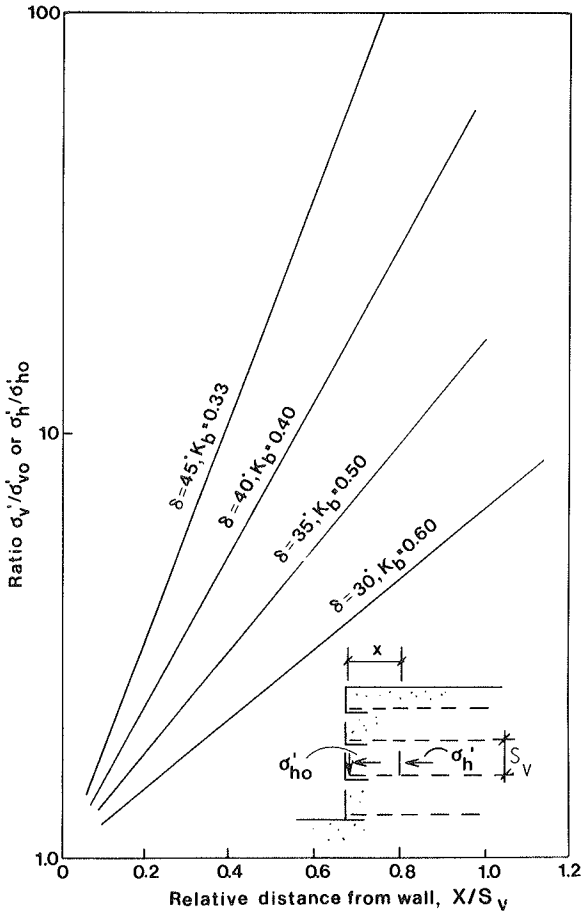

Figure A-67. Increase of σ'_v/σ'_{vo} and σ'_h and σ'_{hc} with increasing distance x/S_v from the face of the retaining wall. [Broms, 1978]

$$L_n = [(\sigma'_h)/(\gamma \tan\delta)] - B \qquad \text{(A-20a)}$$

$$L_{n-i} = (1.3\ T_a)/(Z_{n-i}\tan\delta) \qquad \text{(A-20b)}$$

where the 1.3 factor is intended to be a factor of safety against the possible variations in fabric stresses behind the failure plane.

If it is desired to make the upper fabric layers shorter than the value determined with the foregoing equations, the total lateral earth pressure at the back of the wall elements must be carried by all the fabric layers and the fabric must be ductile enough for redistribution of lateral earth pressures to occur.

If the fabric is not tied to the wall elements, the area of contact between the fabric and horizontal portions of the facing elements must be sufficient to transfer the earth pressure's load to the fabric:

$$B = (1.3\ T_a)/(2S_v\gamma\tan\delta) \qquad \text{(A-21)}$$

If the tensile strain distribution for the selected geotextile in soil is known, Broms suggests that the lateral displacement at the top of the wall may be approximated by: $\Delta \approx 0.2\ \epsilon\ H$ where ϵ is the tensile strain of the fabric at the critical section and H is the height of the wall [(Broms, 1978)].

In addition, external modes of failure should be analyzed as with the Forest Service method.

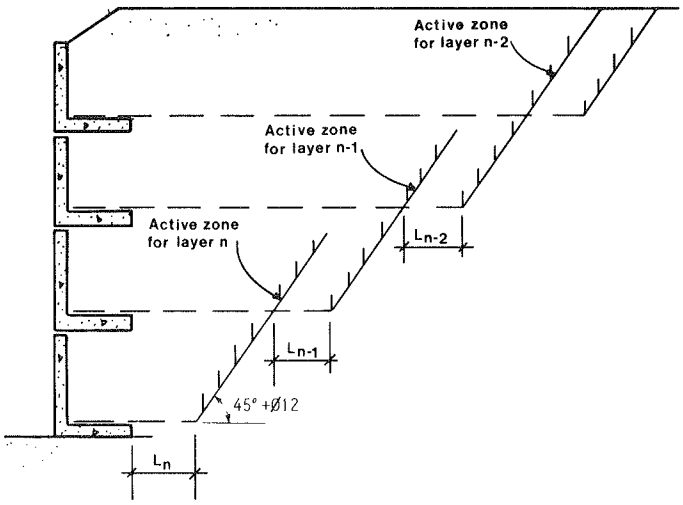

Figure A-68. Active zones of the different layers. [Broms, 1978]

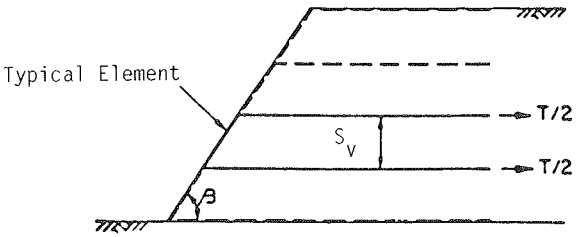

A) Embankment Geometry

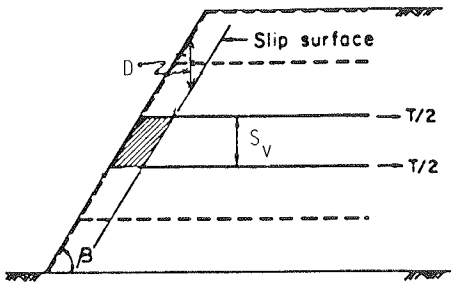

B) Infinite Slope Failure

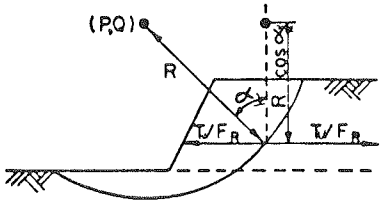

C) Circular Slip Failure

Figure A-69. Geotextile reinforced embankment. [Ingold, 1982]

7.4 Embankment Design

Ingold [1982] proposed a method for the design of fabric-reinforced embankments (Fig. A-69a) in dry cohesionless soils. The analysis involves an adoption of a slip circle technique, with the reinforcement modeled by an equivalent tensile force developing in addition to the restoring moment which is generated by the strength of the soil. A similar approach has also been proposed by Christie and El-Hadi [1977].

The inclusion of geotextile reinforcements into an embankment allows the construction of much steeper side slopes than those feasible for unreinforced embankments. The fabric-reinforced embankment must be checked for two optimal failure modes: superficial failures and deep-seated failures.

7.4.1 Infinite Slope Analysis

Embankments constructed of sands and gravels are susceptible to surface raveling or shallow sliding, which can be analyzed using the simple infinite slope analysis [Duncan and Buchignani, 1975]. Figure A-69b shows a fabric-reinforced embankment with a planar slip surface parallel to the slope batter. The stability of the shaded soil mass shown in the figure is a function of the weight of the soil element and the restoring forces generated by the soil and reinforcement. If a soil element is considered that is bounded by two fabric layers, the slope, and a potential failure plane parallel to the slope but at vertical distance, D, below the slope (Fig. A-69), the weight of the element is:

$$W = N_1 \gamma S_v^2 \cot\beta \qquad \text{(A-22)}$$

where N_1 = ratio of D to S_v, and β = slope angle of the embankment with the horizontal.

The restoring force is generated by the soil and the reinforcement. That portion contributed by the weight of the soil element and friction at the failure plane is:

$$R_s = N_1 \gamma S_v^2 \cos\beta \cot\beta \tan\phi \qquad \text{(A-23)}$$

where R_s = restoring force due to the soil, and ϕ = internal friction angle of the soil.

The tensile force in the fabric can be resolved into a normal force and a force parallel to the failure plane. Conservatively ignoring the latter component of this force, the restoring force contributed by the additional friction on the failure plane caused by the tensile force can be computed as:

$$R_T = T_u \sin\beta \tan\phi \qquad \text{(A-24)}$$

where R_T = restoring force due to reinforcement, and T_u = ultimate tensile strength of the fabric.

The factor of safety for a reinforced embankment subject to infinite slope failure is the ratio of restoring forces to disturbing forces:

$$F.S. = \frac{N_1 \gamma S_v^2 \cot\beta \cos\beta \tan\phi + T_u \sin\beta \tan\phi}{N_1 \gamma S_v^2 \cot} \qquad \text{(A-25)}$$

From this equation the fabric spacing within an embankment can be determined for any given factor of safety.

7.4.2 Slip Circle Analysis

Ingold [1982] proposed the use of Bishop's Modified Method of Analysis [Bishop, 1955] for the determination of the factor of safety of the reinforced embankment with respect to deep circular failures.The horizontal force generated in the reinforcement adds a restoring moment Δm, which is the sum of the product of the individual tensile forces developed in each layer multiplied by their respective moment arms. Figure A-69c shows the force and moment arm for one single layer of reinforcement. The equation for the restoring moment is:

$$\Delta m = \sum T_u R \cos\alpha / F_R \qquad \text{(A-26)}$$

where R = radius of the slip circle, and F_R = $F.S.$ for tensile rupture.

The equation for the factor of safety of the reinforced embankment is the sum of the restoring forces divided by the driving forces:

$$F.S. = \frac{\sum w(1-r_u) \tan\phi / m_\alpha + \sum T_u \cos\alpha / F_R}{\sum w \sin\alpha} \qquad \text{(A-27)}$$

where $m_\alpha = \cos\alpha \left(1 + \frac{\tan\alpha \tan\phi'}{F.S.}\right)$, r_u = pore pressure ratio, W = weight of the slice, and α = angle between a line tangent to the slip circle and horizontal.

The pullout capacity of the reinforcement must also be checked. The bond length should be located outside the critical failure surface and should be calculated by the method discussed previously. Finally, a check should be made for a slip circle passing through the free ends of the reinforcement to assure an adequate factor of safety. It should be noted that the above-described analyses apply to an embankment constructed of dry cohesionless soils and that modification of the analyses would be required for saturated embankments. Such saturated embankments would also require special provisions for erosion protection.

8. CASE HISTORIES

Several of the geotextile-reinforced wall case histories listed in Table A-8 are briefly discussed in this section. More complete details about each of the cases may be found in the indicated references.

8.1 Autoroute A15—Rouen, France, 1971

As a portion of a highway embankment, the first geotextile-reinforced wall was built by the French Highway Administration in Rouen. The purpose of the wall, which was constructed with low quality backfill and founded on very compressible peat (with a natural moisture content of 300 percent), was to test its stability and ability to tolerate deformations caused by the soil–geotextile interaction. The wall was constructed with a vertical face, and a surcharge load was placed on top.

The wall is 13 ft high and 65 ft long. As illustrated in Figure A-70, layers of polyester needle-punched nonwoven geotextile, Bidim U34, were placed extending 16 to 20 ft behind the wall face. The wall face was formed by wrapping geotextile layers

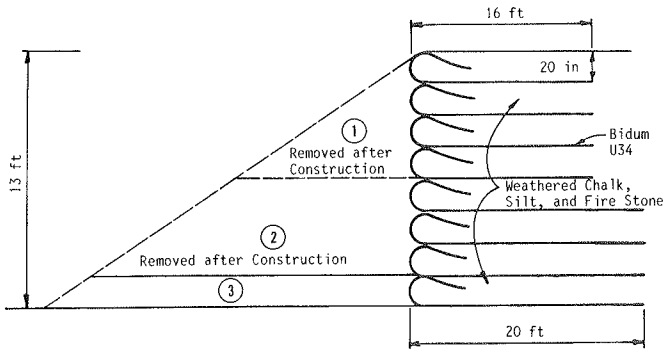

Figure A-70. Autoroute A15.

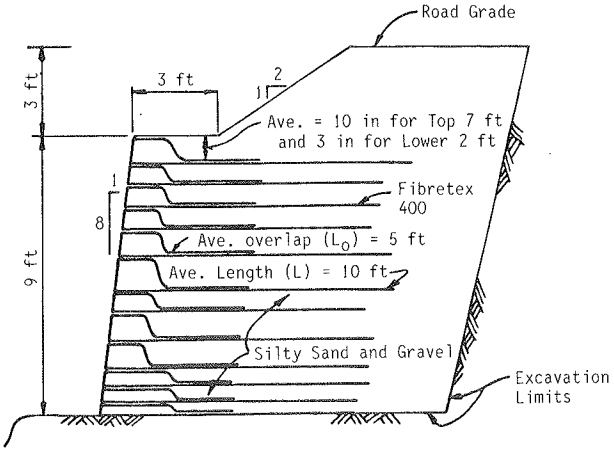

Figure A-71. Illinois River Road.

around 1.6-ft thick backfill layers. A berm was raised on the passive side of the wall as construction proceeded and was partially removed after the end of construction. The purposes of this berm were: (1) to provide stability for the wall and its compressible foundation, and (2) to provide support for a temporary wood-form system for the facing.

Observations of the overall behavior of the wall and foundation have indicated satisfactory performance, even though lateral deformations on the order of 1 in., total settlement on the order of 3 ft, and differential settlements of about 10 in. over a length of 10 ft were recorded.

8.2 Illinois River Road—Siskiyou National Forest, Oregon, 1974

Construction of a road fill became necessary after part of the Illinois River Road was eroded by excessive runoff. Because of the steep natural slopes along which the road was built, slope reconstruction to restore road width was difficult. A geotextile-reinforced wall was therefore selected as a remedial measure by the U.S. Forest Service.

The wall, 9 ft high and 33 ft long, consists of a polypropylene needle-punched nonwoven geotextile, Fibretex 400, placed in horizontal layers with silty sand and granular backfill. The geotextile layers were extended approximately 10 ft behind the wall face and spaced vertically at 8 to 10 in., as shown in Figure A-71. The wall face, which was protected by a gunite layer after construction, was formed by wrapping the geotextile around a compacted sand berm of thickness equal to the vertical spacing of the geotextile layers for the first three layers of backfill, and by wrapping the geotextile layers around rows of burlap bags filled with sand for the remaining layers of the backfill.

Construction of this wall showed that a geotextile-reinforced wall was economical and practical for certain classes of low retaining wall problems. The performance has been satisfactory since construction in 1974.

8.3 Olympic National Forest Road—Shelton, Washington, 1975

Following the satisfactory performance of the Illinois River Road wall, a second geotextile-reinforced wall was built by the U.S. Forest Service as a trial use project. The purposes of this second wall were: (1) to evaluate materials and construction methods, and (2) to measure the wall movements at various locations.

The wall, protected by an asphalt sprayed facing, is 3 to 20 ft high and 164 ft long. It is divided into two sections, each section incorporating two types of geotextiles of different weights. One section used polypropylene needle-punched nonwoven fabrics, Fibretex 400 and 600, and the other section used polyester needle-punched nonwoven fabrics, Bidim C-28 and C-38. As shown in Figure A-72, the heavy geotextiles were used in the lower of two levels and the lighter geotextiles in the top level. Each level was further divided into an upper and lower portion. A 9-in. vertical spacing in the lower portion and a 12-in. vertical spacing in the upper portion were maintained for both the heavy and the light geotextile layers. In all cases, the length of the reinforcement layers was approximately 13 ft.

The backfill material consists of crushed basalt which was locally available. With the exception of the use of a temporary wood-form system to form the wall face, the construction technique involved the same steps as those for the Illinois River Road project, i.e., layout of the geotextile, placement of a compacted berm at the wall face, wrapping of the berm with the geotextile, and backfilling and compaction to final layer thickness.

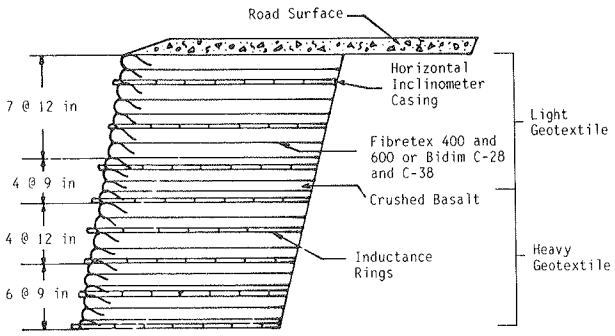

Figure A-72. Olympic National Forest road.

Post-construction behavior of the wall, as recorded one year and a half later, was very satisfactory. Lateral movements on the order of 1.2 in. occurred within the first 6 months, with most deformations occurring within 2 ft of the wall face. No significant difference in movements was observed with the different type of geotextile polymer.

8.4 Barrage De Maraval—Pierrefeu, France, 1976

A geotextile-reinforced wall was constructed on the downstream face of a weir embankment. The wall, 21 ft high and 52 ft long, consists of a polyester woven geotextile, Tri X, placed in horizontal layers in a backfill made of compacted clay and schist colluvium. The geotextile layers were extended 13 and 20 ft behind the wall face and were spaced vertically at 2 ft, as illustrated in Figure A-73. The wall face was obtained by wrapping the geotextile around rounded gravel placed near the facing and applying a resin coating over the facing after the end of construction.

During construction the geotextile-reinforced wall was flooded three times with no adverse consequences.

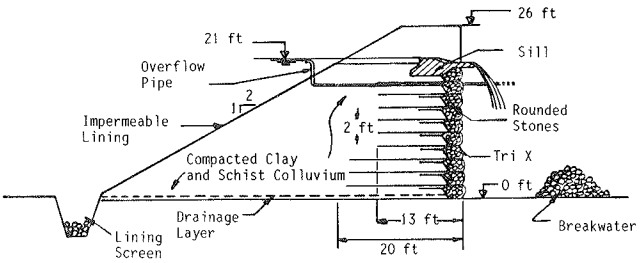

Figure A-73. Barrage de Maraval.

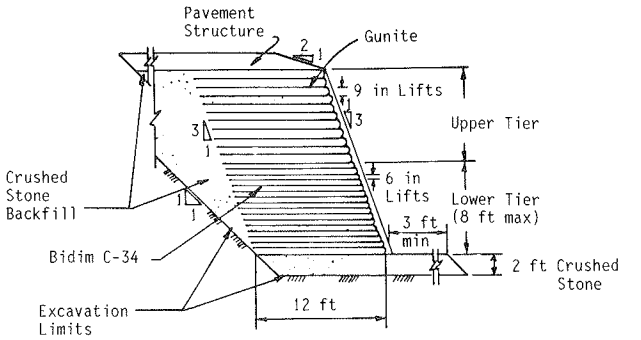

Figure A-74. NY22.

8.5 NY-22—Columbia County, New York, 1980

Two geotextile-reinforced walls were constructed 125 ft apart on the same road to repair shallow slope failures on a hillside embankment. The geotextile-reinforced wall solution was selected by the New York State Department of Transportation as a low cost solution that does not require a significant amount of maintenance.

The walls, 16 ft high and 110 ft long respectively, were made with a polyester needle-punched nonwoven geotextile, Bidim C-34, placed in horizontal layers in a backfill of crushed stone. As shown in Figure A-74, the geotextile layers were extended 12 ft behind the wall face. The layers are vertically spaced at 6 in. for the lower 8 ft of wall and 9 in. for the upper portion of the wall. The wall face, sloping at 1 horizontal to 3 vertical, was obtained by wrapping the geotextile around the backfill layers and applying a gunite layer over the facing after the end of construction. A 2 ft layer of crushed stone was placed beneath the first layer of backfill to increase lateral sliding resistance of the wall along its base.

Settlements measured one year after construction were 1.2 in. at one wall and about 0.4 in. at the other wall. These settlements have not caused noticeable effects on either the roadway structure or the rigid wall facing. No significant lateral movement at either wall was observed one year after construction.

8.6 Camp Hill Road—Willamette National Forest, Oregon, 1981

A geotextile-reinforced wall was constructed to retain fill in conjunction with widening of a road across a slide area. The wall, approximately 28 ft high, was built by the U.S. Forest Service. Innovative use was made of a lightweight sawdust backfill. The light backfill material was used to help maintain slope stability. The geotextile used was a polypropylene slit film woven, Supac 5W, which is placed in horizontal layers in the backfill. The wall face was obtained by wrapping the geotextile around the backfill layers and application of emulsified asphalt coating over the facing at the end of construction.

8.7 Allemond Road—Allemond, France, 1981

In the southern part of France, at Allemond, Electricite de France has built a hydropower plant with a capacity of 1,800 MW. The hydroscheme consists of a high level water basin with a capacity of 180 million cubic yards plus an additional basin with a capacity of 20 million cubic yards.

Problems were encountered during the construction of the hydroscheme because of its location in the side of a mountain and the lack of suitable roads for access to the constructed site. The design and construction of a road located between the mountain and the hydropower plant under construction was particularly difficult.

Possible design solutions given serious consideration were a concrete retaining structure and a reinforced soil structure. Whichever solution was used, the contractors had to be certain that the construction and use of the road did not result in horizontal forces being applied against the hydropower unit. A geotextile-reinforced wall was selected as a solution for the earth retaining structure.

The Allemond embankment is 66 ft high and 492 ft long, and slopes at 2 vertical to 1 horizontal (see Fig. A-75). Locally available gravel and sand were used as fill material. The fill material was sandwiched in 2.6-ft thick layers and supported on the bottom by a 23 ft width of Stabilenka 200, a polyester multifilament woven geotextile. The geotextile was folded

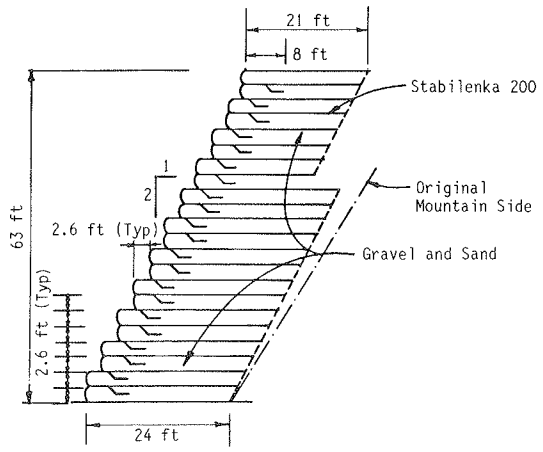

Figure A-75. The Allemond Road.

around the fill and laid back on the top of the fill to ensure sufficient friction resistance within the embankment. This is an unusually high structure for a geotextile-reinforced wall. However, the slope is not as steep as is commonly used for lower walls, thus reducing horizontal stresses.

Protection of the wall face was achieved by spraying of mixture of bituminous material and sand onto the facing.

8.8 Yorkshire Test—West Yorkshire, England, 1981

The purpose of this urban environment test, conducted by the West Yorkshire Council, was to study the feasibility of use of geotextile structures. The trial consisted of two fabric-reinforced walls built alongside an unreinforced wall. The reinforcement used in the trial was ICI "Terram 100", a needle-punched nonwoven geotextile. The length of the reinforcement was 3.3 ft and the height of the walls was 6.6 ft. All three structures were backfilled in 6 in. layers, using crusher run stone and hand ramming. On completion of filling, all sections of the wall, Figure A-76, remained standing, including a wall formed from a single skin of brickwork (4 in. thick) and having no reinforcement. After 6 months, the unreinforced wall collapsed by overturning about the toe. After 12 months the reinforced soil walls still showed no signs of distress.

8.9 Interstate I-70—Glenwood Canyon, Colorado, 1982

Glenwood Canyon is a narrow, steep-walled chasm, underlain by thick deposits of highly compressible soils. Construction of a road through this canyon posed several problems, the most significant being the large differential settlements expected because of the nature of the foundation soil. Because of limited space and excessive cost of vertical drains, it was not possible to consolidate the foundation soil by surcharging. Consequently, a flexible retaining wall system that could adapt to large differential settlements had to be found. Based on this requirement, the Colorado Division of Highways studied, in addition to the Reinforced Earth wall system then fully approved by the Federal Highway Administration, other systems of reinforced soil walls, including geotextile-reinforced walls. The purpose of evaluating

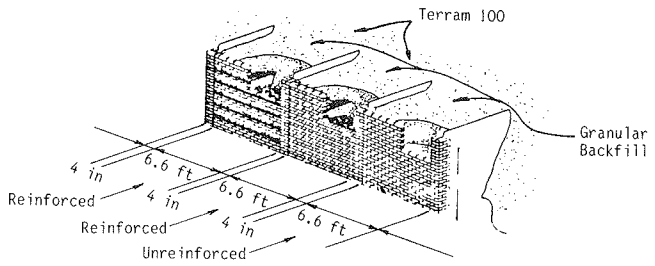

Figure A-76. Yorkshire test.

these other systems was to determine whether one or more could be approved for competitive bidding.

The geotextile-reinforced test wall, shown in Figure A-77, was approximately 15 ft high and 300 ft long. The primary objective of this test wall was to determine the lower stability limits of geotextile-reinforced walls. This was done by dividing the wall into 10 test sections of 30 ft length, each section incorporating a different combination of geotextile strengths, while keeping the geotextile layer spacings constant for all test sections. Since the geotextiles have different strengths, each section would exhibit different factors of safety.

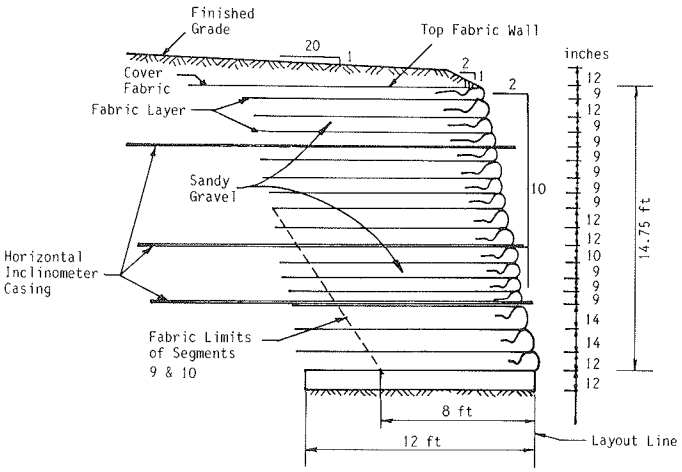

Figure A-77. I-70 Glenwood Canyon.

Four types of nonwoven geotextiles were selected for the tests. Each type was used in two weights. The geotextiles were Fibretex 200 and 400 (polypropylene needle-punched), Supac 4NP and 6NP (polypropylene and needle-punched), Trevira S1115 and S1127 (polyester needle-punched), and Typar 3401 and 3601 (polypropylene heat-bonded). The geotextile layers were extended approximately 13 ft behind the wall face and were vertically spaced 9 to 14 in. The wall face was obtained by wrapping the geotextile around the backfill layers, which consisted of a free draining pit-run, rounded, well-graded, clean sandy gravel, and applying gunite over the facing.

Observations indicated that a relatively large amount of consolidation had taken place in the foundation soil. Although differential settlements of the order of 1 ft over the 300 ft length of wall were recorded after only 3 months, the settlement had not produced significant cracking of the gunite facing. Large lateral deformations anticipated in some sections of the wall had not occurred.

The performance of the wall has been very satisfactory to date.

9. COST COMPARISONS

In the majority of cases, a fabric-reinforced retaining structure may be 20 to 50 percent less expensive than conventional alternatives. This is because the materials cost less, and the simple construction procedures result in lower installation costs. A fabric wall may be especially cost effective where its use permits the use of in-situ soil as backfill material.

Items usually included in a cost estimate are: excavation, geotextile, geotextile installation, backfill and haul, layer placement, and wall face protection or facing panels. In 1983 prices, the cost of a fabric-reinforced soil retaining wall is approximately \$11.50 to \$13.00 per sq ft of wall face. This may be compared with a cost of around \$19.00 per sq ft for a conventional reinforced concrete retaining wall. A breakdown of the unit cost might be as follows:

Item	Cost (\$/ft^2)
Geotextile	\$2.10–2.60
Labor	0.50–1.05
Equipment	0.50–1.05
Backfill, including haul	5.25
Gunite face protection	3.15
Total	\$11.50–13.00

Retaining walls constructed by the U.S. Forest Service in Olympic and Siskiyou National Forests, Shelton, Washington, and Glenwood Canyon, Colorado, all had costs falling within this range.

One may note that the fabric cost is only a small percentage of the total cost, and thus conservative design methods do not result in much greater costs unless this conservatism requires greater excavation and more backfill.

The costs for several of the walls described in the case histories section are listed in Table A-8. Geotextile material costs are given in Table A-10.

10. FUTURE DEVELOPMENTS

Several developments in geotextile-reinforced walls are likely. There is no solution likely to the problem of UV light degradation of geotextiles, although geotextile wall facings must be protected. New types of shielding and protective surfaces may be developed which may be stiffer and more aesthetically acceptable. More detailed knowledge on the long-term durability of various types of fabrics should, however, be obtained.

Geotextile-reinforced wall height will probably not routinely exceed 30 ft to 45 ft, as steel-reinforced earth walls are more efficient for high walls.

Geotextile-reinforced walls are likely to continue to be built in remote areas with difficult access. New, temporary installations may arise for roadways, shelters, or other types of facilities. Landslide repair will remain an important application. Many of the future projects may be for lower cost residential problems.

For small dams of limited width, geotextile-reinforced walls may be used for spillway weirs and embankment walls. Geotextiles may be used in tailings dams for drainage as well as reinforcement.

The important cost advantages of limited equipment requirements, unskilled labor, and inexpensive materials will make geotextile-reinforced walls more popular in the future.

11. DESIGN EXAMPLES

Several design examples which illustrate the U.S. Forest Service design procedure discussed in Section 7 of this chapter are presented in Chapter Five of the main report.

12. REFERENCES

ALFHEIM, S. L., and SORLIE [1977]. "Testing and Classification of Fabrics for Application in Road Constructions," *Proc. International Conference on the Use of Fabrics in Geotechnics,* Paris, Vol. II, p. 333.

ALLEN, T., BELL, J. R., and VINSON, T. S. [1983]. "Properties of Geotextiles in Cold Regions Applications," *Transportation Research Report No. 83-6,* Oregon State University, March.

ALLEN, T., VINSON, T. S., and BELL, J. R. [1982]. "Tensile Strength and Creep Behavior of Geotextiles in Cold Regions Applications," *Proc. 2nd International Conference on Geotextiles,* Las Vegas, Vol. III, p. 775.

BELL, J. R., BARRETT, R. K., and RUCKMAN, A. C. [1983]. "Geotextile Earth Reinforced Retaining Wall Tests, Glenwood Canyon, Colorado," 62nd Annual Meeting, Transportation Research Board, Washington.

BELL, J. R., and STEWARD, J. E. [1977]. "Construction and Observations of Fabric Retained Soil Walls," *Proc. International Conference on the Use of Fabrics in Geotechnics,* Paris, Vol. I, p. 123.

BELL, J. R., STILLEY, A. M., and VANDRE, B. [1975]. "Fabric Retained Earth Walls," *Proc. 13th Annual Engineering Geology and Soils Engineering Symposium,* Boise, Idaho.

BISHOP, A. W. [1955]. "The Use of the Slip Circle in the Stability Analysis of Slopes," *Proc. European Conference on Stability of Earth Slopes,* Vol. 1, pp. 1–13.

BROMS, B. B. [1977]. "Polyester Fabric as Reinforcement in Soil," *Proc. International Conference on the Use of Fabrics in Geotechnics,* Paris, Vol. I, p. 129.

BROMS, B. B. [1978]. "Design of Fabric Reinforced Retaining Structures," *ASCE Proc. Symposium on Earth Reinforcement,* Pittsburgh, p. 282.

CHASSIE, R. G. [1983]. "Fabric Retained Earth Walls—Some Case History Examples," 34th Annual Road Builders Clinic, Washington.

CHRISTIE, I. F., and EL-HADI, K. M. [1977]. "Some Aspects of the Design of Earth Dams Reinforced with Fabric," *Proc. International Conference on the Use of Fabrics in Geotechnics,* Vol. I, pp. 99–103.

CII [1982]. Construction Industry International Reprint, April.

COLLIOS, A., DELMAS, P., GOURC, J. P., and GIROUD, J. P. [1980]. "Experiments on Soil Reinforcement with Geotextiles," *Proc. ASCE Symposium on the Use of Geotextiles for Soil Improvement,* Portland, p. 53.

DELMAS, P., GOURC, J. P., and GIROUD, J. P. [1979]. "Experimental Analysis of Soil-Geotextiles Interaction," *Proc. International Conference on Soil Reinforcement,* Paris, Vol. I, p. 29.

DOUGLAS, G. E. [1981]. "Design and Construction of Fabric Reinforced Retaining Walls by New York State," *Transportation Research Record 872,* TRB, National Research Council, Washington, D.C. (1981) p. 32.

DUNCAN, J. M., and BUCHIGNANI, A. L. [1975]. "An Engineering Manual for Slope Stability Studies," University of California, Berkeley, March.

FINNIGAN, J. A. [1977]. "The Creep Behavior of High Tenacity Yarns and Fabrics Used in Civil Engineering Applications," *Proc. International Conference on the Use of Fabrics in Geotechnics,* Paris, Vol. II, p. 305.

GIROUD, J. P. Personal communication.

GIROUD, J. P., GOURC, J. P., BALLY, P., and DELMAS, P. [1977]. "Behavior of a Nonwoven Fabric in an Earth Dam," *Proc. International Conference on the Use of Fabrics in Geotechnics,* Paris, Vol. II, p. 213.

GRAY, D. H., ATHANASOPOULOS, G. and OHASHI, H. [1982]. "Internal/External Fabric Reinforcement of Sand," *Proc. 2nd International Conference on Geotextiles,* Las Vegas, Vol. III, p. 661.

HART, W. J. [1984]. Personal communication.

HOLM, G.,and BERGDAHL, U. [1979]. "Fabric Reinforced Earth Retaining Walls—Results of Model Tests," *Proc. International Conference on Soil Reinforcement,* Paris, Vol. I, p. 53.

HOLTZ, R. D. [1977]. "Laboratory Studies of Reinforced Earth Using a Woven Polyester Fabric," *Proc. International Conference on the Use of Fabrics in Geotechnics,* Paris, Vol. III, p. 149.

HOLTZ, R. D., and BROMS, B. B. [1977]. "Walls Reinforced by Fabrics—Results of Model Tests," *Proc. International Conference on the Use of Fabrics in Geotechnics,* Paris, Vol. I, p. 113.

HOLTZ, R. D., TOBIN, W. R., and BURKE, W. W. [1982]. "Creep Characteristics and Stress-Strain Behavior of a Geotextile-Reinforced Sand," *Proc. 2nd International Conference on Geotextiles,* Las Vegas, Vol. III, p. 805.

INGOLD, T. S. [1979]. "Reinforced Earth Embankments—An Analytical Study," *Internal Report No. 167703/1,* Ground Engineering Limited.

INGOLD, T. S. [1982]. "An Analytical Study of Geotextile Reinforced Embankments," *2nd International Conference on Geotextiles,* Industrial Fabric Association International, Las Vegas.

INGOLD, T. S., and MILLER, K. S. [1982a]. "Analytical and Laboratory Investigations of Reinforced Clay," *Proc. 2nd International Conference on Geotextiles,* Las Vegas, Vol. III, p. 587.

INGOLD, T. S. and MILLER, K. S. [1982b]. "The Behavior of Geotextile Reinforced Clay Subject to Undrained Loading," *Proc. 2nd International Conference on Geotextiles,* Las Vegas, Vol. III, p. 593.

JOHN, N., JOHNSON, P., RITSON, R., and PETLEY, D. [1982]. "Behavior of Fabric Reinforced Soil Walls," *2nd International Conference on Geotextiles,* Las Vegas, Vol. III, p. 569.

JONES, C. J. F. P. [1982]. "Practical Construction Techniques for Retaining Structures Using Fabrics and Geogrids," *Proc. 2nd International Conference on Geotextiles,* Las Vegas, Vol. III, p. 581.

KERN, F. [1977]. "Realisation d'un Barrage en Terre avec Parement Aval Vertical au moyen de Poches en Textile," *Proc. International Conference on Geotechnics,* Paris, Vol. I, p. 91.

KOERNER, R. M., ROSENFARB, J. L., DOUGHERTY, W. W., and MCELROY, J. J. [1980]. "Stress-Strain-Time Behavior of Geotextiles," *Proc. ASCE Symposium on the Use of Geotextiles for Soil Improvements,* Portland, p. 31.

LEE, K. L., ADAMS, B. D., and VAGNERON, J. J. [1973]. "Reinforced Earth Retaining Walls," *ASCE J. Soil Mechanics and Foundations Division,* Vol. 99, No. SM10, p. 745.

LEE, K. L., ADAMS, B. D., and VAGNERON, J. J. [1975]. "Discussion and Closure," *ASCE J. Soil Mechanics and Foundations Division.*

MARTIN, E. 1982. "Light Resistance of Textile Fibers," *Proc. 2nd International Conference on Geotextiles,* Las Vegas, Vol. III, p. 751.

MCGOWN, A., ANDRAWES, K. Z., and KABIR, M. H. [1982]. "Load Extension Testing of Geotextiles Confined in Soil," *Proc. 2nd International Conference on Geotextiles,* Las Vegas, Vol. III, p. 793.

MYLES, B. [1982]. "Assessment of Soil Fabric Friction by Means of Shear," *Proc. 2nd International Conference on Geotextiles,* Las Vegas, p. 787.

MYLES, B. [1984]. Personal communication.

NAVAL FACILITIES ENGINEERING COMMAND, Design Manual NAVFAC DM-7.2, *Foundations and Earth Structures,* U.S. Government Printing Office, Washington, D.C., May 1982.

PASLEY, C. W. [1822]. *Course of Elementary Fortification,* Vol. 2, Ch. 26, London: J. Murray.

PUIG, J., BLIVET, J. C., and PASQUET, P. [1977]. "Remblai Arme avec un Textile Synthetique," *Proc. International Conference on the Use of Fabrics in Geotechnics,* Paris, Vol. I, p. 85.

RAUMANN, G. [1982]. "Outdoor Exposure Tests of Geotextiles," *Proc. 2nd International Conference on Geotextiles,* Las Vegas, Vol. II, p. 541.

SALAMONE, W. G., BOUTRUP, E., HOLTZ, R. D., KOVACS, W. D., and SUTTON, C. D. [1980]. "Fabric Reinforcement Designed Against Pullout," *Proc. ASCE Symposium on the Use of Geotextiles for Soil Improvement,* Portland, p. 75.

SCHWAB, E. F., PREGL, O., and BROMS, B. B. [1977]. "Deformation Behavior of Reinforced Sand at Model Tests Measured by the X-ray Technique," *Proc. International Conference on the Use of Fabrics in Geotechnics,* Paris, Vol. I., p. 105.

SHERARD, J. L., and DECKER, R. S. [1976]. "Dispersive Clays, Related Piping, and Erosion in Geotechnical Projects," 79th Annual Meeting, ASTM, Chicago, Vol. STP 623.

SHRESTHA, S. C., and BELL, R. J. [1982]. "Creep Behavior of Geotextiles Under Sustained Loads," *Proc. 2nd International Conference on Geotextiles,* Las Vegas, Vol. III, p. 769.

SINGH, A., and MITCHELL, J. K. [1968]. "General Stress-Strain-

Time Function for Soils," *ASCE J. Soil Mechanics and Foundations Division,* No. SMI, p. 21.

SOTTON, M., and LECLERCQ, B. [1982]. "Geotextiles and Aging Tests," *Proc. 2nd International Conference on Geotextiles,* Las Vegas, Vol. II, p. 559.

SOTTON, M., LECLERCQ, B., PAUTE, J. L., and FAYOUX, D. [1982]. "Some Answer's Components on Durability Problem of Geotextiles," *Proc. 2nd International Conference on Geotextiles,* Las Vegas, Vol. II, p. 553.

STEWARD, J. E., and MOHNEY, J. [1977]. "Olympic National Forest Wall," U.S. Forest Service, Oregon.

STEWARD, J. E., and MOHNEY J., [1982]. "Trial Use Results and Experience for Low-Volume Forest Roads," *Proc. 2nd International Conference on Geotextiles,* Las Vegas, Vol. II, p. 335.

STEWARD, J. E., WILLIAMSON, R., and MOHNEY, J. [1977]. "Guidelines for Use of Fabrics in Construction and Maintenance of Low-Volume Roads," National Technical Information Service (Revised, 1983).

TERZAGHI, K., PECK R. B. [1967]. *Soil Mechanics in Engineering Practice.* John Wiley & Sons, N.Y.

VAN LEEUWEN, J. H. [1977]. "New Methods of Determining the Stress-Strain Behavior of Woven and Nonwoven Fabrics in the Laboratory and in Practice," *Proc. International Conference on the Use of Fabrics in Geotechnics,* Paris, Vol. II, p. 299.

CHAPTER THREE—PLASTIC STRIPS

Contents

1. INTRODUCTION

1.1 Physical Description

Nonmetallic strip reinforced walls are vertical or sloping walls that consist of linear nonmetallic reinforcing strips embedded in soil backfill and connected to the wall face (also called skin element) (see Fig. A-78). The nonmetallic reinforcing strips used to date have consisted of plastic strips and composites made of plastic strips bonded to a geotextile.

Backfill has typically consisted of granular fill ranging from sand to gravel in size, compacted in lifts with the reinforcing strips. Wall faces have mostly consisted of precast concrete panels.

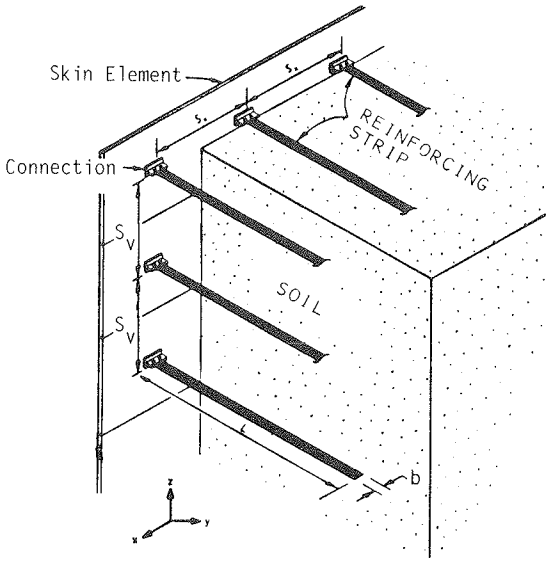

Figure A-78. Schematic of major elements of nonmetallic strip reinforced soil wall.

1.2 History and Development

Nonmetallic strips were introduced to preclude the corrosion associated with metallic reinforcements. Early research was initiated by La Terre Armee, in France, at the experimental reinforced soil wall of Beaulieu near Poitiers, France, in 1970 [Bastick, 1982]. The wall, which supports an access ramp to a bridge, was the first wall constructed using nonmetallic reinforcing strips. The strips used in this experimental structure were made of woven polyester instead of metal. Because of degradation of the polyester strips, backfill was placed against the face of the wall in 1983 to stabilize the wall against potential outwards movement or failure.

During the mid-1970's, separate full-scale studies were performed by the U.S. Corps of Engineers (COE) [Al-Hussaini, 1977] and the U.K. Transportation and Road Research Laboratory (TRRL) [Bodem et al., 1978] on laboratory-fabricated and commercially available nonmetallic reinforcing strips. Varying degrees of success were observed during these test programs. Discussion of each testing program can be found in Section 8 of this chapter, "Case Histories." During the late 1970's and early 1980, two reinforced soil walls varying in height from 13 ft to 26 ft were constructed in Europe using nonmetallic reinforcing strips [John et al., 1982]; early measurements indicated satisfactory short-term performance of these structures.

The only nonmetallic reinforcement strips currently available commercially are the Paraweb and Parastrip strips used in the Websol Frictional anchor system. These strips are manufactured by ICI Fibres.

Recent research related to the use of nonmetallic reinforcing strips has been mainly concerned with determining the long-term mechanical properties, i.e., long-term stress-strain behavior. Polyaramid fibers are also being tested. Because of the lack of information on long-term behavior, large-scale experiments are also being initiated to evaluate durability.

1.3 Proprietary Restrictions

The use of Paraweb and Parastrip strips has proprietary conflict with Vidal's Reinforced Earth patents in the United Kingdom. Because of proprietary restrictions, little technical information is available in the public domain on plastic strip systems. Consequently, this report cannot address plastics in the same detail as done for the other reinforcement systems. Other than limited research [Al-Hussaini, 1977; Al-Hussaini and Perry, 1978], the authors are not aware of full-scale applications in the United States.

2. APPLICATIONS

2.1 Inherent Advantages

Nonmetallic reinforcing strips are considered suitable for some environmental conditions that may be detrimental to metallic reinforcing strips, specifically, highly corrosive regimes where metal strips would have a comparatively high corrosion rate.

2.2 Disadvantages

The nonmetallic Paraweb reinforcing strips currently available are susceptible to changes in their mechanical properties. These changes can, for example, occur over the long term in a humid environment, as discussed in Section 5. Furthermore, because of creep properties, these reinforcing strips have to be designed for lower working stresses than metal strips. When the plastic strips are extensible, larger strains have to occur in a reinforced soil mass to mobilize the full reinforcing forces which the strips can provide, than would be the case for metal strips. In effect, this could limit the economically reasonable height of vertical wall faces. Based on experience with other systems, however, one would anticipate that higher modulus plastic strips will become available.

2.3 Site Conditions Appropriate for Use

Nonmetallic reinforcing strips can potentially be used on almost any site where a reinforced soil wall is being considered. Nonmetallic reinforcing strips have been used in various types of corrosive environments such as tidal river environments [John et al., 1982], which are generally considered not suitable for metallic reinforcing systems without extensive corrosion protection. Connections, which have generally been metallic, should be designed taking environmental conditions into account.

2.4 Routine Applications

Reinforced soil walls using nonmetallic reinforcing strips can be routinely used as retaining walls for main structures, bridge abutments, viaducts, slope stabilization in mountainous areas, and coastal or river protection.

3. MECHANISMS AND BEHAVIOR

3.1 Principle of Soil and Reinforcement Interaction

The transfer of stress between the soil and reinforcement, necessary for the reinforced soil mass to act as a coherent unit, is accomplished primarily through friction for nonmetallic strip reinforcement systems. This mechanism is very similar to the frictional stress transfer of smooth metallic reinforcing strips, and details need not be repeated here (see Chapter Four of the main report and Chapters One and Two of this appendix for more details).

3.2 Behavior and Failure Modes of the Reinforced Soil Material

Experiments by the Corps of Engineers [Al-Hussaini, 1977] on neoprene-coated nylon fabric strips indicated that there might be, in addition to strip breaking and strip pullout, a third possible mode of failure that is caused by excessive deformation of the plastic strip. Because of such excessive deformation, the wall in the Corps of Engineers' tests failed, even though the computed factors of safety against breaking and pullout were greater than one.

3.3 Behavior of the Reinforced Soil Structure

Lateral earth pressure measurements at a distance of 1 ft behind the facing by the Corps of Engineers [Al-Hussaini, 1977] have shown that the actual lateral earth pressure at this location was less than the active Rankine earth pressure. This is most likely because of the extensible nature of the plastic reinforcements in comparison to metallic reinforcements, which can allow lateral stresses in the structure to relax. Hence, the structures should be designed taking into account that the required reinforcing force must be developed in the reinforcement at a strain magnitude that is acceptable for the structure as a whole.

4. TECHNOLOGY

4.1 Description and Fabrication of Components

Nonmetallic strip-reinforced walls generally consist of the following components: reinforcing strip, strip-to-wall face connection, wall face, and soil backfill. The properties of the various nonmetallic reinforcing strips which have been used experimentally and routinely are summarized in Table A-14 together with the properties of metallic strips. Of the nonmetallic strips listed, only Paraweb strips and comnposites are still commercially available.

Paraweb strips are illustrated in the cross section of Figure A-79a. The strips are composed of 10 lanes, each lane containing a given quantity of fibers that are dependent on the tensile strength desired. Thus, the width of the strips may vary from 3.3 to 3.6 in. The fibers used in the manufacture of the strips are high tenacity polyester or polyaramid fibers that are produced by extrusion through dies and then drawn to give strength to the fibers by orienting the molecules. A given quantity of fibers is then grouped together to form a lane and coated with

Table A-14. Properties, dimensions, and costs of the reinforcing strips used in the TRRL experimental wall. [After Bodem et al., 1978]

	Property or cost							
Type of material	Minimum tensile strength (psi)	Minimum yield stress (0.2% proof) (psi)	Dimensions of strip	Cost of material ($ per strip)	Cost of coating ($ per strip)	Cost of punching fixing hole ($ per strip)	Total cost ($ per strip)	Total cost of reinforcement used per standard facing unit area (17.7 in. x 17.7 in.) $
Galvanized mild steel (grade 43/25)	49,315	29,000	2.56 in x 0.12 in x 13 ft.	2.21	1.40 (0.123 lbs/ft^2)	0.42	4.03	4.03
Plastic coated mild steel (grade 43/25)	49,315	29,000	2.56 in x 0.12 in x 13 ft.	2.21	3.92 (15.7 mils thick)	0.42	6.55	6.55
Aluminum coated embossed mild steel (grade CR4) Aludip	52,216	42,060	2.56 in x 0.08 in x 13 ft.	--	--	--	2.10	2.10
Stainless steel (grade 316 S16 rolled)	78,324	58,020	2.68 in x 0.06 in x 13 ft.	7.84	--	0.42	8.26	8.26
Polyester filaments in polyethylene Paraweb	24,658	--	3.46 in x 0.08 in x 13 ft.	1.12	--	--	1.12	2 strips: 2.24 4 strips: 4.48
Glass fibre reinforced plastic (FRP)	29,000	--	3.54 in x 0.12 in x 13 ft.	7.00	--	--	7.00	7.00
Prestressed concrete (grade 43/25)	Maximum direct tensile load (9400 lbs)	--	4.72 in x 2.17 in x 13 ft.	17.64	--	--	17.64	One plank served 2 facing units 8.82

low-density polyethylene (LDPE) which, on cooling, forms a resistant protective outer sheath. In order to minimize the effects of sunlight and oxidation, the LDPE contains carbon black, which also contributes to the stability of the material against chemical degradation.

Paraweb composites are illustrated in the cross section of Figure A-79b. The composites are formed by bonding the polyester or polyaramid plastic strips to Terram 1000, a polypropylene heat-bonded nonwoven geotextile. These composites are available in a wide range, including various combinations of different grades of the polyester or polyaramid reinforced plastic strips and/or the number of strips per unit width.

Strip-wall face connections are typically achieved by sandwiching and pinning the reinforcing strips between steel plates attached to the wall face (see Fig. A-78), or by passing the strips around a bar that has been previously passed through loops preattached into the wall face (see Fig. A-80a), for the case of the Websol Frictional Anchor System.

The wall face typically consists of precast concrete panels. However, other types of facing similar to those used for metallic strip-reinforced walls can also be used.

Soil backfill is genrally granular, ranging in size from gravel to sand.

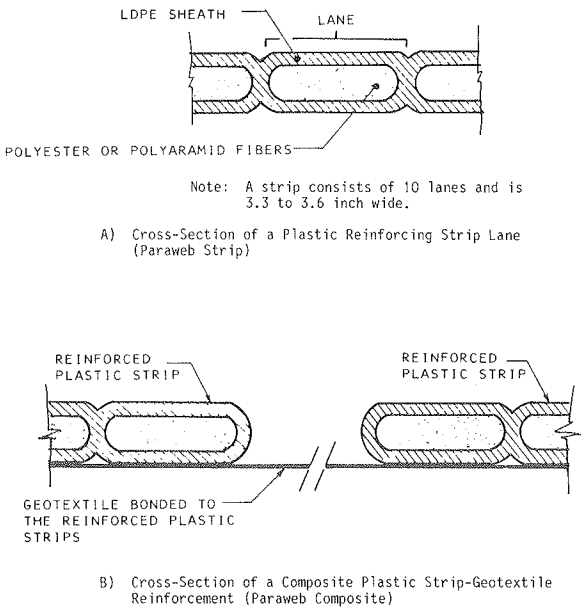

Figure A-79. Paraweb strips and composites.

4.2 Fabrication Quality Control

Fabrication of the nonmetallic reinforcing strips is subject to quality control requirements used in other types of civil engineering structures. In the United Kingdom, the quality of the material must comply with the Agreement Board Roads and Bridges Certificate registered with the Department of Transport. Plastic strips for soil reinforcement purposes are not currently manufactured in the United States.

5. DURABILITY AND SELECTION OF BACKFILL

5.1 Members Susceptible to Degradation

5.1.1 Mode of Degradation

As discussed in Section 4.1 of this chapter, the nonmetallic reinforcing strips commercially available are the Paraweb composites, i.e., plastic strips bonded to a geotextile, and the Paraweb strips, i.e., plastic reinforcing strips only. The modes of degradation of geotextiles are discussed in Chapter Two of this appendix. Only the mode of degradation of the plastic strips is discussed in this section.

The LDPE sheath which surrounds the fibers acts as a protection for the fibers. Consequently, degradation of plastic reinforcing strips can occur as a result of deterioration of either the LDPE sheath or the polyester fibers. Deterioration of the LDPE sheath may in the long term result in a degradation of the polyester fibers. However, studies [Jones, 1982] have shown that, in the long term, degradation could also occur in the fibers when the sheath is intact.

5.1.2 Sheath Degradation

Causes of LDPE sheath deterioration are varied and may be of chemical, physical, or mechanical nature. Brittle-type fractures have been reported to occur in LDPE at forces below the short-term ultimate tensile strength because of the presence of environmental agents such as solvents or oxidative agents [Connolly et al., 1970]. Other forms of failure of a physical nature have been found in LDPE. One is thermal embrittlement of unstressed LDPE leading to fractures. This type of failure is likely to occur in LDPE continuously exposed to temperatures above 60°C. However, at normal temperatures, the likelihood of thermal embrittlement is small. Another form of failure, which is also of a brittle type, has been observed in LDPE subjected to constant stress. This form of failure, which has been interpreted as brittle creep failure, appears to be caused by internal physical changes. Brittle failure of LDPE may also occur when the degree of crystallinity in the LDPE becomes excessive. In LDPE, this can apparently be caused by the manufacturing process. Other plastic products, such as HDPE, may reduce or eliminate these potential problems.

Deterioration of the LDPE sheath also includes damage caused by transportation, storage and site handling, placement of backfill, and anchoring of the strips near the wall facing panels. During transportation, storage and handling, abrasion or contact with any sharp object may result in puncture of the sheath. This same phenomenon may be expected during backfilling when the sheath is in direct contact with sharp and

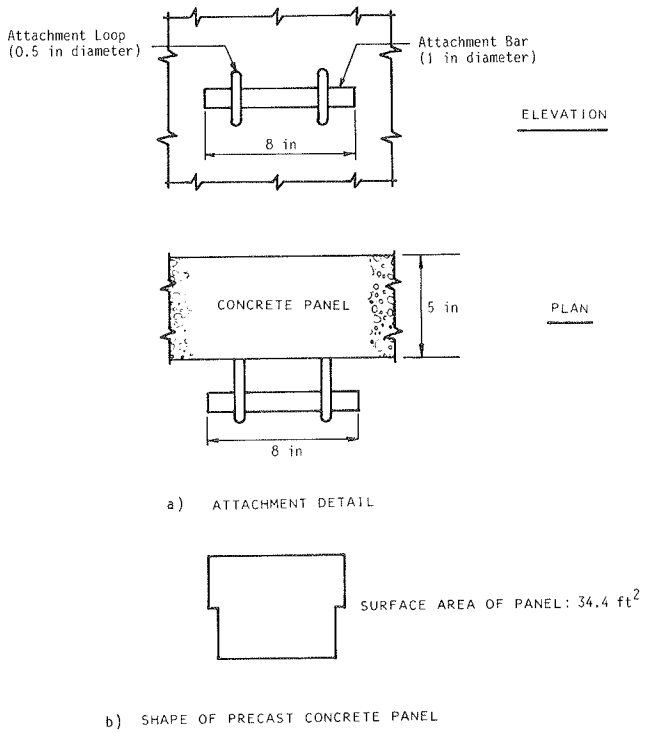

Figure A-80. Wall face precast concrete panel (Websol Frictional Anchor System).

angular fragments of rock. Anchoring of the strips at the wall face is usually done by passing the strips around a bar. In doing so, one side of the strip is in tension, whereas the other is in compression. A permanent state of tension combined with the wide variation of temperature likely to be encountered near the wall facing can lead to the same brittle type of failure discussed above, i.e., brittle failure due to creep and continuous exposure to high temperatures. All of these modes of LDPE sheath deterioration can result in localized openings such as fractures, cracks and tears allowing penetration inside the sheath of environmental agents which may be harmful to the polyester fibers.

Another mode of strip deterioration occurs when sealing at the ends of the strips is improperly executed. The end result is similar to that of LDPE sheath deterioration, i.e., penetration of environmental agents inside the sheath.

5.1.3 Fiber Degradation

In the short term, polyester fibers used in the manufacture of plastic reinforcing strips possess strength properties which remain constant, whether the fibers are wet or dry, and have excellent resistance to a wide range of chemicals. However, under particular conditions, such as long-term immersion in water, and over very long periods of time, the fibers may undergo aging and degradation.

Aging of the fibers is marked by changes in the properties with time due to nonchemical actions. The rate of aging may be influenced by such parameters as temperature and applied stress, but the relationships among these factors and aging are not yet well understood.

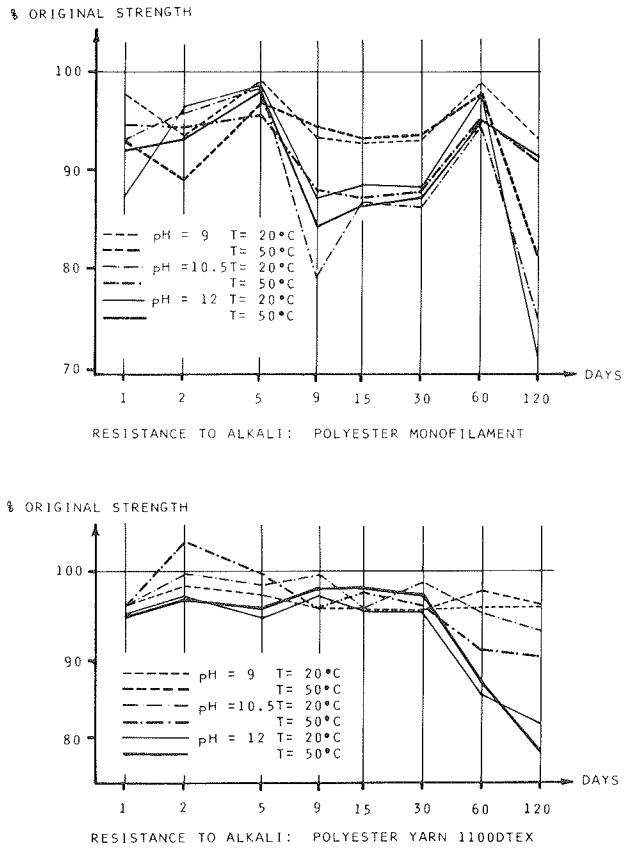

Figure A-81. Effect of alkaline solutions on polyester monofilaments and yarns. [Rhone-Poulenc, 1970]

Degradation may be initiated after long periods of time by simply exposing the fibers to chemicals or a humid environment. Tests have been conducted [Rhone Poulenc, 1970] to determine the effect of alkaline solutions on polyester monofilaments and yarns. After 120 days of immersion in pH solutions between 9 and 12 at temperatures of 20°C and 50°C, some of the monofilaments and yarns lost about 20 percent of their initial strength, as shown in Figure A-81. The effect of humidity on polyester fibers was investigated as early as 1959 by McMahon and his co-workers [McMahon et al., 1959] and Fuzek [1980]. McMahon's test results, although not valid because the tests were carried out at temperatures that could result in changes to the polyester fiber structure, are nevertheless still of great interest. The tests showed that polyester fibers can degrade as a result of hydrolysis generated by absorption of water by the fibers. The degradation rate by hydrolysis is much faster than oxidation or thermal degradation. In the short term, hydrolysis leads to increased elongation for a given stress loading, which results in additional creep. In the long term, hydrolysis causes a loss in tensile strength.

The foregoing results are complemented by the findings of Fuzek [Fuzek, 1980], who showed that at 23°C if kept fully immersed in water for 24 hours, polyester fibers can absorb as much as 7.0 percent of water in weight. Under 100 percent relative humidity, the fibers can absorb up to 1.2 percent in weight, and the amount of absorption can be expected to increase as temperature rises. Below 65 percent relative humidity, the amount of moisture absorption is 0.4 percent in weight and is expected to increase with temperature.

As previously mentioned, hydrolysis causes degradation of the polyester fibers, and, therefore, degradation of the reinforced plastic strips. Also, hydrolysis occurs at a relatively fast rate as compared to oxidation or thermal degradation. Consequently, in order to minimize the potential for degradation, the fibers must be isolated from moisture which generates hydrolysis. Isolation is provided in the short term by the LDPE protective sheath. In the long term, experience has shown that LDPE, in spite of being an effective liquid barrier is permeable to gases, including water vapor. Experiments carried out by British Telecom [Harrison, 1968] on LDPE cable sheath with a thickness of 0.19 in. showed that the core would reach 100 percent relative humidity within a period of 1 to 5 years.

Since it is reasonable to assume that the backfill in all structures will retain some moisture, the reinforced plastic strips may be considered to be in contact with a humid environment of a 100 percent relative humidity for their lifetime. As has been discussed above, LDPE is not effective in the long term as a barrier to moisture vapor. Consequently, it is expected that a similar situation as the one described by British Telecom for cables will occur and that sufficient moisture will permeate the sheath to saturate the polyester fibers after a certain time. Once the moisture is present, conditions are favorable to start a hydrolysis reaction, which in the long term will result in a loss of tensile strength.

It should be pointed out that hydrolysis of polyester fibers is not the only cause of loss in strength. Other factors such as the effect of stress and aging on the fibers should be considered as well. However, the combined effect of both of these factors is still unknown. This lack of understanding unfortunately still precludes the existence of a rational design procedure for allowing for the effects of aging of plastic strips in a specific environment. Much research remains to be done. Such research would be especially valuable if conducted on full-scale structures in a wide variety of environments. Aging can, however, be expected to first result in creep and excessive deformation of structures, rather than sudden failure without warning.

5.1.4 Parameters Determining Rate

Damage to the LDPE protective sheath will expose the polyester fibers to attack by external agents and thus accelerate the degradation process of plastic strip reinforcements. Thus, care should be taken during construction to prevent such damage.

When the LDPE sheath has remained intact after backfilling operations, there still exists potential for strip degradation, as mentioned previously. Among the parameters having a direct influence on rate of degradation are temperature and relative humidity inside the sheath. Also, internal changes in the fiber structure occur at temperatures exceeding 50°C [Fuzek, 1980]. A rise in temperature has the effect of increasing vapor pressure according to thermodynamics laws. The increased vapor pressure results in a higher rate of permeation through the LDPE sheath and, consequently, in a larger quantity of moisture vapor inside the sheath within a given period of time.

Both temperature and relative humidity, by increasing the amount of moisture vapor absorption by the fibers, will accelerate the rate of hydrolysis and thus the rate of degradation of reinforced plastic strips as illustrated in Figure A-82.

5.2 Methods and Tests to Predict Rate of Degradation

At present, there does not exist a method to predict rate of degradation of plastic strips that accounts for all the parameters involved. Such a method would have to include the influence of such factors as damage due to continuously applied stress, damage due to shocks, i.e., transportation, storage, site handling, and placement of backfill, and damage due to temperature variations.

A tentative method, proposed by Jones [1982], to estimate the lifetime of plastic strips assumes that degradation is caused only by hydrolysis of the polyester fibers. This assumption may be reasonable, since hydrolysis occurs at a rate much faster than oxidation or thermal degradation. However, the method may underestimate the loss in strength in a given time because of the influence of other factors such as aging and creep also acting on the strips.

The criterion used by Jones to estimate lifetime of plastic strips is the loss of the original strength. The assumptions he made in estimating this lifetime are as follows: (1) Water vapor permeates through the LDPE sheath whose exterior is maintained at 100 percent relative humidity and interior is completely dry. (2) The polyester fiber gains moisture as humidity of the sheath interior rises; values of moisture absorbed by the fibers to reach equilibrium are as given by Fuzek [1980], i.e., at 20°C, 0.4 percent in weight under 65 percent relative humidity and 1.2 percent in weight under 100 percent relative humidity. (3) Since no data are available regarding variation of moisture absorption with temperature and the amount of absorption is expected to increase with temperature rise, the same values, 0.4 and 1.2 percent, can be conservatively used for temperatures lower than 20°C. (4) The time taken to reach 65 percent relative humidity or 100 percent relative humidity inside the sheath is negligible. (5) Once the relative humidity inside the sheath has reached 65 percent or 100 percent, the rate of absorption of moisture by the fibers is equal to the rate of water permeating through the sheath. (6) After the fibers have absorbed sufficient moisture to reach moisture equilibrium, i.e., after they have absorbed 0.4 percent or 1.2 percent in weight, hydrolysis will begin to occur resulting in degradation.

In order to estimate the lifetime for the plastic strips, data from various sources were used by Jones such as rates of permeation through LDPE [Harrison, 1968], multipliers to apply on permeation rates to account for tempeature increase, polyester moisture absorption values [Fuzek, 1980], and rate of loss in tensile strength due to hydrolysis [ICI Fibres, 1975]. These parameters are presented in Table A-15 and plotted in Figure A-82.

Computations made by Jones showed that the time taken to start a hydrolysis reaction was relatively short as compared to that required to reach significant loss in strength at working temperatures between 20°C and 50°C. Consequently, the lifetime of plastic strip reinforcements could be estimated only on the basis of the time of degradation caused by hydrolysis. As shown in Table A-15, the estimated lifetime for plastic strips to lose 50 percent of their original strength under a temperature of 20°C and a relative humidity of 100 percent inside the sheath would be approximately 26 years.

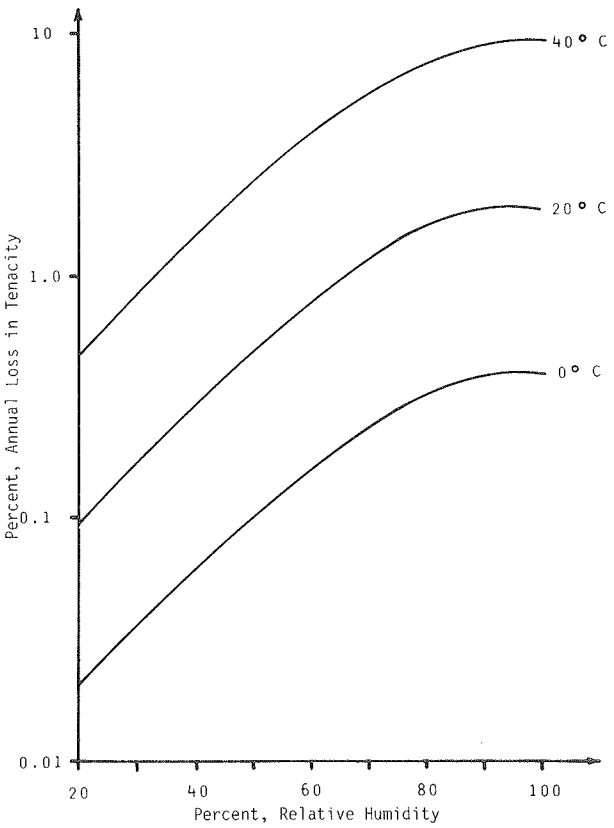

Figure A-82. Effect of hydrolysis on strength of polyester fibers. [ICI, 1975]

Table A-15. Percentage loss in tenacity for the polyester fibers used in the plastic strip reinforcements. [After ICI, 1975]

Temperature	Relative Humidity	Percent Loss in Tenacity, Time, years 1	5	10	25	50
0	65	0.2	1.0	2.0	5.0	10.0
	100	0.4	2.0	4.0	10.0	20.0
20	65	0.9	4.6	9.1	22.7	45.5
	100	1.9	9.4	18.7	46.8	93.6
40	65	4.2	20.8	41.6	>100	
	100	9.4	46.8	93.6		
60	65	22.1	>100			
	100	44.2	>100			

5.3 Selection of Backfill

The requirements for selection of an appropriate backfill material for nonmetallic strip-reinforced soil walls generally follow the guidelines established for metal strip-reinforced soil walls (see Chapter One in this appendix) and are not repeated here.

5.4 General Creep Considerations

The time-dependent stress-deformation behavior of a nonmetallic strip-reinforced wall is of concern because the wall may undergo excessive deformation due to creep of the reinforcing strips, even though adequate factors of safety are provided against other modes of failure. Tests, quoted by ICI [ICI, Paraweb], were conducted to detect any significant movement of polyester plastic strips. After a testing period of 4 years, the plastic strips had elongated only by an additional 0.57 percent when subject to a constant load of 80 percent of their breaking load. Other experiments conducted under similar conditions at 40 percent of the breaking load would have shown a 0.42 percent additional movement after a period of 4 years.

Polyaramid plastic strips have also been tested [ICI, Paraweb]. The elongation of a sample subject to a constant load of 40 percent of the breaking load was only 0.11 percent after a 4-year period.

For the composites made of reinforced plastic strips bonded to a geotextile, consideration should also be given to possible creep of the geotextile. Creep of geotextiles is discussed in Chapter Two of this appendix.

6. CONSTRUCTION

6.1 General Considerations

Many of the construction procedures used for plastic reinforcing strips are similar to those for metallic reinforcing strips. The major difference is the way connections are made to the facing, requiring more care not to damage the reinforcing elements.

6.2 Existing Specifications

In the United Kingdom, construction specifications have been issued by the British Department of Transport for reinforced soil retaining walls and bridge abutments for embankments [British Department of Transport, *Technical Memorandum BE 3/78,* 1978]. For reinforcing systems using plastic strips and geotextiles, specifications have been issued under the name Websol Frictional Anchor System by the Agreement Board Roads and Bridges (Certificate No. 82/22, 1982). The Websol system consists of Paraweb plastic strips installed in the manner shown in Figure A-83 and overlain by a geotextile (Terram). The strips are attached to the wall face by passing the strips around steel bars which have previously passed through the loops, as shown in Figure A-83a; and the loops are themselves pre-attached into the wall face precast concrete panels shown in Figure A-83b. Standards applicable specifically to plastic strips have not yet been developed in the United States.

7. DESIGN METHODS

7.1 General Considerations

Design methodology for plastic-stripped reinforced soil walls should generally follow the methodology used for other reinforced soil walls, as described in Chapter Five of the main report. Because of the lower modulus of plastics than of steel it may be reasonable to use the active lateral earth pressure ratio, K_a, for the entire height of the wall. As explained for Geogrid in Appendix B, it should be ascertained that the strains required to mobilize the design reinforcing force in the plastics are acceptable for the structure as a whole.

7.2 Available Specifications for Design

In the United Kingdom, design of reinforced soil walls, i.e., walls reinforced with metallic or nonmetallic strips, should comply with specifications issued by the British Department of Transport [*Technical Memorandum BE 3/78*]. There are no standards in the United States pertaining specifically to the use of plastic reinforcing strips.

8. CASE HISTORIES

8.1 Transport and Road Research Laboratory—Crowthorne, Berkshire, England, 1978

Based on a preliminary laboratory model, the Transport and Road Research Laboratory (TRRL) conducted experiments on a full-scale reinforced soil wall, 20 ft high, 150 ft long, and 46 ft wide [Bodem et al., 1978]. The objectives of the study were to optimize the use of reinforcing strips in terms of length, spacing, and orientation; make use of on-site materials; and provide data on corrosion or deterioration of the reinforcements.

To study the effects of various fill materials, the structure was built in three separate layers. The first layer consisted of a sandy clay having a fairly low clay content. The second layer was constructed with a free-draining granular material. The final layer consisted of a silty clay with a clay content higher than that selected for the first layer.

Various types of reinforcing strips were used in the study. The properties, dimensions, and cost of these strips are presented in Table A-14. In their selection, consideration was given to cost, resistance to corrosion or other form of deterioration in service, frictional and tensile characteristics, availability, and handling capability.

The plan and elevation view of the full-scale model are shown in Figure A-84. As shown, specific sections were built with several types of reinforcements. Two sections were reinforced with fiber-reinforced plastic (FRP) and Paraweb, while the other sections were reinforced primarily with steel with the exception of one section using concrete planks. A constant vertical spacing of about 1.5 ft was maintained for each layer, and a standard reinforcement length of 13 ft was used behind a wall face made of interlocking concrete panels. For the FRP section, a relatively constant factor of safety against pullout was obtained by varying the width, thickness, and horizontal spacing of the reinforcing strips. For the Paraweb section, the design was based on an elongation criterion rather than on pullout because of the relatively high elongation exhibited by the Paraweb strips, i.e., strain compatibility was considered in design.

Instruments were installed to measure tension in the reinforcing strips, vertical and horizontal earth pressure, pore water pressure, soil temperature and settlement within the fill mass. High pore water pressures developed in the wet clay fill during the construction of the first two layers, and large deformations occurred in the clay layer under these circumstances. The tension in the FRP strips as determined by strain gauges exceeded

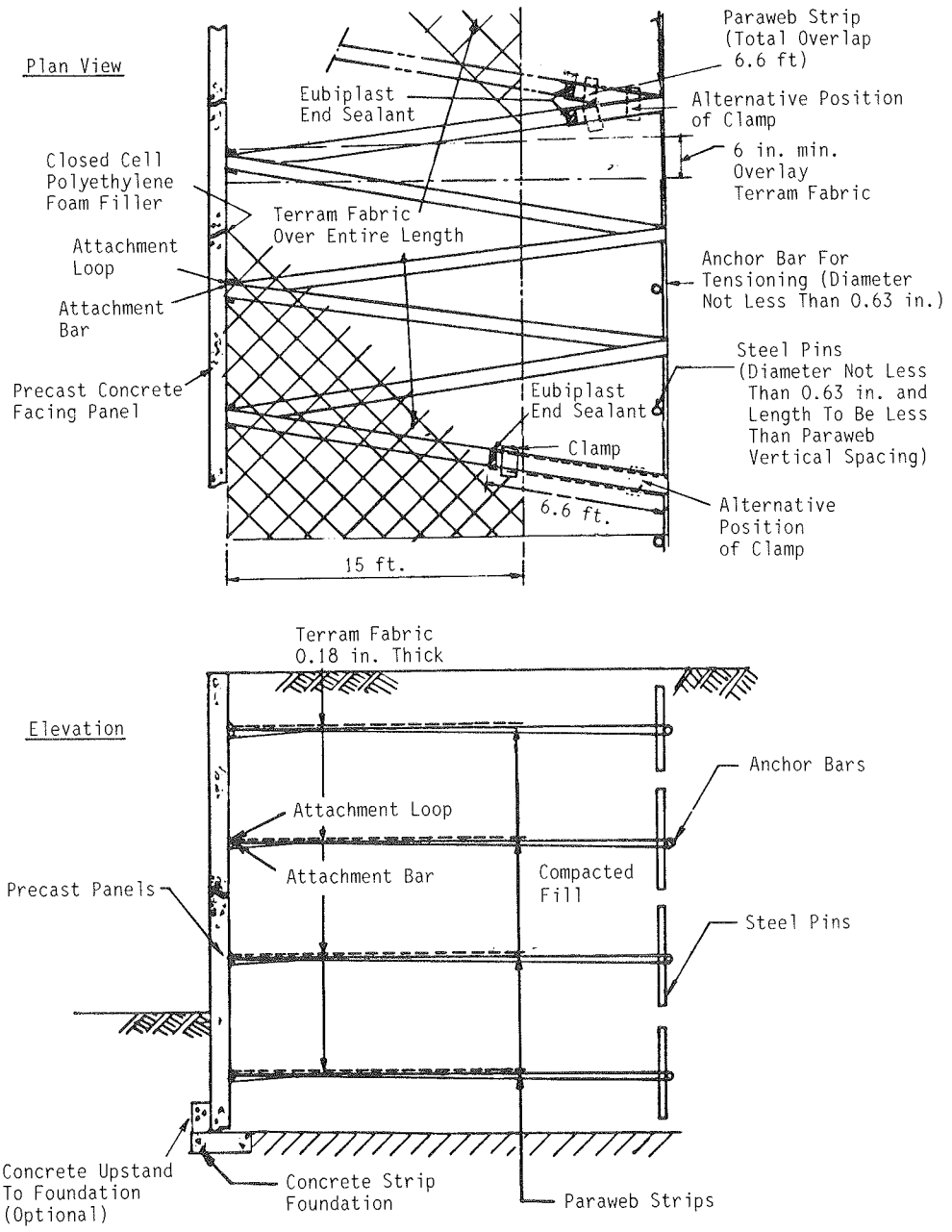

Figure A-83. Websol Frictional Anchor System.

the ultimate strength. Low tensions were recorded in the Paraweb strips due to the tendency of the strips to be displaced towards the facing during plastic failure of the wet clay under the action of the construction equipment. This difficulty was not encountered during the construction of the second layer with the free-draining granular material, nor were any major displacements detected in this level of the structure.

8.2 U.S. Army Waterways Experiment Station—Vicksburg, Mississippi, 1978

An experimental field test was conducted on a 12 ft high textile-membrane strip-reinforced soil wall [Al-Hussaini and Perry, 1978]. The reinforcing strips used in the experiment were made of heavy-duty 4-ply nylon fabric coated with neoprene. Each strip was 0.08 in. thick, 3.94 in. wide, and 10 ft long. The strips were spaced at 2 ft in the vertical direction and at 4 ft in the horizontal direction.

The backfill material used in the construction of the reinforced soil wall was a clean sand. The internal friction angle was equal to 36 deg and the friction angle between the membrane strip and the sand was assumed to be 30 deg.

Instruments, installed to monitor stress and deformation during construction and surcharge loading, indicated that lateral deformation of the skin element was excessive. Since the deformation was much higher than that expected to initiate active

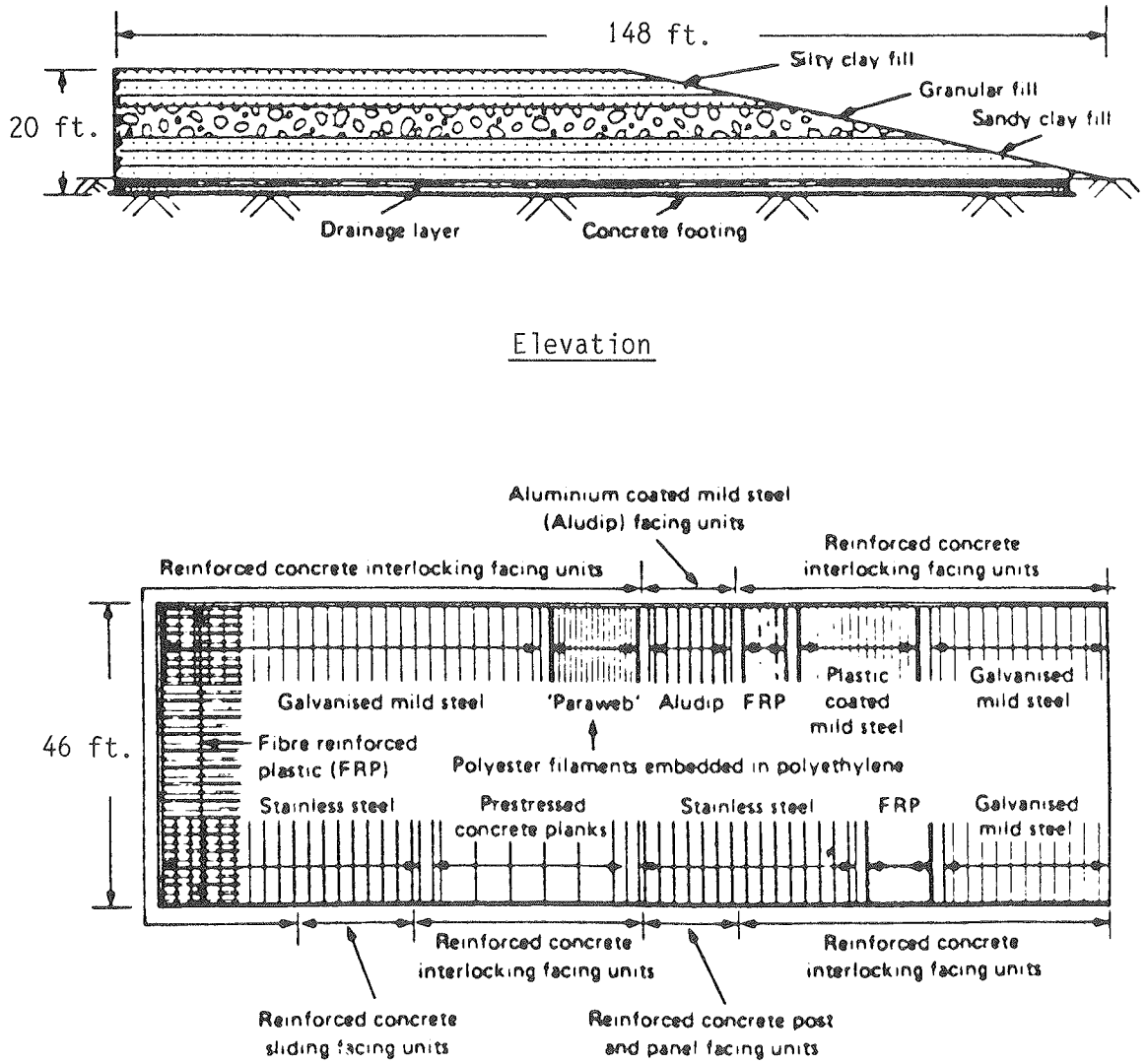

Figure A-84. Transport and Road Research Laboratory experimental wall.

failure in the loose sand, and the design factors of safety against strip breaking and pullout were satisfied, it is highly probable that failure of the wall was caused by the large deformation of the reinforcing strips that may have caused large tension zones and internal cracks. The experiment showed that for materials that exhibit large deformation, such as the 4-ply neoprene-coated nylon strip used in this study, a design based only on criteria of strip breaking and pullout is not adequate and a criterion considering strain compatibility should be incorporated in the design.

8.3 Southampton Wall—Southampton, England, 1979

A reinforced soil retaining wall was constructed using the Websol System to form part of an outfall structure on the bank of the River Itchen at Southampton [John et al., 1982]. The Websol System uses a heat-bonded nonwoven geotextile, Terram 1000, that has Paraweb reinforcing strips attached to it. The reinforcement is usually placed with the fabric on top to absorb the strain of construction traffic. A reinforced soil retaining wall, 13 ft high and 66 ft long, was constructed using single-size 0.6-in. gravel aggregate as a free draining fill material in the lower part. For the upper part, graded crushed rock was specified. Reinforcement of the wall was provided by 20-ft long layers of Paraweb strips and Terram 1000 sheet embedded in the backfill.

The Paraweb strips were attached to the facing panels using mild steel anchorage pins. In order to measure the force on the Paraweb connections at the facing panel, some of the standard connections were strain gauged. Monitoring was performed for several months after construction. The average load at this location remained fairly constant with time, and indicated lateral

earth pressures lower than "theoretical" values. Unfortunately, the reference does not provide sufficient information to verify whether the theoretical value was computed using active or at-rest lateral earth pressures.

A magnet extensometer system was developed to measure strain distribution in the Paraweb strips. The results showed a considerable amount of scatter, but in general indicated local strains to be highest (about 0.6 percent) at a distance of about 6 ft from the facing. This indicates that the forces in the strips were higher at some distance from the facing than at the location where forces were measured. Settlement was monitored by taking levels on top of the facing panels. The line of panels settled between 1.6 and 3.2 in. during the first 6 months, with most of the settlement occurring in the first 3 months.

8.4 Jersey Wall—St. Helier, Jersey, Channel Islands, 1980

A complete vertical section of a new harbor wall, 820 ft long, 26 ft high, constructed using the Websol System, was instrumented with strain gauged connections attached to the facing panels, earth pressure cells buried within the rock fill, inclinometers within the fill, and magnet extensometers bolted to the Paraweb [John et al., 1982].

The results after 2 years had suggested that the performance of the structure was somewhat at variance with the predicted behavior. The load distribution measured in the connections at the facing panels had been fairly uniform with depth rather than increasing linearly with depth. The loads in the reinforcing elements at the connections were once again smaller than "theoretical" values, but it is not evident from the reference how the theoretical values were computed.

8.5 Portsmouth Wall—Portsmouth, England, 1981

An experimental wall was constructed in 1981–1982 at the Geotechnics Field Centre, Portsmouth Polytechnic [John et al., 1982]. The Websol wall is approximately 66 ft long, 16 ft wide and 8 ft high. The facing panels are of timber construction, and backfill consists of single-size 0.79-in. gravel aggregate.

The Paraweb has been strain gauged and inclinometer tubes have been installed within the backfill at various locations. In order to more accurately assess the contribution of the Terram to the reinforcing function, various sections were built with and without incorporation of the Terram sheet. Pullout tests will be carried out on single and multiple Paraweb strips.

Land survey marks have been incorporated in the facing panels, and when all the survey and instrument readings have stabilized pullout and failure tests will be carried out. No data are currently available on the performance of this wall.

9. COST COMPARISONS

A comparison of costs of the various types of reinforcing strips, including the Paraweb, used in the Transport and Road Research Laboratory experimental wall (see Sec. 8.1 of this chapter) is shown in Table A-14. These costs are strictly applicable only to the TRRL wall, and caution should be used to extrapolate these costs for other uses. In particular, note that the reinforcing strips were purchased in relatively small quantities, and the costs are in 1978 dollars.

10. FUTURE DEVELOPMENTS OF SYSTEMS

Nonmetallic reinforcing strips have been developed primarily as an alternate to metal strips for use in corrosive environments. Little research has been conducted to date in this field, especially on the behavior and failure modes of the reinforced soil material or the reinforced soil structure, and the design methods. Design methods for plastic strip-reinforced walls still use features initially developed for metal strip-reinforced walls. This lack of research can be partly attributed to the fact that structures using nonmetallic reinforcing strips have not been as extensively built as those using metal strips.

Present research has been undertaken by the Paraweb manufacturer to determine the long-term effect of continuously applied stress on the polyaramid-reinforced plastic strips.

In the future, several trends with plastic strip-reinforced walls are likely. In the near future, plastic strip-reinforced wall height will probably not exceed 30 to 45 ft, because beyond this height metal strip-reinforced walls are currently more efficient. Because of their nonsusceptibility to corrosion, plastic strip-reinforced walls are likely to be extensively used in harbor, river, and coastal structures. Also, because of their good resistance to a wide range of chemicals (at least in the short term), they may be used as reinforcement in waste management projects. It is also highly likely that more durable plastic strips of higher modulus will be developed.

The relatively low cost of the Paraweb strips, as shown in Table A-8, will likely result in increased use of plastic strip-reinforced soil structures in the future.

11. DESIGN EXAMPLE

Because plastic strips have not often been used, there is not yet a unique design method pertaining to their use. It is likely that either the design methods applying to Reinforced Earth or the methods applying to geotextiles (see Chapter Five of the main report) can readily be adapted. However, it is important that it be recognized that currently available plastics are of relatively low modulus. Hence, it should be verified that the computed forces in the reinforcements will not result in strain magnitudes that are unacceptable for the structure as a whole. When higher modulus plastic strip materials become available strain compatibility will become less of a concern.

12. REFERENCES

AL-HUSSAINI, M. M. [1977]. "Field Experiment of Fabric Reinforced Earth Wall," *Proc. International Conference on the Use of Fabrics in Geotechnics,* Paris, Vol. I, p. 119.

AL-HUSSAINI, M. M., PERRY, E. B. [1978]. "Analysis of a Rubber Membrane Strip Reinforced Earth Wall," *Proc. Symposium on Soil Reinforcing and Stabilizing Techniques,* Syndey, p. 60.

BASTICK, M. [1982]. "Study of the Tergal Webbing Used as Reinforcing Strip for the Reinforced Earth Wall of Beaulieu near Poitiers," *Terre Armee Internationale Informative Report No. 1.*

BODEM, J. B., IRWIN, M. J., POCOCK, R. G. [1978]. "Construction of Experimental Reinforced Earth Walls at the TRRL," Ground Engineering, Vol. II, No. 7, p. 28.

BRITISH DEPARTMENT OF TRANSPORT, *Technical Memorandum BE 3/78* [1978]. Reinforced Earth Retaining Walls and Bridge Abutments for Embankments.

Certificate No. 82/22 [1982]. "Websol Frictional Anchor System," The Agreement Board Roads and Bridges.

CONNOLLY, R. A., DECASTE, J. B., GAUPP, H. L. [1970]. "Marine Exposure of Polymeric, Materials and Cable after 15 Years," *J. Materials,* Vol. 5, p. 339–362.

FUZEK, J. F. [1980]. "Glass Transition Temperature of Wet Fibres, its Measurement and Significance," *ACS Symposium Series No. 127,* Paper 31, p. 515–530.

HARRISON, J. C. [1968]. "The Metal Foil PE Cable Sheath and its Use in the Post Office," Institution of Post Office Electrical Engineers, Paper 229, London.

ICI Industrial Fibres Manual, TAI/3 [1975]. "Chemical Properties of Terylene and ICI Nylon," Edition 2.

ICI, Paraweb, Brochure on *Construction Materials for Soil Reinforcement.*

JOHN, N., JOHNSON, P., RITSON, R., PETLEY, D. [1982]. "Behavior of Fabric Reinforced Soil Walls," *Proc. 2nd International Conference on Geotextiles,* Las Vegas, Vol. III, p. 569.

JONES, M. [1982]. "An Evaluation of the Factors Affecting the Lifetime of Paraweb," *Terre Armee Internationale Informative Report No. 2.*

MCMAHON, W., BIRDSALL, H. A., JOHNSON, G. R., CAMILLI, C. T. [1959]. "Degradation Studies of Polyethylene Terephthalate," *J. Chemical and Engineering Data,* Vol. 4, p. 57–79.

RHONE POULENC INDUSTRIES [1970]. "Reaction of Filaments and Monofilament Polyesters in an Alkaline Solution," Report Included in *Terre Armee Internationale Informative Report No. 1.*

APPENDIX B

PASSIVE RESISTANCE REINFORCEMENT SYSTEMS

CHAPTER ONE—WELDED WIRE WALL AND REINFORCED SOIL EMBANKMENT

Contents

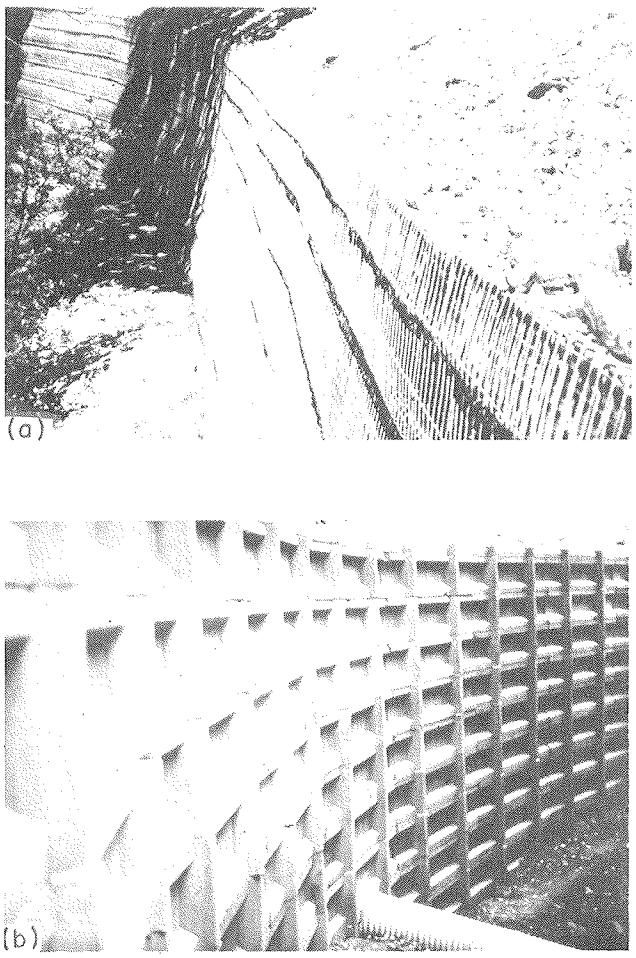

Figure B-1. Typical installations of Welded Wire Wall and Reinforced Soil Embankment: (a) Welded Wire Wall, (b) Reinforced Soil Embankment.

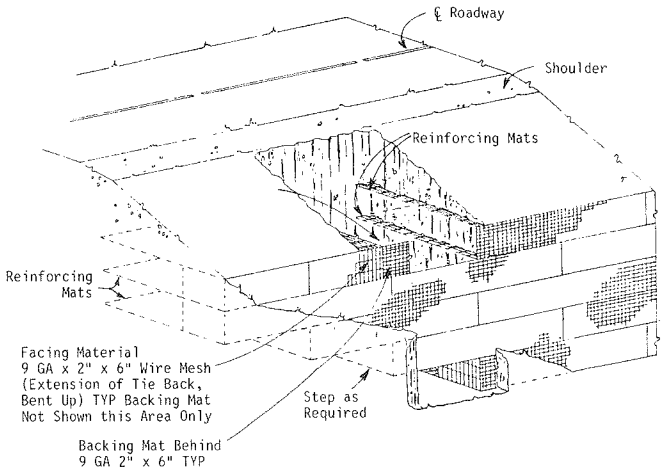

Figure B-2. Schematic of Welded Wire Wall.

1. INTRODUCTION

1.1 General

The Welded Wire Wall and the Reinforced Soil Embankment (RSE) each employs welded wire mesh grid reinforcement within backfill to produce a coherent reinforced soil mass. Both systems were developed by the Hilfiker Retaining Wall Company, with the Reinforced Soil Embankment being an outgrowth of the research and development prompted by the Welded Wire Wall. Commercial use of the Welded Wire Wall began in about 1977, and use of the Reinforced Soil Embankment was initiated in 1983. Both systems have some similarities with the Bar Mat systems described in Chapter Four of this appendix. The development and the design procedures for the RSE and the Welded Wire Wall are somewhat similar. The differences between Welded Wire Wall and RSE are primarily in the finished faces of retaining walls and in the sizing of the reinforcing meshes. Typical installations of each of the two systems are shown in Figure B-1. The selection of one system rather than the other is based primarily on the desired architectural appearance at a given location.

1.2 System Description

1.2.1 Welded Wire Wall

The Welded Wire Wall uses a type of welded wire reinforcing mesh commonly used in concrete slabs. This material is fabricated in 8-ft wide mats of varying lengths and can be ordered according to project requirements.

The mats are placed in alternating layers with compacted backfill to produce a composite material. The thickness of the compacted soil layers between reinforcing mats is 18 in. A portion of each mat, extending outward from the face, is bent upwards for connection to the mat layer immediately above. A schematic drawing of a typical Welded Wire Wall is shown in Figure B-2. For many installations, the wire face of the wall is left exposed as shown; however, other facings are possible. A minimum of 18 in. of soil cover is used above the upper reinforcement layer.

The mats initially used for Welded Wire Wall construction were of 9-gauge wire (W1.7) laid in a 2-in. by 6-in. mesh. This mat was oriented so that the wires spaced at 2 in. were normal to the wall face. Beginning in 1984, substantially heavier wire laid in a 6-in. by 9-in. mesh became the standard for wall construction. Wires spaced at 6 in. are normal to the wall face; the various wire sizes now being used are discussed in detail in Section 7.5 of this chapter under "Design Parameters."

"Backing mats" are installed behind the bent-up face portion of each reinforcing mat during construction. The backing mats, which are made of the original 9-gauge, 2-in. by 6-in. welded wire mesh, are placed so the wires spaced at 2 in. are parallel to the ground, and the 6-in. spacing wires are vertical. Wire screen (¼ in.) is placed behind the backing mat; the screen and the backing mats are installed so that backfill cannot flow out through the openings in the large mesh.

Originally, pea gravel or gravel with ¾-in. maximum particle size was placed against the wire face of walls constructed with the 9-gauge, 2-in. by 6-in. mesh. This allowed adequate compaction near the face with minimal effort and minimized

compression of the face. With the heavier wire mats now being used, this facing gravel has been eliminated.

1.2.2 Reinforced Soil Embankment

The Reinforced Soil Embankment combines reinforcing elements similar to those of the Welded Wire Wall with precast concrete facing elements as shown on Figure B-3 (Orvan Optional Cast-in-Place Concrete Face). The grid reinforcement is a heavy gauge, welded wire mesh in a 6-in. by 24-in. pattern, with the wire at the 6-in. spacing oriented normal to the wall face. The vertical spacing between the reinforcing mats is 24 in. As can be seen on Figure B-3, each reinforcing mat has a wide strip at its head, with pins that fit into holes in the top and bottom of the prefabricated concrete facing panels to anchor both the top and bottom of the facing panels to the reinforcing mats. In 1985, design studies for a new and simpler connection were initiated.

The RSE has a prefabricated leveling pad placed directly on the foundation to which the first layer of wire mesh is attached. The 2-ft-high by 12-ft-wide face panels are then built as high as is required, using the wire mats to retain the soil. A leveling cap for the wall is provided at the top.

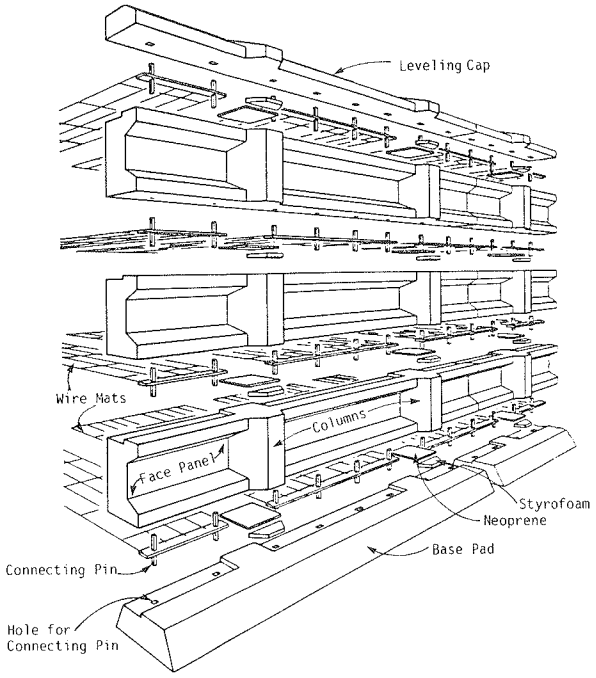

Figure B-3. RSE components.

1.3 History and Development

Development of the Welded Wire Wall by William Hilfiker began in the mid-1970's, with an experimental wall being built in 1975 to confirm feasibility. The first commercial use was in 1977, when Southern California Edison Power Company used the concept to repair portions of powerline access roads constructed in the San Gabriel Mountains of Southern California.

In late summer 1978, Utah State University began a general evaluation of Welded Wire Wall to develop design criteria under the direction of Dr. Loren R. Anderson. A 22-ft-high Welded Wire Wall, in the San Gabriel Mountains, was instrumented and observed during construction. Tests to quantify the pullout resistance of the grid reinforcement were performed, and experimental, instrumented wall segments were constructed and tested. Based on the results of these tests and field measurements, recommendations for design and construction of future Welded Wire Walls were developed by Bishop [1979]. Shortly thereafter, two substantially more detailed studies were performed to refine pullout criteria for the grid reinforcement [Peterson, 1980; Nielsen, 1983], while walls under construction were instrumented and monitored to refine the design and construction procedures.

In 1980, the use of the Wire Wall expanded to larger projects, such as a 750-ft-long, 15-ft-high wall built for the Union Oil Company at their Parachute Creek shale oil development. Upwards of 200 walls were completed by mid-1984, with Welded Wire Wall having been accepted for use in road construction by several states, the Federal Highway Administration, and the U.S. Forest Service.

The first experimental Reinforced Soil Embankment was constructed in 1982, and first commercial use of the system was in 1983 on State Highway 475 near the Hyde Park ski area, northeast of Santa Fe, New Mexico. This installation included four different Reinforced Soil Embankments, for a total of about 17,400 sq ft of wall face. Several additional installations have been completed since.

1.4 Proprietary Restrictions

As of this writing, there are three U.S. patents granted on the Welded Wire Wall and one additional patent pending. The first patent (No. 4117686) essentially covers a grid reinforcement system in which the grid is left extending from the face of the soil which it reinforces, and is bent-up and tied to the next layer of reinforcement; i.e., the basic scheme of the Welded Wire Wall. The second and third patents (Nos. 4329087 and 4391557) are for a wall constructed as described in the first patent, with the modification of a molded or a formed-concrete face. As an option, they include the use of rock bolts to retain the face of the wall if it is to be used where the base width of the wall is restricted by hard rock. A fourth patent, presently pending, is for a recently developed preformed tie for attaching the reinforcing mats to one another on the face of the wall.

The primary U.S. patent for the Reinforced Soil Embankment (No. 4324508) covers the method of connecting the reinforcing grid to the prefabricated concrete panels, as well as how the facing panels fit together. Two other patents that are pending concern the specific pin involved in the hardware connection of the mat to the panels and the shape of the prefabricated concrete facing panel.

The foregoing patents are owned by the Hilfiker Retaining Wall Company. Atlas Industries, Limited, has been licensed by Hilfiker Walls for international administration and distribution of the Welded Wire Wall and Reinforced Soil Embankment. Patents are pending in several countries for both of these retaining wall systems. A subsidiary of Atlas Industries, Gridcote, has been licensed to market the Wire Wall in the United States.

In July of 1984, the Hilfiker Retaining Wall Company entered into an agreement with the Reinforced Earth Company for licensing of certain Hilfiker products. In particular, the RSE system, when constructed with precast panels is presently li-

censed by Reinforced Earth in California, Oregon, Washington, Idaho, Nevada, Utah, Arizona, New Mexico, Colorado, Wyoming, Montana, Hawaii, and Alaska. This licensing is under existing Reinforced Earth patents, due to expire in 1986. The RSE system, when constructed anywhere with a cast-in-place face, or with precast panels outside the noted states, does not come under this agreement. The Welded Wire Wall does not come under the agreement in any way.

2. APPLICATIONS

2.1 Inherent Advantages

The inherent advantages of Welded Wire Wall and Reinforced Soil Embankment are similar to those for most reinforced soil systems and are described in detail in Chapter Three of the main report. The fact that separate facing panels are not used for Welded Wire Wall makes this system unique among methods using metal reinforcement. Equipment for installation or construction of precast or cast-in-place concrete or other types of faces is not needed, and the grid openings at the face permit seeding of slopes when desired.

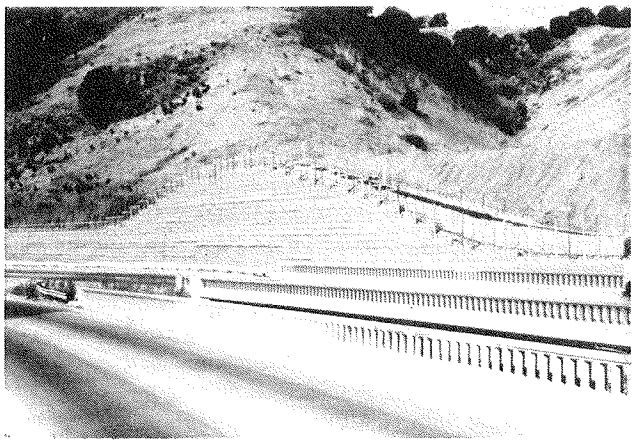

Figure B-4. Photograph of Welded Wire Wall in highway applications.

2.2 Site Conditions Appropriate for Use

The Welded Wire Wall and RSE have no particular restrictions on site conditions different from those that apply to any other reinforced soil structure. As with all retaining walls, embankments, or any soil structure, external stability and settlement considerations must be taken into account. These considerations include both deep and shallow slope stability, as well as sliding, bearing capacity, and overturning. Surface drainage and groundwater conditions must be evaluated thoroughly and either positive control be established or the walls be designed appropriately.

2.3 Routine Applications

Welded Wire Walls and Reinforced Soil Embankments were originally developed as retaining wall systems. An example of Welded Wire Wall used for construction of a highway embankment under limited access or right-of-way conditions is shown in Figure B-4. The Welded Wire Wall and the Reinforced Soil Embankment can be used on steep side hills, near river beds, and in other difficult situations. They can be used both for new highway embankment construction and repair of roads where slipouts, slides, or other problems have occurred. Extensive use has been made of Welded Wire Walls to repair back-country roads (Forest Service and powerline access roads are examples) because of straightforward construction and favorable economics. Because construction is relatively simple and fast, a road embankment failure can usually be repaired rapidly. Other routine applications include construction of bridge abutments as shown in Figure B-5.

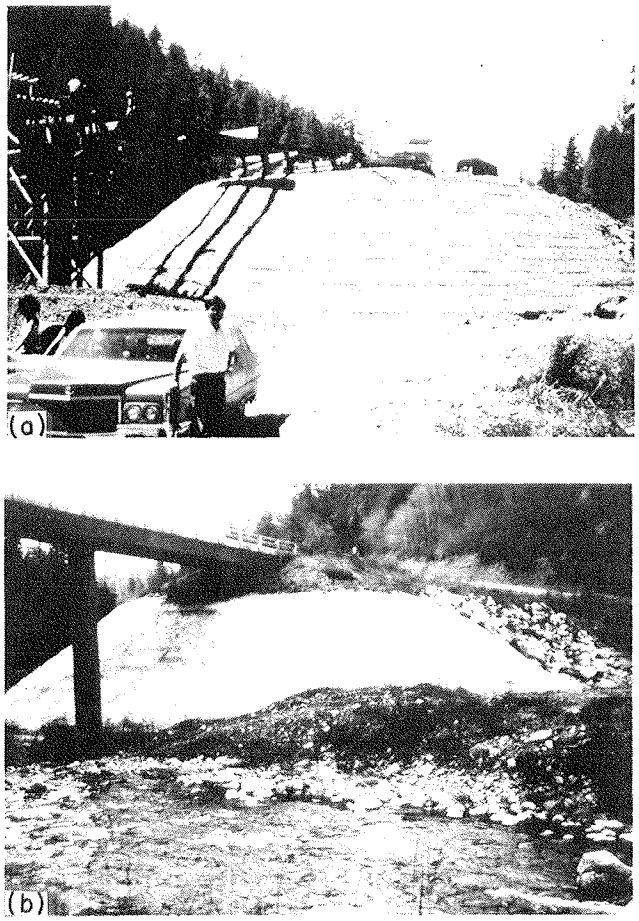

Figure B-5. Photograph of Welded Wire Wall used as bridge abutment: (a) bridge abutment under construction, (b) completed abutment.

2.4 Special Applications

Although the Welded Wire Wall and the Reinforced Soil Embankment are relatively recent developments, a few special

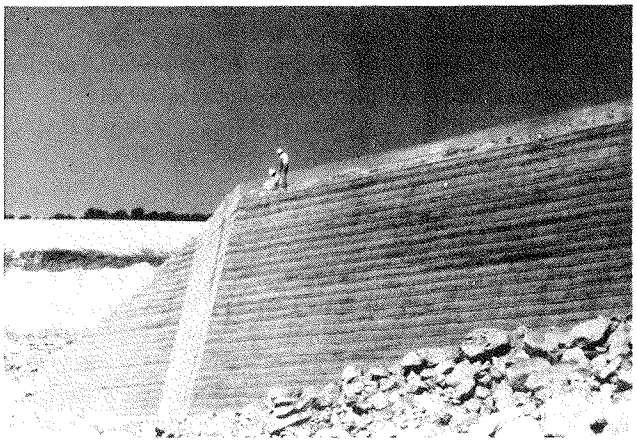

Figure B-6. Photograph of Chevron double wall under construction.

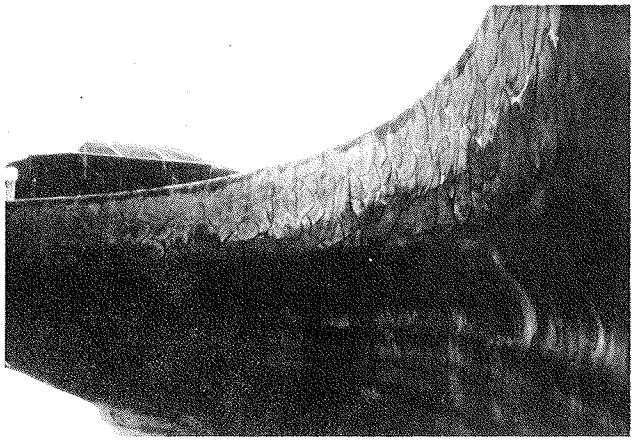

Figure B-7. Photograph of Sequoia Park Zoo cantilever Welded Wire Wall.

applications have been made. A double-faced wall was constructed to a height of 52 ft for containment of material at a shale oil plant in Vernal, Utah, as shown in Figure B-6. Another unusual application was the construction of a slightly cantilevered retaining wall around a specially built enclosure for bears at the Sequoia Park Zoo in Eureka, California. The upper portion of the 12-ft-high wall was cantilevered out about 18 in., as shown in Figure B-7. Cement was applied to the facing mesh by hand for the final finish.

Construction of a working pad over poor foundation soils is another application. Such working pads have been prepared for a high tension powerline tower and for an exploratory oil drill rig. Use in slide stabilization problems has been made of the Welded Wire Wall, with construction of a pair of walls to support a gas products pipeline at the heads of two small landslides, planned for summer of 1985.

3. MECHANISMS AND BEHAVIOR

3.1 Introduction

The pullout resistance of wire mesh reinforcement is generated by passive soil resistance against the transverse wires and frictional soil resistance developed along the longitudinal wires. For typical mesh configurations, passive resistance is the major contributor to total pullout resistance.

The Caltrans studies of grid reinforcement [Chang et al., 1977], which led to the development of Mechanically Stabilized Embankment, formed the basis for the current understanding of the mechanisms and behavior of Welded Wire systems. Using these results as a point of departure, three laboratory studies were performed at Utah State University to evaluate the pullout resistance of welded wire mesh and single longitudinal wires [Bishop, 1979; Peterson, 1980; Nielsen, 1983]. Parameters varied in these tests included soil type, number of transverse wires, number of longitudinal wires, wire diameters, both transverse and longitudinal wire spacing, overburden pressure, and soil type.

3.2 Frictional Resistance

3.2.1 Theoretical Considerations

The frictional resistance generated by the soil–reinforcement interaction can be estimated on the basis of the average stress over the circumference of the wire and the friction angle, δ, between the soil and the reinforcement. The friction angle can be either measured with direct soil-to-steel shear tests or estimated using empirical correlations.

The frictional pullout force for a single wire can be computed as

$$P_f = \sigma_a \, \pi d \, (\tan \delta) L \tag{B-1}$$

where P_f = frictional pullout force; L = length of embedded wire; d = wire diameter; and σ_a = average confining stress, computed as:

$$\sigma_a = \frac{\sigma_v + \sigma_h}{2} = \frac{\sigma_v + K\sigma_v}{2} \, 0.75\sigma_v \tag{B-2}$$

where σ_v, σ_h = vertical and horizontal stress, respectively; and K = lateral earth pressure coefficient, taken as 0.5 for the general case in the above-noted studies [Peterson, 1980 and Nielsen, 1983].

3.2.2 Experimental Data

Studies were performed by Caltrans and by Utah State University [Chang et al., 1977; Peterson, 1980], in which circular bars and single, longitudinal wires were pulled out of soils. These studies generally indicated that measured pullout resistances exceeded theoretically computed values. As discussed in the main report, it has been projected that the difference between the actual and theoretical values is the result of increased local confining stresses due to soil dilation. The difference between the measured and calculated values should decrease with in-

Table B-1. Standard wire sizes.

Size Number	Nominal Diameter		Area	
	in	(mm)	in^2	(mm^2)
W1.7	.148	(3.8)	.017	(11)
W2.5	.178	(4.5)	.025	(16)
W3.4	.207	(5.3)	.034	(22)
W3.5	.211	(5.4)	.035	(23)
W4.0	.226	(5.7)	.040	(26)
W4.5	.239	(6.1)	.045	(29)
W5.0	.252	(6.4)	.050	(32)
W7	.299	(7.6)	.070	(45)
W9	.338	(8.6)	.090	(58)
W9.5	.348	(8.8)	.095	(61)
W12	.391	(9.9)	.120	(77)
W14	.422	(10.7)	.140	(90)
W18	.479	(12.2)	.180	(116)
W20	.505	(12.8)	.200	(129)

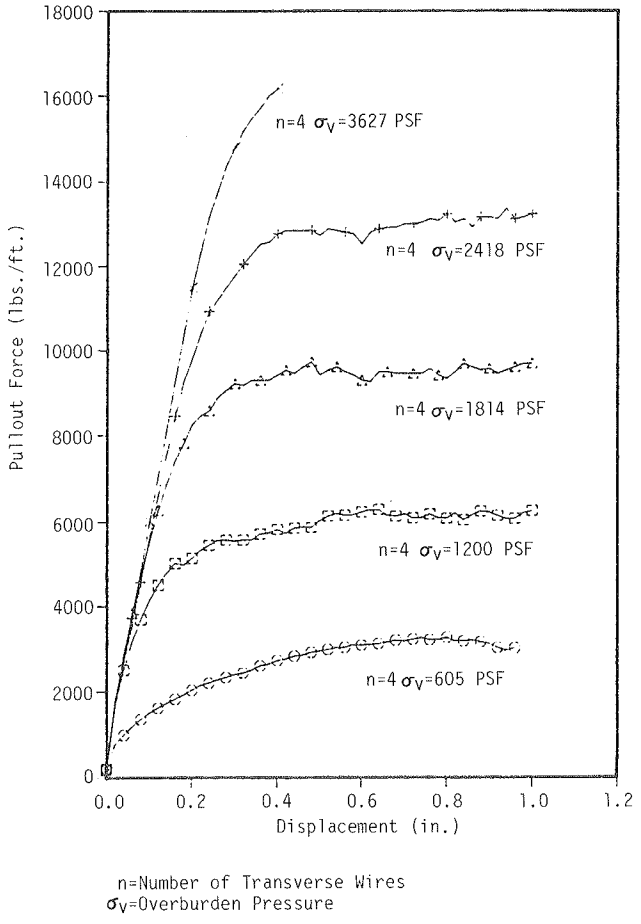

Figure B-8. Wire mesh pullout load-displacement curves for washed sand, ⅜-in. wires. [Nielsen, 1983]

creasing confining stress, i.e., depth, because less dilation occurs under high confining stresses.

Use of values calculated theoretically will thus be conservative for dense granular soils under low confining stress.

3.3 Passive Resistance

3.3.1 Experimental Basis

The tests by Bishop [1979], Peterson [1980], and Nielsen [1983] were performed with three soil types, a silty sand, a clean sand, and a pea gravel. Wire sizes used in these tests were W1.7 (9 gauge), W2.5 (7 gauge), W3.4 (5 gauge), W5 (¼ in.), and W12 (⅜ in.). Nominal dimensions of standard wire sizes are given in Table B-1. Various mesh spacings were used, along with variations in overburden pressure.

A group of typical load-displacement curves is shown in Figure B-8. From these curves, it can be seen that there is a yield point at a displacement of about 0.2 to 0.3 in.

The data from pullout tests, such as those shown in Figure B-8, were reduced as follows. In accordance with FHWA criteria [FHWA, 1983], pullout resistance for a given mesh was read at 0.75-in. displacement. It was assumed that each longitudinal wire within the mesh contributed the same force to total mesh pullout resistance, as was developed by a single longitudinal wire tested under identical conditions. The contribution of the transverse wires to total pullout resistance, P_f, was then computed by subtracting the contribution of the longitudinal wires (which was calculated by Eq. B-1) from the total pullout resistance. The obtained passive resistance force, P_p, was then expressed as a bearing stress by dividing by the total bearing area of the transverse wires, i.e., division by the number, length, and diameter of transverse wires ($n \times L \times d$). The passive resistance stress was then plotted as a function of overburden pressure as shown in Figure B-9.

It is believed that with small meshes the pullout resistance is not as great as would be developed by the sum of the resistances provided by the same number of transverse and longitudinal elements pulled separately. Specifically, passive and frictional resistances may interact in closely spaced grids. Bishop [1979], Peterson [1980], and Nielsen [1983] interpreted the results of pullout tests as indicating that an increase in the number of transverse wires or in the transverse wire diameter gave proportional increases in pullout resistance. This would imply that a direct increase in the bearing area of transverse, reinforcing elements provides a similar, linear increase in pullout resistance, and consequently that:

$$P_t = P_f + P_p \tag{B-3}$$

where P_t is the total resistance to pullout.

A mat having smaller grid openings (with transverse wires spaced less than 20 to 25 wire diameters) is more likely to have interaction of passive and frictional resistances. In this instance, soil may tend to become "locked" within the grid opening, with the consequence that the mat will fail in pullout as a fully rough mat with a surface area the same as total overall area of the wire mat.

Welded Wire Walls and RSE walls generally use mats having mesh sizes with transverse wire spacings ranging from 30 to 43 wire diameters, for the currently used 6-in. by 9-in. mesh. Mesh

sizes used in pullout tests to develop pullout resistance criteria included transverse wire spacings ranged from 24 to 72 wire diameters. The smallest mesh sizes used in the tests may have been within the range where rough mat behavior begins, which could explain some of the data scatter (Fig. B-9). The total mat pullout resistance is given in Section 3.3.3 as the sum of the transverse bearing resistance and the longitudinal frictional resistance, and is considered to be appropriate for the range of mesh sizes used in practice.

3.3.2 Theoretical Considerations

The mechanism of passive resistance development, proposed by Peterson [1980], is that of a bearing capacity failure for a strip footing. Accordingly, the Terzaghi-Buisman bearing capacity equation [Dunn, Anderson and Keifer, 1980] was modified, and correlations with the experimentally derived data were attempted. The Terzaghi-Buisman equation for ultimate bearing capacity of a strip footing per unit length, Q_{ult}, is:

$$Q_{ult} = B\,c\,N_c + \tfrac{1}{2}\gamma\,D_f B^2 N\gamma + D_f N_q B\gamma \qquad \text{(B-4)}$$

where B = footing width (wire diameter, d, for wire wall); c = cohesion; γ = effective unit weight of soil; D_f = overburden height (depth, Z, for wire wall); N_c = cohesion factor; N_q = surcharge factor; and $N\gamma$ = friction factor.

The unit bearing capacity, Q_{ult}, is set equal to the unit pullout force P_p/NW. The footing width, B, is the wire diameter, d, for this instance. Since c is usually very small for soils used as fill, for the range of small wire diameters, d, the first term involving N_c is insignificant, and is dropped. Because the diameter of the wire is so small and is squared in the $N\gamma$ term of Eq. B-4, it may also be ignored. Dividing by d, Eq. B-4 can then be rewritten as:

$$\frac{P_p}{N\,d\,W} = S_v\gamma\,N_q \qquad \text{(B-5)}$$

where N = number of transverse wires; W = width of the mat; d = wire diameter; and S_v = vertical soil depth to mat.

Predictions using this equation were compared with experimental data obtained [Peterson, 1980]. Backfiguring, using Eq. B-4 with known pullout data for one soil type, produced an N_q value of 15.7. Direct shear tests for this soil indicated a soil friction angle of 27 to 30 deg with a resulting N_q factor [Dunn et al., 1980] ranging from 13.2 to 18.4. The average of these two values is 15.8, which provides favorable correlations. Tests in another soil type backfigured to give an N_q of 27.7, which was compared with an N_q of 30.2, derived from soil test data. Several more soil types still need to be tested to verify the general applicability of the bearing capacity equation.

One brief, qualitative study, which was performed in addition to the pullout tests adds some weight to the hypothesis that the bearing capacity mechanism describes the pullout resistance for the larger meshes used in wall construction. This study was a photoelastic stress analysis that was performed to view stress patterns created by the transverse wires [Peterson, 1980]. Patterns viewed were of the same general shape as those predicted (i.e., pressure bulbs) under a strip footing by Westergaard and Boussinesq [Dunn et al., 1980].

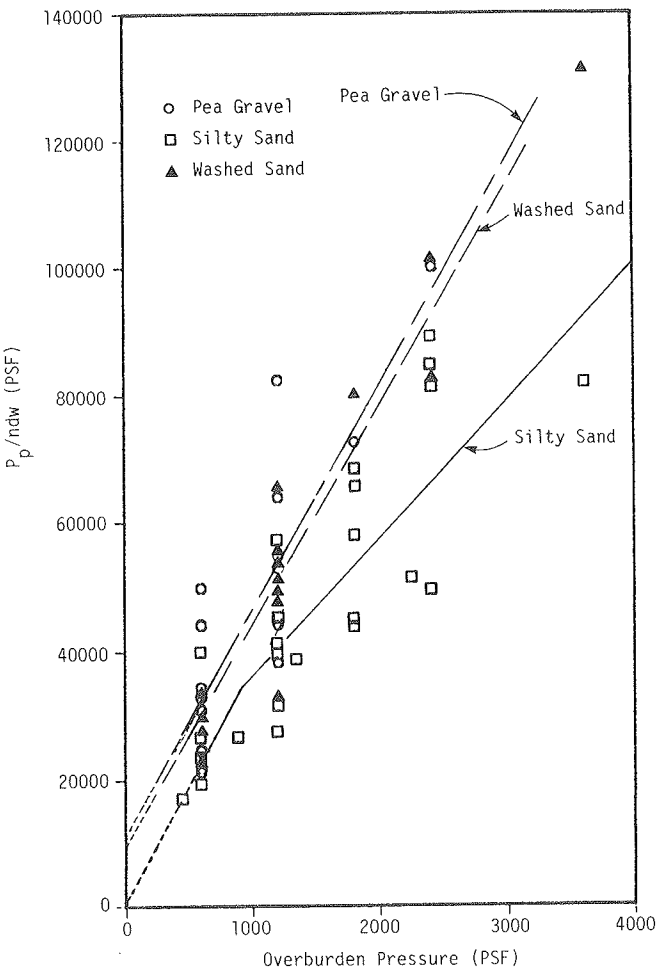

Figure B-9. Pullout test results. [Nielsen, 1983]

3.3.3 Empirical Correlations

To establish correlations among passive resistance and overburden stress, straight lines were fitted to the data for each of the tested soil types [Nielsen, 1983], as shown in Figure B-9. These equations are:

Silty Sand

$$P_t = 2{,}143 \text{ lb/ft} + \sigma_v d[(0.75)\,\pi L_e M \tan\delta + 17.61\,N]\; N\sigma_v d > 113.6 \text{ lb/ft} \qquad \text{(B-6)}$$

$$P_t = \sigma_v d[(0.75)\,\pi L_e M \tan\delta + 36.47\,N] \quad N\sigma_v d \leq 113.6 \text{ lb/ft} \qquad \text{(B-7)}$$

Washed Sand

$$P_t = 633 \text{ lb/ft} + \sigma_v d[(0.75)\,\pi L_e M \tan\delta + 36.8\,N] \qquad \text{(B-8)}$$

Pea Gravel

$$P_t = 712 \text{ lb/ft} + \sigma_v d[(0.75)\,\pi L_e M \tan\delta + 38.1\,N] \quad \text{(B-9)}$$

where P_t = total pullout resistance in pounds per linear foot of mat width; d = wire diameter, ft; L_e = length of mat behind Rankine failure plane, ft; M = number of longitudinal wires per foot of mat width; and N = number of transverse wires behind active zone (on L_e).

Some limitations are readily apparent as reflected by the scatter and the "cohesion intercept" of the two soils which should not have inherent cohesion. Because of the uncertainties inherent to these correlations more conservative relationships are used for design as shown in Section 7.7.

3.4 Behavior and Failure Modes of the Reinforced Soil Mass

In order for the reinforced soil mass to act as a coherent unit, there must be an interaction between the reinforcement and the soil. Part of the overall interaction is derived from shear stress transfer from one reinforcing layer to the next through the contained soil. The vertical spacing of the reinforcement, S_v, must, therefore, be sufficiently small to assure interaction between successive layers of reinforcement.

In addition to the stress transfer between layers of reinforcement, there must be sufficient soil resistance on each reinforcement layer to prevent pullout. The longitudinal wires in the reinforcement must be of sufficient strength to withstand the resistance to pullout developed by the transverse wires.

3.5 Behavior of the Reinforced Soil Structure

The principle of a vertical reinforced soil structure is schematically shown in Figure B-10. Without the reinforcement, the failing wedge would fail away from the resisting zone. The reinforcements transfer the tensile stresses created by the failing zone to the resisting zone, as described in Chapter Four of the main report.

With all other soil reinforcement methods described in this report, the magnitude of the required tensile resistance of the reinforcing members is based on assumptions for lateral earth pressures that range between at-rest or active values, i.e., K_o and K_a conditions, respectively. However, based on tests performed on Welded Wire Wall segments constructed in an earth-pressure cell at Utah State University, and measurements of tensile forces developed in longitudinal wires in full-scale structures [Bishop, 1979], a coefficient of lateral earth pressure of 0.65 has been selected for design of welded wire walls. This design coefficient, hereafter referred to as K_D, corresponds to the coefficient of earth pressure at-rest for a soil with a friction angle of 20 deg, and is about 1.5 times the coefficient of earth pressure at-rest for a soil with a friction angle of 35 deg.

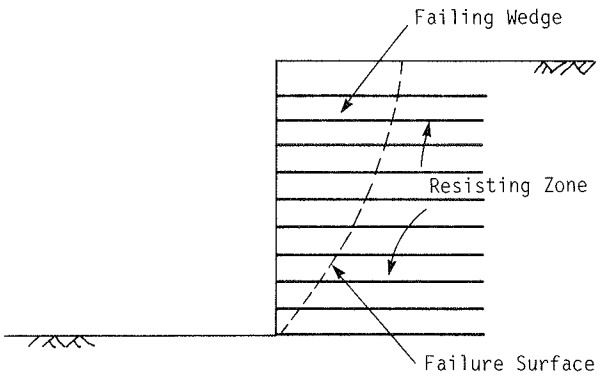

Figure B-10. Schematic illustration of reinforced soil.

This high K_D value possibly results from the continuous nature of the welded wire reinforcement, which would restrict lateral deformation more than the reinforcements of other systems. Backfill compaction may also produce high K values at shallow depths. Data from other soil reinforcement systems may not be directly comparable because the other continuous reinforcements, i.e., geotextiles and Geogrid (Appendix A and Chapter Three of this appendix), are more extensible and would not limit lateral soil strain (which results in horizontal stress relaxation) to the same degree. Bar mats, which in other aspects are similar to wire mesh, are not continuous and would thus probably not limit horizontal stress relaxation to the same degree as the continuous welded wire.

There are some data, especially on walls less than 25 ft high, which have been interpreted as supporting the high design value for lateral earth pressure. Field measurements have been obtained, for example, in a 22.5-ft-high Welded Wire Wall. Locations of strain gauges on a mesh near the bottom of the wall are shown in Figure B-11. Forces measured with each of the strain gauges are plotted as a function of height of fill above the strain gauges in Figure B-12.

The data obtained are also plotted in Figure B-13 in the form of the distribution of tensile forces in the longitudinal wires for five fill heights.

The results in Figures B-12 and B-13 indicate that initially, as fill height increases to a maximum of about 8 ft above the mat, the forces in the wires are indicative of horizontal earth pressure coefficients exceeding 0.7. This is not an unusually high value when compaction-induced lateral earth stresses, combined with the relatively low overburden, are taken into account.

When fill height reached about 9 ft above the mesh, the longitudinal force at a number of the strain gauges decreased significantly, probably because of outward deflection of the wall and a concomitant decrease in lateral earth pressures.

As shown by the data on Figure B-12, strain gauge S12, which was near the rear end of the mesh, did not show the sudden decrease. The Figure B-12 data have been replotted in Figure B-13; as shown on this figure the fact that S12 did not yield implies a significant tensile force near the end of the mat, which is not consistent with expected distributions of tensile force along reinforcements in other systems. Furthermore, the results of laboratory-controlled model tests on Welded Wire, for example, the data in Figure B-14, show tensile force distributions more typical of those measured in other soil reinforcement systems. In this figure, which shows laboratory measurements, the tensile force distribution in a single mat is plotted as a function of increasing simulated overburden height. Because the latter data show good agreement with the tensile force distributions that have been measured in other soil reinforcing systems, it is not certain that the strain gauge S12 data in Figures B-12 and B-13 are reliable, or possibly there was a local stress concentration.

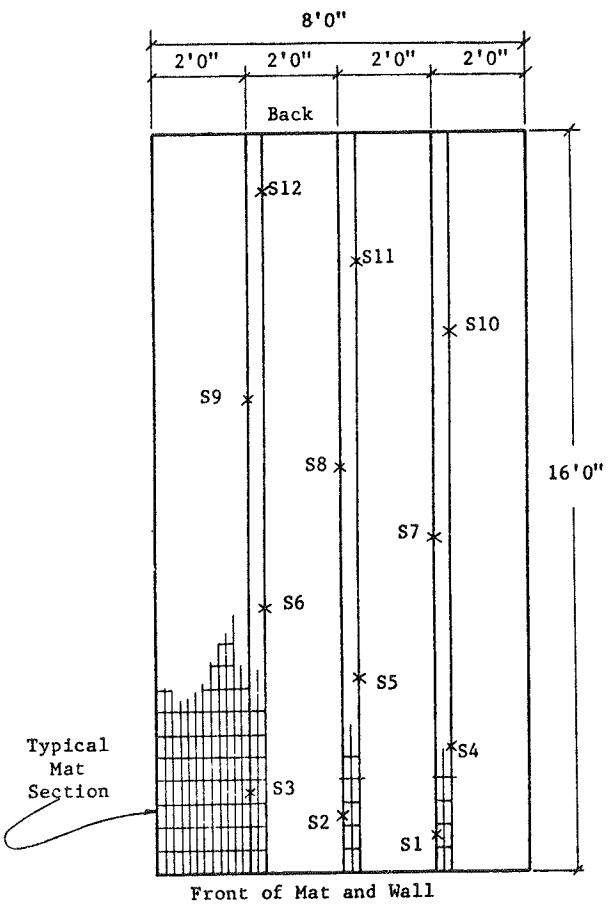

Note: S7 refers to strain gauge number 7.

Figure B-11. Strain gauge distribution for 22.5-ft high wall. [Bishop, 1979]

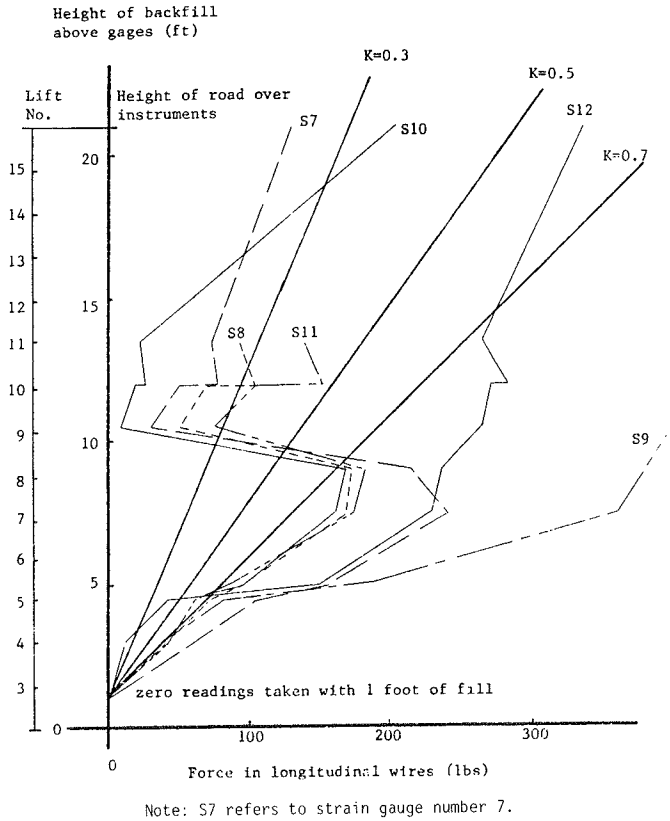

Note: S7 refers to strain gauge number 7.

Figure B-12. Height of fill vs. force in longitudinal wires for a 22.5-ft high wall. [Bishop, 1979]

Because of these uncertainties, further tests on full-scale walls, especially if such tests give results with less data scatter, would be very useful in confirming the high apparent horizontal earth pressure coefficient currently used for design. One such test has already been performed, as described in Section 3.6; it is expected that the results of this test will have a significant influence on the design approach used for Welded Wire structures.

Additional tests on Welded Wire Wall have demonstrated that very low tensile forces exist in the longitudinal wires near the facing. A 4-ft high wire wall segment was constructed in a pressure cell and loaded to approximately 100 ft of simulated soil overburden. The wires at the face of the wall were gradually cut away to verify very low tensile forces near the facing [Bishop, 1979]. During the cutting of the wires, no sudden releases of stress were noted, and the soil between the reinforcements did not cave or ravel outwards, even when the entire face was exposed.

3.6 Most Recent Test Data

In 1985, Utah State University completed a test program on

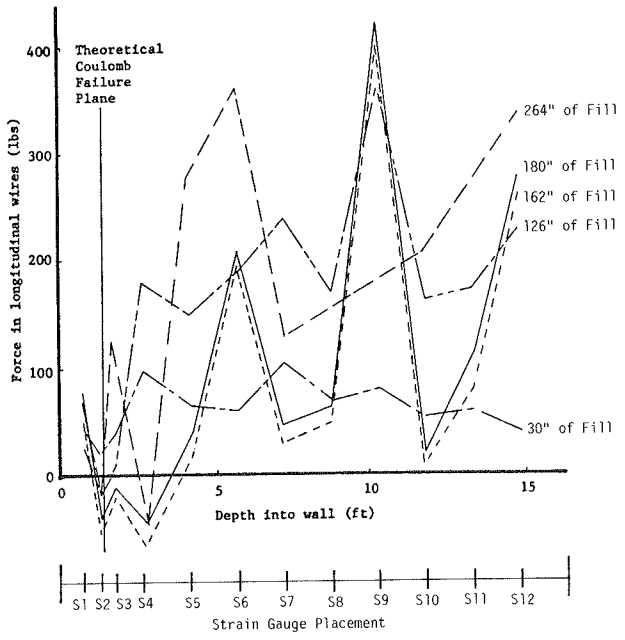

Note: S7 refers to strain gauge number 7.

Figure B-13. Reinforcement stresses for a 22.5-ft high wall. [Bishop, 1979]

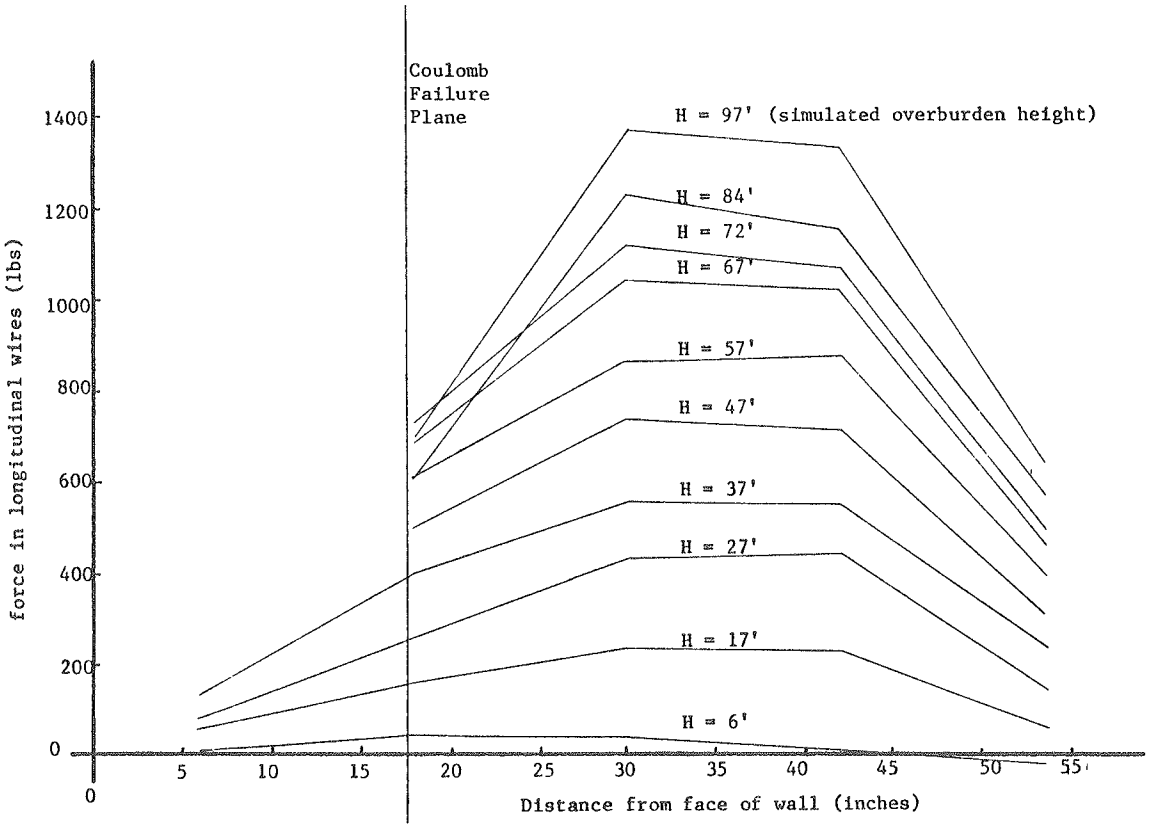

Figure B-14. Reinforcement stresses for a model Welded Wire Wall segment. [Bishop, 1979]

a 55-ft-high wall. The results of this study are briefly described because they may significantly influence future design methodology.

In general, the project involved instrumentation and observation of one of a series of Welded Wire Walls constructed as part of the expansion of Interstate 90 in Seattle, Washington. The instrumented section of Welded Wire Wall was a 55-ft-high wall, having 5 ft of embedment below grade. It was constructed using 44-ft-long mats having a vertical spacing of 18 in., and a standard grid size of 6 in. by 9 in. Size of the longitudinal wires varied from W4.5 to W12.

The purpose of the instrumentation program was to study the relationship between the tension in the longitudinal wires and the height of the wall. The instrumentation program involved measuring the tension in the longitudinal wires (using specially mounted strain gauges) at 15 locations on each of 7 different wires mats, which were spaced throughout the full height of the wall. The wall was completed in July of 1985; monitoring was accomplished during construction and will continue for approximately one year. To facilitate the analyses of results as well as confirm design parameters, pullout tests were performed with facilities at Utah State University, using backfill material from the same source as that used for construction of the wall itself.

The results of this program are especially significant in that the highest wall which had previously been instrumented was 25 ft high. The measurements on this comparatively low structure served as the basis for establishing 0.65 as the coefficient of lateral pressure, *K,* for routine design.

Figure B-15, excerpted from the draft report prepared by Utah State University [Anderson et al., 1985] for the Hilfiker Retaining Wall Company, presents the envelope of K values interpreted for the 55-ft-high wall as well as the resulting recommended K values for use in future design. As can be seen, for wall heights up to about 10 ft, the value of K varies between about 0.6 and 0.8. However, the K value decreases with height, and for wall heights greater than 20 ft, a maximum value of K on the order of about 0.45 was measured. The very high K values measured while the wall was lower were most likely caused by the long mats used in the wall.

As the result of this study, the following design values were recommended by Anderson et al. [1985] for general use in Welded Wire design:

Wall Sections	Coefficient of Lateral Earth Pressure, K
0. to 15 ft high	0.65
More than 20 ft below the top of the wall	0.45
Between 15 and 20 ft from the top of the wall	Straight line interpolation between 0.65 and 0.45

The other result of the study which should influence future design practice relates to the location of the failure plane. Previously a Coulomb failure plane has been assumed. However, from the data measured on this high test section, the location shown in Figure B-16 may be inferred. This location is in general

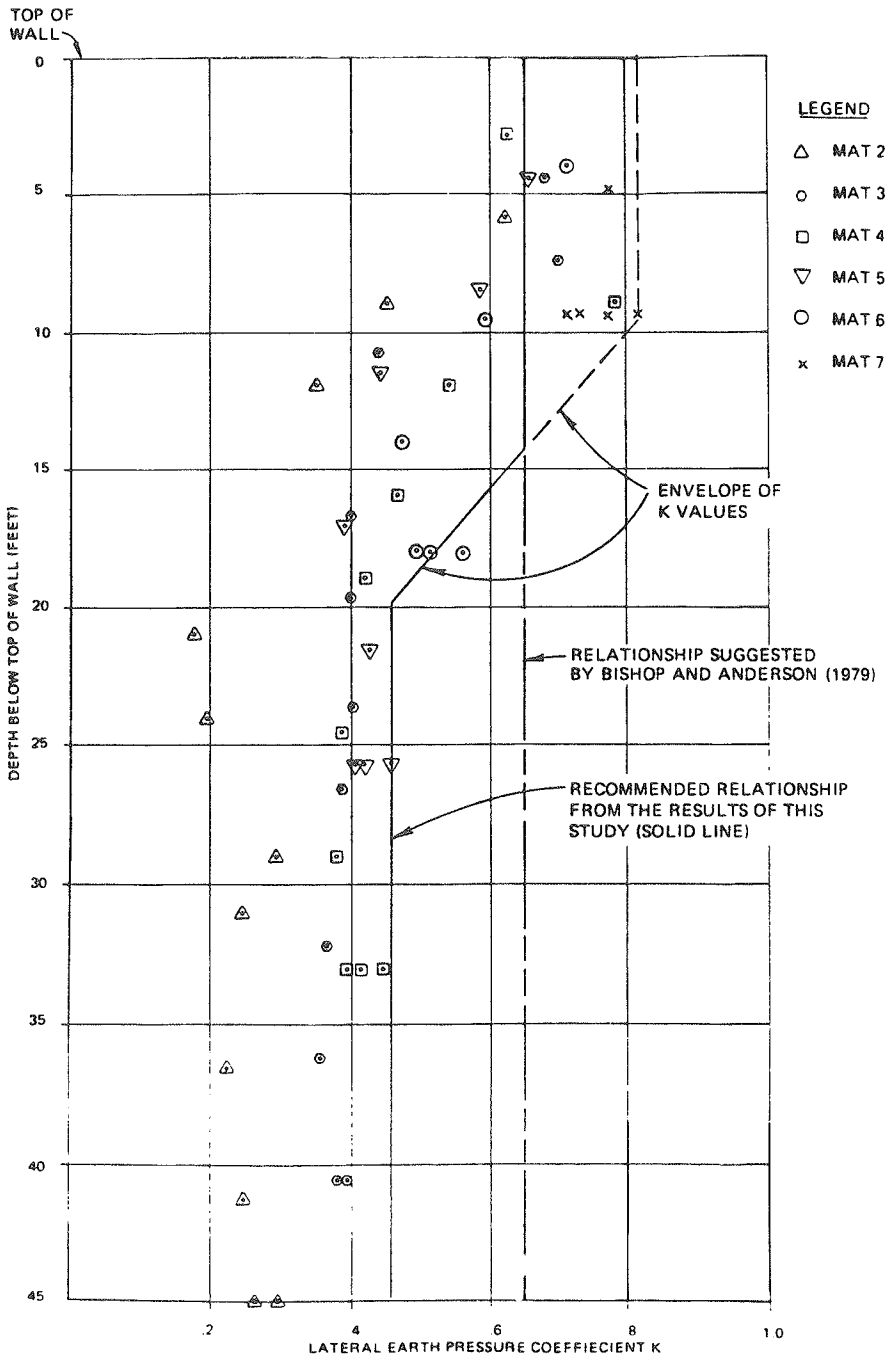

Figure B-15. Relationship between the lateral earth pressure coefficient, K, *and wall height.* [Anderson et al., 1985]

agreement with the failure plane commonly assumed for Reinforced Earth.

4. TECHNOLOGY

4.1 Description of Fabricated Components

The Welded Wire Wall is constructed using standard welded-wire mats, which are 8 ft wide and cut to the needed length. The wires are in a 6-in. by 9-in. mesh; wire sizes presently in use vary, and are discussed in Section 7.5 of this chapter. The backing mat, immediately behind the bent-up face of the wire mat, is cut from 9-gauge, 2-in. by 6-in. welded wire mesh. Behind the backing mat is a quarter-inch galvanized wire screen. The only additional components are rings that clip the mats together, for convenience during construction.

The Reinforced Soil Embankment is also constructed with a wire mat. At the front of each mat is a flat plate to which are

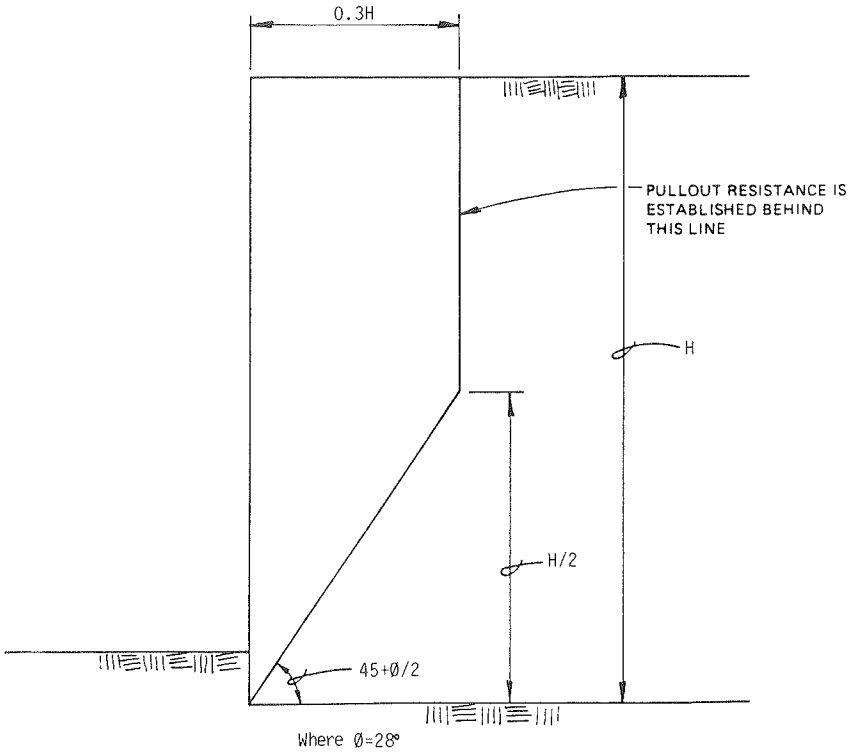

Figure B-16. Location of maximum tensile forces in reinforcements. [Anderson et al., 1985]

fixed connecting pins that fit into the facing panels (Fig. B-3). The facings are precast concrete panels to which the mats are pinned through holes in the top and bottom. A neoprene and a styrofoam pad are used to separate the panels as they are installed; these two pads are placed at the thickened portions (referred to as columns) of the wall panels as shown on Figure B-3. This provides a slight clearance between the panels to allow for dirt and small gravel on the top of the panel, as well as a quick and efficient means to level the panels during construction.

4.2 Fabrication of Components

The welded-wire mats are manufactured at steel wire mills. The mats used are made of cold-drawn steel wire, with a yield strength of 65,000 lb per sq in. Rolls of wire mesh are purchased in bulk and transported to the Hilfiker Retaining Wall Company for fabrication into the Welded Wire Wall mats. This fabrication includes cutting of the mesh to desired lengths, bending the mesh to form the facing, and bending the end wires of the facing to a "preformed tie" for rapid attachment to the next higher mat in the wall. Backing mats of 18-in. width are also cut from standard wire mesh rolls.

Mats for RSE are generally special ordered (because of the larger wire diameters used) and transported to the Hilfiker plant for installation of the connecting bar for attachment to the facing panels. Generally, if a project is within a 300 to 400 mile radius of the plant, facing panels for RSE are precast at the plant and hauled to the project location. If not, a temporary casting yard is set up at a convenient location near the site, for panel manufacture.

Presently, specifications for concrete facing construction vary somewhat, with the specifications in use by the contracting agency most often being used for the facing panels. A 28-day strength at 4,000 psi is always required, with air-entraining additives used. Three cylinders per batch are taken with breakage results being averaged. Tolerances on panel construction are $\pm$ $1/16$ in.

4.3 Fabrication Quality Control

Two ASTM specifications provide the manufacturing standard for the wire mesh used in the Wire Wall and the RSE. ASTM A-82 pertains to the quality of the wire itself, as well as its fabrication into a mesh, and ASTM A-185 (incorporated into ASTM A-82) governs control for the welds connecting the wires. ACI standards for precast concrete are used for the design and casting of the RSE facing panels.

At present, a 0.4 oz per sq ft shop coating of zinc galvanizing is applied to the rolls of wire mesh intended for Welded Wire Walls. Previously, a second coating of zinc galvanizing was applied to the wire mesh to give a 2-oz coating for additional protection against corrosion during the service life. Quality control during this second coating process was questionable; subsequently, it was decided that it is more economical to employ additional steel as sacrificial metal rather than attempt to achieve a satisfactory 2-oz coating of galvanizing. Mats for RSE are not galvanized.

An epoxy-coated mesh, for use in highly corrosive environments, has been developed by the Gridcote Corp. Acceptable standards for the epoxy coating have not, as yet, been selected.

5. DURABILITY AND SELECTION OF BACKFILL

5.1 Members Susceptible to Degradation

The steel components of both Welded Wire Wall and RSE are subject to degradation by electrochemical corrosion as described in Chapter Six of the main report.

5.2 Methods to Predict Rate of Degradation

The method used to predict the degradation of reinforcing mats is to estimate loss of sacrificial steel by uniform wire loss. The corrosion rates used are as follows:

1. *Galvanized Wire Mesh Reinforcing*
   a. Nonsaturated backfill

      initial zinc loss—0.24 mil/yr for first 2 years
      secondary zinc loss—0.08 mil/yr until zinc is depleted
      sacrificial steel loss—0.36 mil/yr

   b. Saturated backfill

      initial zinc loss—0.40 mil/yr for first 3 years
      secondary zinc loss—0.08 mil/yr until zinc is depleted
      sacrificial steel loss—0.36 mil/yr

   c. Backfill subject to heavy deicing salts (applied only to reinforcing within the top 6 ft of the wall)

      initial zinc loss—0.68 mil/yr for first 3 years
      secondary zinc loss—0.08 mil/yr until zinc is depleted
      sacrificial steel loss—0.48 mil/yr

   d. If the resistivity of the backfill is greater than 10,000 ohm-cm for condition a or b, the sacrifical steel loss is reduced to 0.24 mil/yr.

2. *Bare Steel Wire Mesh Reinforcing*
   a. Nonsaturated backfill

      initial sacrificial steel loss—0.72 mil/yr for first 6 years
      secondary steel loss—0.36 mil/yr

   b. Saturated backfill

      initial sacrificial steel loss—0.94 mil/yr for first 6 years
      secondary steel loss—0.36 mil/yr

   c. Backfill subject to heavy deicing salts (applied only to reinforcing in top 6 ft of wall)

      initial sacrificial steel loss—1.6 mils/yr for first 6 years
      secondary steel loss—0.48 mil/yr

   d. If the resistivity of the backfill is greater than 10,000 ohm-cm for condition a or b, the initial sacrificial steel loss is reduced to 0.47 mil/yr and secondary steel loss is reduced to 0.24 mil/yr.

For these rates to be applicable, the backfill must meet these conditions:

pH range	4.5 to 9.5
Resistivity	$\geq$ 1,000 ohm-cm
Chlorides	< 200 ppm (except for when dealing with deicing salts)
Sulfates	< 1,000 ppm

These rates for the uniform reduction in wire diameter can be used in a simple equation to estimate the final diameter of the wire at the end of the desired design life of the proposed structure:

$$\sum_{i=0}^{N_y} (d_i - C_R) = d_f \qquad \text{(B-10)}$$

where N_y = design life in years; d_i = initial wire diameter for each succeeding year, in.; d_f = final wire diameter, in.; and C_R = corrosion rate, in./yr; 1,000 mils equals 1 in..

It should be remembered that reinforcing for the Welded Wire Wall comes with a 0.4 oz per sq ft shop coating of zinc galvanizing, while mats for the RSE have no zinc coating.

It is important that the soil pH and resistivity be determined accurately. Tests should be run on backfill materials in the form that they will be placed, i.e., at the specified water content and degree of compaction. The potential long-term changes in pH and resistivity, for example, caused by seepage or other environmental factors must also be considered.

As noted in Section 4.3, an epoxy-coated mesh for use in severely corrosive soils is under study. This involves application of a heavy (5 to 10 mil) epoxy coating to mats after they are otherwise prepared. Because of the difficulties in applying this to the smaller wires involved in the Welded Wire Wall mats, and because it is felt that this type of protection will be required with a concrete face, it is anticipated that only RSE construction will involve epoxy-coated mats. Epoxy coating can now be provided on an "as-required" basis.

5.3 Selection of Backfill—Geotechnical Criteria

A large variety of backfill materials may be used for construction of the Welded Wire Wall or RSE. Low-quality backfill materials (fine-grained silt and clay soils) have not been extensively used. Wire walls with up to 30 to 40 percent fines (soil particles, by weight, passing the No. 200 sieve) have, however, been designed and constructed.

The Federal Highway Administration, in providing guidelines for Welded Wire Walls, issued a bulletin [FHWA, 1983] with backfill specification which reads in part:

> *Application*—The select backfill specifications for all internally reinforced soil systems such as, Reinforced Earth, Retained Earth, fabric walls, Hilfiker Welded Wire Walls, etc., should be prepared based on the following:
>
> Gradation and Plasticity

Sieve Size	Percent Passing
6-inch	100
3-inch	100–75
No. 200	15*–0

Plasticity Index (P.I.) shall not exceed 6

* Results of laboratory and field pullout tests have indicated that all materials having up to 25 percent passing the No. 200 sieve will provide adequate pullout and frictional resistance. However, some materials having 15 to 25 percent passing the No. 200 sieve may produce problems related to frost susceptibility, compaction and drainage. Backfill requirements therefore, should be determined on an individual project basis by taking into consideration the specific backfill characteristics of the anticipated borrow source. The maximum percent passing the No. 200 sieve may be increased to 25 only when all backfill criteria are satisfied.

The intent of this FHWA guideline is to preclude the use of "low quality" backfills until a sufficient amount of testing and evaluation can be done to allow their use on a standard basis for federal projects. For general use, the Hilfiker Retaining Wall Company recommends a 6-in. maximum size, nonsaturated, durable granular soil with a PI less than 10. When considering the possible use of backfill not satisfying these criteria, potential problems such as lower strength and increased creep potential must be recognized, evaluated, and allowed for in design.

6. CONSTRUCTION

6.1 General

Both Welded Wire Wall and RSE are simple to construct. Five to eight workers are usually adequate. The placement and compaction of backfill, rather than placement of the reinforcement elements, are usually the limiting factors in construction. Production rates are usually on the order of 400 to 700 sq ft of wall face per working day, with the highest reported production rate being about 1,100 sq ft per day. These rates are dependent on many factors, such as site access, weather, availability of backfill, availability of adequate equipment, and competent workers.

6.2 Phases of Construction

Typical construction of a Welded Wire Wall or RSE can be divided into three phases: site preparation, wall construction, and capping of the wall at project completion. Site preparation includes clearing of the site, excavation as required, and preparation of the work and storage areas. Wall construction begins when the wire mats (or in the case of the RSE, the initial leveling course of precast facing elements) are first placed and backfill placement begins. Capping is required to complete the top lift and finish the structure.

Following wall completion, some wire walls have been seeded at the face to promote growth and thereby obscure the wire facing. A gunite, molded or formed concrete facing can also be incorporated into the wire wall face.

6.3 Site Preparation

Preparation of the construction area begins by clearing vegetation, debris, and other deleterious materials from the site. Excavation of loose soil and rock should be conducted so that the wall is founded on competent, undisturbed natural soil, or on compacted structural fill. In performing the excavation, line and grade for the wall alignment should be established. The excavation should be cleaned to natural soil to allow for benching of the wall into competent material. If necessary, portions of the wall may be founded on replacement structural fill; fill should be granular material and compacted to 95 percent of standard Procter (ASTM D-698). The face of the wall should be stepped back from the face of the excavation or fill; this embedment, usually on the order of 1 to 3 ft, enhances bearing capacity, reduces settlement, and protects the wall against, for example, erosion from surface runoff. Temporary drainage for the construction period must be established and is especially important when poorer quality backfills are used.

6.4 Placement of Different Components

6.4.1 Welded Wire Wall

The general construction sequence for Welded Wire Walls is shown in Figure B-17, and Figure B-18 shows photographs of a wall under construction. The construction is initiated by placing the first level of mats directly on the prepared foundation. Mats at each end of the excavation may be trimmed (lengthwise) to fit the excavation as needed. Only transverse wires should be cut. The wall face may be curved as required to conform to a specified alignment. Convex curves may be formed by overlapping the back of the mats, while concave curves are formed by leaving a space between the back of the mats with the face of the mats still touching. Embedment depths should be predetermined to ensure that the necessary resistance to pullout is still achieved on a concave curved wall which has spaces between the backs of the mats.

Following the layout of the reinforcement mats, backing mats and the quarter-inch screen are placed against the back portion of the face of the wall. The backing mats are cut to the same length and width as the reinforcement mats, 8 ft, and are placed to span from center-to-center of the reinforcement mats, thus achieving a better continuity between the reinforcement mats at the face.

Subsequent to placement of the backing mats and wire screen, backfill operations can begin. Soil is placed over the mats up to and against the wall face and compacted to 95 percent of the maximum dry density as determined by ASTM D-698. Care should be taken to prevent heavy construction equipment from coming into direct contact with the reinforcing mats to avoid local damage. A total fill thickness of 18 to 20 in. should be placed on the reinforcing mat before the next layer of reinforcing can be placed.

Compaction at the face of the wall is critical, both because it must be done carefully to avoid damaging the wire facing and to preclude compression at the completed face. Prior to initiating the use of the heavier gauge wire mesh now in service, it was standard procedure to place gravel immediately behind the wall face, for a depth of about 6 to 12 in. This could easily be compacted by rodding and minimized compression of the 9-gauge wire mesh forming the face. With the heavier wire mesh this procedure has been eliminated and backfill is placed directly against the face.

Compaction of the backfill can be accomplished using standard construction and hauling equipment routed continuously over the fill surface. At the outside edge of the fill it is generally helpful to run a hand-compaction unit, such as a wacker or

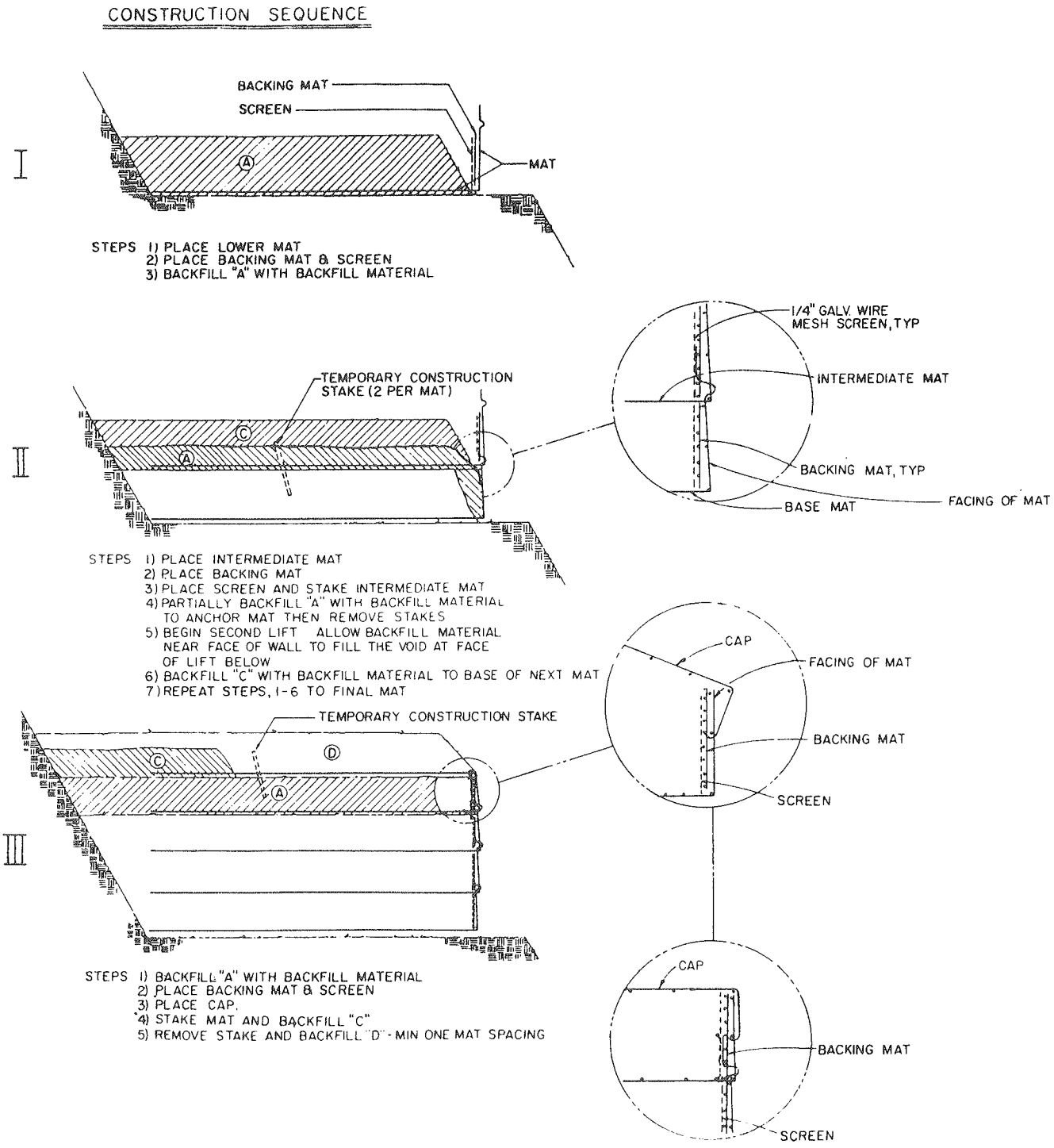

Figure B-17. General construction sequence for Welded Wire Wall.

vibratory drum roller, to achieve the needed density. Typically, the face of the wall is battered at a ratio of 1 in 12, with flatter face slopes possible, as desired.

Capping of the wall is accomplished by using prongless reinforcing mats for the second to last layer of reinforcement. The last layer of reinforcement is a series of mats with hooks on the face which are inverted and attached to the prongless mats. A minimum of 18 in. of fill is then placed on this top mat to complete the wall.

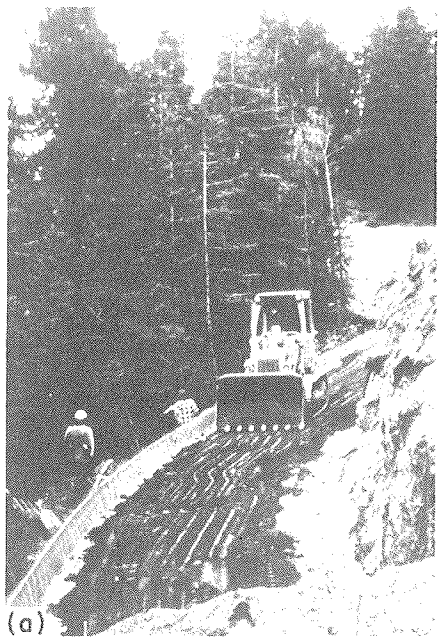

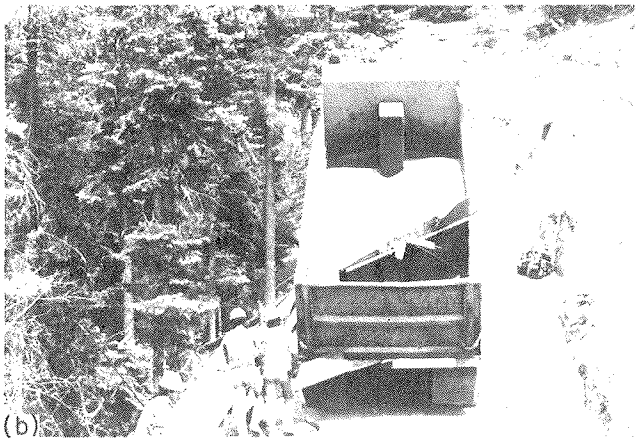

Figure B-18. Photograph of Welded Wire Wall construction: (a) initial backfill placement on wire mats, (b) placement of gravel fill at the face of a Wire Wall constructed with the 9 gauge, 2 in. by 6 in. mesh.

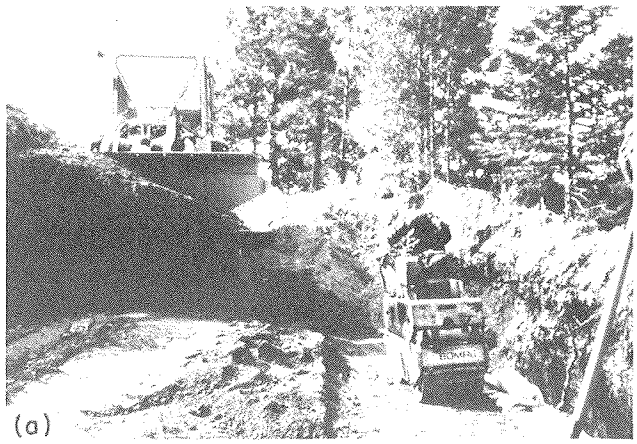

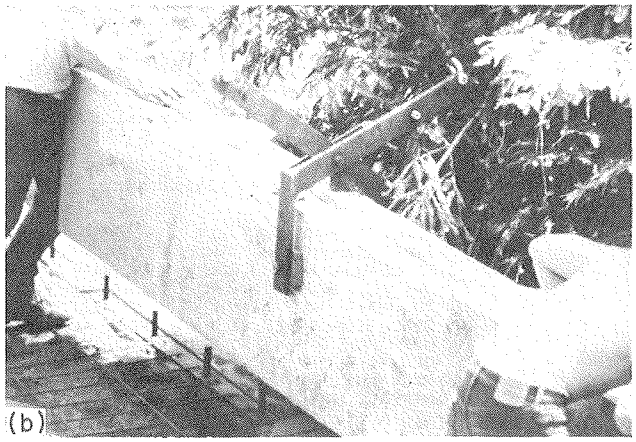

Figure B-19. Photograph of an RSE wall under construction: (a) compaction behind the RSE facing panels, (b) installation of RSE facing panel.

6.4.2 Reinforced Soil Embankment

Construction of the RSE is begun on the prepared foundation by placing base sections for the wall panels along the wall face alignment (Fig. B-3). Overexcavation to form a slot for this base course or placement of 6 in. of fill behind the base sections is needed to provide a level surface for the mat layer which is attached to the top of the base sections. The first layer of reinforcing mats is then laid down with the pins at the front of the mats inserted in the holes of the base sections.

The first lift of full-sized facing panels can be installed when the top of the base section has been cleaned off, and the neoprene and styrofoam pads have been placed at the thickened (or column) sections of the facing panels. These pads preclude any point bearing from small particles left on top of each facing panel as the next one is placed above it. The styrofoam pad (Fig. B-3) is slightly thicker than the neoprene pad and consequently tilts the facing panel slightly inward. Backfill operations are begun, and a 2-ft thickness of soil is placed behind and up to the facing panel. As the backfill is compacted into place, the styrofoam pad under the front of the column of the facing panel is gradually compressed and the facing panel tilts forward slightly to a nearly vertical position (typically, the wall face is battered at 1 to 48, to avoid the "falling over" look of a vertical face).

The next layer of reinforcing mats is installed along with the next course of facing panels, using the same procedures. This procedure continues until the top of the wall is reached, when a course of precast caps is laid on top of the last course of full-sized facing panels. Eighteen inches of fill is then placed on the top layer of mats, and the wall is completed. An RSE under construction is shown in Figure B-19.

6.5 Construction Equipment

Standard equipment for placement and compaction of backfill, as for any earthwork project, is required for construction of Welded Wire Wall and RSE walls. This equipment (e.g., front end loaders) may also be used for handling the reinforcing mats.

For RSE construction, a small crane with a telescoping boom is generally effective for handling the concrete facing panels; front loaders and backhoes are frequently used. The Hilfker Retaining Wall Company provides a special clamp for gripping and handling RSE panels at their single balance point. As with all of the reinforcing systems which can be used in embankment construction, Welded Wire Wall and RSE construction can be performed on a large scale, with a full spread of earth moving equipment.

6.6 Work Organization

Crews can be broken into two groups for the wall construction, with one responsible for mass backfill placement and compaction, including the pouring of the gravel against the Wire Wall face, and the second responsible for layout of the wire mats in the construction area and compaction of the soil near the wall face. Two to four individuals are needed for placement of the mats and compaction of the soils near the face, while two or three workers are needed for placement of the mass backfill.

6.7 Quality Control

It is important that the reinforcing mats not be damanged, and in particular that the longitudinal wires not be cut or welds broken during construction operations. Damaged mats should be replaced.

Facing panels for the RSE must be handled and placed with the care standard to the placement of any precast element. They are designed and balanced to be handled from one point at the center of the panel and are comparatively easy to pick up, move into place, and align.

Backfill should be checked on a regular basis at random locations for proper compaction. It is important that proper compaction be done near the wall face to minimize any bulging of the wire face, due to later compression of the soil.

6.8 Construction Specifications

At the present time, there are no standard specifications for wall construction. The Hilfiker Retaining Wall Company does provide a construction booklet and on-site technical assistance.

7. DESIGN

7.1 Internal Versus External Stability

The design of Welded Wire Walls and RSE walls, like that of any other type of reinforced soil system, must take both internal and external stability into account. The internal stability of the wall deals with the ability of the reinforced soil mass to act as a coherent unit. This is accomplished through a transfer of stress from the soil to the reinforcement. Two criteria are analyzed: the tension in the reinforcement, and the resistance of the reinforcing elements to pullout.

The external stability refers to stability failures outside the reinforced zone: bearing capacity at the toe of the wall, sliding of the reinforced soil mass as a unit, and overturning about its base. Classical soil mechanics analyses may be used for the analysis of these potential failure modes.

7.2 Site Conditions

7.2.1 Soil Parameters

The natural soils at the site should be studied to determine the adequacy of on-site material as backfill and the competency of the proposed foundation. The foundation soils should be thoroughly evaluated for analysis of external stability and to determine beforehand what, if any, potential for settlement exists. Potential differential settlements should be estimated; this includes consideration of the settlement potential at the toe of the proposed wall to evaluate what allowance should be made in the slope of the wall face to allow for tilting. Abrupt changes in foundation soils, such as stiff or dense soil (or rock) adjacent to soft ground, where both would serve as part of the wall foundation, should be carefully evaluated, as discontinuities could cause high, detrimental stresses within the wall.

7.2.2 Water

A primary consideration in construction and long-term performance is control of surface and groundwater. Surface drainage should be established toprevent seepage into and saturation of the soil backfill. Likewise, internal drainage should be installed, if necessary, to control groundwater and preclude backfill saturation. The only alternative is to design for the saturated case.

7.2.3 Topography

Occasionally, in steep rocky terrain, a portion of the wall base may have to be constructed against a rock outcrop. Situations are possible in which either the base width of the wall will be narrower than desired, or excavation of rock will be required. The latter alternative is expensive and seems somewhat illogical in that very competent material has to be removed. A system has been designed by which rock bolts can be used to support the lower portions of the wall until the wall has reached a sufficient height that the design reinforcement lengths can be used. To support the wall between rock bolts, tubular steel sections are installed. The wall is restrained by these "beams" which transfer the load to the anchors installed in the rock. Essentially this means a tied-back "foundation wall" would be constructed first, with a reinforced soil wall (either Welded Wire or RSE) built on top. While this system presents some promise for very limited access situations, it has yet to be installed and tested. A conceptual sketch is shown on Figure B-20. Further analysis and evaluation of this combination system would appear advisable.

7.3 Loading and Boundary Conditions

Externally, Welded Wire Wall and RSE are designed as gravity retaining walls, with a base width equal to the length of the

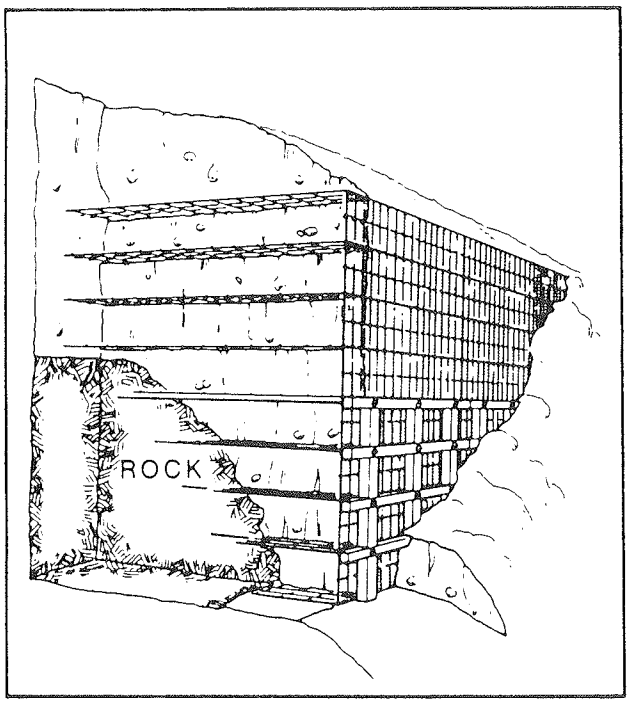

Figure B-20. Schematic of Welded Wire Wall with rock anchors.

mats. Design forces against the back and top of the wall are evaluated, and it must be verified that the base width is sufficient to provide adequate resistance against sliding and a sufficient bearing capacity.

For internal analyses, horizontal shear forces (from such sources as sloping backfill above the wall or bridge decks founded on the wall), vertical external loads (such as traffic loads), horizontal soil pressures from the nonreinforced zone and the weight of the reinforced mass must be considered.

7.4 Internal Stability Evaluation

Two conditions must be separately satisfied: (1) tension—the wire reinforcing must be sized to provide sufficient tensile resistance without rupture; and (2) pullout—the mats must be extended a sufficient length behind the theoretical failure plane to preclude failure by pullout.

7.5 Design Parameters

Fixed design parameters are the yield strength of the wire (65,000 psi), longitudinal and transverse wire spacing (unless specially ordered), and the vertical spacing between the mats (fabrication equipment is set up to bend only 18-in. faces). Consequently, the variable reinforcement parameters are wire diameter and the length of the mats.

On most projects it is economically beneficial to use standard wire sizes and mesh configurations. Prior to 1984, wire sizes ranged from W1.7 to W3.4, with a 2-in. by 6-in. mesh size. With the development of a simpler method to couple the wire face to the mat above it, heavier longitudinal wire sizes, W4.5, W7, W9, and W12, are now in routine use. The W12 is the largest wire size that is given a standard shop coat of 0.4 oz per sq ft of zinc galvanizing. For each of these longitudinal wires, the transverse wires used are W3.5, W3.5, W4.0, and W5.0, respectively. The corresponding mesh size is 6 in. by 9 in. The longitudinal wire sizes used for RSE design are W7, W9.5, W12, W14, W18, and W20 laid in a 6-in. by 24-in. mesh, with the transverse wires being W7 for the W7 longitudinal wire size and W9.5 for the rest. Pertinent design data for wire sizes are given in Table B-1.

7.6 Design Approach

The equations used for wall design were empirically derived. Tensile forces in the wire are determined by evaluating the lateral pressures in the soil at each level of the mats. The wire is sized to preclude failure by rupture at the end of the service life, and the mat length is sized to provide adequate pullout resistance.

In practice, the wire mats used are generally uniform with respect to wire size throughout the wall height. Two or three changes, at most, are made for high walls. This means that the factor of safety against a rupture failure generally varies from a minimum for the most highly stressed mats at the base of the wall to a high value at the top where lateral forces are the least. The length of the mats into the resistant zone and the overburden-imposed weight are the primary factors controlling pullout resistance for a given soil. Hence, length of the reinforcing mats is an important design consideration. In practice, however, it is often found that the base width required for adequate resistance against sliding, rather than the length required for pullout resistance, controls design.

7.7 Current Design Practice

Design of the longitudinal wires is based on the equation:

$$\frac{\text{Allowable tensile force}}{\text{Horizontal load on wire}} = \frac{f_a A_R}{K_D \sigma_v S_v S_H} \geq 1.0 \quad \text{(B-11)}$$

where f_a = allowable wire stress; A_R = cross-sectional area of the wire after allowance for corrosion (i.e., the estimated wire diameter at the end of the structure design life); K_D = 0.65, the empirically derived design lateral earth pressure coefficient (as discussed in Sec. 3.6, this value may be decreased to 0.45 for sections of wall more than 20 ft below the top); σ_v = vertical stress caused by overburden and external loads at the depth of the considered wire; S_H = spacing between longitudinal wires; and S_v = vertical spacing between mats.

When computing the vertical stress, σ_v, vertical loads on top of the wall may be reduced using a dispersion angle of 2 vertical to 1 horizontal. Eccentricity of such loads can be allowed for using Meyerhof's equations as described in Chapter Five of the main report.

Traffic along the top of the wall is treated as a simple vertical surcharge; a standard H-20 highway load requires an equivalent of about 2 ft of soil be added in design calculations. Freeway traffic loads will require up to 5 ft.

Although not explicitly cited in available Welded Wire literature, horizontal stip loads, F_H, applied on the upper portion

of the wall can be allowed for as shown in Figure B-21. The magnitude of the shear stress at the ground surface, τ_o, is computed by dividing the horizontal force per linear foot, F_H, by the base width of the loaded strip, B. This shear stress is dispersed with depth at an angle of 2 vertical to 1 horizontal. For a reinforcement located at depth, Z, the additional tensile load per unit length of wall caused by the applied line load can then be computed as:

$$F_T = \tau_o\left(1 - \frac{Z}{2B}\right)S_v \qquad \text{(B-12)}$$

The dispersion angle of 2 vertical to 1 horizontal, and hence Eq. B-7, applies only to granular backfill with an internal friction angle of about 35 deg. The more general case, for other friction angles and placement of the strip load at some distance from the face is discussed in Section 7 (in Chapter Two, "Anchored Earth," of this appendix) and also in Chapter Five of the main report.

When combined vertical and horizontal strip loads are considered, eccentricity of the loads should be considered in accordance with Meyerhof's methods as described in Appendix A, Chapter One, Section 7.

The Federal Highway Administration [FHWA, 1982] requires that 0.55 f_y be used for the allowable steel stress, f_a, on federal aid projects. This is generally the value for f_a used for all designs, unless otherwise specified for a specific project.

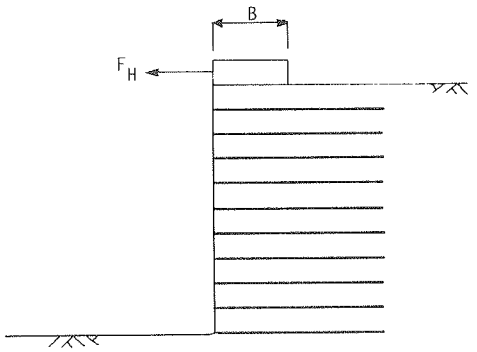

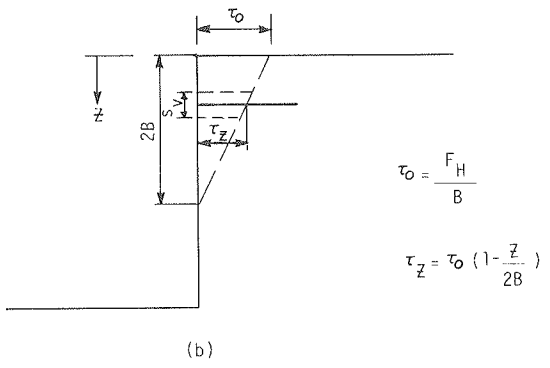

NOTE: Applies Only to Granular Backfill With $\phi \approx 35°$

Figure B-21. Method for computing reinforcement force caused by a horizontal strip load.

The adequacy of pullout resistance is then evaluated. First, the lateral earth pressures which must be resisted by each mat are evaluated to determine mobilized pullout forces. A lateral earth pressure coefficient of $K_D = 0.65$ is used in these calculations. Horizontal loads caused by exterior loading are allowed for using the methods described above. Only that portion of the mat extending beyond a theoretical Rankine failure plane, i.e., a plane with an inclination of $45° + \phi'/2$ to the horizontal (Fig. B-22) is considered effective in mobilizing pullout resistance. The computed pullout forces are compared with pullout resistance; the factor of safety for each mat should be 1.5. Additionally, the entire lateral force within the wall is compared to the summation of each mat's individual resistances to pullout. Again, an overall factor of safety of 1.5 or greater should be obtained. If needed, the length of the mat should then be extended or, if more economical, a differenct mat with larger diameter wires should be used. The following equations are currently used to evaluate resistance to pullout of the mats:

Silty Sand:

$$P_t = 2{,}140 \text{ lb/ft} + \sigma_v d\,[(0.75)(\pi L_e M)\tan\delta + 18\,n]\,n\,\sigma_v d > 114 \text{ lb/ft} \qquad \text{(B-13)}$$

$$P_t = \sigma_v d\,[(0.75)(\pi L_e M)\tan\delta + 36\,n]\,n\,\sigma_v d \leq 114 \text{ lb/ft} \qquad \text{(B-14)}$$

Washed Sand:

$$P_t = \sigma_v d\,[(0.75)(\pi L_e M)\tan\delta + 37\,n] \qquad \text{(B-15)}$$

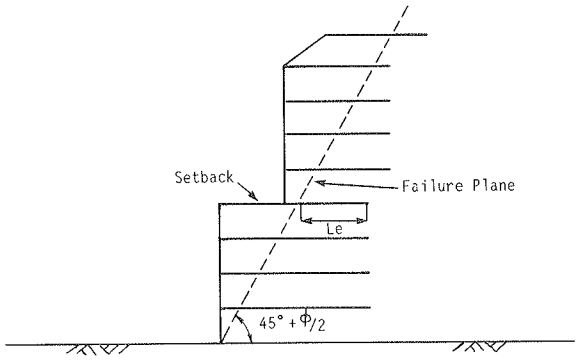

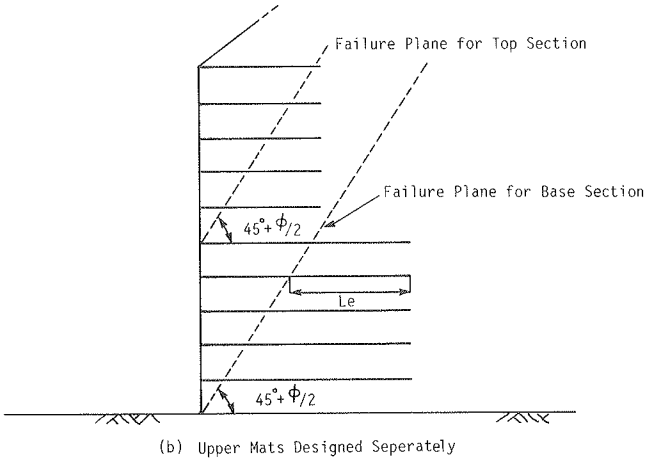

Figure B-22. Wall configurations.

Pea Gravel:

$$P_t = \sigma_v d\,[(0.75)(\pi L_e M)\tan\delta + 38\,n] \qquad \text{(B-16)}$$

where P = total pullout resistance in pounds per linear ft of wall length; L_e = length of embedment behind Rankine failure plane (Fig. B-19); $\tan\delta$ = friction factor between soil and reinforcement; M = number of longitudinal wires per transverse foot of mesh; and n = number of transverse wires behind the active zone, i.e., within L_e.

It should be verified that the spacing of transverse wires is sufficient that the development of full passive resistance on each transverse wire is possible; otherwise the multiplier, n, may not be valid. (See Chapter Four of the main report.)

Finally, the possible pullout failure of the mat by slip along planes adjacent to the mat, but in the soil, should also be evaluated. That is, the pullout resistance of a fully rough sheet with $\delta = \phi$, having the same total plan dimensions as the wire sheet, should not be exceeded. (See Chapter Four of the main report.)

The design approach described above pertains to Welded Wire Wall where the wire mats are continuous along the length of the wall. As shown in Figure B-3, this continuity does not exist with RSE panels, where the mats are spaced to provide room for the panel "columns." The average tensile reinforcement and pullout resistances for RSE per linear foot wall length are currently assumed to be 80 percent of the value computed for continuous mats.

7.8 Special Design Cases

7.8.1 Intermediate Mats

The use of intermediate mats for high or heavily loaded walls is being considered. Loading conditions that would require tensile reinforcement greater than that obtained by W12 wire in a 6-in. by 9-in. grid (for mats spaced vertically at 18 in.) would use this option. Rather than go to a larger wire size (which could not be obtained with a shop coat of galvanizing) or a finer mesh (which would require twice the inventory of wire mesh), intermediate mats may be set at a vertical spacing of 9 in. This will allow use of a smaller, stock wire and mesh size and not require altering the fabrication equipment producing the 18-in. bent-up face. The intermediate mats would be laid down 9 in. above the primary mats without attaching them to the wire face. Placement of the intermediate mats can be discontinued when the construction has reached a height above which they are no longer needed.

7.8.2 Benched Walls

A benched-wall design, as shown in Figure B-22a, where the face is stepped back 1 to 5 ft every three to six layers of reinforcement is occasionally used where aesthetics or access considerations make it desirable. The average slope of the face is thus less than vertical, with the result that shorter mats can be used on the upper portion of the wall.

Another suggested version of the stepped-wall design is to step the reinforcement internally while maintaining a vertical face (Fig. B-22b). Current design methodology is to treat each "step" of the wall separately, with the lower portions being designed to withstand the forces imposed by the portions above.

Design of this type of wall is done by initially sizing the entire wall as a unit (i.e., as a wall with uniform, not stepped, reinforcement), using external stability criteria. Once the overall sizing is done, internal design is begun by dividing the wall into two or three different sections, each having a uniform reinforcement length (e.g., Fig. B-22b). Each of these sections must be designed to withstand both the vertical and horizontal forces imposed on it by the remaining sections on top. Figure B-23 presents the freebodies for a two-segment wall, with the relevant forces. The reinforcement in the lower section must be sufficient to resist the entire pullout force created by the full height wall. This requirement may result either in lengthening of the mats slightly or in the need for heavier gauge wire.

A substantial horizontal shearing force exists at the interface between the two segments. This shear force must be transmitted fully by sliding resistance between the two segments. Presently, this shear force is assumed to be distributed to the mats in the lower section of wall in the same triangular distribution as that of the horizontal shear force imposed by a strip footing (Fig. B-21, Eq. B-12).

The behavior of walls with stepped reinforcement lengths is not yet fully understood (see Chapter Four of the main report) and both analytical and experimental studies are needed to verify and calibrate proposed design procedures.

7.9 Application under Special Loading Conditions

The Wire Wall and the RSE can generally be tailored to meet most any condition for which a reinforced soil structure can be

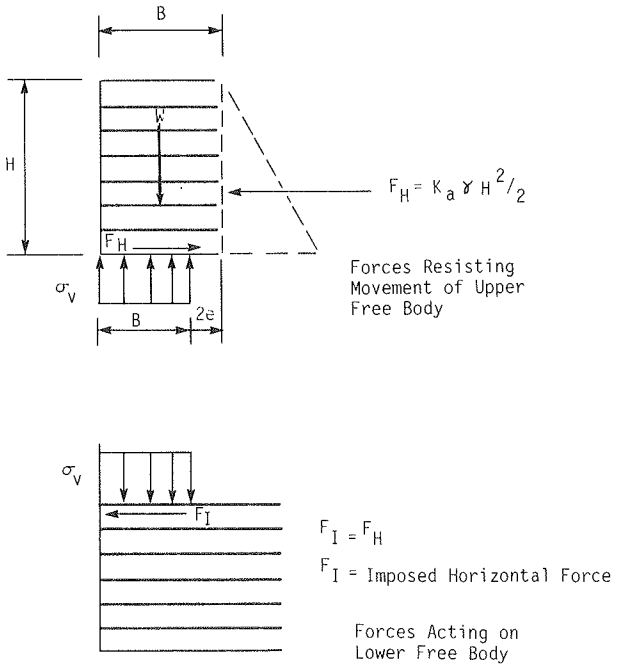

Figure B-23. Schematic illustration of wall with stepped reinforcement lengths as free bodies.

used. Some of these conditions, such as a short base width supplemented by rock bolts and two types of stepped walls, are described in previous sections.

Seismic loading conditions also constitute special conditions to which the Wire Wall or RSE may be subjected. At the present time, only a very approximate design approach is in use. The procedure is simply to apply a horizontal force in the critical direction for stability. This is usually determined by determining the potential ground acceleration and multiplying it by the mass of soil in the wall to give the equivalent horizontal earthquake force. This pseudostatic approach is believed to be conservative.

7.10 Limitations of Current Design Practice

Current design practice does not yet account adequately for low-quality backfill materials. Pullout tests and instrumentation of full-scale walls constructed with these soils are needed.

The seismic design of the Wire Wall and RSE systems needs to be further evaluated. Also, the internally stepped wall design discussed previously should be more fully investigated by observation and instrumentation to better define the nature and any limitations of the stress transfer between wall segments.

8. CASH HISTORIES

8.1 General

Since the use of Welded Wire Walls began, more than 200 walls have been constructed in a variety of situations. In addition to specific research and development programs, several walls have been instrumented during construction to provide data on behavior. Many more have been subjected to various types of intermittent observations. A great deal of the useful design and construction data has been gained from such observations of full-scale, in-service installations. For those (relatively few) walls which have incurred in-service problems, deficiencies have generally been traced to improper design or poor construction, as opposed to system inadequacies. Presented in this section are three examples from which useful lessons were drawn for both design and construction purposes.

8.2 San Gabriel Wall, California, 1979

During the fall of 1979, a large Welded Wire Wall to date was constructed in the San Gabriel Mountains, near Mt. Wilson, in Southern California. It was built to correct a slip-out that occurred on a power line access road for the Southern California Edison Power Company. Prior to construction, it was decided to make extensive use of the wall for inservice observations, and a formal study was initiated.

Maximum height of the wall was 22½ ft and overall length was 120 ft. A 2½-ft thick road base was added on top. Every five lifts, a 3-ft step-back was made at the wall face. Nine-gauge wire in a 2-in. by 6-in. mesh was used.

The wall was instrumented by placing strain gauges on two different mats, each placed at different levels in the wall. Figure B-11 shows the location of the strain gauges, and Figures B-12 and B-13 show strain gauge measurements made during the course of the wall construction. Section 3.5 briefly discusses some aspects of the wall behavior. In addition to the strain gauges, four extensometers were installed at each of the two levels of strain gauges, at increasing depths into the wall, to correlate yield of the wall face with stress measurements in the reinforcing. Also, settlement plates in the wall mass and survey monuments on the wall face were installed. A more complete evaluation and discussion of the wall's performance during and after construction is presented by Bishop [1979].

Based on measurements and observations of this wall, the factor $K_D = 0.65$ was chosen for the design coefficient of lateral earth pressure. The equation for design of tensile reinforcement (Eq. B-11) was also chosen as being the most appropriate method to design the longitudinal wires.

The most significant construction lesson learned from this wall was the difficulty in compacting soil against the face of the wire mesh. Several different techniques were tried, including the use of mechanical hand compaction equipment and regular tamping of the soil with a shovel handle through the mesh of the wire layer above. These were not particularly successful, and compression of several of the lower layers at the face was observed, especially following heavy rainstorms during and after the wall construction. Based on this experience, it was decided to use the facing gravel that was specified for the lighter 9-gauge wire, used until 1984.

8.3 Union Oil Shale Mine Access Road, Colorado, 1980

In 1980, a 750-ft long, 14½-ft high Wire Wall was constructed at the Union Oil Shale Mine near Parachute, Colorado. Shown in Figure B-24, this wall was constructed on talus-covered slopes for the purpose of widening an existing narrow road winding up a mountainside. This was one of the first "large" projects utilizing the Welded Wire Wall, and it included the first attempts at mass backfill placement. Placement of gravel at the face of the wall was successfully done using a Redi-mix truck with its chute directed along the inside of the wall face, as shown for another project in Figure B-18b.

There were nine lifts constructed, the top four being stepped-back about 3 ft. During the construction of the eighth and ninth lifts, the wire wall face was pushed outwards by construction equipment. The result was that the soil directly behind the pea gravel, and the face was mildly distorted. Substantial compression took place during completion of the wall. Due to buckling, a slightly overhanging face formed in some places. However, the integrity of the wall was not compromised, and structural behavior thus far has been satisfactory.

8.4 Interstate 580 Wall, California, 1982

In 1982, a Welded Wire Wall was constructed on Interstate 580, about 5 miles east of Hayward, California. The wall was constructed to serve as a temporary retaining structure to facilitate new grading. This vertical faced wall ranged in height from 6 ft to 30 ft and was about 450 ft long. The top 10½ ft of the wall were designed as an internally stepped wall, as depicted in Figure B-22b. The reinforcing mats in this top section were substantially shorter than those in the bottom sections of the wall, and were designed as discussed earlier, in Section 7.8.2 of this chapter.

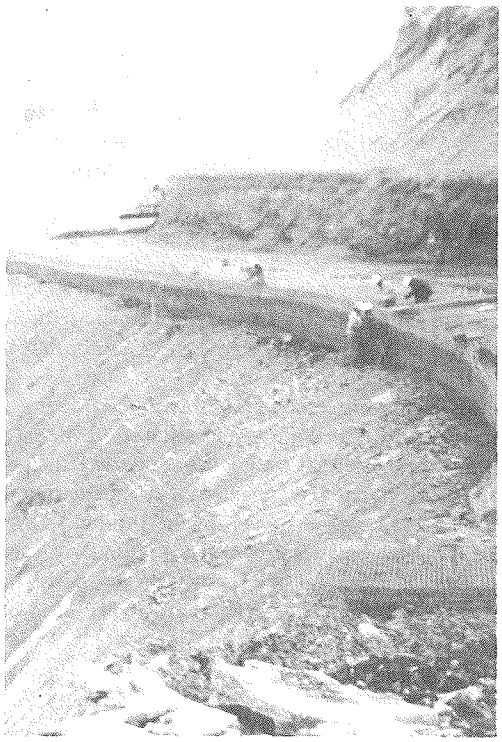

Figure B-24. Photograph of Union Oil Wire Wall under construction. Note: This wall was constructed using mass backfill placement techniques. Mats made of 9-gauge wire were used. This photograph shows a gravel envelope at the face and an intricate method of tying together successive layers of reinforcement. With wire sizes now in use, no facing gravel is required and a simple method of interlocking the mats is used.

Following construction, observations of the overall wall performance indicated that a 100-ft section of the upper portion of the wall was gradually tilting outward. Cracks began appearing at the back of the wall. At one point a significant fissure on the order of 2 ft wide was apparent. Remedial backfilling did not solve the problem.

An investigation of the wall was conducted, and the following conclusions were reached. Initially, the client had specified a granular backfill, and that an internal angle of friction of 38 deg would be appropriate for design. Excavation and testing of representative soils indicated the backfill used was a sandy clay with a "moderate" potential for expansion. The soil was found to have a water content generally well in excess of optimum and above the plastic limit. The angle of friction of the saturated soil was not measured, but was judged to be substantially lower than 38 deg. Ultimately it was felt that the primary cause of the problem with this structure was poor drainage of surface water. Whereas the original plans called for positive drainage on top of the wall, in actuality, water was allowed to pond and seep into the back of the wall and saturate the backfill material. The low quality backfill material, when saturated in a series of wet and dry cycles, experienced both expansion as well as creep.

It should be noted that the wall was of a configuration (internally stepped) that is not yet fully understood. It is thus possible that the unusual configuration may have contributed to the excessive movement.

Remedial measures that involved removal of the top four layers of mats and their replacement with much longer mats were initiated. The backfill material was required to be a silty sand with a maximum of 20 percent fines, a P.I. less than 10, and a minimum angle of internal friction of 34 deg. The drainage of surface waters across the top of the wall was altered so that no further water migration into the wall could occur. The wall has performed satisfactorily since completion of this work.

9. COSTS

Labor and material costs vary from site to site depending on access, available materials, and local economic conditions. Typical costs (for 1984) are given in terms of cost per square foot of wall face. Wire Wall components delivered to the job site range from $6.00 to $14.00 per sq ft. This encompasses a range of wall heights from around 6 ft to 60 ft. This price includes technical assistance from an on-site technical representative. Erection costs range from about $2.00 to $3.00 per sq ft, and backfill costs will usually range from $2.50 to $5.00 per cu yd for placement and compaction. Additional costs may be encountered with more labor-intensive wall construction such as in severely limited access areas, use of select backfill, and with placement of internal drains. Generally, for walls ranging from 6 to 60 ft high, completed construction costs will range from $12.00 to $26.00 per sq ft of face.

Recently, a project by the U.S. Forest Service in Region IV, Manti-Lasalle National Forest, involved construction of a 248-ft long Wire Wall [Fitzgerald, 1983]. A 163-ft portion of the wall was built on an 80-ft radius, and the wall varied in height from 6.5 to 22.5 ft, with 19 different wall heights along its length. An internal drain system, which included underdrain pipe and filter cloth, was installed. Access was comparatively restricted, and construction was probably more labor-intensive than for most installations. The Forest Service reviewed several types of retaining wall systems and chose the Wire Wall because of its low cost, flexible construction, and working area required for the construction. The final, in-place construction costs of the wall (including excavation, select backfill, facing gravel, and wall materials) was $22.79 per sq ft of wall face.

For walls from 6 to 60 ft high, RSE components range from $10.00 to $20.00 per sq ft delivered to the site. Erection costs range from $3.00 to $5.00 per sq ft and typical backfill costs from $2.50 to $5.00 per cu yd. Costs for walls ranging from 6 to 60 ft will therefore range from about $20.00 to $30.00 per sq ft.

Wall material costs noted above were provided by the Hilfiker Retaining Wall Company, as were erection costs. Backfill and overall construction costs were obtained from general experience of both the Hilfiker Retaining Wall Company and the author, which also included records from specific projects, such as the one noted herein.

10. FUTURE DEVELOPMENTS OF THE SYSTEM

10.1 Required Research

The primary need for future research is a study of low-quality backfills for wall construction, verification of present design

procedures, and further verification of the high lateral earth pressure coefficient used for design. These studies should include both pullout resistance and overall assessment of performance of full-scale structures. Additional research is also needed on corrosion protection and seismic design.

10.2 Anticipated Future Trends

It is anticipated that both the Wire Wall and the RSE will continue to be used primarily in retaining wall applications. Slope stability problems, such as slide stabilization, as well as routine embankment construction for highways are anticipated to be the primary areas of general use.

11. DESIGN EXAMPLE

11.1 General

Several design examples with 6-in. by 2-in. welded wire mesh reinforcements are presented in Chapter Five of the main report. The design example presented below is based on the more recent 6-in. by 9-in. grid.

11.2 Problem

Consider a 22½-ft high wall with a uniform surcharge:

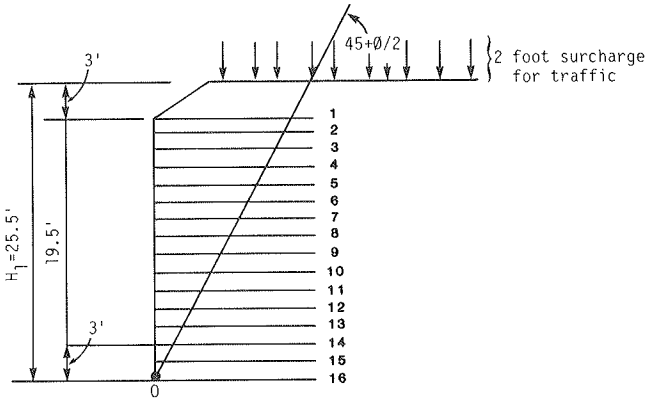

The surcharge will consist of 3 ft of fill on the top of the wall to establish the desired grade, and an allowance for traffic loads of an additional 2 ft, for a total design load of 5 ft of surcharge. The wall height of 22½ ft allows for a total of 15 layers at 18 in. thickness each (standard mat spacing). The 3 ft of embedment at the toe enhance bearing capacity and passive resistance and help protect the toe from being undercut by erosion.

It is assumed that the native soil, a silty sand, can be used as backfill; soil parameters are as follows: $\gamma = 110$ pcf; $\phi = 33°$; $c = 0$; $\delta = 14°$; pH = 6.5; resistivity = 4,000 ohm-cm; design life of 75 years; and negligible sulfate and chloride content. It is known that the backfill will not be saturated.

11.2.1 External Stability

Length of the mats (depth of the wall) is sized initially by required sliding resistance. It is assumed that deep stability has been checked and an adequate safety factor established. To evaluate sliding, loading must be determined.

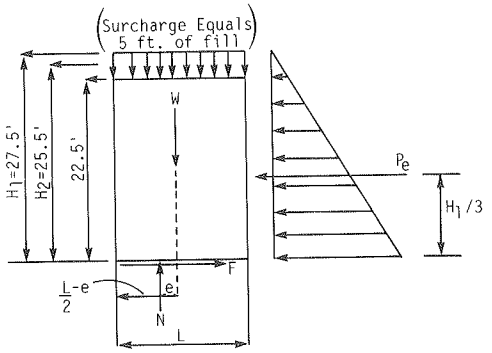

Sliding. Use a sliding factor of safety of 1.5 and ignore passive resistance from embedded portion at the toe. From the freebody diagram, this can be expressed as follows: $F.S. = \frac{F}{P_e} = 1.5$, or $F = 1.5\ P_e$, with $F = N \tan \phi = 27.5\ L\ (110) \tan 33°$ and $P_e = \frac{1}{2} K_a \gamma H_1^2 = \frac{1}{2}\ (0.3)\ 110\ (27.5)^2$, in which $K_a \tan^2 (45 - \phi/2)$; therefore: $27.5\ L\ (110) \tan (33°) = [0.5\ (0.3)\ 110\ (27.5)^2]1.5$, $L = 9.5$ minimum. Use $L = 10$ ft.

Bearing Capacity. Since settlement will take place during construction, base the allowable bearing pressure on the ultimate bearing capacity with a safety factor of 2.0. A trapezoidal distribution of bearing pressure is assumed in this example: $q_{ult} = \frac{1}{2} B \gamma N_\gamma + \gamma D(N_q - 1)$, where N_γ and N_q are bearing capacity factors. For $\phi = 33°$, $N_\gamma = 35.6$ and $N_q = 26.3$.

The width B is the length, L, of the mats. Since the base is loaded eccentrically, e, an effective width B' must be used. $B' = L - 2e$.

$$e = \frac{M_{centerline}}{N} = \frac{P_e\ (H_1/3)}{N} = \frac{\gamma K_a (H_1^2/2) H_1/3}{H_1 L \gamma} \frac{K_a H_1^2}{6L}$$

$$e = \frac{K_a H_1^2}{6L} = \frac{0.3\ (27.5)^2}{6(10)} = 3.78 \text{ ft}$$

$$B' = 10 - 2\ (3.78) = 2.44 \text{ ft}$$

$$q_{ult} = 0.5(2.4)\ 110(35.6) + 110(3)\ (26.3 - 1) = 13{,}043 \text{ psf}$$

$$q_a = 6{,}525 \text{ psf}$$

Since the resultant is outside the middle third of the base, the maximum bearing pressure must be calculated on the basis of a triangular pressure distribution (see sketch below).

The base of the triangle will be: $\left[3\left(\frac{L}{2} - e\right)\right]$ = base, and the area of the triangular pressure distribution must equal the normal force N: $0.5 q_{max}\ (3)\left(\frac{L}{2} - e\right) = N = H_1\ L$; $q_{max} = (2H_1L)/3[(L/2) - e]$.

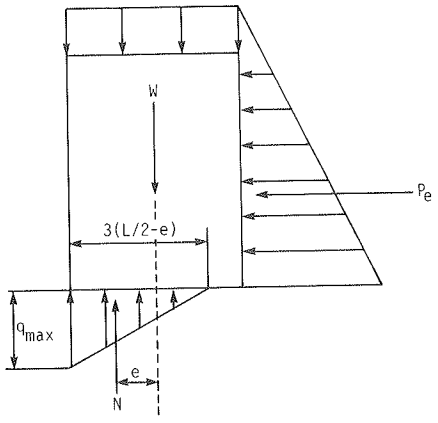

For a mat length of 10 ft: $q_{max} = \dfrac{2(27.5)\ 10(110)}{3\left(\dfrac{10}{2} - 3.78\right)} = 16{,}530$ psf > 6,525 psf. Since $q_{max} > q_a$, increase mat length. Try $L = 14$ ft. Thus:

- $e = \dfrac{K_a H_1^2}{6} = \dfrac{0.3\ (27.5)^2}{6(14)} = 2.7$ ft.
- $B' = 14 - 2\ (2.7) = 8.6$ ft.
- $q_{ult} = 0.5(8.6)(110)(35.6) + 110(3)\ (26.3 - 1) = 25{,}188$ psf.
- $q_a = 12{,}594$ psf.
- $q_{max} = \dfrac{2(27.5)\ 14(110)}{3\left(\dfrac{14}{2} - 2.7\right)} = 6{,}566$ psf < 12,594 psf. Use 14-ft long mats.

Overturning. Taking moments about the toe (Point "0"), the ratio of overturning moment to resisting moment should be 2.0 or greater. Resisting moment = $\widehat{M_0} = \frac{1}{2} L\ W = \frac{1}{2} L\ (H_2 L)$. Overturning moment = $\widehat{M_0} = \frac{1}{3} H_1 P_e = 9.2\ (\frac{1}{2} K_a H_1^2)$.

Note: For resisting moment, ignore the 2-ft surcharge load for traffic load (live load). This is conservative. $\dfrac{\widehat{M_0}}{\widehat{M_0}} = \dfrac{\frac{1}{2} L\ H_2 L\gamma}{9.2\ (\frac{1}{2}) K_a \gamma H_1^2} = \dfrac{L^2 H_2}{9.2\ K_a H_1^2} = \dfrac{14^2\ (25.5)}{9.2\ (0.3) 27.5^2} = 2.4 > 2.0.$

11.2.2 Internal Stability—Design of Wire Mats

Corrosion. A 100-year design life is desired. With a zinc galvanizing of 0.4 oz/sf, and assuming that the zinc unit weight is 490 lb/cf, the thickness of the zinc is estimated at 0.6 mil. Using the degradation rates for galvanized wire mesh (Section 5.2), it is estimated that the zinc will last 3 years (0.6 − 0.24 − 0.24 − 0.08 = 0.04; round to 3 years). Estimate the final wire diameter at the end of the remaining 97 years with Eq. B-10: $\sum_{i=0}^{N} (d_i - C_R) = d_f$, where d_i is the initial wire diameter the first year and d_{i+1} thereafter; C_R is 0.36 mil/yr, 0.0036 in./yr (see Fig. B-12); and d_f is the final wire diameter.

For W4.5 wire, the initial, d_i, diameter is 0.239 in. and d_f is 0.204.

Tension in wires. $f_y = 65{,}000$ psi; diameter for design = 0.204 in.; area = 0.33 in.^{2} = A_R; and $f_a = 0.55(65{,}000) = 35{,}750$ psi.

By using Eq. B-6, $\dfrac{f_a A_R}{K_D\ \sigma_v\ S_H H_v} \geq 1.0$, where $K_D = 0.65$ (assumed for design); $\sigma_v = \gamma H_1 = 110(27.5) = 3{,}025$ psf = 21.0 psi, critical case, deepest reinforcing layer; $S_H = 6$ in. (for a 6-in. by 9-in. mesh); and $S_v = 18$ in. Thus, $\dfrac{35{,}750\ (0.033)}{0.65(21.0)\ 6(18)} = 0.793 < 1.0$.

Try next standard wire size W7 with $d = 0.299$ in. Final diameter is $d_f = 0.264$ in.; $A_R = 0.055$; $\dfrac{35{,}750\ (0.055)}{0.65(21.0)\ 6(18)} = 1.3 > 1.0$.

At this point, economics must be considered in the design. There are three options to pursue for the construction of the Wire Wall, depending on the volume of wall to be built (transverse length). The first is that the entire wall can be built with the W7 wire, or change to W4.5 wire can be made part way up the wall, where stresses decrease to allow this, as a second option. The third is to use W4.5 throughout, with intermediate mats (i.e., $S_v = 9$ in.) in the lower part of the wall where the stress requires it. Costs of the different mats and problems involved with handling would have to be weighed.

For the purpose of this example, it will be assumed that the wall requires a low volume and would, therefore, be constructed entirely of W7 wire mesh. In reality, because price is based on weight of steel purchased, the cost savings obtained by changing over to the lighter mats as soon as possible would probably more than offset the nominal charge of handling mats with two different wire sizes.

Pullout. The final diameter for the transverse wire (W3.5), as determined by the methods discussed above, is 0.176 in. Only the portion of the mat behind the potential failure plane can provide pullout resistance, with the pullout resistance limited by the available tensile capacity of the longitudinal wires in the mat. A factor of safety of 1.5 should be obtained for each mat, or an overall factor of safety of 1.5 for the entire wall against pullout failure, or both.

The following table presents calculations for available pullout resistance of each mat. The following variables are used: P_t = total pullout resistance per transverse foot of wall; L_e = length of mat behind the failure plane; σ_v = overburden stress; n = number of transverse wires in L_e; $d = d_F$ = final diameter of transverse wires; M = number of longitudinal wires/foot of mat, which is 2 for the 6-in. by 9-in. mesh; and δ = soil-steel friction angle, $\frac{2}{3}\phi = 22°$ for this case.

P_t is derived from the silty sand Eqs. B-13 and B-14. L_e for any reinforcement layer at depth, Z, below the top of the wall can be determined as follows: $L_e = L - (H - Z) \tan(45 - \phi/2)$.

Mat #	L_e (in.)	n(9" spacing)	σ_v (psf)	$n_{\sigma_v d}$	P_t (lb/ft)
1	21	3	550	24	898
2	31	4	715	42	1,562
3	41	5	880	65	2,387
4	51	6	1045	92	3,435
5	60	7	1210	124	4,545
6	70	8	1375	161	5,268
7	80	9	1540	203	6,086
8	90	11	1705	275	7,448
9	99	12	1870	329	8,495
10	109	13	2035	388	9,640
11	119	14	2200	452	10,880
12	129	15	2365	520	12,215
13	139	16	2530	594	13,645
14	148	17	2695	672	15,163
15	158	18	2860	755	16,782
16	168	19	3025	843	18,496

The pullout resistance, P, should now be compared with the pullout force per unit width of wall, calculated by: $F = K\ \sigma_v\ S_v$ ($K = 0.65$).

Calculations for the factor of safety in pullout (pullout resistance P divided by the pullout force F) for each mat are shown in the table below.

Considering only dead load, $F = 0.65\ (316)5.75 = 1{,}181$ lb/ft.

The factor of safety for tensile rupture of longitudinal wires is also shown in the table above. This factor of safety is determined by dividing the ultimate tensile resistance available by the force in longitudinal wires: $FS_{rupture} = \dfrac{f_y A_R M}{F} = \dfrac{(65{,}000\ \text{psi})(0.055\ \text{in.}^2)(2/\text{ft})}{F} = \dfrac{7{,}150\ \text{lb/ft}}{F}$, where M is the number of longitudinal wires per transverse foot of mesh, and F is the calculated pullout force for each individual mat. The

Mat #	Pullout Force (lbs/ft)	F.S. in pullout	F.S. in rupture	Internal F.S. min.
1	1181*	0.76	6.05	0.76
2	697	2.24	10.26	2.24
3	858	2.78	8.33	2.78
4	1019	3.37	7.02	3.37
5	1180	3.85	6.06	3.85
6	1341	3.93	5.33	3.93
7	1502	4.02	4.76	4.02
8	1663	4.48	4.30	4.30
9	1824	4.66	3.92	3.92
10	1984	4.86	3.60	3.60
11	2146	5.07	3.33	3.33
12	2307	5.29	3.10	3.10
13	2468	5.55	2.90	2.90
14	2629	5.77	2.72	2.72
15	2790	6.02	2.56	2.56
16	2951	6.27	2.42	2.42

*For mat #1 $F = K_v S_v \quad _v = 110 \times \frac{5.75}{2} = 316$ psf

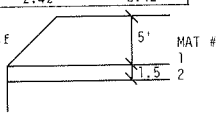

actual internal factor of safety for each mat is the minimum of the factors of safety in rupture and pullout.

At this point the designer has several options with regard to *F.S.* against pullout of the top mat including: (1) ordering the top (capping) mats an extra 12 in. longer to achieve a *F.S.* > 1.0; (2) reevaluating the need for a 3-ft layer of soil on top of the wall (minimum requirements are 18 in.; unless the extra fill is needed to establish grade, do not use it); and (3) bending the upper mat down into the backfill.

Checking overall factor of safety for the minimums listed: $\frac{F.S._{\min}}{\#\text{ mats}} = 3.1$.

Unless this project were administered by an agency which specifically required a pullout *F.S.* of 1.5 for *each* mat, a *F.S.* for pullout greater than 1.0 for the top mat would be satisfactory. If needed, the top mat could be ordered longer to provide the required factor of safety.

12. REFERENCES

ANDERSON, L. R., SHARP, K. D., WOODWARD, B. L., and WINWARD, R. F., [1985]. "Performance of the Rainier Avenue Welded Wire Retaining Wall, Seattle, Washington," Prepared for The Hilfiker Company, Eureka, California and Washington State Dept. of Transportation, Olympia, Washington.

BISHOP, J. A. [1979]. "Evaluation of a Welded Wire Retaining Wall," Masters Thesis, Utah State University, Logan, Utah.

BISHOP, J. A., and ANDERSON, L. R. [1979]. "Performance of a Welded Wire Retaining Wall," Report to the Hilfiker Company, Utah State University, Logan, Utah.

CHANG, J. C. [1974]. "Earthwork Reinforcement Techniques," California Division of Highways, *Transportation Laboratory Research Report, CA-DOT-TL-2115-9-74-37.*

CHANG, J. C., HANNON, J. B., and FORSYTH, R. A. [1977]. "Pull Resistance and Interaction of Earthwork Reinforcement and Soil," Presented at the 56th Annual Meeting of the Transportation Research Board, January 1977.

DUNN, I. S., ANDERSON, L. R., and KIEFER, F. W. [1980]. *Fundamentals of Geotechnical Analysis,* John Wiley and Sons, New York, p. 267.

FEDERAL HIGHWAY ADMINISTRATION [1982]. Letter to the Hilfiker Pipe Company, March 11, p. 3.

FEDERAL HIGHWAY ADMINISTRATION [1983]. Memorandum: Hilfiker Welded Wire Wall Update, Feb. 18.

FITZGERALD, T. [1983]. "Welded Wire Walls: A Solution to Diversity of Retaining Wall Needs," Engineering Field Notes; Forest Service, USDA, Washington, D.C., Vol. 15, pp. 7–19.

NIELSEN, M. R. [1983]. "Pullout Resistance of Welded Wire Mats Embedded in Soil," Masters Thesis, Utah State University, Logan, Utah.

PETERSON, L. M. [1980]. "Pullout Resistance of Welded Wire Mesh Embedded in Soil," Masters Thesis, Utah State University, Logan, Utah.

UNITED STATES DISTRICT COURT, Northern District of California [1984]. *The Reinforced Earth Company v The Hilfiker Pipe Company and William K. Hilfiker,* No. C-83-1243-WHO, San Francisco, California, April 11.

CHAPTER TWO—ANCHORED EARTH

Contents

1. INTRODUCTION

Anchored Earth is an earth retention system patented in the United States (Patent No. 4407611) and elsewhere by the Transport and Road Research Laboratory, Crowthorne, England [Murray and Irwin, 1981a]. Like most earth reinforcement systems, high strength tensile members are incorporated with the soil to form a composite material.

An Anchored Earth retaining wall has concrete facing panels from which steel rods, bent to form anchors at their ends, project into the earth to resist the soil pressure on the facing. The rods extend through the facing panels in slots and are secured by nuts. The facing units are typically lap jointed laterally, and the anchors extend through adjacent overlapping portions. Unlike other earth reinforcement methods described in this report, which are designed on the premise that frictional stress or passive resistance develops along the entire embedment length of the reinforcement, Anchored Earth is designed on the basis that passive resistance is developed only at the deformed ends of the reinforcing members.

Figure B-25 shows two types of low fabrication cost anchors. The preferred type of anchor is the triangular shape incorporating a short length of weld.

Figure B-26 is a general view of an assembly of facing units and anchor members.

To date, Anchored Earth remains in its experimental stages, encompassing model tests, a pilot scale structure, and a recently constructed full-scale embankment [Jones et al., 1985].

2. APPLICATIONS

2.1 Inherent Advantages

Round steel bar is used to form the anchors of an Anchored Earth wall. The surface area of a round bar is, for a given cross-sectional area, less than that for a strip, thus reducing the surface area exposed to corrosion and hence the quantity of corrosion protection required. The low surface area of a rod compared to a strip does, however, mean that less frictional resistance area is available.

Both types of anchor illustrated in Figure B-25 offer the advantages of low fabrication cost, ease of handling, and good pullout resistance. The pullout resistance is not as sensitive to the surface characteristics of the anchor as other reinforcement systems because passive resistance on the anchor head contributes the majority of the pullout resistance. This implies that a variety of surface protections to guard against corrosion can be employed, particularly over the length of bar between the connection and the start of the anchor bend. This could prove advantageous near the facing where differential aeration can occur [Murray and Irwin, 1981b].

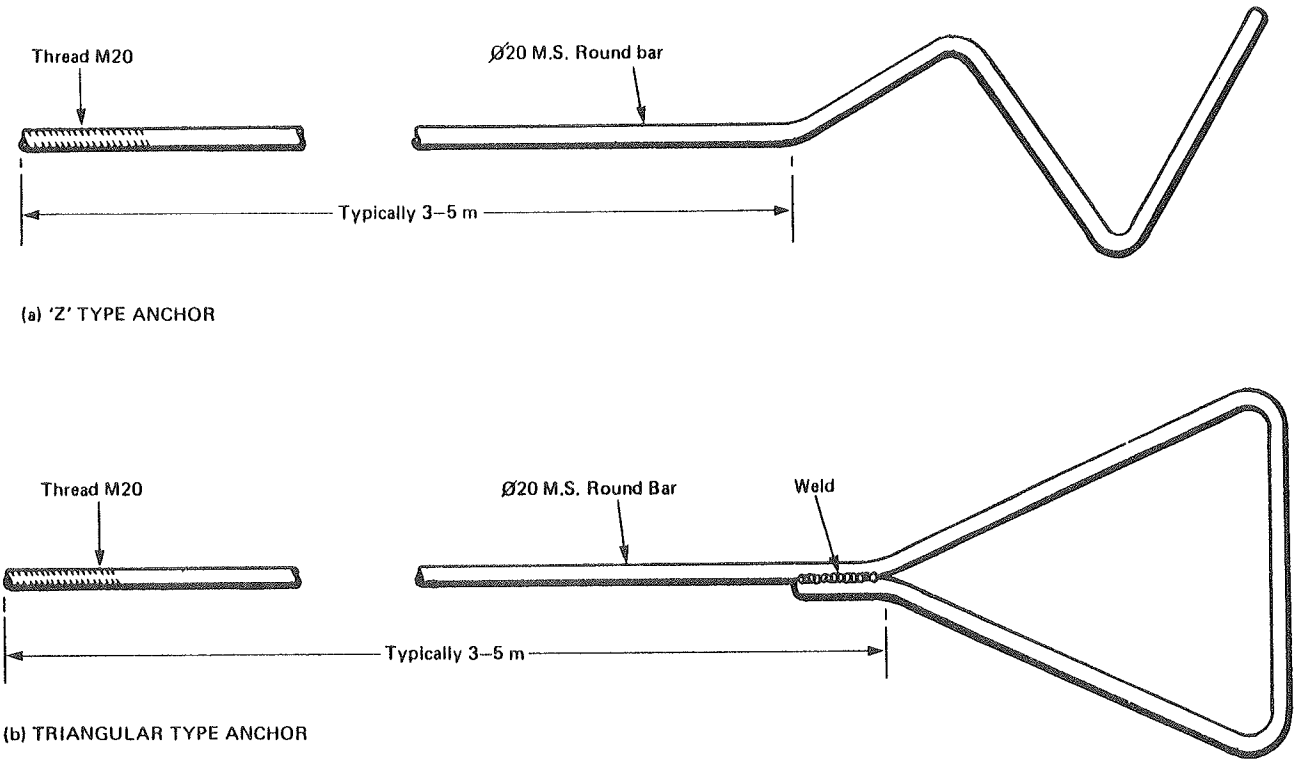

Figure B-25. Types of TRRL anchors. [Murray and Irwin, 1981b]

Anchored Earth, like other reinforcement methods depending primarily on passive resistance, is likely to be more efficient in cohesive soils than methods that rely predominantly on friction.

Finally, the anchors can be shorter than equivalent frictional flat strips because the zone in which the anchor force is developed is small relative to the zone required to develop frictional resistance on, for instance, the strips in Reinforced Earth. Hence, the anchor need not extend as far behind potential failure surfaces as a reinforcement strip.

2.2 Routine and Special Applications

Because Anchored Earth is a system in its early stages of research and development, none of its applications can be considered as routine. However, with continued development and use in practice, the system will probably find applications similar to those of other reinforcement systems. It is likely that Anchored Earth will prove especially beneficial in areas where clean granular backfill is not readily available.

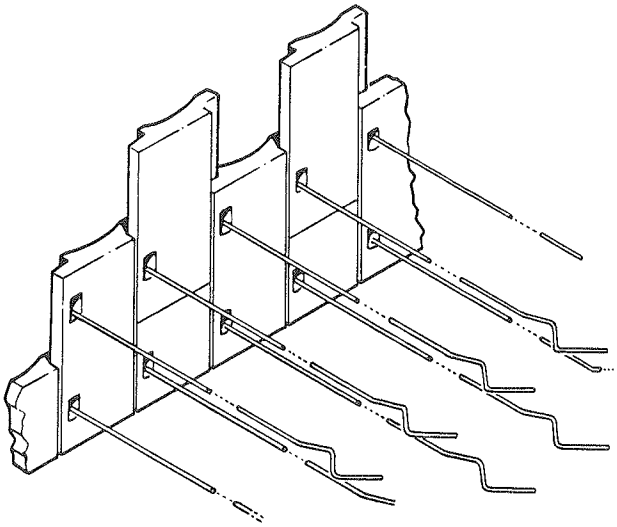

Figure B-26. Schematic arrangement of TRRL Anchored Earth System. [Murray and Irwin, 1981b]

3. MECHANISMS AND BEHAVIOR

In common with other soil reinforcement types, Anchored Earth resists the horizontal pressure from a mass of earth by imparting tension along the reinforcing members. In Anchored Earth, load transfer is presumed to be developed mainly through passive resistance between the soil and bent anchor surfaces.

The published experimental work on Anchored Earth to date has concentrated on obtaining relative performance data between anchors and reinforcing strips rather than obtaining detailed information on Anchored Earth behavior. Small-scale and full-scale pullout tests have been performed on Anchored Earth models and composite materials and the results of these tests compared with data from similar tests on equivalent Reinforced

Earth systems. Nearly all these tests were conducted at the government Transport and Road Research Laboratory, Crowthorne, in the United Kingdom.

3.1 Laboratory Pullout Tests—Analysis for Pullout Resistance

To evaluate pullout resistance, model plane reinforcing strips and anchors were tested in a specially constructed apparatus, schematically shown in Figure B-27 [Murray, 1983 and Murray and Irwin, 1981b].

Two types of dry sand were used in the tests. The sand was placed and compacted in thin layers, the reinforcing member placed, and filling with sand continued until the container was full. A normal confining load was applied to the sand, and pullout load on the reinforcing element was increased in increments until failure.

Model anchors were formed from 0.09-in. (2.3-mm) diameter mild steel rods, while model strips were made from thin brass of 0.002 in. (0.05 mm) thickness and 1.0 in. (2.5 cm) width.

The relationships between pullout force and applied normal stress for model anchors and strips are shown in Figure B-28. The pullout resistance of the anchors in the two sands is very similar and is higher than the pullout resistance of strip reinforcements for the investigated confining stress range.

At present, no definitive procedures are available for predicting the performance of anchor elements. (This is the case for soil anchors in general, because although a great deal of research effort has been applied over many years to anchor behavior, the methods available have not always proven to be reliable.) However, a functional relation incorporating the principal factors governing pullout capacity of an anchor can be developed: Pullout resistance = f(area, width, thickness, shape and stiffness of the reinforcement, the internal angle of friction of the soil, and the soil normal pressure).

An analytical approach based on the failure mode and zone shown in Figure B-29 has been developed by Murray [1983] to describe pullout resistance.

The radius of the logarithmic spiral defining the boundary slip field, R, is determined as follows:

$$R = R_o \exp(\theta \tan \phi') \tag{B-17}$$

where R_o = length of one side of the triangle defining an anchor element, and θ = subtended angle as shown on Figure B-29.

From geometry (Fig. B-29):

$$R_o = w/(2 \cos \alpha_1) \tag{B-18}$$

where w is the base width of a triangular element.

$$R = \frac{w}{2 \cos \alpha_1} \cdot \exp(\theta \tan \phi') \tag{B-19}$$

$$R_f = \frac{w}{2 \cos \alpha_1} \cdot \exp[(\pi - \alpha_1) \tan \phi'] \tag{B-20}$$

where α_1 = the angle measured from the base of the isoceles

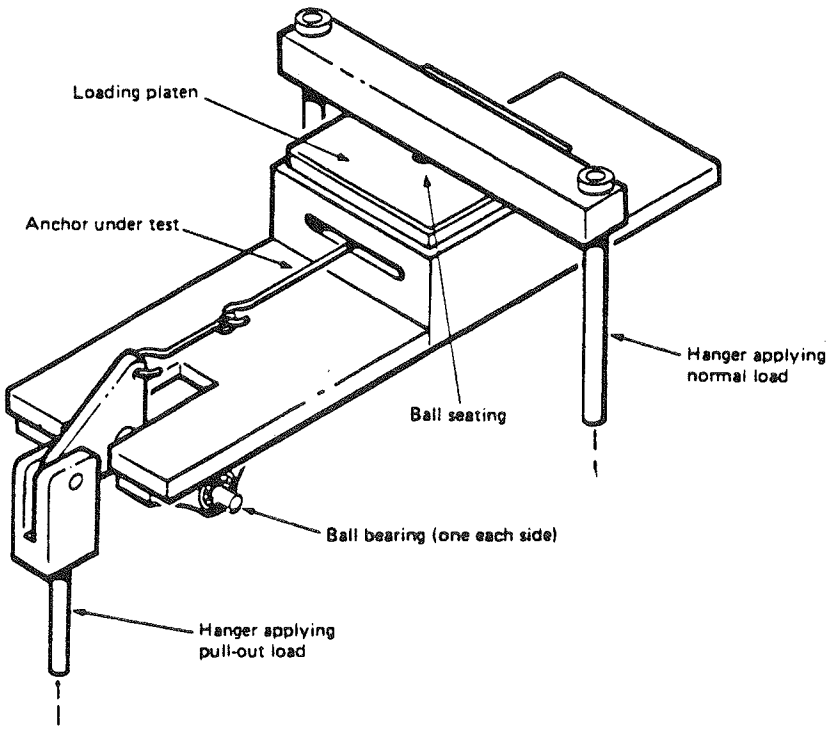

Figure B-27. Apparatus used for laboratory pullout tests. [Murray and Irwin, 1981b]

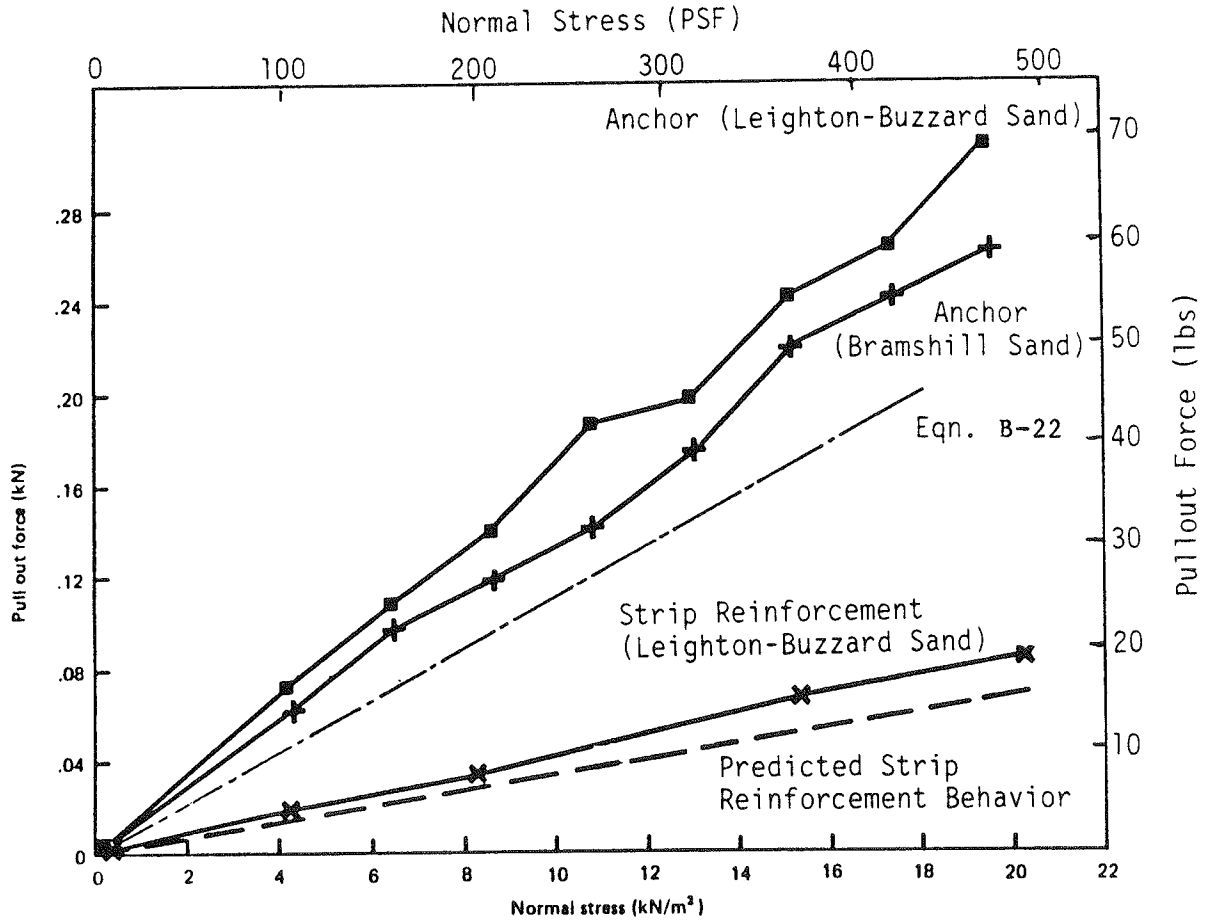

Figure B-28. Results of laboratory pullout tests on both anchors and reinforcing elements. [Murray, 1983]

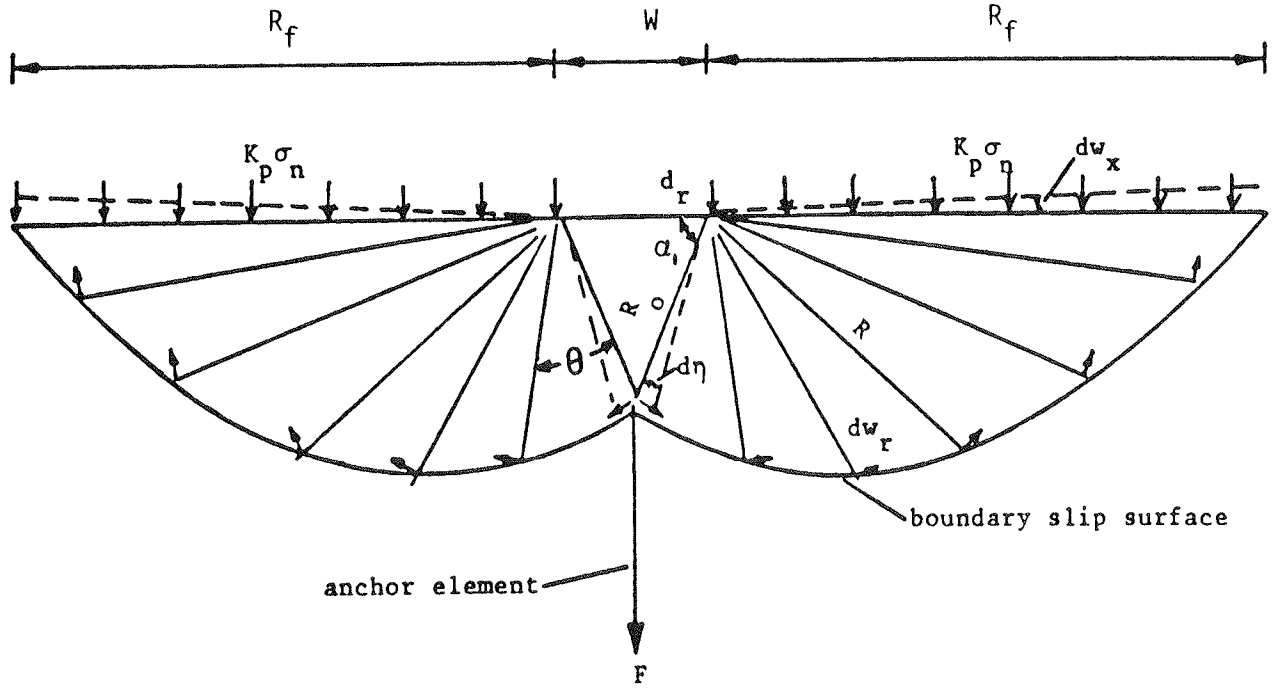

Figure B-29. Geometry assumed in analysis of anchor pullout. [Murray, 1983]

triangle, defining the plan area of the anchor, to one of the equal side legs; and R_f = final radius of the logarithmic spiral defining the boundary slip field.

Assuming that gravity forces can be ignored because the element is in a uniform vertical stress field, and using a virtual work derivation, Murray [1983] showed that anchor pullout force, P, may be written as:

$$P = \frac{K_p \sigma_v' \, w \, t}{\cos \alpha_1} \cdot [\exp 2(\pi - \alpha_1) \tan \phi'] \quad \text{(B-21)}$$

Using Eq. B-25 and the following parameters,
$\alpha_1 = 70$; 1.2 radians
$w = 1.51$ in. (4 cm)
$t = 0.09$ in. (2.3 mm)
$\phi' = 33°$
$K_p = 3.36$

we can calculate the relation between pullout force and normal stress presented in Figure B-28. Calculated pullout resistances appear to underestimate the measured values. An alternative, simpler analysis for anchor pullout capacity has been presented by Jones et al. [1985]. They consider two possible mechanisms of soil flow around an embedded anchor during pullout, as shown in Figure B-30.

In the first case (Fig. B-30a), the pullout force is mobilized by the soil bearing pressures on the anchor bar. The pullout force may be calculated in terms of the surface area of the anchor on which bearing develops, A_b, and the bearing pressure, σ_b, thus

$$P = \sigma_b \cdot A_b \quad \text{(B-22)}$$

For the case of the triangular anchor

$$P = \sigma_b \cdot 2wt \quad \text{(B-23)}$$

where t is the thickness of the anchor element.

To express bearing stress as a fraction of the vertical effective stress, σ_v', Jones et al. [1985] suggest the value,

$$\sigma_b = 4K_p \sigma_v' \quad \text{(B-24)}$$

where K_p is the coefficient of passive earth pressure.

This gives a pullout force:

$$P = (4 \, K_p \sigma_v') \cdot (2wt) = 8wt \, K_p \sigma_v' \quad \text{(B-25)}$$

The alternative mechanism of soil flow during pullout, shown in Figure B-30b, considers the soil contained by the triangular anchor to be fixed. Thus the surface area of the anchor for bearing is reduced, and an additional frictional component of resistance to pullout is added, Figure B-30b. The pullout resistance may be expressed

$$P = \sigma_b \cdot wt + \sigma_v \cdot \tan \phi \cdot 2A_{TR} \quad \text{(B-26)}$$

where A_{TR} is the plan area of the triangular region of the anchor element.

The lower value of pullout resistance calculated from Eqs. B-25 and B-26 should be used for design.

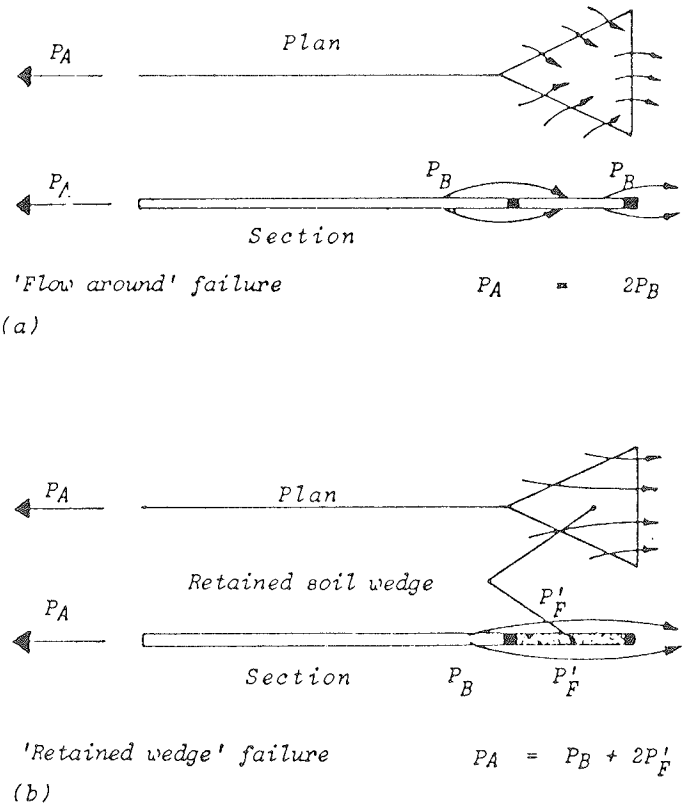

Figure B-30. Flow of soil around a triangular anchor for pullout. [Jones et al., 1985]

3.2 Model Studies

Model tests described by Murray and Irwin [1981b] were performed in specially constructed apparatus to compare the pullout resistance of Anchored Earth and Reinforced Earth. Each model wall was essentially cubical, with dimensions of 3.3 ft and precautions were taken during the tests to minimize boundary effects.

The anchors or strip reinforcements were connected to identical facing with a pin arrangement. Horizontal spacing between elements was 2.4 in. (6 cm) for both types of element. The anchors were manufactured from 0.09-in. (2.3-mm) diameter rod deformed to the same anchor dimensions used in the laboratory pullout tests. The effective length of the anchor after fabrication was 1.18 ft (0.36 m). The strip reinforcements were made from the thin brass shim also employed in the laboratory tests. Their overall length was 1.3 ft (0.4 m) and width was 0.39 in. (1 cm).

Both models were constructed to a height of 2.8 ft. A strip load, 4 in. (10 cm) wide, was applied to each model in increments at a distance of 1.0 ft (0.3 m) behind the face to induce a pullout-type failure.

Pullout failure of the Reinforced Earth model occurred when it was subjected to a strip load of 27 lb/ft (390 N/m). The Anchored Earth strip load was increased to 116 lb/ft (1,690 N/

m); because there was still no evidence of imminent failure, the strip load was removed. This model was then reloaded with the strip load positioned at a distance of 0.8 ft (0.25 m) from the face, and the test was terminated when the applied load reached 170 lb/ft (2,470 N/m).

The strip load was then relocated with its center at a distance of 1.4 ft (0.42 m) from the face. This load was applied slightly behind the anchors, at the location where it had been calculated that a Coulomb type failure wedge would emerge at the surface. The model failed when the strip load reached 69 lb/ft (1,006 N/m).

The results of the foregoing tests are given in Table B-2 [Murray and Irwin, 1981b]:

The Anchored Earth model thus exhibited greater capability of resisting concentrated strip loads than the strip reinforcement system. Pullout failure for the Anchored Earth model was not induced with the strip load located above the anchored region, and loading could presumably have continued until the rods failed in tension. The collapse that ultimately did occur was probably a consequence of a failure surface forming behind the upper anchors and propagating downwards and outwards.

Further tests were conducted to evaluate if the reinforcement stiffness was a major contributor to the observed differences in behavior of the strip reinforcements and the Anchored Earth elements [Murray, 1983]. When the thickness of the strips was increased to 0.07 in., rather than the 0.002 in. of the first test series, behavior of the Anchored Earth and strip reinforcement systems was essentially identical. Thus, the stiffness of linear reinforcements can be an important factor in the ability of a reinforced mass to support external loads.

Table B-2. Summary of strip load tests on Reinforced Earth and Anchored Earth walls.

Type of model	Distance from face to center of strip load (feet)	Maximum applied strip load per foot (pounds per foot)	Condition of model
Earth Reinforcement system	1.0	27	Failure
Anchored Earth	1.0	116	No indication of imminent failure
Anchored Earth	0.8	170	No indication of imminent failure
Anchored Earth	1.4	69	Failure

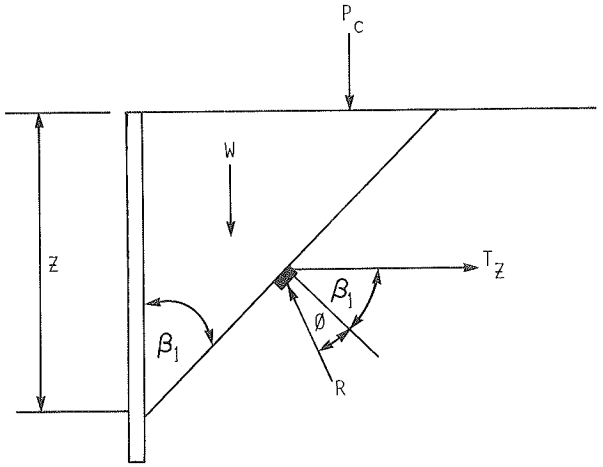

(a) Schematic Illustration of Forces on Wedge

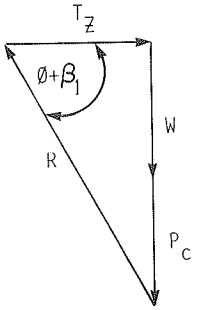

For Unit Width:

$W=\frac{1}{2}\gamma Z^2\tan\beta_1$

For Equilibrium:

$T_Z\tan(\emptyset+\beta_1)=W+P_C$

$\therefore P_C=T_Z\tan(\emptyset+\beta_1)-\frac{1}{2}\gamma Z^2\tan\beta_1$

(b) Polygon of Forces

Figure B-31. Schematic illustration of collapse force computation.

3.3 Computation of Collapse Load

Assuming that strip loading of an Anchored Earth wall will induce a wedge-shaped failure (Fig. B-31a) and using a polygon of forces to compute the collapse load (Fig. B-31b), it can be shown that:

$$P_c = (T_Z \tan(\phi + \beta_1) - \tfrac{1}{2}\gamma Z^2 \tan\beta_1) \quad \text{(B-27)}$$

where P_c = collapse strip load per unit width; T_Z = the total pullout resistance for the anchors at wall depth Z; and β_1 = inclination of failure plane relative to vertical.

Provided any increase in pullout resistance caused by the presence of the strip load is ignored, T_Z can be obtained by summing all of the individual anchor pullout resistances. According to the analysis by Murray [1983], with closely spaced anchor elements Eq. B-21 cannot be fully satisfied because of interference from adjacent elements (Fig. B-32). The minimum boundary of the slip field (with maximum interference from adjacent anchors) will be $\pi/2$, while the maximum will be π as defined by Eq. B-21. Clearly the actual boundary to the slip field will be somewhere between these limits, and it will depend on the spacing between anchors. Assuming the boundary is midway between the above two (i.e., at 3 $\pi/4$), the equation for the resistance offered by a single element at any depth within the reinforced earth mass, P_Z, may be derived by substituting $3\pi/4$ for π in Eq. B-21 as follows:

$$P_Z = \frac{K_p \gamma Z\, wt}{\cos\alpha_1} \exp\left[2\left(\frac{3\pi}{4} - \alpha_1\right)\tan\phi'\right] \quad \text{(B-28)}$$

The total resistance per unit width of Anchored Earth to a depth Z is obtained by summing the resistances given by Eq. B-28, for those elements which extend beyond the slip plane:

$$T_Z = \frac{(N_Z)(N_Z + 1)(S_v \times K_p \times \gamma \times w \times t)}{2 \times S_H \times \cos\alpha_1} \exp\left[2\left(\frac{3\pi}{4} - \alpha_1\right)\tan\phi'\right] \quad \text{(B-29)}$$

where N_Z = the number of layers of reinforcing elements in a

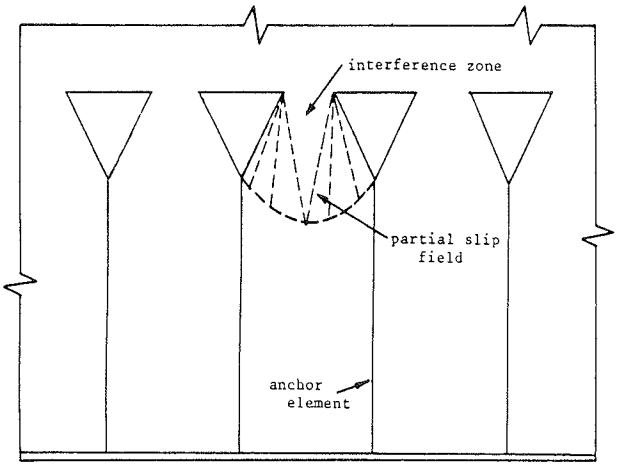

Figure B-32. Interference between closely spaced anchor elements. [Murray, 1983]

vertical profile to depth Z; S_v = vertical spacing of reinforcing elements; and S_H = horizontal spacing of reinforcing elements.

The term $(N_Z + 1)\, S_v/2$ is the average value of Z for anchors at uniform vertical spacing.

For a wall of height H, subjected to a collapse strip load P_c, the most critical wedge will pass through the bottom of the wall. This can be inferred by studying the polygon of forces on Figure B-31 and Eqs. B-27 and B-28: the reinforcing force T_Z increases linearly with depth, while the weight of the failing wedge increases with the square of depth.

Thus Eq. B-27 can be rewritten as:

$$P_c = T_H \tan(\phi + \beta_1) - \tfrac{1}{2}\gamma H^2 \tan \beta_1 \qquad \text{(B-30)}$$

Using Eq. B-30 and assuming the β_1 angle to be $45° - \phi'/2$. The collapse load for the model described in Section 3.2 of this chapter can be computed as 183 lb/ft [Murray, 1983]. Because this value exceeds the 170 lb/ft reached in the model tests without failure, a comparison of computed and observed failure loads is not possible.

From Eqs. B-21 and B-28 it is clear that the efficiency of Anchored Earth would be improved if the elements were arranged to permit the maximum possible size of slip field to develop. This can be accomplished by increasing horizontal spacing and reducing vertical spacing for a given number of elements. It would also theoretically be advantageous to stagger the elements between alternate layers such that they were more uniformly spread through the fill, but this may entail construction difficulties.

3.4 Full-Scale Pullout Tests

Full-scale pullout tests were performed [Murray, 1983] with Z and triangular-type anchors as well as galvanized mild steel reinforcements embedded in Bramshill sand. The dimensions of the anchor elements, as shown in Figure B-33, were about 9 ft long, 1.3 ft wide, and 0.63 and 0.79 in. diameter. The smooth galvanized strips were of the same length, 2 to 4 in. wide and 0.1 in. thick. Confining stress was applied to simulate up to about 8 ft (2.5 m) of fill on the reinforcing elements. Two dial gauges were mounted to monitor movement of the elements during and after application of incremental loads.

Typical obtained load versus deflection relations for the Z-type anchors for both 16-mm and 20-mm (0.63-in. and 0.79-in.) diameter bars are shown in Figure B-34 together with the results for a strip reinforcing element, while pullout force is shown as a function of confining stress in Figure B-35. As shown

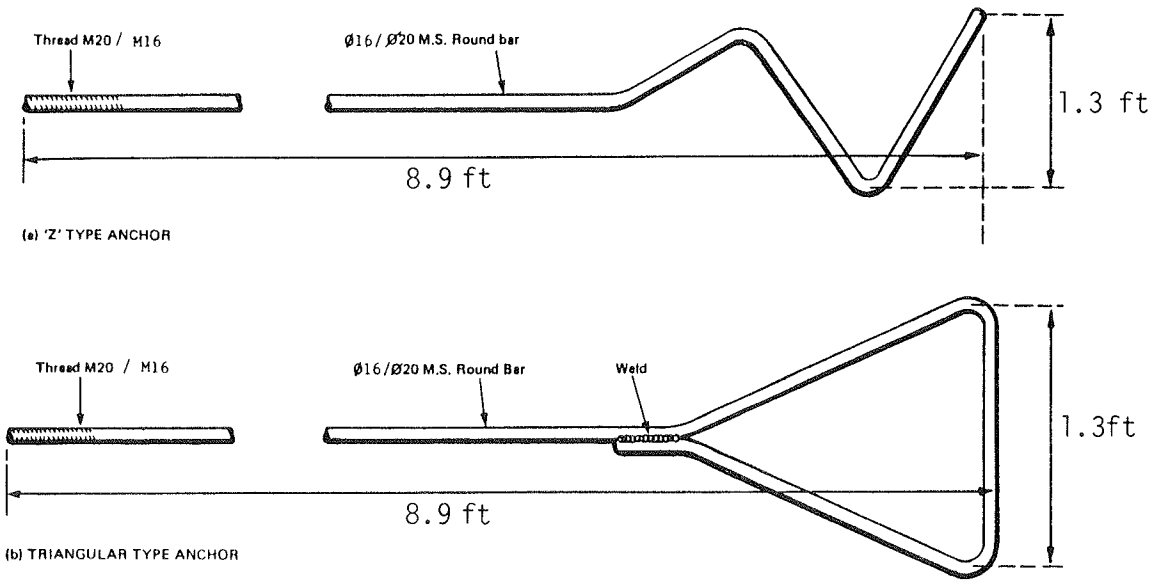

Figure B-33. Types of TRRL anchors used in study. [Murray, 1983]

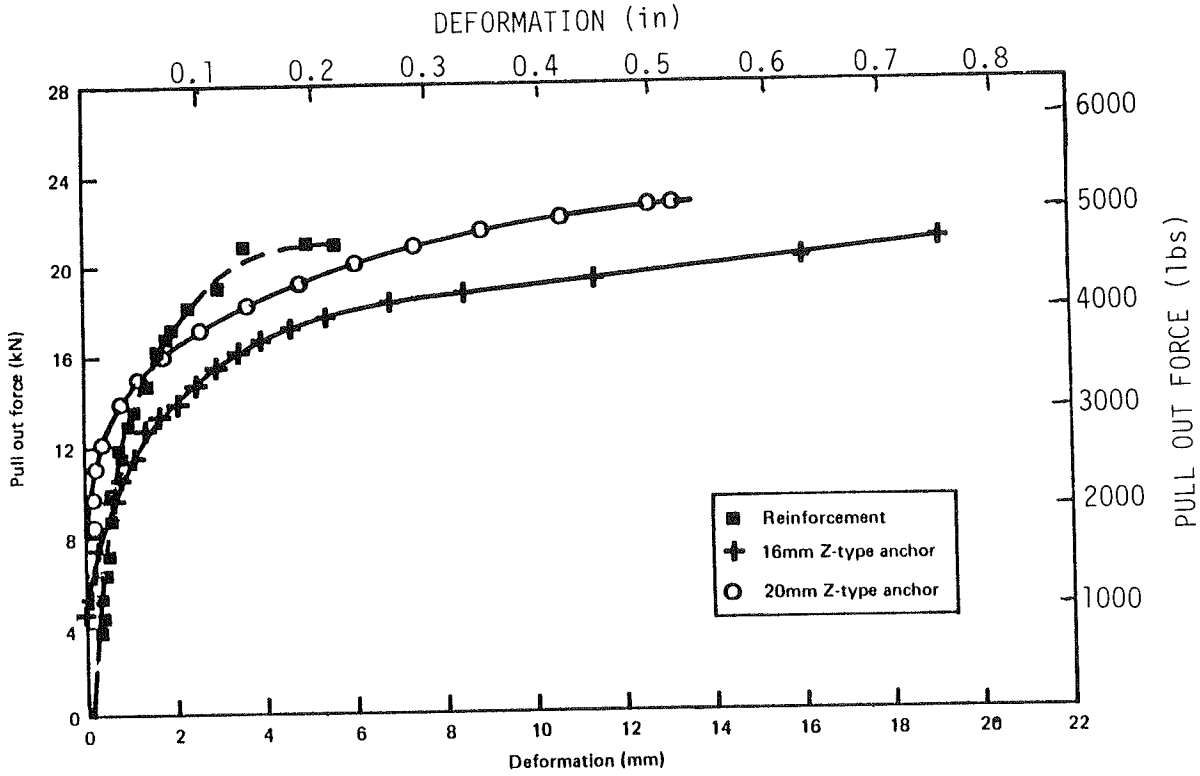

Figure B-34. Relations between pullout force and deformation for anchor and reinforcing elements in full-scale tests. [Murray, 1983]

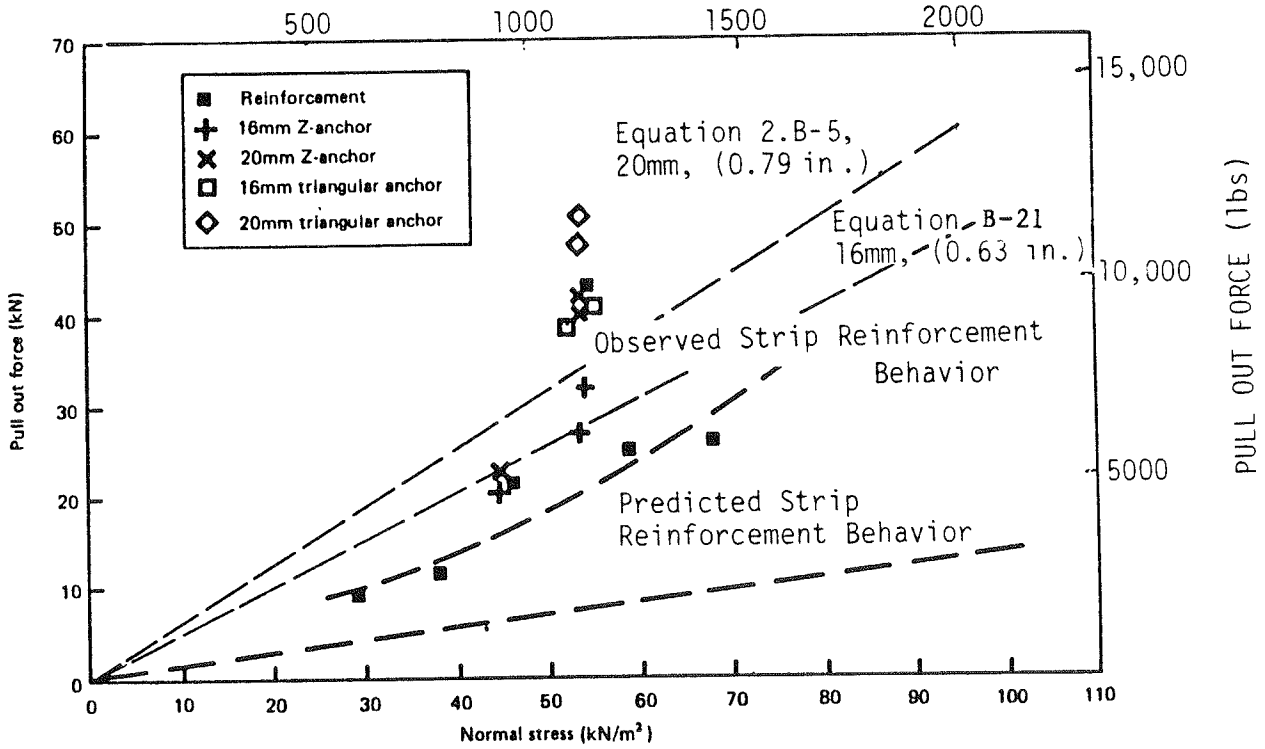

Figure B-35. Overall results of full-scale tests on anchors and reinforcing elements. [Murray, 1983]

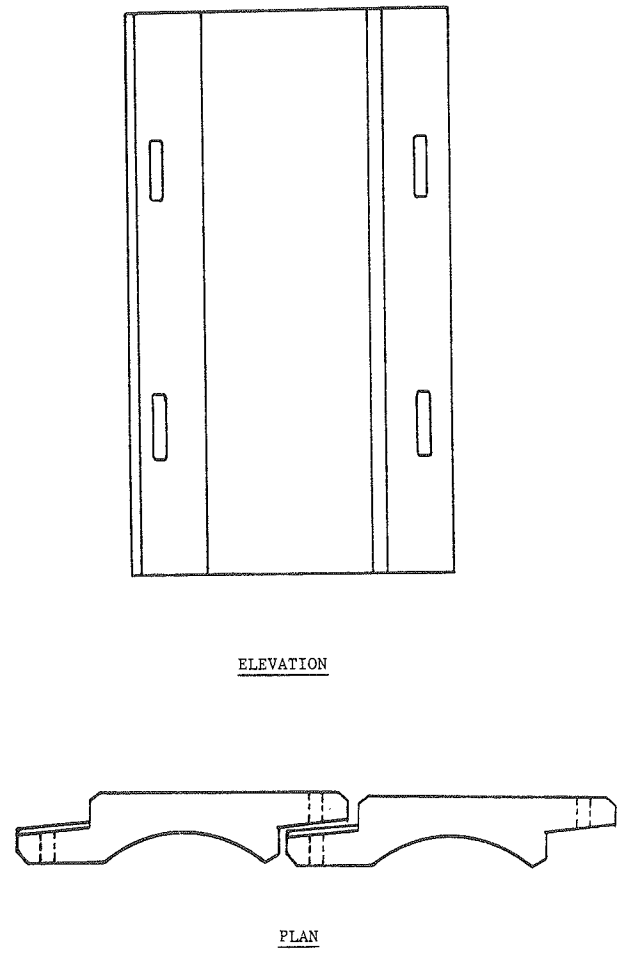

Figure B-36. Details of facing unit.

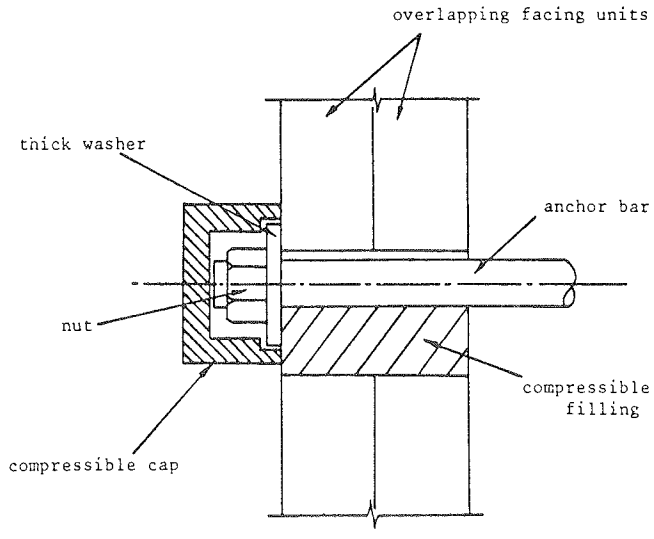

Figure B-37. Details of anchor/facing connection.

in Figure B-34, the anchors exhibit a similar form of deformation versus force relation at pullout to that obtained for the reinforcing elements, which implies that as the anchor reaches the limiting condition, soil at the failure state flows around the slip lines and the anchor moves forward into soil which has not yet failed.

Even with the relatively low values of normal stress which were applied, the pullout resistance of the triangular anchor of 0.79-in. diameter rod had already obtained the yield limit of the mild steel bar. The *Z*-type anchor produced lower values of resistance. However, even for the *Z* anchors, pullout resistance was sufficient that 0.79-in. diameter anchors could be spaced at 3.3 ft both vertically and horizontally in a 33-ft high wall. This suggests that a very economical design would be feasible. The reinforcing elements also provided good resistance in pullout and, as indicated in Figure B-35, reached values twice those estimated from shear box tests assuming zero dilatancy.

Pullout resistances predicted with Eq. B-21 are also shown in Figure B-35. The predicted values agree well with, or underestimate, the results obtained for both sizes of triangular element. However, the prediction overestimates the resistances for the *Z* anchors, and the equation would therefore require some modification prior to its application for design computations. On the basis of the limited data currently available, a simple procedure would seem to be to assume that deformation of the anchor zone would reduce the size of the slip field and that Eq. B-28 rather than Eq. B-21 applies.

4. TECHNOLOGY—DESCRIPTION OF ANCHORED EARTH COMPONENTS

4.1 Anchors

The anchors are formed from mild steel bars of 0.6 to 0.8 in. (15 to 20 mm) diameter having a screw threaded portion at one end. The anchor length could be sized according to specific project requirements. Of the two anchor types shown in Figure B-25, the simplest is the *Z*-type, where a double reverse bend is formed over a short length. The triangular type of reinforcement incorporates a short length of weld to prevent the anchor from being distorted when subjected to a pullout force. The latter is likely to be more expensive to produce, but its greater pullout resistance as determined from the preliminary tests (Section 3 of this chapter) may compensate for the additional cost (see Section 3).

4.2 Facing Panels

The facing elements for Anchored Earth are rectangular precast reinforced concrete panels (see Fig. B-36). Adjacent panels are overlapped at the edges, as shown in Figure B-36.

4.3 Anchor and Facing Connections

The anchors are fastened to the facing units by passing the threaded end of the anchor rods through slots in adjoining facing units (see Fig. B-37). The protruding rods and attached nuts can be housed in recesses cast in the facing panels, which are then capped to provide a flush appearance. Because of the bolt connection, misalignment or slack of the facing units during

construction can be corrected, provided such correction does not overstress the anchors.

By virtue of the slotted connections between facings, some relative movement between adjacent units can be accommodated. In addition, some differential settlements can be accommodated without creating undue stress in the system, because relative movement can occur between the anchors and the facing.

The reduction in cross-sectional area of an anchor because of threading for the bolt connection is about 15 percent.

5. DURABILITY AND SELECTION OF BACKFILL

5.1 Durability Considerations

Within the Anchored Earth system, the components most susceptible to degradation are the steel anchors themselves and their metallic fastenings. As with other metallic reinforcements, the anchors are subject to electrochemical corrosion as described in detail in Chapter Six of the main report. Galvanizing can be employed to initially retard corrosion of the steel.

Triangular-type anchors (Fig. B-25) when manufactured from pregalvanized steel may be particularly subject to corrosion because of the short length of weld used. Some special protection, such as coating, may be needed, or the anchor could be galvanized after bending and welding.

In Chapter Six of the main report, methods for predicting the rate of corrosion of metallic reinforcements are presented for other systems with metal components. Similar concepts may be applicable for Anchored Earth, but remain to be further investigated. To date, there has not been developed a specific method for the prediction of corrosion of Anchored Earth elements.

5.2 Selection of Backfill

Because Anchored Earth is in its experimental stages, and only one full-sized reinforced soil structure has been constructed to date, proven specifications for backfill material do not yet exist. As more experience is gained, optimal backfill characteristics for use with Anchored Earth will probably be developed. Backfill specifications used for reinforcement systems that have been further developed (e.g., Reinforced Earth, VSL Retained Earth) can be used as a guide for selecting backfill for Anchored Earth until more experience with the system is gained.

6. CONSTRUCTION

No detailed construction procedures for Anchored Earth exist at present. However, as actual structures are built with Anchored Earth, standard procedures and construction details will no doubt be developed. Many of the construction details used for other earth reinforcement systems—as described in the other method-specific appendixes—would be applicable to Anchored Earth.

The European Patent Application for Anchored Earth describes a construction sequence including the following details.

The facing units are set on a strip footing of concrete to provide initial support and leveling. For the first course, alternating half height panels are interposed between normal height panels to provide a castellated profile. The facing panels should initially be supported by props or other suitable means.

A layer of earth fill is placed behind the flat faces of the facing units and compacted up to the level of the lower row of slots.

Anchors are laid flat on the surface of the layer of fill and their respective screw-threaded ends are passed through the aligned slots in the overlapping spurs of the facing units, after which a nut is attached.

Normal height facing units are next placed on top of the half height ones, after which a further layer of earth fill is placed on the first layer of anchors and compacted up to the level of the second row of slots.

The process is repeated until the design wall height is reached. Half height facing panels are, of course, required at the top to level the wall.

It is desirable that the slots be closed off to prevent migration of water or backfill. This may be by the use of foam rubber or polystyrene inserts, by shield-plates carried by the anchors, or other suitable means. It is also desirable to place compressible joining material between the facing units to prevent damage during construction, increase flexibility, and to reduce water leakage. Foam rubber, bitumen-impregnated tape or other similar treatment can be applied on the surface of the half lap joints between facing units to provide an effective sealing medium.

7. DESIGN METHODS

Anchored Earth walls have been designed in accordance with the U.K. Department of Transport Design Memorandum for Reinforced Earth Walls [Jones et al., 1985]. The main elements of these rules are summarized below.

7.1 External Stability

The external stability assessment for an Anchored Earth retaining wall is the same as that for other reinforced soil systems. The reinforced soil system must be able to withstand the external loads, including the horizontal earth pressure from the soil being retained behind the reinforced soil mass and loads applied to the top of the wall without failure by: sliding along the base of the wall, overturning about the toe of the wall, bearing capacity failure of the foundation soil, or general slope instability.

7.2 Internal Analysis

The Tie Back Wedge design method as adopted by the Department of Transport in their *Technical Memorandum BE 3/78* can be used for the design of Anchored Earth retaining walls [Murray, 1981]. This method considers the stability of individual reinforcements and the ability of the sum of the reinforcements to prevent sliding wedge type failures within the reinforced soil mass.

7.2.1 Tension Failure

The maximum tensile force T_i to be resisted by the ith layer

of elements at a depth Z_i below the top of the wall may be obtained from the summation of the forces arising from the height of fill above the anchors and from externally applied loads. Mathematically this may be expressed as

$$T_i = T_{Zi} + T_{wi} + T_{Si} + T_{Fi} + T_{Mi} \qquad \text{(B-31)}$$

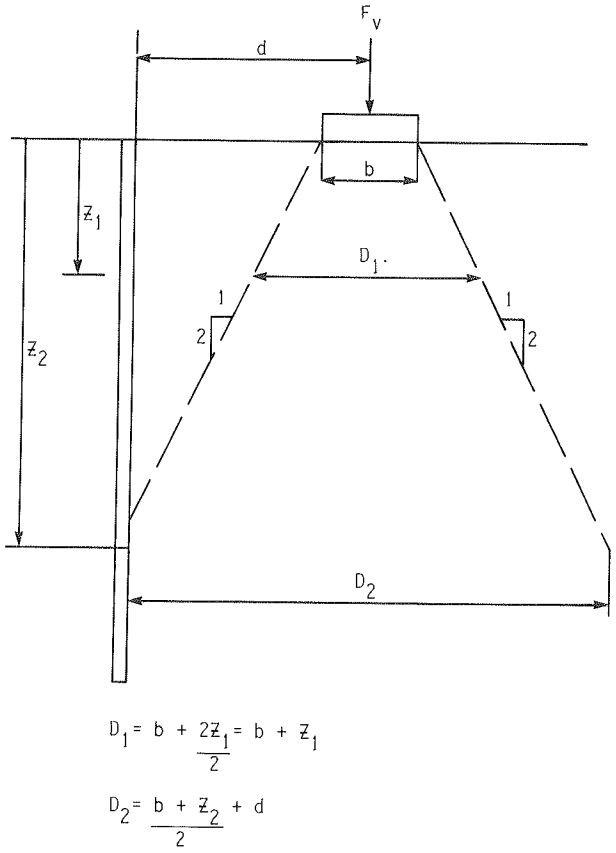

Figure B-38. Schematic illustration of vertical strip load dispersal.

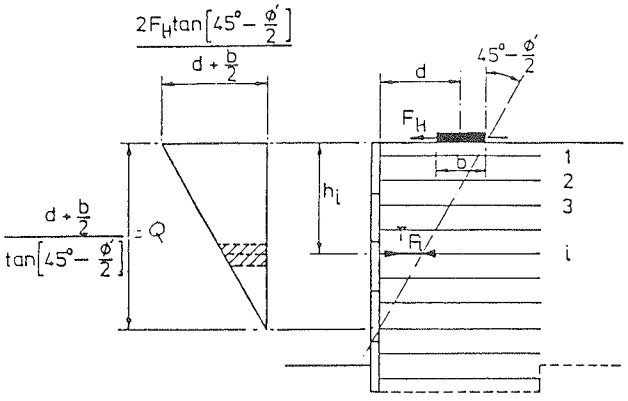

Figure B-39. Internal local stability—dispersal of horizontal shear through reinforced fill. [Department of Transport, 1978]

where T_{Zi} = tensile force derived from the height of reinforced fill above a layer of reinforcement; T_{wi} = tensile force derived from a uniform surcharge on top of the wall; T_{Si} = tensile force derived from a vertical strip load applied to the top of the wall; T_{Fi} = tensile force derived from a horizontal force applied to the top of the wall; and T_{Mi} = tensile force caused by external bending moments acting on the wall.

These tensile force components can be computed as follows:

1. Height of reinforced fill above the layer of elements. The tensile force caused by the height of fill above the anchors can be computed as:

$$T_{Zi} = [K_a \gamma Z_i - 2c' \sqrt{K_a}] S_v \qquad \text{(B-32)}$$

where K_a = coefficient of active earth pressure; Z_i = height of reinforced soil above the level of the ith layer of elements; and c' = effective cohesion of the soil.

2. Uniform surcharge on top of the wall. The tensile force caused by a uniformly distributed surcharge on top of the wall can be computed as:

$$T_{wi} = K_a W_s S_v \qquad \text{(B-33)}$$

where W_s = uniformly distributed surcharge on top of the wall.

3. Combined effect of height of fill and uniform surcharge. According to the British code, *Technical Memorandum BE 3/78,* the tension caused in the reinforcements by the combined effect of self-weight and uniform surcharge should never be less than $\gamma_{EF} S_v (Z_i + [W_s/\gamma])$ where γ_{EF} is the unit weight of an equivalent fluid with half the density of water.

4. Vertical strip load. If a vertical strip load of magnitude F_v is applied to a footing of width b at a distance d behind the wall facing (Fig. B-38), vertical load dispersion can be taken, similar to other soil reinforcement systems, at a slope of 2 vertical to 1 horizontal. The tensile force caused by the strip load can be computed as:

$$T_{Si} = K_a S_v \frac{F_v}{D_i} \left[1 + \frac{6e_1}{b^2}\right] \qquad \text{(B-34)}$$

where e_1 = eccentricity of a vertical strip load with respect to the center line of the contact area of the load on the top of the wall, and D_i = width over which line load F_v is dispersed at depth Z_i. From geometry (Fig. B-38):

$$D_i = (Z_i + b), \text{ if } Z_i \leq 2d - b \qquad \text{(B-35)}$$

$$D_i = d + \left[\frac{Z_i + b}{2}\right], \text{ if } Z_i > 2d - b \qquad \text{(B-36)}$$

Note: The second term in the square brackets both for T_{si} and D_i may be ignored when $Z_i > 2b$.

5. Horizontal strip load. If a horizontal force of magnitude F_H is applied to a strip contact area of width b on top of the wall at distance d behind the facing (Fig. B-39), dispersal of the horizontal load F_H, from the contact area on top of the wall, may be taken as shown in Figure B-39. The tensile force caused by the dispersed load may be computed as:

$$T_{Fi} = \frac{2S_v F_H}{Q}\left[1 - \frac{Z}{Q}\right] \tag{B-37}$$

where Q is the depth where the horizontal load is fully dispersed (Fig. B-39). This depth is computed as:

$$Q = \frac{d + \frac{b}{2}}{\tan\left(45° - \frac{\phi'}{2}\right)} \tag{B-38}$$

6. Overturning. The pressure of the soil behind the reinforced block causes overturning moments that increase the vertical stresses in the soil close to the face of the wall causing an additional tension,

$$T_{Mi} = \frac{6K_a S_v M_i}{L_i^2} \tag{B-39}$$

where L_i = length of reinforcement at the ith level, and M_i = bending moment about the center of the reinforcement at the ith level arising from the external horizontal force on the back of the reinforced mass per unit length of wall.

In a simple example of granular fill behind the reinforced zone and assuming a horizontal pressure equal to the active value acting at one-third of the wall height, the overturning moment would be $M = P_a H/3$.

7. Local stability requirements. Expressions for the ith layer cross-sectional area and anchor dimensions required to satisfy local stability requirements are given below:

$$a_{si} \geq \frac{T_i}{P_{at}} \tag{B-40}$$

$$P_{pullout}\, i \geq \frac{T_i}{2} \tag{B-41}$$

where a_{si} = total structural cross-sectional area parallel to the face of the wall, of the ith layer of reinforcing elements at the connection with the facing, per foot "run" of wall; P_{at} = basic permissible axial tensile stress on reinforcing elements; and $P_{pullout}$ = pullout resistance of anchors per lineal foot "run" of wall at the level considered.

Equation B-40 is a rupture criterion, while Eq. B-41 is a pullout criterion with a factor of safety of 2.

7.2.2 Forward Sliding of the Upper Portion of a Wall on Any Horizontal Plane

The British soil reinforcement specification (*Technical Memorandum BE 3/78*) specifies that a factor of safety of 2.0 should be used when analyzing sliding of an upper portion of a reinforced soil structure relative to a lower portion. In Anchored Earth, such sliding could occur either as fill sliding on fill within any layer or as fill sliding on reinforcing elements and fill.

7.2.3 Wedge Stability

Internal stability of Anchored Earth may be evaluated by analyzing the stability of a series of wedges as shown in Figure B-40 and finding the most critical wedge. To simplify the analysis, each wedge is assumed to behave as a rigid body, and friction between the facing and the fill is ignored.

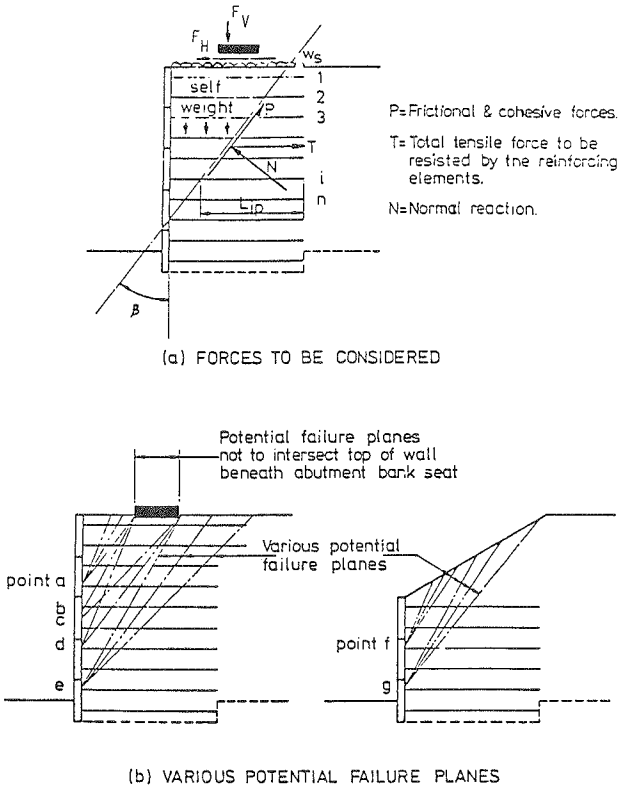

Figure B-40. Internal wedge stability. [Department of Transport, 1978]

Where applicable, the following loads and forces should be considered in the analysis (see Fig. B-40a): (1) self-weight of the fill in the wedge; (2) uniformly distributed surcharge, W_s; (3) vertical loading, F_V; (4) horizontal loading, F_H; (5) frictional and cohesive forces acting along the potential failure plane; and (6) the normal reaction on the potential failure plane.

For convenience, the wedges are normally selected so that they pass through an anchor element at the wall facing. The angle of the failure surface, β, with the wall facing is varied as shown in Figures B-40a and B-40b to find the maximum required anchoring force, T. The computed required anchoring force for each level of reinforcements should not exceed the pullout resistance of the elements anchoring the wedge. Equation B-29 may be used to compute the anchoring force. It should also be verified that the allowable stress in the anchor elements is not exceeded.

8. CASE HISTORIES

Following the results obtained from model studies and large-scale pullout tests, the Transport and Road Research Laboratory investigated the Anchored Earth system at full scale. This has led to the first engineering application of Anchored Earth—a retaining wall on the Otley By-Pass, England, designed by the West Yorkshire Metropolitan County Council. Because of the

relative lack of performance data, the full-scale pullout tests are also described as a case study.

8.1 Full-Scale Pullout Tests

Murray [1983] describes the experiment in detail. The structure's height and length were 10.5 ft (3.2 m), and 33 ft (10 m), respectively. A uniform surcharge was applied to simulate a 16-ft (5-m) equivalent height.

Both "Z"-type and triangular-type anchors were incorporated. The anchors were fabricated from 0.79-in. (20-mm) diameter mild steel rod of initial length 9.8 ft (3 m). The effective length was about 8.9 ft (2.7 m).

The reinforced concrete facing panels were 4.3 ft (1.3 m) high, 2.0 ft (0.6 m) wide, and nominally 4.7 in. (120 mm) thick. The vertical and horizontal spacings of slots, and therefore of anchor elements, were 25.6 in. (650 mm) and 23.6 in. (600 mm), respectively. The wall footing consisted of wooden railway ties bedded into the sand foundation.

The fill was Bramshill sand with an average dry unit weight of 119.3 lb per cu ft (18.74 kN/m^3) and an internal angle of friction ϕ' of 33 deg.

The wall was instrumented to record the movement of the facing, the applied load on the anchors, the tension in the anchors, and the horizontal pressure on the facing.

On completion of construction, a strip load was applied parallel to the facing at a distance of 3.3 ft (1 m) behind the wall. A maximum stress level of 820 psf (39.4 kN/m^2) was applied in four increments. A complete set of measurements was recorded after each increment of 1.4 lb per sq in. (9.84 kN/m^2) had been applied. The strip load was then removed, and a uniform surcharge was applied in four increments up to a maximum stress of 820 psf (39.4 kN/m^2). Again a complete set of measurements was taken after each increment.

Finally, tests were carried out to establish the limiting pullout resistance of each of the 20 anchors.

The vertical pressure distributions, as obtained by averaging the results from two profiles located near the base of the structure, at the end of construction and following the application of a uniform surcharge of 820 psf are shown in Figure B-41. The higher vertical pressures near the wall face indicate that the retained soil was exerting an overturning moment.

The recordings of horizontal pressure acting on the facing versus the depth of fill above the pressure cells are shown in Figure B-42. The highest horizontal pressure was reached with limited fill above the pressure cell. As the facing deflected, this pressure first decreased and then remained approximately constant even though a further 10 to 12 ft of fill was placed.

The average anchor tensions from both sets of anchors at a depth of 7.3 ft (2.4 m) are shown in Figure B-43 as a function of fill height above the anchors. Initially the anchor tension was

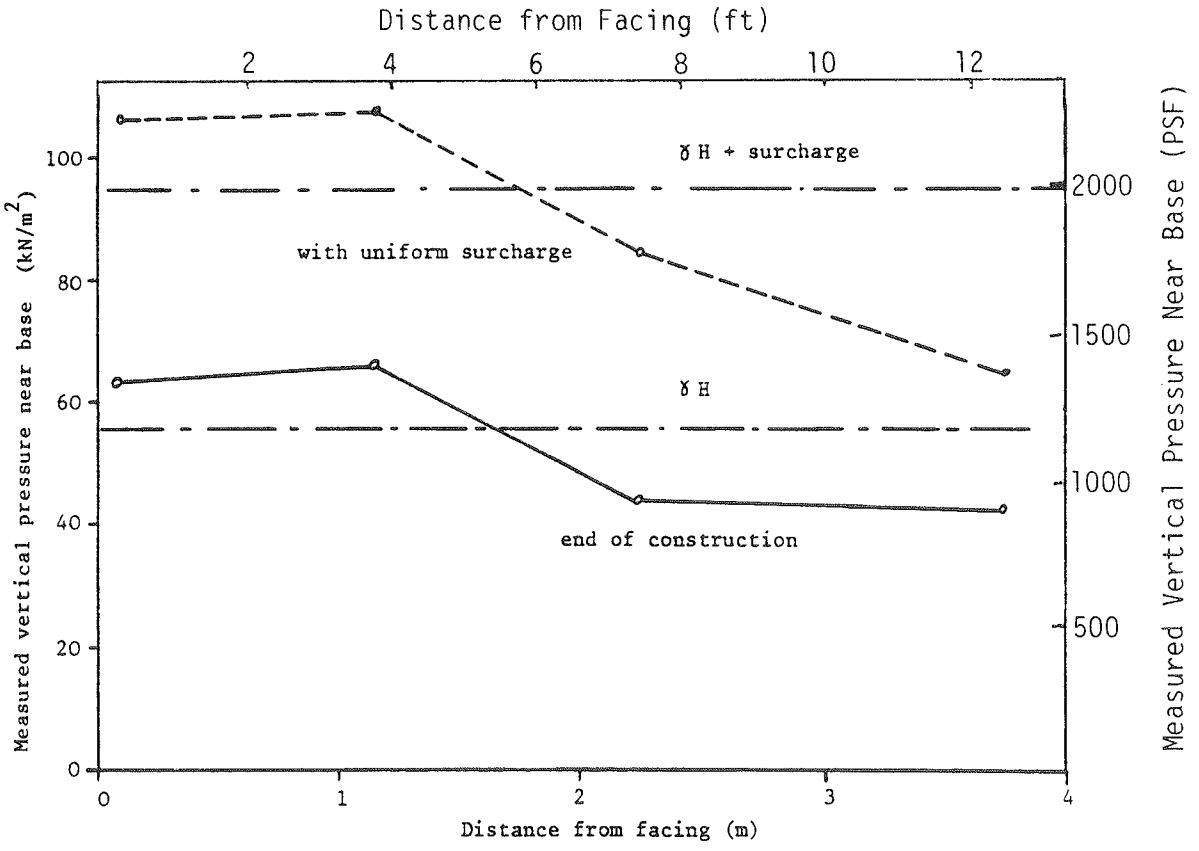

Figure B-41. Distributions of vertical pressure near base. [Murray, 1983]

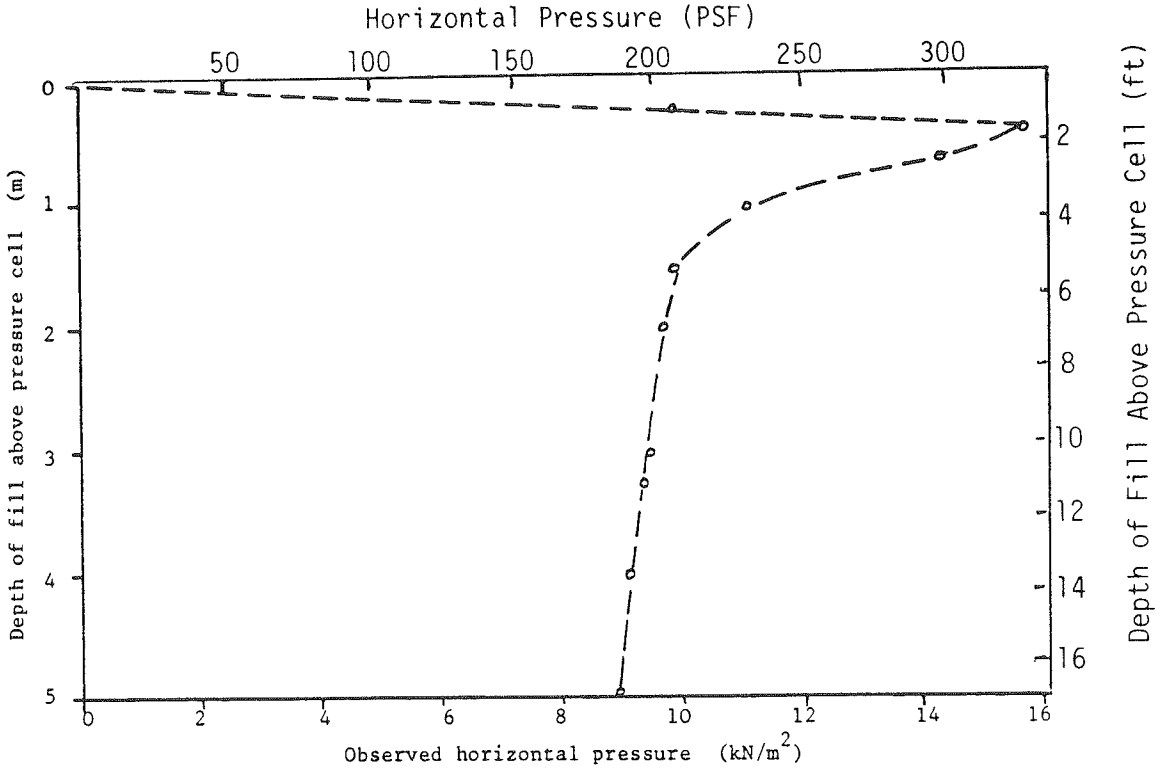

Figure B-42. Relation between depth of fill above pressure cell and horizontal pressure on facing. [Murray, 1983]

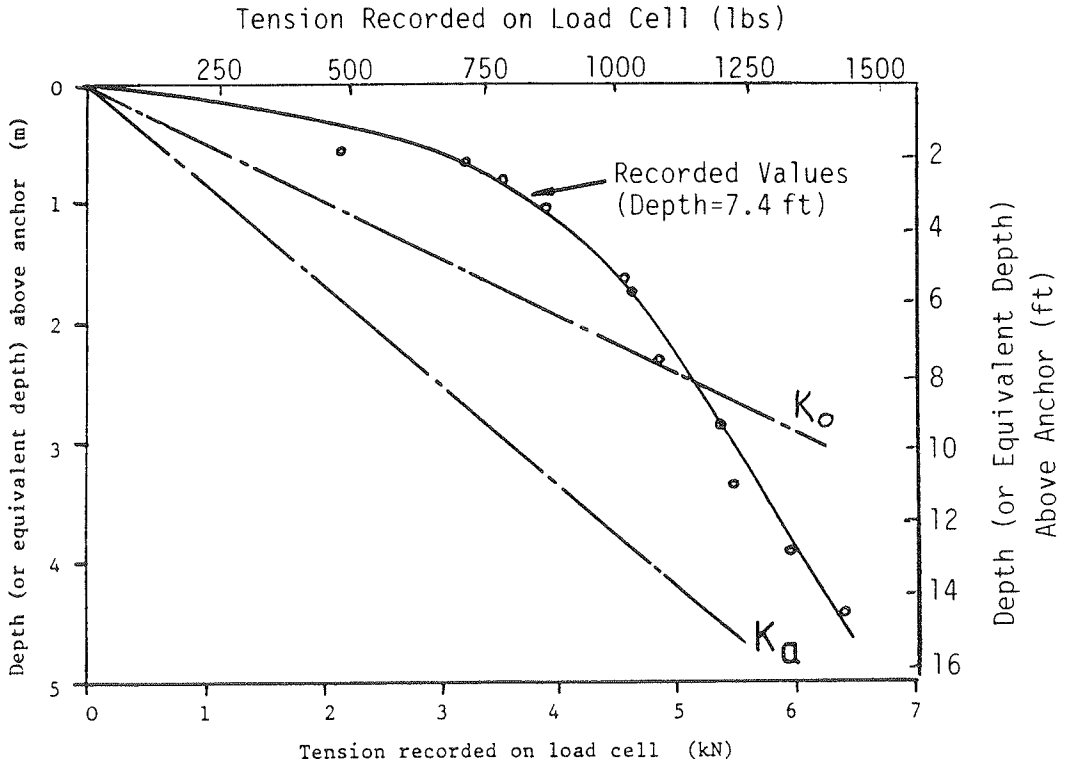

Figure B-43. Typical relations between depth of fill above anchor and measured tension. [Murray, 1983]

significantly greater than the K_o value, but as the depth of fill increased beyond about 3 ft (1 m) the lateral earth pressure coefficient reduced and approached the active value at an equivalent depth of about 16.4 ft (5 m).

The vertical profile of anchor tension at the end of construction is shown in Figure B-44. Each point is the average value of four cells at a particular depth. Tension distributions based on the at-rest and the active earth pressure conditions are also shown. The reductions of force in the elements near the base of the structure compared to elements higher in the wall are probably because the footing prevents sufficient movement near the base to allow full mobilization of anchor tension.

The variation of horizontal movement of the facing with depth at the end of construction is shown in Figure B-45. Greatest movements were noticed in the areas of the wall containing triangular elements. Peak movements of both anchor types occurred at a depth of 3.3 ft (1 m). The magnitude of movement was reasonably small, about ½ in., and an initial inward batter could be used during construction to obtain a vertical wall.

After construction of the test embankment was complete, pullout tests were conducted. Relations between pullout force and anchor movement are shown in Figure B-46. For both triangular and "Z"-type anchors the vertical stress acting was 1,250 psf (60 kN/m^2). The results indicate that greatest resistance was obtained from the triangular anchors but, at the ultimate condition, about twice as much movement occurred. Pullout resistance can be plotted as a function of anchor movement as shown in Figure B-47. This presentation of the data suggests that ultimate pullout force and the magnitude of anchor movement are related.

Assuming that the bent portions of the anchors were of the same dimensions as those used in the pullout tests described in Section 3.3 of this chapter (see Fig. B-33) and the same material properties cited for the laboratory tests with Bramshill sand ($\phi' = 33°$, $K_p = 3.36$), pullout resistances can be computed with Eq. B-21 and B-28. The computed pullout values are also shown in Figure B-46. Equation B-21 shows reasonable agreement with the values measured on the welded anchors, while Equation B-28 underpredicts the values measured on the "Z"-type anchors.

The results of all the pullout tests are summarized in Table B-3. The efficiency of an anchor is defined as the ratio of pullout resistance to ultimate tensile strength expressed as a percentage. Table B-3 indicates that the efficiency of the triangular anchors is quite high, and when pullout resistance is plotted as a function of confining stress (Fig. B-48) the data indicate that the welded triangular elements would be 100 percent efficient at an overburden pressure of 1,670 lb per sq ft (80 kN/m^2). This corresponds to about 14 ft of dry fill above the anchor. With extrapolation of the data it appears that about 25 ft (7.5 m) of fill would be needed for a "Z"-type anchor to achieve 100 percent efficiency. For greater depths of fill, the ultimate load capacity of anchors would be determined by their tensile strength, in

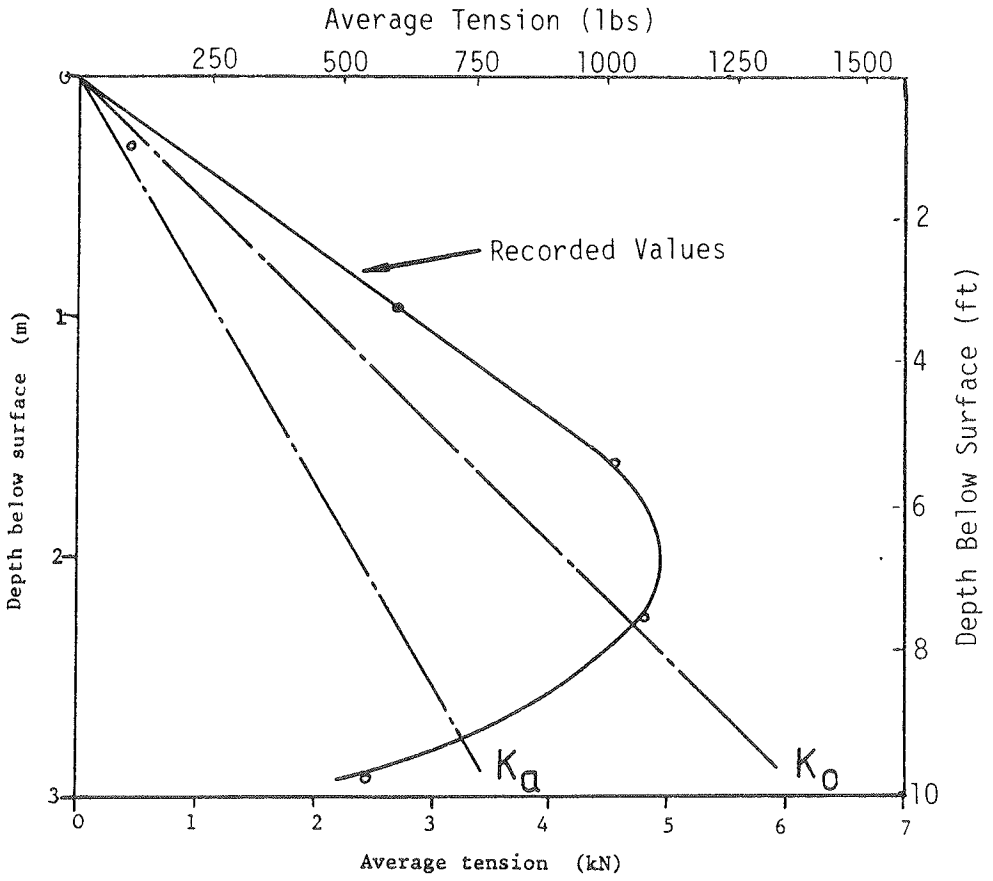

Figure B-44. Vertical distribution of average anchor tension at end of construction. [Murray, 1983]

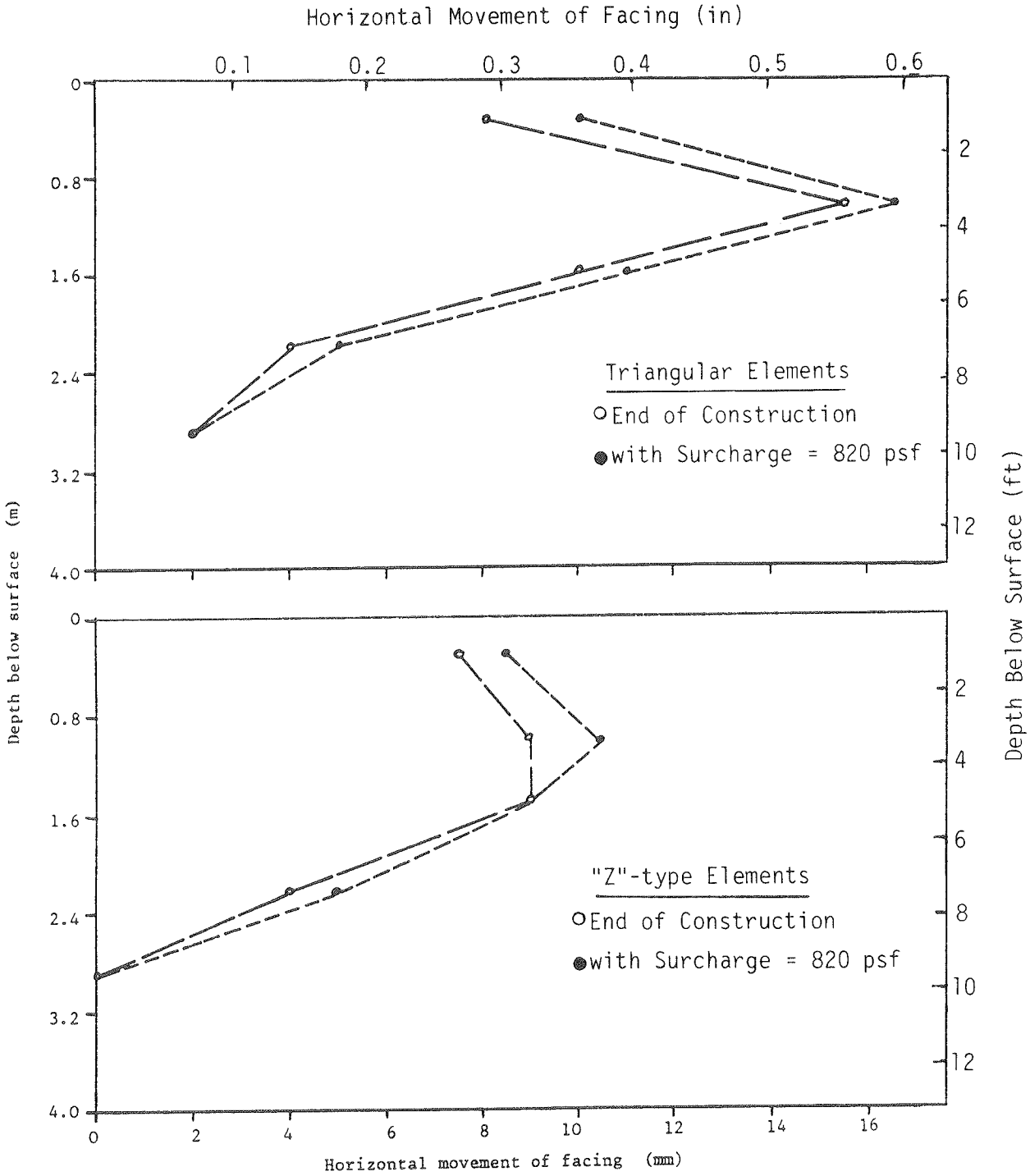

Figure B-45. Variation of horizontal movement of facing with depth at end of construction and after application of uniform surcharge. [Murray, 1983]

which case steel, having a higher ultimate tensile resistance, would be most economic for use as anchors.

Figure B-49 compares the available pullout resistances with the forces measured in the anchors after wall construction to give the factor of safety against failure by pullout. The results are presented in terms of safety factor versus vertical stress above the element. Average safety factors for triangular and "Z"-type anchors are about 10 and 6, respectively. A safety factor of 2 is normally considered adequate.

Significant conclusions drawn from the experiment data include the following. Anchor Earth should be as easy to construct as other reinforced soil systems because of the simple connection

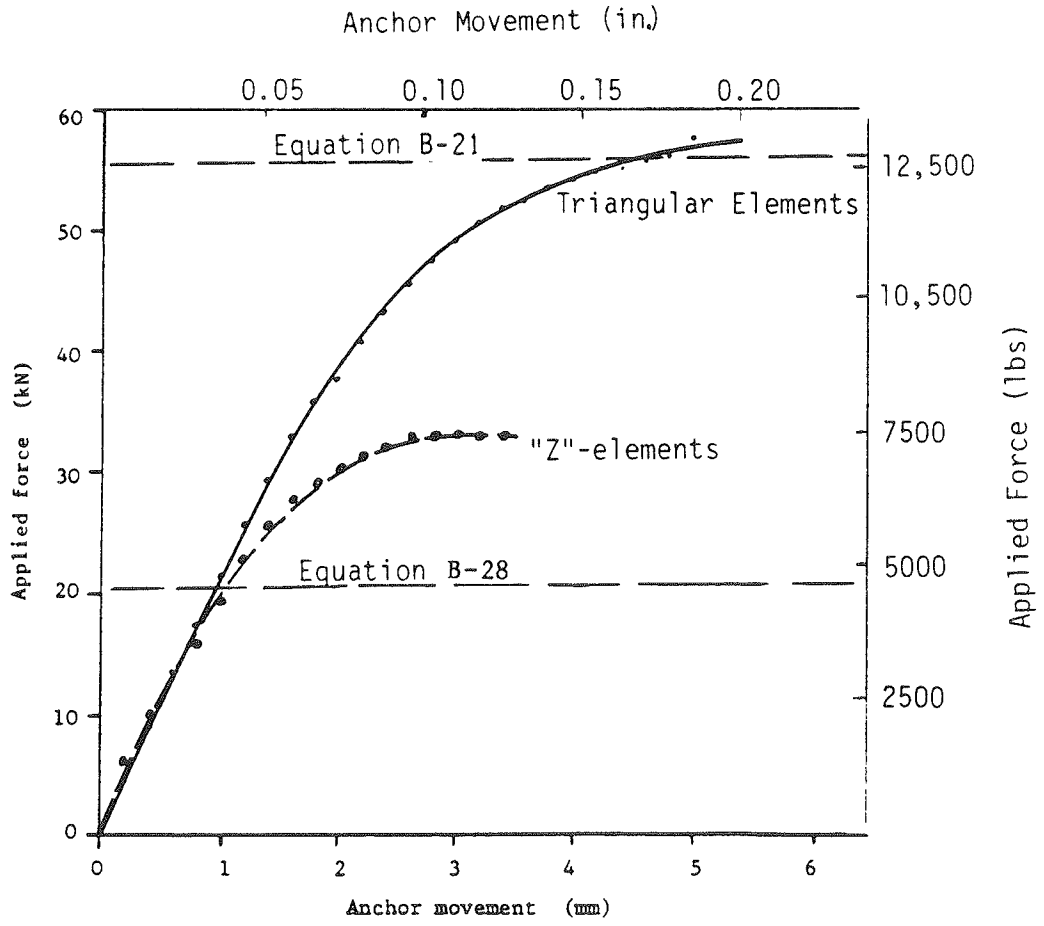

Figure B-46. Relation between applied force and anchor movement. [Murray, 1983]

arrangement and the type of facing unit employed. The large horizontal pressures induced by construction equipment need careful consideration; otherwise, damage or excessive movement of the wall may occur. Greater horizontal movements of facing units are associated with triangular-type anchors than with Z-type anchors, possibly because of the development of a larger slip field, but total movement remains reasonably small. Finally, greater pullout resistance is provided by the triangular type-anchors than by Z-type anchors.

8.2 Silver Mill Hill Retaining Wall—A660 Otley By-Pass, Yorkshire, England

The first application of Anchored Earth was described by Jones et al. [1985]. The Otley By-Pass, at the site of the wall, follows the course of an old railway cutting below the hillside known as the Chevin. The area has a long history of instability and numerous different types of landslides and mudflows have occurred. These overlie mudstone which dips at approximately 10 deg in the direction of the cutting slope. At the site of the wall the top of the mudstone is just below the old track bed level.

The retaining wall supports a road at the top of the cutting and a bank seat to a footbridge. The wall is 280 ft (85 m) long with a maximum height of 20 ft (6.2 m).

The anchors are triangular in shape and formed from 0.79-in. (20-mm) diameter, cold-worked steel reinforcement. Their effective length is about 16.4 ft. Vertical and horizontal spacings of anchors are approximately 20 in. (500 mm) and 48 in. (1,200 mm), respectively. The anchor width for most anchors is 26 in. (650 mm). Near the top of the wall some 36-in. (900 mm) and 48-in. (1,200 mm) wide anchors were used to improve pullout resistance.

The facing units are precast, prestressed concrete planks 47 in. wide, 6 in. thick, and of varying heights to suit the wall profile. Gaps between units are filled with a Neoprene sealant. The connecting bolts and washers were covered by a compressible cap. The units and bolt caps are hidden by a 7-in. thick masonry facing. The final wall profile was battered 1 in 40.

9. COST COMPARISONS

No direct cost comparisons with other earth reinforcement systems have been performed to date. However, production costs, when considering equivalent volumes of steel, are lower for round bars than for strips, and the length of reinforcement required may be less for Anchored Earth than for some of the other reinforcement systems. More accurate cost comparisons will be possible once several full-scale Anchored Earth structures have been constructed.

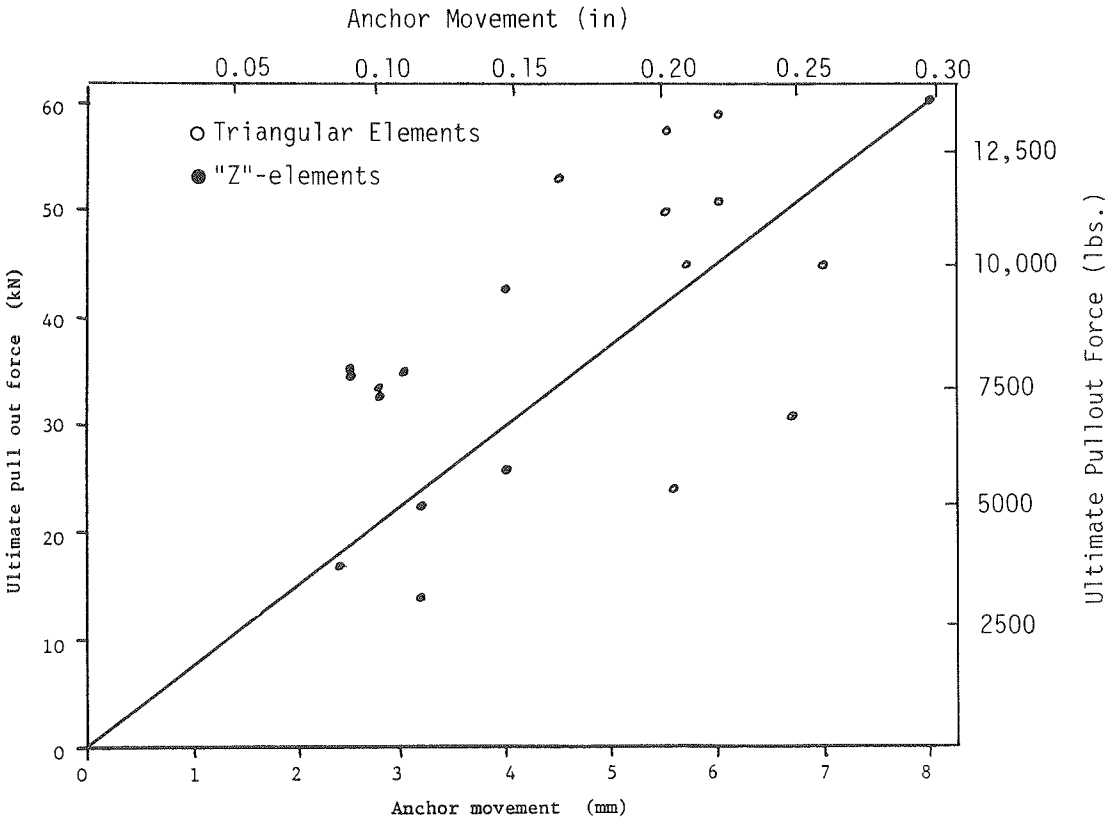

Figure B-47. Relation between ultimate pullout force and anchor movement. [Murray, 1983]

10. FUTURE DEVELOPMENTS

The Anchored Earth system is still in its early stages of development. Construction and instrumentation of full-scale Anchored Earth structures are required in order to develop optimal and cost-effective construction procedures, evaluate and improve technology (facing panels, anchors), evaluate the mechanisms of soil-reinforcement interaction and the behavior of the reinforced soil structure, develop a proven and reliable design methodology, evaluate cost effectiveness relative to other reinforcement systems, and increase designer confidence.

The system can also be developed further by additional laboratory and theoretical investigations of the effects of anchor stiffness, anchor geometry, and soil type on stress transfer and anchor behavior. The Otley By-Pass embankment is the first full-scale application of Anchored Earth. More experience must be gained by construction of other projects before Anchored Earth is used as routinely as some of the other earth reinforcement systems.

11. DESIGN EXAMPLE

Because Anchored Earth is still a system under development, a general design methodology has not yet been adopted. It seems reasonable to expect that a design methodology similar to that in Chapter Five of the main report will be developed.

Table B-3. Summary of pullout test results. [Murray, 1983].

Anchor Type	Normal Stress (Psi)	Pullout Force (Kips)	Movement At Limiting Pullout Force (In.)	Efficiency (Percent)
'z' - type	5.16	3.82	0.09	22
"	"	3.15	0.13	
Triangular	"	5.39	0.22	39
"	"	6.97	0.26	
'z' - type	6.93	5.84	0.16	34
"	"	5.05	0.13	
Triangular	"	10.12	0.28	63
"	"	10.12	0.22	
'z' - type	8.70	7.42	0.11	46
"	"	7.42	0.11	
Triangular	"	11.46	0.24	76
"	"	12.93	0.22	
'z' - type	10.47	7.87	0.10	49
"	"	7.87	0.12	
Triangular	"	13.26	0.24	84
"	"	13.49	0.32	
'z' - type	12.22	9.55	0.16	55
"	"	7.87	0.17	
Triangular	"	11.24*	0.22*	73*
"	"	11.91*	0.18*	

*Damage to facing panel, test stopped.

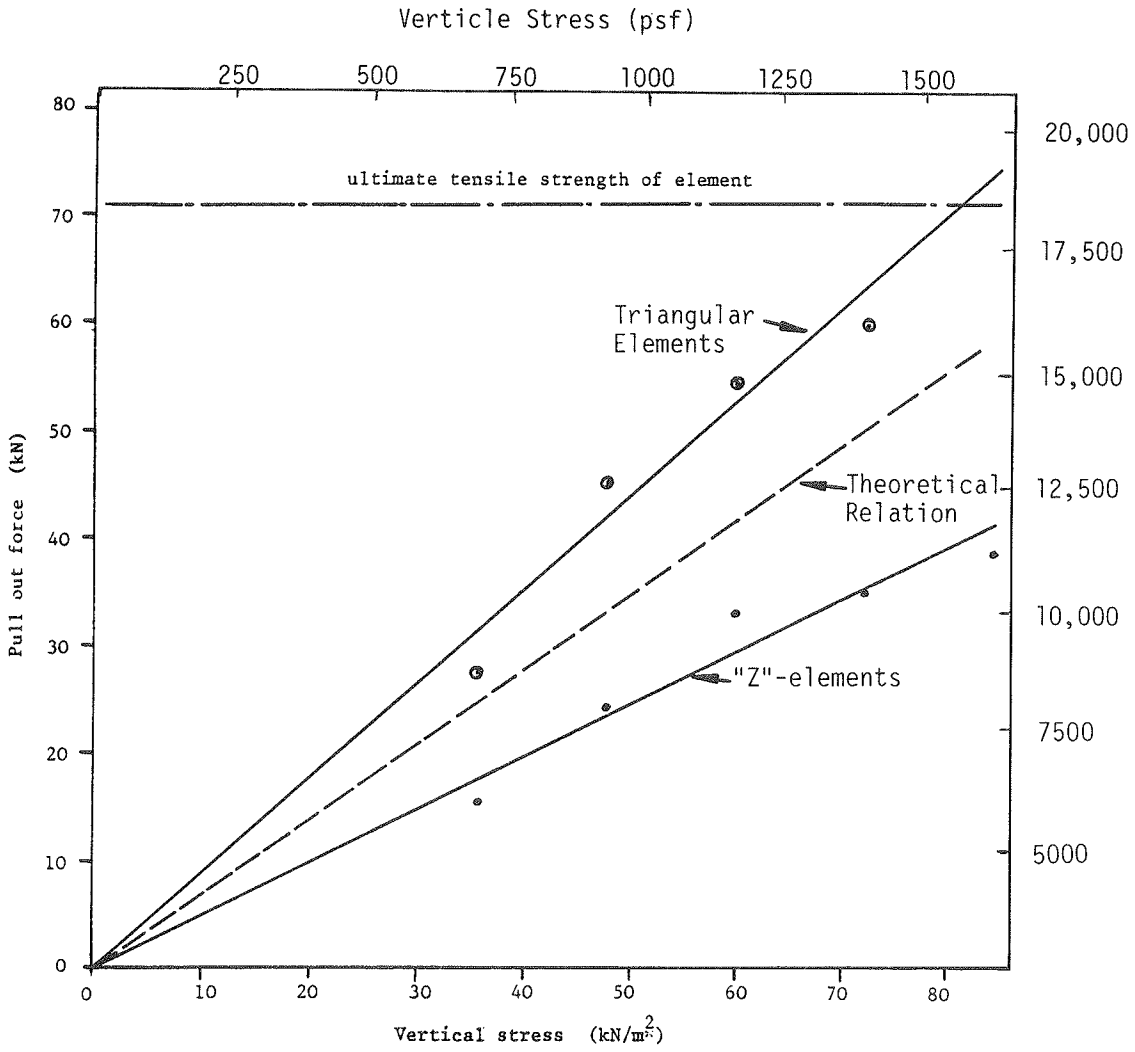

Figure B-48. Relation between pullout force and vertical stress. [Murray, 1983]

12. REFERENCES

DEPARTMENT OF TRANSPORT [1978]. "Reinforced Earth Retaining Wall and Bridge Abutments for Embankments," *Technical Memorandum (Bridges) BE 3/78,* Highway Procedure and Legislative Division, London.

JONES, C. J. F. P., MURRAY, R. T., TEMPORAL, J. and MAIR, R. J. [1985]. "First Application of Anchored Earth," *Proc. 11th International Conference on Soil Mechanics and Foundation Engineering,* San Francisco, Vol. III, pp. 1709–1712.

MURRAY, R. T. [1981]. Private communication with Author (Richard A. Jewell) December.

MURRAY, R. T. [1983]. "Studies of the Behaviour of Reinforced and Anchored Earth," Ph.D. Thesis, Heriot-Watt University, Edinburgh.

MURRAY, R. T. and IRWIN, M. J., [1981a]. "Anchored Earth Structure," European Patent Application No. 81303913.3. European Patent Office.

MURRAY, R. T., and IRWIN, M. J. [1981b]. "A Preliminary Study of TRRL Anchored Earth," *TRRL Supplementary Report 674.*

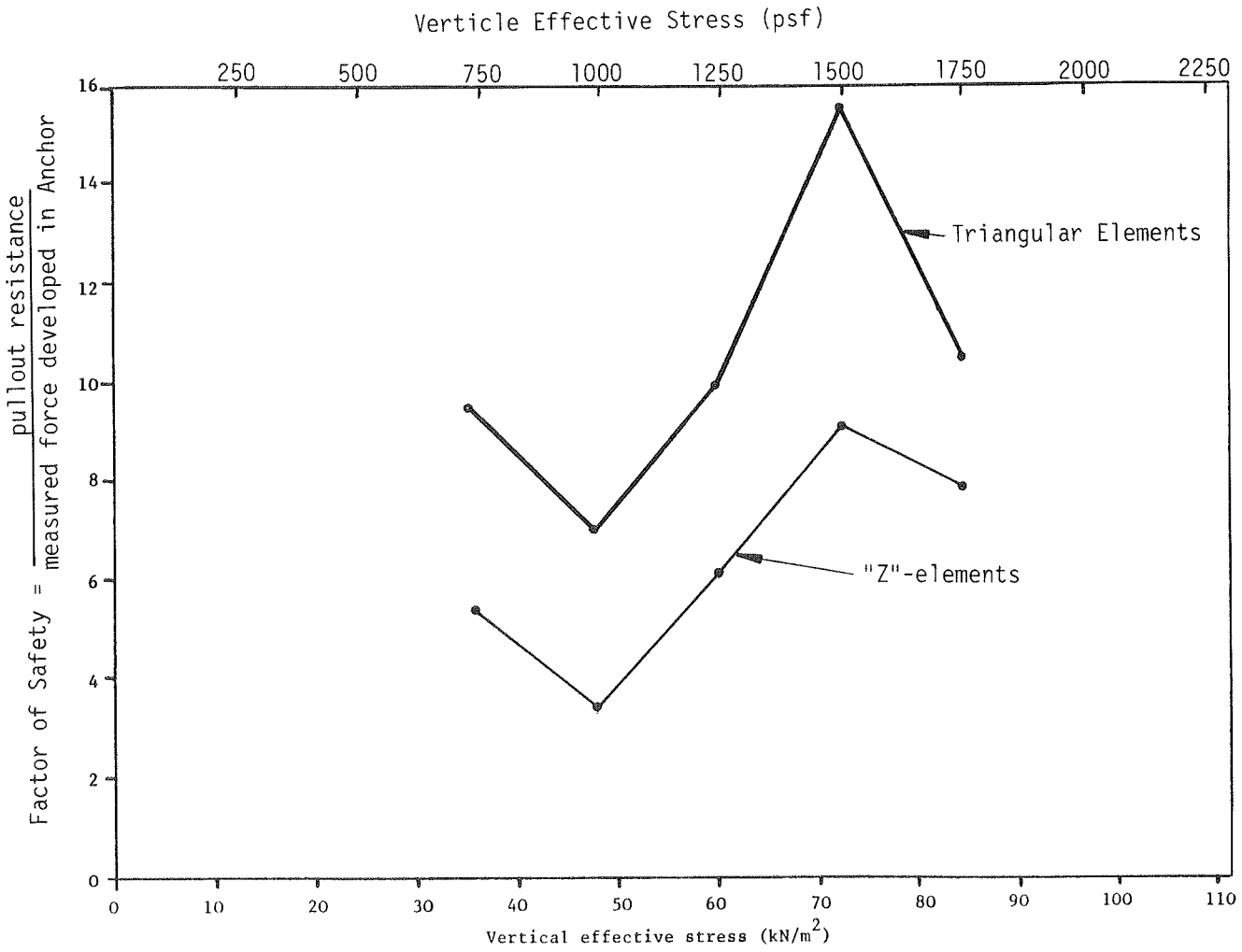

Figure B-49. Relations between factor of safety against pullout versus vertical effective stress. [Murray, 1983]

CHAPTER THREE—**GEOGRIDS**

Contents

1. INTRODUCTION

1.1 Physical Description

Geogrids are tensile resistant polymeric grid mats which can be included within a soil mass to create a reinforced soil structure. A composite construction material with improved tensile and compressive properties results from the interaction of alternate layers of soil backfill and geogrid reinforcements. With geogrids, the mechanism of stress transfer includes both soil friction on horizontal reinforcement surfaces and passive resistance (also referred to as horizontal soil bearing or just soil bearing) against transverse members of the grid.

A schematic diagram of a geogrid-reinforced soil wall is shown in Figure B-50. The major components of the wall are the geogrid reinforcements, the soil backfill, and the facing elements.

Geogrid reinforcements are produced and marketed under the trade name "Tensar" by Netlon Limited in the United States, United Kingdom, and elsewhere. Tensar geogrids are manufactured from high-strength grades of high-density polyethylene or polypropylene using a stretching process. Both uniaxial-oriented grids (Tensar SR2) and biaxial-oriented grids (Tensar SS1, SS2, and SS3) are available.

Compacted granular soils are usually used for the soil backfill, but poorer backfill soils (e.g., clays, pulverized fuel ash) have also been used. Geogrids have also been used successfully with poorer quality soils for slope repair applications.

Facings for geogrid-reinforced soil structures can be formed by looping the reinforcement at the face (and seeding or guniting the exposed soil) or attachment to structural elements (e.g., gabions, concrete panels).

Figure B-51 presents geometric terminology for grid reinforcement used in this chapter.

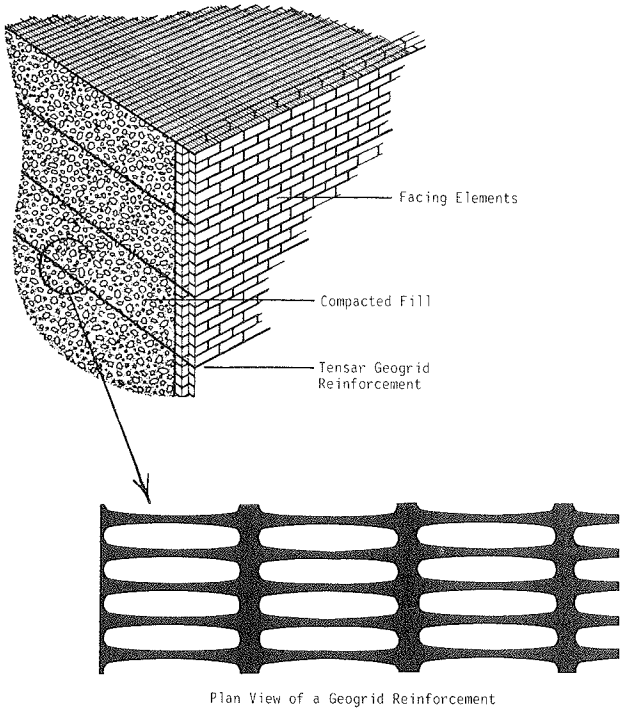

Figure B-50. Schematic diagram of a geogrid-reinforced soil wall.

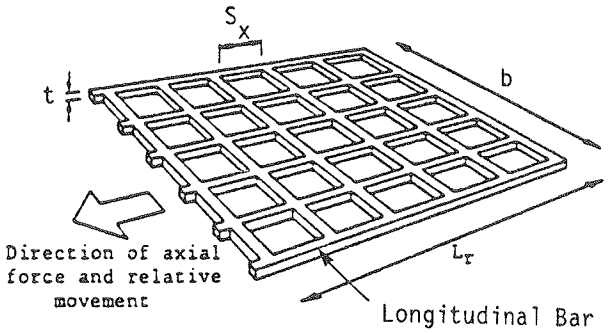

$A_r = bL_r$ Grid surface area

α_s Fraction of grid surface area that is solid

α_b Fraction of grid width b available for bearing

Figure B-51. Definition of geometry of a grid reinforcement. [Jewell et al., 1984a]

1.2 History and Development

The first engineering applications of grid-type reinforcement involved the use of metallic grids, which are susceptible to corrosion. This limitation led to the development of polymer grid reinforcements, which because of their inert nature, can be used in more aggressive environments. Polymer grids can be handled easily because of their light weight and flexibility.

The physical properties of polymers can be improved by copolymerization and other molecular processes, and by stretching [Wilding and Ward, 1981]. Tensar SR2, a high density polyethylene reinforcement grid which incorporates this technology, was developed in the late 1970's [Mercer, 1979] and was made available by Netlon Limited in 1980. Laboratory testing of this geogrid [Netlon Limited, 1984a] has provided data on the load deformation behavior and long-term strength. A number of other types of Tensar geogrids have also been produced by Netlon Limited. Tensar SR2 geogrids have now been applied successfully in reinforced slopes and walls. Much of the ongoing work with geogrids was described at the International Symposium on Polymer Grids in Civil Engineering, London, March 1984.

1.3 Proprietary Restrictions

There are currently no proprietary restrictions to the use of Tensar geogrids. However, the grids themselves are patented.

2. APPLICATIONS

Polymer grids have been used for the construction of vertical soil walls and reinforcement of steep soil slopes. They can be used for structures such as bridge abutments. Construction has often involved new types and arrangements of wall facings or the use of alternative fill materials such as pulverized fuel ash. Embankment and slope failures have been repaired with reinforcement by polymer grids in both the United States and the United Kingdom.

2.1 Inherent Advantages

Inherent advantages include: (1) Resistance to soil environments—Polymer materials are relatively inert and appear to provide good resistance to decay in most soil environments. They are believed also to resist most forms of biological attack and may be useful in fine-grained and clay soils which are typically considered aggressive. (2) Form and handling—Polymer grids are relatively light and are supplied in rolls of 3.3 ft width. This provides ease of handling and construction, particularly for slope applications, where continuous layers of reinforcement are often used. (3) Jointing and connections—Geogrids are easily connected and joined. Connections may be made by using a rod, Figure B-52, or by stitching with synthetic cord. Grids also provide flexibility for connections with the facing and do not require a reduction in the cross-sectional area of the reinforcement at the joint. However, these joints may be the source of "slack" in the system, which could be the source of unacceptable deformation.

2.2 Site Conditions for Use

Geogrids may be used at any site, provided the external stability of the reinforced soil structure can be satisfied.

2.3 Routine and Special Applications

It would be premature to classify any of the slope reinforcement applications of grids as routine. However simple design methodology already exists for applications with vertical and sloping soil faces less than about 35 ft in height and for slope failure repair. The increased loads on the reinforcement and facing, and the more severe consequences of failure for soil faces higher than 35 ft, place these applications in the category of "special" design.

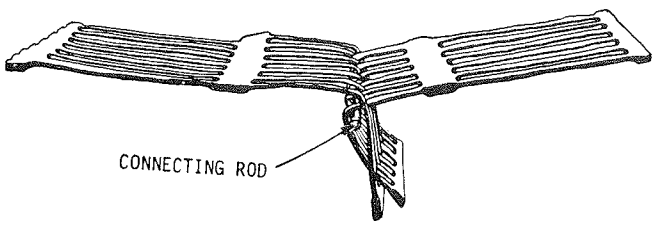

Figure B-52. Schematic diagram of geogrid connection.

3. MECHANISMS AND BEHAVIOR

3.1 Interaction between Reinforcement Grids and Soil

Three aspects of behavior need to be considered for a design of a reinforced soil embankment, two of which are illustrated in Figure B-53. There must be sufficient sliding resistance to prevent gross outward movement of soil blocks along the surface of a reinforcement layer in the soil. Sufficient reinforcement length must also be provided to ensure that the required axial forces may be developed in the reinforcements by bond to maintain equilibrium, i.e., sufficient pullout resistance must exist. Thirdly, the stresses developed in the reinforcements should not exceed the tensile strength.

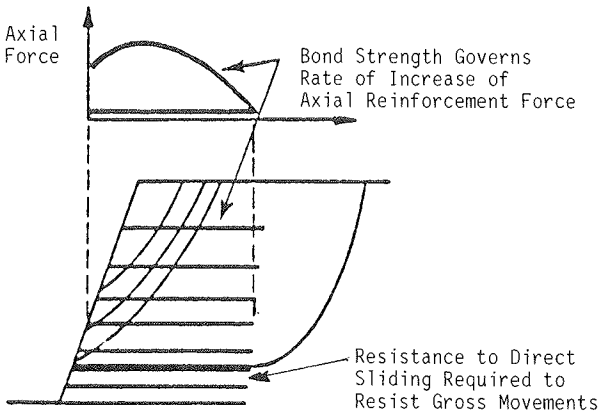

Figure B-53. Two mechanisms of failure in a reinforced soil embankment. [Jewell et al., 1984a]

3.1.1 Mechanisms of Interaction

The three main mechanisms of soil-reinforcement interaction are: (1) soil friction on plane surfaces of the reinforcement that are parallel to the direction of relative soil and reinforcement movement, (2) soil passive resistance on reinforcement surfaces that are substantially normal to the direction of relative soil and reinforcement movement, and (3) soil shearing over soil through the apertures in a reinforcement grid.

3.1.2 Direct Sliding Resistance

The loading condition for direct sliding is a gross outward shearing force tending to cause a block of soil overlying a plane of reinforcement to shear over the reinforcement and the underlying soil. The three mechanisms of interaction that may contribute resistance to such direct sliding are schematically shown in Figure B-54:

1. *Influence of soil particle size.* The size of the backfill soil particles relative to the size of grid apertures can influence direct sliding resistance of a soil block in the ways shown schematically in Figure B-55.

Soil made up of particles in the fine sand or silt sizes has sufficient kinematic freedom to rupture in zones of varying orientations that when the soil moves relative to the grid, sliding would be across the surface of the rib bearing members (Fig. B-55A).

For a coarser sand, the direct sliding mechanism would change to a rupture zone formed mostly in the soil with the only soil-to-grid sliding occurring on the smooth top surfaces of the bearing members (Fig. B-55B). Hence a significant portion of the failure plane would consist of soil-to-soil contacts.

If the soil contains particles of a similar size to the grid apertures, these would likely become lodged against the grid bearing members and extend into the soil on either side of the grid (Fig. B-55C). If a number of particles were lodged in this way, the soil would no longer be able to take advantage of the smooth top surface of the bearing members, and the rupture zone would be forced away from the grid fully into the soil. In this case, the shear resistance to direct sliding would equal the full shear resistance of the soil.

Finally, grid reinforcement could be placed in soils with particles too large to penetrate the grid apertures (Fig. B-55D). The resistance to direct sliding in this case could be very low because in the extreme, shear resistance might be provided only by soil particles in contact with the smooth plane grid surface areas. The irregularity in the surface profile of the grid in this case would be insignificant to the scale of the soil, so that little benefit from that source could be expected. The shear resistance to direct sliding could therefore be reduced to the resistance of the soil shearing on a smooth sheet of the reinforcement material. However, in the field the grid is likely to have undulations in the compacted soil, and these should improve the overall direct sliding resistance.

The influence of soil paticle size on direct sliding resistance is shown qualitatively in Figure B-56. Direct sliding resistance is expressed as a factored reduction on the soil direct shear resistance, $F_{ds}\tan\phi_{ds}$ as explained below.

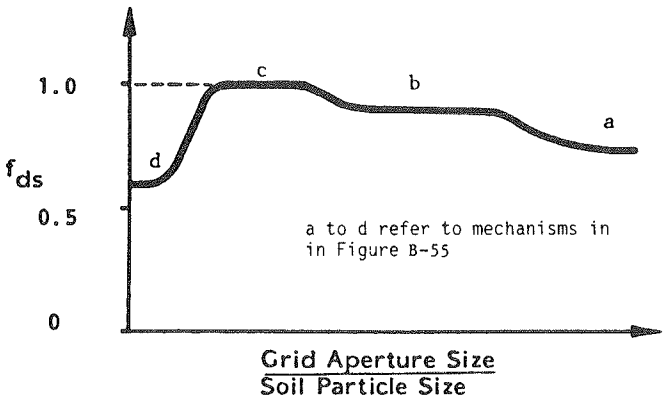

Figure B-56. Schematic illustration of the influence of particle size on the resistance to direct sliding, $f_{ds}\ tan\phi_{ds}$. [Jewell et al., 1984a]

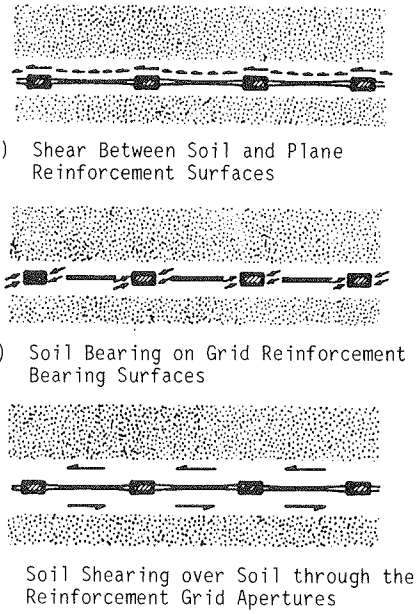

Figure B-54. Three mechanisms resisting direct sliding. [Jewell et al., 1984a]

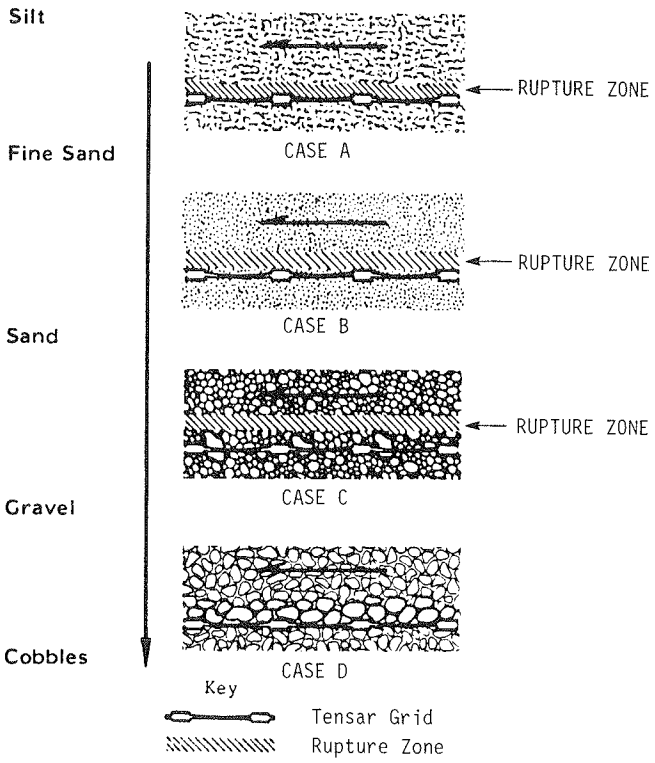

Figure B-55. Qualitative effect of increasing soil particle size on direct sliding. View in cross-section across direction of sliding. [Jewell et al., 1984a]

2. *Theoretical expressions for direct sliding resistance.* The basic equation for direct sliding resistance can be expressed in terms of the two contributions from (1) shear between soil and the plane surface areas of the grid, and (2) the soil shearing over itself in the grid apertures. Direct sliding resistance can be described by a general expression, which neglects any contribution due from the transverse members in bearing:

$$f_{ds}\tan\phi_{ds} = \alpha_{ds}\tan\delta + (1 - \alpha_{ds})\tan\phi_{ds} \qquad \text{(B-42)}$$

where f_{ds} = coefficient of resistance to direct sliding; ϕ_{ds} = angle of friction for soil in direct shear; δ = angle of skin friction for soil on plane reinforcement surfaces; and α_{ds} = fraction of grid surface area that resists direct shear with soil.

The parameter α_{ds} has been introduced so that one general expression can be used to describe the four different values of direct sliding resistance envisaged in Figures B-55 and B-56. Equation B-42 can be rearranged to give an expression for f_{ds},

$$f_{ds} = 1 - \alpha_{ds}\left(1 - \frac{\tan\delta}{\tan\phi_{ds}}\right) \qquad \text{(B-43)}$$

The effect of the soil particle size shown in Figures B-55 and B-56 can now be seen from Eq. B-43. A reduction in the value α_{ds} results in an increase in direct sliding resistance f_{ds}, during the change from case a to b to c (Fig. B-55). Indeed, when the rupture zone is forced away from the grid, case c, $\alpha_{ds} = 0$ and $f_{ds} = 1.00$. In the extreme case of large particles resting directly on the grid plane surfaces rather than penetrating the apertures, case d in Figure B-55, $\alpha_{ds} = 1.00$ resulting in a reduction of direct sliding resistance to:

$$f_{ds} = \frac{\tan\delta}{\tan\phi_{ds}} \qquad \text{(B-44)}$$

In the field this equation may not be entirely true for large particles. If Tensar is placed in such particles, it would deform and there would not be a planar surface of Tensar for the particles to slide on. Hence f_{ds} in such particles may approach unity.

Where the soil particles penetrate the grid apertures and where the soils shear along the entire available Tensar surface, a suitable value of maximum direct sliding resistance would be given by Eq. B-42 or Eq. B-43 adopting a value $\alpha_{ds} = \alpha_s$, where α_s is the fraction of solid surface area in a grid (Fig. B-51). This corresponds to case a in Figures B-55 and B-56.

3. *Comparison with experimental results.* A comprehensive series of tests has been carried out to investigate the influence of particle size on direct sliding resistance [Jewell et al., 1984a]. Two types of polymer grid, Tensar SR1 and Tensar SR2, were used. Seven different grading curves gave relative soil particle sizes ranging from silts to gravels (Fig. B-57).

The lower portion of a large direct shear box was first filled with compacted soil almost to the top, the grid placed so as to be flush with mid-plane, then the upper half of the box was filled, and a vertical load was applied before shearing.

The results of tests on the grid Tensar SR2 with a minimum aperture width 0.7 in. (17.3 mm) are summarized in Figure B-58. The coefficient of direct sliding resistance f_{ds} is shown plotted against the ratio of minimum aperture width to the average particle size (D_{50}). At low ratios of aperture width to soil particle size, tests were carried out on soil type G and the grid Tensar SR1. The test results were obtained by clipping out alternate rib members and then pairs of rib members to increase the grid size, and the results are summarized in Figure B-59.

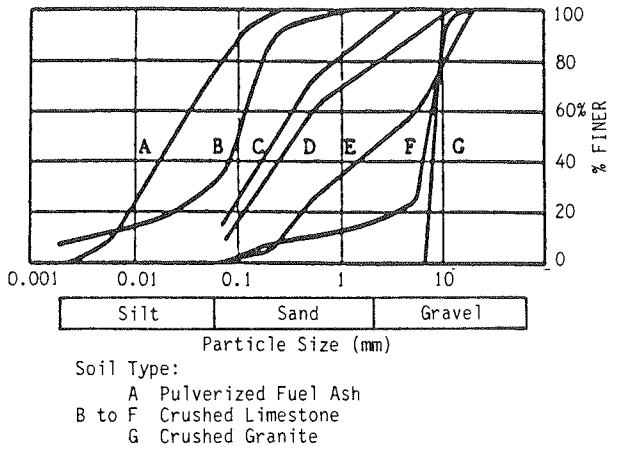

Figure B-57. Soils tested during investigations of direct sliding resistance. [Jewell et al., 1984a]

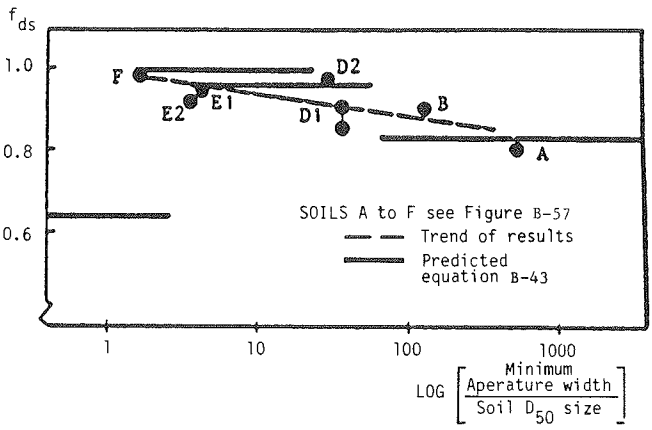

Figure B-58. Measured peak direct sliding resistance f_{ds} for granular soils over Tensar SR2 grid reinforcement. [Jewell et al., 1984a]

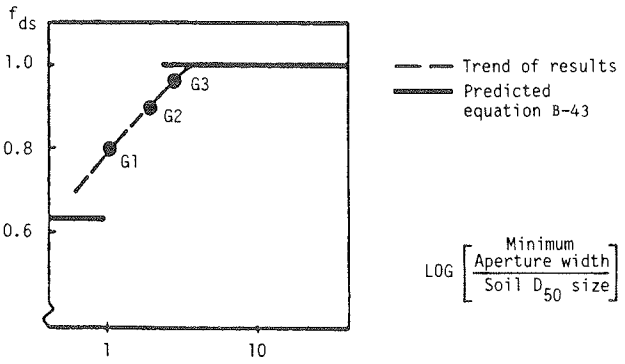

Figure B-59. Measured peak direct sliding resistance f_{ds} for granular soils over Tensar SR1 grid reinforcement. [Jewell et al., 1984a]

The trend of the experimental results, shown dotted in Figures B-58 and B-59, confirms the expected qualitative variation of direct sliding resistance with soil particle size. Predictions of f_{ds} given by Eq. B-43 are compared with the experimental results in Figures B-58 and B-59. The predicted values are found to bound the experimental data well.

On the basis of the data available, it is recommended that Eq. B-43 with a value of $\alpha_{ds} = \alpha_s$ would give a suitably conservative value of direct sliding resistance for design when,

$$\frac{\text{Minimum grid aperture dimension}}{\text{Average soil particle size}} > 3 \qquad \text{(B-45)}$$

3.1.3 Pullout Capacity

Resistance to geogrid pullout is developed by the following two stress transfer mechanisms, as illustrated in Figure B-60: (1) soil friction on plane surface areas of the reinforcement, and (2) soil passive resistance on reinforcement surfaces substantially normal to the direction of relative movement between the soil and the reinforcement.

Friction between soil and plane surfaces. The shear force, P_f, that can be developed between the soil and the horizontal plastic surface depends on the angle of skin friction and the normal efffective stress between the soil and the reinforcement surface. (Note that P_f does not include the frictional component of soil grains sliding over one another or bearing resistance.)

$$P_f = 2A_r\alpha_s \cdot \gamma' z \cdot \tan\delta \qquad \text{(B-46)}$$

where γ' = effective unit weight of the soil; z = depth of embedment of the grid being considered; and A_r = area of the grid, i.e., length times width of the mat rather than just the grid members (gross area).

Soil passive resistance on transverse grid members. The passive resistance of soil bearing on grid members is a problem similar in kind to the base pressure on deep foundations in soil. In Chapter Four of the main report, theoretical and experimental considerations for this mechanism of stress transfer are discussed in detail.

Theoretical expressions for pullout capacity. It is convenient to express the pullout capacity of grid reinforcement in terms of the total surface area of the grid A_r. The bond strength can then be given as a bond coefficient multiple, f_b, of the angle of friction for the soil, thus:

$$f_b \tan\phi = \alpha_s \tan\delta + f_{bearing} \tan\phi \qquad \text{(B-47)}$$

The first term represents the contribution from friction; and the second term, that from passive resistance. Dividing Eq. B-47 by tanϕ gives a general expression for the bond coefficient,

$$f_b = \alpha_s \frac{\tan\delta}{\tan\phi} + f_{bearing} \qquad \text{(B-48)}$$

For a fully rough continuous sheet, α_s would be unity, tanδ would equal tanϕ, and there would be no component from bearing. Hence, f_b would equal unity. For a grid, this value of f_b cannot be exceeded, because failure of the soil at a small distance from the grid will occur preferentially. Hence, f_b is

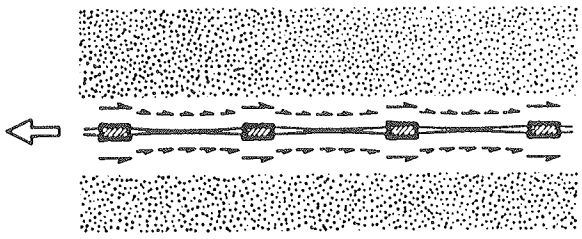

A) Friction Between Soil and Plane Surfaces

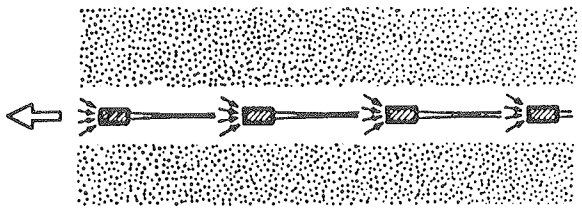

B) Soil Passive Resistance on Reinforcement Surfaces

Figure B-60. The two mechanisms for stress transfer between a geogrid and soil. [Jewell et al., 1984a]

limited to a maximum value of 1.0. The maximum pullout resistance, P_{max}, that could be developed in a frictional soil would be for the case where the transverse bearing members are close enough together so that the grid and its contained soil act as a rough sheet of thickness, t, being pulled through the soil. For this case (see Fig. 40 of main report):

$$P_{max} = 2S_{opt} n \sigma_v' \tan\phi \qquad \text{(B-49a)}$$

where n is the number of transverse bearing members, and S_{opt} is the optimum spacing.

The same resistance developed by bearing would be

$$P_{max} = \alpha_b t \sigma_b' n \qquad \text{(B-49b)}$$

Combining Eqs. B-49a and B-49b gives an expression for the optimum spacing to thickness ratio:

$$\left(\frac{S}{t}\right)_{opt} = \frac{\sigma_b'\ \alpha_b}{\sigma_v'\ 2\tan\phi} \qquad \text{(B-50)}$$

There would be no increase in pullout resistance for values of S/t less than the optimum value. Use of smaller transverse member spacings would be uneconomical. Greater spacings will result in a system that is not capable of developing the full passive bearing resistance that could be mobilized within the area of reinforcement.

The reduction in the bearing component of the pullout resistance for spacings S_x greater than S_{opt} can be expressed as:

$$f_{bearing} = \frac{\left(\frac{S}{t}\right)_{opt}}{\frac{S_x}{t}} \qquad \text{(B-51)}$$

Equations B-50 and B-51 may thus be rewritten as:

$$f_{bearing} = \frac{\sigma_b'}{\sigma_v'} \frac{\alpha_b^t}{S_x} \frac{1}{2\tan\phi} \qquad \text{(B-52)}$$

The coefficient of pullout resistance for a reinforcement grid in soil can now be written in a general form:

$$f_b = \alpha_s \frac{\tan\delta}{\tan\phi} + \frac{\sigma_b'}{\sigma_v'} \frac{\alpha_b^t}{S_x} \frac{1}{2\tan\phi} \qquad \text{(B-53)}$$

The parameters of Eq. B-54 can be simply determined except, perhaps, the value of σ_b'/σ_v'. In Chapter Four of the main report, the theoretical and experimental variation of σ_b'/σ_v' with ϕ is developed. These values may be used, or alternatively, the ratio of σ_b'/σ_v' may also be measured directly in a pullout test.

Influence of soil particle size. Soil particle size is likely to affect pullout capacity in a similar way to its effect on direct sliding resistance as described earlier, i.e., larger particles are likely to improve bond strength. There are no test data for the influence of soil particle size on pullout resistance for a grid. According to Jewell [1980], as long as the combination of grid and soil meets the criteria suggested for direct sliding, i.e., Eq. B-45 $\left(\frac{\text{Minimum grid aperture dimension}}{\text{Average soil particle size}} > 3\right)$, then the value of maximum bond coefficient calculated from Eq. B-52 should provide a reasonably conservative value for design.

3.1.4 Influence of Pore Water Pressure

The expressions for direct sliding resistance and pullout capacity have been derived in terms of an effective normal stress between the soil and the reinforcement grid. The magnitude of this normal stress is directly reduced by pore water pressures.

3.1.5 Cohesive Soils

The resistance to direct sliding and the pullout capacity for reinforcement grids in clay soils under drained loading conditions could be predicted with the above equations if appropriate values of drained effective friction angle are used. Until there are data on performance, however, it is recommended that direct measurements of sliding resistance and pullout capacity be made to select design values.

The case of reinforced clay soils subject to rapid undrained loading conditions has not been considered. Both laboratory and field measurements will be required to select design values for grids reinforcing clay in undrained loading.

The pullout resistance per unit width of grid reinforcement in cohesive soil has not been studied. A tentative approach might be to consider the soil resistance on the bearing elements in a manner similar to a conventional bearing capacity equation. This approach would lead to:

$$P_B = n(N_c S_u + \sigma) t\, \alpha_b \qquad \text{(B-54)}$$

where P_B is the pullout resistance per unit width developed by bearing on n bars; N_c is a bearing capacity factor applicable to undrained soil at depth; S_u is undrained shear strength; t is the thickness; σ is total vertical stress; and n is the number of bars against which bearing is developed.

The total bearing resistance against the bearing members cannot exceed the force required to cause failure on a plane within the cohesive soil parallel to the grid, i.e.,

$$\alpha_b n(N_c S_u + \sigma)t \leq 2nS_x S_u \qquad \text{(B-55)}$$

The multiplier 2 is used because failure would have to occur on planes on either side of the grid. Ignoring the contribution of total stress to bearing (which is likely to be relatively small), this simplifies to:

$$N_c \leq \frac{2S_x}{t\alpha_b} \qquad \text{(B-56)}$$

For Tensar SR2, the ratio S_x/t is about 23. Considering that N_c values are likely to range between about 9 and 20 and that α_b is less than one, this S_x/t ratio when inserted in Eq. B-56 indicates that Tensar SR2 will develop pullout resistance not only from bearing but also from adhesion on portions of the grid area. It is likely that the soil-to-Tensar adhesion would be lower than the undrained shear strength of the soil. Until more data become available on the adhesion-to-undrained shear strength ratio, it would appear conservative when evaluating pullout resistance to only allow for cohesive soil bearing on the Tensar bearing elements, and to compute the soil resistance with a bearing capacity factor, N_c, equal to 9. Studies would be needed to confirm this approach prior to its application.

3.2 Strain Compatibility

The magnitude of tensile strain at any point along a reinforcement cannot exceed the tensile strain generated in the adjacent soil in the direction of the reinforcement. Any slippage or incompatibility would reduce the tensile strain in the reinforcement below that in the adjacent soil. This logical supposition has been demonstrated by direct measurements of soil and reinforcement strains in the case of sand reinforced by extensible reinforcement and loaded in direct shear [Jewell, 1980].

Strain compatibility need not be considered in design with inextensible reinforcements, but the following factors are important for design with extensible reinforcements. The magnitude of strain required to mobilize the soil shear strength must be compatible with the tensile strain required in the reinforcement needed to mobilize the design value of reinforcement force. Also, the outward face deflections that would result from tensile strain in the reinforcement must be compatible with any deformation serviceability requirements.

The relationship between mobilized shear strength and development of soil tensile strain has not been important for most geotechnical design problems. Consequently, there are few published data readily available. Between 3 and 6 percent principal tensile strain normally develops in compact granular soils up to peak stress ratio when the soil is deforming under plane strain conditions [Jewell, 1980].

Jewell et al. [1984b] and McGown et al. [1984a] suggested that until data from laboratory and field measurements provide a better understanding of strain compatibility between soils and extensible reinforcement, stability should be calculated on the basis of residual soil strength. These strength values should be slightly conservative, because the shear strength of compacted granular soil is likely to exceed the residual value.

The appropriate allowable stress for polymers with time-dependent properties would be either the force that would cause the limiting strain at the end of the design life under the worst expected conditions of temperature and in service environment, or the maximum allowable reinforcement force, whichever is less (see Section 4 of this chapter). For most applications, the acceptable reinforcement tensile strain would probably be on the order of 3 to 5 percent for extensible reinforcements.

3.3 Behavior of Grid-Reinforced Soil Structures

Reinforcement contributes to the stability of a reinforced soil structure in two ways: (1) Reinforcement directly improves the shear resistance of the soil, thus allowing the reinforced soil mass to stand on a steep slope (Fig. B-61A). (2) The reinforced zone holds the unreinforced soil mass in equilibrium without exceeding the allowable bearing stresses of the underlying soil (Fig. B-61B), or sliding along its base. As illustrated in Figure B-61C, however, the change in loading due to the steepened slope must not overstress weak strata that may be present beneath the reinforced soil mass.

Recent work to devise design charts for steep geogrid-reinforced slopes founded on stable foundations introduced four criteria to determine a satisfactory reinforcement layout [Jewell et al., 1984b; Netlon Limited, 1984b]: (1) When unreinforced soil "stands" at a steep unstable slope, there is a tendency for the outer wedge of soil to slide outwards. The total force ΣT_i in Figure B-62A must be greater than T to prevent sliding. Sufficient reinforcement layers, carrying a safe design load, are needed to provide this force. (2) The effective pullout length of the upper reinforcement must be sufficient to withstand local pullout (Fig. B-62B). (3) The reinforcement length at the base of the slope must give the desired margin of safety against outward sliding of soil along the interface between the grid and the soil (Fig. B-62C). (4) The reinforcement length not only must satisfy 2 and 3 but also provide a zone of reinforced soil which, if acting as a rigid block, would not cause tension at the heel (Fig. B-62D).

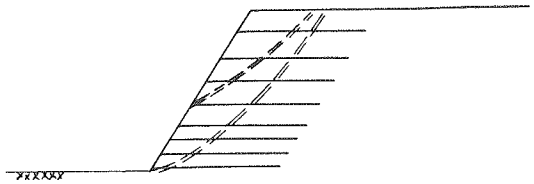

A. Reinforcement directly increases shear resistance to resist shear failures in the oversteepened slope

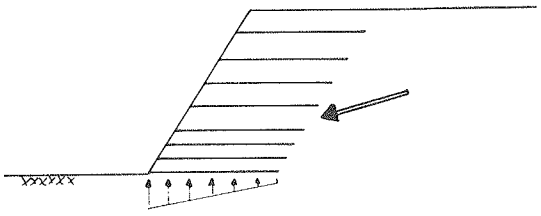

B. The reinforced zone resists the thrust from the retained soil.

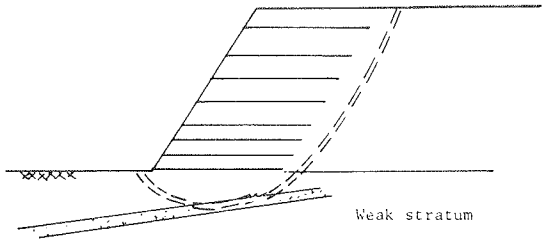

C. Loading from the steepened slope must not overstress more deep seated soil layers

Figure B-61. Action of reinforced soil in slope applications.

4. TECHNOLOGY OF TENSAR GEOGRIDS

4.1 Manufacturing Process

The Tensar process orients the molecular structure of prepunched polymer sheets by drawing or stretching under con-

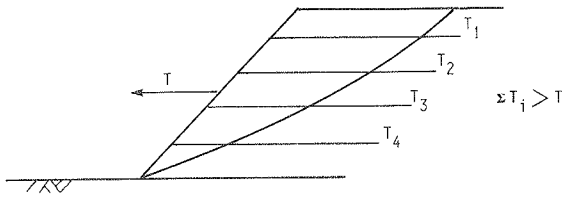

A) Reinforement provides maximum required gross force.

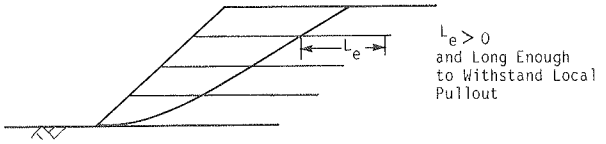

B) Reinforcment must contain the critical mechanism from A.

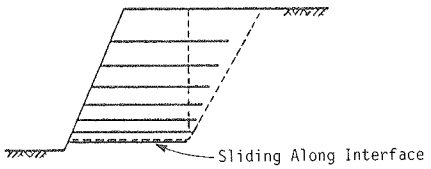

C) Reinforcment zone must resis direct outward sliding.

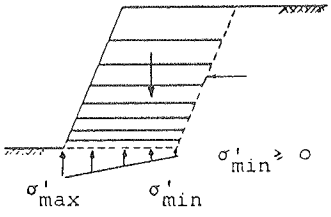

D) No tensile effective stress on the base.

Figure B-62. Criteria to determine a satisfactory layout of grid reinforcement.

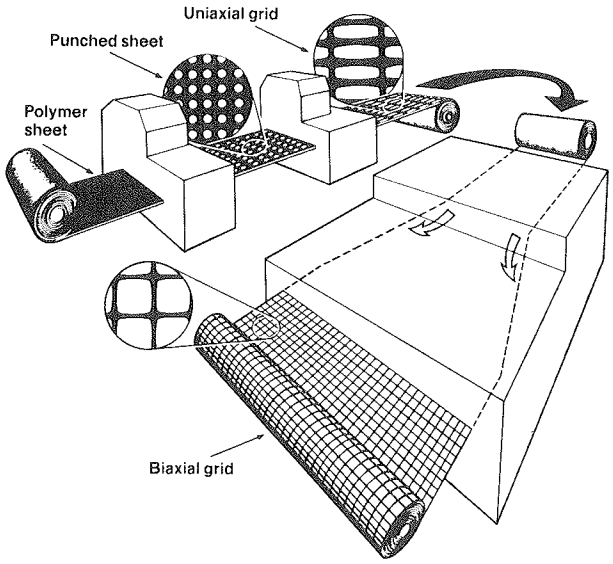

Figure B-63. Tensar manufacturing process. [Netlon Ltd., 1984a]

trolled conditions to produce grids with enhanced stiffness and tensile strength.

The first stage consists of punching evenly spaced holes in a sheet of polymer. The perforated polymer sheet is then heated and longitudinally stretched to produce a grid with a highly regular structural form (Fig. B-63). The properties of the grid are strongly influenced by the original punched hole layout and the degree of stretching. Tensar SR2, produced in this manner, has improved stiffness and strength characteristics in the direction of stretching.

A uniaxially oriented grid can be drawn or stretched at 90 deg to the first drawing stage to produce a biaxially oriented grid (Fig. B-63). Biaxial grids have similar properties in the two orthogonal directions.

4.2 Description of Fabricated Components

4.2.1 General Considerations

Tensar SR2 is a uniaxial polymer grid specifically designed for use as a reinforcing element in earthworks. Biaxial Tensar grids, SS1 to SS3 and GM1, are also available for use in site stabilization, road applications, gabions, or other situations where loading is expected in more than one direction.

The geometric terminology used to describe uniaxial and biaxial geogrids is illustrated in Figures B-64 and B-65. Specific geometric dimensions for the Tensar SR2 geogrids and Tensar SS1 to SS3 geogrids are shown in Figure B-66.

4.2.2 Polymer Materials

Tensar SR2. Tensar SR2 is manufactured from a co-polymer grade, high density polyethylene (HDPE) [Ward, 1984]. The polymer can be classified by the standard tests shown in Table B-4. Prior to the production of Tensar SR2, 2.5 percent by weight of carbon black is added to the polymer to provide ultraviolet light protection.

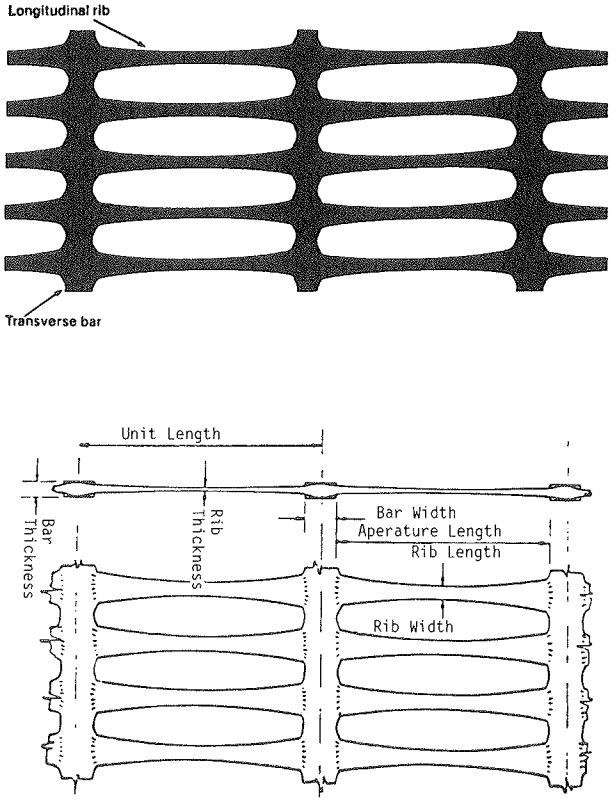

Figure B-64. Geometric terminology for uniaxial Tensar grids. [Netlon Ltd., 1984a]

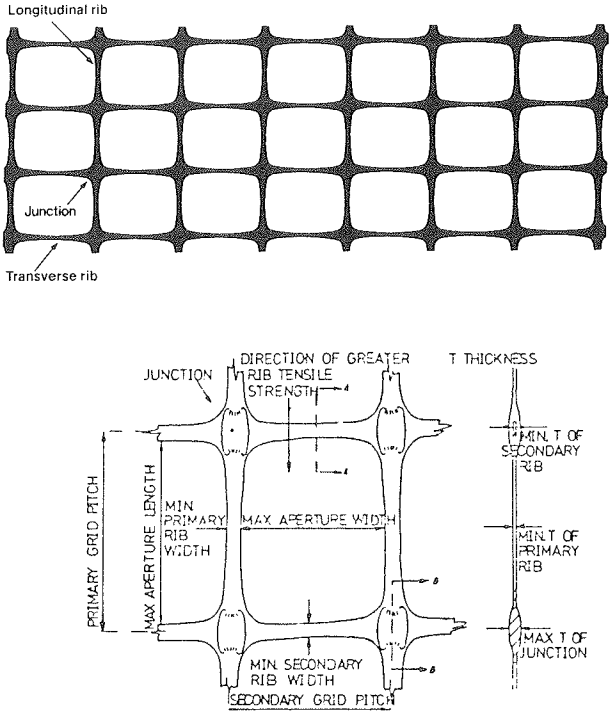

Figure B-65. Geometric terminology for biaxial Tensar grids. [Netlon Ltd., 1984a]

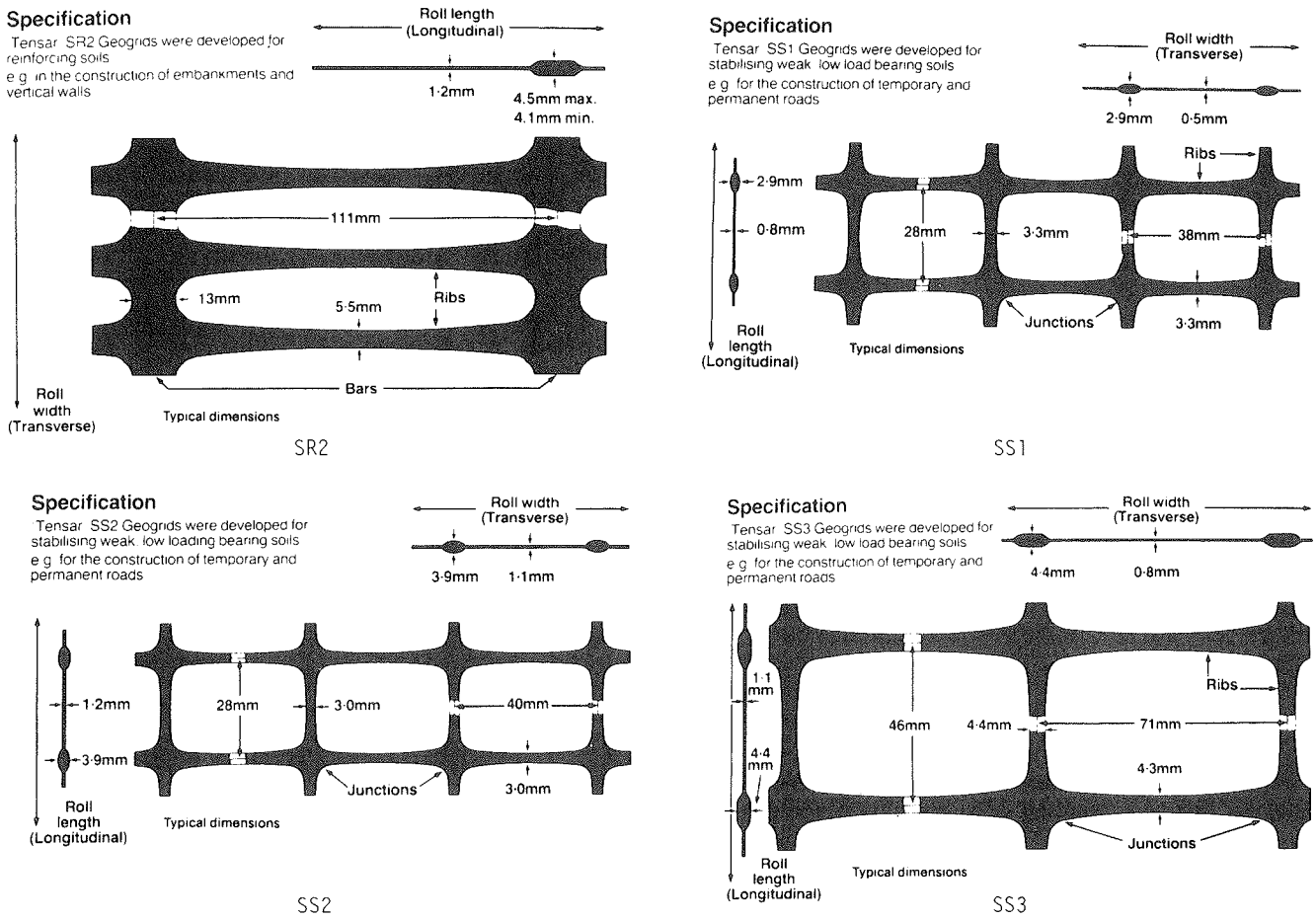

Figure B-66. Geometric terminology for Tensar Geogrids SR2, SS1, SS2, SS3.

Table B-4. Specifications for Tensar SR2. [Netlon Limited, 1984a]

CONSTITUENT POLYMER - PHYSICAL AND CHEMICAL PROPERTIES

Vicat Softening Point (°C)	BS 2782 102 D	121
Shore Hardness (D)		65
Stress Crack Resistance (Hrs)	ASTM D-1693B	300
Tensile Strength (MN/m^2)	BS 2782 320A	24
Elongation at Failure (%)	BS 2782 320A	>300
Abrasion Resistance (Mg/1000 cycles)	Taber CS-17	300

Properties of the HDPE polymer include: (1) Ultraviolet light resistance—With continual exposure in a temperate climate, the minimum outdoor life of HDPE stabilized with 2.5 ± 0.5 percent well-dispersed carbon black is claimed by the manufacturer to be in excess of 15 years [Netlon Limited, 1984a]. (2) Chemical resistance—HDPE is reported to be chemically inert [Netlon Limited, 1984a] to a wide range of chemicals and has no solvent at ambient temperatures. HDPE is generally inert to chemicals other than strongly oxidizing acids because of its chemical structure [Ritchie, 1968]. (3) Temperature resistance—HDPE does not become brittle until very low temperatures are reached. This is usually measured by a cold bend test, BS 2782, Method 104A. A maximum service temperature range for Tensar SR2 is given as −50°C to +80°C [Netlon Limited, 1984a]. (4) Biological resistance—HDPE has good resistance to microbiological attack and reportedly does not biodegrade when buried [Dolezal, 1967].

Biaxial Tensar grids. The biaxial Tensar grids with SS nomenclature are manufactured from a homo-polymer grade polypropylene with 2.5 percent carbon black added to provide protection against ultraviolet light [Netlon Limited, 1984a]. Classification of the polymer by standard tests gives the results shown in Table B-5. Polypropylene has similar chemical, temperature, and biological resistances to those described for HDPE.

4.3 Fabrication Quality Control

To test the geometry of production material, Netlon Limited selects 5 ft long, full-width samples at random from a production batch and trims the selected samples to a whole number of ribs (see Fig. B-67). Ten random measurements are taken of the aperture lengths, aperture widths, rib widths, and thicknesses from both uniaxial and biaxial grids. Similarly, selected samples

Table B-5. Specifications for Tensar SS2. [Netlon Limited, 1984a]

CONSTITUENT POLYMER - PHYSICAL AND CHEMICAL PROPERTIES

Vicat Softening Point (°C)	BS 2782 102 D	148
Shore Hardness (D)		74
Stress Crack Resistance (Hrs)	ASTM D-1693B	
Tensile Strength (MN/m^2)	BS 2782 320A	37
Elongation at Failure (%)	BS 2782 320A	300
Abrasion Resistance (Mg/1000 cycles)	Taber CS-17	18-28

are also tested for mass per unit area (which must satisfy a minimum value) and for tensile stress versus strain and creep properties. Typical results on Tensar SR2 samples are shown on Figure B-68.

4.4 Mechanical Properties of Tensar SR2

4.4.1 General Behavior of Polymer Materials

Within Tensar grids, both the cross-sectional area of polymer and the amount of drawing experienced by the polymer vary with position in the rib and the bar. Thus, stress parameters for individual grid portions differ from one another. Consequently, it is convenient to define stress–strain behavior not for the material but for the grid as a whole, as follows: (1) Instead of stress, use load per unit overall width of the grid, measured as kN/m or lb/ft. This is preferable to load per rib because the number of ribs in a given width of grid varies with the grid type. (2) Instead of polymer strain, use overall strain, i.e., increase in length divided by original length. (3) Instead of secant modulus, use secant stiffness expressed as load per unit grid width divided by overall strain. A similar definition would apply for tangent stiffness.

To measure these parameters in Tensar, it is essential that test specimens contain at least 15 ribs and 5 bars to obtain representative values [McGown et al., 1984b].

The conditions for comparison tensile tests on polymer grids that are recommended by McGown et al. [1984b] and Netlon Limited [1984a] are as follows:

Temperature:	20°C ± 2°C
Relative humidity:	65% + 5%
Constant strain rate:	0.33 10^{-3}/sec (2% per min).

4.4.2 Typical Design Data for Tensar SR2

The results of short-term tests are not adequate for design purposes because sustained loading of polymer materials will induce creep. Hence, creep and constant strain rate tests must be performed to establish design parameters. Creep test data for Tensar SR2 at 20°C and 65 percent ±5 percent relative humidity, as reported by McGown et al. [1984b] and Netlon Limited [1984a], are summarized in Figure B-69.

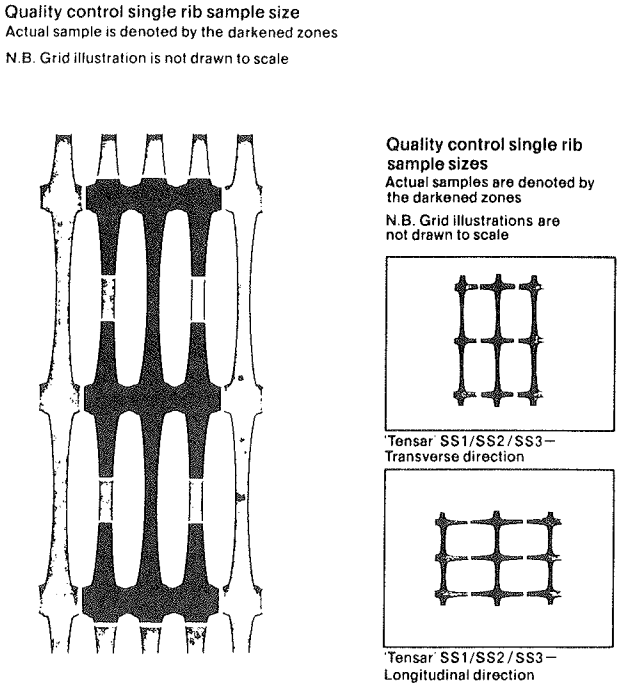

Figure B-67. Quality control sample size. [Netlon Ltd., 1984a]

The creep data may be plotted in the form of isochronous curves that are more useful for design purposes (Fig. B-70). These curves show that for Tensar SR2 at 20°C much of the time-dependent deformation occurs in the first 100 hours to 1,000 hours of loading, which is of the same order of magnitude as the construction phase of medium size embankment and retaining wall projects. Such creep could be the source of wall facing alignment difficulties.

The data may also be plotted in a fashion recommended by Ward [1984] and Wilding and Ward [1978] for the determination of the critical stress or load below which long-term equilibrium would be established. This form of data presentation is shown in Figure B-71.

From the results in Figure B-71 a limit of 10 percent overall strain has been identified "below which rupture is unlikely to occur by ductile yield" [McGown et al., 1984b]. The 10 percent overall strain limit translates by extrapolation to a load of slightly more than 2,000 lb/ft for loading periods of the order of 120 years (Fig. B-70).

The identification of a "critical strain" for Tensar SR2 is similar in concept to the "critical stress" phenomenon described by Ward [1984].

The results of constant strain rate tests on Tensar SR2 at various temperatures [McGown et al., 1984b] indicate peak strength to be a function of both temperature and rate of loading (Fig. B-72). These results also indicate that there is a tendency for stress–strain behavior to change from ductile to brittle with decreasing temperature.

The *Structural Plastics Design Manual* [Heger et al., 1978] recommends that polymer materials intended to support loads for long periods should be considered as nonductile. Long-term tests accelerated by elevated temperatures should allow an assessment of the possibility of failure by nonductile behavior for Tensar SR2, and are in progress [Netlon Ltd., 1984a].

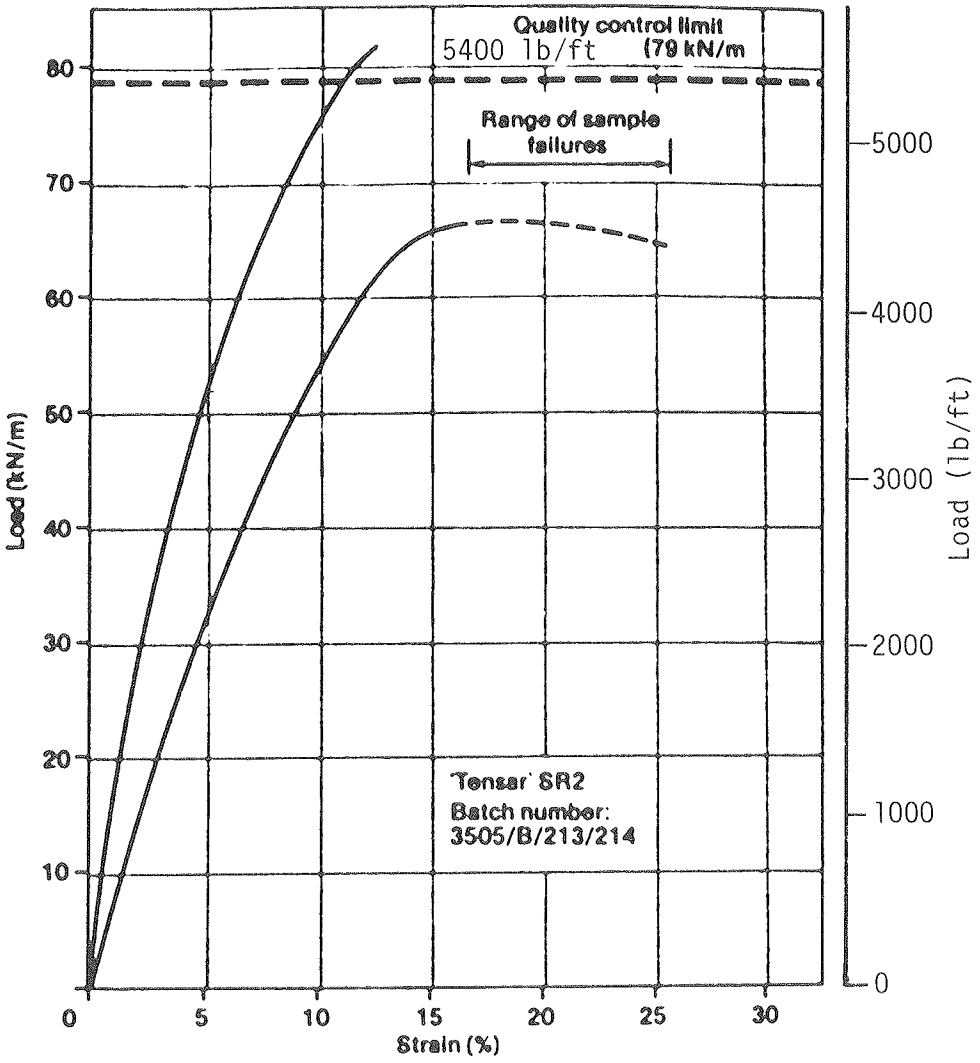

Figure B-68. Typical tensile test results for Tensar SR2. [Netlon Ltd., 1984a]

4.4.3 Recommendations for Design

Netlon Limited [1984a] has made the following recommendations for design: (1) The long-term strength for Tensar SR2 suitable for design lives between 1 year and 120 years is 2,000 lb/ft. This is a characteristic value that, on the average, should be exceeded by 19 out of 20 samples. (2) The effects of construction (including damage to the grid), creep, and other conditions "in service" can be allowed for with a single partial factor, γ_m. The partial factor is used to divide the laboratory characteristic strength to give the characteristic strength in service. The suggested values of γ_m for Tensar SR2, assuming careful construction procedures, are given in Table B-6.

5. DURABILITY AND SELECTION OF BACKFILL

5.1 Durability Aspects of Tensar Geogrids

5.1.1 Suggested Approach

Tensar geogrids have not been available for a sufficient period that durability can be predicted on the basis of observed performance. Hence, durability design must allow for factors that are believed to have an influence on service life. These include time and temperature, which have been shown to have a significant influence on stress–strain behavior. The material response is determined largely by the crystal and network molecular structure of the polymer [Wilding and Ward, 1981; Ward, 1984]. Another factor is mechanical damage to the polymer material (abrasion, scratches, and notches caused by handling and installation), which raises the stress level near the point of damage. Also, the molecular structure of the polymer, which controls stress–strain behavior, may be changed by radiation or chemical exposure. Microbiological organisms can sometimes break down or biodegrade the polymer material.

Currently, these parameters can only be investigated by performing idealized laboratory tests to assess stress–strain–time–temperature relationships for the polymer determined on ideal specimens (undamaged) under standardized laboratory conditions over a relevant combination of time and temperature conditions. To "accelerate" time, it is necessary to perform elevated temperature tests. The effect of chemical exposure and microbiological attack in the soil environments intended for use must

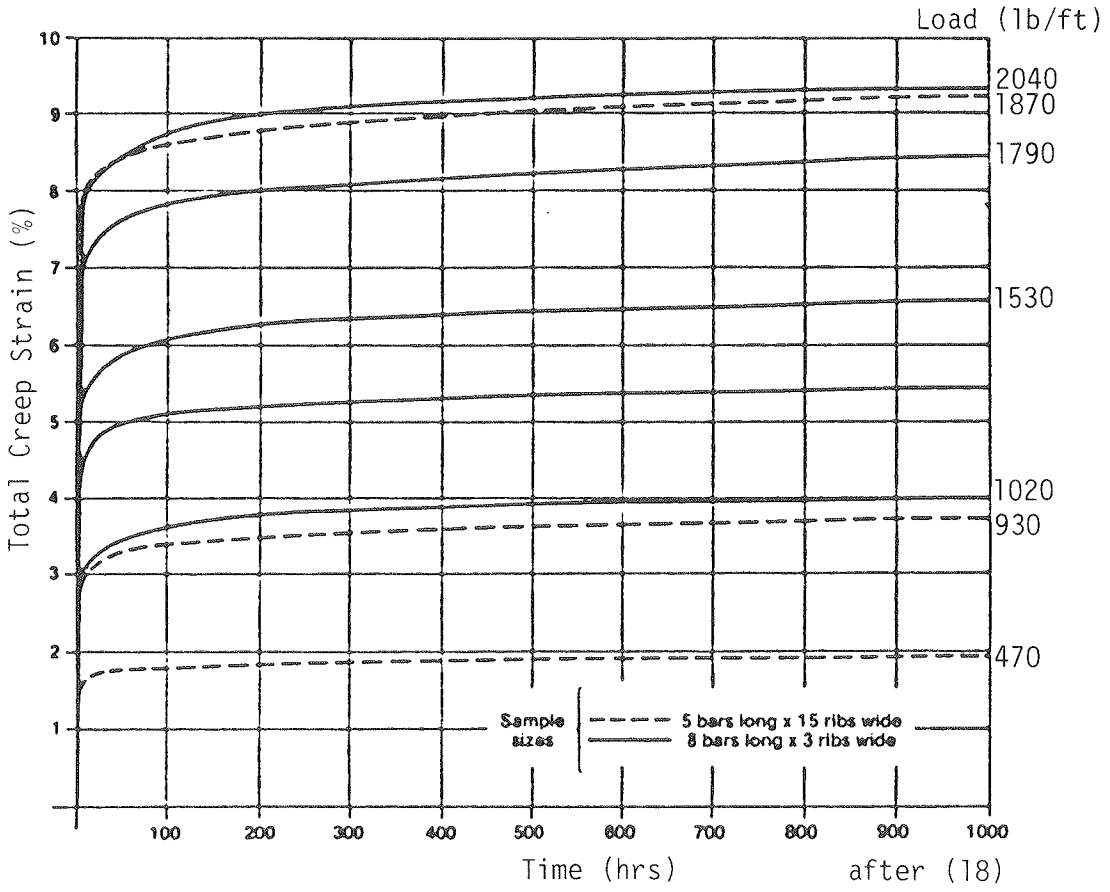

Figure B-69. Typical creep curves for Tensar SR2 at 20°C. [Netlon Ltd., 1984a]

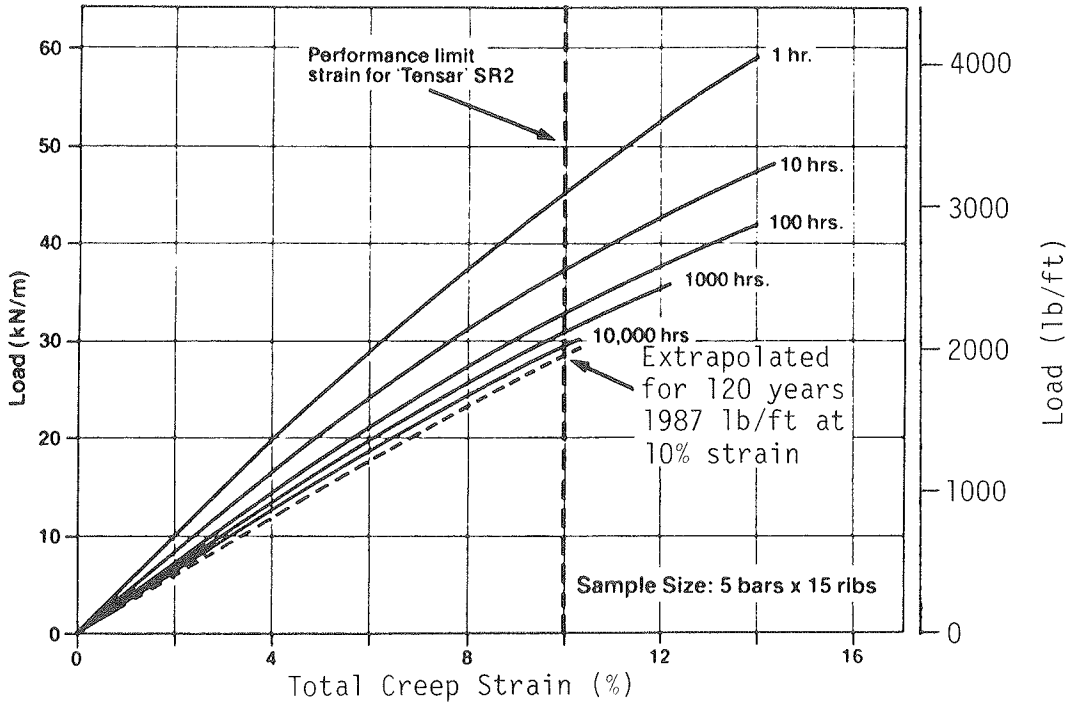

Figure B-70. Isochronous curve (SR2) at 20°C. [Netlon Ltd., 1984a]

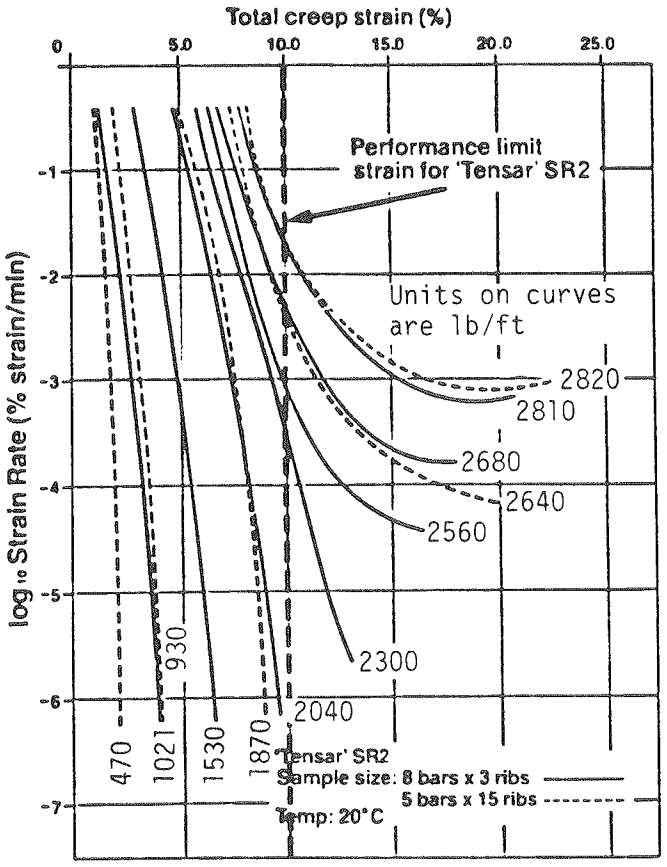

Figure B-71. Creep strain rate against total creep strain (Sherby-Dorn Plot) for Tensar SR2 at 20°C. [Netlon Ltd., 1984a]

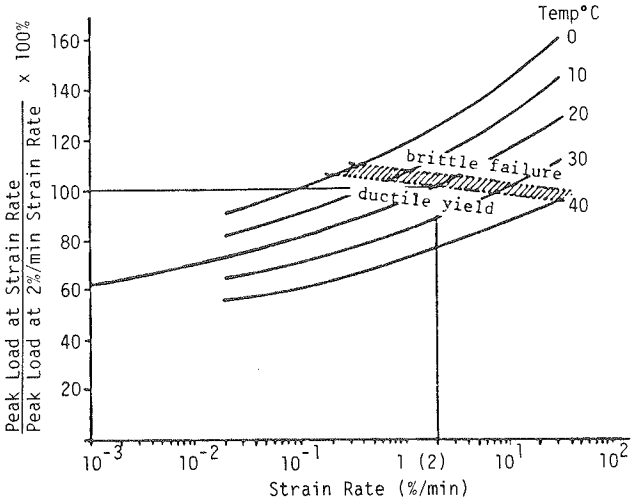

Figure B-72. Temperature/strain rate correction for SR2. [McGown et al., 1984]

also be assessed. These effects include absorption of the chemical, chemical attack on the polymer material, or the initiation of stress cracking. Finally, the effect of construction damage is of interest. Polymer reinforcements can be artificially damaged by notching (to allow the effect of the severity of damage to be assessed) and tested, or alternatively samples recovered from a range of construction conditions may be tested. The samples can also be tested in the presence of a stress cracking agent over a similar range of time and temperatures as undamaged samples.

To extend our knowledge of Tensar behavior it would be advantageous to also test samples in soil environments containing chemical concentrations that are not currently considered suitable for long-term use.

The complex interaction between these factors can then be organized into ideal behavior which would provide a design datum, and departures from ideal behavior caused by different mechanical and environmental conditions of use.

The influence of the soil should be reduced to an assessment of the mechanical damage to the polymer reinforcement that is likely during construction (particularly compaction) and the chemical and biological conditions that could be encountered in service.

5.1.2 *Durability of Tensar SR2*

Chemical and microbiological resistance. In the absence of solar radiation, many polymers show a high degree of stability.

Table B-6. Suggested range of partial factors of safety. [Netlon Limited, 1984a]

Basic Soil Type	Particle Size (mm)	Suggested Partial Factors of Safety γ_m
Boulders	200	Limited to 75 mm max size. Sand carpet or alternative protection to be used with this type of fill material.
Cobbles	75 60	
Gravels	Coarse 20	1.5-1.6
	Medium 6	1.3-1.5
	Fine 2	1.25-1.4
Sands	Coarse 0.6	
	Medium 0.2	1.1-1.25
	Fine 0.06	
Silts	Coarse 0.02	Not normally used in construction.
	Medium 0.006	
	Fine 0.002	
Clays		1.1-1.3
Pulverized Fuel Ash		1.1-1.25

Aging tests on polyethylene under such conditions showed "no evidence of any marked change" in physical properties or in short term stress–strain behavior [Moates, 1976]. Polyethylene is generally inert to chemicals other than oxidizing acids [Ritchie, 1968].

There is extensive field experience with polyethylene to support these observations [Heger et al., 1978]. HDPE has been used in buried pipe applications for potable water, effluent, and gas distribution for up to 30 years. HDPE pipe for gas is supplied for a 50-year minimum service life. The resistance of HDPE to acid soils is also known to be good. HDPE has been used to sheath metal pipes in order to reduce (or eliminate) corrosion.

The remaining question then is whether the HDPE data can be extrapolated to Tensar. The Tensar manufacturing process stretches or orients the HDPE polymer. Orientation is known to reduce the permeability of the polymer, and is not expected to reduce the chemical resistance compared to the nonoriented material.

Influence of mechanical damage. Visual classification of damage as well as short-term strength tests have been completed with samples of Tensar compacted into a variety of soils. The work, carried out by Netlon Limited [1984a], resulted in the set of proposed partial factors shown in Table B-6. These partial factors are used to adjust ideal properties to give in-service properties.

Although the partial factors in Table B-6 are intended to give an in-service long-term strength [Netlon Limited, 1984a], it must be expected that mechanical damage is likely to reduce stiffness as well. As a first estimate, the same partial factors could be used to reduce ideal stiffness to an in-service stiffness.

There is need for further tests on mechanical damage. Longer term tests on damaged samples are clearly a high priority. Tests on artificially damaged specimens would provide a datum from which to assess the results from field-damaged specimens.

5.2 Selection of Backfill

5.2.1 General

Evaluation of backfill should include: (1) a conventional site investigation and laboratory test program to provide the parameters needed for geotechnical analyses and design, and (2) an assessment of the degradation characteristics (i.e., chemical concentrations, temperature, and so forth) of the backfill soil.

5.2.2 Assessment of Geotechnical Aspects

Parameters to describe the pullout resistance and also the direct sliding resistance, between the soil and the reinforcement, must be determined. These parameters include internal angle of friction of the soil, angle of skin friction between the soil and reinforcement material, and unit weight of the soil.

Knowledge of groundwater conditions is as important for reinforced soil walls as for conventional retaining walls, and appropriate measurements and tests must be carried out for their assessment.

The use of grid reinforcement ordinarily does not limit the choice of soil fill, provided the durability criteria are satisfied (Section 5.1 of this chapter), and stability of the structure can be obtained.

Two factors become increasingly significant when "poorer" backfill soils are used: (1) porewater pressures and consolidation require more complex analyses and result in time-dependent deformations; and (2) for a given slope angle and height, lower fill shear strengths and higher end of construction porewater pressures require significantly more reinforcement to provide stability (Section 7 of this chapter).

5.3 Existing Specifications

There are no specifications for polymer reinforcements, although there is now an urgent need for such documents.

6. CONSTRUCTION

The construction of a geogrid-reinforced slope can use conventional techniques, equipment and construction control, with only minor modifications to allow for the inclusion of the reinforcing elements and slope facing.

6.1 Installation Methods and Tolerances

6.1.1 Compaction of Fill

The placement and compaction of fill can be carried out using conventional equipment in accordance with standard specifications.

Grid reinforcement should be laid directly on the surface of a layer of compacted fill and covered with the next layer of fill. This fill should be spread over the grid using a tracked vehicle, or other suitable equipment, working on the newly placed fill. Care should be taken to control the timing and rate of placing of fill material to ensure that grids are not damaged by compaction or site vehicles. Vehicles should not travel directly on exposed reinforcement.

6.1.2 Types and Placement of Grids

Uniaxial grids—Tensar SR2—are generally adopted as the main reinforcement. Biaxial grids can be used as intermediate layers to provide local stability at the face of the slope or if reinforcement in both horizontal directions is required.

When positioning the grids, particular attention should be given to ensure that they are placed in the correct directions. The reinforcement is generally laid horizontally in continuous strips of the required length. In most embankment applications, no joints or overlaps are required between the adjacent lengths of reinforcement and so they are simply laid side by side. However, provisions such as pinning the grid to the fill using U-shaped rebar may be made to maintain the position of the grid.

The vertical position of each layer of grids should not deviate more than one-half the minimum compacted layer thickness of the fill from the position shown on the drawings. In addition, two successive reinforcement layers should not be placed at opposing extremes of this tolerance.

The variation in the vertical position along each grid layer should not exceed half the minimum compacted layer thickness of the fill from the position shown on the drawings.

6.1.3 Facing Arrangements

Facings are provided to retain fill material and prevent slumping and erosion of faces. Tensar can readily be used with a variety of facings, including polymer grid reinforcements turned up at the face of the slope and returned into the embankment below the next reinforcement layer (Fig. B-73). Secondary grids can be installed to provide stability at the face (Fig. B-74). A regular layout of short lengths of reinforcement of 12-in. to 20-in. spacing may provide resistance to slumping, and a separate treatment provides resistance to surface erosion. For example, a polymer grid may be fastened to the face of the slope to hold a seeded mulch until vegetation cover is established, with the root map providing face protection. Gabion baskets or structural elements (concrete panels) can be used for steep reinforced slopes and abutments. The reinforcement should be attached to the back of the gabions or other elements (Fig. B-75).

Formwork can be erected to support the face during the construction of steep slopes. It can take the form of a lightweight system of scaffold tubes and boards. Fine mesh can be used to prevent loss of soil, and seeding can promote the growth of grasses and vegetation to provide a natural reinforcement to the surface and a pleasing appearance to the slope [Szymonick et al., 1984; Busbridge, 1984].

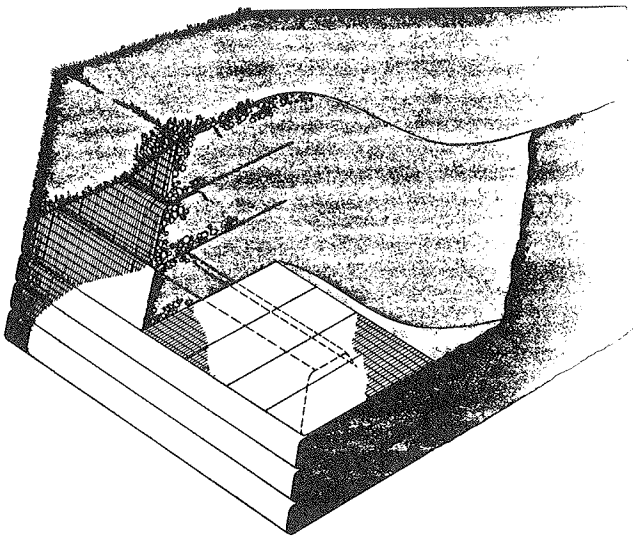

Figure B-73. Facings formed by wrap-around reinforcement. [Netlon Ltd., 1984b]

6.2 Quality Control for Polymer Reinforcements

Visual inspection of the reinforcement on-site with a check on the specified geometry should be frequently carried out to check the physical quality of the supplied material.

Regular index testing of reinforcement samples will, like the visual inspection, provide a general check that the supplied material meets the specification.

Index testing shares the shortcomings of other rapid tests and is not sufficient to check the mechanical properties appropriate to long-term loading conditions. As a part of site quality control, especially for large projects, there is a need to check the mechanical properties of random samples and the polymer compound used to manufacture the reinforcement.

Finally, because the influence of construction damage to the polymer reinforcement may be significant, samples of reinforcement should be recovered after installation so that damage, if any, can be assessed.

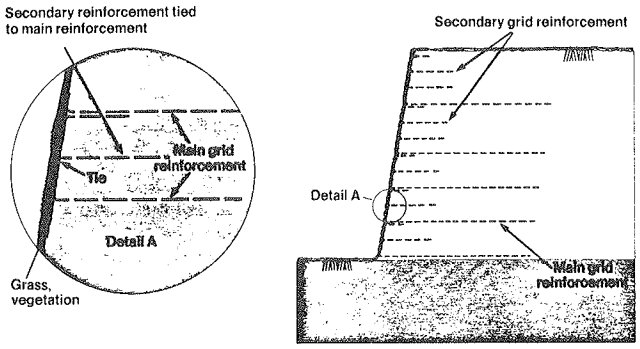

Figure B-74. Facing provided by secondary grid reinforcement. [Netlon Ltd., 1984b]

7. DESIGN METHODS

7.1 Introduction

Design of vertical walls with grid reinforcement systems is also discussed in the Bar Mat and Welded Wire chapters of this appendix. Provided that strain compatibility is verified, i.e., that Tensar will strain sufficiently to mobilize required reinforcing forces and that this magnitude of strain is acceptable, those design methods can readily be adapted for geogrid-reinforced vertical walls as well. Hence, the design procedures are not repeated in this chapter.

Because geogrid is also well suited to reinforcement of steeply sloping (30 deg to 80 deg from horizontal) soil wall or embankment faces, design for these applications is discussed in detail, with particular reference to the use of simplified design charts.

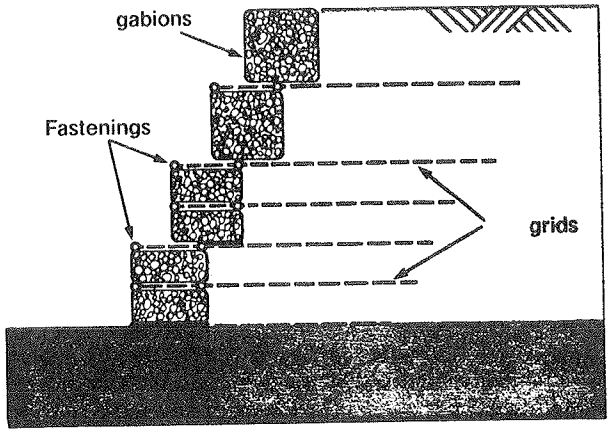

Figure B-75. Gabion facings. [Netlon Ltd., 1984b]

7.2 Safety Factors and Assumptions for Design

7.2.1 Design Parameters

The selection of appropriate safety factors is not yet well defined for extensible polymer reinforcement. As with other soil reinforcement systems, the design safety factors should result in safe and economic designs over a wide range of cases.

For long-term reinforcement, the two most important parameters of geogrid reinforcement are: (1) their characteristic strength in the soil environment (in service); and (2) the long-term relationship between sustained stress and cumulative strain (for example, 100-year isochronous curve).

Jewell et al. [1984b] recommended the following design values for the stability analysis of slopes reinforced with Tensar SR2, which has an allowable strain (Fig. B-71) of 10 percent.

Soil strength. A soil strength value measured at large strains would be appropriate for design with polymer grid reinforcement, and the residual strength friction angle ϕ_r' may be used. For clay fills under drained conditions, i.e., long term, it would be appropriate to assume zero effective cohesion. The short-term stability of such clay fills should be verified using undrained strength parameters.

Polymer reinforcement strength. The strength appropriate to service conditions in the ground at the end of the design life of the structure is appropriate for design. Ideally, this value should be selected on the basis of the most severe expected conditions. However, in practice, probably conservative design strengths are selected on the basis of partial factors of safety.

Overall safety factor. A conventional overall safety factor of the order 1.3 to 1.5 is appropriate. For simplicity, the overall safety factor can be applied to the design value of reinforcement strength.

Geometry. The slope height and slope angle are usually well defined by specific site conditions.

Loads. The maximum expected value of loads which can occur simultaneously should be taken. The soil unit weight, pore water pressures, and surcharge loading may all attain their maximum values at the same time.

7.2.2 Design Charts for Grid-Reinforced Embankments and Slopes

A design procedure for determining a suitable layout of grid reinforcement for embankments with side slopes in the range 30 deg to 80 deg, constructed on stable foundations, has been presented in chart form [Jewell et al., 1984b]. This provides a simple method for producing a preliminary design which quantifies the amount of polymer grid reinforcement required and suggests a practical layout of grids.

The design charts are based on well-established limit equilibrium methods of analysis. They were derived from results provided by the computer program WAGGLE, which has been written for the limit equilibrium analysis of reinforced soil [Netlon Limited, 1984b; Binnie and Partners, 1981]. Results obtained with this program are consistent with those of limit analyses published by Chen [1975] for unreinforced vertical walls and also those for naturally stable slopes published by Bishop and Morgenstern [1960].

The method of analyses used in WAGGLE, as schematically shown in Figure B-76, is based on two-part wedge analyses (see Chapter Four of main report). Wedge nodes are established (Fig. B-76a), and a search is made at each node for the most critical combination of the two wedge angles. A value of mobilized reinforcement force is included in the equilibrium equations at each point that reinforcement intersects a wedge surface. Design proceeds iteratively; a trial reinforcement layout is analyzed, revised, and reanalyzed until a satisfactory solution is found.

The charts developed with WAGGLE considered the following cases (Fig. B-77): (1) embankment slopes built over a competent level foundation that will not be overstressed by the constructed slope; (2) uniform slope with a horizontal crest; (3) uniform surcharge W_s along the slope crest; (4) slope angles with the horizontal in the range 30 deg to 80 deg; (5) soils with effective stress strength parameters in the range $c' = 0$ and $\phi' = 20$ deg to 40 deg; (6) porewater pressures in the slope expressed by the coefficient r_u in the range 0 to 0.5 [Bishop and Morgenstern, 1960]; and (7) polymer reinforcement grids with constant length placed adjacently in horizontal layers. The design strength for the reinforcement grid allows for construction effects, environmental conditions in the soil, and time effects on reinforcement mechanical behavior during the design life of the structure.

7.2.3 Steps for Design Chart Development

The maximum horizontal force T (Fig. B-76), required to hold the slope in equilibrium when the soil and porewater pressures are at their design values, was first determined. If each reinforcement layer can support a maximum force P per unit width, the minimum number of reinforcement layers N required for equilibrium is given by the ratio T/P.

The minimum length L for the reinforcement layers was then determined to ensure adequate wall stability and pullout resistance. Because practical reinforcement layouts are likely to be divided into zones containing layers at an equal vertical spacing, calculations were required to derive practical spacing arrangements that will not lead to local overstressing in any reinforcement layer.

7.2.4 Assumptions and Criteria for Chart Development

Gross horizontal force for equilibrium. The maximum horizontal force, T, required to hold a slope in equilibrium was estimated using the two-part wedge program WAGGLE (Fig. B-76). This force was calculated to provide equilibrium of the critical two-part wedge with the soil shear strength fully mobilized.

Minimum allowable reinforcement length. Three main criteria were identified which govern the selection of the minimum allowable reinforcement length: (1) Internal stability of reinforced soil mass—Reinforcement layers must have sufficient length to prevent pullout of reinforcements under the required design forces (Fig. B-78a). (2) Sliding along base—The reinforcement length must be sufficient to prevent outward sliding along the interface between the soil and a reinforcement layer (Fig. B-78b). (3) Overturning of reinforced soil mass—The reinforced zone, acting as a rigid block, must be wide enough to resist the outward thrust of the unreinforced soil in the slope

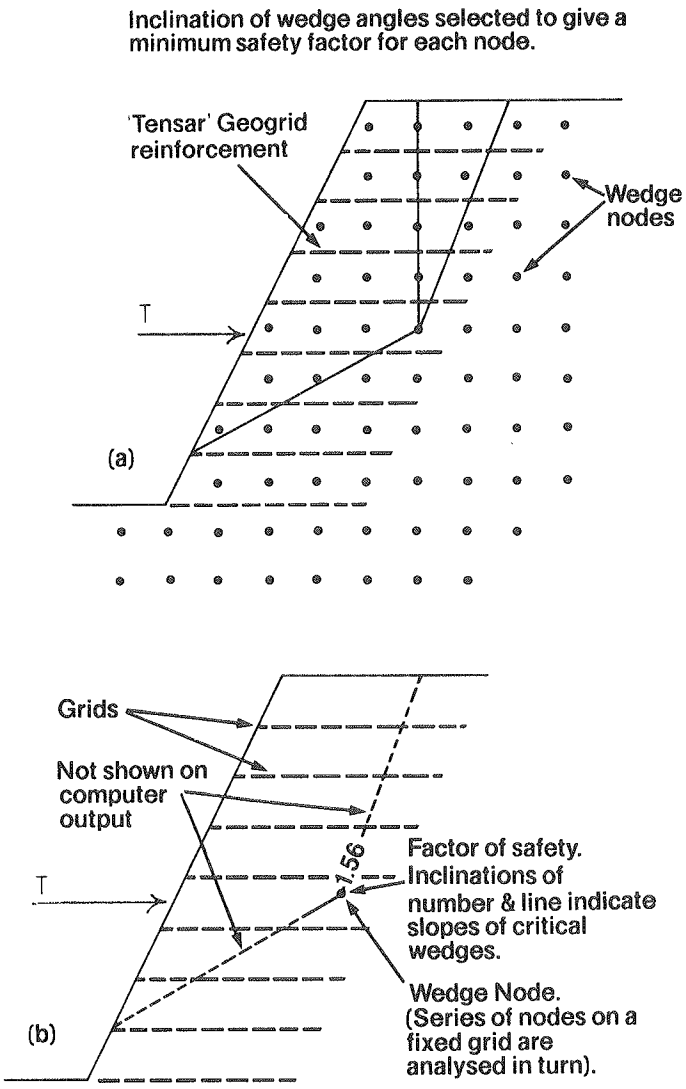

Figure B-76. Definitions for two-part wedge failure mechanisms. [Jewell et al., 1984b]

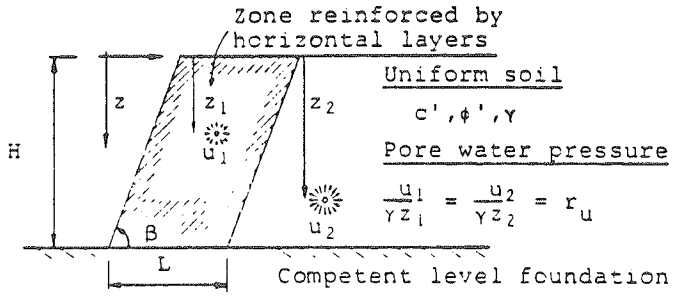

Figure B-77. Definitions for the slope cases examined in design charts. [Jewell et al., 1984b]

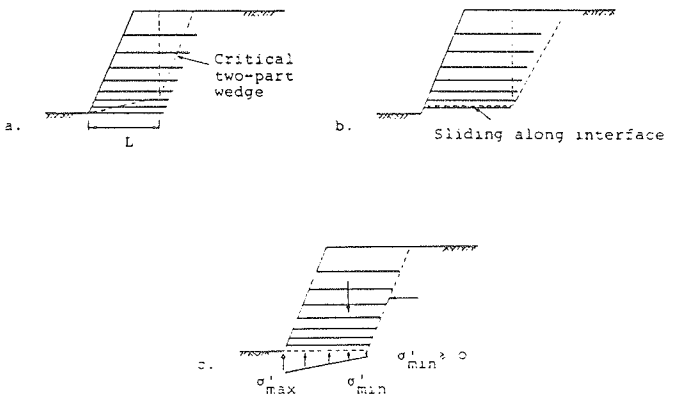

Figure B-78. Criteria to determine the minimum allowable reinforcement length. [Jewell et al., 1984b]

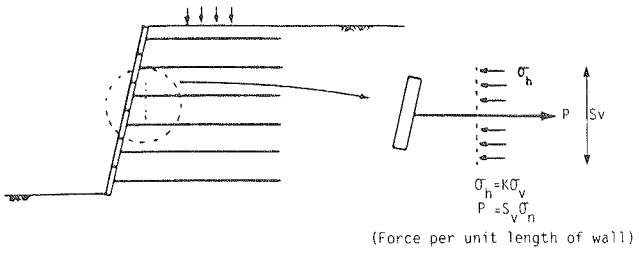

Figure B-79. Concept of local stress equilibrium in reinforced soil slopes.

interior without developing tensile vertical effective stresses anywhere along its base (Fig. B-78c).

Reinforcement spacing. If reinforcement were to be locally overstressed because of unfavorable distribution, the risk of rupture in the reinforcement which could lead to progressive collapse of the reinforced slope would be greatly increased.

The concept of local stress equilibrium in reinforced soil slopes is shown in Figure B-79. Locally, a continuous reinforcement layer at a vertical spacing S_v is required to hold in equilibrium the horizontal soil stresses σ_H, in which case the local mobilized value of reinforcement force P (force per unit transverse length) would be:

$$P = S_v \sigma_H = S_v K \sigma_v \qquad \text{(B-57)}$$

where K is the coefficient of lateral earth pressure.

For steep slopes, where the vertical stress approximately equals the overburden pressure, and provided the lateral earth pressure ratio, K, remains constant with depth, the reinforcement layers would carry approximately equal forces P throughout the slope if the vertical spacing was varied as the inverse of depth. For a constant value of P with depth,

$$S_{vz} = \frac{P}{K \gamma z} \qquad \text{(B-58)}$$

where S_{vz} is the vertical reinforcement spacing at depth z.

The ideal change in vertical spacing with depth is shown in Figure B-80. With the current lack of knowledge about the

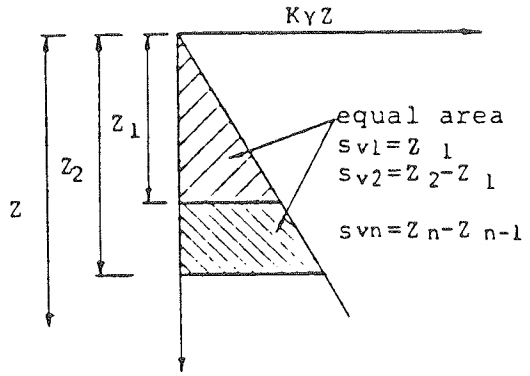

Figure B-80. Change of vertical spacing with depth to provide equally loaded reinforcements. [Jewell et al., 1984b]

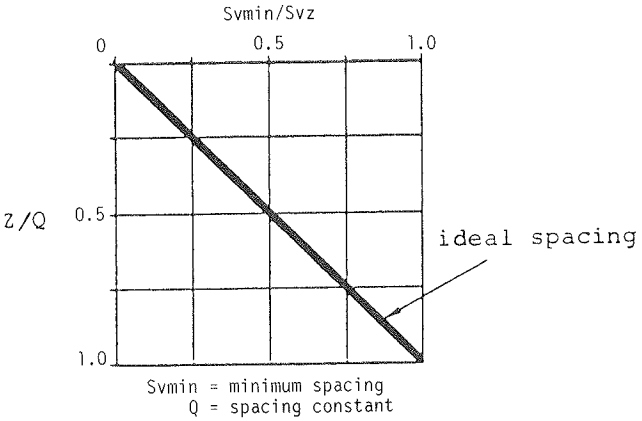

Figure B-81. Variation of spacing S_{vz} *with depth to load reinforcement layers equally.* [Jewell et al., 1984b]

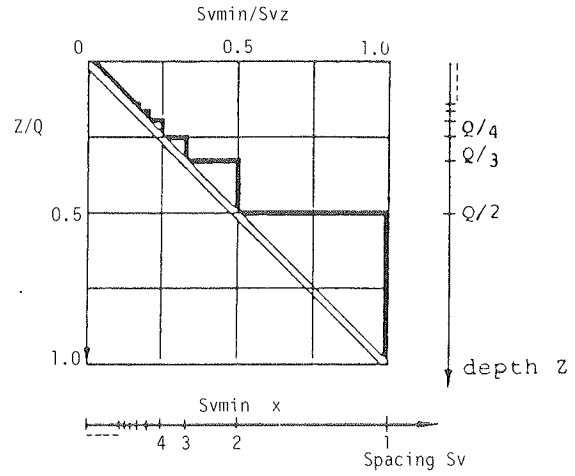

Figure B-82. Zones for reinforcement layers spaced equally at multiples of compaction layer thickness. [Jewell et al., 1984b]

effect of reinforcement spacing on reinforcement forces and overstressing, it would be prudent to space reinforcement layers on the assumption that each layer may locally have to support the horizontal stresses in the soil as shown in Figure B-79, and described by Eq. B-57.

The calculation of spacing arrangements for reinforcement is simplified by defining a spacing constant Q for the slope, in terms of a minimum spacing, S_{vmin}, to be used.

$$Q = \frac{P}{K\gamma S_{vmin}} \tag{B-59}$$

Using Q, the relationship between the maximum allowable spacing of any given depth, S_{vz}, and the depth below the crest of the slope, z, can be reduced to the nondimensional form shown in Figure B-81.

In practice, the actual spacings should be selected as multiples of the compaction layer thickness. Setting the compaction layer thickness equal to S_{vmin}, the maximum depth to which reinforcement spaced at S_{vmin}, $2S_{vmin}$, $3S_{vmin}$ . . . iS_{vmin} may be used can be calculated from the equation,

$$Z_{iy} = \frac{QS_{vmin}}{iS_{vmin}} = \frac{Q}{i} \tag{B-60}$$

To use reinforcement efficiently, the largest allowable spacing should be used at any depth, to give the stepwise distribution shown in Figure B-82. This chart, for example, shows that if z/Q is larger than 0.5, the vertical reinforcement spacing S_v should be equal to S_{vmin}. For depth values between z/Q values of 0.33 and 0.5, S_v can be $2S_{vmin}$.

7.2.5 Design Charts

The charts for three assumed values of pore pressure ratio r_u = 0, 0.25, and 0.50 are shown in Figures B-83, B-84, and B-85, respectively. The terminology used on these charts is schematically defined on Figure B-77.

The charts may be used with the following steps:

1. Define the required embankment dimensions and surcharge loading.
2. Select design values or soil properties and porewater pressures.
3. Determine the earth pressure coefficient K and the length of reinforcement L from the charts.
4. Choose the in-service design strength properties for the reinforcement (Sec. 4.4.9) and an overall factor of safety.
5. Calculate the reinforcement factored design strength P, by dividing the in-service value by the overall safety factor.
6. Choose a minimum vertical reinforcement spacing, S_{vmin}, equal to compaction lift thickness and calculate the spacing constant $Q = P/K\gamma S_{vmin}$ (see Section 7.2.3 of this chapter).
7. Perform a tabular calculation for the number and spacing of reinforcement layers. Start at the bottom of the slope (depth H) and place the first reinforcement layer at foundation level. The number of layers in the first zone of equal spacing can be calculated by dividing the thickness of the zone by the required spacing of the reinforcement (see Sec. 7.2.3 and Fig. B-82). The result is unlikely to be a whole number, and it is sufficient to round down to the nearest integer number of layers, and add the remaining thickness to the overlying zone, repeating the

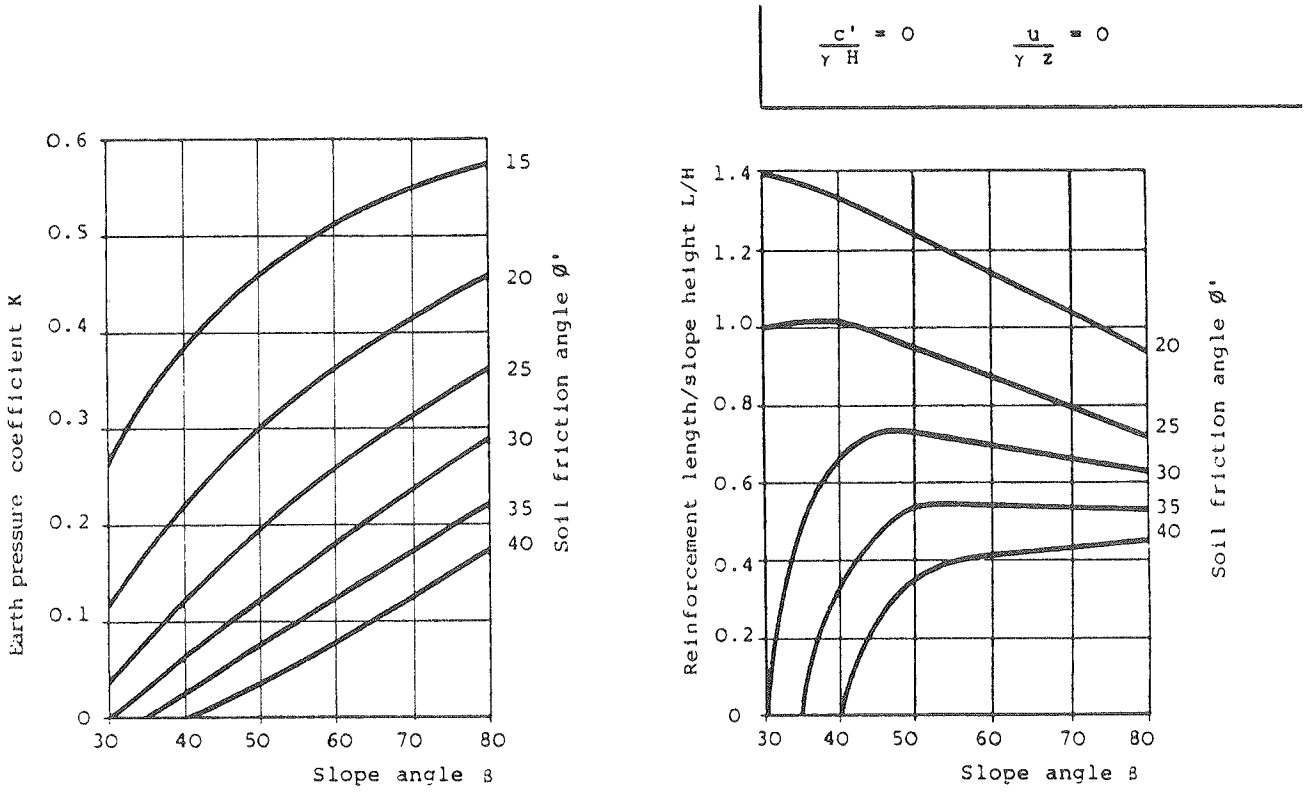

Figure B-83. Simplified design chart with pore pressure coefficient equal to zero. [Jewell et al., 1984b]

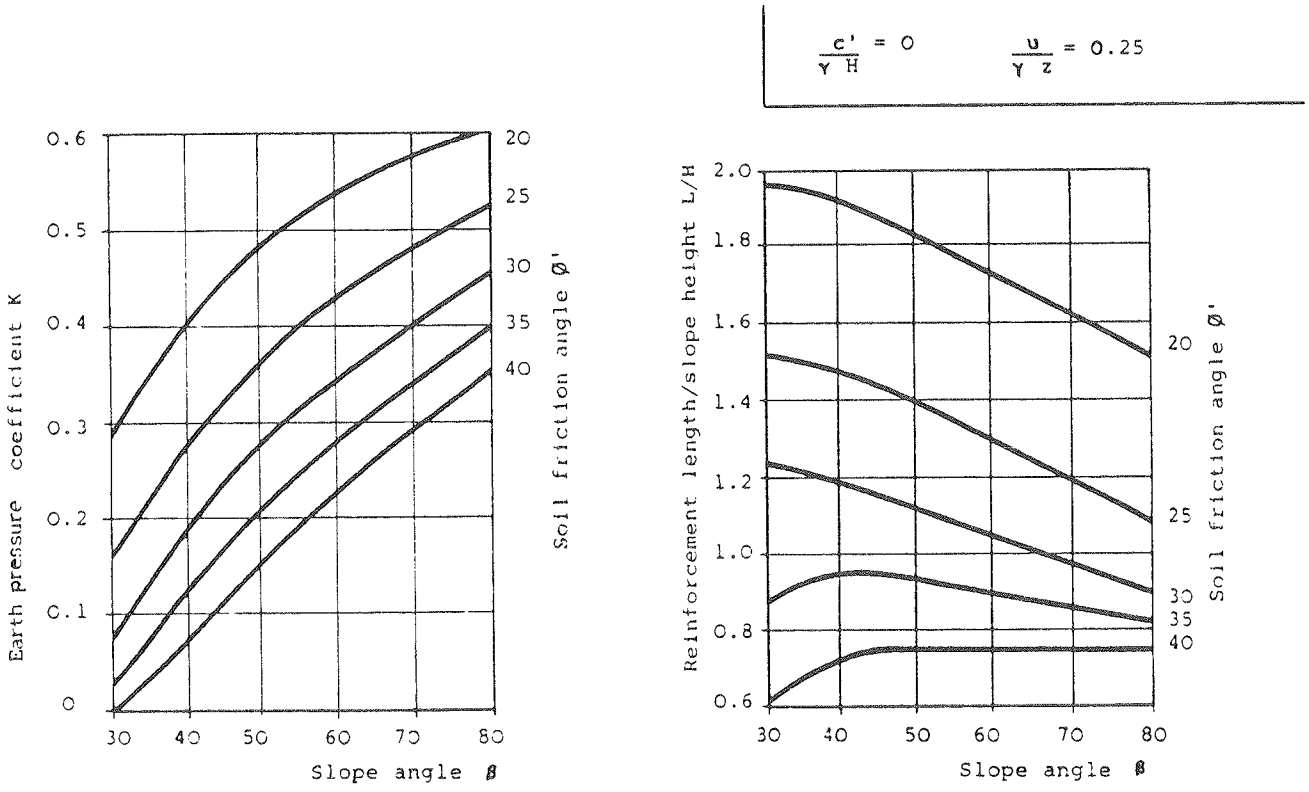

Figure B-84. Simplified design chart with pore pressure coefficient equal to 0.25. [Jewell et al., 1984b]

process to the top of the slope, giving the elevations of each reinforcement layer and the total number of layers N.

8. Check the result by calculating the total horizontal force required for equilibrium,

$$T = \tfrac{1}{2}K\gamma H^2 \qquad \text{(B-61)}$$

and checking that the total required force divided by the calculated number of layers gives a required force per layer less than the factored design strength,

$$T/N < P \qquad \text{(B-62)}$$

7.2.6 Design Chart Example

The example is taken from the technical guidelines for the design and construction of steep reinforced embankments over stable foundations issued by Netlon Limited [1984b].

The problem is to determine a suitable reinforcement layout to provide equilibrium in a 20-ft high embankment with a slope angle 70 deg built from compacted granular soil.

1. The embankment dimensions are shown in Figure B-86 and there is no surcharge loading.

2. The large strain value of shear strength is taken to be $c' = 0$, $\phi' = 29°$, and the maximum density $\gamma = 121$ pcf. The slope is fully drained and $r_u = 0$.

3. The earth pressure coefficient from Figure B-83 is $K = 0.25$. The reinforcement length to embankment height ratio $L/H = 0.69$ from Figure B-83, giving a reinforcement length $L = 13.5$ ft.

4. The in-service characteristic strength suggested by the manufacturer of Tensar SR2 in granular soils is the ideal laboratory value (2,000 lb/ft) divided by a partial factor 1.1 to 1.4 dependent on soil type (see Sec. 4.4.3) to account for possible construction damage, creep, and long-term loss of strength. In this case taking a partial factor 1.3 gives an in-service design strength, $\frac{2{,}000}{1.3} = 1{,}530$ lb/ft.

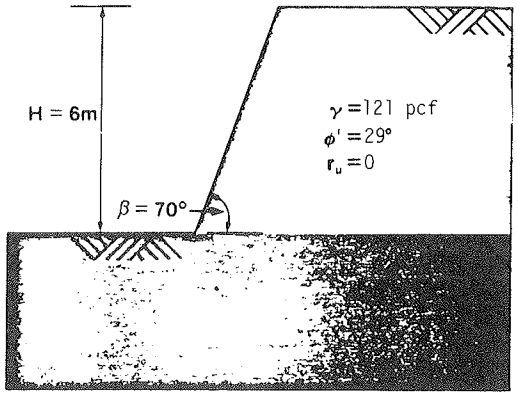

Figure B-86. Slope geometry and soil properties for the design example. [Netlon Ltd., 1984b]

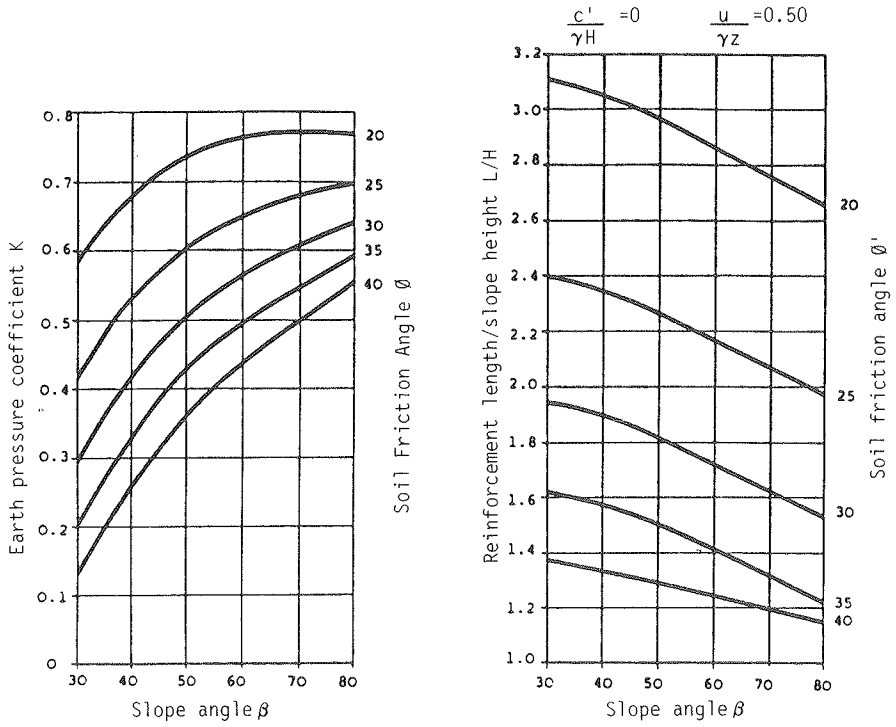

Figure B-85. Simplified design chart with pore pressure coefficient equal to 0.50. [Jewell et al., 1984b]

5. Selecting an overall design safety factor 1.35 fives a factored design strength $P = \frac{1,530}{1.35} = 1,130$ lb/ft.

6. An assumed minimum spacing for the reinforcement S_{vmin} = 9 in. gives a value for the spacing constant $Q = \frac{P}{K\gamma S_{vmin}} =$ 50.6 ft.

7. The depths and thickness of the zones of equal reinforcement spacing may be calculated (see Fig. B-82) and these are shown in Figure B-87.

8. The total horizontal force required to provide equilibrium is $T = \frac{1}{2} K\gamma H^2 = 5,860$ lb/ft.

9. The calculated number of reinforcement grids is 8 (Table B-7, Fig. B-88), giving the check $\frac{5,860 \text{ lb/ft}}{8} = 732$ lb/ft < 1,130 lb/ft, which is sufficient.

8. CASE HISTORIES

Grid reinforcement has been most frequently used in slope applications, especially for the repair of slope failures. Ten case histories are summarized in Tables B-8 and B-9. Those in Table B-8 have been described in greater detail than those in Table B-9. The steep 80 deg reinforced soil slope described in Szymonick et al. [1984] has been included for this review in the wall section.

Synopses of four of the main case histories [Forsyth and Breber, 1984; Szymonick et al., 1984; Devata, 1984; Bonaparte and Margason, 1984] are given in Section 9 where cost comparisons are described. The main features of all the case histories shown in Tables B-8 and B-9 are described in the following.

8.1 Retaining Walls

Details of the four retaining wall case histories are summarized in Table B-10. A cross section of the Oregon wall is shown in Figure B-89, and the cross section for the Sunderland wall is shown in Figure B-90. The cross section for the 20-ft high wall at Dewsbury is similar to that shown in Figure B-91.

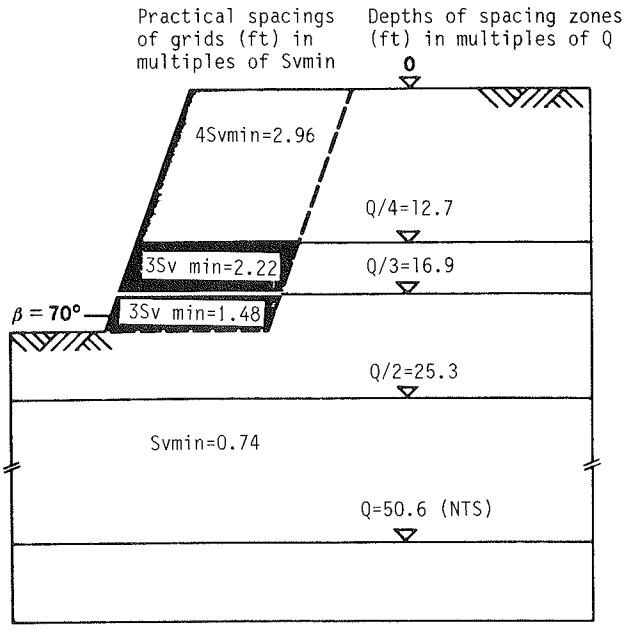

Spacing of Grids in Zone (ft)	Depth to Bottom of Zone (ft)	Thickness of Zone (ft)
Svmin=0.74	Q=50.6	——
2Svmin=1.48	Q/2=25.3	20-16.9=3.1
3Svmin=2.22	Q/3=16.9	16.9-12.7=4.2
4Svmin=2.96	Q/4=12.7	12.7-0=12.7
		Height=Σ=20.0

Figure B-87. Depth and thickness of reinforcement spacing zones for the design example. [Netlon Ltd., 1984b]

Table B-7. Number of reinforcement layers in each zone as drawn in Figure B-88. [Netlon Limited, 1984b]

Spacing in zone (ft)	Thickness of zone (ft)	Calculated number of grids	Chosen number of grids	Remainder (ft)
		Initial grid at base	1	
1.48	2.79	2.79/1.48 = 1.89	1	0.89 x 1.48 = 1.32
2.21	4.23	(4.23 + 1.32)/2.21 = 2.50	2	0.8 x 2.21 = 1.10
2.95	12.70	(12.7 +1.10)/2.95 = 4.67	4	0.67 x 2.95 = 2.0
		Total	8	

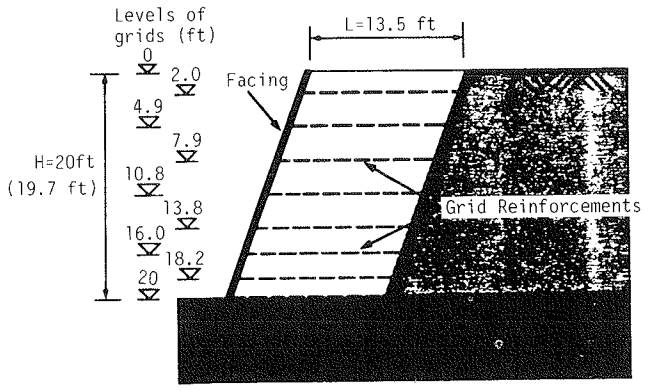

Figure B-88. Positions of eight reinforcement layers as calculated in Table B-7. [Netlon Ltd., 1984b]

Table B-8. Summary of six main case histories.

	Walls	Slopes	Slip Repairs
References	Szymonick et al., (1984); Pigg and McCafferty (1984)	Devata (1984)	Forsyth and Bieber (1984); Szymonick et al., (1984); Busbridge (1984)
Height	10 ft to 30 ft	23 ft	30 ft to 40 ft
Slope Angle	80° to 90°	45°	30° to 80°
Fill Type	granular	glacial till	granular

Table B-9. Summary of four case histories with limited details.

	Walls	Slopes	Slip Repairs
References	Paul (1984); New Civil Engineer (1984)	Elwell and McGloin (1984)	Netlon Limited (1983)
Height	20 ft to 23 ft	29 ft	30 ft
Slope Angle	90°	45°- 70°	17°
Fill Type	granular	granular	clay

Design details. Three of the four walls were designed using methods devised for Reinforced Earth walls modified for the case of polymer reinforcement material. Design of the Oregon wall was based on the method developed for geotextile reinforcement by Bell et al. [1975] and Whitcomb and Bell [1979]. A "working force," 2,200 lb/lin. ft, which was greater than the manufacturer's presently recommended value, was adopted for the Tensar SR2 reinforcement. A safety factor of 2.0 for dead loading conditions was adopted in conjunction with conventional "peak" soil shear strength parameters.

Although not directly stated, the same value of 2,200 lb/lin. ft was almost certainly adopted for Tensar SR2 in the design of the Sunderland wall [Pigg and McCafferty, 1984]. A value of friction angle of 35 deg was used in design for the compacted colliery shale fill to give a minimum safety factor 2.0.

Facing. The types of facing used are given in Table B-10.

For the Oregon wall the reinforcement was wrapped around to form the face. Early in construction of the Oregon wall, loss of material at the face and bulging caused problems [Szymonick et al., 1984]. Two contributing factors were (1) soil particles could pass through the grid apertures at the face; and (2) temporary formwork supporting the face deflected significantly during placement of the backfill at the wall face.

Both factors were recognized and rectified, and an improved method of support was devised [Szymonick et al., 1984]. Systems for supporting wall and slope faces made by wrapping with reinforcement are described by Paul [1984].

Conventional interlocking concrete panels were selected for the Sunderland wall. A variation was tried at the Dewsbury trial wall (Fig. B-91). In this case the concrete panels were held between continuous upright I-section columns, to which the reinforcement was attached.

Instrumentation and measurements. No instrumentation was reported on the Newport, Dewsbury, and Lancashire walls. Maximum face movements were reported for the Sunderland wall to be less than 2 in. vertical settlement and less than 1.2 in. outward movement.

The Tensar SR2 was strain gauged to give extensions at one point on the reinforcement during construction of the Dewsbury trial wall. Although detailed surveys of face deflectors and deflections at the joint between the face and grid reinforcement were carried out, the data have not yet been published.

General comment. In all cases, the retaining wall structures served their intended purpose well. In no case did the extensibility of the Tensar SR2 reinforcement result in undue face movements. Face deflections and serviceability criteria were not mentioned as an important aspect of design or subsequent performance.

Table B-10. Details of retaining wall case histories.

Reference	Szymonick et al. (1984) Busbridge (1984)	Pigg & McCafferty (1984)	Paul (1984)	New Civil Engineer (1984)
Date built	1983	1981	1981	1983
Site	Near Newport, Oregon, USA	Low Southwick, Sunderland, U.K.	Preston, Lancashire U.K.	Dewsbury, Yorkshire U.K.
Height-H	30 feet	11.5 feet	23 feet	20 feet
Slope angle β	80°	90°	90°	90°
Fill type	crushed basalt	burnt colliery shale	sand	sandstone derivative
c', ϕ'	0, 40°	0, 35°	--	--
γ	140 pcf	127 pcf	--	--
Reinforcement	Tensar SR2	Tensar SR2	Tensar SR2	Tensar SR2
L/H	0.54	0.89	--	1.00
Min. spacing S_{vmin}	1 foot	1.6 feet	--	--
Pore water	0	0	0	0
Facing	wrap around	concrete panels	wrap around	concrete panels

There are two aspects of time-dependent behavior, i.e., creep strains and loss of strength, which cannot be commented on until further time has passed for these structures. Information on long-term "in-service" strength for the grids could be obtained from recovered samples (preferably of materials that have been supporting forces) tested in creep under loads of the order of the assumed "working force."

8.2 Embankments and Slopes

Details of the two case histories are summarized in Table B-11, and a cross section of the embankment in Brampton, Ontario, is shown in Figure B-92.

Design details. The size of the reinforced zone required to maintain the unreinforced interior in equilibrium was calculated for the Brampton Ontario embankment to give a safety factor 1.5 against outward sliding movements [Devata, 1984]. The reinforcement spacing within the reinforced zone was determined by limit equilibrium calculations. A minimum value of

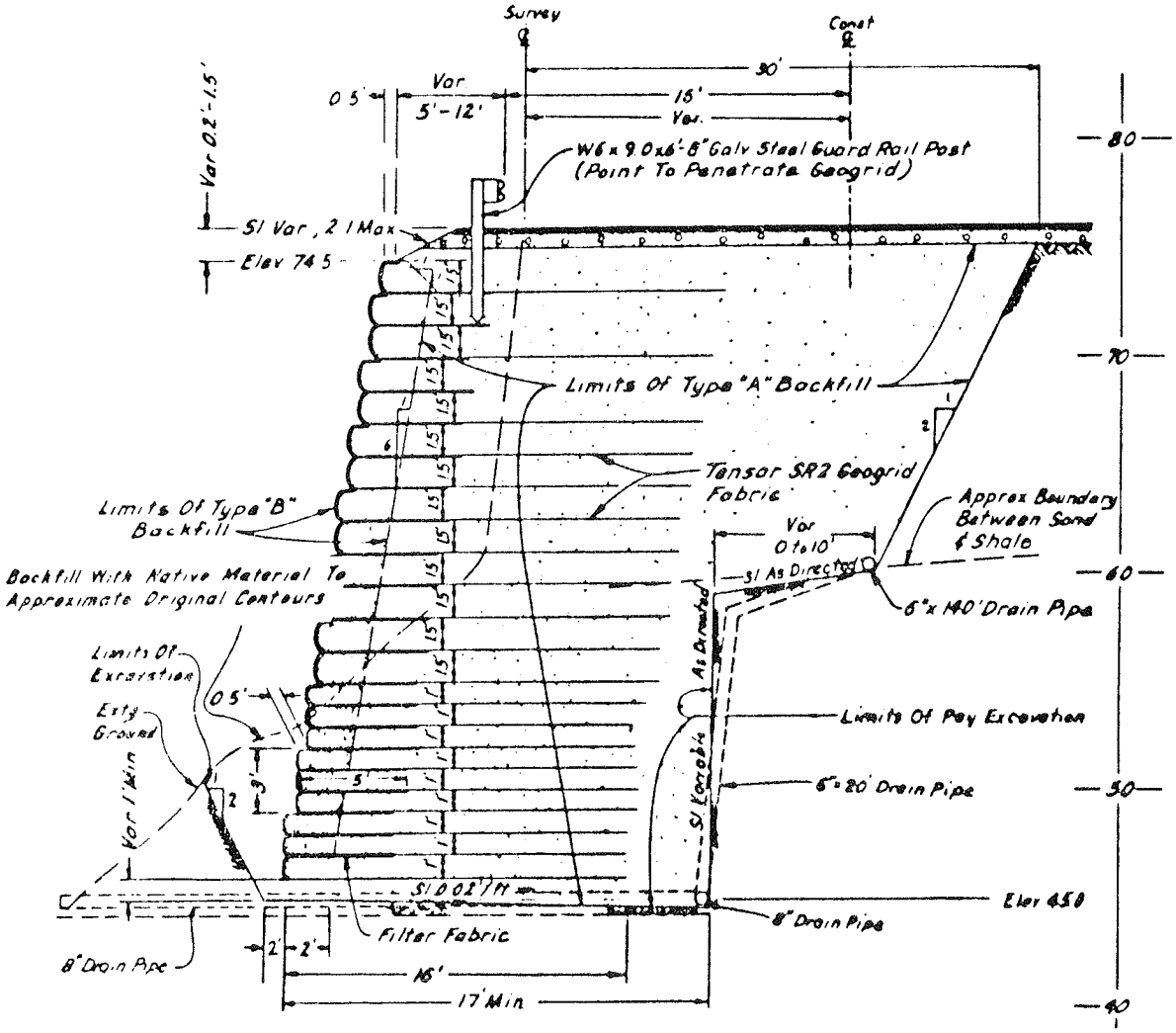

Figure B-89. Reinforced soil wall near Newport, Oregon. [Szymonick et al., 1984]

safety factor of 1.30 was used for shear surfaces in the reinforced fill. A "limiting force" of 2,200 lb/ft was used for the Tensar SR2.

Facing. Because of problems of frost penetration in Ontario, the surface of the reinforced zone was formed from a 5 ft thickness of granular fill, reinforced at 10-in. vertical spacings by a biaxial Tensar grid SS1 (see Fig. B-92). The face of the embankment was covered with topsoil and seeded, with a mesh pegged over the surface.

The steep reinforced fill in Cleveland, U.K., formed an abutment to a pile supported bridge crossing a river. A gabion facing was selected because it was sufficiently flexible to accommodate differential settlements during consolidation of the underlying estuarine deposits, and sufficiently robust to resist erosion from high river flows.

Instrumentation and measurements. An extensive instrumentation of a second portion of embankment is planned at the Brampton, Ontario, site where it is hoped to measure horizontal soil strains and reinforcement strains.

General comments. The same general comments made for the retaining wall case histories apply here. Both embankments served their design purposes, and no undue soil movements were observed during or subsequent to construction.

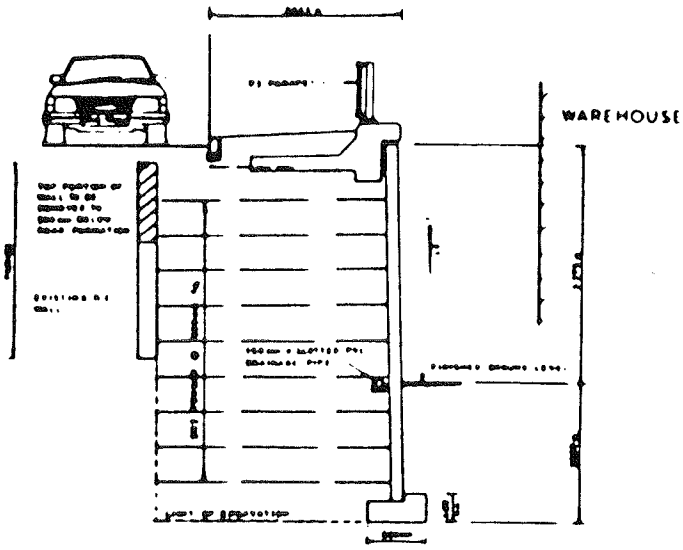

Figure B-90. Reinforced soil wall at Low Southwick, Sunderland, U.K. [Pigg and McCafferty, 1984]

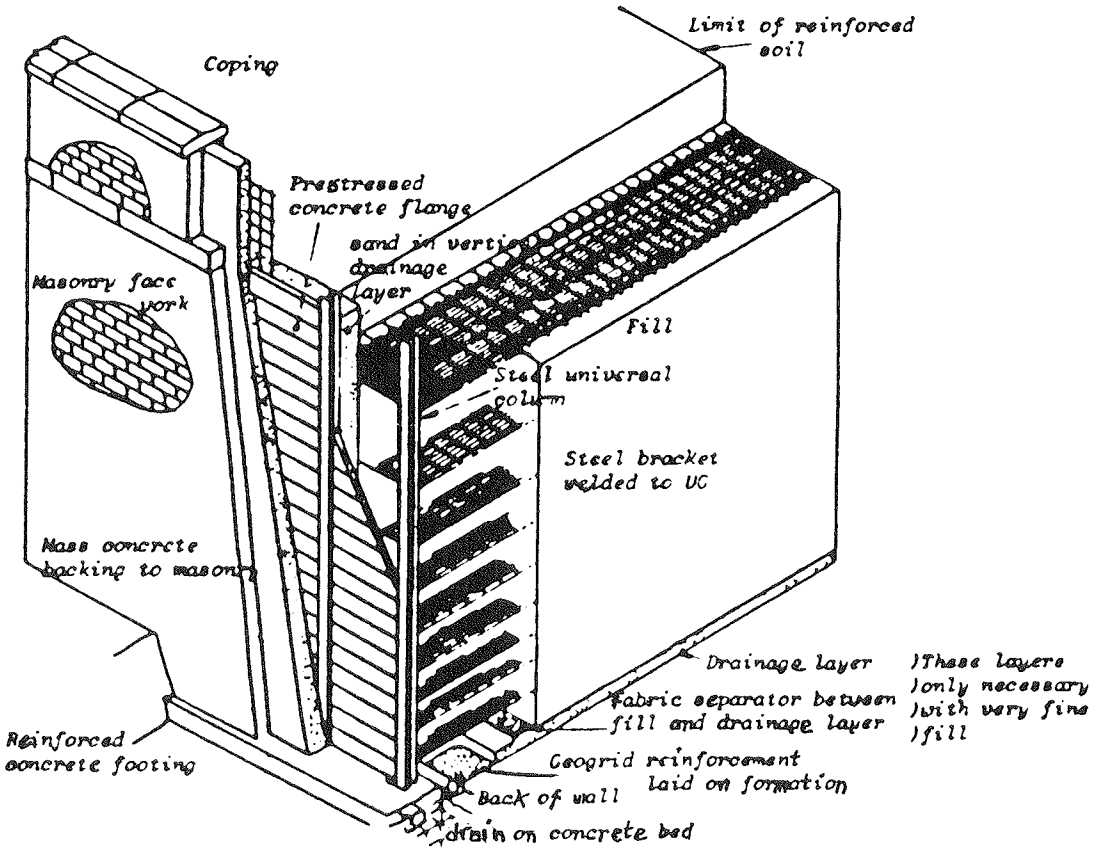

Figure B-91. Reinforced soil arrangement similar to the trial wall at Dewsbury, Yorkshire, U.K. [Jones, 1984]

Table B-11. Details of embankment and slope case histories.

Reference	Devata (1984)	Elwell and McGloin (1981)
Date built	1983	1980
Site	Brampton, Ontario, Canada	Greatham, Cleveland, U.K.
Height - H	23 ft	11.5 ft
Slope angle β	45°	45° and 70°
Fill type	glacial till	crushed limestone
c', ϕ'	0, 31°	--
γ	140 pcf	--
Reinforcement	Tensar SR2	Tensar SR1
L/H	0.36 to 1.57	--
Min. spacing S_{vmin}	3.3 ft	--
Pore water	0	0
Facing	multiple short reinforcements	gabion

8.3 Slope Failure Repairs

Details of three slope failure repair case histories are given in Table B-12. These cases were repair of slopes to approximately the pre-failure slope geometry. Cross sections for the three reinstated slopes are shown in Figures B-93 (La Honda, California), B-94 (Waterdown, Ontario), and B-95 (M1 Motorway, Nottinghamshire, U.K.).

Design details. Limit equilibrium methods were used in the design of all the three case histories.

The analysis for the La Honda case was done with a slip circle analysis. The horizontal force required to hold the slope repair in equilibrium with a conventional safety factor 1.2 was calculated. The force which could be provided by each layer of Tensar SR2 was taken to be 460 lb/lin. ft, and sufficient layers were incorporated at equal spacing to provide the required force.

Circular and noncircular slip surfaces were examined in the analysis for the repair at Waterdown, Ontario. A safety factor of 1.3 was required, and the Tensar SR2 reinforcement could provide 1,100 lb/ft per layer, or a lesser value governed by bond, in order to provide the additional horizontal force for equilibrium.

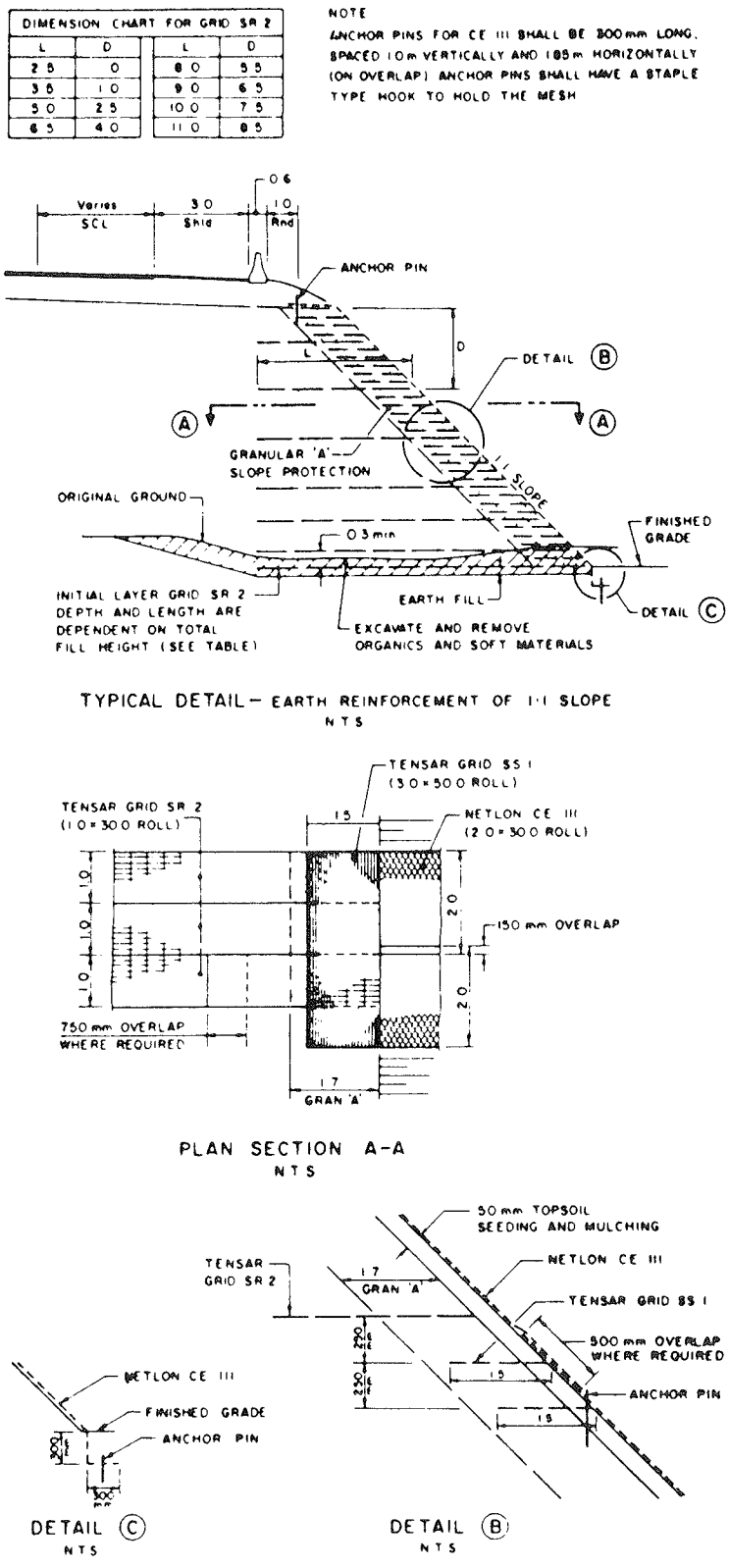

Figure B-92. Reinforced embankment at Brampton, Ontario, Canada. [Devata, 1984]

The cut slope failure in clay on the M1 Motorway was almost certainly triggered by a high water table [Netlon Limited, 1983]. Two-part wedge surfaces were used in the analysis for the repair.

Facing. Wraparound facing was adopted at all three sites. Busbridge [1984] recommends that for slopes steeper than 45 deg, temporary support should be used to provide reaction against which fill can be compacted. He believes the inclusion of short, closely spaced reinforcements at the embankment face (as in the Brampton case history) is easier to construct than wrapping the reinforcement at the face.

For flat clay slopes (e.g., M1 Motorway), the construction of a wraparound face was also time consuming. Again regular, closely spaced reinforcement at the face might have been a preferable method of providing surface stability.

Table B-12. Details of slope failure repair case histories.

Reference	Forsyth, Bieber (1984)	Busbridge (1984)	Netlon Ltd. (1983)
Date built	1984	1982	1982
Site	La Honda, California, USA	Waterdown, Ontario, Canada	M1 Motorway, Nottinghamshire, U.K.
Height-H	30 ft	15 ft and 18 ft	30 ft
Slope angle β	45° to 48°	34° and 45°	17°
Fill type	granular	till	clay
c', ϕ'	50 psf, 32°	0, 35°	0, 25°
γ	--	127 pcf	133 pcf
Reinforcement	Tensar SR2	Tensar SR2	Tensar SR2
L/H	0.66	0.64 and 1.00	0.61 to 0.80
Min. spacing S_{vmin}	2.0 ft	3.9 ft	4.9 ft
Pore water	0	0	Water table and seepage at 2/3 H
Facing	wrap around	wrap around	wrap around

Instrumentation and measurements. A program of instrumentation was planned for the slope repair at La Honda. Soil movements were to be measured by an inclinometer, three horizontal extensometers, and from surface surveys. The results from the planned instrumentation are not yet published.

General comments. The stabilization and reinstatement of slope failures using polymer grid soil reinforcement appears to be attractive and cost effective. Ease of construction at difficult sites is a particular benefit.

8.4 Special Applications

Grid reinforcement was used to form a steeply sloping abutment to support a road at the head of a slip failure zone, Figure B-96 [Bonaparte and Margason, 1984]. The reinforced soil abutment was founded on the hard claystone underlying the weathered clay in which the slip had occurred. The grid reinforcement was wrapped around to provide the facing.

The aim of the abutment is to isolate the road from any subsequent movements of the unstable slope. Unlike the other case histories, the steeply sloping reinforced abutment is partly supported by the fill placed up the slope face. The full design loading would only occur if slip movements occurred in front of the reinforced mass and the abutment face became fully or partially self-supporting.

Four alternative methods of forming the abutment were gabions, concrete cribbing, a conventional concrete retaining wall, and soil reinforcement. The polymer grid-reinforced abutment was the least expensive alternative.

9. COST COMPARISONS

Information on construction costs for polymer grid-reinforced soil applications is included in four publications (see Table B-13). Synopses of each case are given in the following sections.

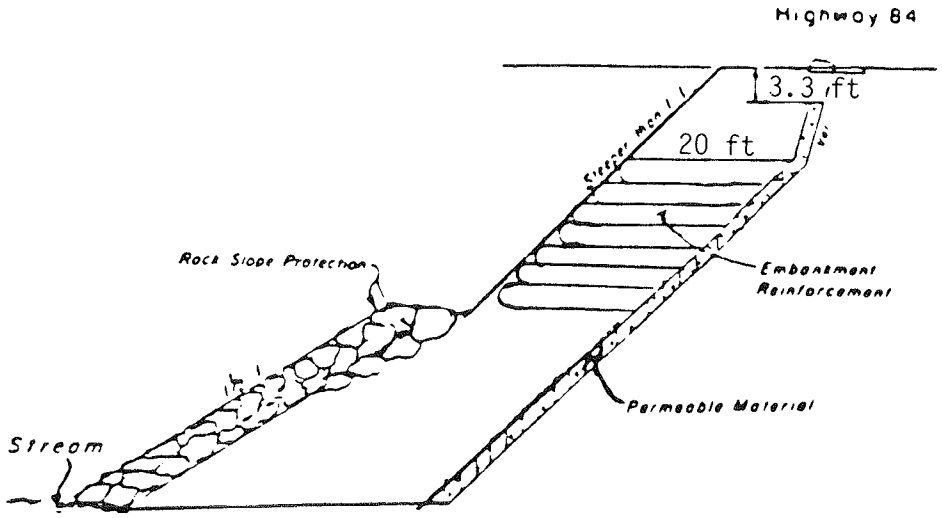

Figure B-93. Slope failure repair at La Honda, California. [Forsyth and Bieber, 1984]

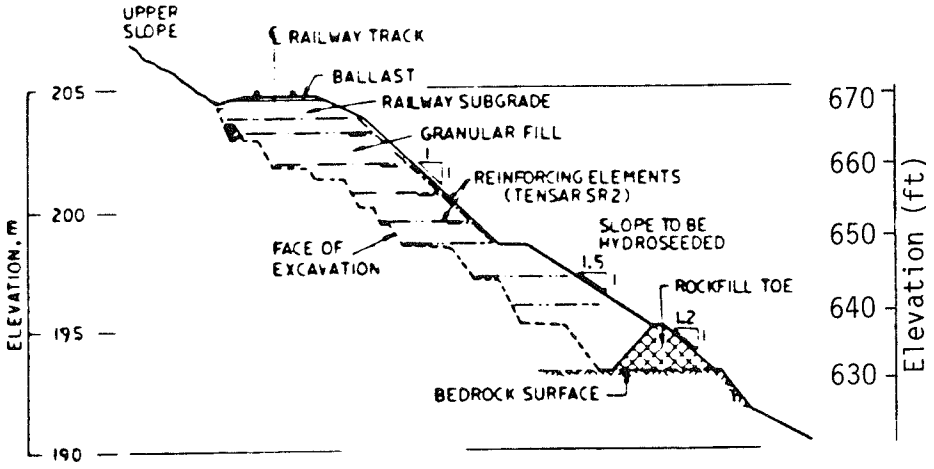

Figure B-94. Slope failure repair at Waterdown, Ontario, Canada. [Busbridge, 1984]

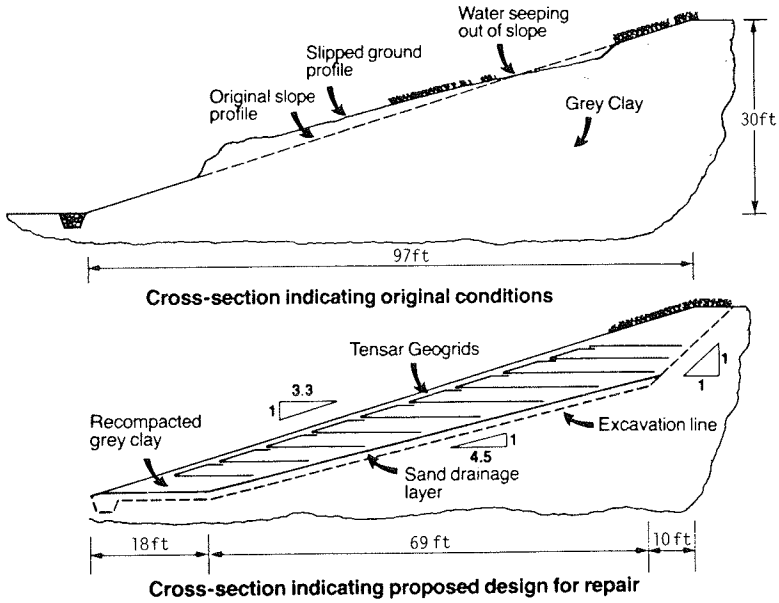

Figure B-95. Slope failure repair adjacent to the M1 Motorway, Nottinghamshire, U.K. [Netlon Ltd., 1983]

9.1 Embankment Construction, Brampton, Ontario

For a provincial highway project in Brampton, Ontario, property acquisition costs and other problems necessitated the design of retaining structures or steep side slopes for a 23-ft high embankment [Devata, 1984].

The proximity of the east side of the highway to recently constructed industrial buildings was such that standard side slopes of 2 horizontal to 1 vertical could not be constructed without the acquisition of private property at great expense and lengthy delays. The steepest slope that could be constructed without acquiring new property was 1:1. It was necessary, therefore, to consider the various options in some detail to determine the most economical solution.

The options were: (1) to construct an earth retaining structure which could be built without acquiring new property; (2) to construct a rockfill embankment with side slopes of 1¼ horizontal to 1 vertical, which would require some additional property; and (3) to construct a 1:1 side slope of earth fill reinforced with synthetic tensile elements.

Table B-14 shows a comparison of the costs of the various alternatives considered including property costs for the east side of the highway for a total length of about 0.6 mile.

These studies showed that a steep side slope reinforced with synthetic tensile elements was considerably cheaper than other alternatives, and the method was therefore selected.

9.2 Retaining Wall, Newport, Oregon

The Oregon State Highway Division constructed a near vertical Tensar SR2 geogrid-reinforced wall to stabilize a landslide on the Oregon Coast [Bell et al., 1984; Szymonick et al., 1984]. The wall was approximately 33 ft high and 164 ft long at the

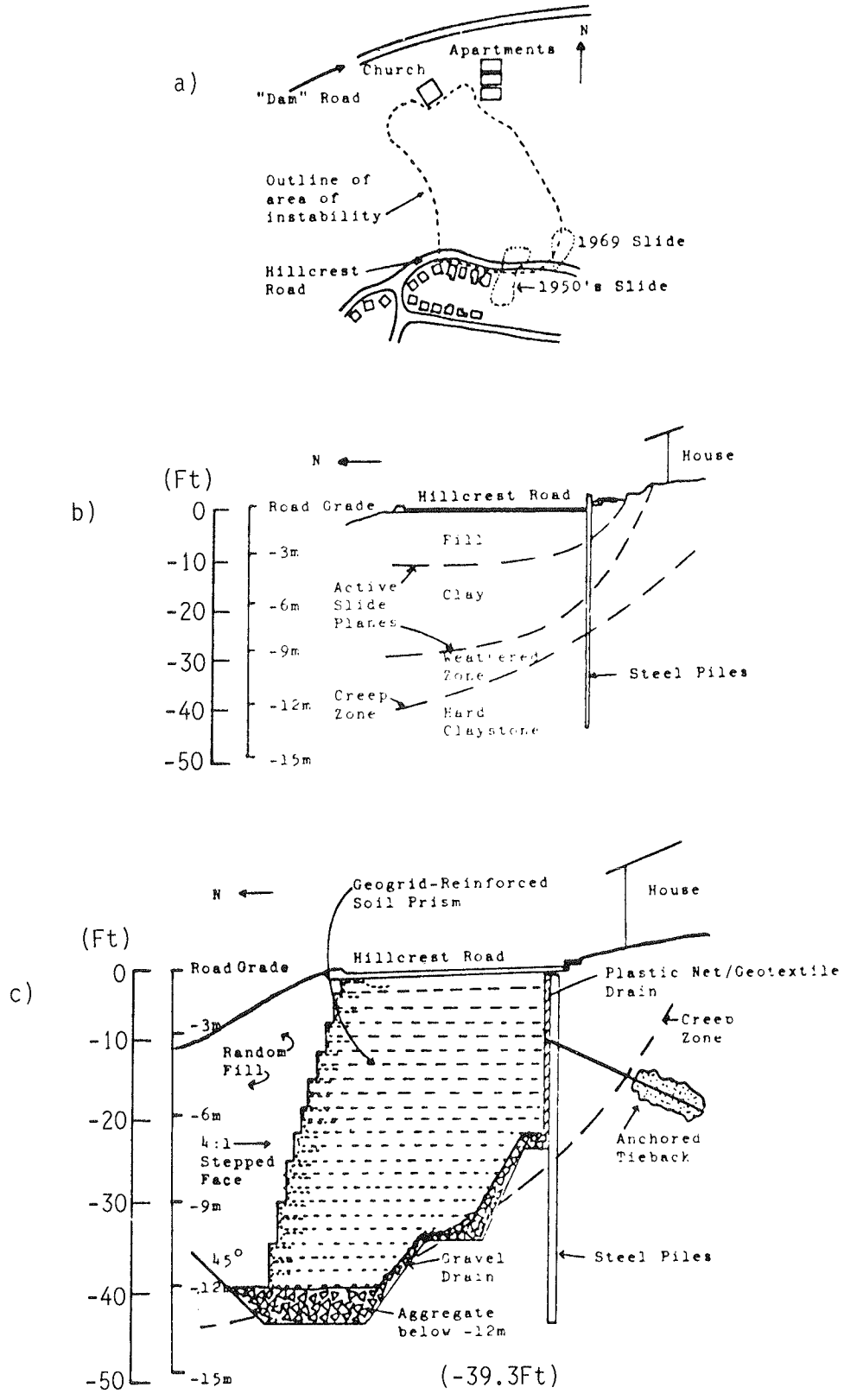

Figure B-96. Special application at the head of a slope failure in San Pablo, California. [Bonaparte and Margason, 1984]

Table B-13. Summary of published cost case histories.

Applications	Embankment	Retaining wall	Slope failure repair	Theoretical study
Location and/or Reference	Brampton Ontario (Devata, 1984)	Newport Oregon (Szymonick, et al., 1984)	La Honda California (Forsyth & Bieber, 1984)	Paul (1984)
Costs for polymer grid reinforced soil solutions	X	X	X	X
Comparative costs of alternative constructions	X			X
Statement of relative cost of alternatives	X	X	X	X

Table B-14. Cost comparison, Brampton, Ontario (millions of Canadian dollars).

Construction Method	Construction Costs	Property Costs	Total Costs
Reinf. Conc. Wall	1.52	Nil	1.52
Bin Wall	1.42	Nil	1.42
Reinf. Earth Wall	1.38	Nil	1.38
1½:1 Slope (Rockfill)	0.93	0.30	1.23
1:1 Slope (Reinforced with 'Tensar')	0.48	Nil	0.48
2:1 Slope (Earthfill)	0.30	0.90	1.20

top. The site was adjacent to a state park, and special considerations were given to providing a natural appearance. Sod was placed behind the grid to establish vegetation on the face of the wall, but was unsuccessful.

Three alternatives were considered by the Oregon State Highway Division for stabilizing the slide. The first alternative was a tie-back soldier pile wall with precast concrete panels and a lightweight backfill. The second alternative was a nonwoven geotextile retaining wall with a gunite facing. The geogrid wall, the third alternative, was chosen over the other two alternatives for two reasons: (1) The geogrid retaining wall had the lowest estimated cost; and (2) it was believed that the open face of the geogrid wall would allow establishment of vegetation on the wall to provide a natural appearance compatible with the surroundings of the state park.

The engineers estimated the project cost to be $165,802, the low bid was $166,328, and the actual cost was $183,395. This translates to $23.70/sq ft of wall face. The in-place cost for the geogrid including the geogrid material, forming, and handling was $0.61/sq ft of grid and $11.15/sq ft of wall face.

9.3 Slope Failure Repair, La Honda, California

As a result of a series of storms almost unprecedented in their intensity and duration in January 1982, the toe of the highway embankment on Route 84 near La Honda was eroded by the action of a stream causing a slipout [Forsyth and Bieber, 1984]. Site geometry required restoration of a 46-ft high embankment with slopes greater than 1:1. Polymer grid, metal grid (bar mat), and tire wall reinforcement options were examined.

The cost of the reinforcement materials are given as follows:

Tensar SR2
$64{,}550\ ft^2$ at $\$0.42/ft^2 = \$27{,}000$ (1982)

Tire reinforcement
$51{,}640\ ft^2$ at $\$1.26/ft^2 = \$65{,}000$ (1982)

Metal grid reinforcement
$22{,}160\ ft^2$ at $\$6.25/ft^2 = \$138{,}600$ (1982)

The solution using Tensar SR2 grid was selected.

9.4 Theoretical Cost Comparisons

A theoretical study was conducted on the costs of alternatives for blast protection embankments [Paul, 1984]. The case examined was for a 28-ft high structure with a crest width between 3.3 ft and 6.6 ft. Three alternatives were: (1) a vertical concrete cantilever wall backed by an unreinforced slope, (2) an unreinforced embankment, and (3) a steepened embankment reinforced on both sides with wraparound facing (Tensar SR2).

The estimated costs for the alternatives were £426.8, £312.5, and £289.6, respectively, per foot length.

10. FUTURE DEVELOPMENTS

10.1 Polymer Reinforcement Properties

There is an urgent need for further testing to provide a wider basis for the selection of long-term properties for polymer reinforcements.

In the case of Tensar SR2, there is a need for elevated temperature testing to accelerate time effects, and further long-term creep tests over a range of temperatures.

Additionally, more test data to show the influence of site damage on polymer reinforcement properties are urgently required.

There would be great benefits to all designers if independent tests on polymer materials could be conducted—particularly for the long-term properties. These data would be most useful if the tests were done following internationally accepted procedures and conditions.

10.2 Field Measurements

There is an urgent need for detailed measurements on field constructions. Again, because of the cost and effort required to obtain a comprehensive set of data these should perhaps be carried out with central funding, perhaps on a national test bed site.

For polymer reinforcement, the relationship between stress (or force) and strain (or overall deformations) is indeterminate. It is essential that both the variation of tensile strain along the reinforcement *and* the variation of tensile stress are both measured. For polymer grids the axial force would be measured on load carriers inserted at points along the reinforcement length.

These data would provide important information both on the stress strain properties of polymer reinforcement in service and on the magnitude of mobilized bond stresses between the reinforcement and soil.

10.3 Soil-Reinforcement Interaction

The two main mechanisms of interaction, passive resistance and frictions have been identified. The magnitude of bond stress for grids needs to be further investigated to give values for design. Useful information will be derived from field measurements.

10.4 Strain Compatibility

There is a paucity of data on strain compatibility for soil reinforced by extensible reinforcements. More information is needed on which to base the selection of maximum allowable tensile strains in the design of reinforced soil. Additional studies to show the relationship between mobilized soil shear strength and tensile strain in soils tested under plane strain conditions are needed.

10.5 Reinforced Clay and Waste Materials

The use of "poor" fill materials through reinforcement is one of the most attractive possibilities of the technique. Polymer grid reinforcement should be particularly suited for this case. Investigations are needed both at laboratory and field scale.

11. DESIGN EXAMPLES

Several design examples that are not based on the design charts, but instead follow general reinforced soil design methodology, are provided in Chapter Five of the main report. In the following sections, three design cases of geogrid-reinforced slopes and embankments are compared with the solution derived from the simplified design charts. These illustrate the close similarity between what was eventually selected for construction and the design chart solution. The examples also serve to show the wide variety of safety factors that have been used, and highlight the need for a more uniform approach to selecting safety factor values.

11.1 Summary of Case History Details

Three reinforced soil slope projects were reported as case histories at the recent Symposium on Applications of Polymer Grid Reinforcement in Civil Engineering, held in London during March 1984. All three reinforced slopes support highway or road works, and the key data are summarized in Table B-15.

The assumptions about parameters and safety factors for the case histories are given in sufficient detail by the authors to allow a chart design to be derived for comparison with the reinforcement layout that was adopted.

11.2 Reinforced Slope at Newport, Oregon

The 9m high, 80 deg slope reported by Bell et al. [1984] and Szymoniak et al. [1984] was constructed in 1983 to support a road lost by a slip failure. A crushed basalt fill was reinforced by Tensar SR2 polymer grid reinforcement in the arrangement shown in Figure B-97. The chart design for this slope would proceed as follows.

1. The slope height H was 9m and the slope angle β was 80.6 deg. The "dead load" case was the most severe for design, so no surcharge was included.
2. Peak strength for the crushed basalt was $c' = 0$, $\phi' = 40°$ with a unit weight of 22 kN/m^3. The fill was free draining and

Table B-15. Summary of case histories for back analysis.

Reference	Bell et al. Szymoniak et al.	Forsyth and Bieber	Devata
Date built	1983	1984	1983
Site	Nr Newport, Oregon, USA	La Honda, California, USA	Brampton, Ontario, Canada
Height	9m	9.5m	9.5m
Slope angle	80°	48°	45°
Fill type	Crushed basalt	Granular	Glacial till
c', ϕ'	0, 40°	2.5, 32°	0, 31°
γ	22 kN/m^3	-	22 kN/m^3
Pore water	0	0	0
Reinforcement	Tensar SR2	Tensar SR2	Tensar SR2
L/H	0.54	0.63	0.36 to 1.57
Min. spacing v	0.30m	0.6m	1.0m
Facing	wrap around	wrap around	multiple short layers

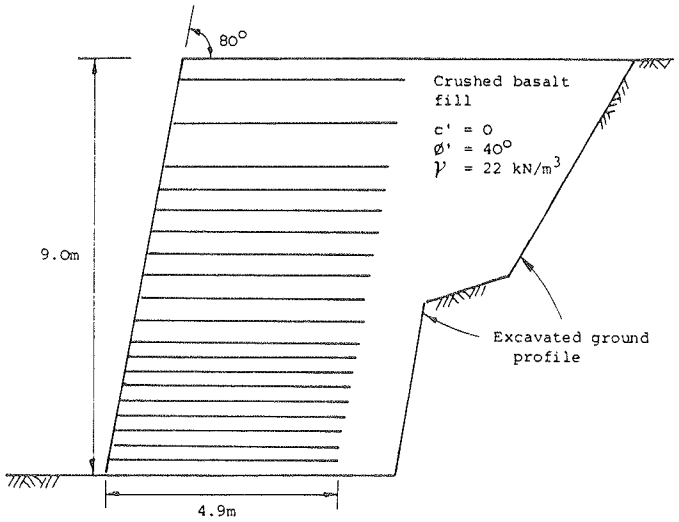

Figure B-97. Reinforcement arrangement for slope at Newport, Oregon. [After Szymoniak et al., 1984]

no pore water pressures were assumed. A factor would normally be applied to peak strength parameters to derive a design soil strength. It is not clear whether the authors applied such a factor. A factor of 1.3 has been assumed for the design chart calculations, and the design friction angle for the soil is therefore:

$$\phi' = \tan^{-1}\left(\frac{\tan 40}{1.3}\right) = 32.8°.$$

3. Values for K and L/H are determined from the charts for $r_u = 0$ in Figure B-83, with design values $\phi' = 32.8°$, $\beta = 80°$: $K = 0.25$ and $L/H = 0.58$.

Thus the required length of reinforcement is: $L = 0.58 \times 9.00 = 5.22$m.

4. The authors took 40 percent of the short-term strength of Tensar SR2 as a working value and applied a partial factor of 2.0 to this value for design. They took the short-term strength for Tensar SR2 as 79 kN/m.

5. The factored reinforcement strength for design is: $P = (79 \times 0.4)/2.0 = 15.8$ kN/m.

6. The smallest vertical reinforcement spacing in the authors' design was 0.3m, and the same value has been adopted for the minimum reinforcement spacing v. The spacing constant Q for the reinforced slope may be calculated: $Q = \frac{P}{K\gamma v} = \frac{15.8}{0.25 \times 22 \times 0.30} = 9.58$m. This satisfies the condition $H \leq Q$, indicating that a sufficiently small vertical spacing has been adopted.

7. The maximum depth for each zone of equal spacing and the thickness of each zone may be determined from Q. The results are shown below.

Reinforcement spacing (m)	Depth to base of Zone (m)	Thickness of Zone (m)
0.30	9.58	4.21
0.60	4.79	1.61
0.90	3.18	3.18

The layout for the reinforcement may now be calculated.

Spacing (m)	Thickness (m)	Calculated no. of layers	Whole no. of layers	Thickness remainder (m)
		Foundation layer	1	
.30	4.21	4.21/.30 = 14.03	14	.03 x .30 = .01
.60	1.61	(.01+1.61)/.60 = 2.70	2	.68 x .60 = .42
.90	3.18	(.42+3.18)/.90 = 4.00	4	0 x .90 = 0
	9.00m		21 layers	

The chart design gives a reinforcement layout of 21 layers of equal length 5.2m spaced as shown in Figure B-98. The layout is similar to the adopted design shown in Figure B-97, which comprised 20 layers of equal length 4.9m.

Alternative analysis. The critical state strength for the soil backfill has been suggested as an appropriate design value for the soil strength when using extensible polymer reinforcements [Jewell et al., 1984; McGown et al., 1984a]. It is interesting to compare a design on this basis to the one adopted in the Oregon project. A typical value for the critical state strength of a crushed basalt would be $\phi'_c = 35°$. This value is equivalent to a partial factor of 1.2 applied to the peak strength $\phi' = 40°$.

If it was assumed that the specific safety factor 2.0 for the "dead load" case examined by the authors was a single-lumped value, the partial factor to be applied to the reinforcement after applying 1.2 to the soil strength, would be 1.67. The factored reinforcement strength would be: $P = (79 \times 0.40)/1.67 = 18.9$ kN/m.

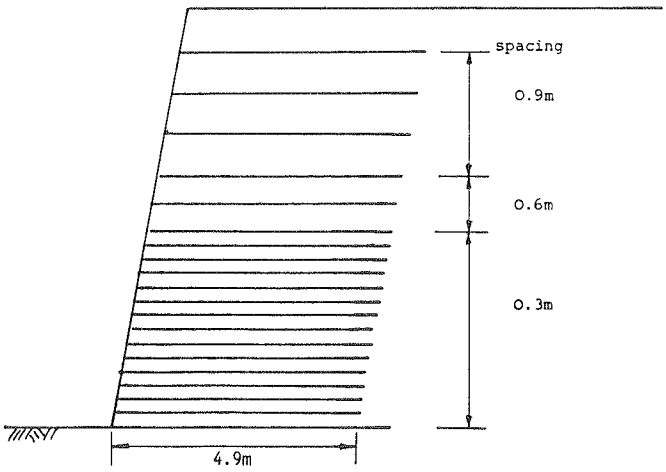

Figure B-98. Design chart reinforcement arrangement for slope at Newport, Oregon.

The chart in this case gives, from Figure B-83, $K = 0.22$, $L/H = 0.53$, and the reinforcements would have equal length 4.8m. The spacing constant, $Q = 13.0$, and the tabular calculation give 17 layers of reinforcement. The results are shown below.

		Back analysis case I	Back analysis case II	As built
Partial Factors	Soil	1.3	1.2	?
	Reinforcement	2.0	1.67	2.0
No. of Layers		21	17	20
Reinforcement Length (m)		5.2	4.8	4.9

11.3 Reinforced Slope at La Honda, California

Forsyth and Bieber [1984] report the case of a reinforced slope 9.5m high and with a slope angle 48 deg which was built to support a road damaged by a slip failure.

The key data for the case history are summarized in Table B-15. Values for the unit weight and surcharge loading are not given by the authors and have been assumed to be $\gamma = 19$ kN/m^3 and $Ws = 5$ kN/m^2.

The fill strength has cohesive and frictional components. The design solution for $c' = 0$ is described below, and results for the case allowing for soil cohesion are also given for comparison (based on charts that are not yet published).

1. Design parameters for the slope geometry are $H = 9$m, $\beta = 48°$, and $W_s = 5$ kN/m^2. The effective height $H' = 9.5 + 5/19 = 9.76$m.

2. The soil shear strength is $c' = 0$, $\phi' = 32°$, $\gamma = 19$ kN/m^3, and $r_u = 0$ (free draining fill). These values were used directly for design by the authors.

3. From the charts $K = 0.08$, $L/H = 0.65$, and $L = 0.65 \times 9.76 = 6.3$m.

4. The reinforcement was Tensar SR2, and the design

strength was selected directly with a value of 6.7 kN/m.

5. A minimum safety factor of 1.2 was required for the design, which gives a factored reinforcement strength: $P = 6.7/1.2 = 5.6$ kN/m.

6. Choosing a minimum reinforcement spacing $v = 0.3$m gives: $Q = \dfrac{5.6}{0.08 \times 19 \times 0.3} = 12.28$m.

7. A combined table summarizing the reinforcement layout calculation is shown below:

Spacing (m)	Depth to zone base (m)	Thickness of zone (m)	Number of layers	Whole no.	Thickness remainder (m)
		Foundation layer		1	
.30	12.28	3.62	3.62/.30	12	.02
.60	6.14	2.05	2.07/.60	3	.27
.90	4.09	3.83	4.10/.90	4	.50
		9.50m		20 layers	

Forsyth and Bieber adopted reinforcement of constant length 6.0m, at a standard spacing of 0.6m, giving 16 layers in the slope.

When repeated, allowing for the soil cohesion $c' = 2.5$ kPa, the chart design gives: $K = 0.05$; $L/H = 0.59$.

The tabular calculation gives a reinforcement arrangement with 15 layers, each of length 5.8m.

The results for the case history are summarized below. As with unreinforced slopes, soil cohesion has a marked effect on stability. The chart design solution closely matches the reinforcement layout that was adopted.

		Back analysis case I	Back analysis case II	As built
Soil Strength	c' (kPa)	0	2.5	2.5
	ϕ'	32°	32°	32°
No. of Layers		20	15	16
Reinforcement Length (m)		6.3	5.8	6.0

11.4 Reinforced Slope at Brampton, Ontario

Devata [1984] reports the case history of a 9.5m high embankment to support a highway. Constructed from a glacial till reinforced with Tensar SR2 grids, the embankment slope was formed to an angle of 45 deg.

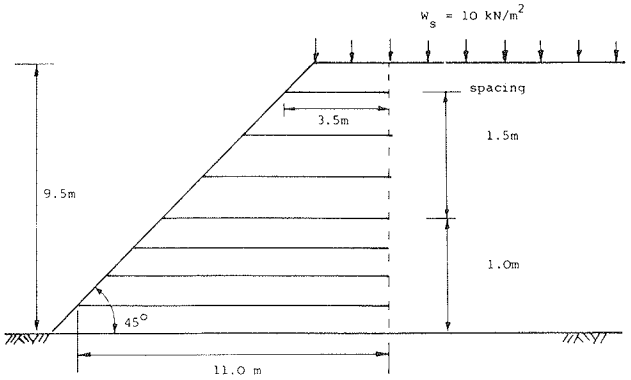

Figure B-99. Reinforcement arrangement for slope at Brampton, Ontario. [After Devata, 1984]

1. Design parameters for the slope are $H = 9.5$m, $\beta = 45°$, and $W_s = 10$ kN/m^2.

2. The soil shear strength is $c' = 0$, $\phi = 31°$, $\gamma = 22$ kN/m^3, and zero porewater pressures were assumed by the authors. A minimum factor of safety of 1.3 was specified, which gives a design soil strength $\phi' = 24.8°$.

3. From the charts in Figure B-83: $K = 0.17$; $L/H = 1.0$.

The length of the reinforcement layers is: $L = 1.0 \times (9.5 \times 10/22) = 10.0$m.

4. & 5. The factored design strength for the reinforcement was selected directly by the authors as $P = 32$ kN/m.

6. Choosing a minimum spacing 0.3m, the spacing constant $Q = 28.5$m.

7. A combined table summarizing the reinforcement layout is given below.

Spacing (m)	Depth to zone base (m)	Thickness of zone (m)	Number of layers	Whole no.	Thickness remainder (m)
		Foundation layer		1	
.30	28.52				
.60	14.26				
.90	9.51	2.83	2.83/.90	3	.13
1.20	7.13	6.67	6.80/1.2	5	.80
		9.50m		9 layers	

The reinforcement layout for the Brampton slope had 8 layers with lengths varying between 11.0m and 2.5m, as shown in Figure B-99. The chart design gives 9 reinforcement layers of equal length 10.0m, as shown in Figure B-100.

11.5 Comments on Design Examples

The simplified design charts provide a rapid "hand calculation" method of deriving preliminary reinforcement layouts for steep slopes. The final choice of a reinforcement layout is based on limit equilibrium calculations and a degree of engineering judgment.

The major shortcomings revealed by the back-analysis is the wide range of safety factors and values currently inserted into the design. There is urgent need for guidance to provide a more uniform level of safety in reinforced slope designs.

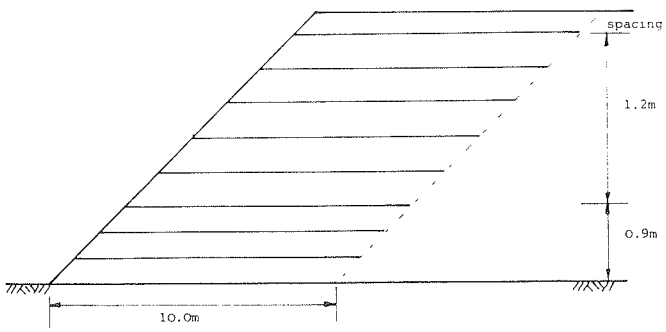

Figure B-100. Design chart reinforcement arrangement for slope at Brampton, Ontario.

12. REFERENCES

ASTM D-1693 [1980]. "Environmental Stress-Cracking of Ethylene Plastics," *ASTM Annual Book of Standards,* Part 36.

BELL, J. R., STILLEY, A. N. and VANDRE, B. [1975]. "Fabric Retained Earth Walls," *Proc. 13th Annual Eng. Geo. and Soils Engineering Symposium,* Moscow, Idaho.

BELL, J. R., SZYMONICK, T. and THOMMEN, G. R. [1984]. "Construction of a Steep State Geogrid Retaining Wall for an Oregon Coastal Highway," *Proc. International Symposium on Polymer Grid Reinforcement in Civil Engineering,* London.

BINNIE and PARTNERS [1981]. "A Computer Design Method for Reinforced Soil Structures Using Limit Equilibrium Analysis," Reinforced Soil Group, *TN/8292/A.* London.

BISHOP, A. W., and MORGENSTERN, N. [1960]. "Stability Coefficients for Earth Slopes," *Geotechnique,* 10, 129–150.

BONAPARTE, R., and MARGASON, E. [1984]. "Repair of Landslides in the San Francisco Bay Area, *Proc. International Symposium on Polymer Grid Reinforcement in Civil Engineering,* London.

BS 2782 [1976]. Part 3: Methods 320A to 320F, "Determination of Tensile Strength, Elongation and Elastic Modulus."

BUSBRIDGE, J. R. [1984]. "Stabilisation of Canadian Pacific Railway Slip at Waterdown Ontario Using Tensar Grids," *Proc. International Symposium on Polymer Grid Reinforcement in Civil Engineering,* London.

CHEN, W. F. [1975]. *Limit Analysis and Soil Plasticity,* Elsevier, New York, pp. 341–398.

DEVATA, M. S. [1984]. "Geogrid Reinforced Earth Embankments with Steep Side Slopes," *Proc. International Symposium on Polymer Grid Reinforcement in Civil Engineering,* London.

DOLEZAL, B. [1967]. "Micro-organisms and Plastics," British Plastics, p. 105.

ELWELL, P. A., and MCGLOIN, D. J. [1981]. "How to Defeat That Sinking Feeling—An Embankment Construction in Tidal Waters," *Chartered Municipal Engineer,* Vol. 108, March.

FORSYTH, R. A., and BIEBER, D. A. [1984]. "La Honda Slope Repair with Geogrid Reinforcement," *Proc. International Symposium on Polymer Grid Reinforcement in Civil Engineering,* London.

HEGER, F. J., CHAMBERS, R. and DIETZ, A. G. H. [1978]. *Structural Plastics Design Manual,* Phases 2 and 3, Chapters 5 to 10, Prepared under contract to ASCE. U.S. Government Printing Office, Washington.

JEWELL, R. A. [1980]. "Some Effects of Reinforcement on the Mechanical Behavior of Soils," Ph.D. Thesis, University of Cambridge.

JEWELL, R. A., MILLIGAN, G. W. E., SARSBY, R. W. and DUBOIS D. [1984a]. "Interaction Between Soil and Geogrids," *Proc. Symposium on Polymer Grid Reinforcement in Civil Engineering,* London.

JEWELL, R. A., PAINE, N., and WOODS, R. I. [1984b]. "Design Methods for Steep Reinforced Embankments," *Proc. Symposium on Polymer Grid Reinforcement in Civil Engineering,* London.

JONES, C. J. F. P. [1984]. "Constructional Details of Retaining Walls with Tensar Geogrids," *Proc. International Symposium on Polymer Grid Reinforcement in Civil Engineering,* London.

MCGOWN, A., PAINE, N. and DUBOIS, D. [1984a]. "The Use of Geogrid Properties in Design," *Proc. Symposium on Polymer Grid Reinforcement in Civil Engineering,* London.

MCGOWN, A., ANDRAWES, K. Z., YEO, K. C. and DUBOIS, D. [1984b]. "The Load-Strain-Time Behaviour of Tensar Geogrids," *Proc. Symposium on Polymer Grid Reinforcement in Civil Engineering,* London.

MERCER, F. B. [1979]. "Plastics Material Mesh Structure," U.K. Patent Application GB 2 304 191 A.

MOATES, R. C. [1975, 1976]. *RAPRA Members Journal,* July/August (1975), p. 53, Mar./Apr., 1976, p. 19.

NETLON LIMITED [1983]. "Stabilisation of a Slip Failure in a Cutting on the M1," *Case Study.*

NETLON LIMITED [1984a]. "Test Methods and Physical Properties of Tensar Geogrids," *Technical Guidelines.*

NETLON LIMITED [1984b]. "Guidelines for the Design and Construction of Embankments over Stable Foundations Using Tensar Geogrids," *Technical Guidelines.*

New Civil Engineering [1984].

PAUL, J. [1984]. "Economics and Construction of Blast Embankments Using Tensar Geogrids," *Proc. International Symposium on Polymer Grid Reinforcement in Civil Engineering,* London.

PIGG, J. R., and MCCAFFERTY, W. R. [1984]. "The Design and Construction of a Reinforced Retaining Wall at Low Southwick," *Proc. International Sumposium on Polymer Grid Reinforcement in Civil Engineering,* London.

RITCHIE [1968]. *Vinyl and Allied Polymers,* Volume 1, Iliffe Books.

SZYMONICK, T., BELL, J. R., THOMMEN, G. R. and JOHNSEN, E. L. [1984]. "A Geogrid Soil Wall for Landslide Correction on the Oregon Coast," 63rd *Annual Meeting,* Transportation Research Board, Washington, D.C.

WARD, I. M. [1984]. "The Orientation of Polymers to Produce High Performance Materials," *Proc. Symposium on Polymer Grid Reinforcement in Civil Engineering,* London.

WHITCOMB, W. and BELL, J. R. [1979]. "Analysis Techniques for Low Reinforced Soil Retaining Walls and Compression of Strip Sheet Reinforcements," *Proc. 17th Engng. Geol. and Soils Engng. Symposium,* Moscow, Idaho.

WILDING, M. A., and WARD, I. M. [1978]. "Tensile Creep and Recovery in Ultrahigh Modulus Linear Polyethylene," *J. Polymer,* 19, pp. 969–976.

WILDING, M. A., and WARD, I. M. [1981]. "Routes to Improved Creep Behaviour in Drawn Linear Polyethylene," *Plastics and Rubber Processing and Applications I.*

CHAPTER FOUR—BAR MATS

Contents

1. INTRODUCTION

Systems that employ bar mats for soil reinforcement currently include VSL Retained Earth, Mechanically Stabilized Embankment, Georgia Stabilized Embankment, and Reinforced Soil Embankments. VSL Retained Earth, Mechanically Stabilized Embankment (MSE), and Georgia Stabilized Earth (GAS), collectively referred to as bar-mat walls, are described in this chapter. Reinforced Soil Embankment is provided by the same vendor as Welded Wire Wall and is designed in accordance with the same procedures. Thus, it is discussed in Chapter One, "Welded Wire Wall," of this appendix.

1.1 Physical Description

There are three major components to a bar-mat reinforced soil wall: precast concrete facing elements, reinforcements, and compacted backfill (Fig. B-101). The facing elements of VSL walls are hexagonal in shape, as shown in Figure B-102, while other bar-mat systems employ different facing shapes.

The reinforcement mats consist of either W11 or W20 steel bars placed in a rectangular grid with prescribed longitudinal and transverse spacing (Fig. B-103). Each mesh may have 4, 5, or 6 longitudinal bars, depending on specific design requirements. The overall length of the mats depends on the geometry of the site, external loading, and the physical properties of both the backfill material and the earth to be retained.

A well-compacted granular material is normally specified as backfill. Proper drainage behind the wall may be required in order to assure adequate soil-to-reinforcement interaction and to limit creep. The bar-mat reinforcements used by the California and Georgia Departments of Transportation, Mechanically Stabilized Embankments (MSE) and Georgia Stabilized Embankments (GAS), respectively, and VSL Corporation are reasonably similar to one another, but facing panel details differ. The facing panels used by VSL have already been described. The facing panels used by Caltrans are essentially rectangular precast concrete elements as shown in Figure B-104, and those used by the Georgia Department of Transportation are shown in Figure B-105.

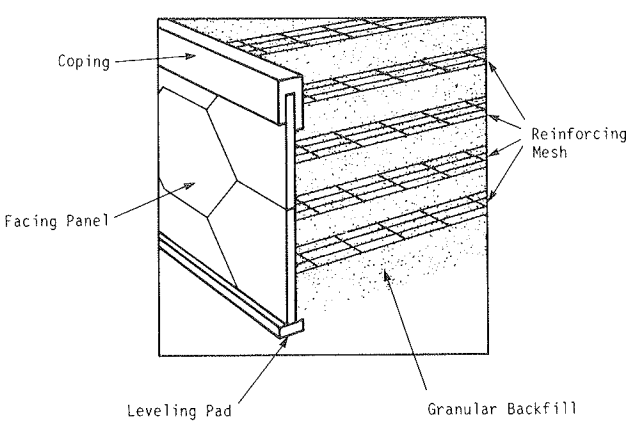

Figure B-101. Schematic illustration of VSL Retained Earth wall.

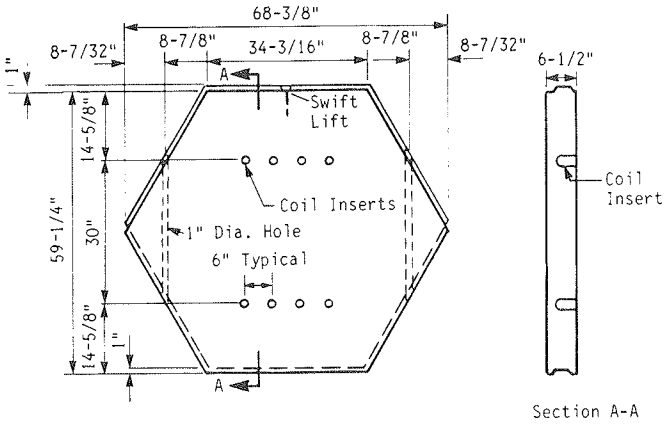

Figure B-102. Typical hexagonal VSL facing panel. [VSL Corp., 1983]

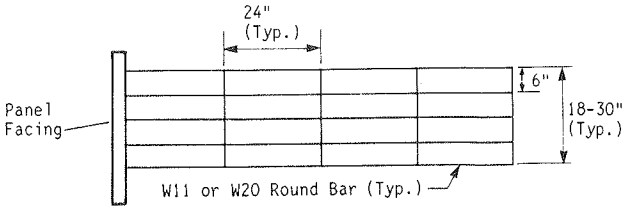

Figure B-103. Plan view, VSL bar mesh.

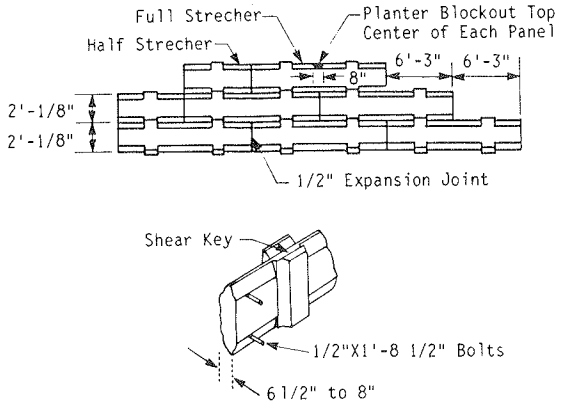

Figure B-104. Mechanically Stabilized Embankment facing panel. [Chang et al., 1981]

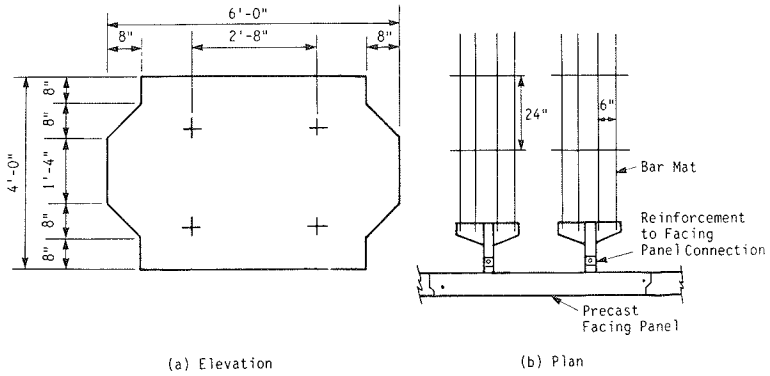

Figure B-105. Georgia Stabilized Embankment facing panel.

Because the reinforcement mats used in the three systems are similar, design approaches and methodology are similar in concept; they do, however, differ somewhat in detail with regards to assumptions about potential failure surface and earth pressure coefficient.

1.2 History and Development

The California Department of Transportation built the first Reinforced Earth wall in the United States in 1972 to repair a landslide on Route 39 in the San Gabriel Mountains just north of Los Angeles [Chang et al., 1974]. After completion of this project, a large direct shear device was built in 1973 to study the pullout resistance of other types of reinforcing systems [Chang, et al., 1977]. A series of tests were run on No. 3 rebar mats, longitudinal No. 3 reinforcing bars, individual flat steel strips, and a solid plate. The test results showed that for the same surface area of steel reinforcement, the bar-mat reinforcement exhibited approximately 5 to 6 times the pullout resistance of the other tested reinforcement configurations (Fig. B-106).

The successful results of these tests led to the construction in 1975 of the first bar-mat reinforced soil walls, near Dunsmuir, California. The two walls, required for the realignment and widening of Interstate Highway 5, had maximum heights of 18 and 20 ft (Fig. B-107). Since then, several additional walls have been constructed by Caltrans.

The first VSL Retained Earth wall was constructed in 1981, in Hayward, California. The wall was required when the City of Hayward made plans for a street widening and grade separation. The height of the wall varies from 4 to 20 ft, and it extends 300 ft in length. Because this was the first VSL Retained Earth installation, extensive evaluation by city, state, and consulting engineers was required. All parties concurred that the VSL Retained Earth design fulfilled the project requirements, and the system was approved. The project was completed in August 1981, and it has performed satisfactorily since that time. Since the completion of the Hayward wall, 36 VSL Retained Earth projects, containing over 100 walls, have been completed or are under construction through mid-1984, totaling some 700,000 sq ft of wall face.

1.3 Proprietary Restrictions

Mechanically Stabilized Embankment is licensed under a Reinforced Earth Company patent in accordance with an agreement dated May 1976. VSL Retained Earth and the Georgia Stabilized Embankment are also licensed under a Reinforced Earth Company patent. VSL Corporation does, however, have a patent pending on the button-head-connection used to fasten the reinforcing mesh to the precast facing panel. This connection is described in Section 4.1 of this chapter.

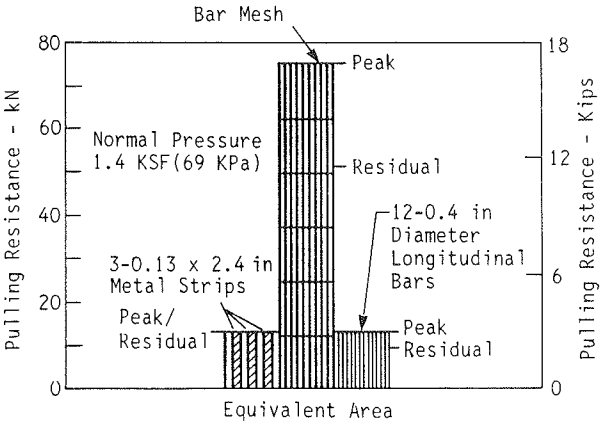

Figure B-106. Pullout test results—bar mat vs strip. [Forsyth, 1978]

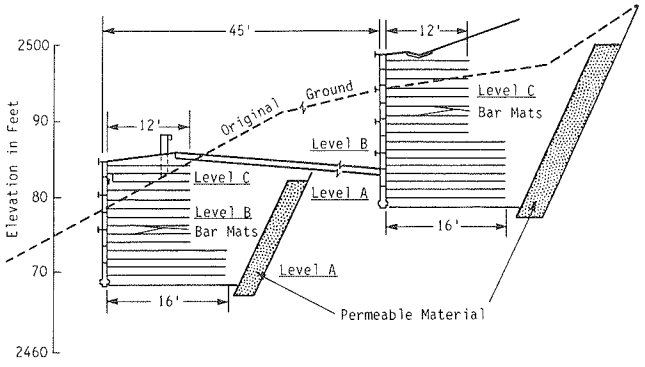

Figure B-107. Cross-section Dunsmuir walls. [Chang et al., 1981]

2. APPLICATIONS

2.1 Inherent Advantages

The technical advantages of bar-mat reinforced soil are the same as the advantages of other earth wall systems as described in Chapter Three of the main report.

2.2 Site Conditions Appropriate for Use

Bar-mat walls, like any other retaining wall, must satisfy external stability requirements. The site must be shown to exhibit both deep and shallow slope stability. There must be adequate resistance to sliding of the base of the wall over the existing ground. The wall must also be safe with respect to bearing capacity failure and overturning. Any site where these requirements can be met is considered appropriate.

2.3 Routine Applications

Bar-mat walls are routinely used for highway embankments. Other applications include stabilization of landslides, bridge abutments, retaining walls, and embankments or retaining walls over compressible foundation soils. In effect, any situation requiring a vertical or near vertical elevation change of more than a few feet could constitute a potential application.

2.4 Special Applications

Bar-mat walls have been constructed since 1975. Most of the walls constructed to date can be considered routine applications. However, the California Department of Transportation has made substantial progress with the use of poor quality backfill (as described in Section 8.4 of this chapter) for structures near Baxter, California. As bar-mat walls become more widely used, designers will no doubt realize many new applications.

3. MECHANISMS AND BEHAVIOR

3.1 Principle of Soil and Reinforcement Interactions—Experimental Basis

The soil-to-reinforcement interaction in bar-mat systems can be broken down into two components: frictional resistance, which is developed through contact between the longitudinal bar reinforcements and the soil particles, and passive resistance, which is developed by the soil bearing directly on the transverse members of the reinforcing mesh.

In 1973, the California Department of Transportation built a large direct shear device to measure the pullout capacity of different types of soil reinforcement. The test facility consisted of a rigid steel box 20 in. high, 36 in. wide, and 54 in. long. Soil was placed and compacted in the box with the reinforcement located at mid-height. Normal pressure was applied to the specimen through a series of hydraulic rams at the top of the backfill. During pullout tests, the deformations of the reinforcement were measured by two extensometers, one located at the front and one at the back of the specimen. The normal loads and pull loads were measured by load cells [Chang, et al., 1977; Forsyth, 1978].

Tests were run on several different reinforcement configurations as shown in Figure B-108. The reinforcement configurations included a No. 3 rebar mat with longitudinal bars 4 in. on center, and transverse bars 8 in. on center; longitudinal No. 3 rebars; individual flat steel straps; and a solid plate.

The results of these tests are shown in Figure B-106, in which pullout resistance is shown as a function of reinforcement area exposed to the soil. These tests showed the bar-mats to be highly efficient. It was also observed that the bar-mat reinforcement did not fail by slipping as did strips and longitudinal bars in comparison tests. Instead, the bar mat and soil failed together in a bearing-capacity-type failure.

The VSL Corporation, in an attempt to develop a more complete understanding of the soil-to-reinforcement interaction, has since performed over 80 laboratory pullout tests using a box 54 in. long, 36 in. wide, and 24 in. deep. In the test procedures used by the VSL Corporation, increasing horizontal loads are applied, while the same vertical load is maintained. After each increment in horizontal load, deflection is monitored until movement has stopped, at which time the horizontal pullout load and dial indicator readings are taken. The test is continued until horizontal displacement exceeds 3/4 in. [Bloomfield, 1984].

An empirical correlation to predict pullout resistance has been developed by the VSL Corporation based on the results of the large-scale pullout tests. To develop this correlation, an empir-

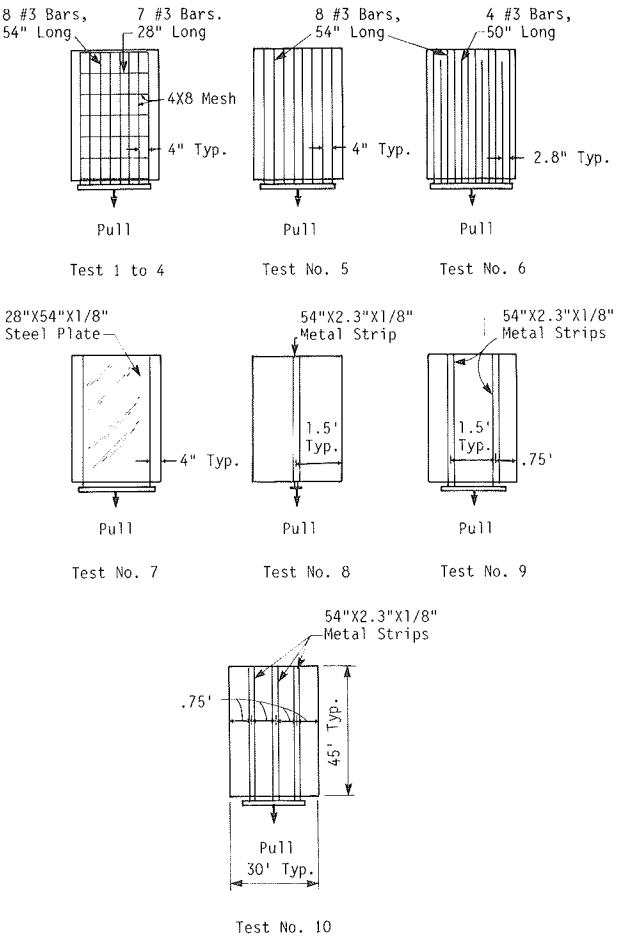

Figure B-108. Reinforcement configuration for large direct shear test. Forsyth, 1978]

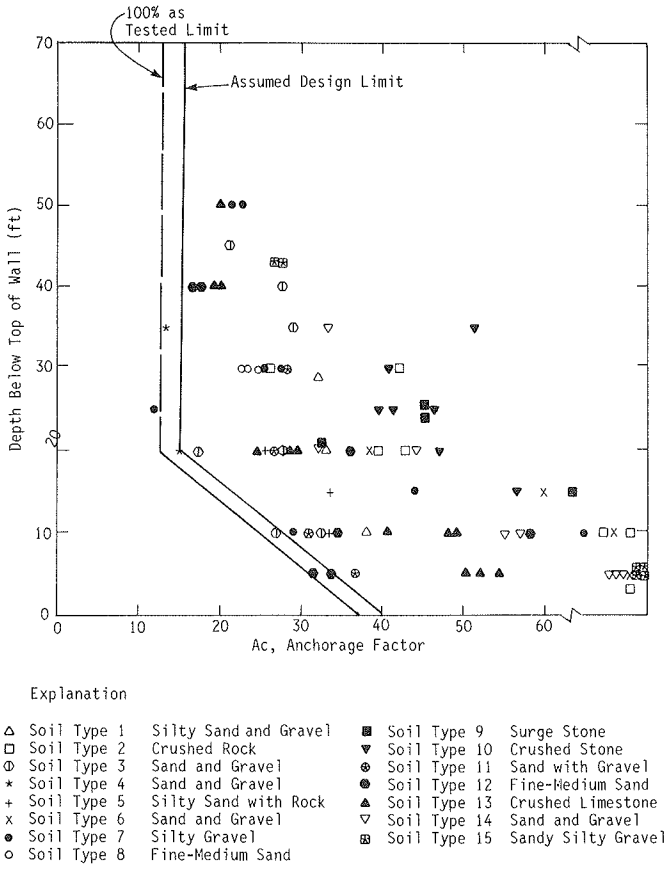

Figure B-109. Pullout test results—VSL bar mat. [Bloomfield, 1984]

ical factor, referred to as anchorage factor, A_c, was defined. The pullout capacity is expressed as a function of bar diameter, width of mesh, number of transverse bars, and unit weight of the soil according to:

$$\text{Pullout resistance} = A_c\, \gamma\, d\, b\, n\, z \qquad \text{(B-63)}$$

where A_c = anchorage factor; γ = unit weight of the soil: d = bar diameter; b = width of mesh in the transverse direction; n = number of transverse bars behind the potential failure surface; and z = depth of mesh from top of fill.

The line labeled "Assumed Design Limit" in Figure B-109 has been approved by the Federal Highway Administration as a boundary limit for A_c for design purposes.

3.2 Behavior of the Reinforced Soil Structure

In order for a bar-mat wall to act as a monolithic mass, the reinforced soil mass must have coherence, as discussed in the main report. The reinforced soil mass can be broken down into two regions, an active zone and a resistance zone, as schematically shown in Figure B-110. The demarcation between these two zones is the potential failure surface within the reinforced soil mass. Because the active zone is tending to move away from the resisting zone, and because bar-mat pullout resistance is developed in the resisting zone, it can be expected that the location of maximum tensile stress in a given bar mat will exist where this bar mat crosses from the active to the resisting zone.

Bar-mat walls have been found, through instrumentation of VSL walls in Hayward, California [Al-Yassin, 1983], and in Hot Springs, South Dakota [VSL Corporation Files], as well as a Mechanically Stabilized Embankment wall in Dunsmuir [Forsyth, 1978], to have a curved locus of maximum tensile stresses. The loci of maximum tensile stresses for the aforementioned walls and four Reinforced Earth walls are shown in Figure B-111. Because this locus corresponds to the assumed potential failure surface, the data in Figure B-111 imply that the failure surface is curved rather than linear. The potential failure surface can be reasonably approximated by the bilinear surface already shown in Figure B-110. For the lower half of the wall, the surface follows the Rankine failure surface, and for the upper half of the wall it is approximated by a vertical line located at a distance of $0.3H$ from the face of the wall [Bloomfield, 1984]. VSL Retained Earth walls are designed based on this assump-

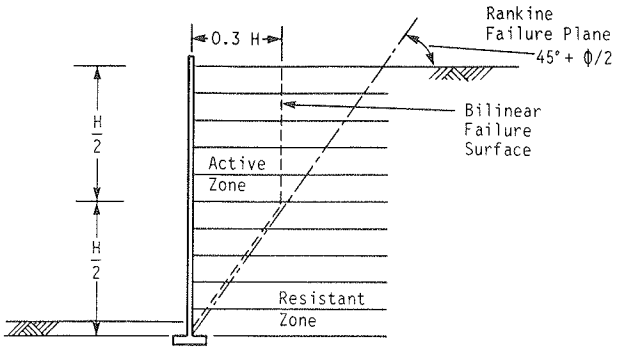

Figure B-110. Bilinear failure surface.

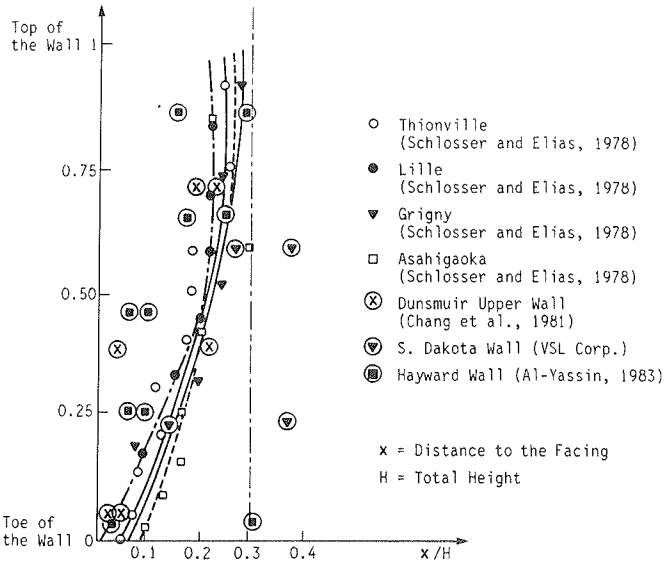

Figure B-111. Locus of maximum tensile forces in experimental Reinforced Earth, Caltrans, and VSL Retained Earth walls. [Bloomfield, 1984]

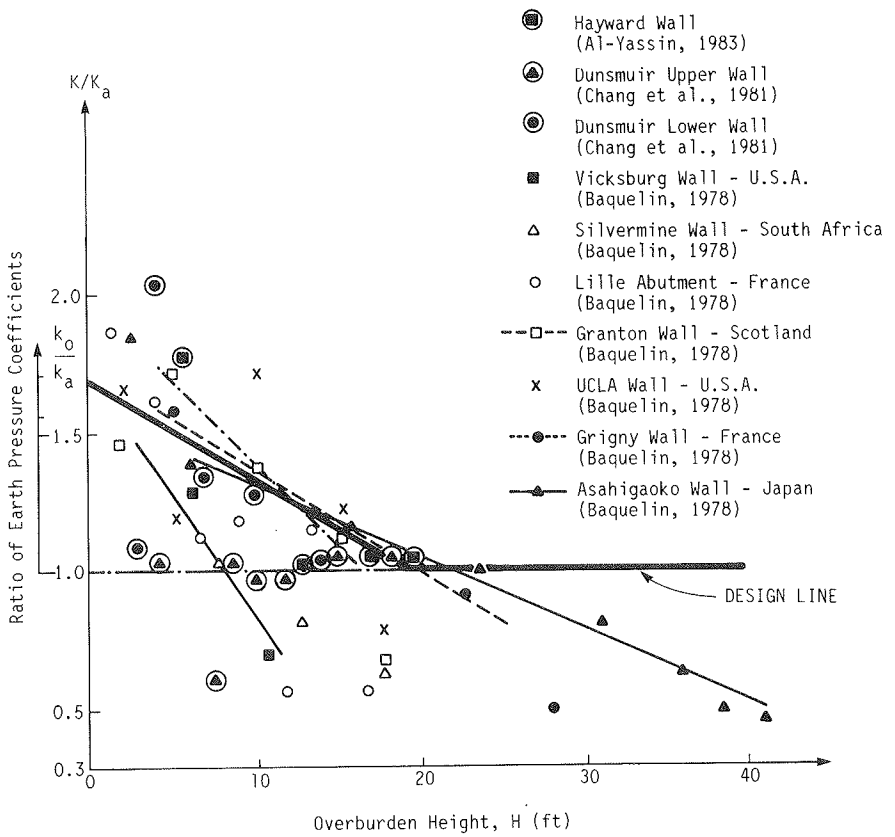

Figure B-112. Variation of earth pressure coefficient with depth for several instrumented walls. [Bloomfield, 1984]

tion, while MSE and GAS walls are designed assuming a linear Rankine failure surface.

The internal stability of a reinforced soil wall, i.e., its ability to act as a coherent unit, is dependent on the reinforcements being able to withstand the horizontal stresses applied to them without pulling out of the soil or rupturing. The horizontal stress to be transferred to the reinforcement is dependent on the vertical effective stress and the coefficient of lateral earth pressure within the reinforced soil mass. Data from a VSL wall at Hayward, California, and two MSE walls at Dunsmuir have been analyzed to determine the variation of the earth pressure coefficient, K, with depth. This variation is shown in Figure B-112 together with lateral earth pressure coefficients measured on Reinforced Earth walls. The majority of data for the bar-mat walls plot along the coefficient of active earth pressure, K_a, line. However, there is considerable scatter; the VSL Corporation, therefore, uses the same assumptions regarding lateral stresses as used by the Reinforced Earth Company. A value of the coefficient of earth pressure at rest, K_o, is used at the top of the wall with a linear decrease to K_a at a depth of 20 ft. This results in higher horizontal design loads than if an active earth pressure coefficient were used for the full height of the wall. MSE and GAS systems are designed assuming an active earth pressure coefficient for the full height of the wall.

4. TECHNOLOGY

4.1 Description of Fabricated Components

4.1.1 Precast Facing Panels

The most frequently used facing panel for VSL Retained Earth is shown in Figure B-102. The panel is hexagonal in shape, measuring 68⅜ in. wide, 60¼ in. high, and 6½ in. thick. Panels of other thicknesses can also be obtained. Two 1-in. diameter holes are precast into the facing panels and 5/8-in. diameter bars are inserted into these holes to provide alignment between facing elements. Two rows of coil inserts, spaced 30 in. apart, are used to connect the bar-mats to the facing elements.

The panels are reinforced with No. 4 rebar (see Fig. B-113) and are designed to withstand the maximum tensile force allowable in the bar mesh. A swift lift is also inserted into the precast panels to facilitate handling and erection as shown in Figure B-102.

There are several other standard types of facing panels used in VSL Retained Earth systems, including: end elements, cap panels, and first lift half panels as shown in Figure B-114.

The Mechanically Stabilized Embankment system uses essentially rectangular facing elements as shown in Figure B-104. These panels are 12½ ft long, 2 ft high, and 8 in. thick (6½ in. thick after 1984). The length of these panels allows four bar mats to be connected to each panel.

The Georgia Stabilized Embankment uses a precast face panel

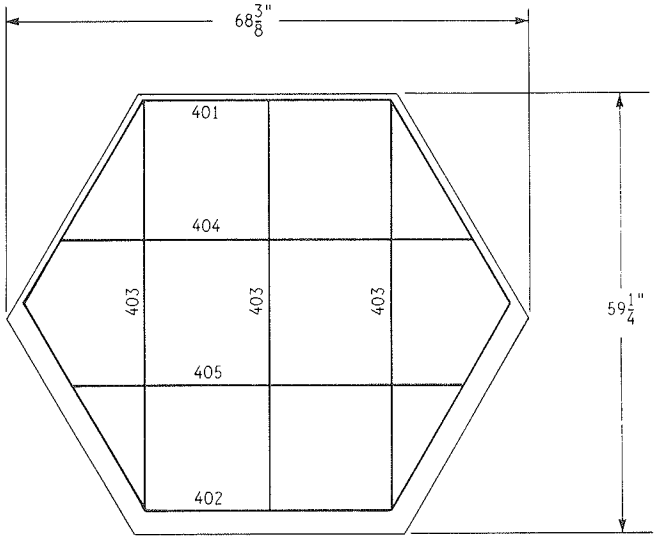

All Bars #4 Grade 40

BAR NO.	LENGTH	SHAPE
401	8'1"	
402	7'10½"	
403	4'7½"	
404	4'7"	
405	4'4"	

Figure B-113. Reinforcing steel for a typical VSL panel. [VSL Corp., 1983]

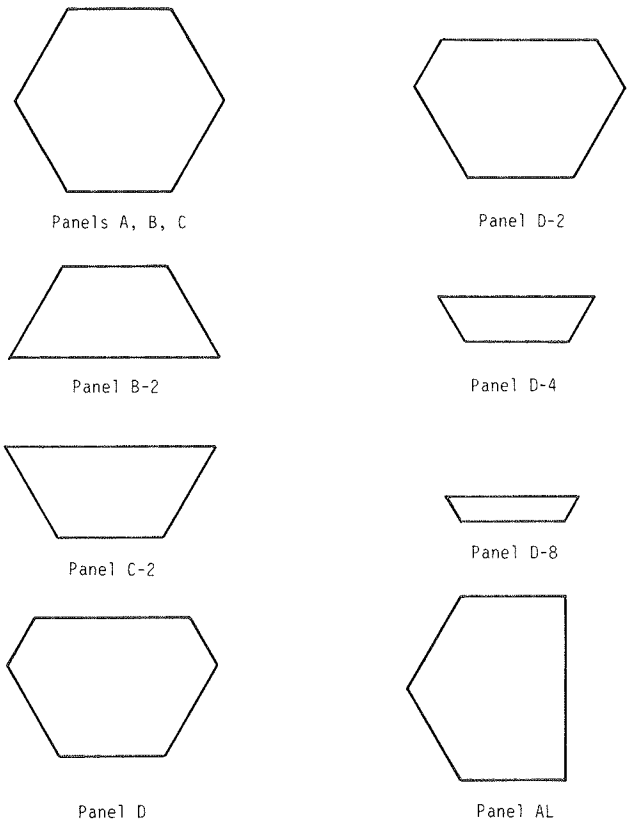

Panel A: Standard Hexagonal Panel - used for major portion of wall.

Panel B: Hexagonal Panel, Flat Bottom - used for Baseline Panel.

Panel C: Hexagonal Panel, Coping Tie in at Top of Panel - used for top of wall.

Panels D-2, B-2, D-4, C-2, D, AL: Odd Shape Panels - used for accomadating non-level bottom, top of wall, or for edge of wall.

Figure B-114. Standard VSL facing panels.

4 ft high and 6 ft long (Fig. B-105). Two levels of reinforcement are attached to each panel. The horizontal center-to-center spacing of the reinforcement meshes is 2 ft 8 in. Four reinforcing mats are attached to each facing unit.

4.1.2 Soil Reinforcing Mats

Reinforcing mat is shop fabricated from W11 and W20 steel bars. The longitudinal bars are spaced 6 in. on center, and the transverse bars are spaced 2 ft on center, with 12- and 18-in. spacings sometimes used. Each mesh element may have 4, 5, or 6 longitudinal bars (Fig. B-103). The intersections between longitudinal and transverse members are welded prior to galvanization.

The attachment ends of the VSL mats have cold-formed button heads on each longitudinal bar (Fig. B-115). Prior to factory button heading, an attachment bolt is placed on each longitudinal bar. The attachment bolts are used to make the field connection to the coil loop inserts, precast into the back of the facing panels, as schematically shown in Figure B-115.

4.2 Fabrication Quality Control

4.2.1 Concrete Facing Panels

The specification developed by Caltrans (1984 Interim Caltrans Specifications) and also used by the VSL Corporation requires that the concrete has a minimum compressive strength of 4,000 lb/sq in. at 28 days, and that the cement conforms to AASHTO M-85. The compressive strength of the concrete facing panels is determined on a lot basis, with a lot consisting of all batches of concrete or panels produced in 7 working days. The number of samples required to be tested is tabulated in Table B-16.

Standard 6- by 12-in. test specimens are prepared in accordance with ASTM C-31. A minimum of four cylinders is cast for each sample. Two of the cylinders are cured in the same manner as the panels and tested at 7 days. The other two cylinders are cured in accordance with ASTM C-31 and tested at 28 days. Compressive strength testing is conducted in accordance with ASTM C-39.

The compressive strength of a lot of facing panels is considered acceptable if the 28-day strength of test results (a test result is the average compressive strength of two cylinders) of all samples for any lot is larger than 4,000 lb/sq in. The lot is also accepted if no individual 28-day compressive strength test result falls below 3,600 lb/sq in. and the average 28-day compressive strength of all test results for the lot is greater than or equal to the limits tabulated in Table B-17 [Juran, 1982].

All precast facing panels are manufactured to the following tolerances: dimensions within 3/16 in., angular distortion with regard to the height of the panel less than 0.125 in. in 5 ft, and

Table B-16. Number of panels tested by VSL; requirement as a function of fabrication rate.

Daily Production	Number of Samples
Less than 50 panels	1
50-100 panels	2
100-150 panels	3
Greater than 150 panels	5

Table B-17. Facing panel strength acceptance criteria.

Number of Tests	Average of All Lot Acceptance Tests Greater than the following (psi)
3-7	4000 + 0.33 R*
8-15	4000 + 0.44 R*
Greater than 16	4000 + 0.46 R*

surface defects on formed surface measured on a length of 3 ft not more than 0.125 in.

4.2.2 Soil Reinforcing Mat

The specifications developed by Caltrans (1984 Interim Caltrans Specifications) and also used by the VSL Corporation for bar-mat reinforcements require that the cold drawn wire meet the quality control specifications of ASTM A-82. It is also required that the welding of connections at intersection points be performed in accordance with ASTM A-185 specifications. When the bar mats have been welded, they are galvanized in accordance with ASTM A-123, which requires a minimum zinc coating of 2.0 oz/sq ft of steel.

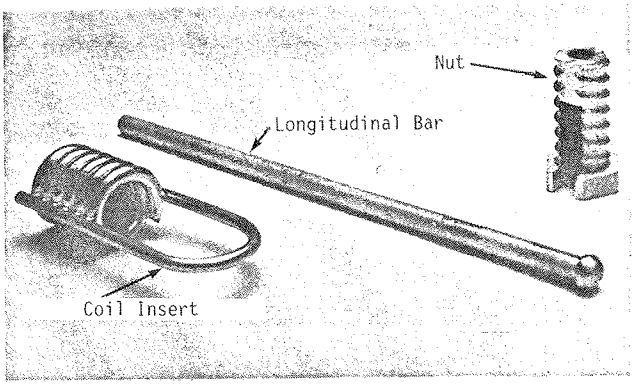

(a) Components of Button Head Connection

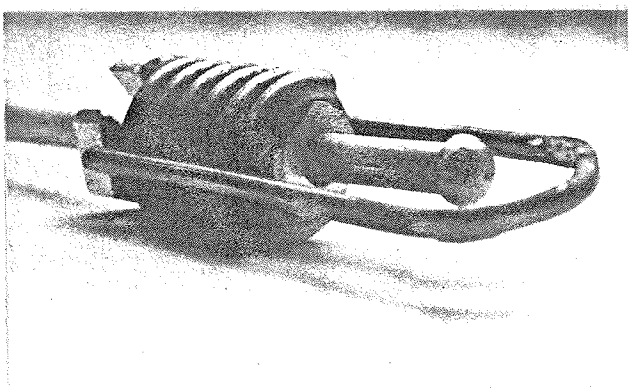

(b) Assembled Button Head Connection

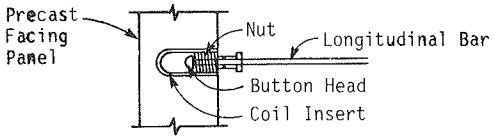

(c) Schematic

Figure B-115. Button head connection.

5. DURABILITY AND SELECTION OF BACKFILL

5.1 Members Susceptible to Degradation

Like all steel buried for extended periods, the bar-mat reinforcements are susceptible to degradation; both the steel and the zinc used for galvanizing are subject to electrochemical corrosion. A detailed description of corrosion of metal reinforcements is provided in Chapter Six of the main report.

5.2 Predicting Corrosion Rate

The method used for providing a design allowance against corrosion by Caltrans is described in Chapter Six of the main report. The method for predicting corrosion loss developed by the Reinforced Earth Company is commonly used for durability design of VSL Retained Earth. Details of the method are presented in Chapter Six of the main report.

In the United States, it is customary to design the reinforcement cross section so that, with allowance for corrosion, sufficient section will remain at the end of the design life so that the yield stress of the metal will not be exceeded.

5.3 Selection of Backfill

All VSL Retained Earth walls and most MSE and GAS embankments constructed to date have used granular soil as the backfill material. Granular soil is preferred because these soils are free draining, have a high friction coefficient, are easy to handle and place, transfer stress to the reinforcement with limited strain, and exhibit little or no creep. However, one Mechanically Stabilized Embankment has been constructed by Caltrans with a low quality, sandy silt backfill [Hannon and Forsyth, 1984] and has performed quite satisfactorily since its completion. The VSL Corporation requires the backfill material used for their standard walls to satisfy the specifications given in Table B-18.

Table B-18. VSL Retained Earth backfill specifications.

Gradation Requirements		Corrosion Considerations	
Sieve Size	Percent Passing	Chlorides	Less than 200 ppm
6"	100	Sulfates	Less than 1000 ppm
3"	75-100	Resistivity	Greater than 3000 ohm-cm
#200	0-25	pH	5-10

If the percent passing the No. 200 sieve is between 15 to 25 percent, it is also required that the plasticity index not exceed 6 percent, that a minimum compaction of 95 percent ASTM D-698 can be achieved, and that the friction angle of the compacted soil not be less than 34 deg at this degree of compaction. Similar, but somewhat less stringent, specifications are also listed in the 1984 Interim Caltrans Specifications for Mechanically Stabilized Embankments and Abutments.

6. CONSTRUCTION

6.1 Construction Equipment

A bar-mat reinforced soil can be constructed with a minimal amount of construction equipment. A small crane is required for the handling and erection of the precast facing panels. Front-end loaders are normally used for loading dump trucks and for spreading the backfill at the site. Scrapers are sometimes used when the volume of backfill to be placed is sufficient. Vibratory rollers are required for compaction of most of the fill, while small hand-operated compactors are used for compaction near the face.

The walls are simple to erect, using only standard tools; e.g., nylon slings for unloading precast panels and reinforcement, shovels, wrecking bars, levels, crescent wrenches, claw hammers, sledge hammers, 2- by 4-in. stock lumber and wooden wedges.

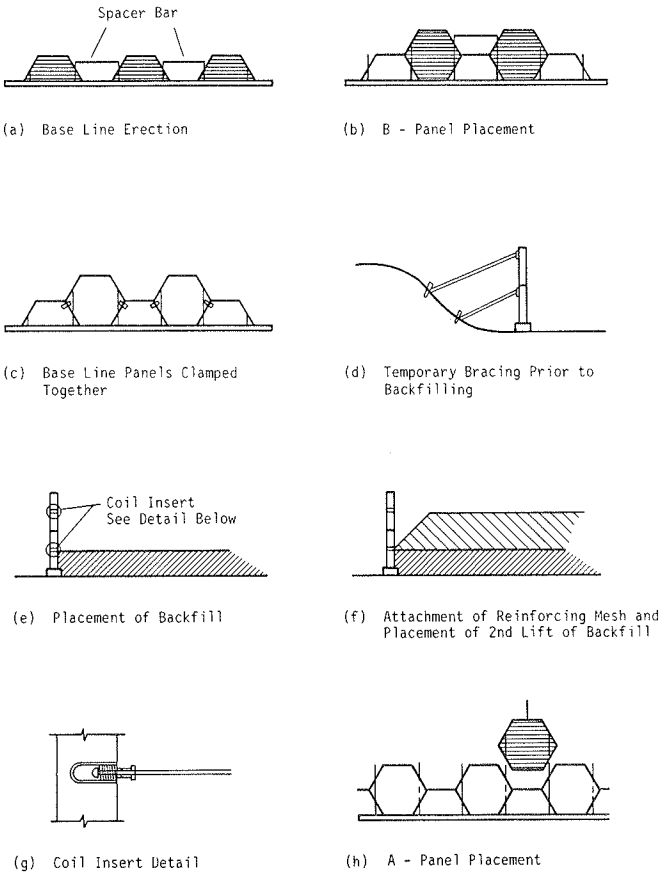

Figure B-116. Erection procedure.

6.2 Work Organization

Typically, a 4 to 5 man crew is used for the construction. Tasks to be performed include operation of the crane for setting precast panels, erection of precast members and installation of bar mats, operation of loader(s) and vibratory roller(s) for controlled placement of backfill, and spreading and compaction of backfill at the wall face.

A crew of this size can produce, on an average daily basis, 800 to 1,000 sq ft of wall face, with maximum output of 1,500 sq ft per day possible.

6.3 Site Preparation

The area where the retained earth soil mass is to be placed is graded level to a width equal to or greater than the length of the reinforcing mesh plus 6 in. Unsuitable material, for example, material of insufficient bearing capacity, at the base of the wall is removed and replaced with compacted backfill.

6.4 Erection Procedure

The erection procedure described below refers specifically to VSL Retained Earth [VSL Erection Manual, 1983]. With only minor variations in detail, similar procedures are used for MSE and GAS.

A concrete leveling pad is constructed along the lines and grades specified for the base of the facing in contract drawings. This concrete is allowed to cure at least 24 hours prior to setting the precast facing panels. The leveling pad, which is not a structural member, is provided only to facilitate the erection of the concrete panels.

Erection can begin subsequent to the establishment of a wall facing line. For VSL Retained Earth, half panels (Fig. B-116) are placed on top of the leveling pad, making sure the outside face of the panels are flush with the wall line. Each panel is battered to the inside approximately ¼ in. to compensate for the outward movement which is required to mobilize reinforcement. The next step is the placement of full-height panels (Fig. B-116b), which are properly centered. These are battered to the same angle as the course of half-panels. The first course of full- and half-panels is clamped and temporarily braced to maintain alignment and batter during the backfill operation (Figs. B-116c and B-116d). No bracing is required on subsequent courses because the reinforcing bar mesh will support the wall face.

After the base line has been erected and braced, filter cloth is typically placed over all joints on the fill side of the facing panels to prevent fines from migrating from behind the wall.

The first layer of backfill is placed and compacted to the level of the first row of coil inserts (Fig. B-116e). The coil insert is filled with "No-Oxide"-type grease to prevent electrochemical corrosion at the connection between facing panel and reinforcement. The reinforcing mats are laid on top of the fill and connected to the wall face by screwing the coil bolts, on the end of the mesh, into the coil inserts (Fig. B-115 and Fig. B-116g). The backfilling operation is then continued up to the next lift of coil inserts. Backfill is generally not placed immediately behind the wall (Fig. B-116f) until the next row of reinforcement is attached to the wall face.

Cork of ¾ in. thickness is typically used as a filler between all horizontal panel joints. The filler is used to provide a uniform

bearing surface between adjacent panels. Wooden wedges may be used between horizontal facing joints to achieve the correct batter.

The backfill is placed up to the next level of bar mesh, the bar mesh is installed as above, and this sequence is repeated for the remainder of the wall. The wooden wedges are then removed to complete the wall.

7. DESIGN METHOD

7.1 Internal vs. External Stability

The design of VSL Retained Earth walls, like that of any other type of earth wall system, must take both internal and external stability into account. The internal stability of the wall deals with the ability of the reinforced soil mass to act as a coherent unit, while external stability pertains to failures outside the reinforced zone. Classical methods of soil mechanics analyses may be used for the analysis of these potential external failure modes.

7.2 Site Conditions

Site conditions may govern certain aspects of the design. The foundation soil must have adequate strength, or it will not be capable of supporting the reinforced soil mass, thus causing external instability. If the groundwater table is above the bottom of the wall, the design must be altered to take into account the additional hydrostatic pressure on the wall face. The effective unit weight of the soil should be used for stability calculations for that portion of the wall below the water table.

Existing topography can also affect the design of the wall. For example, a rock outcropping can limit the length of reinforcement. This might necessitate increasing the width of the bar mats from 4 longitudinal bars to 6.

7.3 Loading Conditions

Traffic loads are treated as uniform surcharge loads, with the assumption that this load acts behind the reinforced soil mass for stability calculations and on top of the reinforced soil mass for maximum horizontal stress calculations (Fig. B-117). MSE design assumes a uniform permanent 2-ft surcharge load for representing traffic. This is a conservative approach which gives the most severe loading conditions in both cases.

Heavy truck traffic can be represented by a line load and the use of Boussinesq stress distributions integrated over the appropriate intervals to determine horizontal and vertical stresses within the soil.

7.4 Design Parameters

The mat spacing for a VSL Retained Earth wall is fixed at a vertical spacing of 30 in. and a horizontal center-to-center spacing of 52 in. For MSE walls, these dimensions are 12 to 24 in. vertical and 75 in. horizontal, whereas for GAS systems the vertical and horizontal dimensions are 24 and 32 in., respectively.

As the precast concrete facing panels dictate bar-mat spacings, the remaining design parameters are the embedment length of the reinforcement, the diameter of the bars, the number of

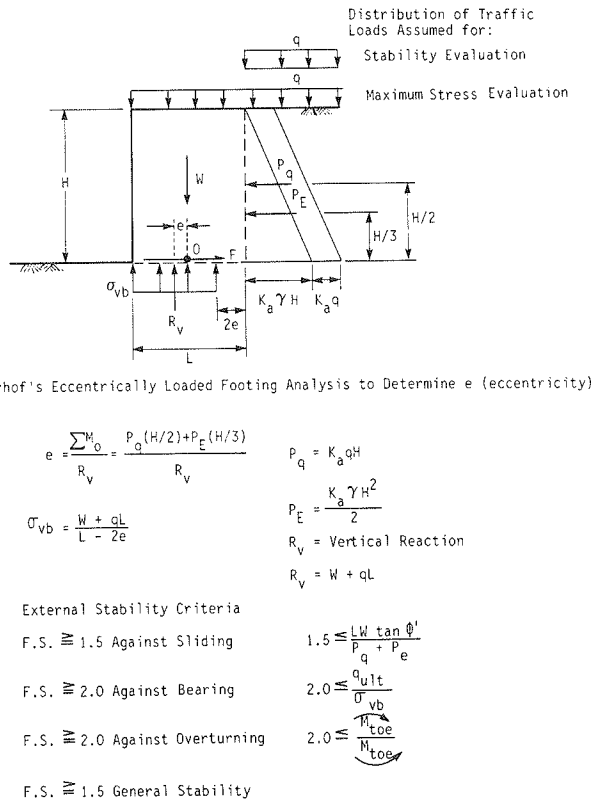

Figure B-117. Location of uniform loads.

longitudinal and transverse bars, and the quality of the backfill material.

7.5 Design Procedure

7.5.1 Internal Stability

Two criteria must be checked to assure internal stability. First, the reinforcement must be strong enough to withstand the stresses induced in it from the soil without rupturing. The reinforcement must also be able to withstand this force without pulling out of the soil.

7.5.2 Bar Size and Number of Longitudinal Bars

As discussed in Section 3.2 of this chapter, the coefficient of earth pressure used for the design of VSL Retained Earth walls varies linearly from an assumed coefficient of earth pressure at rest, K_o, at the top of the wall to an active earth pressure coefficient, K_a, 20 ft below the top of the wall (Fig. B-112). For MSE and GAS walls, the lateral earth pressure coefficient is assumed to be the active, rather than the at-rest, value for the full height of the wall. For design the horizontal stress, σ_h, at any depth within a wall is determined as follows:

$$\sigma_h = K \sigma_{vb} \tag{B-64}$$

where K = coefficient of earth pressure as determined from Figure B-112 for VSL, or K_a for MSE and GAS, and σ_{vb} = vertical stress at any depth using a Meyerhof [1953] distribution

to account for eccentric loading (see the design section of the main report, Chapter Five, and Fig. B-117).

If the vertical spacing between reinforcement mats is S_v and the horizontal center-to-center spacing between reinforcement mats is S_M, the total horizontal load, F_H, to be resisted by a given layer of reinforcement is:

$$F_H = \sigma_h S_M S_V \tag{B-65}$$

The tensile stress in the longitudinal bars is a function of F_H, as well as the number, M, and diameter, d, of the longitudinal bars used. The tensile stress, f_m, is equal to:

$$f_m = \frac{4F_H}{M\pi d^2} \tag{B-66}$$

The allowable tensile stress in the reinforcement as recommended by the American Association of State Highway and Transportation Officials is 0.55 times the tensile yield strength, f_y, of the steel. For the standard bars used as reinforcement in VSL Retained Earth walls, the tensile yield strength is 65,000 lb/sq in., and the allowable stress, f_a, is 35,750 lb/sq in.

7.5.3 Required Embedment Length

From field observations and model tests it has been shown that as the wall deforms, an active wedge of soil develops behind the wall face. This wedge has the internal boundaries as shown by the bilinear failure surface in Figure B-110. To stabilize this active wedge of soil, the reinforcing bar mat must extend beyond the failure surface into the fixed soil mass a minimum anchor distance L_e. The anchor length of the reinforcement, L_e, can be determined by dividing the horizontal load on any layer of reinforcement (Eq. B-65) by the pullout capacity of the reinforcement (Eq. B-63). With a transverse member center-to-center spacing of S_x, the anchor length, L_e, can be computed as:

$$L_e = \frac{S_x S_M S_y \sigma_h FS}{A_c \gamma z\, b\, d} \tag{B-67}$$

where FS is an appropriate factor of safety.

7.5.4 External Stability

The overall stability of the wall system can be evaluated by checking three potential failure modes: overturning, sliding on the base, and bearing capacity at the toe. Classical methods of soil mechanics can be used to check the external stability of the bar-mat walls. Analysis of external stability is covered in detail in the main report.

8. CASE HISTORIES

There have been relatively few instrumented bar-mat walls constructed to date. These are listed in Table B-19.

8.1 VSL Retained Earth Wall, Hayward, California

A VSL Retained Earth Wall was constructed in Hayward, California, to support an embankment for an overpass [Al-Yassin, 1983]. The wall height ranges from a minimum of 4 ft to a maximum of 20 ft. The surface area of the wall measures 3,700 sq ft. The wall supports a fill that slopes at an angle of 26 deg from the horizontal and extends a distance of approximately 50 ft behind the back of the wall (Fig. B-118).

Two sections of this wall, A and B, were instrumented with strain gauges (Figs. B-118 and B-119). Alternating vertical layers of reinforcement were instrumented. Field measurements were taken from the start of construction and continued for a period of approximately 1 year after the wall was completed.

The data from the strain gauges were reduced and plotted as lateral earth pressure as shown in Figures B-120 and B-121 [Al-Yassin, 1983]. The theoretical earth pressures for K_o and K_a conditions, using both the vertical stress as determined by the Meyerhof distribution and as determined by the overburden only are also plotted on these graphs. The lateral earth pressure in the upper part of the wall was close to the at-rest value for the entire time the wall was monitored. However, there appears to be a significant reduction in lateral earth pressure with time in the lower part of the wall. This might be caused by movement in this section of the wall, thus allowing the active condition to develop. The eventual earth pressure distribution at Section AA (Fig. B-120) is consistent with that used in the design procedure for VSL Retained Earth walls, while the eventual earth pressure at Section BB (Fig. B-121) is consistent with the MSE and GAS design procedures. The VSL, MSE, and GAS procedures for computing lateral earth pressures are described in Section 7.5.2 of this chapter.

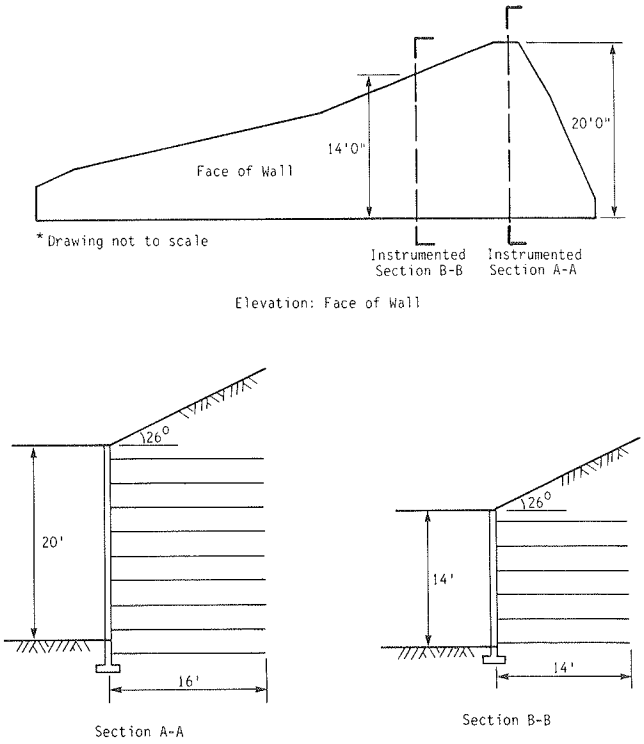

Figure B-118. Elevation and cross-section of Hayward wall.

8.2 VSL Retained Earth Wall, Hot Springs, South Dakota

A new bridge over an existing street was to be constructed on U.S. Highway 18 in Hot Springs, South Dakota [VSL Corporation, Project Files]. Four retaining walls were required to achieve the elevation changes necessary for this overpass (Fig. B-122).

VSL Retained Earth walls were chosen for this site because of the economic advantage earth walls have over conventional reinforced concrete walls and for their aesthetics. Hot Springs is situated in an historical area, which made the appearance of the wall of paramount importance. The precast facing panels were subsequently designed with a textured and colored surface to complement the surrounding native sandstone.

The structures were monitored on this project because this was the first VSL Retained Earth wall supporting a bridge abutment. Strain cells and tilt plates were installed to test the conformance of the walls to the design criteria. The wall performed to the satisfaction of the South Dakota Department of Transportation over the period of time the instruments were monitored.

8.3 Mechanically Stabilized Embankment, Dunsmuir, California

The realignment and widening of Highway I-5 near Dunsmuir, California, required three retaining walls [Chang et al., 1981]. The California Department of Transportation chose to install two Mechanically Stabilized Embankment walls and one Reinforced Earth wall for this project. This was the first project to use the Mechanically Stabilized Embankment system of earth wall construction.

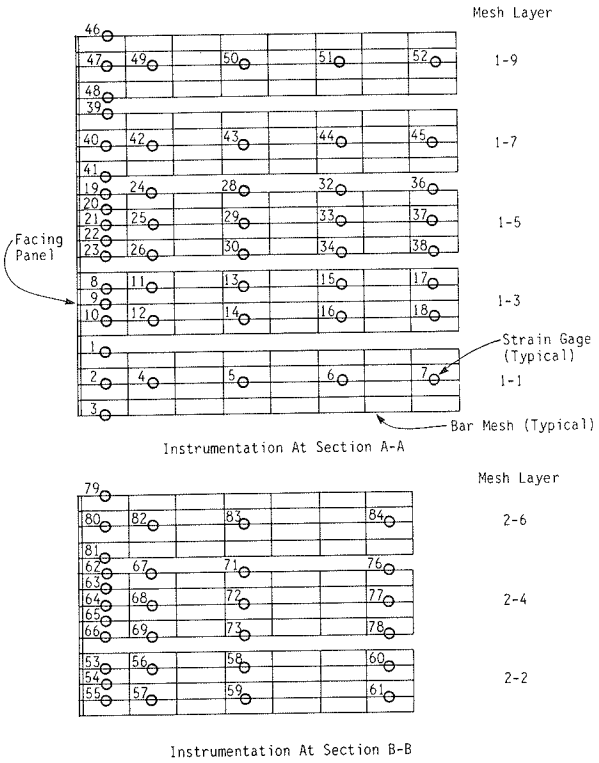

Figure B-119. Hayward wall instrumentation. [Al-Yassin, 1983]

Table B-19. Case histories of bar-mat walls.

Reference	Project Location & Date	Description	Backfill	Instrumentation	Comments
Al-Yassin & Shen (1983) Al-Yassin (1983)	Hayward California (1981)	Wall height 4-20 ft. surface area 3,700 SF wall was used as grade separation	gravelly sand	strain gauges on mesh, face of wall movements read optically	1st VSL RETAINED EARTH wall performance satisfactory
VSL Corp. Files	Hot Spring South Dakota (1982)	4 walls plus 2 bridge abutments wall height 0-30 ft. surface area 17,000 SF	granular	strain gauges load cells tilt plates	1st VSL RETAINED EARTH bridge abutment architectural precast facing
Chang et al. (1981)	Interstate 5 Near Dunsmuir California (1975)	Two MSE walls upper wall 20 ft high lower wall 18 ft high	granular	strain gauges corrosometer probes concrete pressure cells soil pressure cells settlement cells	1st MSE wall horizontal and vertical movements after the wall was complete were very small
Hannon and Forsyth (1984)	I-80 near Baxter, CA (1982)	Four MSE walls max wall height 16 ft.	silt 49% passing #200 sieve	strain gauges pressure cells reference monuments plumb points piezometers	performance after six months was satisfactory

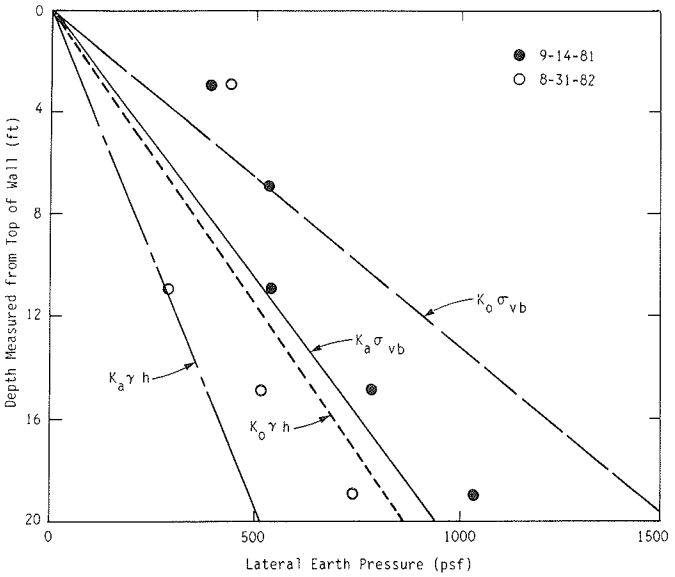

Figure B-120. Lateral earth pressure near face of wall—Section A-A. [Al-Yassin, 1983]

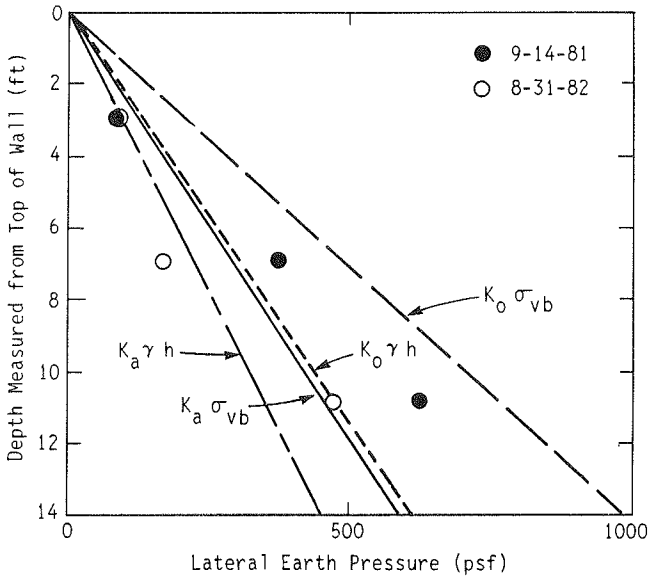

Figure B-121. Lateral earth pressure near face of wall—Section B-B. [Al-Yassin, 1983]

The two Mechanically Stabilized Embankment walls are located below the Siskiyou Elementary School. The upper and lower walls (Fig. B-107) are 20 and 18 ft high, respectively. The lower wall, which was constructed first, was completed in October 1975. Construction on the upper wall did not start until the following spring, and it was completed in August 1976.

The 20-ft high Reinforced Earth retaining wall was approximately 2,000 ft away along the highway. Both the Reinforced Earth wall and the Mechanically Stabilized Embankment walls are located on a soft foundation material. Expected settlement for the walls was calculated at 18 in., thus precluding the use of conventional reinforced concrete retaining walls unless they were pile-supported.

The performance of the retaining walls was monitored by a series of strain gauges, corrosometer probes, pressure cells located on the concrete facing panels, pressure cells located within the backfill, settlement sensors to measure vertical settlement, reference monuments to measure horizontal and vertical movement at the top of the walls and plumb points to measure horizontal and vertical movements at the face of the wall. Both the Mechanically Stabilized and Reinforced Earth systems performed satisfactorily during the period of monitoring.

During the construction of the Mechanically Stabilized Embankment walls, there were two construction difficulties. The more serious one was that the proper fit of the precast panels along curved alignments was difficult to achieve. As a result of this difficulty, the facing panel design was modified to facilitate constructing curved walls. The second problem, which was minor in cause but a potential safety hazard, was that some of the panels toppled before they were secured to reinforcing mats. The contractor was required to make sure all facing panels were secured to reinforcing mats prior to stopping work for the day and further problems did not occur.

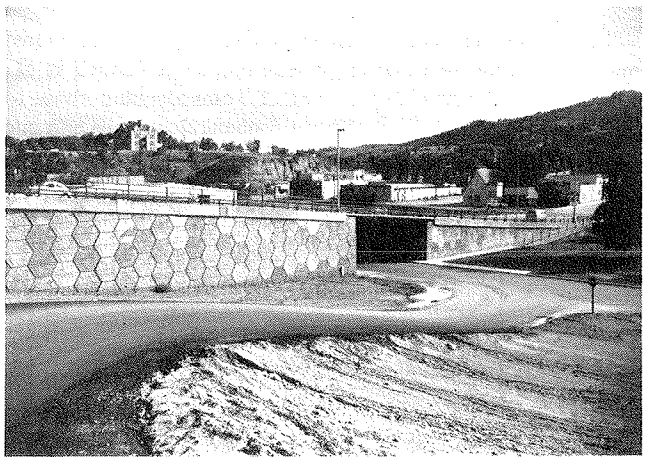

Figure B-122. Hot Springs, South Dakota, VSL Retained Earth wall.

8.4 Mechanically Stabilized Embankment, Baxter, California

Four Mechanically Stabilized Embankment walls were required for the widening of a ½ mile long stretch of Interstate 80, near Baxter, California [Hannon and Forsyth, 1984]. As low quality backfill material was to be used for the first time in MSE for these retaining walls, two of the four walls were instrumented with strain gauges, pressure cells, reference monuments, plumb points, and piezometers, to monitor the effects of using a low quality backfill. Maximum wall height was 16 ft.

The material used for the embankments was classified as "SM" or sandy silt by the Unified Soil Classification System. About 50 percent of the material passed the No. 200 sieve, which is considered excessive for most reinforced soil walls.

Furthermore, the on-site material is not free-draining and is subject to considerable strength loss when saturated. A subsurface drainage system was therefore required as shown in Figure B-123.

Construction commenced on July 9, 1982. In mid-September construction was stopped for one week because of intermittent rain. The fine-grained backfill material became partially saturated and required additional time to dry out before work could be resumed. Construction was forced to stop more than once following rains because of the inability to achieve proper compaction owing to the higher water content of the backfill.

The wall was completed in the fall of 1982. Monitoring of the wall during and after the record rainfall of the 1982–1983 winter showed no significant lateral or vertical wall movements. The major conclusion from this study was that fine-grained soils have been shown to be an acceptable backfill material when used with bar-mat reinforcement and an appropriate drainage system.

9. COSTS

Cost comparisons of bar-mat walls with other types of reinforced soil structures are inevitably site-specific. However, some generalized unit costs for Georgia Stabilized walls, taken from two Georgia Department of Transportation projects bid in April and June of 1984, indicate the overall wall price, excluding traffic barriers and coping, to be about $25.00/sq ft. This average was determined for over 49,000 sq ft of wall face, with the height of wall varying from 8 to 22 ft. These costs are, of course, site-specific and very dependent on material availability, local wage rates, local taxes, local insurance, and local material costs.

10. FUTURE DEVELOPMENTS OF THE SYSTEM

Future research on bar-mat walls is likely to concentrate on three areas: (1) durability of reinforcements, (2) use of fine-grained soil for backfill, and (3) field instrumentation to better define working stresses and deformations.

Research on durability aspects would improve the current understanding of the mechanisms of corrosion of buried metals under high stress and how to more accurately estimate the rate of corrosion under varying soil conditions.

The wall constructed at Baxter, California, has already demonstrated the ability of bar-mat reinforcements to perform effectively in fine-grained soils. However, more research and experience are needed before cohesive soils can be readily accepted as backfill material.

More bar-mat walls need to be instrumented in the future to better define the loci of maximum stresses for design and to determine the earth pressures acting within the reinforced soil mass.

11. DESIGN EXAMPLE

Several design examples for mechanically stabilized walls are given in Chapter Five of the main report.

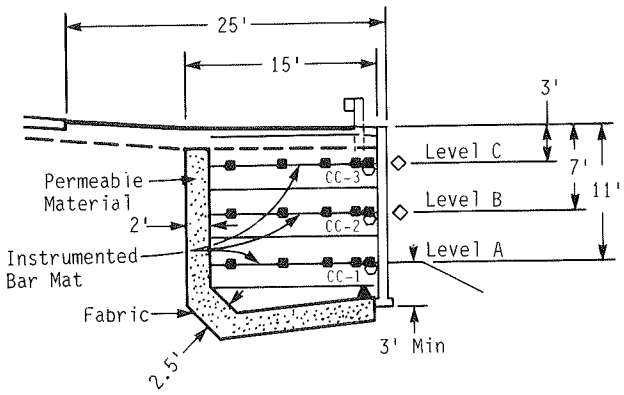

LOCATION 1, Station 383 + 60 (H=14')

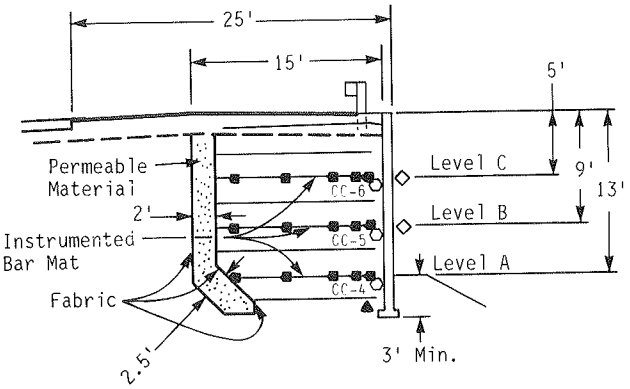

LOCATION 2, Station 399 + 30 (H=16')

CODE	SYMBOL	DESCRIPTION
SG	■	STRAIN GAGES (2 EACH)
CC	○	CONCRETE PRESSURE CELLS
PP	◇	PLUMB POINTS
P	▲	PIEZOMETERS

Figure B-123. Baxter, California MSE wall, instrumentation sections. [Hannon and Forsyth, 1984]

12. REFERENCES

AL-YASSIN, Z. [1983]. "VSL Retained Earth—Hayward Test Results," Report to the VSL Corporation, January.

AL-YASSIN, Z. and SHEN, C. K. [1983]. "Field Behavior of a Retained Earth Structure," *Proc. International Conference on Case Histories in Geotechnical Engineering,* St. Louis, Missouri.

BAQUELIN, F. [1978]. "Construction and Instrumentation of Reinforced Earth Walls in French Highway Administration" *Proc. ASCE Symposium on Earth Reinforcement,* Pittsburgh, April, pp. 186–201.

BLOOMFIELD, R. A. [1984]. "Proposed Design Modifications—VSL Retained Earth," VSL Corporation, January.

CHANG, J. C., FORSYTH, R. A., BEATON, J. K. [1974]. "Performance of a Reinforced Earth Fill," *Transportation Research Record 510,* TRB, National Research Council, Washington, D.C.

CHANG, J. C., HANNON, J. B., FORSYTH, R. A. [1977]. "Pull Resistance and Interaction of Earthwork Reinforcement and Soil," *Transportation Research Record 640,* TRB, National Research Council, Washington, D.C.

CHANG, J. C., HANNON, J. B., FORSYTH, R. A. [1981]. "Field Performance of Earthwork Reinforcement," *CA/TL-81/06,* California Department of Transportation, Sacramento, California, November.

FORSYTH, R. A. [1978]. "Alternate Earth Reinforcements," *Proc. ASCE Symposium on Reinforced Earth,* Pittsburgh, April, pp. 358–370.

HANNON, J. B., FORSYTH, R. A. [1984]. "Performance of an Earthwork Reinforcement System Constructed with Low Quality Backfill," *Transportation Research Record 965,* TRB, National Research Council, Washington, D.C.

JURAN, I. [1982]. "Design of Reinforced Earth Structures," Notes from the Louisiana State University Short Course of Reinforced Earth, *Report GE-82/02.*

MEYERHOF, G. G. [1953]. "The Bearing Capacity of Foundations Under Eccentric and Inclined Loads," *Proc. 3rd International Conference on Soil Mechanics and Foundation Engineering,* Vol. I, Zurich, Switzerland, pp. 440–445.

SCHLOSSER, F. and ELIAS, V. [1978]. "Friction in Reinforced Earth," *Proc. ASCE Symposium on Earth Reinforcement,* Pittsburgh, April, pp. 735–763.

VSL CORPORATION [1983]. *Field Erection Manual,* March 1983.

VSL CORPORATION, *Project Files.*

APPENDIX C

SOIL NAILING

CHAPTER ONE—SOIL NAILING IN EXCAVATIONS

Contents

1. INTRODUCTION

1.1 Physical Description of Nailed Soil Retaining Systems

Soil nailing is a method of reinforcing in-situ soils of various types using passive inclusions to retain excavations or stabilize slopes as shown in Figure C-1. The technique has been used to stabilize highway slopes, to construct inclined retaining structures, to construct vertical retaining structures [Stocker et al., 1979; Shen et al., 1981a; Cartier and Gigan, 1983; Guilloux et al., 1983], and in tunneling [Louis, 1979] and other civil and industrial projects [Louis, 1981].

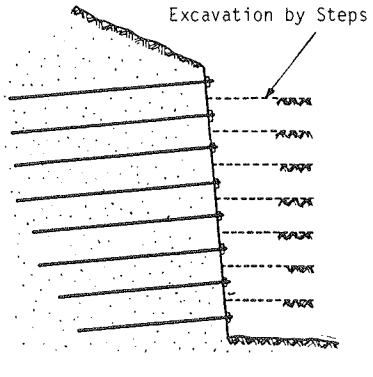

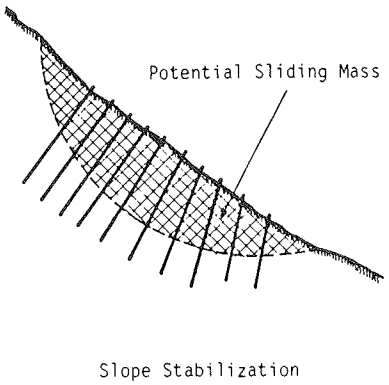

Figure C-1. Main applications of soil nailing.

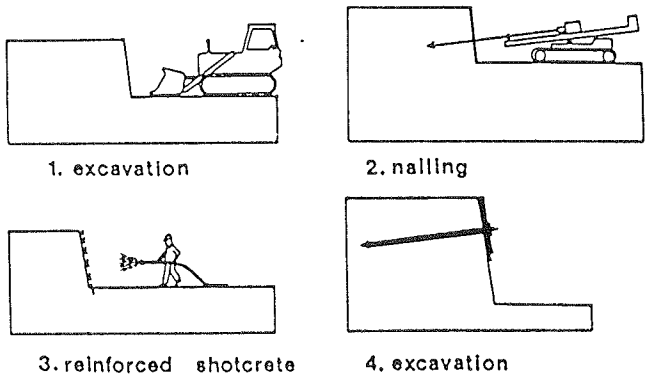

Figure C-2. Construction process.

In nailed soil retaining structures, the inclusions are generally steel bars or other metal elements which can resist tensile stresses, shear stresses, and bending moments. They are either placed in drilled boreholes and grouted along their total length or driven into the ground. The inclusions are not prestressed, and their "density" is approximately one bar per 5 to 65 sq ft, thus providing an anisotropic apparent cohesion. The outside facing of the structure, which ensures local stability between the reinforcement layers, can consist of a thin layer of shotcrete 4 to 6 in. thick with wire mesh or steel mesh reinforcing between nails.

Figure C-2 shows the different phases of soil nailing construction in excavations. Successive incremental excavations with a height of 3 to 6 ft are generally stable, provided the in-situ soil has some short-term cohesion. The design and geometry of the structure are dependent on the technique used to install the bars. There are two typical methods: (1) "micro piles," consisting of long and very strong inclusions (of about 50 to 100 kip strength in tension) grouted in a predrilled borehole at a wide spacing (about one bar per 30 to 60 sq ft); and (2) "hurpinoise," a term used to refer to nailing with shorter and less resistant bars (10 to 35 kip strength in tension) that are driven into the soil at a close spacing (approximately one bar per 5 sq ft).

1.2 History and Development

In-situ reinforcement of soil by resistant inclusions is a very old technique. In recent decades this method has been widely used in tunneling and in the stabilization of rock slopes by using passive metallic anchors grouted in the rock mass. The purpose of such reinforcement is to limit stress reduction from rebound and the opening of preexisting discontinuities (i.e., spalling) by restraining deformations, thus creating a mass where rock blocks are locked together. During the last decade, the so-called "Austrian Tunneling Method" developed by Rabcewicz [1964, 1965] has been frequently used to replace conventional methods of tunnel construction. By reinforcing the ground around the tunnel, while at the same time allowing some yielding, the loads on the tunnel supports are greatly reduced. A comparison with conventional tunnel support is shown schematically in Figure C-3.

In-situ soil nailing for tunneling consists of protecting the excavation by a continuous skin of shotcrete about 4 to 12 in. thick. Because of the method of construction, this surface layer perfectly fits the irregularities of the section and can even fill voids and cracks in the surrounding ground. The shotcrete skin is usually reinforced with a wire mesh, and is supported by short bars (10 to 20 ft long) that are driven or grouted into place. The shotcrete skin is applied immediately after a total or even a partial section of the tunnel has been excavated, and thus it restrains rebound of the surrounding ground.

The somewhat similar technique of soil nailing in excavations has been developed mainly in Europe, particularly in Germany and France. In France, the first applications concerned inclined railway retaining walls in cut slopes. They were constructed in 1972 and 1974 and are described by Rabejac and Toudic [1974] and by Hovart and Rami [1975]. Figure C-4 shows a typical section of the first of these two retaining walls.

Soil nailing is presently used in Europe for construction of temporary retaining structures in excavations [Schlosser and Juran, 1979; Schlosser, 1983; Guilloux et al., 1983; Louis, 1979]. A few of these structures have been instrumented to develop a data base for incorporation into design methods [Stocker et al., 1979; Gassler and Gudehus, 1981; Schlosser, 1983].

In North America, the behavior of a lateral earth support system similar to the European system has been investigated by Shen et al. [1978, 1981a and 1981b]. This lateral earth support system was developed to replace conventional soldier pile and bracing systems and has been successfully used in excavations as deep as 60 ft. A typical section of this system is shown in Figure C-5.

In parallel with the development of soil nailing, the somewhat similar system called root piles [Lizzi and Carnavale, 1979], has also been used to retain excavations and stabilize slopes. The

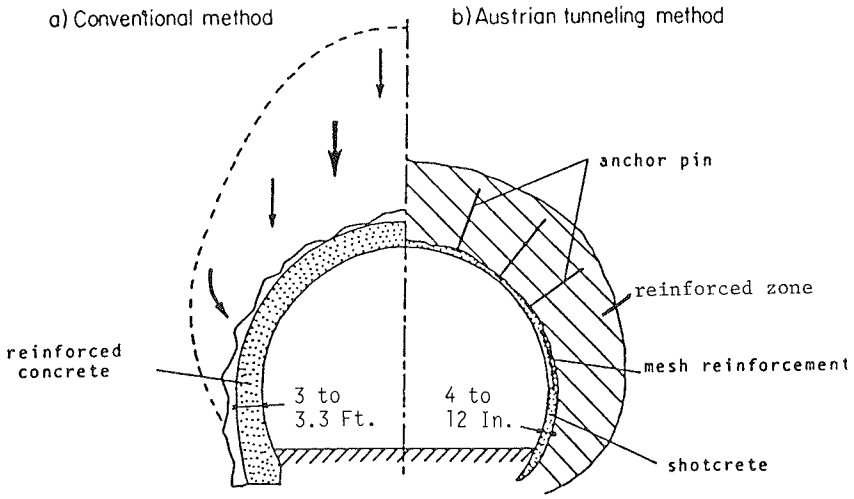

Figure C-3. Schematic comparison of the Austrian tunneling method and the conventional method

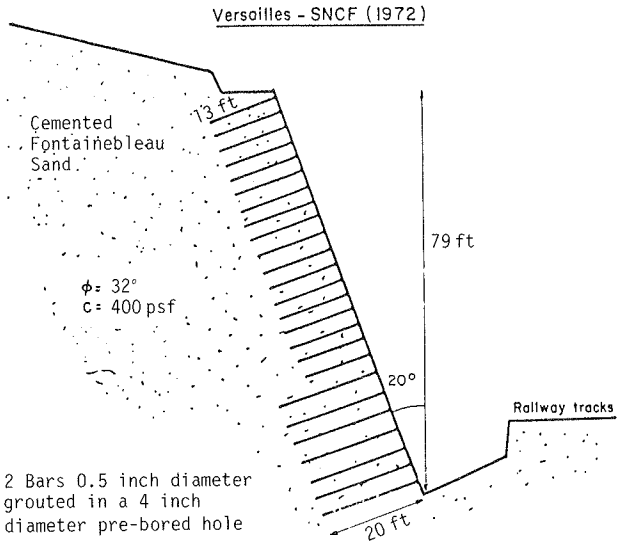

Figure C-4. First application of soil nailing retaining walls

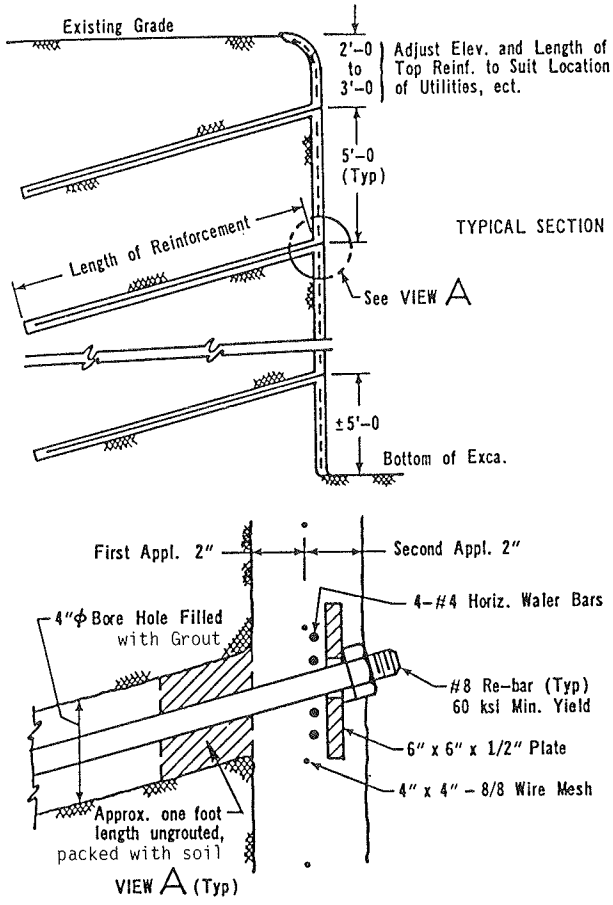

Figure C-5. Construction details of lateral earth support system. [Shen et al., 1978]

main difference between root piles and soil nailing is that the reinforcing bars in root piles are normally grouted under high pressure (115 to 150 psi) and that the alignments of the reinforcing members differ. The high pressure grouting has two major effects. First, it significantly increases the adherence of the bars to the in-situ soil and thus enables a reduction in the length of the reinforcements. Secondly, because the grouting is under pressure rather than gravity feed, it enables installation of the bars at any desired orientation, thus providing the possibility of creating a criss-crossing effect in the reinforced soil mass [Schlosser and Juran, 1979], producing a quasimonolithic gravity retaining structure of soil and very closely spaced root piles. This reinforced soil mass can be analyzed in the same manner as a gravity retaining structure constructed of reinforced concrete.

Soil nailing in excavations is still limited primarily to temporary structures because of the difficulties associated with evaluating the corrosion rate of steel bars in the in-situ ground and in producing low cost reinforcing elements with high resistance to corrosion. Recently, efforts have been made in France to develop new types of reinforcements to make structures more durable. Of particular interest are the high adherence tube nails developed by Solrenfor (Fig. C-6) and the prestressed multi-reinforced nails developed by Intrafor-Cofor (Fig. C-7). In these two types of reinforcements, the steel bars are enclosed in grout to protect against water penetration.

1.3 Proprietary Restrictions

There are no proprietary restrictions on the use of soil nailing. However, different types of prefabricated facing and reinforcements, i.e., the components used for construction, have been patented and are subject to proprietary restrictions. Examples of such patented reinforcing elements are the Solrenfor and Intrafor-Cofor nails shown in Figures C-6 and C-7.

2. APPLICATIONS

2.1 Inherent Advantages

In comparison to conventional excavation retaining systems (such as massive concrete walls, soldier pile walls, cast-in-place slurry walls, and internal bracing systems) the technique of in-situ soil nailing presents some special advantages: (1) *Low cost*—In soil nailing, the in-situ ground is used as one of the main structural elements in the retaining structure, the other structural element being the relatively low-cost nails. The shotcrete

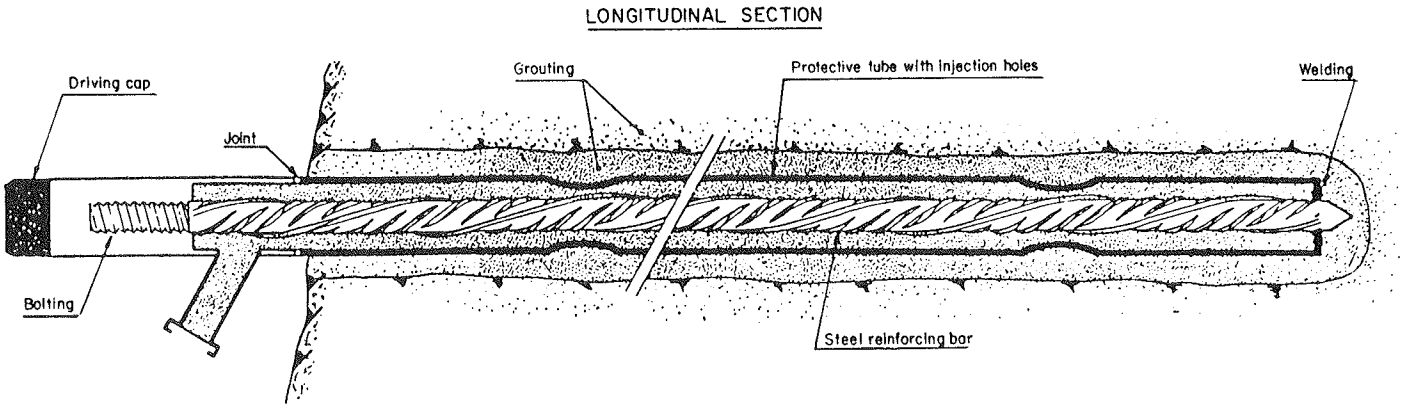

Figure C-6. "TBHA" nail patented and developed by SOLRENFOR for permanent structures.

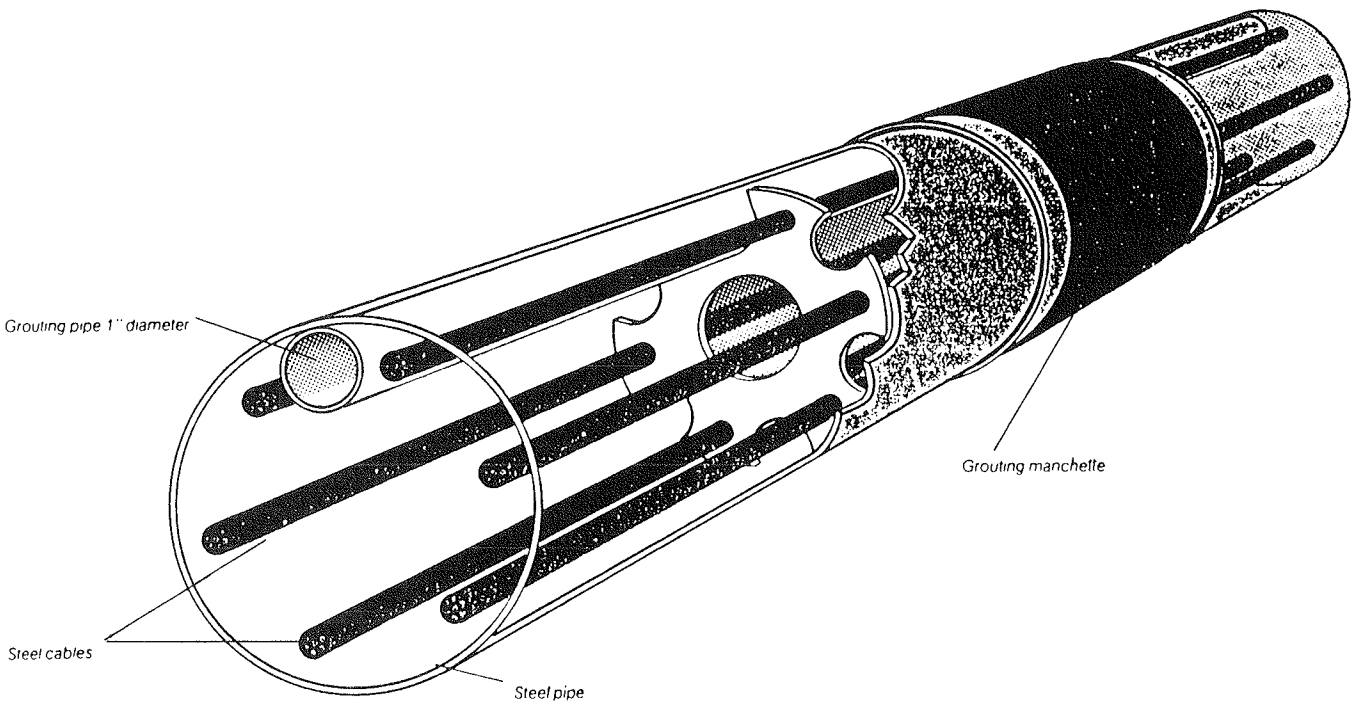

Figure C-7. Prestressed multireinforced nail "INTRAPAC" developed by INTRAFOR-COFOR (France).

or prefabricated facing has only a local role, preventing the collapse of the soil at the face between the nails. The facing is, therefore, relatively thin and inexpensive. The low cost of the elements can provide significant savings in construction materials relative to conventional solutions, which generally require thick reinforced concrete facings or prestressed ground anchors. (2) *Light construction equipment*—Soil nailing can be done using simple drilling and grouting equipment (drilling by vibropercussion and grouting generally by gravity). The handling of equipment is relatively easy because of staged construction, and the technique is thus of a particular interest in sites with difficult access. (3) *Adaptability to site conditions*—There is flexibility in the application of the system, because the staged construction process allows the geometry of the structure, the inclination of the facing, and the density and dimensions of the reinforcements to be adapted to the site conditions and soil characteristics exposed at different levels during excavation. (4) *Easy operation in heterogeneous soils*—In heterogeneous ground, where boulders or hard rocks may be encountered in softer layers, soil nailing is generally more feasible than other techniques such as slurry walls and soldier piles, because it involves only small-diameter drilling for the installation of the inclusions. An interesting example is the application of nailing in the construction of an underground parking lot in the French Alps as described by Guilloux et al. [1983]. As part of the temporary construction, it was necessary to build retaining walls to depths of nearly 70 ft in compact moraine with boulders. The initial design considered a soldier pile wall with three levels of prestressed ground anchors, but the piles were considered too difficult to install. Soil nailing, which was selected as an alternate, was successfully used to significantly reduce the time and cost of construction. (5) *Flexibility*—Nailed soil retaining structures are more flexible than classical cast-in-place reinforced concrete retaining structures. Consequently, these structures can conform to deformation of surrounding ground and withstand larger total and differential settlements. This characteristic of soil nailing can provide economical support for excavations on unstable slopes.

2.2 Site Conditions Appropriate for Use

Soil nailing can be used in a wide variety of excavation sites, but is of particular interest in mountainous areas, where a combination of reinforced soil embankments and soil nailing can result in an optimum design minimizing the excavation necessary for the reinforced soil retaining structures.

The following limitations inherent to soil nailing must be considered during design: (1) *Clayey soils*—In clayey soils, an increase of the degree of saturation can significantly reduce the soil-reinforcement friction or adhesion. Furthermore, increase in saturation can also result in an increase in the tensile reinforcement forces because of the associated decrease in shear strength of the supported soil. Hydrostatic porewater pressures may also be detrimental, while creep displacements of the soil may cause an excessive lateral displacement of the facing. Guilloux and Schlosser [1982] described a failure of a 15-ft high nailed soil wall in a plastic clay. Suitable designs for soil nailing in clayey soils may, therefore, require a high density of long reinforcements, in which case they may be more costly than conventional solutions. (2) *Soil-reinforcement displacements*—The mobilization of the soil-reinforcement interaction in nailed soil retaining structures requires a relative displacement of soil and reinforcements, which is a function of the type of the soil and of the reinforcements. Therefore, in urban sites the potential use of this technique can be limited by the necessity to avoid movement of structures in the immediate vicinity. In most cases, however, the displacement necessary to mobilize the tensile forces in the reinforcements is reasonably small, of the order of several millimeters. Full-scale experiments [Guilloux and Schlosser, 1982; Cartier and Gigan, 1983; Gassler and Gudehus, 1981; Shen et al., 1981] have demonstrated that the maximum lateral displacements of nailed soil walls do not usually exceed 0.2 percent to 0.3 percent of the wall height (Fig. C-8). The displacements without prestressing in a nailed soil wall are of the same order of magnitude as those in a prestressed multi-anchor system.

2.3 Routine and Special Applications

To date, soil nailing has been primarily used as a retaining system for highway slopes, for excavations in mountainous areas, for stabilization of railway slopes, and for tunnel facing. A few typical soil nailing projects are summarized in Table C-1.

To date, soil nailing in excavations has mainly been used for temporary structures for two reasons: (1) the facing technology does not yet conveniently provide for an aesthetic facing of the technical quality for permanent structures, and (2) there are still remaining concerns about longevity aspects, because the corrosion rate in heterogeneous ground is difficult to evaluate. However, permanent structures as high as 80 ft have been constructed in France.

It has also been demonstrated [Gassler and Gudehus, 1981] that these structures can withstand both static and dynamic vertical loads at their upper surfaces without excessive movement.

At the present state of practice, special applications of soil nailing are still rather limited. However, in a further development of the current tunneling techniques, the method can be used for support of circular shafts using metal panels and anchoring bolts as shown in Figure C-9.

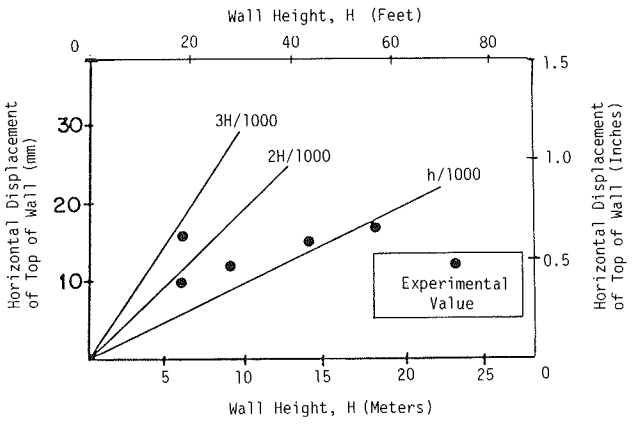

Figure C-8. Nailing retaining structures—displacements of the facing. [Guilloux and Schlosser, 1984]

Table C-1. Some typical soil nailing projects.

Type of structure	Type of soil	Height of structure (ft)	Type of reinforcements	Length of reinforcements (ft)	Spacings (ft) V X H
Railway retaining structure (Versailles) (1972) Temporary	cemented fine sand $\phi' = 32°$ $c' = 400$ psf	79	grouted bars 2 bars/reinf 0.5 inch dia.	13 to 20	3.3x3.3
Urban retaining structure (Nice) (1975) Temporary	sandy marl $\phi' = 35°$ $c' = 200$ psf	36	grouted bars	26	6.6x10
Urban retaining structure (Paris) (1976) Temporary	silty colluvium and sand $\phi' = 20°-35°$	39	driven tubes 40/49 mm	20	2.5x2.5
Retaining structure for underground parking (French Alps) (1980) Temporary	compact moraine $\phi' = 55°$ $c' = 0$	46	grouted bars 1 inch dia.	23 to 30	6.6x10
Cut slope retaining structure (French Alps (1981) Permanent	clayey soils $c' = 0$ $\phi' = 28°$	20	grouted bars 1 inch dia.	30 to 33	6.6x6.6
Excavation retaining structure (Lyon) (1984) Permanent	sand with sandstone layers	98	grouted bars 1 inch dia.	20 to 46	varying (average 6.6x10)
Excavation retaining structure (southeast France) Temporary	calcareous marl $\phi' = 35°$ $c' = 400$ psf	36	grouted bars 1 to 1¼ inch dia.	23 to 39	6.6x10
Retaining structure (Paris) Temporary	remolded, stiff marl $\phi' = 25°$ $c' = 0$	30	grouted bars 1¼ inch dia.	33	4x5
Excavation retaining structure (France) Temporary	weathered shale $\phi' = 45°$ $c' = 0$	62	grouted bars 1 to 1¼ inch dia.	16 to 30	3.3x6.6
Excavation for facing of tunnel entrance (Rosti)	marl, calcareous marl	131	--	--	--

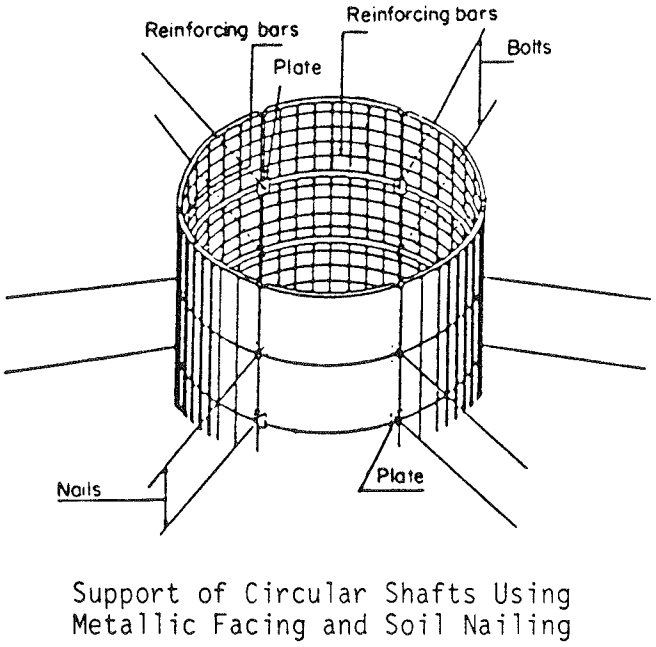

Figure C-9. Example of nailed soil shaft. [Louis, 1981]

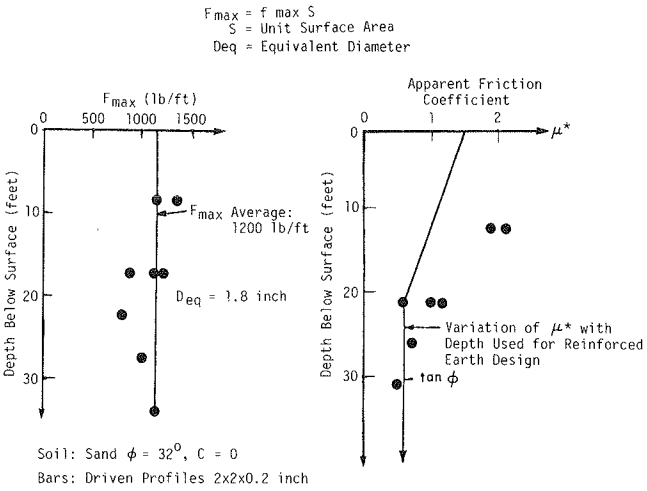

Figure C-10. Soil-reinforcement friction in a nailed soil wall with driven bars. [Cartier and Gigan, 1983]

3. MECHANISMS AND BEHAVIOR

3.1 Principles of Soil-Reinforcement Interaction and Behavior of the Nailed Soil Material

The soil-reinforcement interaction in nailed soil retaining structures can involve two fundamental mechanisms: friction along the reinforcements and passive earth resistance against surfaces normal to the pullout direction. The mobilization of these two mechanisms is dependent on both the orientation of the reinforcements relative to the potential sliding surface, and on the bending stiffness of the reinforcements.

3.1.1 Friction

Full-scale pullout tests on bars buried in a nailed soil wall [Cartier and Gigan, 1983] have demonstrated that the mobilization of the soil-reinforcement friction along the driven bars is comparable with observations on reinforced soil walls. As shown in Figure C-10, measured values of the apparent friction coefficient μ^* in a nailed soil wall correspond reasonably well to those proposed by Schlosser and Guilloux [1979] for the design of Reinforced Earth walls (Chapter One in Appendix A).

The results of pullout tests, as shown in Figure C-11, indicate that the relative soil-to-reinforcement displacement necessary to mobilize friction is small (0.08 to 0.12 in.). The soil-reinforcement friction in in-situ nailed soil can vary significantly depending on the technology used to install the inclusions, i.e., driving into the in-situ ground, placing in boreholes and grouting with or without pressure, placement in an embankment, and so on.

An attempt has been made to use the value of the limit skin friction, f_{max}, on the nail surface to calculate pullout resistance according to:

$$f_{max} = \mu^* \gamma h \qquad \text{(C-1)}$$

where μ^* = apparent coefficient of friction between the soil

and the reinforcement; γ = effective unit weight of the soil; and h = height of fill above the reinforcement.

As shown in Figure C-10, the value of f_{max} appears approximately constant with depth. For preliminary design, the value of f_{max} can be estimated on the basis of recommendations for the design of friction piles using available correlations based on in-situ or laboratory test results.

The soil-reinforcement friction is strongly dependent on the type and density of the soil. In dense granular soils, dilatant behavior can increase normal stress on the inclusion, as discussed in the main report. Values of maximum skin friction ranging from less than 2,100 psf for a relatively loose sand up to about 12,300 psf for dense granular soils have been measured [Guilloux and Schlosser, 1982]. For cohesive soils, the maximum skin friction is generally lower, particularly in the case of soft clays, and decreases significantly when the soil is saturated.

Although correlations between the available maximum skin friction and the characteristics of the in-situ soil are helpful for a preliminary design [Guilloux and Schlosser, 1982], pullout tests on the actual inclusions are recommended to provide reliable design values for a particular case.

3.1.2 Passive Earth Thrust on the Reinforcements

Although tensile forces constitute the dominant reinforcing mechanism, passive lateral earth resistance can develop against the nail on either side of a potential failure surface, when reinforcing elements are rigid (see Fig. C-12). To illustrate the effect of the rigidity of the reinforcement on the soil-inclusion interaction, the two limiting cases of flexible and completely rigid reinforcements can be considered. As shown in Figure C-12, a flexible reinforcement will deform until equilibrium is reached. However, the rigid reinforcement will resist the deformation; consequently, passive lateral earth thrust will be mobilized at both sides of the potential sliding surface, and shear stress will be developed on the cross section of the reinforcement to maintain the equilibrium requirements. Rigid reinforcements, dependent on alignment, may thus have to withstand shearing forces and bending moments as well as tensile forces.

To investigate mobilization of passive resistance, Juran et al. [1981] performed direct shear tests on large silty sand samples ($2 \times 2 \times 1.3$ ft), reinforced by passive bars of different diameters placed perpendicular to the failure surface. These experiments enabled measurement of the stresses in the bars, their displacements, and the displacement of the soil. Both apparent cohesion and apparent internal friction angle of the reinforced soil mass during shearing could be inferred from the test results. The reinforcement–soil interaction was also analyzed using a two dimensional numerical finite element model in which a row of bars was represented by an equivalent plate, and plane strain conditions were assumed to prevail [Juran et al., 1983].

This study showed that the relative displacement x (the ratio of the displacement of the upper box to the length of the shear surface), necessary to fully mobilize shear resistance and bending stiffness of the reinforcements, depends on the rigidity of the reinforcements relative to the soil and on the spacings of the inclusions.

Figure C-13a shows the failure envelopes of both the nailed soil and the nonreinforced soil as measured in the experiments and interpreted from the finite element analysis. Failure has been defined by a relative displacement, x, of 10 percent. As

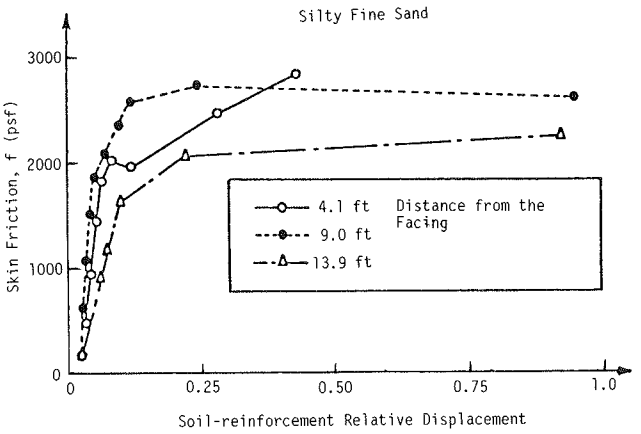

Figure C-11. Measured mobilization of the limit skin friction in a pullout test on a nail. [Cartier and Gigan, 1983]

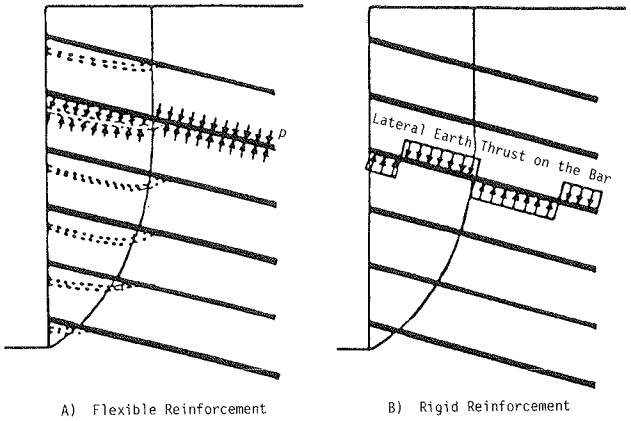

Figure C-12. Effect of the rigidity of the reinforcement.

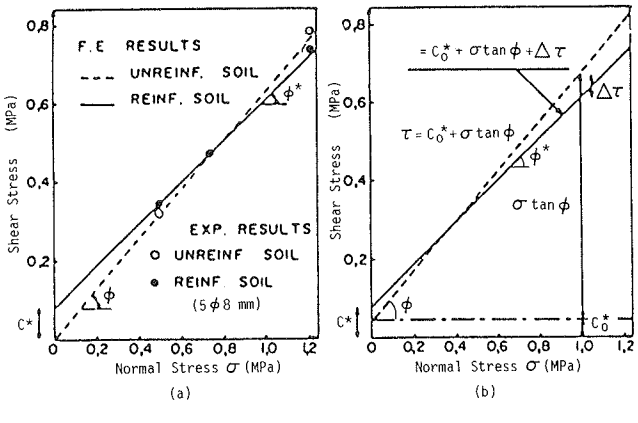

Notes: 1MPa = 10.4 Tons Per Square Foot

$C_0^* = \frac{\Sigma V_0}{A}$ where V_0 = Shear force on each nail, A = Area of failure surface

Figure C-13. Failure curves of reinforced and unreinforced soils—direct shear tests. [Juran et al., 1983]

schematically shown in Figure C-13b, the overall shear resistance of the reinforced soil can be divided into three components: (1) the apparent cohesion C_o^* due to the shear forces, V_o, mobilized in the bars: $C_o^* = \Sigma V_o/A$ (where A is the area of the shear surface); (2) the frictional shear stress, τ_s, mobilized in the soil along the potential failure surface away from the bars, which is equal to σ' tan ϕ; and (3) the difference in frictional shear stresses between reinforced and nonreinforced soil, $\Delta\tau$, which is caused by the effect of the reinforcing bars on the stresses and displacements of the soil.

Hence, the total shearing resistance of the reinforced soil can be written as:

$$\tau = C_o^* + \sigma' \tan \phi + \Delta\tau \qquad \text{(C-2)}$$

The finite element results show that the shear forces mobilized in the bars, V_o, and the corresponding values of the apparent cohesion C_o^*, are practically independent of the applied normal stress σ'. However, the effect of the reinforcing bars on $\Delta\tau$ is highly dependent on the applied normal stress; in fact, $\Delta\tau$ varies from positive for low normal stresses to negative for high normal stresses. Consequently, the total apparent cohesion C^* is greater than C_o^*, and the apparent internal friction angle of the reinforced soil ϕ^* is smaller than the internal friction angle of the soil ϕ (see Fig. C-13).

This finite element results (Figs C-13 and C-14) show that the bars modify the stress and strain fields which develop in the reinforced soil. As shown in Figure C-12b, they restrain the shear displacement of the soil along the failure surface in the vicinity of the reinforcements and, consequently, as shown in Figure C-13b, reduce the shear stress in the soil and the mobilized internal friction angle of the reinforced soil. However, they create an anisotropic apparent cohesion and increase the global shear resistance.

The mobilization of both the apparent cohesion C^* and the portion of cohesion due to shear forces in the reinforcement bars C_o^*, as functions of relative displacement, x, is shown in Figure C-14. These results indicate that a relatively large displacement ($x > 4$ percent) is necessary in order to fully mobilize the apparent cohesion. At this displacement, the soil around the bars (or the equivalent plates) attains a limit state of stress,

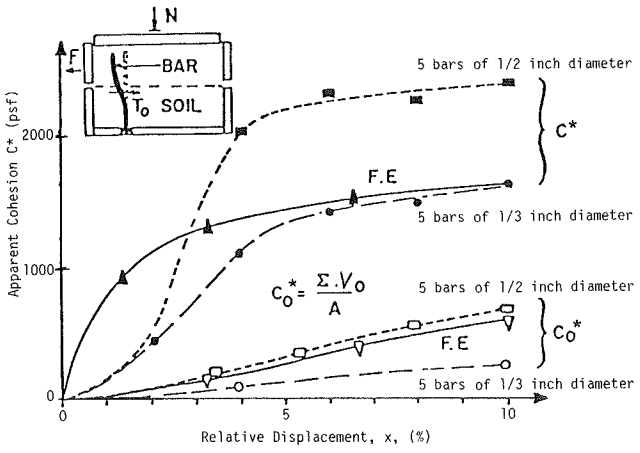

Figure C-14. Mobilization of the apparent cohesion of the nailed soil. [Juran et al., 1983]

and the passive lateral earth thrust on the bars is, therefore, practically fully mobilized. In the actual case of a row of bars, a progressive plastic flow of the soil will occur because the spacing between the bars is too wide, and the soil–bar interaction is not sufficient to prevent the flow of soil between the inclusions.

In order to evaluate the shear forces V_o and the apparent cohesion C_o^*, a further analysis was performed in which the bars were considered as laterally loaded vertical piles supported by horizontal springs with spring coefficients, E_s, which can vary during the loading. This analysis is similar in concept to the p-y analysis commonly used to evaluate pile behavior under lateral loading. The loading due to the lateral thrust of the sliding zone is simulated by imposing a lateral earth thrust on the bars $p(z)$ that is proportional to the relative displacement.

$$p(z)D = E_s\,[y(z) - g(z)] \qquad \text{(C-3)}$$

where $y(z)$ = lateral displacement of the bar; $g(z)$ = lateral displacement of the soil itself away from the bars; and D = diameter of the bar.

The differential equation for the elastic bending of the bars provides a solution for the distributions of the shearing stresses and bending moments as a function of the relative displacements. This solution involves a useful design parameter, L_o, referred to as the transfer length of the bar which characterizes the relative rigidity of the bar and the soil:

$$L_o = \sqrt[4]{\frac{4EI}{K_s D}} \qquad \text{(C-4)}$$

where EI = bending stiffness of the bar; K_s = modulus of lateral soil reaction; and D = diameter of the bar.

At large displacement, the soil is assumed to exhibit plastic behavior; the limit lateral pressure of the soil on the bar is therefore expected to be entirely mobilized. Brinch-Hansen

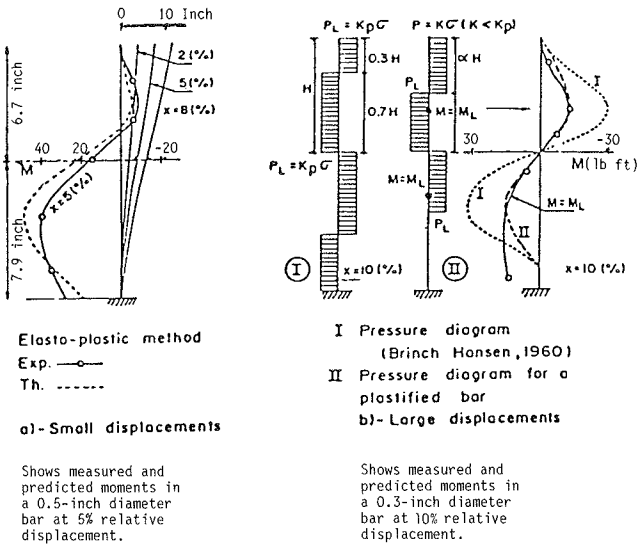

Figure C-15. Theoretical and experimental distributions of moments in the reinforcements of a nailed soil-direct shear test. [Cermes 1982 in Juran 1983]

[1960] developed a relatively simple method for representing stress distribution along a pile under these conditions.

Figure C-15a shows a comparison between the predicted and measured distributions of bending moments in a 0.5-in. diameter steel bar at a relative displacement of $x = 5$ percent. This comparison illustrates that this simplified model of soil–bar interaction may provide a reasonable approach for the evaluation of the mobilization of the bending stiffness of the reinforcements in nailed soil structures.

At large relative displacements the passive soil resistance, which can be developed on the bar, is assumed to be entirely mobilized at both sides of the failure surface. The soil around the bar is therefore assumed to exhibit a rigid plastic behavior, and its lateral earth thrust on the bar can be calculated in accordance with the procedures developed by Brinch-Hansen [1960]; the results of such computations are shown in Figure C-15b. The limit earth pressure, P_L, on the inclusion can be evaluated as discussed later in this chapter.

Figure C-15b also shows a comparison of the predicted and measured distributions of bending moments in a 0.3-in. diameter steel bar at the reasonably large relative displacements of $x =$ 10 percent. It was observed that plastic hinges had formed in the bar at this displacement. Consequently, the Brinch-Hansen diagram overestimated the possible moments in the bars. The moment diagram was therefore modified to take into account the yielding of the bars at points where the maximum bending moments attained the limit bending resistance ($M = M_1$). This comparison shows that such an approach may provide an upper limit to the lateral earth thrust of the soil when it actually undergoes a plastic flow between the bars.

3.1.3 *Effect of the Inclination of the Reinforcements with Respect to the Failure Surface*

The effect of the orientation of the reinforcements in a frictional soil has been studied by Jewell [1980]. He performed direct shear tests on sand samples reinforced by passive bars and grids placed at different orientations with respect to the failure surface. The reinforcements were longitudinally "ideally stiff" and practically inextensible with respect to the sand. The test results showed that the development of tensile forces in the reinforcements during a direct shearing of a reinforced soil mass depends mainly on the orientation of the reinforcements with respect to the failure surface. As shown in Figure C-16, the maximum increase of the shear strength of a sand sample reinforced by passive bars or grids is reached when the reinforcement is oriented in the same direction as the principal tensile strain increment which would have occurred in the unreinforced sand at failure. When the reinforcement is oriented in a direction of a compressive strain increment, it may result in a decrease of the shear strength of the soil. If the potential failure surface in the reinforced soil mass is considered to be a zero extension plane, these results suggest that inclining the reinforcement downwards or vertically in an unstable slope or excavation can significantly reduce the efficiency of the reinforcing system.

Jewell concluded that the reinforcements have two main effects: reducing the average shear stress carried by the soil and increasing the average normal stress on the failure surface. The total shear resistance of the reinforced soil mass along the failure plane can be written as:

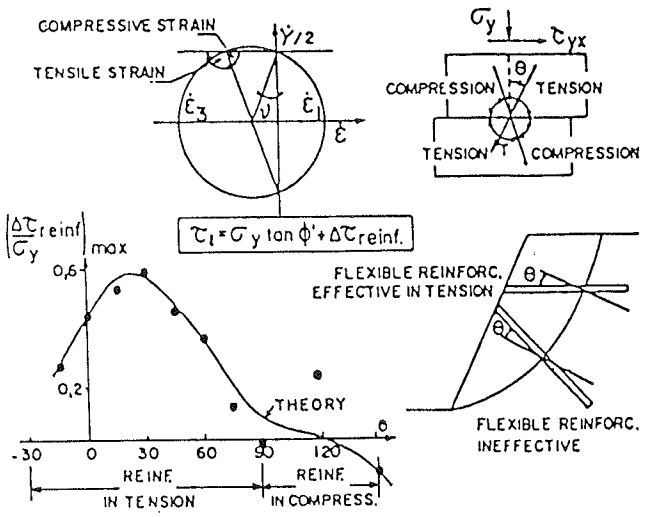

Figure C-16. Increase in the shear strength of sand versus orientation of reinforcement. [Jewell, 1980]

$$\tau = \sigma \tan\phi' + \frac{T_{max}}{A_{cr}x}[\cos\theta \tan\phi' + \sin\theta] \quad \text{(C-5a)}$$

or

$$\tau/\sigma = \tan\phi' + \frac{\Delta\tau_{reinf}}{\sigma} \quad \text{(C-5b)}$$

where T_{max} is the lesser of P or R_T, respectively, the limit pullout resistance and the tensile resistance (rupture strength) of the reinforcement; σ and $\Delta\tau_{reinf}$ are, respectively, the applied normal stress and the increase of the overall shear resistance due to the reinforcement; A_{cr} is the cross-sectional area of the failure surface; θ is the angle between the reinforcement and the normal to the failure plane; and ϕ' is the friction angle of the nonreinforced soil.

As shown in Figure C-16, this theoretical solution agrees fairly well with the experimental results. However, no consideration has been given to the mobilization of the bending stiffness of the reinforcements.

Equation C-5 at first appears inconsistent with the data shown on Figure C-13 in that the equation would imply an increase in friction angle for a nail perpendicular to a failure surface, whereas Figure C-13 shows a decrease. However, Eq. C-5 pertains to a friction angle measured from the origin, whereas the Figure C-13 friction angle allows for a cohesion intercept.

There is an interesting aspect of Eq. C-5. For the range of confining stresses and lengths of bars where failure is by pullout (rather than rupture), the ratio of T_{max} to σ remains approximately constant. Hence, an apparent friction angle ϕ^* can be defined by the ratio $\tan\phi^* = \tau/\sigma = \tan\phi + (\Delta\tau_{reinf})/\sigma$.

However, when failure is by rupture, the ratio of T_{max} to σ will decrease with increasing confining stress and cannot be considered as an intrinsic soil characteristic because its value depends on the applied stress. Hence, ϕ^* will decrease with increasing confining stress. Equation C-5 does not allow for bending stiffness of the reinforcing members, which, in fact, can

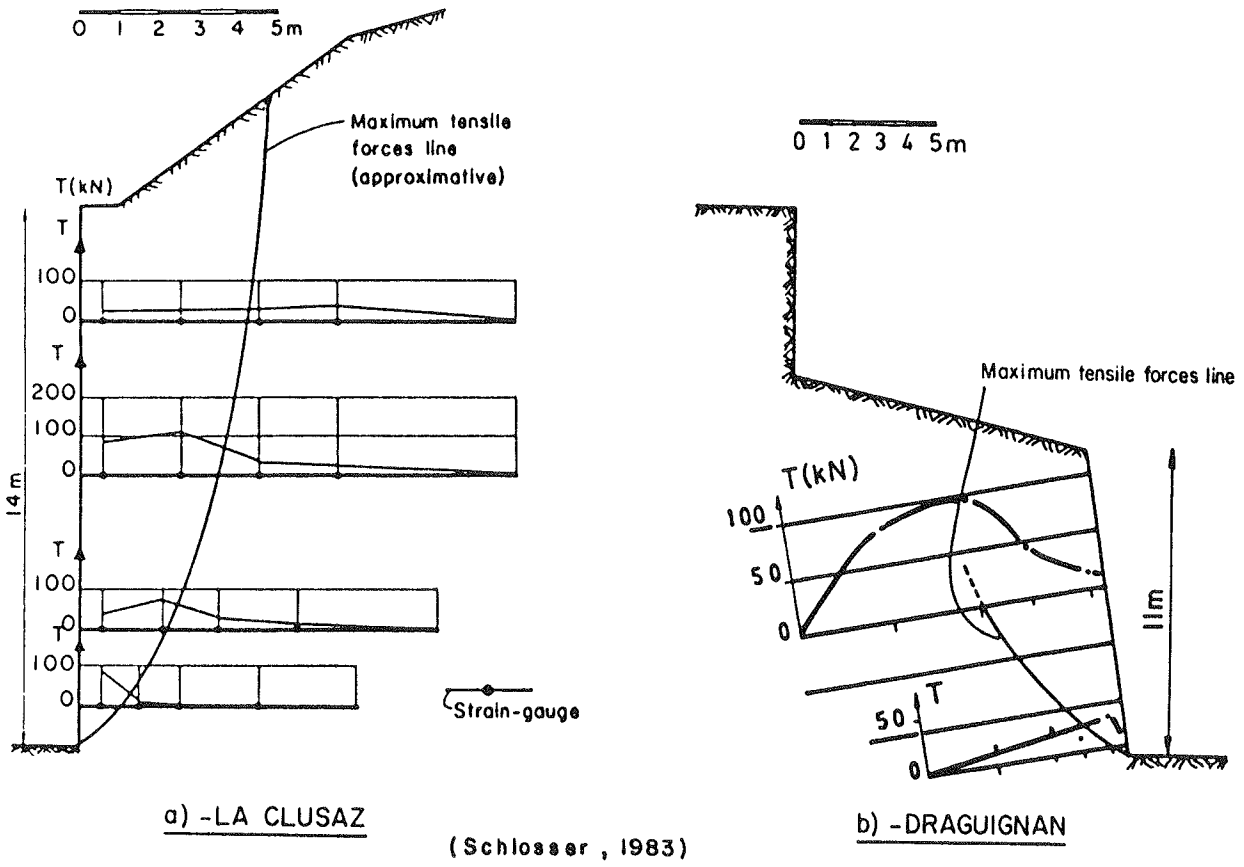

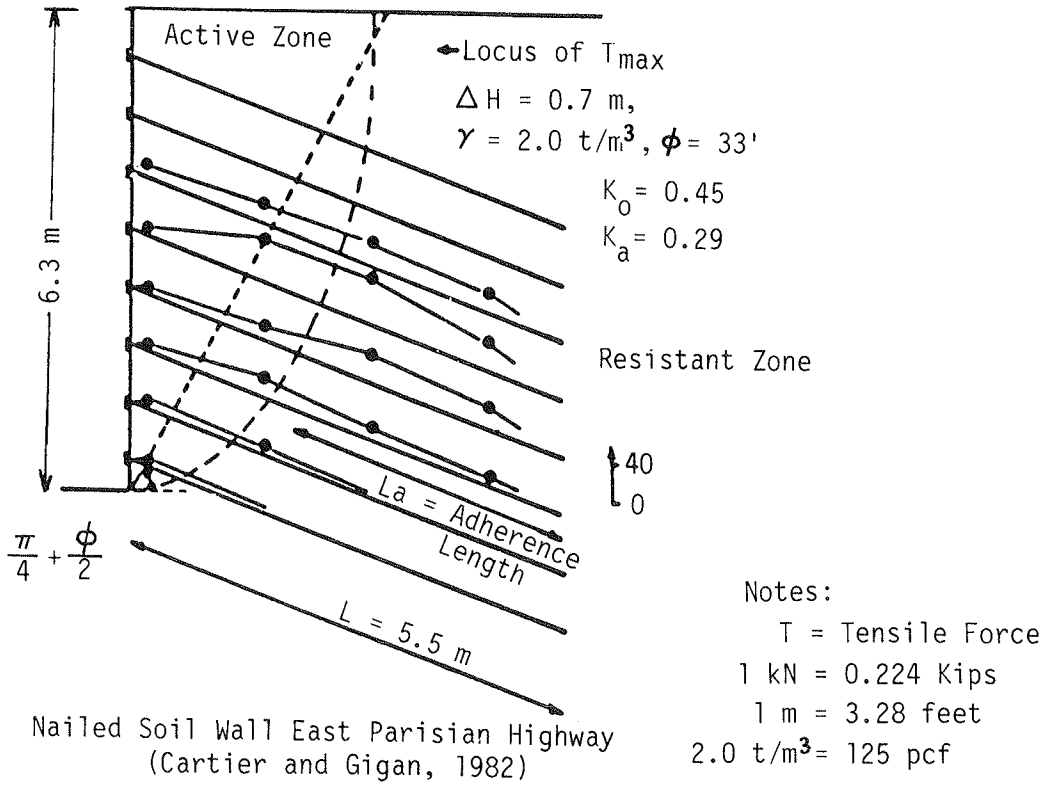

Figure C-17. Tensile forces distribution in nailed soil walls.

have a significant influence on optimal orientation of the reinforcements.

3.1.4 Failure Mechanisms of the Nailed Soil Material and Related Design Criteria

The analysis of soil-reinforcement interaction in nailed soil retaining structures shows that failure can be caused by the following mechanisms: tension failure of the reinforcements, i.e., rupture; slippage of the reinforcements, or pullout failure; bending failure of the reinforcements; and plastic flow of the soil between the reinforcements.

A methodology to take into consideration these different failure mechanisms in design of nailed soil retaining structures is described in Section 7 of this chapter.

3.2 Behavior of Nailed Soil Retaining Structures

Several full-scale experiments have been done on nailed soil retaining structures [Stocker et al., 1979; Gassler and Gudehus, 1981; Shen et al., 1981a and 1981b; Cartier and Gigan 1983; Schlosser, 1983; Guilloux et al., 1983]. Figure C-17 shows the tensile force distributions measured in three nailed soil retaining structures: the Clusaz wall in compact moraine, the Draguignan wall in calcareous marl, and the "Hurpinoise" Paris wall in silty fine sand. The Clusaz wall and the Draguignan wall were constructed using Dywidag bars placed in prebored holes and grouted along their total length, whereas the Paris wall was built with an "hurpinoise" facing and rather flexible nails, which were driven into the ground by percussion. In spite of the differences between the construction methods, the loci of the maximum tensile forces are quite similar to those observed on imported embankment Reinforced Earth walls. The reinforced soil mass can be separated into two zones: (1) an "active zone" behind the facing in which the shear stresses generated on the surfaces of the reinforcements are directed outward causing an increase of the tensile forces in the reinforcements; and (2) a "resistant zone" in which the shear stresses mobilized to prevent the sliding of the reinforcements are directed inward, towards the free end of the reinforcements. The portion of the reinforcement in the resistant zone, called the adherence length, must be long enough so that the total skin friction mobilized along the soil-reinforcement interface in this portion of the reinforcement can withstand the mobilized pullout force.

As in other reinforced soil structures, the boundary of the active zone (i.e., the locus of the maximum tensile forces) in nailed soil walls is quite different from the Coulomb failure plane. In the case of vertical, unloaded reinforced soil walls it has been demonstrated that the locus of maximum tensile forces is practically vertical at the upper part of the structure and is generally located at a distance of about 0.3 H from the facing (with H being the height of the wall). In a vertical unloaded nailed soil wall, the construction process and the inclination of the reinforcements appear to result in a larger active zone; i.e., the locus of the maximum tensile forces is at a distance greater than 0.3H from the face.

The upper zones of soil in a nailed soil structure appear to maintain nearly a K_o state of stress, most probably because the maximum horizontal displacements do not exceed 0.2 to 0.3 percent of the height. An example of field measurements showing such behavior is shown on Figure C-18. This mechanism is quite different from that of classical rigid retaining walls which generally rotate slightly around their toe, allowing the soil to progressively attain an active stress state. As shown in Figure C-18, the distributions of maximum tensile forces measured in reinforcements in both Reinforced Earth and nailed soil walls are quite different from the triangular lateral active earth pressure predicted by the Rankine theory. In the upper portions of these reinforced soil structures, measured distributions are generally near to K_o state of stress, while the lateral earth pressure coefficient decreases with depth.

Figure C-18 also shows the effect of the construction process on the distributions of maximum tensile forces in Reinforced Earth walls and nailed soil walls. The two structures shown in Figure C-18, the Lille Reinforced Earth wall [Juran et al., 1978] and the Paris nailed soil wall [Cartier and Gigan, 1983], are of the same height (H = 18 ft), they both have granular backfill materials and flexible reinforcements with similar spacings. The differences in the construction processes lead to different distributions of the maximum tensile forces, characterized essentially by higher tensile forces in the upper reinforcements and lower tensile forces in the lower reinforcements of the nailed excavation.

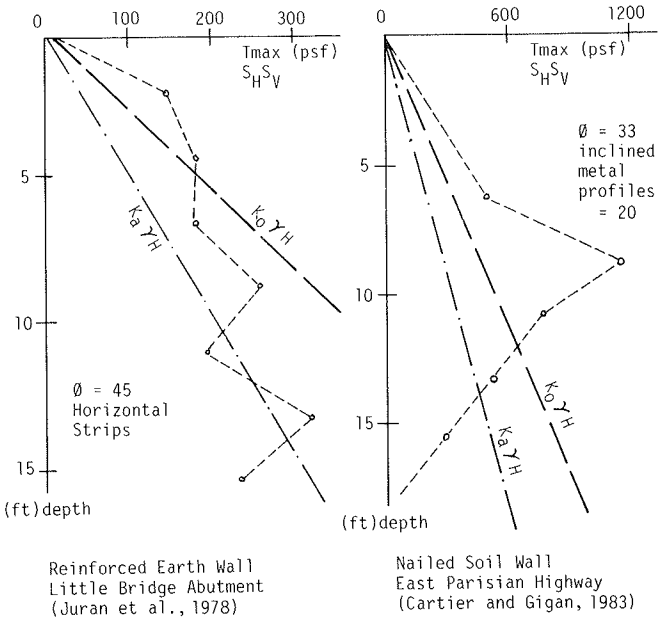

Figure C-18. Distribution of maximum tensile forces measured in the reinforcements in Reinforced Earth and nailed soil retaining walls.

To investigate the consequences of the difference between reinforced soil embankment construction and soil nailing excavation construction on the behavior of the structures, both laboratory model studies and finite element analyses have been carried out in the Ecole Nationale des Ponts et Chaussees [Juran et al., 1984 and 1985].

3.2.1 *Effect of Construction Process*

Figure C-19 shows that the construction process has a significant effect on the displacement y of the facing and on the variation with depth of the maximum tensile forces T_{max} in the inclusions as measured respectively in the laboratory scale models of Reinforced Earth walls and nailed soil walls. In the latter case, the model was built up placing the soil, the inclusions, and the facing layer by layer and restraining any displacement of the facing during the construction by placing the sand at both sides of the facing. When the model was built up to its final height an excavation was carried out mobilizing the tensile (and eventually shear) forces in the inclusions from the top down. Identical thin flexible strips were used as reinforcements in both models.

It can be observed that the excavation process leads to displacements that are larger at the top of the wall and decrease with the depth, whereas the backfilling process in the case of Reinforced Earth leads to a more uniform displacement with depth. In both cases the maximum displacement is of about $y_{max}/H = 1.2$ percent (H being the height of the model wall). This magnitude of displacement exceeds that observed on actual structures where y_{max}/H is generally less than 0.3 percent.

The observed effect of the construction process on the variation with depth of the maximum tensile forces measured in the inclusions of the Reinforced Earth and nailed soil model walls is quite consistent with that observed on actual structures as shown in Figure C-18. The excavation process leads to larger tensile forces at the top of the nailed soil wall and smaller tensile forces in the lower part of this wall as compared with the variation with depth of the maximum tensile forces in the inclusions of the Reinforced Earth wall.

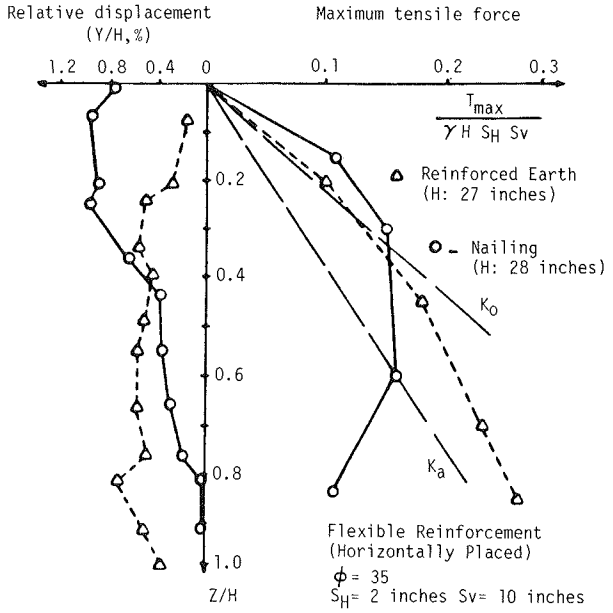

Figure C-19. Effect of the construction mode on the facing displacements and on the maximum tensile forces. [Juran et al., 1984]

3.2.2 *Effect of the Inclination of the Reinforcement*

Figure C-20 shows the effect of the inclination of the inclusions on the displacements of the facing and on the maximum tensile forces in a Reinforced Earth model wall. Increasing the inclination of the inclusions from $\beta = 0°$ (horizontal reinforcement) to $\beta = 20°$ (downwards tilt of reinforcement away from facing) leads to larger displacements of the facing, and the maximum tensile forces variation with depth approaches that corresponding to the active lateral earth pressure, characterized by the Rankine coefficient of active earth pressure, K_a.

Figure C-21 shows the results of finite element analyses which were undertaken to interpret the observations on the laboratory model walls [Juran et al., 1985]. In this finite element analysis a discrete representation of the soil and the reinforcements in the composite reinforced soil mass was developed. The soil was considered as an elastoplastic material, the reinforcements were assumed to have an elastic behavior, and the soil-reinforcement interaction was simulated using special interface elements with oriented failure criteria. As shown in Figure C-22, the theoretical results agree fairly well with the experimental observations on the model walls. Increasing the inclination of the inclusions in a nailed soil wall leads to much larger displacements of the facing. These large displacements are associated with a decrease of the maximum tensile forces in the inclusions corresponding to an evolution of the state of stresses in the soil from a K_o state of stresses in the case of horizontal reinforcements, to a K_a state of stresses in the case of inclined inclusions.

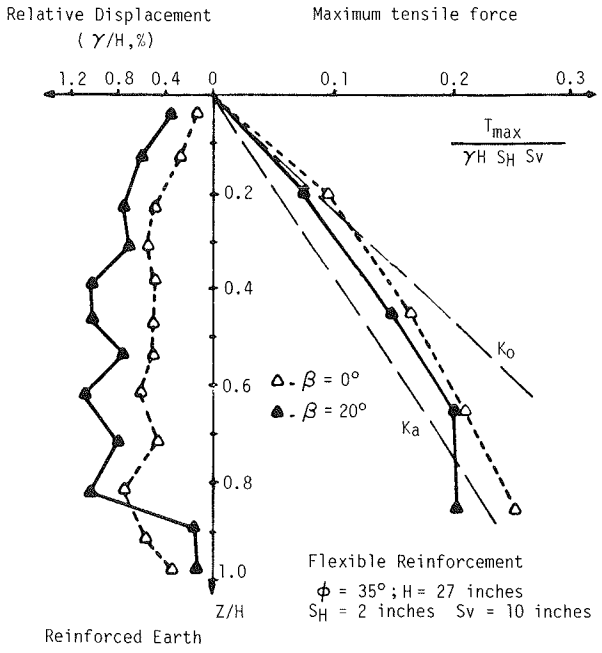

Figure C-20. Effect of the inclination of the inclusions on the facing displacements and on the maximum tensile forces in a Reinforced Earth wall. [Juran et al., 1984]

Figure C-22 shows that the inclination of the inclusions has a significant effect on the shape of the maximum tensile forces line (locus of maximum tensile force) in the actual structure under normal working conditions and on the shape of the failure surface observed on the model walls. Both the finite element

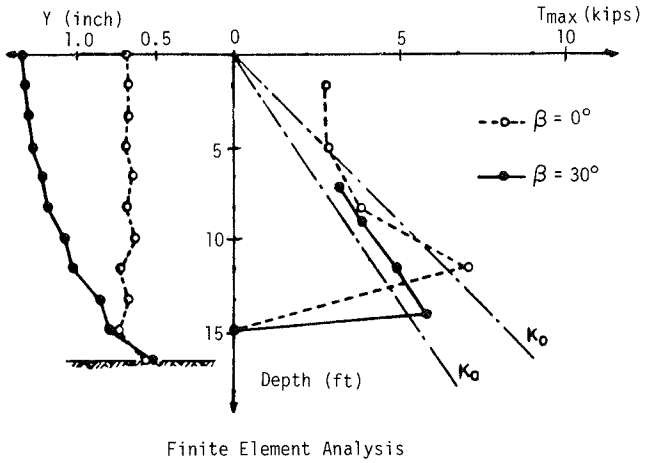

Figure C-21. Effect of inclusion inclination on the displacement of facing and on the maximum tensile forces. [Juran et al., 1985]

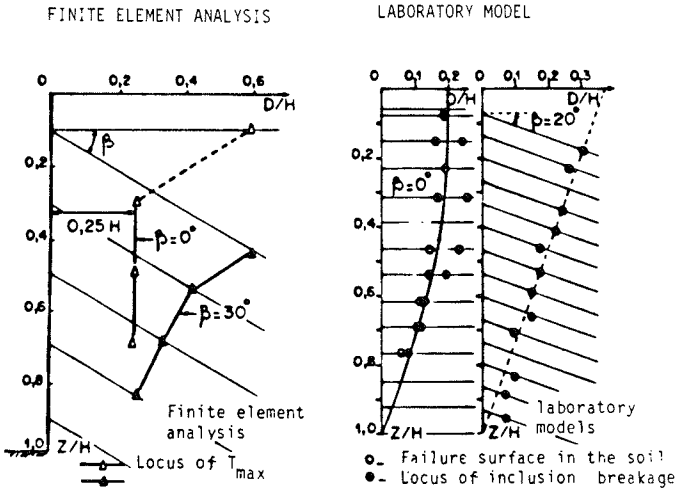

Figure C-22. Effect of the inclination of the inclusions on the locus of maximum tensile forces. [Juran et al., 1985]

analyses and the model walls indicate that near the upper part of the wall the maximum tensile forces line in the actual structure and the failure surface corresponding to the propagation of reinforcements breakage in the model wall are practically perpendicular to the inclusions. Consequently, the inclination of the inclusions leads to a larger active zone which must be taken into account for an adequate evaluation of the effective adherence length of the inclusions.

3.2.3 Effect of the Bending Stiffness of the Reinforcements

As indicated in Section 3.1.2, the passive lateral earth thrust on a rigid inclusion at both sides of the potential failure surface in a nailed soil wall results in a mobilization of shear forces and bending moments in the inclusion. However, as discussed in Section 3.1.2, the displacement of the soil in the direction perpendicular to the inclusion (which is necessary in order to mobilize the shear and bending resistances of the inclusion) is significantly larger than that required to generate tensile forces in the reinforcements. Therefore, as long as the soil displacements are small, under normal working conditions, the bending stiffness of the inclusions has practically no effect on the behavior of a structure. Figure C-23 (left portion) shows the results of the finite element analysis of the behavior of two identical walls, 5 m high, with two different types of inclusions (flexible inclusions and rigid inclusions made of bars of 2 in. diameter). Figure C-23 (right portion) shows the experimental measurements of the maximum tensile and shear forces in the inclusions of two identical nailed soil model walls with two different types of inclusions (flexible inclusions made of linear aluminum strips 0.1 mm thick and rigid inclusions made of channel-shaped metallic profiles 0.2 mm thick). Both the finite element results and the experimental observations on the laboratory models indicate that under normal working conditions the shear forces, V, mobilized in the inclusions are significantly smaller than the maximum tensile forces, T_{max}, and that the bending stiffness has practically no effect on either the displacements of the facing or the tensile forces in the inclusions. These observations pertain to a wall at working stress conditions rather than at failure.

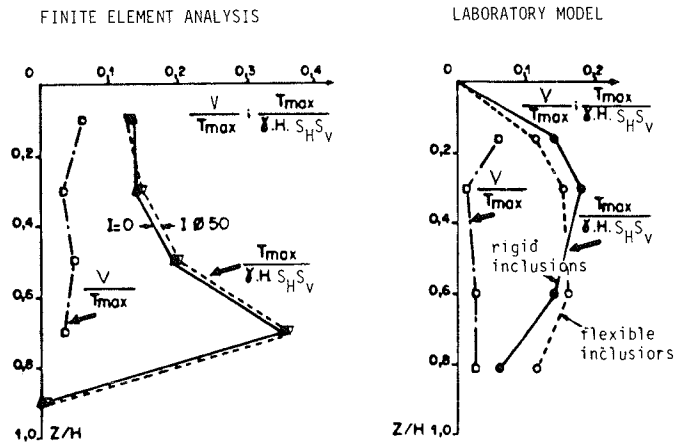

Figure C-23. Effect of the bending stiffness of the inclusions on the maximum tensile forces. [Juran et al., 1985]

However, the laboratory models have demonstrated that the bending stiffness can have a significant effect on the failure mechanisms when the rotational kinematics of the active zone cause relatively large soil displacements perpendicular to the inclusions. Figure C-24 shows the failure surfaces observed in the reinforced soil and the locus of breakage points of the reinforcements in different nailed soil model walls. In these walls the flexible inclusions were made of linear aluminum strips, 0.1 mm thick, and the rigid inclusions were made of polystyrene strips, 6 mm thick.

It is interesting to note that the failure surfaces in the soil observed with both the flexible and the rigid inclusions are quite similar. However, in the case of flexible reinforcemens, the failure surface in the soil develops along the potential rupture locus of the inclusions, whereas in the case of rigid inclusions it seems that the failure surface in the soil and the locus of the inclusion rupture points do not coincide. This experimental observation can be explained by the analysis of the soil-reinforcement interaction illustrated schematically in Figure C-12. In the case of rigid inclusions, because of the symmetry of the distribution

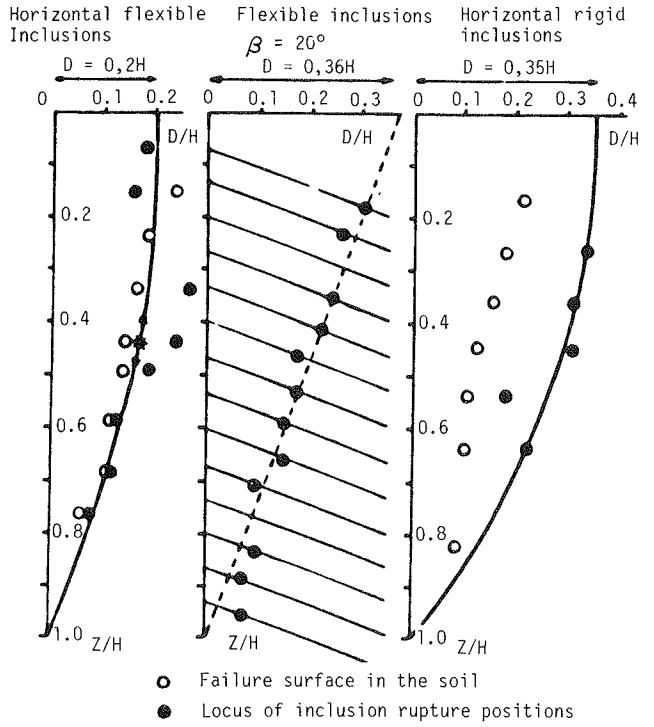

Figure C-24. Effect of inclination and bending stiffness on the failure of a nailed soil model wall. [Juran et al., 1984]

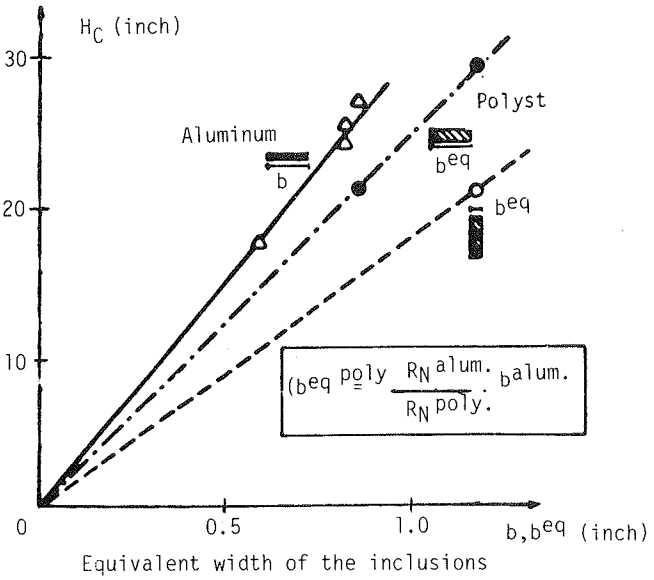

Figure C-25. Effect of the bending stiffness on the failure height of a nailed soil model wall. [Juran et al., 1984]

of the passive lateral earth thrust on the inclusion with respect to the potential failure surface, the bending moment at the locus of maximum tensile and shear forces is equal to zero. In fact the moment reaches its maximum value some distance behind this locus. Therefore, if the reinforcement's rupture in the model walls was caused by excessive bending, the locus of the breakage points should be located behind the failure surface which developed in the soil as shown in Figure C-24.

Figure C-25 shows that the bending stiffness also has a significant effect on the failure height of nailed soil model walls; model walls were constructed with reinforcements of different materials (and thus different moduli). When the model reinforcements were sized to have the same rupture strengths, the walls did not fall at the same height. Increasing the bending stiffness of a particular reinforcement in the vertical plane (by rotating the orientation) also allowed construction of a higher model prior to failure. However, further research and more laboratory model studies are still required to develop a better understanding of the effect of reinforcement bending stiffness on the behavior of nailed soil retaining structures.

4. TECHNOLOGY

4.1 Introduction

Because there are no proprietary restrictions on the application of the basic concept of soil nailing and no specifications govern the selection of the construction elements, the technology of soil nailing has been developed using different types of construction elements (reinforcements and facings), and several processes are used to install the components. This wide range of components is also the result of the fact that most of the structures to date have been temporary. With the current move towards the development of permanent soil nailing installations, special patented nails and prefabricated panels are beginning to appear.

4.2 Description of Fabricated Components

4.2.1 The Nails

The resistant element of the nail is the steel, which can be either mild steel or high-strength steel. These steel elements can be either driven into the ground or placed in prebored holes and contained with a suitable grout.

Driven reinforcements. A wide range of reinforcing elements can be used. Generaly, simple and low-cost metal rods and bars made of mild steel with a yield strength of 50 ksi are used. Their diameters vary from about ½ to 1 in. The tensile resistance of these elements is therefore relatively low (10 to 35 kip) and they are closely spaced (about two bars per 10 sq ft). At the present time, no protection against corrosion has been developed for this type of reinforcement, and mild steel remains the most economical material commonly used.

Drilled reinforcements. These are reinforcements made of high-strength steel (yield strength 150 ksi). Their diameter varies from 0.5 to 1.5 in., and they are more expensive than mild steel bars. Generally, one bar is placed per borehole (4 to 6 in. diameter), with spacings varying from 3 to 10 ft. They are normally grouted into the boring by gravity rather than by high pressure. The characteristics of the available high-strength reinforcements commonly used in France are given in Table C-2. Specially ribbed bars can be used to improve the adherence with the grout and to facilitate the attachment of the bar to the facing plates using special bolts which fit the ribs of the bars. Figure C-26 shows a Dywidag bar with these ribs.

New types of nails. Two new types of nails have been developed in France for use in permanent retaining structures. They have been specially designed to prevent microfissuring of the grout

Table C-2. High strength reinforcements commonly used in France.

PRODUCER	DIAMETER (inch)	ELASTIC LIMIT STRESS (ksi)	YIELD STRESS (ksi)
DYWIDAG	0.60 0.80	128	156
	1.00 1.25 1.42	120	150
	1.00 1.25 1.42	156	178
GEWI	0.80 0.87 0.98 1.10 1.42 1.57 1.97	60	69

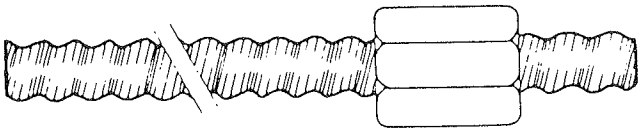

Figure C-26. High-strength steel nail—type Dywidag.

either by prestressing (bar developed by INTRAFOR-COFOR, Fig. C-7) or by preventing water entering into the microfissures of the grout by using a casing in a similar manner as for prestressed ground anchors (bar developed by SOLRENFOR, Fig. C-6).

4.2.2 The Facing

There are three kinds of facings: (1) with fragmented rock, e.g., chalk, marl, and shale, the facing usually consists of a welded wire mesh to prevent block falls (Fig. C-27a); (2) with soils, the facing generally consists of shotcrete (4 to 12 in. thick), which may or may not be reinforced (Fig. C-27b); and (3) prefabricated panels that are now being developed for permanent structures. Figure C-28 shows metallic panels which have been developed by Louis [1981] and by SOLRENFOR for inclined facings. In this case, each panel is rectangular and is attached at its four corners to the nails.

The attachment of grouted reinforcements to the facing (mesh or shotcrete) is generally made by bolting the bars to a square steel plate 0.6 to 0.8 in. thick and 12 to 16 in. wide (see Fig. C-27a). The attachment of driven bars to the facing is generally made by cladding or another suitable method.

The facing must be structurally designed to take into account the bending moment and tensile stresses induced by the soil pressures and nail forces.

4.3. Fabrication of Components and Quality Control

Except for recent developments for permanent structures, no prefabricated element is used in soil nailing, and there are only two fabricated components: the grouted reinforcements and the shotcrete.

4.3.1 Fabrication and Quality Control of Grouted Reinforcements

After the boreholes have been drilled, the bars are placed and sealed with cement grout. Generally the boreholes are inclined slightly downwards from the facing to enable gravity filling. In some cases, grouting is performed under small pressure using a packer placed close to the facing.

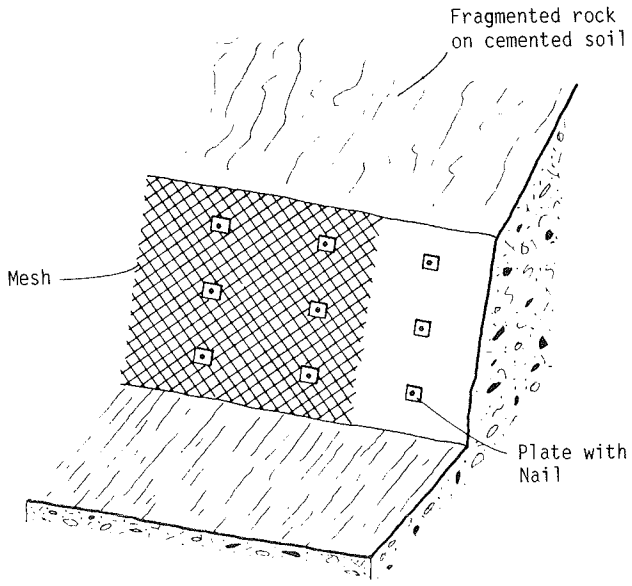

a) Welded wire mesh

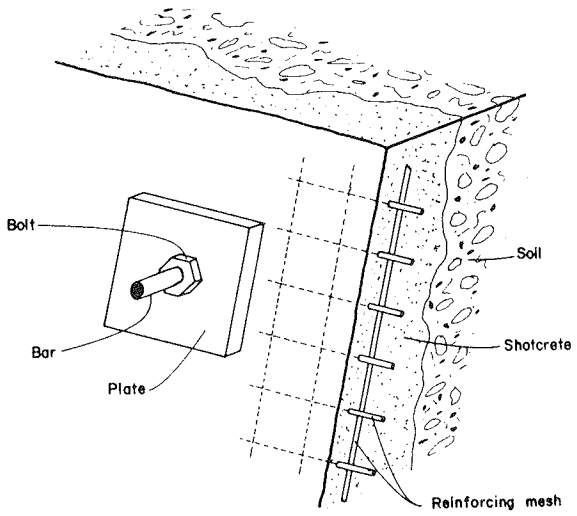

b) Shocrete facing

Figure C-27. Classical types of facing in soil nailed retaining structures.

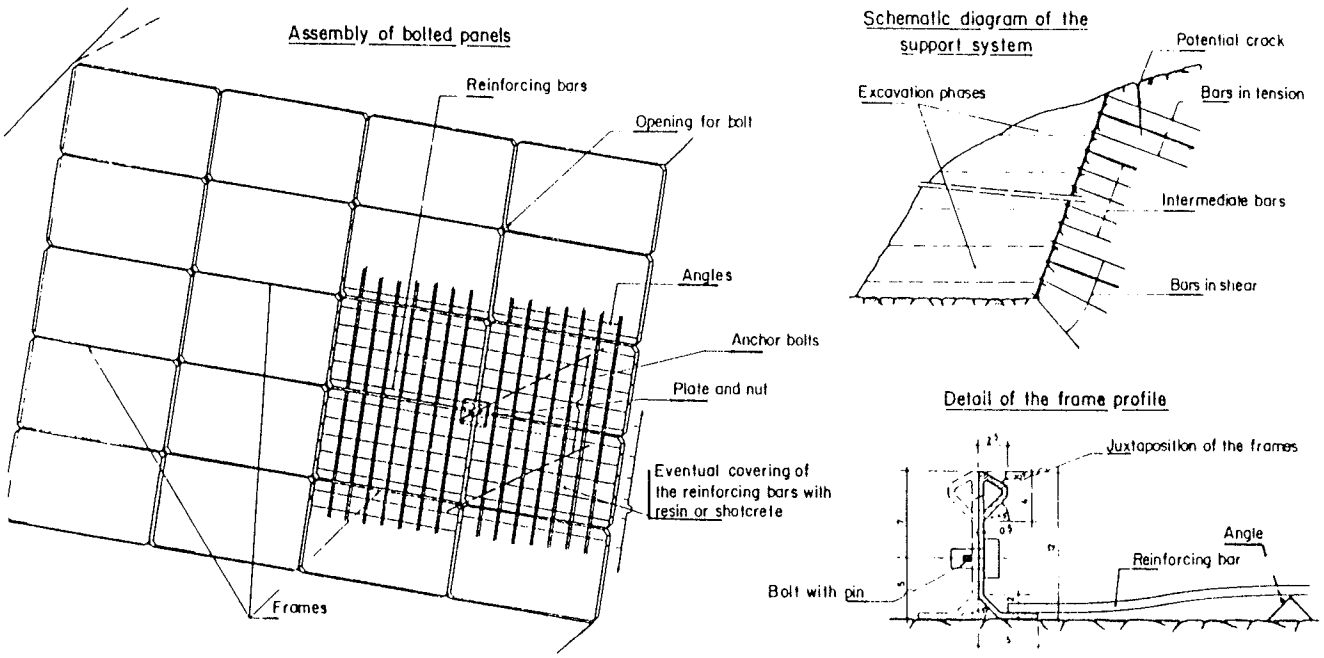

Figure C-28. Facing with prefabricated metallic panels. [Louis, 1981]

To evaluate the quality of the bond between the reinforcements and the in-situ ground, it is recommended that pullout tests be done on bars grouted along a small length (6 to 10 ft) in each of the different soil types encountered. As indicated in Figure C-29, the bar is sometimes protected by a casing along a certain distance from the facing in order to test the grouting without influence of edge effects.

4.3.2 Fabrication and Quality Control of the Shotcrete Facing

Shotcrete is a concrete applied to a soil surface using special equipment. The maximum aggregate size is usually limited to 0.4 to 0.6 in. There are presently both a dry and a wet method for placement.

As indicated on Figure C-30, in the dry method, water is introduced at the end of the transport of the dry cement and granular material by compressed air. In the wet method, the wetted mixture (cement, granular material) is transported under pressure by means of a concrete pump. The granular material must be well graded. Figure C-31 shows a typical range of grading curves for granular materials to be used. Conventional admixtures to accelerate the concrete setting and special admixtures to reduce creep of the hardened concrete are usually used.

The composition of the shotcrete must be determined taking into account the loss of granular material rebounding off the surface being shotcreted. Thus, the percentage of cement must be greater than that used in classical concrete. The minimum quantity of cement for a shotcrete application is usually taken at about 18 lb/cu ft.

It is generally necessary to reinforce the shotcrete. Typically, reinforcement consists of welded wire mesh, with wire diameters varying from 0.2 to 0.4 in. This mesh is generally attached to short and small diameter nails driven into the soil. The minimum dimension between the outer edge of shotcrete facing and the mesh should be at least 1 in.

Quality control of the shotcrete generally consists of projecting samples into boxes and measuring the mechanical properties of these samples in the laboratory. At least one control test for every 100 cu yd of shotcrete is normally performed.

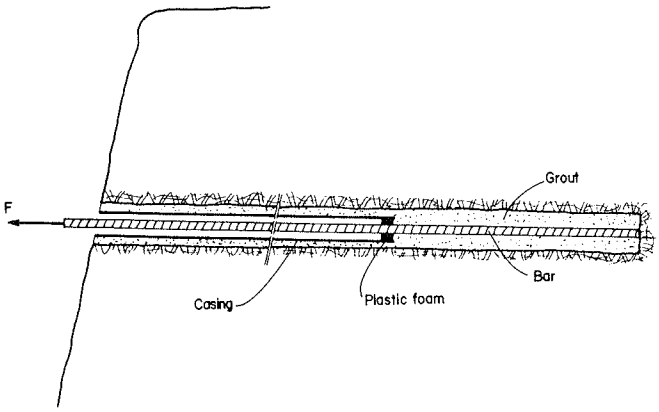

Figure C-29. Pullout test to control the grouting and to measure soil-reinforcement friction.

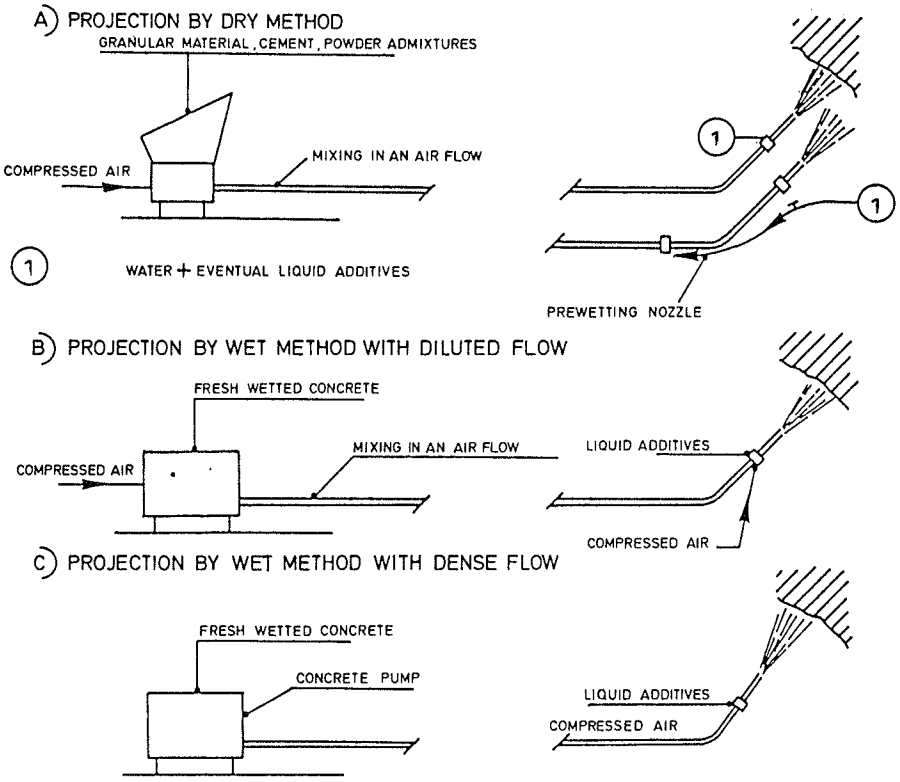

Figure C-30. Different techniques of shotcreting.

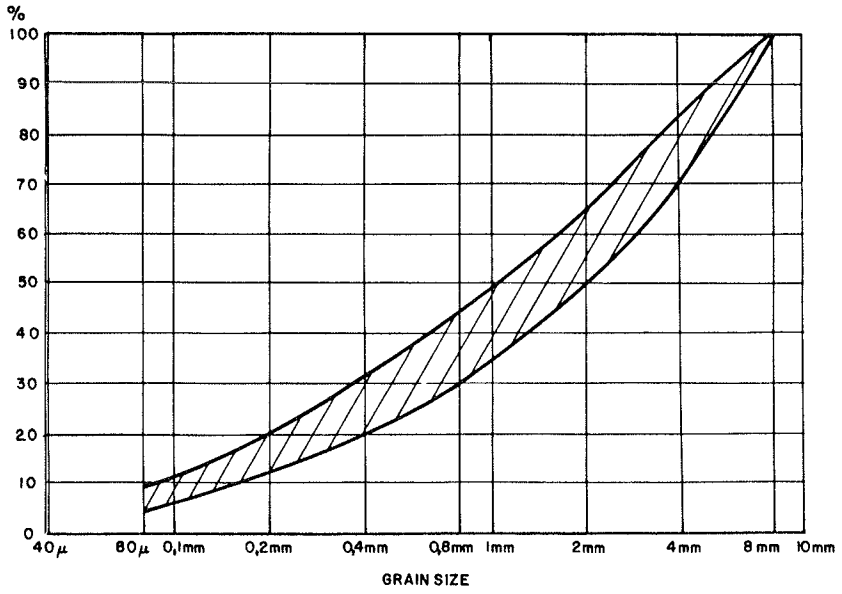

Figure C-31. Typical range of grading curves for granular material in shotcreting.

5. DURABILITY AND EVALUATION OF IN-SITU GROUND

5.1 Corrosion of Steel Bars

5.1.1 Corrosion of Mild Steel and of High-Strength Steel

The components most susceptible to degradation are the steel reinforcing bars. The types of corrosion vary in mild and high-strength steel.

With mild steel, the corrosion is relatively uniform and occurs on a large part of the surface of the steel in contact with the soil. This type of corrosion has been described in detail in Chapter Six of the main report. The decrease in tensile strength of a steel bar is directly related to the loss of thickness due to corrosion. Thus, the main parameter concerning the service life of the structure is the rate of corrosion, i.e., the rate of loss of metal at the surface of the bar in contact with the soil.

Unlike mild steel, the corrosion of high-strength steel under tensile stresses develops at the interface of the crystals, progressively from the surface to the inside of the steel, and is called "intergranular corrosion." This type of corrosion is much more difficult to analyze and predict. For safety, it must currently be assumed that it is not possible to predict the decrease in tensile strength of a bar subjected to intergranular corrosion.

5.1.2 Corrosion of Steel Bars Surrounded with Grout

When the steel bar is surrounded with grout there is no direct contact between the soil and the steel, and the mechanism of corrosion is different. It is only the microcracking of the grout which enables the steel to be in contact with water and oxygen, thus resulting in corrosion. The degree of microcracking, as well as the thickness of the grout around the bar, influences the propagation of the corrosion.

In the case of grouted mild steel bars, it can be assumed that the presence of the grout has no effect and that the rate of corrosion is the same as for mild steel directly buried into the ground. This is conservative, but sufficient information is not presently available that can justify any other method.

In the case of grouted, high-strength steel bars, the prediction of corrosion rate is very complicated, and no rational calculation can be done at present.

5.1.3 Special Reinforcing Bars for Permanent Structures

Nailed soil walls are being more commonly used as permanent structures. Hence, special measures must be taken to prevent corrosion. As shown in Figures C-6 and C-7, special types of bars have been designed in order to protect high-strength steel.

In one case, the steel bar and the surrounding grout are protected by a casing made of steel (SOLRENFOR nail, Fig. C-6) or of plastic. This is commonly used to protect prestressed ground anchors by preventing the flow of water through the microcracks towards the steel bar. In this case, there is no corrosin of the steel until the degradation or corrosion of the casing occurs.

The second case consists of prestressing high-strength bars (INTRAFOR-COFOR nail, Fig. C-7) in a cement grout inside a plastic tube. This prestressing prevents microcracking of the grout, which remains always in compression. In this case the steel bars are assumed to retain their initial mechanical properties indefinitely.

5.2 Parameters Controlling Corrosion

Parameters controlling corrosion rates in mild steel are described in Chapter Six of the main report and are, therefore, not repeated here.

5.3 Evaluation of In-Situ Ground

Soil nailing is suitable for use in a wide range of soils. However, soft clays may not be suitable because the low values of the soil-to-bar friction and adhesion can lead to uneconomical structures. This type of soil is often susceptible to creep, particularly at high water content.

Loose cohesionless soils (silts, sands) have practically no short-term cohesion and can be unstable during the excavation phases, particularly at high water content. In such soils the construction stages must be considered thoroughly prior to construction and actual construction must proceed with due care.

From a geotechnical viewpoint, the in-situ soils must be evaluated with about the same level of detail as for an excavation using more conventional excavation bracing.

6. CONSTRUCTION

Other than site clearance, no particular preparation is required prior to construction.

As illustrated in Figure C-2 there are three main repetitive phases in the construction process: (1) excavation of a limited height, (2) nailing and drainage, and (3) placing of the facing.

6.1 Excavation

The excavation process is carried out using small conventional earthwork equipment starting at the top and progressing in incremental steps towards the bottom. Generally, each step is less than 10 ft in height, and is commonly limited to 5 ft. The cut slope must be properly excavated to assure minimum disturbance of the ground, and special care must be taken to prevent local instabilities that could induce movement in the upper part of the nailed soil wall.

Generally, the short-term cohesion of the soil is sufficient to ensure local stability of each excavated step. However, different methods can be used to increase this stability if necessary, such as excavation by alternate plots, which enables mobilization of arching, or inclination of the cut slope, which increases the safety factor with respect to local sliding considering the short-term cohesion of the soil. The latter generally results in the entire slope being inclined.

For long walls, the optimum construction process consists of carrying out the excavation, the shotcreting and the nailing, successively, starting from one side of the wall and progressing along the same level to the other side.

6.2 Nailing

The nailing process should be carried out as soon as possible after the excavation has been completed in order to prevent a significant decrease of the short-term cohesion of the soil or loss of material by erosion or seepage discharge.

With driven bars, a small vibropercussion hydraulic hammer is used to drive the bars at the design inclination. This technique is rapid and economical and enables driving 4 to 6 bars per hour. However, it is limited by the length of the bars (maximum length of 60 ft) and by the heterogeneity of the soil (boulders, etc.). In addition, it is difficult to control the orientation of bars if they deflect during driving.

In the case of grouted bars, a borehole has to be drilled. The nailing process depends on the ability of the borehole to stand open without collapse of the surrounding soil. In stiff soils the boreholes tend to be stable, and the drilling can be carried out using a down hole rotary percussion drilling device with compressed air. As illustrated in Figure C-32, the bars are installed using centering rings to keep the bars centered and a grouting tube is placed at the same time downwards to the bottom of the hole. Gravity cement grouting is then performed from the bottom of the hole upwards through the tube using a pump, and the tube is progressively pulled out during the grouting.

In loose soils, a bentonite drilling mud can be used during drilling to maintain the stability of the borehole. After the drilling, a grouting tube is placed, and the cement grout is placed by gravity, progressively replacing the bentonite. When the borehole is completely filled with the cement grout, the bars are pushed into the hole with centering rings.

Another process that can be used in loose soils is to drill the borehole with a hollow stem continuous flight auger. Once the hole has been advanced to the desired depth, the reinforcing bar is placed inside the stem of the auger. Grout is then pumped down the auger stem while the auger is gradually withdrawn, thus filling the annular space between the bar and the soil.

Casing may be required in some cases (particularly in horizontal boreholes) to maintain the stability of the boreholes. When borings are horizontal or inclined upwards, grouting can be performed under pressure.

6.3 Drainage

There are generally two systems of drainage in a nailed soil wall: (1) Deep drainage with slotted tubes that are generally longer than the reinforcing bars in order to prevent any saturation of the wall. These drains, called "French drains," are generally plastic tubes about 2 in. in diameter and they are inclined at an angle of 5 deg to 10 deg with respect to the horizontal. The spacing between these drains depends on the site conditions, but it generaly does not exceed 1 drain per 100 sq ft. (2) Shallow drainage with small steel or plastic pipes (12 to 15 in. long) in order to prevent accumulation of water behind the facing. The pipes are about 4 in. in diameter. Their spacing depends on the site conditions and normally approximates the spacing between the nails.

6.4 Placing of the Facing

Welded wire mesh or prefabricated panels are generally attached by cladding or more commonly by bolting to the grouted bars. In the case of driven bars, shotcrete facing is generally used. The required thickness is obtained by successive layers of shotcrete, and special care must be taken to provide a uniform thickness of facing. An aesthetic finish, if required, should be provided as an additional layer without disturbing the previous layers of shotcrete.

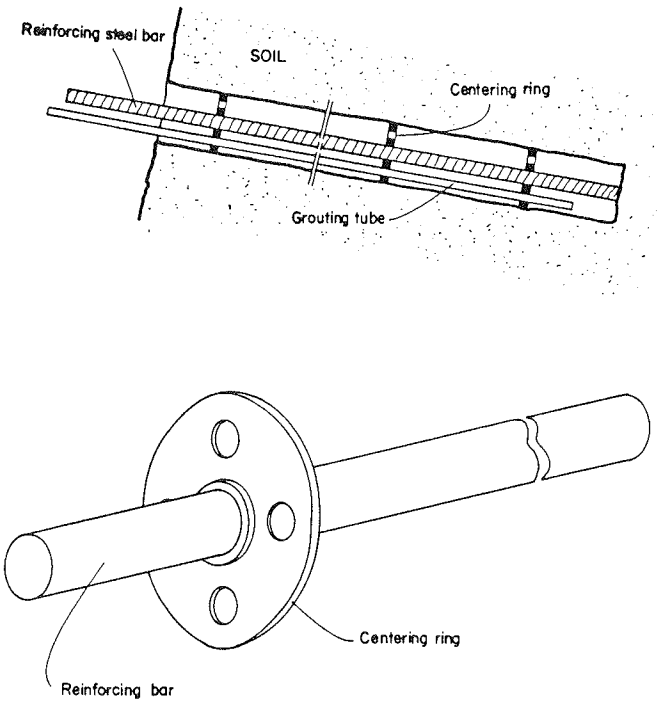

Figure C-32. Installation of the grouted bar. [After INTRAFOR-COFOR, France]

6.5 Attachment of the Nails to the Facing

The nails are attached to the facing using small plates (see Section 4.2.2). These plates are placed either on the wire mesh or on the shotcrete facing, after which the nails are bolted (Fig. C-27). In the case of driven bars, no special attachment is used.

7. DESIGN METHODS

7.1 Introduction

There are three different design methods currently used for soil nailing. All three are based on limit equilibrium analysis in which the potential failure surfaces throughout the soil mass are examined. The Davis method proposed by Shen et al. [1981] and the method developed by Gassler and Gudehus [1981] consider only the tensile capacity of the reinforcement when assessing the stability of the reinforced soil mass, while the French method [Schlosser, 1983] also considers the effects of the shear capacity and bending stiffness of the nails on the overall stability of the in-situ reinforced soil mass.

7.2 Preliminary Design and Design Parameters

7.2.1 Preliminary Design

Soil nailing can be used in a wide variety of soils and at sites with highly variable subsoil conditions. Hence, it is difficult to provide general recommendations for a preliminary design that are not site-dependent. However, on the basis of the available experience with both driven and grouted reinforcement bars, guidelines for preliminary design have been developed in graphical form as shown in Figures C-33 and C-34 [Guilloux and Schlosser, 1982]. These figures show, respectively, the variations of the ratio L/H (where L is the length of reinforcing bar, and H is the height of vertical face) and the cumulative length of bars per square foot of facing versus the angle of internal friction, ϕ, of the soil in actual soil structures. The relationships shown in Figures C-33 and C-34 are only intended to be used for preliminary design, specifically to determine whether soil nailing is feasible for a particular project. A more vigorous design must follow to assure the stability of the excavation.

7.2.2 Design Parameters

The main design parameters of a nailed soil system concern the mechanical properties of the soil and the inclusions, as well as the parameters characterizing the different mechanisms of soil-reinforcement interaction described in Section 3. They can be classified in the following six main groups: (1) Mechanical properties of the in-situ ground, particularly soil type and internal friction angle. (2) Mechanical properties of the reinforcements, specifically the tensile and shearing resistances and the bending stiffness. (3) Parameters related to the soil-reinforcement interaction by friction, particularly the limiting unit effective friction, f_{max}, which can be mobilized along the inclusion in the specific ground under consideration. The limit skin friction, f_{max}, may be computed using similar methods commonly used for friction pile design. However, in-situ pullout tests should still be performed to verify the design values. (4) Parameters related to the normal soil-reinforcement interaction by lateral earth thrust on the reinforcement, particularly the limit passive pressure of the soil and the modulus of lateral soil reaction. These parameters can be deduced using p-y analyses or pressuremeter tests. The p-y analysis method, which is commonly used in the United States to predict lateral pile behavior, is described in detail in many pile design references such as Tomlinson [1981]. The methodology is also briefly described in Section 3.2, Chapter Two, of this appendix. (5) Geometrical properties of the reinforcements (thickness, shape, length) and of the structure (vertical and horizontal spacings between the reinforcements; inclination of the reinforcements and of the facing). (6) Parameters related to the method of reinforcement installation, e.g., type of the facing and grouting parameters.

7.3 Design Approaches

Two approaches generally used for the design of reinforced soil retaining structures can be adapted for design of nailed soil excavation. The first approach is based on the analysis of the local equilibrium conditions of the active zone which is bounded by the failure surface. This failure surface, which develops in the soil along the maximum tensile forces line, is assumed to be either a logarithmic spiral or a circle. It is assumed that the failure is caused by a progressive breakage of the inclusions and that at failure, the soil resistance to shearing is entirely mobilized all along the considered failure surface. The limit analysis approach proposed by Juran [1977] for the design of Reinforced Earth walls (see Appendix A, Chapter One, "Reinforced Earth") can also be adapted to design of nailed soil retained excavations [Juran et al., 1984] to provide a solution for the locus and to evaluate design values of the maximum tensile (and shear) forces in each reinforcement. However, the application of this limit analysis approach is limited to cases involving homogeneous ground and simple geometry.

As far as nailed soil retaining structures are concerned, the in-situ ground is often heterogeneous. Furthermore, both the construction process and the geometry of the structure often

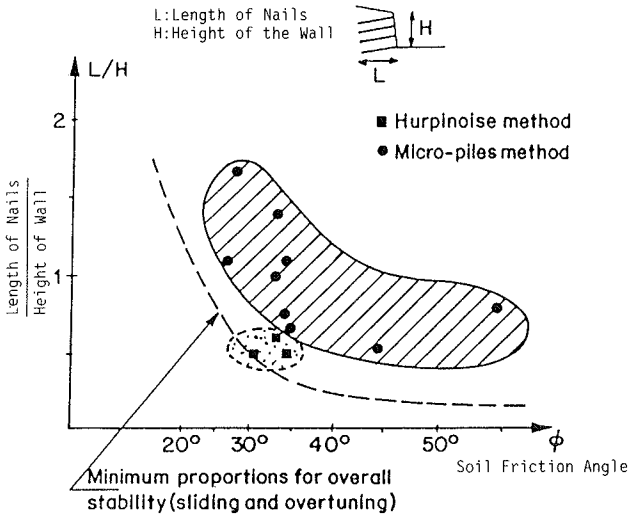

Figure C-33. Geometry of nailing structures. [Guilloux and Schlosser, 1982]

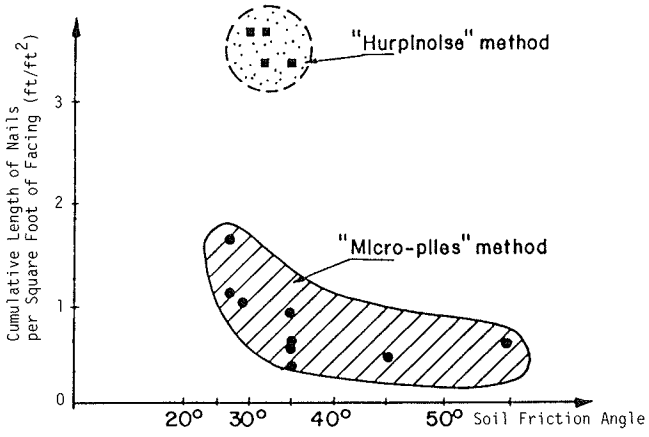

Figure C-34. Nailing structures—cumulative length of bars per square foot of facing versus angle of internal friction of soil. [Guilloux and Schlosser, 1982]

have to be adapted to actual site conditions exposed only during construction. Hence, for the same structure, reinforcements of different types, lengths and inclinations, as well as facings with different slope angles may sometimes be required. These considerations severely limit the use of this approach for practical nailed soil design.

The second design approach is based on a general stability investigation of the nailed soil structure and its surroundings. Classical slope stability analysis methods can be adapted to evaluate the safety factor with respect to failure along potential circular or wedge-shaped sliding surfaces, taking into account the available shearing, tensile and pullout resistances of the reinforcements crossing the failure surfaces. This design approach does not provide a solution for the locus and values of the maximum tensile forces in each of the reinforcements, but is limited to the evaluation of a global safety factor with respect to failure of the soil or the reinforcements. However, it provides an efficient working tool to solve engineering problems related to heterogeneous soils, structures of complicated geometry, failure modes involving both internal and external stability aspects, and water flow in slopes.

The design methods that are based on the second approach and that are presently available involve different assumptions regarding the definition of the safety factors, the mobilization of the stresses (bending moment, shear and tensile forces) in the reinforcements, the shape of the failure surface, and the type of soil-reinforcement interaction.

7.4 The Davis Design Method

The limit design procedure developed by Shen et al. [1981b] assumes that the failure surface for an in-situ reinforced slope can be represented by a parabolic curve passing through the toe of the wall. The assumption is based on results of a finite element analysis of in-situ reinforced soil [Bang, 1979], which was used to develop contours of factor of safety for a potential failure surface as shown schematically in Figure C-35. The potential failure surface deduced from the finite element analyses passes more or less through the toe of the wall and forms a curved surface.

A classical method-of-slices slope stability analysis is used to evaluate the contribution of the nails to overall stability. Only tensile forces are considered to be developed in the reinforcements. These tensile forces are divided into the components parallel and perpendicular to the failure plane. The normal force and tangential component in each reinforcement crossing the potential failure surface are added to the resisting forces mobilized in the soil when determining the factor of safety of the entire mass. To perform the stability analysis, two conditions must be considered separately. One condition considers a failure surface that extends beyond the reinforced zone, as shown in Figure C-36, while a second condition considers a failure surface that is entirely within the reinforced soil mass. As with conventional slope stability analyses, direct computation of the factor of safety is not possible because the equations for both the driving force and the resisting force contain the factor of safety as a variable unknown term. Accordingly, the solution process is an iterative method most readily done by computer. A computer program specifically developed to calculate the global factor of safety for in-situ reinforced soil is presented by Shen et al. [1981b].

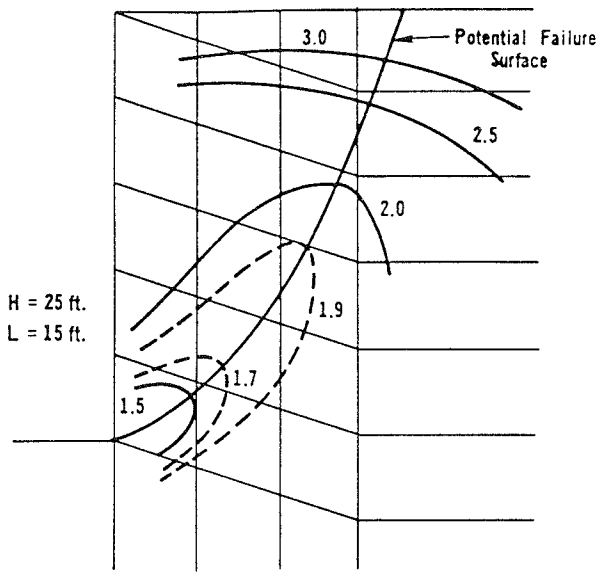

Figure C-35. Contours of factor of safety.

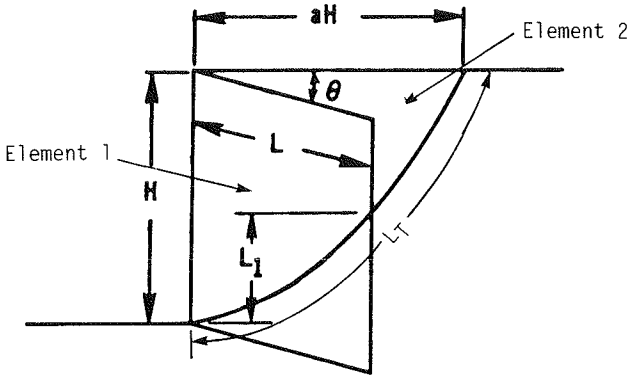

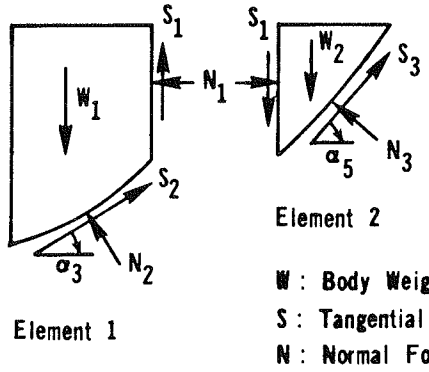

Figure C-36. Free body diagram when the failure surface extends beyond the reinforced soil mass. [Shen et al., 1981]

The *stability calculation* for the first condition, i.e., a failure surface extending beyond the reinforced soil mass, is summarized below. Detailed derivations of the stability calculations for both conditions are described by Shen et al. [1981b].

Figure C-36 shows the assumed potential failure surface and the free body diagram. Forces S_2 and S_3 developed by soil-to-soil shear are assumed to be parallel to the corresponding chords. The force equilibrium equations for element 1 are thus:

$$N_2 = (W_1 = S_1)\ (\cos \alpha_3) - N_1 \sin \alpha_3 \qquad \text{(C-6)}$$

$$S_2 = (W_1 - S_1)\ (\sin \alpha_3) + N_1 \cos \alpha_3 \qquad \text{(C-7)}$$

where W_1 = weight of element 1; S_1 = tangential force between elements 1 and 2 (assumed to be vertical); α_3 = angle between horizontal and failure surface for element 1; $N_1 = \frac{1}{2} K\gamma (H-L_1)^2$; and K = soil stress ratio = σ_h/σ_v, which can be estimated using K_o, the at rest earth pressure coefficient.

The force equilibrium equations for element 2 are expressed by:

$$N_3 = (W_2 + S_1)\ (\cos \alpha_5) + N_1 \sin \alpha_5 \qquad \text{(C-8)}$$

$$S_3 = (W_2 + S_1)\ (\sin \alpha_5) - N_1 \cos \alpha_5 \qquad \text{(C-9)}$$

where W_2 = weight of element 2, and α_5 = angle between horizontal and failure surface for element 2.

The total driving force, S_D, along the assumed failure surface is:

$$S_D = (W_1 - S_1) \sin \alpha_3 + (W_2 + S_1) \sin \alpha_5 + N_1 (\cos \alpha_3 - \cos \alpha_5) \qquad \text{(C-10)}$$

The total resisting force, S_R, along the failure surface consists of the developed shear strength of the soil, plus the additional shear strength developed in the soil due to the normal component of the reinforcement force and the tangential component of the reinforcement force. The total resisting force can be expressed as follows:

$$S_R = c'L_T + N_3 \tan \phi_2' + N_2' \tan \phi_1' + T_T \qquad \text{(C-11)}$$

where L_T = length of the entire failure arc; N_3 = normal reaction on failure surface in element 2; ϕ_1' = developed friction angle for element 1 = ϕ_1/FS_ϕ; ϕ_2' = developed friction angle for element 2 = ϕ_2/FS_ϕ; c' = developed cohesion = c/FS_c; FS_ϕ = factor of safety with respect to friction; FS_c = factor of safety with respect to cohesion; $N_2' = N_2 + T_N$; T_N = normal component of axial tensile force in the reinforcing members, and T_T = tangential component of axial tensile force in the reinforcing members.

To solve the equation for resisting force, S_R, both T_N and T_T must be known. The axial force in each reinforcing member, therefore, must be determined before the resisting force and overall factor of safety can be evaluated.

The force in each reinforcing member is obtained by calculating the frictional resistance of the portion of the member behind the assumed failure surface. The frictional resistance is the skin friction developed between the reinforcing member and the surrounding soil and can be determined as follows:

$$T = \pi D\ L_e\ (\sigma_N \tan \phi_a' + C_a')/S_H \qquad \text{(C-12)}$$

where T = force in the resisting member per unit length of wall; D = diameter of reinforcement; L_e = effective adherence length of the reinforcement behind the failure surface; ϕ_a' = mobilized soil-to-reinforcement friction angle; C_a = soil-to-reinforcement adhesion; $\tan\phi_a'$ = developed soil-to-reinforcement frictional coefficient tan (ϕ/FS_g); C_a' = developed cohesion at soil-to-reinforcement interface = C_a/FS_g; σ_N = average normal stress; S_H = horizontal spacing between reinforcements; and FS_g = factor of safety with respect to pullout resistance parameters.

The frictional resistance of each reinforcing member cannot exceed the yield strength of the member. Once the frictional resistance of each reinforcing element has been determined, the overall stability of the excavation can be computed for the assumed failure surface. The driving force and the resisting force developed along the assumed failure surface must be in equilibrium ($S_D = S_R$) and the overall factor of safety is obtained when:

$$FS_c = FS_\phi = FS_g,\ \phi_a = \phi_i \text{ (internal soil friction angle) and } C_a' = C_a \qquad \text{(C-13)}$$

Both the driving force and resisting force contain a variable factor of safety, thus making direct solution impossible. However, the problem can be solved by an iteration method which quickly converges.

Limit analyses performed in accordance with the foregoing procedures have been compared with the results of finite element analysis performed by Bang [1979] on an in-situ reinforced soil excavation. Figure C-37 shows the predicted potential failure surfaces for a 25-ft deep excavation with 15-ft nails, using the two methods; the results are in good agreement.

7.5 The French Method

The general stability analysis approach developed by Schlosser [1983] considers the reinforced soil mass as a composite material and follows procedures reasonably similar to the Davis method; however, four failure criteria are considered (Fig. C-38).

7.5.1 Shear Resistance of the Soil

The classical Mohr-Coulomb's failure criterion, $\tau = c + \sigma \tan \phi$, is used, where c and ϕ are the cohesion and the internal friction angle of the soil, respectively.

7.5.2 Soil-Reinforcement Friction

The mobilized tensile force T must be balanced by the effective friction along the soil-to-reinforcement interface in the resistant zone behind the failure surface.

For a circular inclusion with diameter D, assuming that the limit skin friction f_{max} is constant all along the length of the reinforcement behind the failure surface, L_e, the mobilized pullout resistance, T_m, can be evaluated as:

$$T_m < \pi D L_e f_{max} = T_{p1} \qquad \text{(C-14)}$$

where T_{p1} is the pullout force.

From limited experimental data [Cartier and Gigan, 1983] it appears that the limit unit skin friction, f_{max}, that is actually mobilized along a given inclusion in a given type of soil is

practically constant, independent of the depth. A preliminary estimate of f_{max} can be made based on available correlations with either laboratory or in-situ test results. In France, correlations developed by Bustamante and Gianeselli [1981] for friction pile design are used. However, these estimates cannot yet be considered reliable for soil nailing. Pullout tests on actual reinforcements are therefore necessary to determine a reliable value of f_{max} to be used for design.

7.5.3 Normal Interaction Between the Soil and the Reinforcement

As shown in Section 3, the normal interaction between the soil and a relatively rigid reinforcement results in a progressive mobilization of the passive lateral earth thrust on the reinforcement. This lateral earth pressure p must be less than the maximum passive resistance that can be mobilized in the soil. In French practice, this lateral earth pressure is maintained at a value lower than the creep pressure p_f determined in a pressuremeter test. It should be possible to extend the p-y analyses commonly used for the design of laterally loaded piles in the United States to establish criteria for the upper limit of this lateral earth pressure. In the absence of such criteria, the upper limit can be considered as $p_{lim} = p_{ult}/2$, where p_{ult} is the ultimate lateral pressure value of a p-y curve.

The shear forces and the bending moments mobilized in the inclusion are calculated considering the equation of the elastic bending of the inclusion and assuming that the soil can be represented by a series of elastoplastic springs. The response of the soil to loading is thus characterized by a lateral reaction modulus K_s. The solution to the equation of the elastic bending of the inclusion involves a design parameter corresponding to the relative rigidity of the inclusion and the soil termed the transfer length, as defined in Eq. C-4.

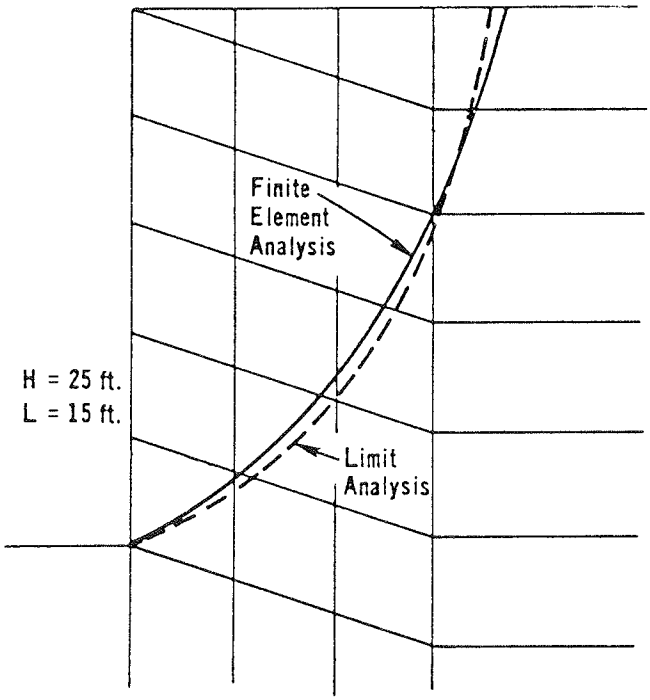

Figure C-37. Comparison of predicted potential failure surface. [Shen et al., 1981]

As shown in Section 3, the computation of lateral forces developed on the nails requires an additional assumption concerning the displacement of the soil away from the inclusion. This displacement is difficult to predict, so for practical design purposes the rather restrictive assumption has been adopted that

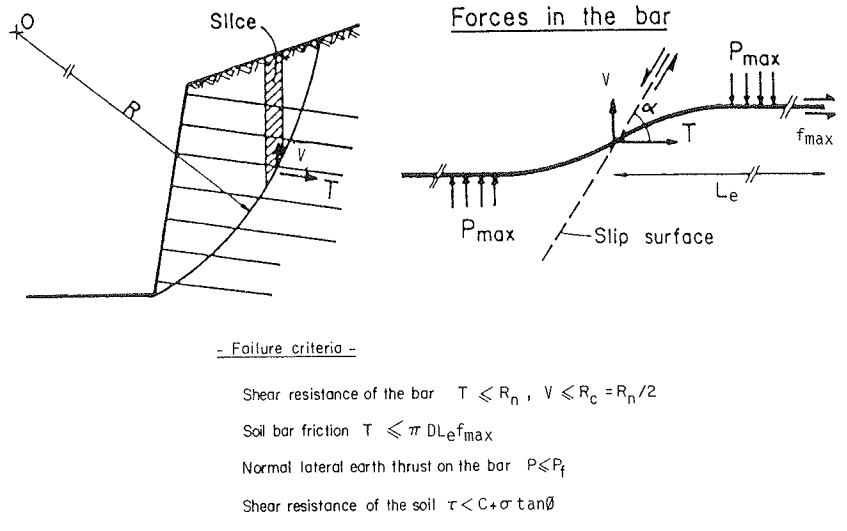

Figure C-38. Design of nailed soil walls by a slope stability analysis method. [Schlosser, 1983]

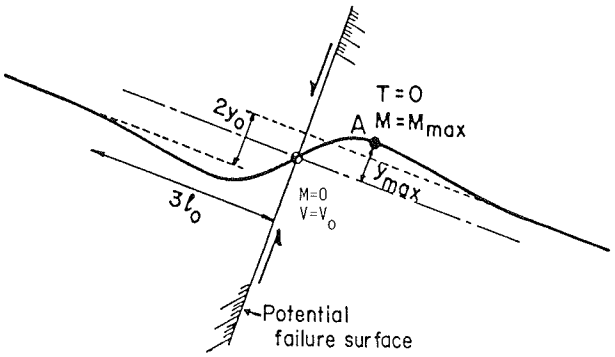

Figure C-39. Theoretical solution for an infinitely long bar adopted for design purposes. [Schlosser, 1983]

planes initially perpendicular to the failure surface remain perpendicular to this surface at any stage of the sliding, as schematically shown in Figure C-39.

Generally, in nailed soil structures, the length of the reinforcements L is much greater than three times the transfer length, L_o. Theoretically, the reinforcements can therefore be considered as infinitely long, and the displacement of the soil in the absence of the inclusion is therefore equal to the distance $2y_o$ between the two extremities of the inclusion (Fig. C-39). Simple solutions are available for the maximum shear force, V_o, mobilized at the point (o) of the intersection with the failure surface, and the maximum bending moment mobilized at a distance of $(\pi/4)L_o$ from point (o).

These equations are:

$$V_o = p\,\frac{D}{2}\,L_o \quad (p < p_{lim}) \tag{C-15}$$

$$M_{max} = 0.16\,pDL_o^2 < M_p \tag{C-16}$$

where M_p is the limit bending resistance of the inclusion, and p is the passive pressure on the bar, with an upper limit p_{lim}.

Limiting the normal pressure to the smaller of either (1) the p_{lim} value or (2) the earth pressure corresponding to formation of a plastic hinge in the nail, the maximum shear force in the inclusion is defined by the lesser of:

$$V_o = \frac{D\,L_o}{2}\,p_{lim} \tag{C-17a}$$

or

$$V_o = \frac{D\,L_o}{2}\,[M_P/(0.16DL_o^2)] \tag{C-17b}$$

7.5.4 Strength of the Inclusion

When the inclusion has to withstand both tensile and shearing forces, denoted, respectively, by T and V, the design criterion is derived from an analysis of the Mohr's circle for the stresses in the inclusion (Fig. C-40) considering that the metallic reinforcing element follows Tresca's failure criterion:

$$\frac{T^2}{R_n^2} + \frac{V^2}{R_c^2} < 1 \tag{C-18}$$

where R_n = tensile strength of the reinforcement, and R_c = shearing strength of the reinforcement; $R_c = R_n/2$.

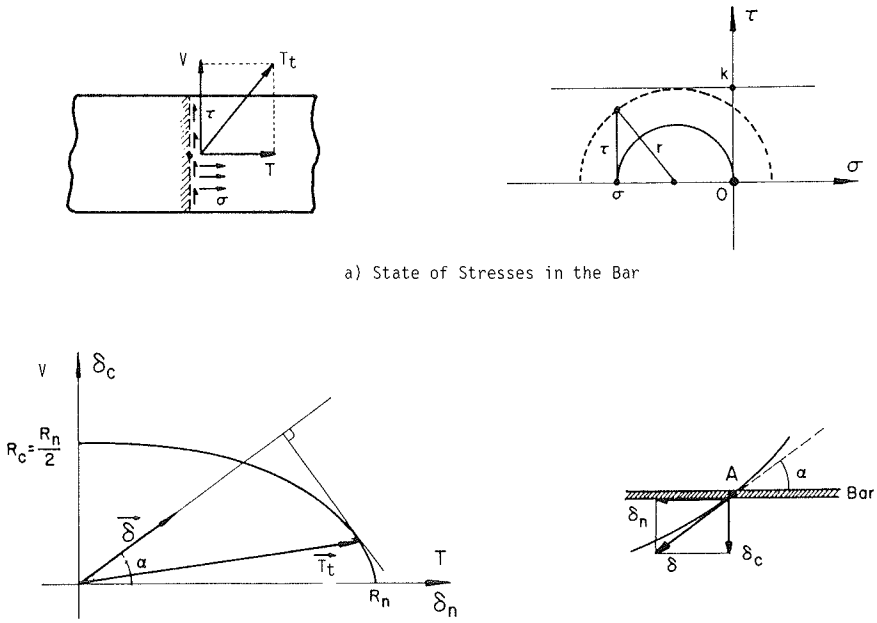

Figure C-40. Determination of the maximum force in the bar. [Schlosser, 1983]

Figure C-40a shows the Mohr's circle for the state of stresses in the inclusion. The tensile and shear forces, T_f and V_f, respectively, mobilized in the inclusion at failure depend on the inclination, α, of the tangent to the failure surface with respect to the considered reinforcement. The failure criterion (Eq. C-18) and the actual total force $\vec{T}$ mobilized in the inclusion (with tensile and shear components T and V), and the displacement vector $\vec{\delta}$ (with normal and tangential components δ_n and δ_c) can be represented on the same axes as shown in Figure C-40b. The principle of maximum plastic work implies that at the point $\vec{T}_T(T,V)$ corresponding to the failure state of stresses in the bar, the tangent to the ellipse representing the failure surface must be orthogonal to the direction of the displacement vector $\vec{\delta}$. From the principle of maximum work and the Tresca failure criterion it can be shown that the tensile and shear forces at failure of a nail can be computed as a function of α as:

$$V_f = \frac{R_c}{\left[1 + 4\tan^2\left(\frac{\pi}{2} - \alpha\right)\right]^{\frac{1}{2}}} \text{ and } T_f$$

$$= 4V_f \tan\left(\frac{\pi}{2} - \alpha\right) \text{ with } R_c = R_n/2 \quad \text{(C-19)}$$

It should be noted that for $\alpha = 0$ only a tensile force develops in the inclusion, whereas for $\alpha = \pi/2$ only a shear force is mobilized.

In the case of grouted bars, it is possible to consider the compressive strength of the grout provided that the bar is located at the center of the composite bar and grout.

For practical application of this complex multicriteria analysis method, a computer program, TALREN, was developed by the French geotechnical company TERRASOL in 1980. A flow chart for this program is shown in Table C-3. In this program, different safety factors are considered with respect to the different failure criteria.

Shear resistance and tensile strength of the inclusion. Generally R_n is defined by the elastic limit of the inclusion and $R_c = R_n/2$. Hence "safe design values" are assigned to the tensile and shear forces in the reinforcements and no safety factors are considered with respect to their tensile and shear resistances ($FS = 1$ with respect to the assigned "safe design values" of R_n and R_c).

Soil inclusion normal pressure. Although it is difficult to accurately evaluate the creep pressure of the soil, the value of the creep pressure p_f measured by pressuremeter is considered as a "safe design value." Therefore, no safety factor is applied with respect to the limit normal pressure on the inclusion p_{lim} which is taken to be equal to the creep pressure p_f. This method can be extended by substituting the value of $\frac{1}{2}\, p_{ult}$ (where p_{ult} is the ultimate lateral pressure of the p-y curve) for p_{lim}. By limiting the normal pressure to p_{lim}, a safety factor of about 2 is obtained with respect to the ultimate normal pressure p_{ult}.

Soil inclusion friction. FS is taken equal to that considered with respect to the shear resistance of the soil and generally has to be equal or greater than 1.5.

Shear resistance of the soil. A minimum value of $FS = 1.5$ is generally required relative to overall slope stability.

The driving moment and the resisting moments due to forces developed in the reinforcements and to the mobilized shear resistance of the soil must be in equilibrium ($M_D = M_R$). The stability analysis uses an iterative procedure, and therefore provides a value of safety factor FS with respect to the pullout resistances of the reinforcements and with respect to the ultimate shear resistance of the soil along the potential failure surface.

7.6 Comparison of Design Methods with Experimental Data

Shen et al. [1981] performed a centrifuge study on a model of a nailed soil excavation retained with grouted nails. They used their design method to predict the acceleration at which failure would occur.

Figure C-41 shows the computed and measured accelerations causing failure, while Figure C-42 shows typical shear strain distributions in the soil deduced from measurements of the soil displacements on in-flight photographs of the failure state. The potential failure zone is shown by the shaded area of maximum shear strains. It is compared with the potential failure surface predicted by the stability analysis. The measured and computed failure surfaces, particularly the measured and computed values of the maximum width of the active zone (Fig. C-43), are in good agreement. Shen et al. concluded that these centrifugal model tests provide substantial experimental support to their design procedure. Further measurements on full-scale structures loaded to failure are, however, still needed to further verify design methods.

7.7 Design of Facing Elements

The purpose of the facing element design is threefold: to prevent local failure of the soil between the nails, to allow for selection of an appropriate welded wire mesh, and to allow for selection of appropriate shotcrete facing.

The design of the wire mesh and shotcrete facing can follow normal structural design procedures provided that the local soil pressure on the facing can be computed.

To evaluate the lateral soil pressure on the facing, the simplified geometry schematically shown on Figure C-44a is used. S_H and S_v are, respectively, the horizontal and vertical spacings between the reinforcements. It is assumed that because of the arching effect above the considered section, the overburden pressure above DC is transferred to the surrounding soil and that the soil resistance to shearing is mobilized only on the lower base of the prism ABCD. Analysis of the local equilibrium leads to an upper limit for the average normal stress on the facing which is equal to:

$$p = \frac{1}{2}\gamma\, S_v \tan^2(45 - \phi/2) \quad \text{(C-20)}$$

The total force applied on the considered section of facing is:

$$P = pS_HS_v = \frac{\gamma S_H S_v^2}{2}\tan^2(45 - \phi/2) \quad \text{(C-21)}$$

This force should be less than the working tensile force T in the reinforcement. The wire mesh is considered to behave as a membrane (Fig. C-44b) supported by the nails. For simplicity, the stability in the vertical and horizontal directions is studied independently, and available solutions, based on the theory of

Table C-3. TALREN (Terrasol) flow chart of computer program.

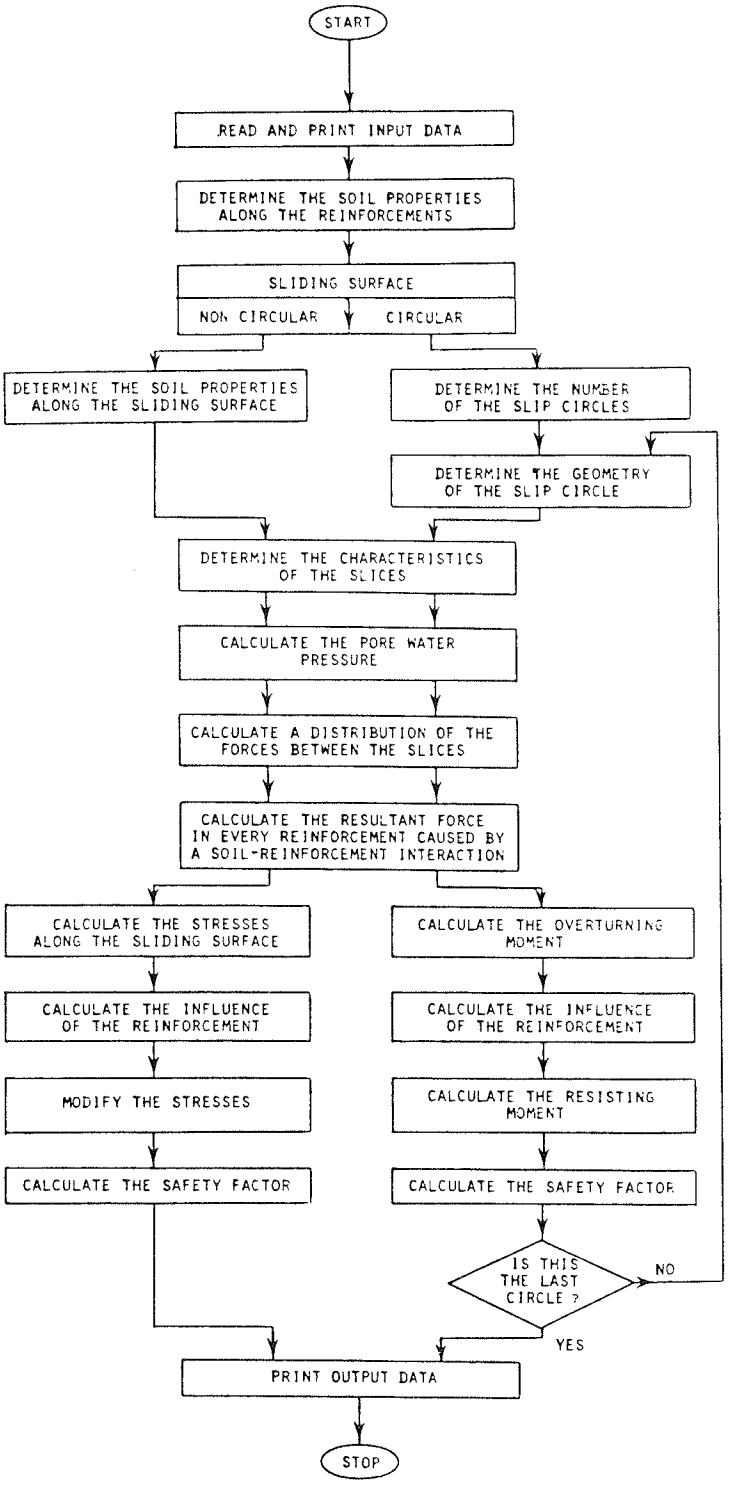

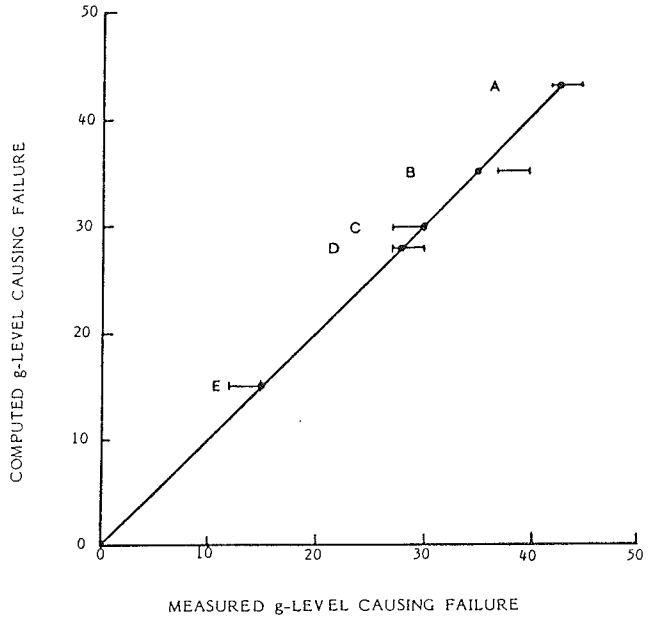

Figure C-41. Centrifuge model tests—computed and measured g levels causing failure. [Shen et al., 1981]

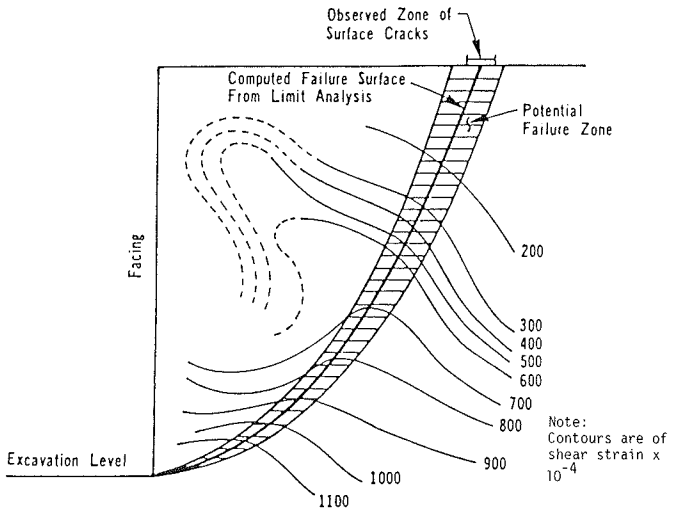

Figure C-42. Centrifuge model tests—a typical maximum shear strain contour of a centrifuge model at failure (45g) (Model A). [Shen et al., 1981]

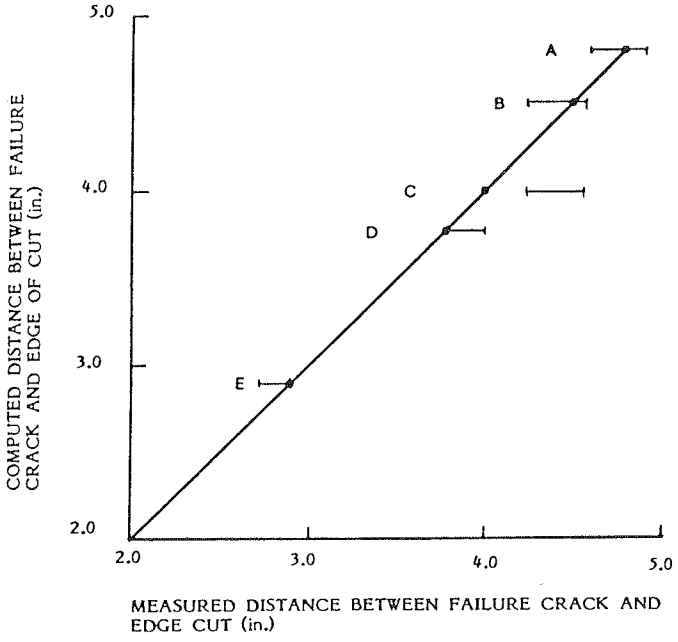

Figure C-43. Centrifuge model tests—computed and measured distance between failure crack and edge of cut. [Shen et al., 1981]

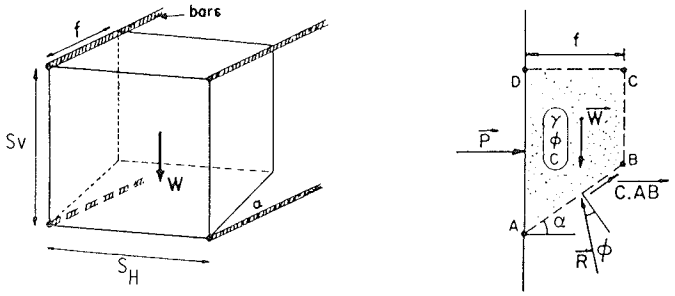

a) Local stability analysis of the soil failure wedge behind the facing (Terrasol, 1983)

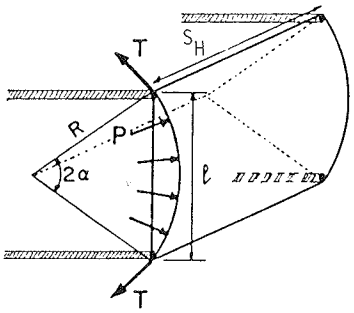

b) Design of welded wire mesh (Terrasol, 1983)

Figure C-44. Principles of design of the facing.

membranes, are used to calculate the required horizontal and vertical reinforcements per linear meter (length or height) of the wall. The design of the reinforced shotcrete facing can be done considering each concrete layer as a beam or raft of width S_v (vertical spacing between the reinforcements) on simple supports formed by the reinforcements. It is then possible to calculate the moments in the shotcrete layer and to determine the necessary reinforcements following usual structural design procedures.

7.8 Limitations of the Current Design Methods

The design procedure outlined in the previous sections provides only a global safety factor and does not enable any evaluation of the maximum tensile and shear forces mobilized in a given reinforcement at a specific location. Furthermore, observations on full-scale structures have shown that the effect of the tensile forces mobilized in the upper reinforcements on the overall stability of the structure is larger than predicted. In fact, according to the French method discussed above, as the potential failure surface at the upper part of the wall is practically vertical, tensile forces in the upper reinforcements should be zero ($\alpha_0 = \pi/2$; Eq. C-19). However tensile forces develop at these upper reinforcements and they affect the behavior and stability of the structure.

As the design procedure is based on limit equilibrium, no consideration is given to the strain field which develops in the reinforced mass and to the allowable displacements of the structure. This limitation, of course, is also associated with slope stability analyses by classical methods. In that case the safety factor and the anticipated displacements are related empirically.

Whereas both full-scale experiments and laboratory model tests have been used to investigate the different mechanisms of soil-reinforcement interaction and the potential failure modes with respect to static loads, there presently are practically no experimental measurements available to evaluate the effect of induced vertical and horizontal vibrations caused by dynamic loads on the behavior of the structure. Consequently, there is currently no specific rational design procedure with respect to dynamic loading. However, in present design practice, dynamic loads can be considered approximately using pseudostatic procedures [Seed and Whitman, 1970].

8. CASE HISTORIES

8.1 Observations on Full-Scale Structures

8.1.1 Failure of a Nailed Soil Retaining Wall [Guilloux and Schlosser, 1982]

The Eparris wall, 15 ft high and 15 ft wide, was built using steel bars placed in boreholes and grouted under low pressures to retain an excavation in a plastic clay (Fig. C-45). Several months after the end of construction, during a period of heavy rains, the walls failed in a kinematic mode corresponding to that of a failure by pullout of the reinforcements; i.e., the top of the wall moved away without any translation of the toe.

Pullout tests on inclusions after failure showed that for the steel bars that were placed in a 4-in. borehole and grouted under low pressure, the mean value of soil–bar friction was about 1 kip/ft. This value was lower than the theoretical value used in the design which varied from 1 kip/ft to 5 kip/ft. The general stability analysis approach described in Section 7 was then used to analyze the stability of this wall using the measured values of friction and gave a factor of safety equal to 1.0.

8.1.2 Full-Scale Loading Tests on Nailed Soil Retaining Structures

Full-scale experiments on instrumented, nearly vertical nailed soil walls in cohesionless soils were carried out and analyzed by Stocker et al. [1979] and Gassler and Gudehus [1981]. The tests were done using driven bars in medium sand of rather low density (bulk density $\gamma = 102$ lb/ft^3; residual friction angle $\phi = 35$ deg). Figure C-46 shows the general set-up of four large-scale tests. Three tests (A, B, C) approached plane strain conditions by use of 1.5-in. thick vertical bentonite-cement walls on each side of 23-ft long sections, and one test (D) was performed using a protruding edge. The reinforced soil body was brought to failure by strip loads (A, B, C) or a rectangular load, respectively (D). In test A, failure was induced by pulling out the lowest row of nails and excavating an additional 3 ft. An additional dynamic load equivalent to maximum traffic load [Gassler, 1977] was applied in test C.

A cross section of each of the nailed soil walls was instrumented as shown in Figure C-47. Forces were measured along selected nails by hydraulic cells and strain gauges, and earth

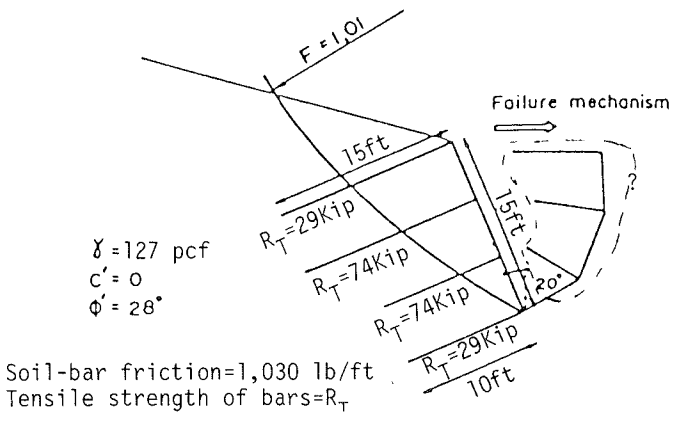

Figure C-45. Eparris wall—analysis of failure using the slope stability design method. [Guilloux et al., 1983]

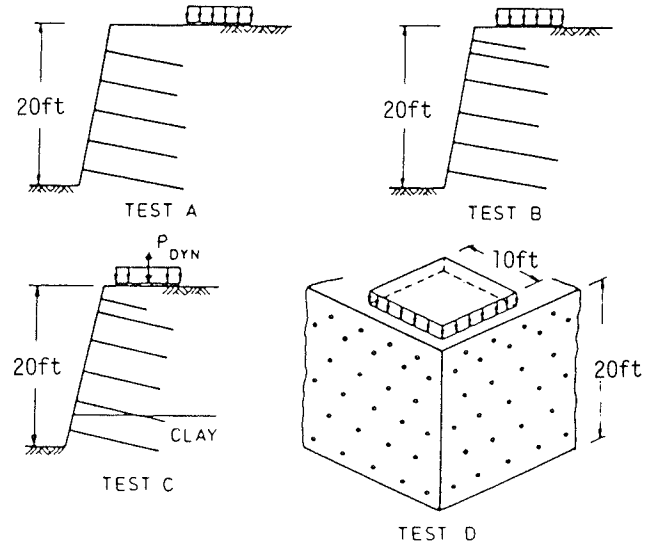

Figure C-46. Large-scale tests in sand. [Gassler and Gudehus, 1981]

pressures behind the shotcrete wall were measured by hydraulic cells. Horizontal displacements within the earth body were measured by inclinometers in boreholes. Surface displacements were determined by surveying methods. The loading device consisted of H-beams and force-controlled hydraulic jacks held by deep-grouted anchors.

Figure C-48 shows typical horizontal displacements during the construction and due to surcharge loads in a plane strain case. These displacements generally did not exceed 0.2 to 0.3 percent of the wall height. Under surface loads there was an additional bulging of the cut slope not exceeding 0.3 percent of the wall height. Global failure was induced by the surface loads and was defined by the load level at which no further load increment could be applied. It was characterized by a fast drop of the hydraulically applied load and a significant increase of horizontal displacements. The failure was caused by slippage of the reinforcements and approximated a rigid body sliding along a circular failure surface, as shown in Figure C-49a.

Typical tensile force distributions caused by the surface loads along the reinforcements are shown in Figure C-49b. Typical earth pressures, measured by means of Glotzl cells behind the shotcrete, are shown in Figure C-50 after excavation (a) and due to surface loads (b). The resultant lateral earth pressure force due to self-weight amounted to about 50 percent of the computed Coulomb's active earth thrust, and the distribution of the earth pressure was marked by a significant reduction relative to Coulomb theory near the toe. The additional earth thrust due to surface loads reached a peak value of about 70 percent of the Coulomb lateral earth thrust.

This significant reduction in the lateral earth thrust as compared to that predicted by the Coulomb theory was attributed to an overall cohesion caused by the nails, and it was recommended that a reduced earth pressure be considered for design purposes. However, these results do not agree with those reported by Cartier and Gigan [1983], who carried out a full-scale experiment on a nailed soil retaining wall also using driven bars in a sandy soil (see Sec. 3). Cartier and Gigan have shown (as illustrated in Fig. C-18) that although the earth pressure is lower

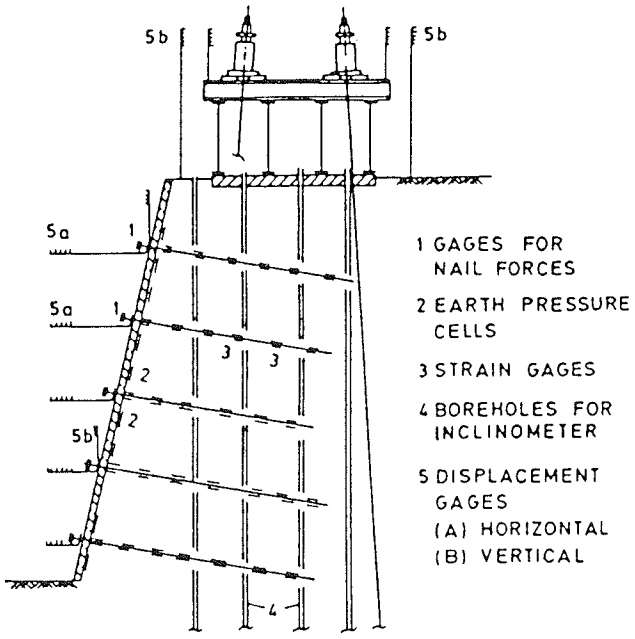

Figure C-47. Measuring facilities of the test walls. [Gassler and Gudehus, 1981]

than the Rankine active earth pressure in the lower part of the structure, in the upper part the tensile forces mobilized in the nails can be greater than even the lateral earth thrust of a soil at a K_o state of stresses. In this case the total lateral earth thrust can be larger than that predicted by the Coulomb method.

The apparent differences between the observations reported on the two full-scale experiments mentioned above cannot yet be fully explained. They may be partially due to the fact that because of the soil-inclusion interaction the lateral active earth pressure measured at the facing, as was done by Gassler and

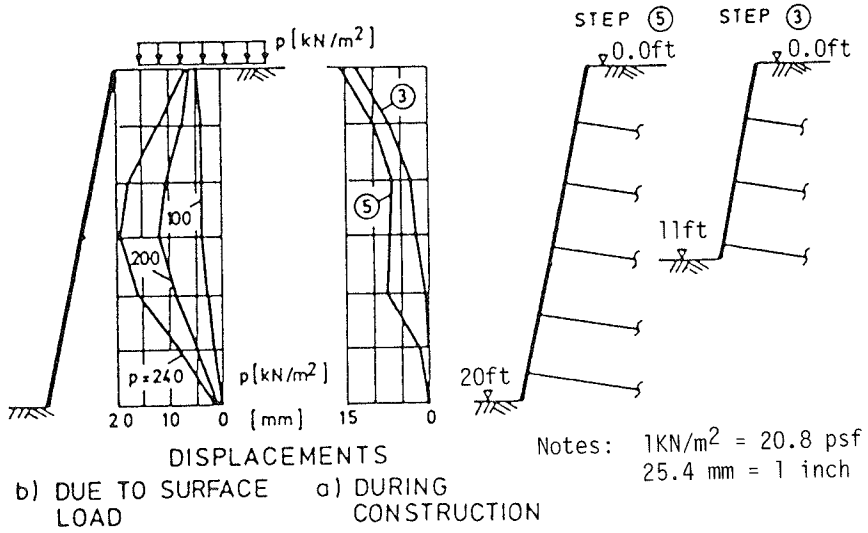

Figure C-48. Horizontal displacements of test C. [Gassler and Gudehus, 1981]

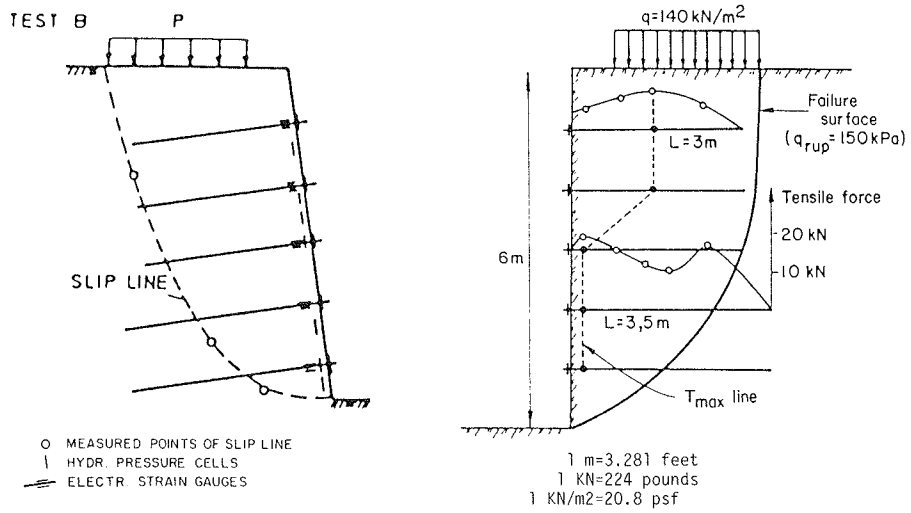

a) Failure mode of the nailed soil wall

b) Typical distribution of tensile forces due to the surface load

Figure C-49. Experimental results of a full-scale loading test on a nailed soil wall. [Stocker et al., 1979]

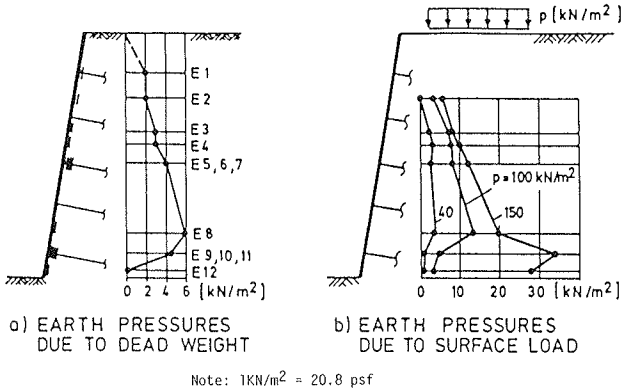

Figure C-50. Earth pressures on the cut slope. [Gassler and Gudehus, 1981]

Gudehus [1981], was lower than the forces measured at a certain distance from the facing, as was done by Cartier and Gigan, [1983]. However, it is probable that factors such as differences in construction techniques, installation methods used to insert the inclusions, facings, and site conditions are the primary causes.

8.1.3 Field Prototype Studies in the United States [Shen et al., 1981]

The first well-documented application of the technique of soil nailing in the United States was at a foundation excavation site in Portland, Oregon. A limited amount of field instrumentation was installed to monitor the system performance. A field test, carried out in the summer of 1979 at the University of California, Davis, involved extensive instrumentation and data collection. The main results of these two studies have been summarized by Shen et al. [1981a,b].

A nailed soil wall 30 ft high was excavated in five lifts of approximately equal thickness. The remaining three sides of the excavation were left untreated with slopes of about 45 deg. The geometry of the system and the layout of the reinforcements are shown in Figure C-51a. The soil profile as determined from boring logs is illustrated in Figure C-51b and the reinforcement system is shown in Figure C-5. The nails were placed in boreholes and sealed to the soil by grouting.

The instrumentation and monitoring included inclinometers and a network of surface movement markers which could be monitored by transit survey to allow for measurements of horizontal displacements of the excavation and of the horizontal and vertical movements of the ground surface. Strain gauges welded to each bar were used to measure the magnitude and distribution of the tensile forces in the reinforcements.

The horizontal deflection profiles yielded by the inclinometer for different construction phases are shown in Figure C-52. The experimental results were analyzed using a finite element method considering a two-dimensional reinforced soil system. A composite model was used to describe the reinforced soil system. As indicated by Shen et al. [1981], the procedure used accounted for the composite nature of the reinforced soil system by combining the element stiffness matrices of the soil, the reinforcements, and the bond behavior to produce the composite element matrices. The approximate solution was then selected by minimizing the incremental potential energy of the system. The soil was assumed to behave as a nonlinear inelastic material considering a hyperbolic stress–strain relationship for primary loading and a linear elastic behavior for unloading and reloading.

The following observations were made: (1) The horizontal deflection decreases with increasing depth from the ground surface. (2) The horizontal deflection decreases with increasing distance behind the vertical cut. (3) The horizontal deflection at a given elevation increases as the excavation depth increases. (4) The horizontal deflection tends to be relatively small at depths greater than the current excavation depth.

It is also of interest to note that profiles 5 and 6 were both taken after the final lift of excavation had been completed.

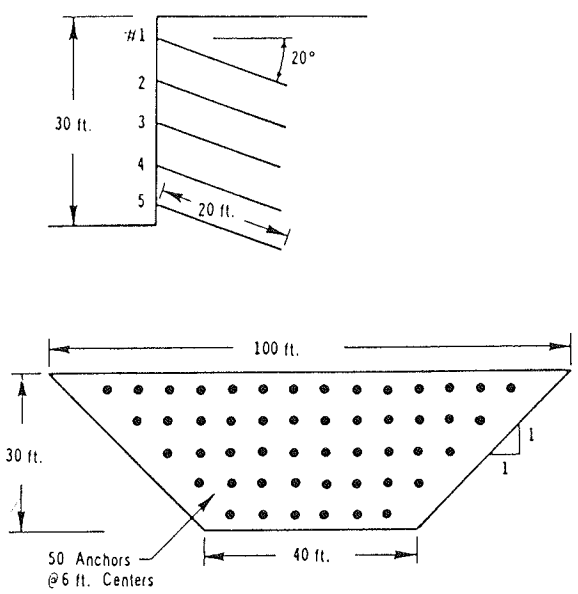

a) Lay out of the nailed soil wall

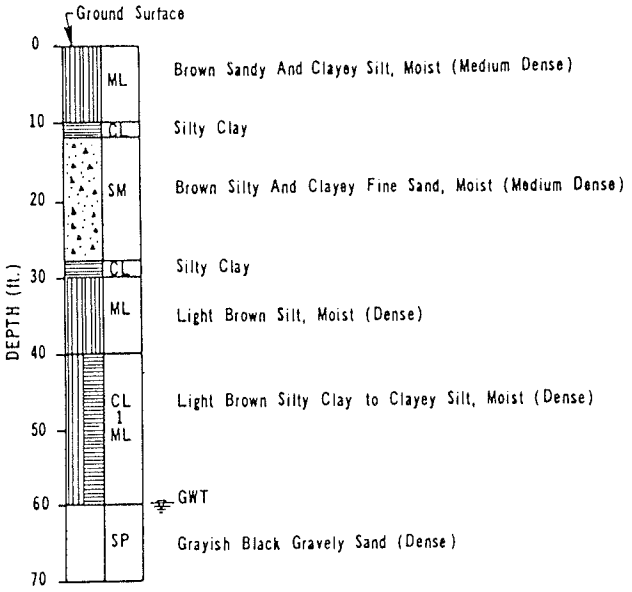

b) A typical boring log - Davis Site

Figure C-51. The Davis prototype of a nailed soil wall. [Shen et al., 1981]

Profile 5 was obtained immediately after excavation completion, whereas profile 6 was recorded 2-weeks later. A comparison of these two sets of profiles reveals that there was a slight amount of post-completion movement. Additional readings were continued throughout the wet winter and spring months. During this period, several earthquakes centered approximately 75 miles southwest of the site occurred; however, no movements greater than those reflected by profile 6 were recorded. The maximum horizontal displacement of the top of the excavation did not exceed 0.2 percent of the excavation depth.

The record of ground surface movements obtained by transit survey (shown in Fig. C-53) resulted in values agreeing well with the inclinometer readings. In both cases the maximum displacements are quite small—approximately 0.8 in. at the center of the uppermost edge of the excavation.

The axial force distributions in the 2nd, 3rd, and 4th level reinforcement members are shown in Figure C-54a. For a given excavation depth, the maximum tensile forces at corresponding levels are approximately of the same magnitude. A rough estimation of the lateral earth thrust based on equivalent soil properties considered by the authors for their finite element analysis shows that the measured tensile forces are of the same order or even greater than the lateral earth thrust of the soil at a K_o state of stresses (Fig. C-54b).

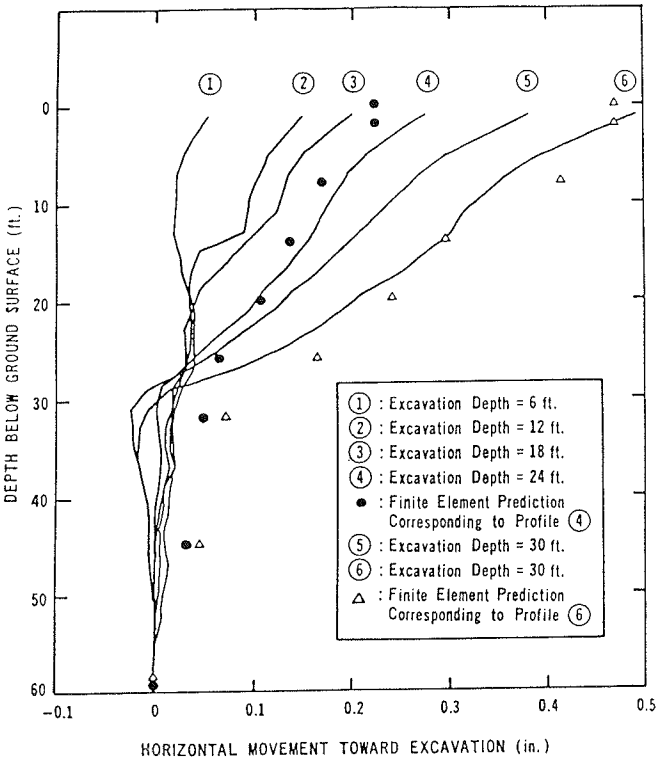

Figure C-52. Horizontal deflection profile at inclinometer No. 1. [Shen et al., 1981]

8.2 Concluding Remarks and Shortcomings in Prediction Methods

In most of the cases described in the literature, the technique of soil nailing offered a useful alternative to more conventional systems generally used for temporary support in deep excavations. In particular, Shen et al. [1981] indicate that it was time saving (e.g., 30 percent less construction time than for a conventional soldier piling and bracing system for the Portland project) and cost-effective (cost of approximately $10/sq ft for the Davis project). The technique requires no heavy equipment

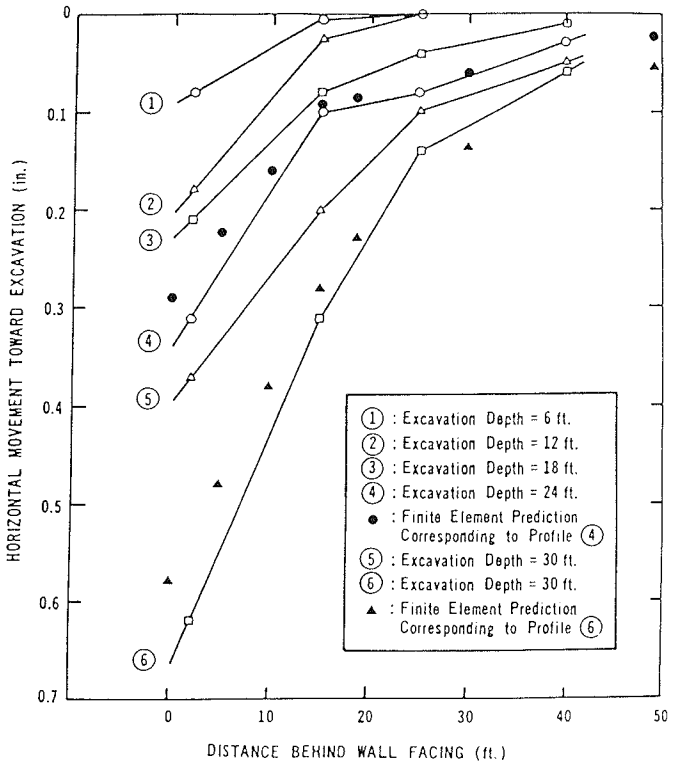

Figure C-53. Horizontal movement of ground surface at the excavation centerline. [Shen et al., 1981]

for pile driving and provides an obstruction-free site for subsequent foundation work.

All of the instrumented structures discussed show that, when the structure is located above the level of the water table, lateral displacements of the retained excavation slope before failure are very small and generally do not exceed 0.5 percent of the excavation depth. This is true even in heterogeneous soils such as the Davis site.

Nailed soil retaining structures can support external surface loads and dynamic traffic loads. These loads do not generally induce large displacements before failure, with measured displacements generally remaining less than 1 percent of the excavation depth [Gassler and Gudehus, 1981].

The slope stability analysis approach currently used for the design of these structures is a limit analysis with respect to an assumed failure along potential circular sliding surfaces. It is therefore difficult to verify the design procedure on the basis of observations on full-scale structures that are not at failure. It has, however, been successfully used to predict failures of both centrifugal models and full-scale structures. As indicated by Juran [1983], the predicted distance from the excavation to the potential sliding surface is generally larger than that to the maximum tensile forces line measured in actual structures. Consequently, this design approach could lead to an overestimation of the required length of reinforcements.

Most failures that have been reported occurred because of pullout of the reinforcements. Post-failure analyses have shown that the failure could be explained by an overestimation of the design value of the limit skin friction which could be mobilized at the soil-reinforcement interfaces. These observations suggest that it is desirable for a safe design of the system to carry out pullout tests on actual reinforcements during the excavation to verify the assumed design value of the limit shear stress.

Most of the case histories discussed earlier yield consistent data concerning the displacements of the retained excavation slopes. However, measured maximum tensile forces in the reinforcements are widely divergent. This is probably mainly because of differences in the construction techniques used to install the facings and the reinforcements, in site conditions, and the wide variety of heterogeneous soils generally encountered. Additional field data and case studies of nailed soil retaining structures are needed to develop simplified design methods capable of predicting the forces mobilized in the reinforcements under the actual working stresses in the structure.

9. COST COMPARISONS

Nailing has not yet been sufficiently used in the United States so that meaningful cost comparisons with other earth retention systems can be made. However, French experience indicates the technique to be competitive.

10. FUTURE DEVELOPMENTS OF THE TECHNIQUE OF SOIL NAILING AND ANTICIPATED RESEARCH TRENDS

The technique of soil nailing is currently used primarily for temporary structures. However, the inherent advantages of this method are leading progressively to its use for permanent structures.

The main difficulty involved in the development of the technique for permanent structures is the evaluation of the corrosion rate of the steel bars in heterogeneous in-situ ground. New types of reinforcements and reinforcement coatings with high resistivity to corrosion are being developed, as are prefabricated panels for use in urban areas.

To increase the confidence of the engineer in the potential use of this technique for permanent structures, further research is required involving both laboratory model studies and full-scale experiments on actual structures to provide a rational basis for the development and verification of appropriate design methods. These methods should integrate the different soil-reinforcement interaction mechanisms discussed in Section 3 and take into account the relative soil-reinforcement displacement necessary to mobilize the resisting forces in the reinforcements.

Nailed soil retaining structures are both flexible and massive, and are therefore expected to have a high resistance to dynamic loads. Consequently, this technique can be of particular interest in seismic zones. As indicated by Shen et al. [1981], several earthquakes centered approximately 75 miles (120 km) southwest of the Davis test site did not cause significant movement of the nailed soil wall. However, the present state of knowledge of the dynamic behavior of this type of structure is extremely limited, and research is required for development of procedures for earthquake resistant design.

11. DESIGN EXAMPLE

11.1 Problem Statement

Using soil nailing, design the support system for a 16-ft deep

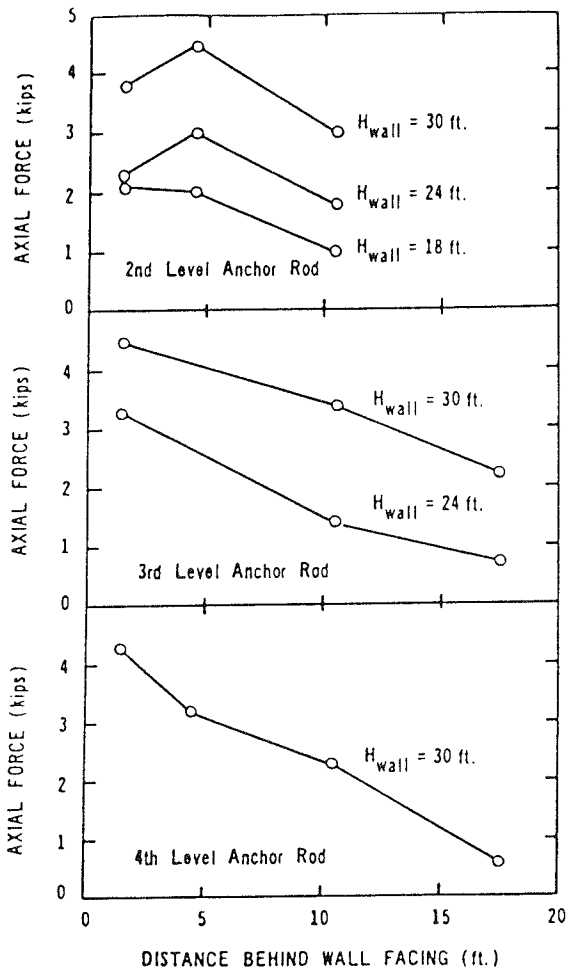

a) Measured axial force distribution in 2nd, 3rd and 4th level anchor rods. (1ft. =0.305m, 1kips = 4.45kN) (Shen et al, 1981)

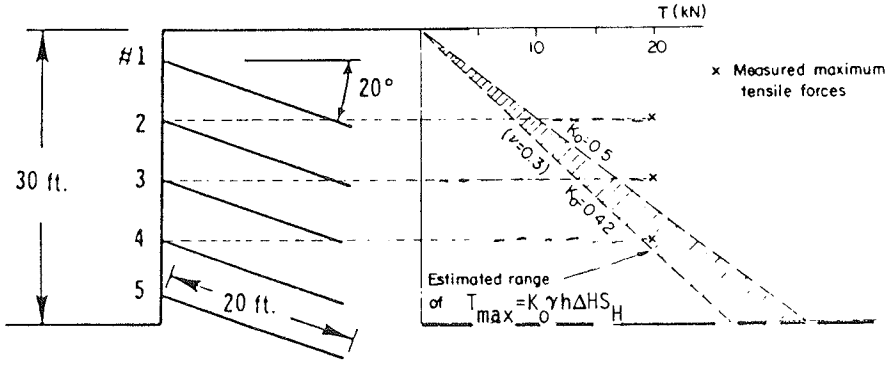

b) Measured and estimated variations of the maximum tensile forces with depth (Shen et al, 1981)

Figure C-54. Axial force distributions measured by Shen et al., 1981.

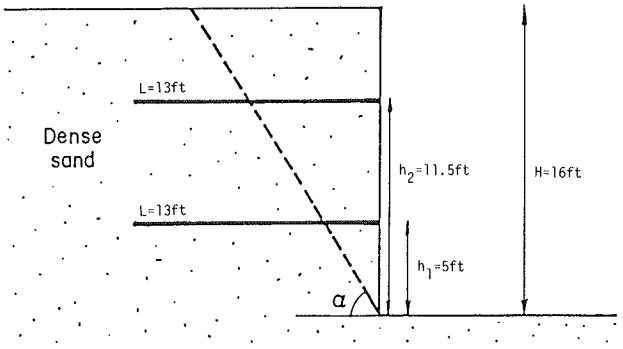

Figure C-55. Design example—cross-section of wall and reinforcement layout.

excavation in dense sand that has the following soil properties: $\gamma = 127$ pcf, $\phi' = 35$ deg, and $c' = 0$. Limit passive pressure of 31 ksf.

Assume that there will be two horizontal layers of 13-ft long reinforcing bars at spacings and locations as shown in Figure C-55. The spacing perpendicular to the page, S_H, is 6.5 ft. The tensile resistance of the bars R_n is 27 kip, which corresponds to the elastic limit of the steel. From pullout tests on grouted bars (diameter of bar plus grout 5 in., or 0.42 ft), at the site, the unit frictional resistance was found to be 4.1 kip/ft of length. Also, the transfer length in accordance with Eq. C-4, namely $L_o = \sqrt[4]{4EI/K_sD}$, is given as 0.66 ft, where D is the diameter of the inclusion (bar plus grout); K_sD is 2.5×10^3 psi; and EI is the bending stiffness of the steel bar only, i.e., excluding grout (diameter 40 mm).

Assume for simplicity that the critical sliding surface is a plane inclined at an angle $\alpha = 60°$ from the horizontal (Fig. C-55). For a first approximation, assume that the reinforcement acts in tension only, i.e., the bars have no shearing resistance ($R_c = 0$). (A second approximation considering both the tensile and shear resistances, R_n and R_c, of the reinforcements is given later in this section.)

11.2 Solution

11.2.1 First approximation ($R_c = 0$)

First, calculate the tensile forces acting at each layer of bars. From the failure criteria, these forces are limited by the lesser of: (1) the maximum allowable tensile force in the bar R_n, and (2) the maximum pullout resistance that can be developed between the bar and the soil, T_p.

From a free body diagram of the sliding wedge (Fig. C-56):

$$\Sigma T_i - P_n \sin\alpha + P_t \cos\alpha = 0 \qquad \text{(C-22)}$$

$$W - P_n \cos\alpha - P_t \sin\alpha = 0 \qquad \text{(C-23)}$$

where P is the earth force on the failure surface. From equilibrium considerations,

$$P_t = P_n \frac{\tan\phi}{FS} \qquad \text{(C-24)}$$

From Eqs. C-22, C-23, and C-24, the factor of safety can be solved as:

$$FS = \frac{W \cos\alpha \tan\phi + \Sigma T_i \sin\alpha \tan\phi}{W \sin\alpha - \Sigma T_i \cos\alpha} \qquad \text{(C-25)}$$

Apply the failure criteria in tension per unit length of wall: $T_i = 1/S_H$ times the lesser of the tensile strength or pullout resistance of the reinforcement, R_n and T_p, respectively. R_n is given as 27 kip, while pullout resistance can be computed as:

$$T_p = \frac{\pi D L_e f_{max}}{FS} = \frac{L - (h_i/\tan\alpha)}{FS} f_{max}\, \pi D \qquad \text{(C-26)}$$

and $\pi D f_{max} = 4.1$ kip/ft (given) $= F_{max}$.

If pullout resistance rather than tensile strength of the reinforcement governs, FS appears on both sides of Eq. C-25 and a trial and error solution is required. For a first trial, assume that factor of safety is equal to 1.5 and compute pullout resistance.

For layer 1:

$$T_{p1} = \frac{[13\text{ft} - (5\text{ft}/\tan 60°)]\ 4.1\ \text{kip/ft}}{1.5} = 27.6\ \text{kip} \qquad \text{(C-27)}$$

The pullout resistance is slightly larger than the given rupture strength. Hence, the tensile strength of the bar governs. Considering the lateral bar spacing S_H of 6.5 ft, the lateral force contribution of the reinforcements per foot of wall is 27/6.5, or 4.1 kip/ft.

For layer 2:

$$T_{p2} = \frac{13\text{ ft} - (11.5\text{ ft}/\tan 60°)\ 4.1\ \text{kip/ft}}{1.5} = 17.4\ \text{kip} \qquad \text{(C-28)}$$

Hence pullout resistance, rather than rupture strength of the reinforcement, governs. The lateral reinforcing force per foot of wall contributed by the second layer of reinforcements, T_2, is therefore 17.4/6.5 or 2.5 kip/ft.

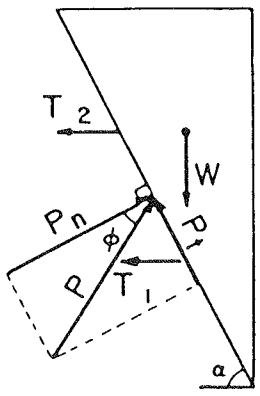

Figure C-56. Design example—first approximation with tension only.

The total horizontal forces are:

$$\Sigma T_i = 4.1 + 2.7 = 6.8 \text{ kip/ft} \qquad \text{(C-29)}$$

The weight of the sliding wedge, per unit length of wall, is:

$$W = \frac{\gamma H^2}{2 \tan\alpha} = \frac{127\ (16)^2}{2 \tan 60} = 9.4 \text{ kip/ft} \qquad \text{(C-30)}$$

Solving for *FS*, from Eq. C-25:

$FS = \dfrac{9.4 \cos 60° \tan 35° + 6.8 \sin 60° \tan 35°}{9.4 \sin 60° - 6.8 \cos 60°} = 1.56$. The value for *FS* is very close to the assumed value of 1.5, and further computations need not be done. If there are substantial differences between the assumed and computed factors of safety, iterative procedures can be used until the values converge.

11.2.2 Second Approximation (Both tensile and shear resistances are considered)

For the second example the shear resistance of the reinforcement is also considered. As indicated in Section 7, at the point where the failure surface passes through the reinforcements, it is assumed (because of symmetry) that the bending moment is zero and the shear stress is a maximum. In this case the four design criteria outlined in Section 7.5 have to be satisfied. The determination of the limit tensile and shear forces in each reinforcing bar is performed following the procedure outlined in the same section.

From a free body diagram of the sliding wedge (Fig. C-57):

$$\Sigma T_i - P_n \sin\alpha + P_t \cos\alpha = 0 \qquad \text{(C-31)}$$

$$W - P_n \cos\alpha - P_t \sin\alpha - \Sigma V_i = 0 \qquad \text{(C-32)}$$

From equilibrium considerations:

$$P_t = P_n \frac{\tan\phi}{FS} \qquad \text{(C-33)}$$

From Eqs. C-31, C-32, and C-33, the factor of safety, *FS*, can be expressed as:

$$FS = \frac{W \cos\alpha \tan\phi + (T_i \sin\alpha - \Sigma V_i \cos\alpha) \tan\phi}{W \sin\alpha - T_i \cos\alpha - \Sigma V_i \sin\alpha} \qquad \text{(C-34)}$$

Because the angle of inclination of the failure plane is not equal to either 0 or 90 deg, the tensile and shear criteria cannot be directly applied as they were in the first approximation above. Instead, the failure criteria to be evaluated are as schematically shown in Figure C-58. In this figure, the following cases are shown:

- *Case 1,* the force that the passive resistance of the soil on the nail can exert exceeds the shear strength, R_c, of the nail, and the pullout resistance of the nail exceeds its tensile strength.
- *Case 2*, the force that can be resisted by passive soil resistance is less than the shear strength of the nail. Hence, the maximum passive force constitutes a failure criterion more restrictive than the shear strength of the nail.
- *Case 3*, the pullout resistance of the nail is less than the rupture strength of the nail. Hence, pullout resistance constitutes a failure criterion more restrictive than the rupture strength of the nail.
- *Case 4*, both the force that can be supported by passive soil resistance and the pullout resistance of the nail constitute more restrictive design criteria than the shear and rupture strength of the nail, respectively.

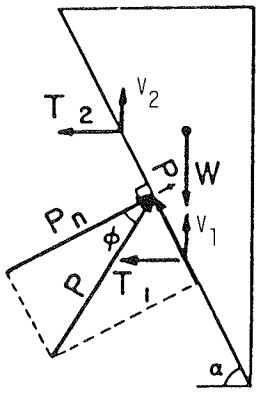

Figure C-57. Design example—second approximation considering shear.

In all four cases, the possible safe design combinations of shear and tensile forces on the nail are indicated by the shaded zones. To use these failure criteria, the limiting soil pullout and lateral resistance must be computed and compared with the allowable tensile and shear forces in the reinforcement to see which case applies. For the given reinforcement strengths of R_n = 27 kip and R_c = 13.5 kip, the nail strength ellipse shown in Figure C-59a can be constructed. For $\alpha = 60°$, the maximum allowable values of tensile and shear forces on the nail, *T* and *V*, respectively, can be computed (see Eq. C-19 in Section 7):

$V \le \dfrac{R_n}{2\sqrt{1 + 4\tan^2(90° - \alpha)}} \le \dfrac{27}{2\sqrt{1 + 4\tan^2(90° - 60°)}} \le$ 8.8 kip. $T \le 4V \tan(90° - \alpha) \le 4(8.8 \text{ kip}) \tan(90° - 60°) \le$ 20.3 kip.

The maximum passive resistance that can be exerted by the soil can be computed by means of Eq. C-15 (Section 7): $V_{max} = P_{max} \dfrac{D}{2} L_o \le R_c$, $V_{max} = \dfrac{(0.42 \text{ ft})(0.66 \text{ ft})(31.0 \text{ ksf})}{4} = 2.1$ kip. By limiting P_{max} to half the ultimate passive value ($P_{max} = P_u/2$), V_{max} can be computed: $V_{max} = 2.1 \text{ kip} \le 8.8$ kip.

Because this value is less than the shear strength R_c of the nail, the shear force that can be resisted is controlled by the passive soil resistance. Determination of the T_T vector is shown in Figure C-59b; this case is similar to case 2 of Figure C-58. Since pullout resistance is greater than rupture strength, but available passive resistance force from the soil is less than shear strength of the nail, the limiting tensile force *T* is calculated from Eq. C-18 (Sec. 7), as follows: $\dfrac{V^2_{max}}{R_c^2} + \dfrac{T^2}{R_n^2} = \dfrac{(2.1)^2}{(13.5)^2} + \dfrac{T^2_{max}}{(27)^2} = 1$; $T_{max} = 26.7$ kip. Allowable tensile force on the bar is thus 26.7 kip.

Determination of the allowable tensile forces to be used in Eq. C-34 is slightly more complex because the term to calculate the soil pullout resistance (see Eq. C-26) also contains the factor of safety *FS*. Thus, an iterative solution is required. To illustrate, first calculate the maximum pullout force for each reinforcement layer with Eq. C-26. Assume *FS* = 1.5 as before. For layer 1, $T_{p1} = \dfrac{[13 - (5/\tan 60°)]\ 4.1 \text{ kip/ft}}{1.5} = 27.6$ kip. But, as shown

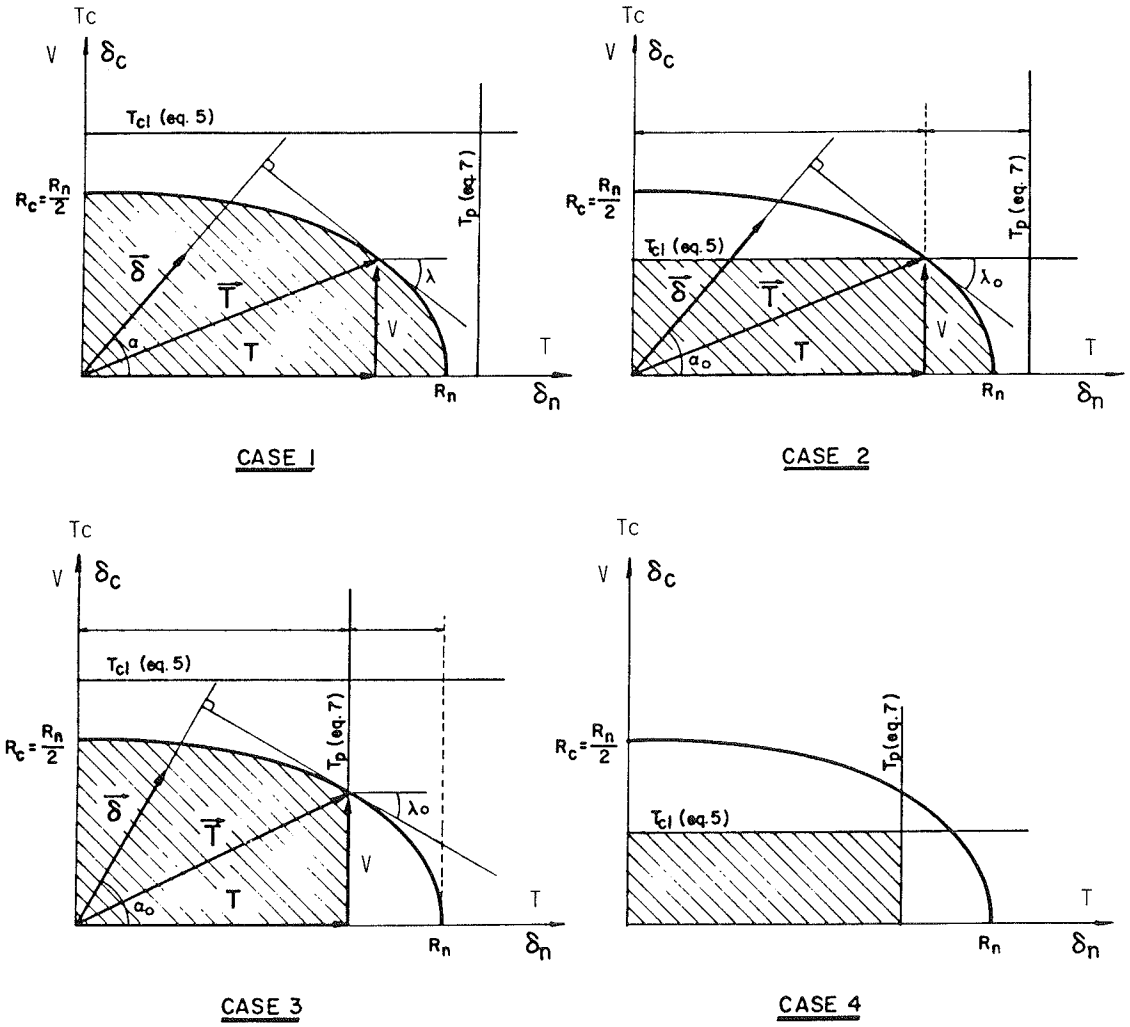

Figure C-58. Examples of the multicriteria analysis for the calculation of allowable tensile and shear forces in the reinforcement.

above, T_{max} = 26.7 kip. Thus, T_{max} controls the maximum allowable force in layer 1.

For layer 2, $T_{p2} = \dfrac{[13 - (11.5/\tan 60°)]\ 4.1 \text{ kip/ft}}{1.5} = 17.4$ kip. Since this value is less than 26.7 kip, T_{p2} controls the resistance of layer 2. The total horizontal force ΣT_i is, per foot run of wall, $T_i = \dfrac{T_1}{S_H} + \dfrac{T_2}{S_H} = \dfrac{26.7}{6.5} + \dfrac{17.4}{6.5} = 6.8$ *kip.*

For the bars in shear, $V_i = \dfrac{V_1}{S_H} + \dfrac{V_2}{S_H} = \dfrac{2.1}{2} + \dfrac{2.1}{2} = 2.1$ kip.

The weight of the sliding wedge is 9.4 kip/ft. From Eq. C-34 and the foregoing values ΣT, ΣV, and α, factor of safety can be computed as FS = 1.60. When different factors of safety are assumed and the calculation process is repeated, the solutions converge at FS = 1.56.

Comparison of the design examples in Sections 11.2.1 and 11.2.2 indicate that allowance for the shear resistance of the bars resulted in only a marginal increase in factor of safety. Thus, the added complexity may, at first glance, appear not to be worth the effort. However, as shown in Section 11.2.3, allowance for shear resistance can, in some cases, influence results significantly.

11.2.3 Second Approximation with Different Soil Parameters

Assume the following soil parameters are typical of the site: ultimate passive pressure P_{ult}, is 63 kip/ft^2; transfer length, L_o, is 1.5 ft.

All other soil parameters, the site conditions and the geometry are identical to those cited in Section 11.1, i.e., the Problem Statement.

The analysis in this case is identical to that previously made. The limiting forces in the reinforcement are shown in Figure C-59a. Then the maximum passive resistance of the soil is determined from Eq. C-15: $V_1 = \dfrac{(0.42 \text{ ft})(1.5 \text{ ft})(63 \text{ kip/ft})}{4} = 9.9$ kip.

Since the value is greater than the shear strength of the bar (V = 8.8 kip), shear in this case is controlled by the strength of the reinforcement. This is similar to case 3 in Figure C-58, as shown in Figure C-60. The allowable tensile load on the reinforcement is computed as 20.4 kip.

Determination of the allowable tensile load in the reinforcement is the same as shown above; a trial and error solution is required. Assuming FS = 1.5, the pullout load, T_{P1}, for layer 1 is computed as 28.2 kip, which is larger than the allowable tensile load on the reinforcement, which has been computed as 20.4 kip. Therefore the latter governs. For layer 2, T_{P2} = 17.8 kip, so it controls. Thus: $T_i = \frac{20.4}{6.5} + \frac{17.8}{6.5}$ = 5.9 kip/ft, and $T_{ti} = \frac{8.9}{6.5} + \frac{8.9}{6.5}$ = 2.7 kip/ft.

From Eq. C-34 with W = 9.4 kip/ft, a factor of safety of 1.83 is first obtained; repeated trials converge at FS = 1.70, which is satisfactory.

Inclusion of the reinforcement's shear resistance has, in this example, significantly increased the factor of safety of the nailed wall.

For a really complete analysis, the limiting bending resistance should also be considered. It is likely that the shape of the failure surface would become rather complex depending on α and the relative magnitude of the limiting tension, shear, and bending forces. As with any slope stability analyses, several failure surfaces must be analyzed to obtain the minimum factor of safety. In practice, a circular sliding surface and the method of slices are usually used to compute the safety factor. With a circular sliding surface, α is not a constant and the determination of the controlling reinforcement forces becomes more complex. Thus, the use of a digital computer to make the calculations and a program which considers all the above factors are needed. However, with the many uncertainties still associated with the design of soil nailing systems, it is not certain that the increased sophistication is warranted. Many systems can be, and in fact have been, designed with consideration only of the tensile resistance of the nail.

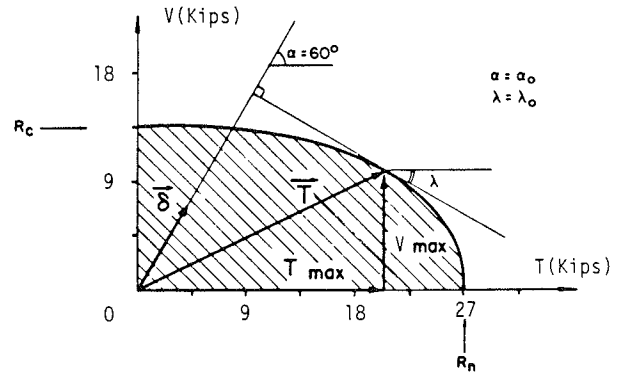

a) Maximum forces in reinforcement (soil not yet included)

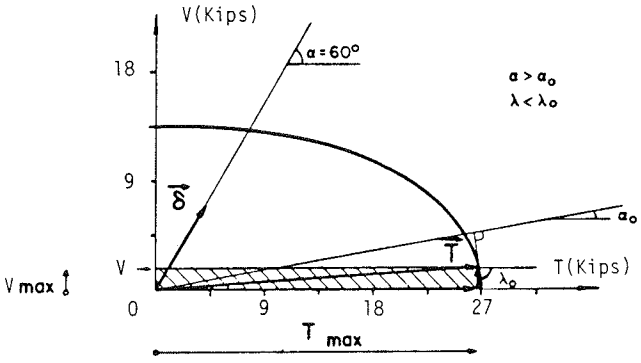

b) Maximum forces limited by passive soil resistance

Figure C-59. Determination of $\vec{T}$ for design example, second approximation.

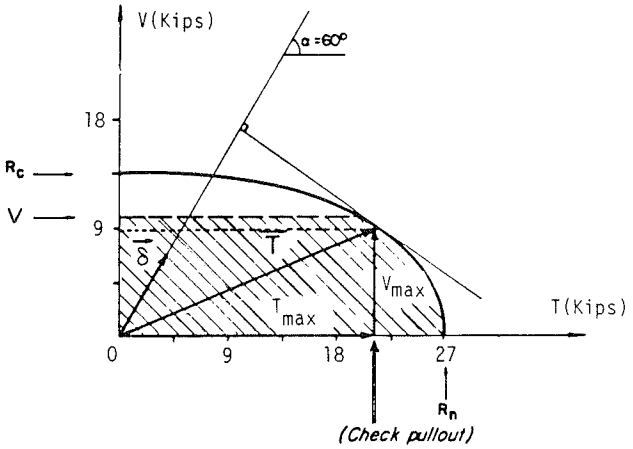

Figure C-60. Calculation of $\vec{T}$ for design example, second approximation with high lateral soil resistance.

12. REFERENCES

BANG, S. [1979]. "Analysis and Design of Lateral Earth Support System," Ph.D. Thesis, University of California, Davis, Calif.

BRINCH-HANSEN, J. [1960]. *Hautprobleme der Bodenmechanik,* Springer-Verlag, Berlin.

BUSTAMANTE, M. G., and GIANESELLI, L. [1981]. "Prevision de la Capacite Portante des Pieux Isoles sous Charge Verticale," *Bull. de Liaison du Laboratoire des Ponts et Chausses,* No. 113.

CARTIER, G., and GIGAN, J. P. [1983]. "Experiments and Observations on Soil Nailing Structures," *Proc. 8th European Conference on Soil Mechanics and Foundation Engineering,* Helsinki.

GASSLER, G. [1977]. "Large Scale Dynamic Test of In-Situ Reinforced Earth," *Proc.,* DMSR 77, Karlsruhe, Vol. 2.

GASSLER, G., and GUDEHUS, G. [1981]. "Soil Nailing—Some Soil Mechanical Aspects of In-Situ Reinforced Earth," *Proc. 10th International Conference on Soil Mechanics and Foundation Engineering,* Vol. 3, Session 12, Stockholm, pp 665–670.

GUILLOUX, A., and NOTTE, G. [1983]. "Experiences on a Retaining Structure by Nailing," *Proc. 8th European Conference on Soil Mechanics and Foundation Engineering,* Helsinki.

GUILLOUX, A., and SCHLOSSER, F. [1982]. "Soil Nailing Practical Applications," *Symposium on Soil and Rock Improvement Techniques,* A.I.T.

GUILLOUX, A., and SCHLOSSER, F. [1984]. "Soil Nailing Practical Applications, *Symposium on Soil and Rock Improvement Technique,* A.I.T.

HOVART, C. and RAMI, R. [1975]. "Elargissement de l'Emprise S.N.C.F. pour la Desserte de Saint-Quentin-en-Yvelines," Revue Travaux.

JEWELL, R. A. [1980]. "Some Effects of Reinforcement on the Mechanical Behaviour of Soils," Dissertation submitted for the degree of Doctor of Philosophy at Cambridge University.

JURAN, I. [1977]. "Dimensionnement Interne des Ouvrages en Terre Armee," Thesis for Doctor of Engineering, Paris.

JURAN, I. [1983]. State-of-the-Art Report "Reinforced Soil Systems—Application in Retaining Structures," *7th Asian Regional Conference on Soil Mechanics and Foundation Engineering,* Haifa.

JURAN, I., and BEECH, J. [1984]. "Theoretical Analysis of Nailed Soil Retaining Structures," *International Symposium on In Situ Soil and Rock Reinforcment,* Paris.

JURAN, I., BEECH J. and DE LAURE, E. [1984]. "Experimental Study of the Behavior of Nailed Soil Retaining Structures on Reduced Scale Models," *International Symposium on In Situ Soil and Rock Reinforcement,* Paris.

JURAN, I., SCHLOSSER, F., LONG, M. F. and LEGEAY, G. [1978]. "Full Scale Experiment on a Reinforced Earth Bridge Abutment in Lille," *Proc. ASCE Symposium on Earth Reinforcement,* Pittsburgh, Apr. 27, 1978, pp. 556–584.

JURAN, L., SCHLOSSER, F., LOUIS, C., KERNOA, M., ECKMANN, B. [1981]. "Soil Reinforcing by Passive Bars," *Proc. 10th International Conference on Soil Mechanics and Foundation Engineering,* Stockholm.

JURAN, I., SHAFIEE, S. and SCHLOSSER, F. [1985]. "Numerical Study of Nailed Soil Retaining Structures, *11th International Conference on Soil Mechanics and Foundation Engineering,* San Francisco.

JURAN, I., SHAFIEE, S., SCHLOSSER, F., HUMBERT, P., GUENOT, A. [1983]. "Study of Soil-Bar Interaction in the Technique of Soil Nailing," *Proc. 8th European Conference on Soil Mechanics and Foundation Engineering,* Helsinki.

LIZZI, F., and CARNAVALE, G. [1979]. "Networks of Root Piles for the Consolidation of Soils: Theoretical Aspects and Tests on Models," *International Symposium on Soil Reinforcement,* Paris.

LOUIS, C. [1979]. "Control and Monitoring in Tunnelling," Report of French Mission to China, Simecsol.

LOUIS, C. [1981]. "Nouvelle Methode de Soutenement des Sols en Deblais," Revue Travaux, No. 553.

RABCEWICZ, L. V. [1964, 1965]. "The New Austrian Tunnelling Method," Parts I to III, Water Power, London, Nov.-Dec. 1964 and Jan. 1965.

RABEJAC, S., and TOUDIC, P. [1974]. "Construction d'un mur de soutenement entre Versailles-Chantiers et Versailles-Matelots," Revue Generale des Chemins de Fer, 93eme annee, pp. 232–237.

SCHLOSSER, F. [1983]. "Analogies et differences dans le Comportement et le Calcul des Ouvrages de Soutenement en Terre Armee et par Clouage du Sol," *Annales de L'Institut Technique du Batiment et des Travaux Publics,* No. 418.

SCHLOSSER, F., and GUILLOUX, A. [1979]. "Etude du Frottement Sable-Armature en Modele Reduit," *International Conference on Soil Reinforcement: Reinforced Earth and Other Techniques,* Vol. I, Paris.

SCHLOSSER, F., and JURAN, I. [1979]. General Report, Session No. 8, "Design Parameters for Artificially Improved Soils," *Proc. 7th European Conference on Soil Mechanics and Foundation Engineering,* Brighton, U.K., September.

SEED, H. B., and WHITMAN, R. V. [1970]. "Design of Earth Retaining Structures for Dynamic Loads," *Proc. ASCE Specialty Conference on Lateral Stresses in the Ground Design of Earth Retaining Structures,* pp. 103–147.

SHEN, C. K., BANG, S. and HERRMANN, L. R. [1981]. "Ground Movement Analysis of an Earth Support System," *ASCE, J. Geo. Eng. Div.,* Vol. 107, No. GT12.

SHEN, C. K., BANG, S., HERRMANN, L. R. and ROMSTAD, K. M. [1978]. "A Reinforced Lateral Earth Support System," *Proc. ASCE Symposium on Earth Reinforcement.*

SHEN, C. K., BANG, S., ROMSTAD, K. M., KULCHIN, L. and DENATALE, J. S. [1981a]. "Field Measurements of an Earth Support System," *ASCE J. Geo. Eng. Div.,* Vol. 107, GT 12.

SHEN, C. K., HERRMANN, L. R., ROMSTAD, K. M., BANG, S., KIM, Y. S., and DENATALE, J. S. [1981b]. "In Situ Earth Reinforcement Lateral Support System," *Report No. 81-03,* Department of Civil Engineering, University of California, Davis, Calif.

STOCKER, M. F., KORBER, G. W., GASSLER, G., and GUDEHUS, G. [1979]. "Soil Nailing," *International Conference on Soil Reinforcement,* Paris, pp. 469–474.

TERRASOL [1980]. "Dimensionnement des Ouvrages en Sol Cloue," Programme TALREN, Rapport Interne, Paris.

TERRASOL [1983]. Rapport Interne.

TOMLINSON, M. J. [1981]. "Pile Design and Construction Practice," Viewpoint Publications, London.

CHAPTER TWO—SOIL NAILING IN SLOPE STABILIZATION

Contents

1. INTRODUCTION

1.1 Description and Classification of Available Techniques

The stabilization of slopes by nailing consists of placing passive linear inclusions capable of withstanding tensile forces, shear forces, and bending moments into an existing or potential sliding surface. The inclusions are generally installed with a uniform density either in a critical zone at the toe of an unstable slope or throughout the sliding or creeping mass, thereby creating a relatively uniform composite cohesive mass of reinforced ground.

Soil nailing may be used to restrain two distinctly different modes of downslope soil movement. The first, referred to as potentially unstable slopes (or simply unstable slopes) in this chapter, is the case where little or no movement occurs but available safety factors along potential sliding surfaces are unacceptably low and a sliding zone can therefore potentially move. In this case the slope is actually under static equilibrium conditions, the failure criterion of the in-situ ground is not violated, and no sliding surface can be observed. The purpose of the reinforcing element is to increase the safety factor. Classical slope stability analysis methods can be adapted to evaluate the effect of resisting forces mobilized in the reinforcements crossing the potential failure surface on the value of the safety factor.

The second case, referred to as creeping slopes, pertains to the situation where movement actually occurs at an unacceptable rate. The upper moving zone is separated from the stable lower zone by either a relatively thin defined failure zone, generally at the interfaces between two different layers, or a larger zone within which the induced shear stresses are of sufficient magnitude to cause a continuous creep. In this case the failure

surface can be detected from in-situ inclinometer measurements, and the safety factor along this surface is known to be 1.0 because the mobilized shear stress is equal to the shear strength of the soil. The purpose of the reinforcing element is to decrease the sliding (or creeping) rate to an acceptable value. The design criteria should therefore allow for consideration of the effect of soil-inclusion interaction on the sliding rate and for the prediction of the development of the corresponding resisting forces in the inclusions as a function of their displacement relative to the soil.

In an unstable slope the reinforcements are generally installed with a rather uniform density throughout the unstable zone. In a creeping slope the reinforcements are generally installed either with a uniform density throughout the creeping zone or in a critical zone at the toe of the slope. The construction process, the choice of the reinforcing element, and the behavior of the reinforced soil system depend on several factors including site conditions, soil type and state (i.e., creeping or unstable slope), inclination of inclusions with respect to the failure surface, spacing of inclusions, and rigidity of the inclusions relative to the soil.

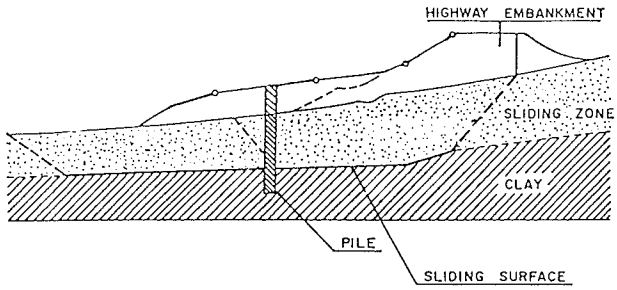

a) Slope stabilization using large diameter piles

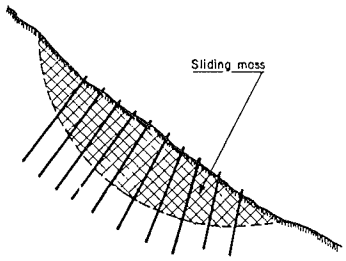

b) Slope stabilization using flexible nails

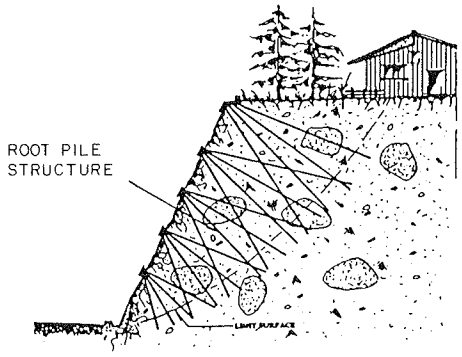

c)Slope stabilization using root piles (Lizzi, 1977)

Figure C-61. Available systems for slope stabilization using soil nailing.

A wide variety of techniques and reinforcing elements, including timber piles, large-diameter piles, micropiles, and driven rails, have been used. The main systems available are the following.

Rigid piles. Large-diameter rigid piles can be used to stabilize landslides [Yamada et al., 1971; Fukumoto, 1972; Kerisel, 1976; Sommer, 1977 and 1979]. One or two rows of piles are generally located at the toe of the slope to provide resistance to the soil tending to slide downslope. The construction process follows conventional pile and pier installation techniques. The row of piles constitutes a relatively rigid screen, which acts as an element of discontinuity in the displacement pattern of the slope (Fig. C-61a).

Flexible inclusions. Small-diameter, flexible structural members, referred to as nails, can also be used. The construction process is quite similar to that for soil nailing in excavations, as described in Chapter One of this appendix. The inclusions (tubes, bars, metallic profiles, rails) are either installed in boreholes and sealed to the ground by cement grouting, or these are simply driven into the ground. The sliding zone is generally uniformly reinforced by the relatively closely spaced inclusions (Fig. C-61b). A relatively high density of the nails causes soil-nail interaction, which, although not yet fully understood, is apparently beneficial to overall stability, providing a global apparent cohesion to the nailed soil mass which is greater than that corresponding to the sum of shear forces mobilized in the inclusions. Because of this interaction, the lateral earth pressure resisted by the group of nails appears to be greater than the earth pressure that a single nail could resist multiplied with the number of nails.

Micropiles (root piles). This system, developed by Lizzi [1971], consists of creating a monolithic rigid block of reinforced soil which extends to a depth below the critical failure surface (Fig. C-61c). The main difference between this system and the soil nailing methods mentioned above is that the behavior of micropiles is significantly influenced by their geometric arrangement [Lizzi and Carnavale, 1979; Schlosser and Juran, 1979]. As a result of the criss-crossed pattern (Fig. C-61c), the micropiles are subject to compression and tension forces that provide the required structural stability of the reinforced slope. Root piles are not considered further in this chapter.

1.2 History

Slope stabilization by rigid piles, flexible nails, and other types of reinforcements is one of the earliest applications of soil reinforcement.

Case histories of railway slope stabilization by timber piles have been reported in Japan as early as the end of the 19th century (1903) when such piles were used as countermeasures against landslides along Noo-Tsutsuishi railway in Niigata Prefecture. Fukuoka [1977a] reported case histories of slope stabilization using reinforced concrete piles in 1955 and steel piles in 1965. At about the same period, cast-in-place concrete piles

started to be used, and subsequently these two types of piles were used jointly combining steel pipe piles reinforced by introducing steel H-piles and filling the voids with concrete.

The French Railway Administration has significant experience with soil nailing, especially in the stabilization of old embankments that were built by the end of the last century and that were undergoing continuous and progressive deformations leading to significant track settlements [Verrier and Merlette, 1981]. Whenever a stabilizing berm could not be used at the toe of the slope, soil nailing was used. Generally, small-diameter piles of low bending stiffness or micropiles were used.

In the United States, early case histories of slope stabilization by different types of inclusions are described by Baker and Yoder [1958].

1.3 Applications

As already mentioned, the two main applications of soil nailing in slopes are to: (1) increase the stability of slopes that are potentially unstable but are not actually at limit static equilibrium conditions; and (2) stabilize slopes that are undergoing creep. Case histories are described in Section 4 to illustrate these applications.

1.4 Inherent Advantages

Nailing techniques can be used economically in different types of soils ranging from soft clays to fissured marls in order to efficiently reinforce potentially unstable slopes and to stabilize creeping soil masses. There are no proprietary restrictions on the use of the various techniques, which are essentially site-dependent. In fact, some of the main advantages of nailing are that the choice of the reinforcing inclusions, the construction process, and the design of the nailed-soil system (geometry, inclination, and density of the reinforcements) can be easily modified during construction to site-specific requirements. Thus, the design can readily be adapted to accommodate available construction equipment and materials.

Furthermore, locally available types of inclusions can often be used (timber piles, rails) to provide efficient, economical, and rapid engineering solutions, especially when temporary ground stabilization during short construction periods is of importance.

1.5 Organization of Chapter

The technology, durability, and installation process of soil nailing by flexible inclusions have been described in Chapter One of this appendix, and details are therefore not repeated here. The following sections address the aspects of soil nailing unique to slopes, including available design approaches, and observations on sites where soil nailing has been used for slope stabilization.

2. MECHANISMS AND BEHAVIOR

2.1 Principles of Soil-Reinforcement Interaction and Related Failure Modes

The soil-reinforcement interaction in a nailed slope depends primarily on the rigidity of the inclusion relative to the soil, on its inclination with respect to the potential failure surface, and on the rate of movement.

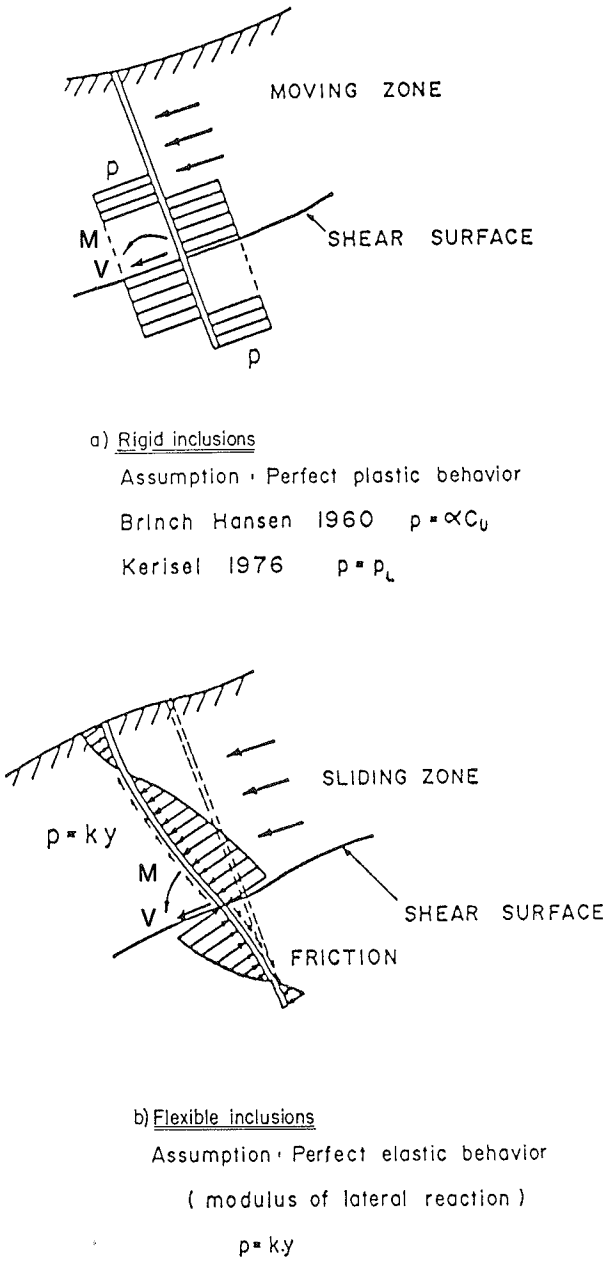

Figure C-62. Soil-reinforcement interaction in an unstable slope stabilized by nailing.

2.1.1 Rigid Inclusions

In the case of rigid inclusions (for example, large-diameter piles), the main mechanism of soil-to-reinforcement interaction is passive soil resistance developed against the face of the inclusion. The relative soil-to-pile displacement required to mobilize the limit earth pressure, p_l, on the pile is small relative to the diameter of the pile. As illustrated in Figure C-62a, it can reasonably be assumed that the limiting passive earth pres-

sure (analogous to the ultimate p value in p-y curves) is entirely mobilized adjacent to both sides of the failure surface [Brinch-Hansen and Lundgren, 1960; Kerisel, 1976]. The passive soil pressure acting on the pile in the unstable zone is transferred to the stable zone by the shear and bending resistances of the pile.

2.1.2 Flexible Inclusions

In the case of flexible, small-diameter inclusions, such as tubes, bars, driven rails, and the like, the relative soil-to-reinforcement displacement required to mobilize the limit lateral earth pressure on the inclusion is sufficiently large (relative to the diameter of the inclusion) to also allow the mobilization of soil-reinforcement friction (Fig. C-62b). Hence, tensile forces can be mobilized in the reinforcements (Fig. C-62b) in addition to shear forces and bending moments. The mobilization of the tensile force in the inclusion depends mainly on its orientation with respect to the failure surface [Jewell, 1980], as discussed in Section 3.1.1 of Chapter One of this appendix.

2.2 Lateral Earth Thrust on Inclusions

2.2.1 Potentially Unstable Slopes

The mechanism of lateral soil resistance developed againt piles subject to horizontal loading has been widely studied [Brinch-Hansen, 1961; Matlock and Reese, 1960; Menard, 1962; Broms, 1964; Baguelin and Jezequel, 1972]. The particular case of a nailed soil, with nails transferring load from one side of a distinct failure surface to the other, has been investigated by laboratory direct shear tests on a silty soil reinforced by a row of vertical steel bars of different rigidities [Juran et al., 1981]. The main results, which are described in more detail in Section 3.1.2 of Chapter One, can be summarized as follows.

The mobilization of the bending stiffness and shear resistance of the inclusions results in an apparent, anisotropic cohesion C^* of the nailed soil. This apparent cohesion can be substantially larger than the additional shear resistance C_o^* due to the bars, i.e., $C_o^* = \Sigma V_o/A$, where ΣV_o is the sum of the shear forces mobilized in the bars and A is the area of the sliding surface. The difference is due to the effect of the inclusions on the displacement and stress fields in the sheared soil, which results in a more uniform stress distribution along the failure surface. This effect, which is not yet fully understood, depends on the normal pressure on the sliding surface and on the density and inclination of the inclusions.

The relative soil-inclusion displacement necessary to mobilize this apparent cohesion is generally much greater than that required to mobilize soil-reinforcement friction. This relative displacement is highly dependent on the relative rigidity of the bars and on the diameter of the inclusion. A simplified model of soil-reinforcement interaction has been proposed by Juran et al. [1981] to simulate the mobilization of the lateral earth pressure on the inclusion. In this model, the nails are considered as laterally loaded vertical piles supported by a lateral series of elastoplastic springs with spring coefficients that may vary during the loading. In this model, the relative rigidity of the bar is characterized by its transfer length:

$$L_o = \sqrt[4]{\frac{4EI}{K_s d}} \tag{C-35}$$

where EI = bending stiffness of the nail; K_s = subgrade modulus of the lateral soil reaction; and d = diameter of the nail.

The spring coefficients, E_s, are computed as the subgrade modulus times the diameter of the nail. Figure C-63 shows the results of a finite element study [Juran et al., 1983] of the effect of the transfer length, L_o, on the displacement, δ, necessary to generate both a required shear force, V_o, in the inclusions and a required increase of the overall factor of safety $\Delta F_s/F_s$ (where F_s is the factor of safety of the unreinforced soil) under a normal stress of σ_v = 2,100 psf. The required displacement decreases as the transfer length increases.

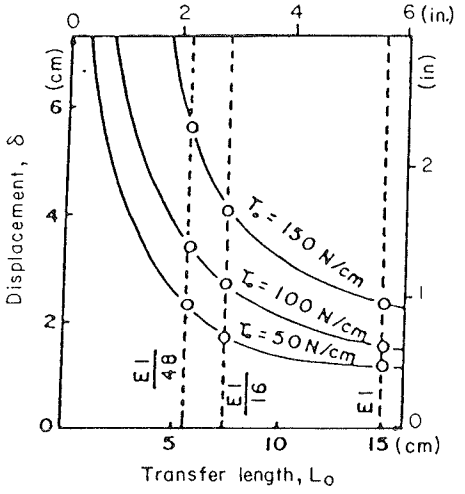

(A) Shear Force in Bars (Vo)

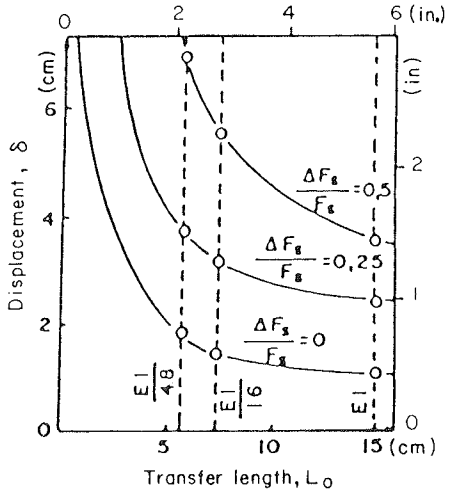

(B) Increase of the Overall Shear Resistance (ΔFs/Fs)

Figure C-63. Effect of transfer length on the displacement necessary to mobilize: (a) shear forces in bars, V_o, and (b) increase of the overall shear resistance (F_s/F_s).

The failure of a nailed soil can be caused either by the yielding of the inclusion due to excessive bending or by a progressive plastic flow of the soil around the inclusion. Consequently, for design purposes, the limit earth pressure on the inclusion has to be less than the limit pressure of the soil. For a factor of safety of about 2, this limit pressure corresponds to about half the ultimate p-value in p-y curves, or to the creep pressure p_f which can be determined from pressuremeter test results.

2.2.2 Creeping Slopes

In the case of a slope undergoing creep, the main role of the inclusion is to reduce the distortion rate, $\dot{\epsilon}$. As shown later, the lateral earth pressure mobilized at the soil inclusion interface depends both on the magnitude of the strain rate, $\dot{\epsilon}$, and its gradient, $d\dot{\epsilon}/dz$, within the zone of creep.

Conceptually, the interaction between the reinforcements and creeping soil may be described as follows. In the nonreinforced creeping soil, the shear stresses mobilized in the soil are equal to the shear strength of the soil at the rate of strain at which creep is occurring.

When subjected to strain-controlled testing, the shear strengths of soils typically increase with increasing strain rate, or decrease with decreasing strain rate. Hence, for a given soil of given strength, high shear stresses can be supported at higher strain rates than at lower strain rates. Conversely, the rate of strain or creep is dependent on the level of shear stress mobilized, with creep rates decreasing if the mobilized shear stresses can be decreased.

When soil nails are inserted into a creeping zone, portions of the driving forces that cause the slope to creep are supported by the nails. Hence, the shear stresses mobilized in the soil decrease, with a consequent reduction in the rate of strain.

To describe this interaction mechanism, it is possible to use the plastic flow equation proposed for soil by Leinenkugel [1976] and considered by Winter et al. [1983] for the design of soil nailing for slope stabilization. According to this equation, the undrained shear strength of a soil at strain rate, $\dot{\epsilon}_c$, is related to the shear strength at a reference strain rate, $\dot{\epsilon}_o$, by a viscosity index I_v as follows:

$$S_u(\dot{\epsilon}_c) = S_u(\dot{\epsilon}_o)\left[1 + I_v \log_e\left(\frac{\dot{\epsilon}_c}{\dot{\epsilon}_o}\right)\right] \qquad \text{(C-36)}$$

where $S_u(\dot{\epsilon}_o)$ is the undrained shear strength at the reference strain rate $\dot{\epsilon}_o$, and $S_u(\dot{\epsilon}_c)$ is the shear strength associated with the strain rate $\dot{\epsilon}_c$. The viscosity index can be determined from undrained triaxial shear tests on saturated consolidated soil samples, according to a special testing procedure described by Leinenkugel [1976]. The test is performed in a standard triaxial cell with the soil specimen being subjected to increasing shear stress under strain-controlled conditions. Once the residual shear strength is reached, strain rates are increased or decreased in increments to evaluate the shear strengths associated with various rates of strain. The test is schematically illustrated in Figure C-64. As a rule of thumb, shear strength typically increases about 10 percent with each log cycle increase in strain rate [Whitman, 1957; Briaud et al., 1984]. Empirical relationships between the liquid limit, w_1, and viscosity index have also been proposed by Gudehus and Leinenkugel [1978].

A creeping zone of soil is schematically illustrated in Figure C-65. Prior to reinforcement, the soil element shown within the zone of creep is undergoing creep or shear strain, at a steady initial distortion rate of $\dot{\epsilon}_i$, where $\dot{\epsilon} = dx/dz$. Because the strain rate is assumed to be steady state (i.e., neither decelerating or accelerating), the shear stresses mobilized in the nonreinforced soil, τ_i, must be equal to the shear strength of the soil at the particular strain rate, S_{u_i}.

When a reinforcing element is included, the mobilized shear stresses in the creeping zone are reduced as a result of the loads transferred to the reinforcement. Thus, for the element dz in Figure C-65, the reduction in mobilized shear stress, $d\tau$, may be written as:

$$p(z)\, d\, dz = S_{eq} \cdot d\tau \qquad \text{(C-37)}$$

or

$$p(z) = \frac{S_{eq}}{d} \cdot \frac{d\tau}{dz} \qquad \text{(C-38)}$$

where p is the lateral earth pressure acting on the reinforcement; d is the diameter of the reinforcement; dz is the height of the soil element; S_{eq} is the equivalent surface of influence of the reinforcing element in the plane of mobilized shear stress; and $d\tau$ is the reduction in mobilized shear stress within the element when rate of distortion is reduced from $\dot{\epsilon}_i$ to $\dot{\epsilon}$.

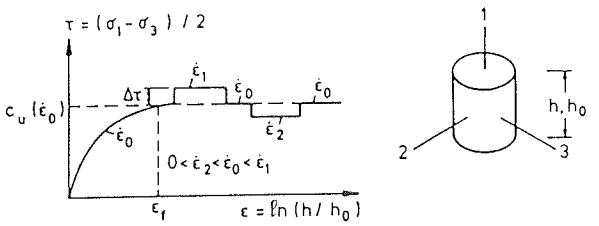

Figure C-64. Undrained triaxial test with jump technique. [Leinenkugel, 1976]

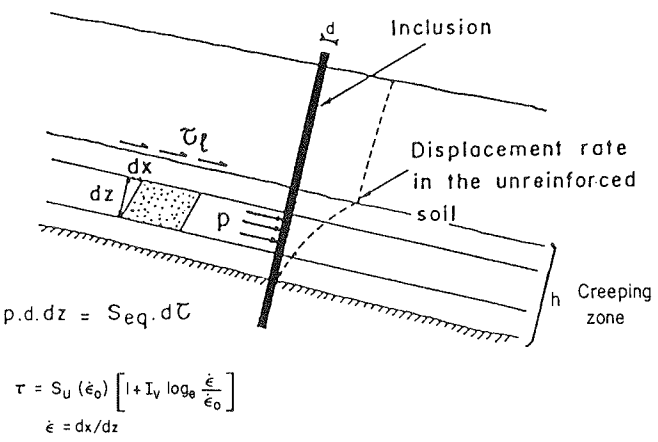

Figure C-65. Mechanism of soil-inclusion interaction in a creeping soil slope. [Schlosser et al., 1983]

To solve Eq. C-38, the function $d\tau/dz$ must be known. However, the mobilized shear stress along the failure surface, separating the upper zone (which undergoes monolithic sliding) from the creeping zone is equal to the soil's undrained shear strength at the particular rate of strain, $\tau = s_u$, and, therefore, in the vicinity of the failure surface:

$$\frac{d\tau}{dz} = \frac{dS_u}{dz} \tag{C-39}$$

The rate of variation of shear stress with depth is assumed to be constant throughout the creeping zone.

Furthermore, for the element dz in Figure C-65, strain rate should be written as:

$$\dot{\epsilon} = \frac{d\dot{x}}{dz} \tag{C-40}$$

Hence, Eq. C-39 may be rewritten as:

$$\frac{d\tau}{dz} = \frac{dS_u}{dz} = \frac{dS_u}{d\dot{\epsilon}} \cdot \frac{d\dot{\epsilon}}{dz} \tag{C-41}$$

By considering the initial strain rate $\dot{\epsilon}_i$, as the reference strain rate, then differentiating Eq. C-36 to obtain $dS_u/d\dot{\epsilon}$, and substitution into Eq. C-38, the following general solution for the lateral earth thrust on the nail, p, may be obtained:

$$p(z) = \frac{S_{eq}}{d} \cdot \frac{S_u(\dot{\epsilon}_i)\, I_v}{\dot{\epsilon}} \left(\frac{d\dot{\epsilon}}{dz}\right) \tag{C-42}$$

This equation can also be written as:

$$p(z) \cdot d \cdot dz = S_{eq} \cdot S_u(\dot{\epsilon}_i)\, I_{v_i} \cdot \left(\frac{d\dot{\epsilon}}{\dot{\epsilon}}\right) \tag{C-43}$$

Integrating along the full depth Z_o of the zone of creep provides the total lateral earth thrust Q_s acting on the pile, as:

$$Q_s = \int_{z_o} p(z) \cdot d \cdot dz = S_{eq} \cdot S_u(\dot{\epsilon}_i)\, I_{v_i} \cdot \ln w = S_{eq} \cdot \Delta\tau \tag{C-44}$$

where $w = \dot{\epsilon}/\dot{\epsilon}_i$ is the required sliding rate reduction factor. $\Delta\tau$ is the reduction in mobilized shear stress (or shear strength) along the failure surface associated with a reduction in creep rate from the initial value $\dot{\epsilon}_i$ to a slower rate $\dot{\epsilon}$.

For these assumptions,

$$\Delta\tau = S_u(\dot{\epsilon}_i) - S_u(\dot{\epsilon}) \tag{C-45}$$

where $S_u(\dot{\epsilon}_i)$, $S_u(\dot{\epsilon})$ are the shear strengths associated with strain rates $\dot{\epsilon}_i$ and $\dot{\epsilon}$, respectively.

2.3 Group Interaction

When a number of reinforcing elements are used at a close spacing in either an unstable or creeping slope, there is a group effect which is not yet fully understood, and for which appropriate mathematical models have not yet been developed. When a single element is inserted into the slope, the total lateral earth pressure that can be withstood by the element is limited by the bending resistance of the element. However, when a group of elements are inserted, the interaction amongst the enclosed volume of soil and the reinforcements modifies the shear strain and shear stress fields along the failure surface within this volume of soil, providing a total lateral resistance that can be greater than the lateral resistance provided by a single element times the number of elements (see also Chapter One, Section 3.1.2). However, as this interaction is not yet fully understood, it is not taken into account in current design methods.

3. DESIGN METHODS

3.1 Design Approaches

Because of the inherently different mechanisms and intents, different design approaches have been developed for limit equilibrium unstable slopes and creeping slopes.

The approach developed for potentially unstable slopes considers the general static equilibrium conditions of the nailed slope and its surroundings. Classical slope stability analysis methods, such as the Fellenius or Bishop methods of slices, have been adapted to evaluate the global safety factor with respect to failure along potential sliding surfaces. The analyses take into account the available tensile, shear, and bending resistances of the reinforcements crossing the potential sliding surfaces, as well as the resistance to shearing of the soil.

For creeping slopes, simplified models of interaction between the creeping soil and the inclusions are used, considering a rigid plastic, or viscoplastic, flowing soil, to predict the lateral earth thrust on the inclusion. This method allows an estimate of the decrease of the creep rate of the slope as a function of the decrease in the mobilized shear stresses in the soil. The reduction in mobilized shear forces must, of course, be balanced by the resisting forces developed in the reinforcements.

3.2 Limit Equilibrium Analysis of Unstable Slopes

The general stability analysis method developed by Schlosser [1983] to investigate the global equilibrium of a reinforced soil mass (described in detail in Chapter One of this appendix) can be used, taking into account the available tensile and shear forces in the reinforcements crossing the potential failure surface. The analysis allows for variations in geometry of potential failure surfaces, of the soil profile, and of the arrangement of reinforcements (inclination, spacings, and length).

The nailed slope is considered a composite mass, and failure criteria for the soil, for the reinforcements, and for the interaction between the soil and the inclusions are satisfied. With the exception of group interaction effects, the different mechanisms of soil-inclusion interaction discussed in Section 2 are all considered in this analysis. The method is of particular interest for the design of slope stabilization by small-diameter, flexible inclusions that have to withstand both tensile and shear forces, as it allows evaluation of the relative soil-to-inclusion displacement which is required to mobilize the shear resistance of the reinforcements. To compute this relative soil-to-inclusion displacement, appropriate lateral load transfer curves, which define the pressure, p, on the inclusion as a function of the soil-to-inclusion displacement, y, are required.

In the United States, lateral pile-to-soil stress versus deflection parameters are normally evaluated as so-called p-y curves, where p denotes the stress developed on the pile at the relative pile-to-soil deflection y. The equations for computing p-y parameters are semiempirical in nature and are based on full-scale lateral pile load tests conducted on piles embedded in sands, as well as in soft and stiff clays.

The shapes of the p-y curves are schematically shown on Figure C-66. The method to compute p-y curves in clays is described by Matlock [1970], and the method to compute p-y curves in sands is described by Reese et al. [1974]. The most commonly used computer program for computing p-y curves is known as COM 624.

In Europe, pile-soil stress versus deflection curves are frequently computed directly from pressuremeter test results because of the similarity between the expanding cavity around the pressuremeter and the mobilization of lateral load against a pile subjected to lateral loading [Menard, 1962 and 1969; Baquelin and Jezequel, 1972; Briaud et al., 1983].

With the lateral stress transfer parameters known, the design of soil nailing for a limit equilibrium unstable slope is similar to the design of soil nailing in excavations (Chapter One). A case history illustrating this design approach is presented in Section 4.2.

3.3 Design of Soil Nailing to Stabilize Creeping Slopes Based on Plastic Soil Behavior

The interaction between a plastically deforming sliding ground (i.e., creeping soil) and stabilizing piles has been investigated both theoretically and experimentally [Fukumoto, 1976; Ito and Matsui, 1975 and 1977; Wang and Yen, 1974]. As Yen [1985] is currently reevaluating the boundary condition assumptions of the Wang and Yen [1974] analysis, only the Ito and Matsui analysis is presented below.

Ito and Matsui [1975] suggested two analytic approaches, considering respectively: (1) plastically deforming soil around

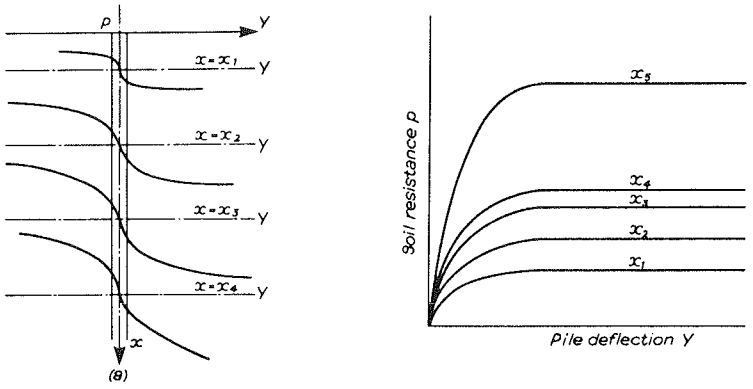

p-y curves for laterally-loaded piles

(a) Shape of curves at various depths x below soil surface

(b) Curves plotted on common axes

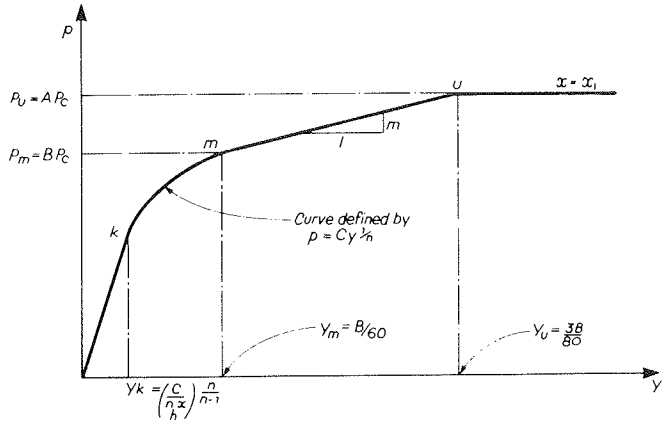

(c) Shape of p-y curve in sand (Reese, Cox and Coop)

Figure C-66. Schematic illustration of p-y curves. [Tomlinson, 1981]

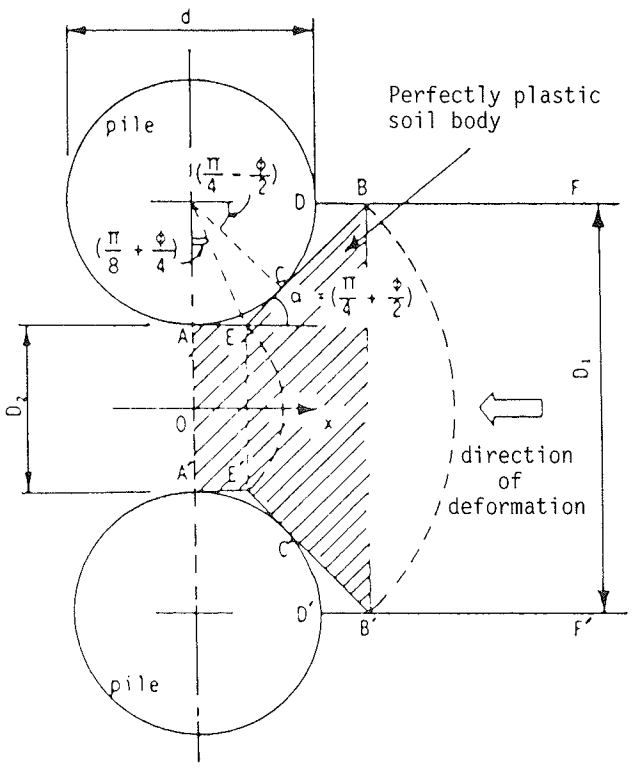

Figure C-67. State of plastic deformation in the ground around piles. [Ito and Matsui, 1975]

the piles (limit analysis approach), and (2) viscoplastic flow of the soil around the piles.

The limit analysis approach, which is considered appropriate only for stiff overconsolidated soils, assumes that the soil just upslope of the piles is in a plastic state (Fig. C-67), and that this soil is a perfectly plastic solid that follows the Mohr-Coulomb yield criterion. The static equilibrium conditions of this plastic solid yield a solution for the lateral force P acting on a unit length of the pile as a function of the pile diameter, the spacings, and the effective strength characteristics of the soil. Typical analytical results based on this method of analysis are shown in Figure C-68. This solution does not take into account soil arching, and no consideration is given to the creep behavior of the sliding ground. Therefore, it cannot be considered valid for normally consolidated, saturated, soft clayey soils.

The viscoplastic flow analysis, intended to be applied in soft soils, assumes that the soil just around the piles behaves as a viscoplastic solid (i.e., as a Bingham solid with a yield stress τ_y and a plastic viscosity η_p) in quasi-steady state of a viscoplastic flow. The sum of the quasi-static lateral force due to the lateral active earth pressure and the viscous shear force due to the soil-pile interaction yields the solution for the lateral force P acting on a unit length of the pile as a function of the pile diameter, the spacings, the soil viscoplastic properties (τ_y and η_p) and the sliding velocity. This second approach incorporates the viscous flow conditions of the creeping soil, but it raises difficulties concerning the boundary conditions at the soil-pile interfaces, the appropriate determination of the viscosity properties of the soil (τ_y and η_p), and the reasonably accurate evaluation of the flow velocity.

3.4 Winter's Pseudostatic Design Approach for Creeping Slopes

More recently, a pseudostatic design approach was proposed by Winter et al. [1983] for creeping cohesive soils. This approach is based on the experimental viscosity law derived by Leinenkugel [1976] for normally consolidated clays and the solution for the horizontal pressure applied by a viscous flowing soil on stabilizing piles [Winter, 1982] presented in Section 2.2.2. It provides a methodology to obtain an optimum design (spacings between the piles and pile geometry) with respect to a required reduction of the sliding rate of the slope, considering the mobilization of an allowable bending moment in the pile.

3.4.1 Design Assumptions

The mechanism of soil-pile interactions considered by Winter et al. [1983] for creeping slopes has been described in Section 2.2.2. The basic assumption is that the mobilized shear stress in the slope equals the shear strength associated with a particular initial strain rate $\dot{\epsilon}_i$. The inclusion of nails reduces the shear stresses in the soil to a lower value. Hence, the slope will creep at a slower rate. If creep continues at this slower rate, the mobilized shear resistance, τ, decreases. The applied shear stress at the failure surface, separating the upper sliding zone which undergoes a monolithic displacement from the creeping zone, stays constant independent of the strain rate. Consequently, equilibrium requirements show that the decrease in the mobilized shear resistance of the soil must be equilibrated by the resisting shear forces developed in the inclusion.

As shown in Section 2.2.2, the reduction of the mobilized shear resistance, $\Delta\tau$, associated with a reduction in strain rate from the initial value, $\dot{\epsilon}_i$, to $\dot{\epsilon}$ is:

$$\Delta\tau = - S_u(\epsilon_i) I_v \log_e \left(\frac{\dot{\epsilon}}{\dot{\epsilon}_i}\right) \qquad \text{(C-46)}$$

It is assumed that each nail or pile has an area of influence (or tributary surface) equal to S_{eq}. For a reduction in mobilized shear resistance in the soil equal to $\Delta\tau$, the nail must support a force equal to $\Delta\tau$ times S_{eq}. This force is balanced by a resisting force, Q, provided by the pile. Hence:

$$Q = S_{eq}\,\Delta\tau = - S_{eq} S_u(\dot{\epsilon}_i) I_v \log_e \left(\frac{\dot{\epsilon}}{\dot{\epsilon}_i}\right) \qquad \text{(C-47)}$$

On the basis of empirical data [Whitman, 1957; Briaud, 1984], it is often assumed that the undrained shear strength of cohesive soils increases by about 10 percent for each $\log_{10}$ cycle increase in strain rate. This corresponds to a viscosity index of about 4 percent. For such soils, Eq. C-47 implies that the rate of creep can be reduced by an order of magnitude if 10 percent of the driving forces are supported by nails.

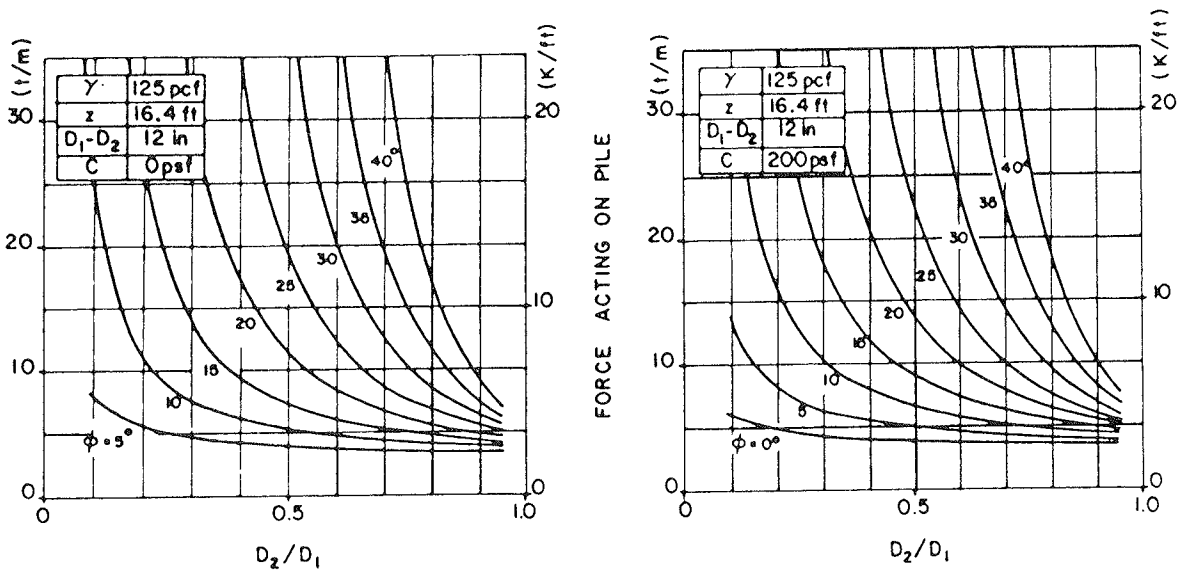

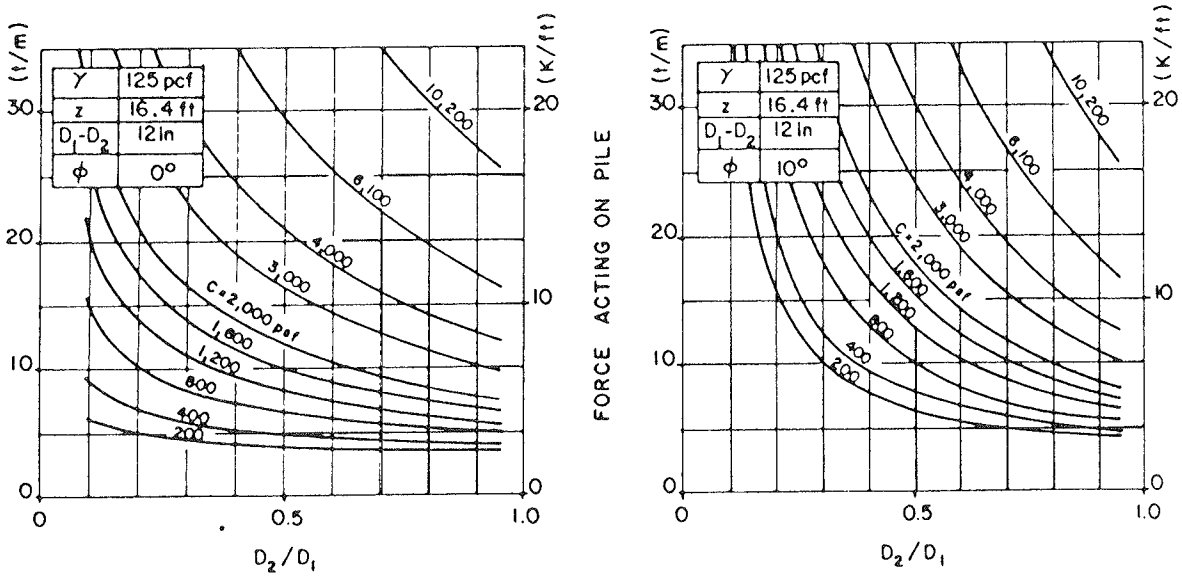

Figure C-68. Typical results of the deformation analysis of a perfectly plastic soil body between rigid piles. [Ito and Matsui, 1975]

An optimal design would satisfy two requirements: (1) The maximum moment, M, in the reinforcement would be practically equal to or near its allowable moment, M_a. (2) The horizontal earth pressure $p(z)$ mobilized on the reinforcement should be high enough so that the shear stress in the soil is sufficiently reduced to result in an acceptable creep rate.

In practice, the upslope/downslope spacing between rows of piles, L, and the diameter, d, of the piles (Fig. C-69) are often dictated by topographical or available construction equipment constraints. Accordingly, the design procedures are aimed at optimizing the spacing between piles in a row perpendicular to the slope, a, and the length of pile embedment below the creeping zone, h.

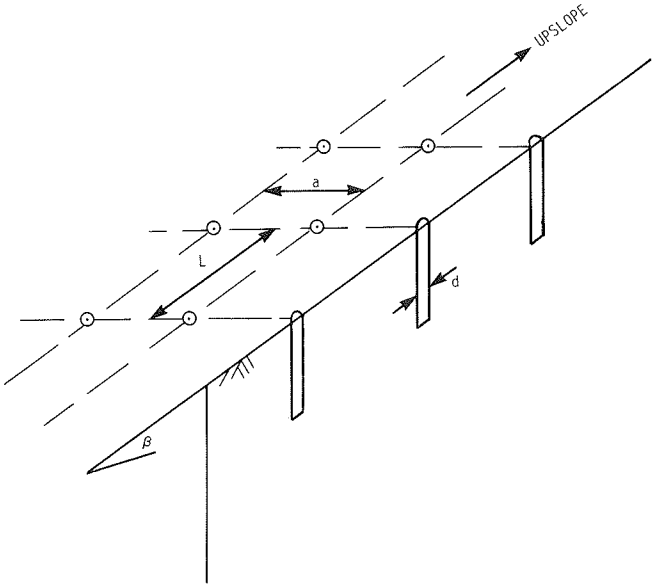

Figure C-69. Definition of spacings a *and* L *and pile diameter* d.

The simplest design procedure is to: (1) Assume the spacing between piles in a row, *a* (Fig. C-69). (2) Calculate the tributary area, S_{eq}, as being equal to row spacing, *a,* times column spacing, *L.* (3) Use Eq. C-47 and the desired reduction in creep rate to compute the shear force exerted on the nail; if the shear resistance of the nail is exceeded, either *a* or *L* can be adjusted. (4) Verify that the allowable bending moment of the nail is not exceeded. To compute the bending moment exerted on the nail, the distribution of the lateral earth pressure on the nail must be known. It can be computed based on simplified bearing capacity methods assuming that the soil undergoes a perfectly plastic flow between the inclusions [Brinch-Hansen, 1961; Wenz, 1963; Fukuoka, 1977b; Ito et al., 1982]. Alternatively, more sophisticated soil-pile interaction methods, such as p-y analyses, or the viscoelastic flow analyses suggested by Ito and Matsui [1975] or Wang and Yen [1974], may be used.

3.4.2 Example of Design Procedure

To illustrate the design procedures, the design case shown on Figure C-70a is considered. The interface between the creeping and noncreeping zones occurs at a depth Z_1, while pile diameter is *d.* The spacing between piles in a row perpendicular to the slope is *a,* while the upslope and downslope spacing between piles is *L,* as shown in Figure C-69. The pile extends a length *h* below the creep and noncreep interface. The entire length *h* is considered effective in transferring load from the creeping to the noncreeping zones, provided this "effective length" is shorter than, or equal to, about three times the transfer length L_o (Eq. C-35).

The upslope and downslope spacing, *L,* and pile diameter, *d,* are assumed given, while row spacing, *a,* and effective length, *h,* are considered design variables to be optimized.

The simplified Brinch-Hansen pressure diagram shown on Figure C-70b is constructed so that it is symmetrical, but of opposite direction, around the interface between the creeping and noncreeping zone. Also, the magnitude of force exerted on the pile per unit length, *P,* is constant with depth, i.e., *P* does not increase or decrease within the zone defined by the effective lengths of pile on either side of the creeping and noncreeping interface.

The dimensions x_o and y_o are defined as shown in Figure C-70b so that $x_o + y_o = h$.

In accordance with the pressure diagram, the bending moment

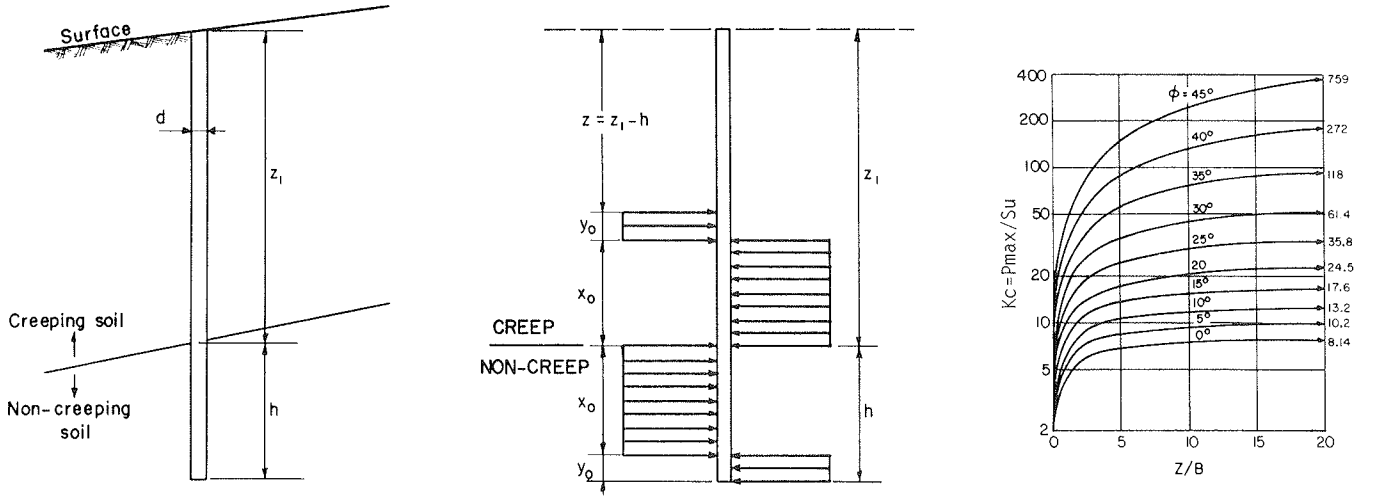

a) Design conditions

b) Idealized pressure diagram (Brinch-Hansen theory)

c) Lateral bearing capacity factors (Brinch-Hansen, after Tomlinson, 1981)

Figure C-70. Parameters for design example.

in the pile at the creeping and noncreeping interface must be zero. Hence:

$$Py_o\left(\frac{y_o}{2} + x_o\right) = P\left(\frac{x_o^2}{2}\right) \quad \text{(C-48)}$$

With $x_o + y_o = h$, x_o and y_o can be shown to equal 0.707 h and 0.293 h, respectively. Thus the total shear force transmitted from the creeping to the noncreeping zone by a single pile, Q_s, is:

$$Q_s = P(0.707 - 0.293)h = 0.414\ Ph. \quad \text{(C-49)}$$

For convenience in using design diagrams developed by Winter et al. [1983], Eq. C-49 is written:

$$Q_s = P(\eta h) \quad \text{(C-50)}$$

By constructing a bending moment diagram, it can be shown that the maximum bending moment acting on the pile is:

$$M_{max} = 0.085\ Ph^2 \quad \text{(C-51)}$$

which, for convenience, is written:

$$M_{max} = P(\lambda h)^2 \quad \text{(C-52)}$$

where $\lambda = 0.292$.

To optimize a and h, the maximum bending moment in the pile, M_{max}, should equal the allowable bending moment, M_a. Hence, from Eq. C-52:

$$P(\lambda h)^2 = M_a \quad \text{(C-53)}$$

From Eq. C-50, Eq. C-53 may be rewritten as:

$$\frac{Q_s}{\eta h}(\lambda h)^2 = M_a \quad \text{(C-54)}$$

while, from Eq. C-47:

$$Q_s = -S_u(\dot{\epsilon}_i)I_v\ a\ L\ \log_e\left(\frac{\dot{\epsilon}}{\dot{\epsilon}_i}\right) \quad \text{(C-55)}$$

Hence:

$$-\left[S_u(\dot{\epsilon}_i)I_v\ a\ L\ \log_e\left(\frac{\dot{\epsilon}}{\dot{\epsilon}_i}\right)\right]\frac{\lambda^2}{\eta}h = M_a \quad \text{(C-56)}$$

From Eq. C-50, Eq. C-55 can be rewritten as:

$$P = \frac{-S_u(\dot{\epsilon}_i)I_v\ a\ L\ \log_e\left(\frac{\dot{\epsilon}}{\dot{\epsilon}_i}\right)}{\eta h} \quad \text{(C-57)}$$

Equations C-55, C-56, and C-57 contain three unknowns, i.e., the force per unit length of pile, P, the spacing between piles in a row, a, and the effective pile length, h.

By assuming a value for h, the value of P can be obtained from the Brinch–Hansen design curves showing the bearing capacity factor K_c (which is defined as the ratio of maximum-lateral earth stress on the pile, P_{max} to undrained strength, S_u) to be applied to shear strength. These curves are shown in Figure C-70c. The depth at the top of the effective height of the pile ($z = Z_1 - h$ in Fig. C-70b) should be used for selecting the bearing capacity factor.

With P and h known, a can be computed from Eq. C-56, while Eq. C-55 may be used to verify that the shear strength of the pile is not exceeded. The h, P, and a values can then be optimized with an iterative procedure. The optimal situation is obtained when the selected value of h and the calculated values of P and a approximately satisfy Eq. C-57. Winter et al. [1983] present a design chart for this process.

3.4.3 Alternate Design Approaches

The design procedure previously outlined is based on simplifying assumptions regarding the distribution of both strain (or strain rate) with depth and also the pressure developed on the pile with depth. It is known that the lateral pressure developed on a pile is dependent on the relative pile-to-soil deflection. Hence, the Brinch–Hansen pressure diagram may not be entirely valid, unless the soil around the pile has reached the state of plastic flow.

To eliminate these assumptions, Winter [1982] generalized Eq. C-42 and performed numerical analyses to evaluate the force P per unit length of pile. To use his solution, it is necessary to know both the initial relative velocity between the soil and the pile, and the initial rate of creep distortion as functions of depth.

Gudehus [1983] developed a design approach based on viscous principles. His analyses are based on the assumptions (1) that the total lateral earth thrust resisted by a number of piles is proportional to the displacement of the creeping mass, (2) that the lateral earth thrust resisted by each pile is equal to the shear force in the pile, and (3) that the shear force in each pile, which is assumed to be equal in all piles, corresponds to the average decrease in mobilized shear resistance in the soil. By computing the displacement field of the creeping soil, and using p-y parameters, he evaluated allowable displacement and sliding rate at a design time after nail installation.

In view of the difficulties associated with evaluating the parameters required for Winter's solution, and the uncertainties of p-y functions in soil subject to creep, the simpler design approaches outlined in Section 3.4.2 appear adequate for practical design. This is especially true when it is considered that additional nails can always be installed if the initial nailing does not adequately reduce the rate of creep.

4. CASE HISTORIES

4.1 Paris-Lyon Railway Embankment [GUILLOUX AND SCHLOSSER, 1984]

About 50 years ago near Yerres, France, the main line of the railway between Paris and Lyon was widened from two to four tracks. However, the "new" embankment experienced large settlements during subsequent years. By the late 1970's nearly 6 ft of ballast and granular materials had been placed under the two new tracks in an attempt to maintain grade. In early 1979, an inclinometer casing was installed at the toe of the embankment, and significant movements were observed; the probable failure surface was detected at a depth of about 10 ft.

A cross section of the embankment showing the various soil layers is shown in Figure C-71, while the location of inclinometer casing and the five rows of nails installed as a remedial measure are shown in Figure C-72. Both the old and new embankments were built directly on the natural ground surface as shown in Figure C-71. The natural soil profile consisted of about 5 ft of top soil, 10 ft of green clays and colluvium, and then marl. The new embankment was constructed of marls and green clays. From a back analysis of the sliding mass and assuming a factor of safety of one, it was possible to evaluate in-situ values of the soil strength parameters assuming fully drained conditions. These parameters were:

New Embankment	Green Clays and Colluvium
$\gamma = 127$ pcf	$\gamma = 127$ pcf
$\phi' = 20°$	$\phi' = 15°$
$c' = 0$	$c' = 0$

The stabilization system consisted of 2-in. diameter perforated steel tubes driven vertically about 5 ft apart up the slope (Fig. C-72b) and at a spacing of 11 ft along the slope. Steel rods of 0.6 in. diameter were then inserted into the perforated tubes and grouted at a pressure of 44 psi. From the grout quantities, it was possible to determine that the average diameter of each nail was about 6 in. The theoretical value of EI used in the stability analysis was 208 psi, with an allowable maximum bending moment of 8,848 lb-ft. The shearing resistance mobilized in each nail was calculated to be about 4,500 to 5,625 lb.

The limiting lateral pile resistance value and soil-spring value used for the embankment materials as well as the natural green clays and colluvium were 10.4 and 167 kip/ft^2, respectively, as interpreted from pressuremeter tests.

Using the computer program TALREN (developed by Terrasol), it was possible to determine that the factor of safety with the nailing installed was 1.38. Inclinometer measurements made for 9 months after installation of the nails showed that the rate of movement of the slope had decreased significantly, and, for the last 3 months of measurements, it had virtually ceased (Fig. C-73).

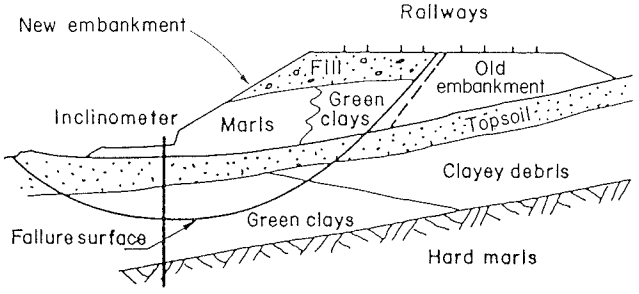

a) SNCF embankment: geotechnical cross-section

Figure C-71. SNCF embankment—geotechnical cross-section. [Guilloux and Schlosser, 1984]

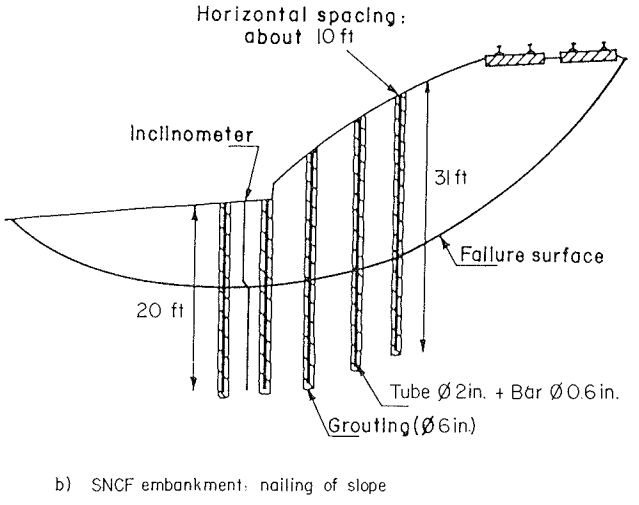

b) SNCF embankment: nailing of slope

Figure C-72. Example of a sliding slope stabilization by nailing. [Guilloux and Schlosser, 1984]

4.2 Large-Diameter Piles [Cartier and Gigan, 1983]

An example of stabilization of a sliding slope by using large-diameter rigid piles is described by Cartier and Gigan [1983]. The cross-section geometry and soil conditions are shown in Figure C-74. In this case, the reinforcement was limited to three rows of cast-in-place concrete piles (16 in. diameter, reinforced by steel H-piles), which were located near the toe of the sliding slope. A rather simple design procedure was developed to assess the effect of the reinforcement on the global safety factor with respect to failure, taking into account the admissible displacement for the stability of the structure. This case illustrates the application of the design approach discussed in Section 3.2 (an analysis under limit equilibrium unstable conditions).

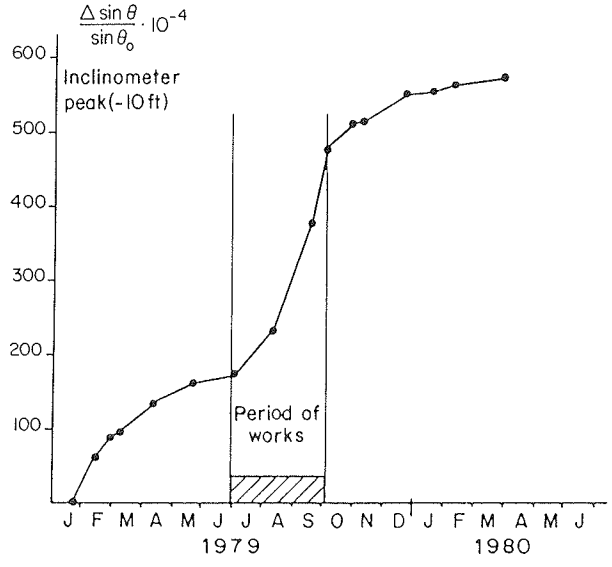

Figure C-73. Inclinometer movements recorded prior and subsequent to nailing. [Guilloux and Schlosser, 1984]

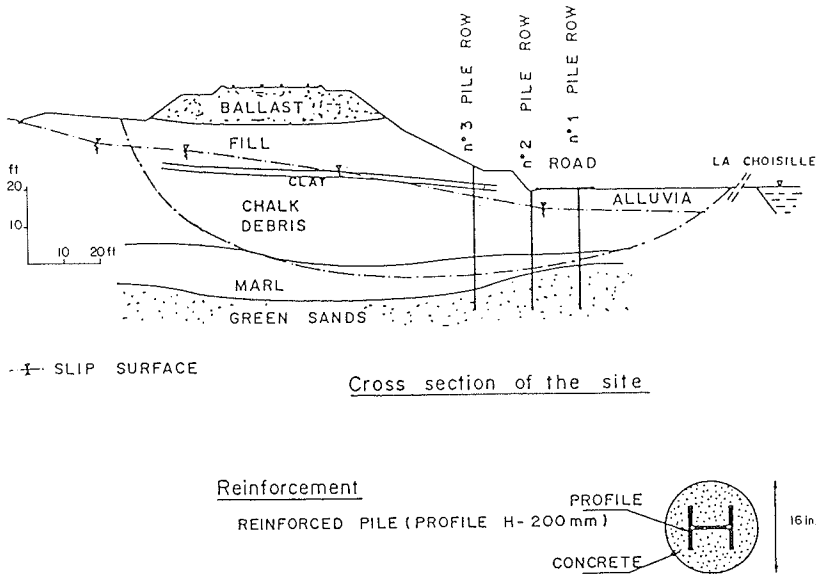

Figure C-74. Example of limit equilibrium slope stabilization. [Cartier and Gigan, 1983]

The principles of the design procedure used by Cartier and Gigan are shown in Figure C-75. It was assumed that the lateral earth pressure exerted by the sliding slope on the pile results in the mobilization of shear forces and bending moments. The shear forces were calculated assuming that the pile was supported by a lateral series of elastoplastic supports (similar to p-y analyses, but deduced from pressuremeter results) and that it was subject to bending loads causing a relative soil-to-pile displacement of $y(z) - g(z)$, where $y(z)$ and $g(z)$, respectively, are the horizontal displacements of the pile and of the soil away from the pile. This approach is similar to that followed in p-y analyses, but the reaction curve of the elastoplastic support ($p(z) = f(y(z) - g(z))$ was deduced from pressuremeter test results. The elastic solution for this laterally loaded pile provided the estimate of the shear force, V, and bending moment, M, in the pile as a function of its relative displacement in the soil.

The safety factor of the reinforced slope with respect to circular sliding was calculated as:

$$F = F_i + \Delta F \qquad \text{(C-58)}$$

where $F_i = M_R/M_D$ is the initial factor of safety before stabilization. Because the slope is unstable, it is assumed to be unity. M_R is the resisting moment due to the shear strength of the soil (Fig. C-75). M_D is the driving moment (Fig. C-75). ΔF is the additional safety factor due to the reinforcement which is given by:

$$\Delta F = \frac{VR\cos\beta - M}{M_D} \qquad \text{(C-59)}$$

where V is the shear force developed in the pile at point A; M is the bending moment in the pile at point A; R is the radius of the sliding surface; and β is the angle between a line perpendicular to the pile and the failure surface (Fig. C-75).

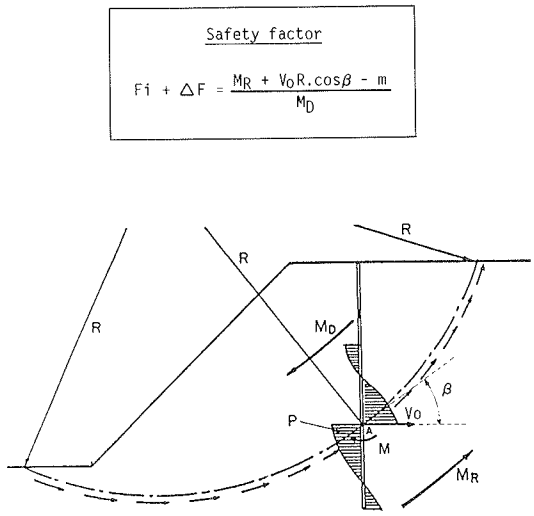

Figure C-75. Slope stabilization by nailing—design principles. [Cartier and Gigan, 1983]

Finally,

$$F = \frac{M_R + VR\cos\beta - M}{M_D} \qquad \text{(C-60)}$$

where F is the factor of safety after stabilization.

Thus, this design procedure enables a simultaneous verification of the four criteria: (1) improvement of the slope safety, $\Delta F/F_i = 20$ percent; (2) normal soil pressure on the pile which has to be less than the yield pressure p_f measured in the pressuremeter test (this is equivalent to a limit p-value in a p-y curve which can be taken as about the ultimate value, p_{ult}); (3) strength of the pile considering an allowable bending moment for the reinforcing materials; and (4) permissible displacement for structures installed on the slope.

The design, using an iterative procedure for optimization, suggested a first alternate with a pile spacing of 31 in. in one row and a second alternate with a pile spacing of about 6.6 ft in three rows. The latter alternate was selected. It should be noted that the design procedure did not take into account any group effect because of the relatively large spacing between the piles.

Cartier and Gigan also reported the measurements of the lateral displacements as measured by inclinometer over a period of 2 years. These measurements demonstrated a gradual stabilization of the slope and a significant decrease of the sliding rate from 4 in. per year prior to stabilization to 0.1 in. per year. The measurements of the deflections of the three rows of piles enabled a backcalculation of the shear forces and bending moments in the piles, an example of which is shown in Figure C-76. It was observed that the lateral earth pressure on the pile was significantly less than the yield pressure of the soil and that the stabilization was obtained with a relatively small increase of the factor of safety.

The pile forces and moments backcalculated from the inclinometer deflections indicated an increase in factor of safety of about 7 percent.

4.3 Stabilization of a Natural Slope under an Embankment, Stahlberg, Germany [Sommer, 1979]

A case history of slope stabilization by large-diameter piles described by Sommer [1979] illustrates the design concepts associated with Winter's design approach (see Sec. 3.4.2). The slope geometry and soil properties are shown in Figure C-77. The 33-ft thick portion of the clayey slope was creeping at a rate of 0.55 in./month. To stabilize the creeping, a row of 10-ft-diameter ferro-concrete piles was installed with a spacing of 30 ft. The ground movement and the position of the shear zone were monitored by inclinometer measurements (Fig. C-78a). The measured lateral earth pressure on the dowel is shown in Figure C-78b.

The following slope data were used in the design: inclination of the failure surface, $\beta = 7°$; depth of the failure surface below the initial ground surface, $z_1 = 50$ ft; initial sliding velocity, $v_i = 0.6$ in./month; length of failure surface, 430 ft.

Soil characteristics (see Fig. C-77) used in the design were $S_u(\dot{\epsilon}_i) = 840$ psf, $\gamma = 134$ pcf, $W_1 = 60$ percent, and $I_v = 3$ percent.

Pile diameter was 9.9 ft, while spacing was equal to 3 pile diameters.

The actual design did not allow entire mobilization of the allowable bending moment of these large-diameter piles and, therefore, the Brinch–Hansen diagram cannot be used. Furthermore, as shown in Figure C-78b and discussed below, the field measurements indicated that the measured lateral earth pressure on the pile was lower than the values calculated using the Brinch–Hansen equations. Rather than being constant with depth, as implied by the Brinch–Hansen solution, the measured pressures on the pile increased nearly linearly with depth and a triangular earth pressure distribution with an effective height, h_{eff}, of about 43 ft above the failure surface could be considered.

In accordance with the principles outlined in Section 4.3.2, the expected lateral earth pressure on the pile would have been about 7.5 S_u. This is because the ratio of $(z_1 - h)/d$ was about 5 (see Section 3.4.2 and Fig. C-71c). In fact, the field-measured ratio was about 4.5 (Fig. C-78b).

From Eq. C-55, the reduction in strain rate associated with the forces mobilized in the pile can be computed as:

$$\log_e\left(\frac{\dot{\epsilon}}{\dot{\epsilon}_i}\right) = \frac{Q_s}{S_u\,(\dot{\epsilon}_1)\,I_v a L} = \frac{\frac{1}{2}\,P_{max}\,h_{eff} d}{S_u(\dot{\epsilon}_1)\,I_v a L} \approx 2.5 \qquad \text{(C-61)}$$

With the values cited for shear strength, viscosity index, pile diameter, pile spacing, and maximum pressure on the pile in conjunction with an assumed L value equal to the length of the sliding zone (427 ft), the ratio $\dot{\epsilon}/\dot{\epsilon}_i$ backcalculated from Eq. C-61 is about 0.08. The actual ratio, as reported by Sommer [1979], was about 0.1, which is in reasonably good agreement.

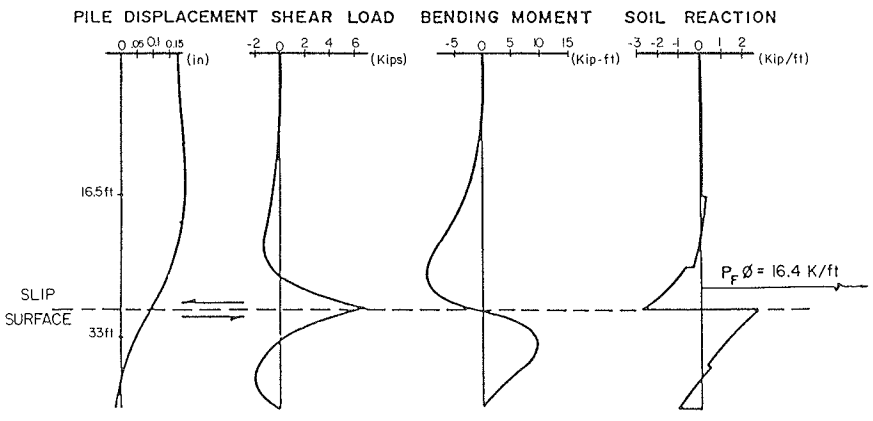

Figure C-76. Measured displacement profile and back-calculated lateral soil reaction, shear forces, and bending moments in the inclusions. [Cartier and Gigan, 1983]

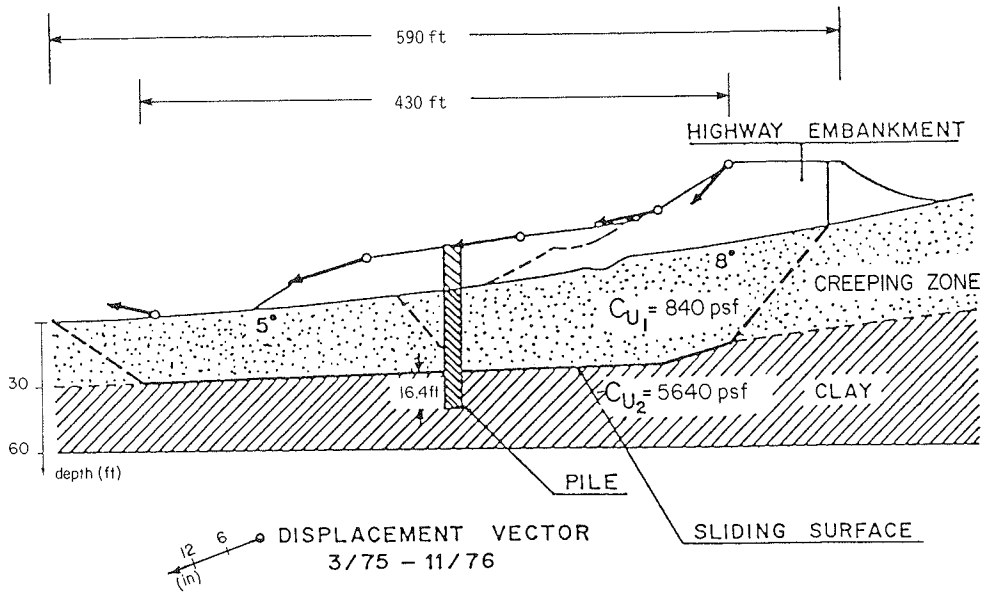

Figure C-77. Sliding slope stabilization by large-diameter piles. [Sommer, 1979]

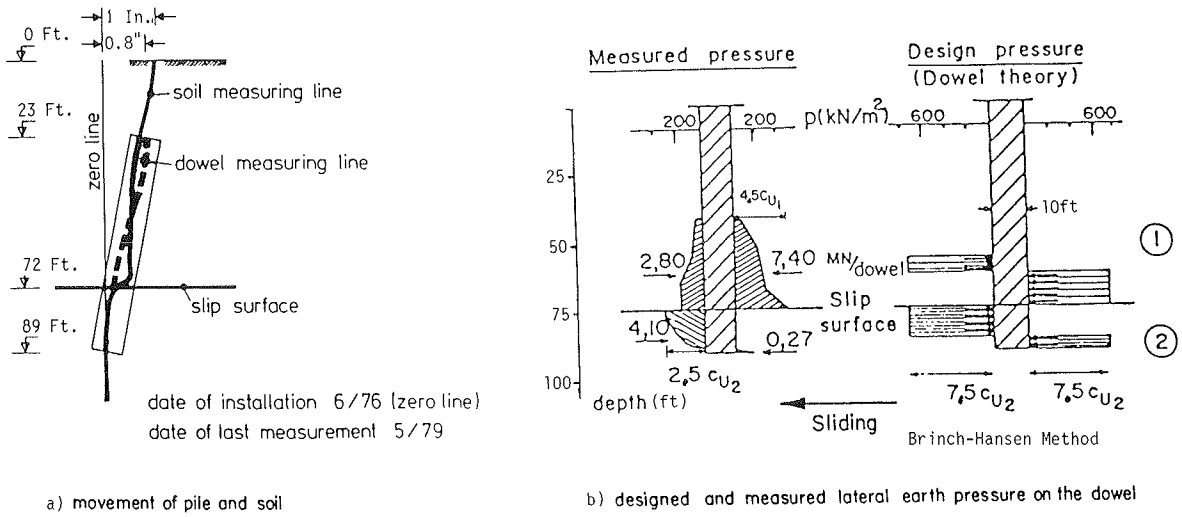

Figure C-78. Sliding slope stabilization by large-diameter piles—design and observations. [Sommer, 1979]

5. CONCLUSIONS

Potentially unstable slopes can be designed in a manner similar to soil nailing in excavations. The design methodology for creeping slopes does not yet take all mechanisms into account. Hence, this methodology should be viewed as an approximate way to get spacings and numbers of piles, rather than as an exact design.

It should be remembered that displacement is required to mobilize reinforcing forces. In creeping slopes it may take a long time for these forces to be fully in effect. Consequently, it may not appear as if much has been accomplished immediately after insertion.

To further develop and improve design techniques, more full-scale field measurements and laboratory data are needed.

6. REFERENCES

BAGUELIN, F., and JEZEQUEL, J. F. [1972]. "Etude Experimentale du Comportement des Pieux Sollicites Horizontalement," *Bull. de Liaison des Laboratoires des Ponts et Chaussees,* No. 62.

BAKER, R. F., and YODER, E. J. [1958]. "Stability Analyses and Design of Control Works in Landslides and Engineering Practice," *HRB Special Report 29,* National Research Council, Washington, D.C., pp. 189–216.

BRIAUD, J. L., GARLAND, E., and FELIO, G. Y. [1984]. "Rate of Loading Parameters For Vertically Loaded Piles in Clay," *Proc. Offshore Technology Conference,* OTC 4694, Houston.

BRIAUD, J. L., SMITH, T., and MEYER, B. [1983]. "Pressuremeter Gives Elementary Model for Laterally Loaded Piles," *Proc. International Symposium on In Situ Testing,* Ecole Nationale des Ponts et Chaussees, Paris, Vol. 2.

BRINCH-HANSEN, J., and LUNDGREN, H. [1960]. *Hautprobleme der Bodenmechanick—Berlin,* Springer-Verlag, Berlin.

BRINCH-HANSEN, J. [1961]. "The Ultimate Resistance of Rigid Piles Against Transversal Forces." *Bull.,* Danish Geotechnical Institute, No. 12.

BROMS, B. B. [1964]. "Lateral Resistance of Piles in Cohesive Soils," *ASCE J. Soil Mech. Found. Div., Proc.,* Vol. 90, SM2, pp. 27–63.

CARTIER, G., and GIGAN, J. P. [1983]. "Experiments and Observations on Soil Nailing Structures.," *Proc. 8th European Conference on Soil Mechanics and Foundation Engineering,* Helsinki.

FUKUMOTO, Y. [1972]. "Researches on the Behavior of Piles for Preventing Landslides," *J. JSSMFE,* Vol. 12, No. 2, pp. 61–73.

FUKUMOTO, Y. [1976]. "The Behavior of Piles for Preventing Landslides," *J. JSSMFE,* Vol. 16, No. 2, pp. 91–103.

FUKUOKA, M. [1977b]. "The Effect of Horizontal Loads on Piles due to Landslides," *Proc. 9th International Conference on Soil Mechanics and Foundation Engineering,* Specialty Session 9, Tokyo, pp. 1–16.

GRAY, D. H. [1978]. "Role of Woody Vegetation in Reinforcing Soils and Stabilizing Slopes," *Symposium on Soil Reinforcement and Stabilizing Techniques,* pp. 253–306, Sydney.

GUDEHUS, G. [1983]. "Design Concept for Pile Dowels in Clay Slopes," *Proc. 8th European Conference on Soil Mechanics and Foundation Engineering,* Discussion, Specialty Session 5, Helsinki, Vol. 3.

GUDEHUS, G., and LEINENKUGEL, H. J. [1978]. "FlieBdruck und Fließbewegungen in Bindigen Boden: Neue Methoden, Vortrage Baugrundtagung, Berlin.

GUILLOUX, A., SCHLOSSER, F. [1984]. "Soil Nailing Practical Applications," *Symposium on Soil and Rock Improvement Techniques,* A.I.T.

ITO, T., and MATSUI, T. [1975]. "Methods to Estimate Lateral Force Acting on Stabilizing Piles," *J. JSSMFE,* Vol. 15, No. 4, pp. 45–59.

ITO, T., and MATSUI, T. [1977]. "The Effect of Piles in a Row on the Slope Stability," *Proc. 9th International Conference on Soil Mechanics and Foundation Engineering,* Spec. Sess. 10, Tokyo, pp. 81–86.

ITO, T., MATSUI, T. and HONG, W. P. [1982]. "Earth Pressures on Piles in a Row Due to Lateral Soil Movements," *J. JSSMFE,* Vol. 22, No. 2, Tokyo, pp. 71–81.

JEWELL, R. A. [1980]. Dissertation submitted for the Degree of Doctor of Philosophy at Cambridge University.

JURAN, I., SCHLOSSER, F., LOUIS, C., KERNOA, M. and ECKMANN, B. [1981]. "Soil Reinforcing by Passive Bars," *Proc. 10th International Conference on Soil Mechanics and Foundation Engineering,* Stockholm.

JURAN, I., SHAFIEE, S., SCHLOSSER, F., HUMBERT, P. and GUENOT, A. [1983]. "Study of Soil-Bar Interaction in the Technique of Soil Nailing," *Proc. 8th European Conference on Soil Mechanics and Foundation Engineering,* Helsinki.

KERISEL, J. [1976]. "Theorie du Clouage et Application au Pont de Puteaux," Rapport Interne SIMECSOL, Paris.

LEINENKUGEL, H. J. [1976]. "Deformations und Festigkeitsver Halten Bindiger Erdstoffe," Experimentelle Ergeßnisse und Ihre Physikalische Deutung Veroffentl. Inst. f. Bodenmech. u. Felsmech. 66, Karlsruhe.

MATLOCK, H., and REESE, L. C. [1960]. "Generalized Solutions for Laterally Loaded Piles," *ASCE J. Soil Mechanics and Foundations,* ASCE 86.

MATLOCK, H. [1970]. "Correlations for Design of Laterally Loaded Piles in Soft Clay," *Offshore Technology Conference,* Paper No. OTC 1204.

MENARD, L. [1962]. "Comportement d'une Fondation Profonde Soumise a des Efforts de Renversement," Sols—Soils 3.

MENARD, L. et al. [1969]. "Regles d'Utilisation des Techniques Pressiometriques et d'Exploitation des Resultats Obtenus pour le Calcul des Fondations. Contraintes et Deformations dans un Pieu Soumis a des Efforts Horizontaux," Notice Speciale No. 2 D/62/69, Centre d'Etudes Geotechniques, Paris.

REESE, L. C., COX, W. R., and KOOP, F. B. [1974]. "Analysis of Laterally Loaded Piles in Sand," *Proc. Offshore Technology Conference,* Houston, Texas, Paper No. OTC 2080.

SOMMER, H. [1977]. "Creeping Slope in a Stiff Clay," *Proc. 9th International Conference on Soil Mechanics and Foundation Engineering,* Specialty Session 10, Tokyo, pp. 113–118.

SOMMER, H. [1979]. "Stabilization of Creeping Slope in Clay with Stiff Element" *Proc. 7th European Conference on Soil Mechanics and Foundation Engineering,* Brighton, U.K.

TOMLINSON, M. J. [1981]. "Pile Design and Construction Practice," Viewpoint Publications, London.

VERRIER, G., and MERLETTE, P. [1981]. "Construction des Remblais Ferroviaires, une Technique Particuliere: Le Clouage," Travaux, March.

WANG, W. L., and YEN, B.C. [1974]. "Soil Arching in Slopes," ASCE, *J. Geotech. Eng. Div.,* Vol. 100, No. GTl, pp. 61–78.

WENZ, K. P. [1963]. "Uber die Große des Seitendrucks auf Pfahle in Bindigen Erdstoffen," Veroffentl. Inst. f. Bodenmech. u. Felsmech., 12, Karlsruhe.

WHITMAN, R. V. [1957]. "The Behavior of Soils Under Transient Loadings," *4th International Conference on Soil Mechanics and Foundation Engineering,* Longon, Vol. I, p. 207.

WINTER, H., [1982]. "Similarity Analysis for Numerical Methods in Geomechanics," *Proc. 4th International Conference Num. Meth. Geomech.,* Edmonton.

WINTER, H., SCHWARZ, W., and GUDEHUS, G. [1983]. "Stabilization of Clay Slopes by Piles," *Proc. 8th European Conference on Soil Mechanics and Foundation Engineering,* Helsinki, Vol. 2.

YAMADA, G., WATARI, M. and KOBASHI, S. [1971]. "Phenomena and Countermeasures of Landslides," Sankaido, pp. 338–339.

YEN, B. C. [1985]. Telephone communications with W.C.B. Villet.

APPENDIX D

BIBLIOGRAPHY

REINFORCED EARTH

Alimi, I., Bacot, J., Lareal, P., Long, N. T., and Schlosser, F. [1977]. "Etude de l'Adherence Sols-Armatures," *Proc. 9th International Conference on Soil Mechanics and Foundation Engineering,* Tokyo, July, Session 1/3, pp. 11–14.

Al-Yassin, Z., and Hermann, L. R. [1979]. "Finite Element Analysis of Reinforced Earth Walls," *International Conference on Soil Reinforcement: Reinforced Earth and Other Techniques,* Paris, March, Vol. I.

American Society of Civil Engineers [1978]. "Soil Improvement: History, Capabilities and Outlook," Report by the Committee on Placement and Improvement of Soils of the Geotechnical Engineering Division, February, p. 182.

Bassett, R. H., and Last, M.C. [1978]. "Reinforcing Earth Below Footings and Embankments," *Proc. ASCE Symposium on Earth Reinforcement,* Pittsburgh, April, pp. 202–231.

Boden, J. B., Irwin, M. J., and Pocock, R. G. [1977]. "Construction of Experimental Reinforced Earth Wall at the TRRL Symposium on Reinforced Earth and Other Composite Soil Techniques," Edinburgh, *Supplementary Report No. 57,* Transport Research Laboratory, U.K.

Chang, J. C., Beaton, J. L., and Forsyth, R. A. [1974]. "Design and Field Behavior of the Reinforced Earth Embankment—California Highway 39," presented at the Jan. 21–25, 1974, ASCE National Water Resources Engineering Meeting, held at Los Angeles, California, and submitted to the *ASCE J. Geotech. Eng. Div.* for publication.

Colloque International sur le Renforcement des Sols: Terre Armee et Autres Techniques, Association Amicale des Ingenieurs Anciens Eleves de l'Ecole National des Ponts et Chaussees, Paris, March.

Corte, J. F. [1977]. "La Methode des Elements Finis Appliquee aux Ouvrages en Terre Armee," *Bull. de Liaison des Laboratoires des Ponts et Chaussees,* No. 90.

Darbin, M. [1979]. "Developpements de la Terre Armee dans le Monde," *International Conference on Soil Reinforcement: Reinforced Earth and Other Techniques,* Paris, March, Vol. I.

Elias, V., and McKittrick, D. P. [1979]. "Special Uses of Reinforced Earth in the United States," *International Conference on Soil Reinforcement: Reinforced Earth and Other Techniques,* Paris, March, Vol. I.

Hausmann, M. R. [1976]. "Strength of Reinforced Earth," *ARRB Proc.,* Vol. 8.

Hausmann, M. R., and Lee, K. L. [1978]. "Rigid Model Walls with Soil Reinforcement," *Proc. ASCE Symposium on Earth Reinforcement,* Pittsburgh, Apr. 27, 1978, pp. 400–428.

Haviland, J. E., Bellair, P. J., and Morrel, V. D. [1968]. "Durability of Corrugated Metal Culverts," *Highway Research Record 242,* HRB, National Research Council, Washington, D.C.

Juran, I. [1983]. State-of-the-Art Report "Reinforced Soil Systems—Application in Retaining Structures," *7th Asian Regional Conference on Soil Mechanics and Foundation Engineering,* Haifa.

Juran, I., and Schlosser, F. [1979]. "Etude Theorique des Efforts de Traction Developpes dans les Armatures des Ouvrages en Terre Armee," *International Conference on Soil Reinforcement: Reinforced Earth and Other Techniques,* Paris, March, Vol. I.

King, R. A., Nabisadeh, H., Clarke, A. J. P., and Dawson, J. L. [1979]. "Studies on the Corrosion of Metals in Reinforced Earth," *International Conference on Soil Reinforcement: Reinforced Earth and Other Techniques,* Paris, March, Vol. II.

Leonard, R., Hermann and Zaynab, Al-Yassin [1978]. *ASCE Symposium on Earth Reinforcement,* Pittsburgh.

Long, N. T., Schlosser, F., Guegan, Y., and Legeay, G. [1973]. "Etude des Murs en Terre Armee sur Modeles Reduits Bidimensionnels," Laboratoire des Ponts et Chaussees, *Rapport de Recherche 30,* 1974.

Proc. Symposium on Soil Reinforcing and Stabilizing Techniques, University of New South Wales, Sydney, Oct. 16, 1978.

Proc. 7th European Conference on Soil Mechanics and Foundation Engineering, Design Parameters in Geotechnical Engineering, Brighton, U.K., Sept. 1979.

Reinforced Earth Structures [1980]. "Recommendations and Rules of the Art," French Ministry of Transport, August, Translation.

Richardson, G. N. [1976]. "The Seismic Design of Reinforced Earth Walls," Soil Mechanics Laboratory, *Report 7699,* University of California, Los Angeles.

Richardson, G. N., and Lee, K. L. [1975]. "Seismic Design of Reinforced Earth Walls." *ASCE J. Soil Mechanics and Foundation Division,* Vol. 101, No. GT2, pp. 167–188.

Romanoff, J. (1957). "Underground Corrosion," *National Bureau of Standards Circular 579.*

Symposium on Earth Reinforcement, *Proc.,* ASCE Annual Convention, Pittsburgh, Apr. 1978.

Symposium on Soil Reinforcement: Reinforced Earth and Other Techniques, Paris, Mar. 1979.

Schlosser, F. [1972]. "La Terre Armee dans l'Echangeur de Sete," *Revue Generale des Routes et des Aerodromes,* No. 480, Oct. 1972.

Schlosser, F. [1972]. "La Terre Armee—Recherches et Realisations," *Bull. de Liaison des Laboratoires des Ponts et Chaussees,* No. 62, Nov.-Dec.

Schlosser, F., and Guilloux, A. [1981]. "Le Frottement dans le Renforcement des Sols," *Revue Francaise de Geotechnique,* No. 16.

Schlosser, F., and Juran, I. [1979]. General Report, Session No. 8, "Design Parameters for Artificially Improved Soils," *Proc. 7th European Conference on Soil Mechanics and Foundation Engineering,* Brighton, U.K., September.

Schlosser, F., Juran, I., and Jacobsen, R. M. (1983). "Soil Reinforcement," General Report, *8th European Conference on Soil Mechanics and Foundation Engineering,* Helsinki.

Schlosser, F., and Long, N. T. [1972]. "Comportement de la Terre Armee dans les Ouvrages de soutenement," *Proc. 5th European Conference on Soil Mechanics and Foundations,* 1 (111a-9), pp. 299–306.

Schlosser, F., and Long, N. T. [1973]. "Etude due Comportement du Materiau Terre Armee," *Annales de l'Institut Technique du Batiment et des Travaux Publics,* Serie: Materiaux, No. 45, April.

Schlosser, F., and Long, N. T. [1974]. "Recent Results in French Research on Reinforced Earth," *ASCE J. Construction Division,* Vol. 100, No. C03, Proc., Paper 10800, Sent., pp. 223–237.

Schlosser, F., and Vidal, H. [1969]. "La Terre Armee," *Bull. de Liaison Laboratoires Routiers Ponts et Chaussees,* Ref. 797, pp. 101–144.

Vidal, H. [1966]. "La Terre Armee,"*Annales de l'Institut Technique du Batiment et des Travaux Publics,* Paris, Nos. 223–229, Jul.–Aug., pp. 888–938.

Westergaard, H. M. [1938]. "A Problem of Elasticity Suggested by a Problem in Soil Mechanics Contrib. Mechanics of Solids," Timoshenko 60th Anniversary Vol., Macmillan, New York.

Yang, Z. [1972]. "Strength and Deformation Characteristics of Reinforced Sand," Ph.D. Dissertation, University of California at Los Angeles, 235 pp.

GEOTEXTILES

Bell, A. L., and Green, H. M., [1982]. "Factors Influencing the Selection of Woven Polypropylene Geotextiles for Earth Reinforcement," *Proc. 2nd International Conference on Geotextiles,* Las Vegas, Vol. III, p. 689.

Woodward-Clyde Consultants Project Files [1983].

WELDED WIRE WALL AND REINFORCED SOIL EMBANKMENT

Anderson, L. R. [1984, 1985]. Associate Dean, USU College of Engineering, Logan, Utah, personal communication.

Hannon, J. B., and Forsyth, R. A. [1984]. "Performance of an Earthwork Reinforcement System Constructed with Low Quality Backfill," Presented at the 63rd Annual Meeting of the Transportation Research Board, Washington, D.C.

Hilfiker, W. K. [1984, 1985]. Hilfiker Retaining Wall Co., Eureka, Calif., personal communication.

Lee, K. L., Adams, B. D., and Vagneron, J. M. J. [1972]. "Reinforced Earth Retaining Walls," *Report No. 7233,* University of California, Los Angeles, School of Engineering and Applied Science, Los Angeles, Calif.

Nelson, K. F. [1984]. Salvage, Heber, Nelson and Associates, Inc., Eureka, Calif., personal communication.

Vidal, H. [1969]. "The Principle of Reinforced Earth," *Highway Research Record, 282,* HRB, National Research Council, Washington, D.C., 1969, pp. 1–16.

GEOGRID

Andrawes, K. Z., McGown, A., Wilson-Fahmy, R. F., and Mashhour, M. M. [1982]. "The Finite Element Method of Analysis Applied to Soil-Geotextile Systems," *Proc. 2nd International Conference on Goetextiles,* Las Vegas, Vol. 3.

Arthur, J. R. F., Dunstan, T., Al-Ani, Q. A. J. L. and Assadi, A. [1977]. "Plastic Deformation and Failure in Granular Media," *Geotechnique,* 27, No. 1 53–74.

ASTM D-618 [1977]. "Standard Methods of Conditioning Plastics and Electrical Insulating Materials for Testing," *ASTM Annual Book of Standards,* Part 35.

ASTM D-638 [1980]. "Standard Test Method for Tensile Properties of Plastics," *ASTM Annual Book of Standards,* Part 35.

ASTM D-2990. "Standard Test Methods for Tensile, Compressive and Flexural Creep and Creep Rupture of Plastics."

Atkinson, J. H. [1981]. *Foundations and Slopes,* McGraw-Hill.

Bassett, R. H., and Last, N. C. [1978]. "Reinforcing Earth Below Footings and Embankments," *Proc. ASCE Symposium on Earth Reinforcement,* Pittsburgh, pp. 202–231.

Blanchier, A., and Gielly, J. [1982]. "Study of Stability of Filling-up Slopes Reinforced by Layers of Geotextile," *Proc. 2nd International Conference on Geotextiles,* Las Vegas.

Boenig, H. V. [1966]. *Polyolefins—Strucutre and Properties,* Elsevier, New York.

Bolton, M. D. [1981]. "Limit State Design in Geotechnical Engineering," *Ground Engineering,* 14, No. 6, pp. 39–46.

Bolton, M. D., Choudhury, S. P. and Pang, P. L. R. [1978]. "Reinforced Earth Wall: A Centrifugal Model Study," *Proc. ASCE Symposium on Earth Reinforcement,* Pennsylvania.

BS 2051 [1972]. "Methods of Test for Textiles—Glossary of Terms Relating to the Conditioning and Testing of Textiles," British Standard Institution, London.

Chang, J. C., Hannon, J. B., and Forsyth, R. A. [1977]. "Pull Resistance and Interaction of Earthwork Reinforcement and Soil," *Transportation Research Record 640,* TRB, National Research Council, Washington, D.C.

Christie, I. F. and El Hadi, K. M. [1979]. "Some Aspects of the Desgin of Earth Dams Reinforced with Fabric," *Proc. Ist International Conference on Geotextiles, Paris.*

CIRIA [1977]. "Rationalisation of Safety and Serviceability Factors in Structural Codes," *Report 63,* 226 pp.

Comite Europeen de Beton [1970]. "International Recommendations for the Design and Construction of Concrete Structures," Cement and Concrete Association.

Dansk Inteniorforening [1978]. "Code of Practice for Foundation Engineering," Danish Geotechnical Institute, *Bull.,* No. 32, p. 52.

Department of Transport (UK) [1978]. "Reinforced Earth Retaining Walls and Bridge Abutments," *Technical Memorandum (Bridges) BE 3/78,* London.

Gassler, G., and Gudehus, C. [1981]. "Soil Nailing—Some Aspects of a New Technique," *Proc. 10th International Conference on Soil Mechanics and Foundation Engineering,* Stockholm. Vol. 3.

Gudehus, G. [1972]. "Lower and Upper Bounds for Stability of Earth-Retaining Structures," *Proc. 5th European Conference on Soil Mechanics and Foundation Engineering,* Madrid., Vol. 1.

Harrison, W. J., and Gerrard, C. M. [1972]. "Elastic Theory Applied to Reinforced Earth," *ASCE J. Soil Mechanics and Foundation Division,* SM 12, December.

Hausmann [1976]. "Strength of Reinforced Soil," *Proc. 8th Aust Road Resh. Conference,* Vol. 8, Sec. 13.

Heger, F. J., Chambers, R., and Dietz, A. G. H. [1982]. *Structural Plastics Design Manual,* Phase 1, Chapters 1 to 4, Prepared under contract to ASCE, U.S. Government Printing Office, Washington.

Herrmann, L. R., and Al-Yassin, Z. [1978]. "Numerical Analysis of Reinforced Soil Systems," *Proc. ASCE Symposium on Earth Reinforcement,* Pittsburgh, pp. 428–457.

Hueckel, S. M., and Kwasniewski, J. [1961]. "Scale Model Tests on the Anchorage Values of Various Elements Buried in Sand," *Proc. 5th International Conference on Soil Mechanics and Foundation Engineering,* Paris.

Ingold, T. S. [1982]. "An Analytical Study of Geotextile Reinforced Embankments," *Proc. 2nd International Conference on Geotextiles,* Las Vegas.

Ingold, T. S., and Miller, K. S. [1982]. "Analytical and Laboratory Investigations of Reinforced Clay," *Proc. 2nd International Conference on Geotextiles,* Las Vegas, Vol. 3.

Juran, I., and Schlosser, F. [1978]. "Theoretical Analysis of Failure in Reinforced Earth Structures," *ASCE Symposium on Earth Reinforcement,* Pittsburgh, pp. 528–555.

Kerisel, J. [1961]. "Deep Foundations in Sands. Variation of Ultimate Bearing Capacity with Soil Density, Depth, Diameter and Speed," *Proc. 5th International Conference on Soil Mechanics and Foundation Engineering,* Paris.

McGown, A., Andrawes, K. Z., Wilson-Fahmy, R. F., and Brady, K. C. [1981]. "Strength Testing of Geotechnical Fabrics," *TRRL Supplementary Report 703.*

Ministere des Transports [1979]. "Les Ouvrages en Terre Armee. Recommendations et Regles de l'Art," LCPC, Service d'Etudes Techniques des Routes et Autoroutes.

Ministry of Transportation and Communications [1980]. *Ontario Highway Bridge Design Code,* MTC, Ontario.

Mitchell, J. K. [1978]. "Soil Improvement—History, Capabilities and Outlook," ASCE, New York.

Murray, R. T., and McGowan, A. [1982]. "The Selection of Testing Procedures for the Specification of Geotextiles," *Proc. 2nd International Conference on Geotextiles,* Las Vegas.

National Geotechnical Societies of the European Economic Community [1983]. "Model Code Proposed as a Base Document for Eurocode EC7 Foundations," Preliminary Draft Chapters 1, 2, 4, 6.

Naylor, D. J. [1979]. "A Study of Reinforced Earth Walls Allowing Strip Slip," *Proc. ASCE Symposium on Earth Reinforcement,* Pittsburgh, pp. 618–643.

Ogorkiewicz, R. M. [1974]. *Thermoplastics Properties and Design,* Wiley.

Peterson, L. M. [1980]. "Pullout Resistance of Welded Wire Mesh Embedded in Soil," M. Sc. Thesis, Utah State University.

Phan, T. L., Segrestin, P., Schlosser, F., and Long, N. T. [1979]. "Stability Analysis of Reinforced Earth Walls by Two Slip Circle Methods," *Proc. International Conference on Soil Reinforcement,* Paris, pp. 119–123.

Potyondy, J. G. [1961]. "Skin Friction Between Cohesive Granular Soils and Construction Materials," *Geotechnique,* 11, No. 4, 339–353.

Poulos, H., and Davis, E. H. [1978]. *Elastic Solutions for Soil and Rock Mechanics,* Wiley.

Prandtl, L. [1921]. "Uber die Eindringungsfestigkeit platisher Baustoffe und die Fetsigkeit von Schneiden," *Zeitschrift fur Angewandte Mathematik und Mechanik,* 1:1, 15–20.

Reissner, H. [1924]. "Zum Erddruckproblem," *Proc. 1st International Conference Applied Mechanics,* 295–311, Delft.

Romstad, K. M., Al-Yassin, Z., Herrmann, L. R., and Shen, C. K. [1978]. "Stability Analysis of Reinforced Earth Retaining Structures," *Proc. ASCE Symposium on Earth Reinforcement,* Pittsburgh, pp. 685–713.

Roscoe, K. N. [1970]. "The Influence of Strains in Soil Mechanics," *Geotechnique,* 20, No. 2, 129–170.

Rowe, P. W. [1962]. "The Stress Dilatancy Relation for Static Equilibrium of an Assembly of Particles in Contact," *Proc. Roy. Soc. A,* 269, 500–527.

Rowe, R. K., and Davis, E. H. [1982]. "The Behaviour of Anchor Plates in Sand," *Geotechnique,* 32, No. 1, 25–41.

Schlosser, F., and Long, N. T. [1973]. "Etude de Comportement due Materiau Terre Armee," *Annales de l'Institut Technique du Batiment et des Travaux Publics,* Suppl. No. 304, Ser. Mater. No. 45.

Schlosser, F., and Long, N. T. [1974]. "Recent Results in French Research on Reinforced Earth," *ASCE J. Const. Div.,* Vol. 100, No. CO3, pp. 223–237.

Schlosser, F., and Juran, I. [1979]. "Design Parameters for Artificially Improved Soils," General Report, *Proc. 7th European Conference on Soil Mechanics and Foundation Engineering,* Vol. 5, Brighton.

Schlosser, F., Jacobsen, H. M., and Juran, I. [1983]. "Soil Reinforcement," General Report, *Proc. 8th European Conference on Soil Mechanics and Foundation Engineering,* Vol. 3, Helsinki.

Segrestrin, P. [1979]. "Design of Reinforced Earth Structures Assuming Failure Wedges."

SERC/Netlon Limited [1984]. *International Symposium on Polymer Grid Reinforcement in Civil Engineering,* London.

Sherby, O. D., Dorn, J. E. [1956]. "Anelastic Creep of Polymethyl-Methacrylate," *J. Mech. Phys. Solids,* 6, p. 145.

Simpson, B., Pappin, J. W., and Croft, D. D. [1981]. "An Approach to Limit State Calculations in Geotechnics," *Ground Engineering,* 14, No. 6, pp. 21–26.

Smith, A. K. C., and Wroth, C. P. [1978]. "The Failure of Model Reinforced Earth Walls," *Proc. ASCE Symposium on Earth Reinforcement,* Pennsylvania.

Stoker, M. F., Korber, G. W., Gassler, G., and Gudehus, G. [1979]. "Soil Nailing," *Proc. International Conference on Soil Reinforcement,* Paris, pp. 469–474.

Taylor, D. W. [1948]. *Fundamentals of Soil Mechanics,* Wiley, New York, pp. 455–461.

Truss, R. W., Duckett, R. A., and Ward, I. M. [1981]. "Effect of Hydrostatic Pressure on the Yield and Fracture of Polyethylene in Torsion," *J. Matertials Science,* 16.

Vesic, A. B. [1963]. "Bearing Capacity of Deep Foundations in Sand," *Highway Research Record 39,* HRB, National Research Council, Washington, D.C.

Vidal, H. [1969]. "La Terre Armee," *Annales de l'Institut Technique du Batiment et des Travaux Publics,* Paris, Nos. 223–229, 888–939.

BAR-MATS

Darbin, M., Jailloux, J. M., and Montvelle, J. [1982]. "Performance and Research on the Durability of Reinforced Earth Reinforcing Strips," *Proc.,* Short Course on Soil and Rock Improvement Technologies including Geotextiles, Reinforced Earth and Modern Piling, November.

Vidal, H. [1969]. "The Principle of Reinforced Earth," *Highway Research Record 282,* HRB, National Research Council, Washington, D.C.

SOIL NAILING IN EXCAVATIONS

Bang, S., Shen, C. K., and Romstad, K. M. [1980]. "Analysis of an Earth Reinforcing System for Deep Excavation," *Transportation Research Record 749,* TRB, National Research Council, Washington, D.C.

Bangratz, J. L., and Gigan, J. P. [1984]. "Methode Rapide de Calcul des Massifs Cloues," Laboratoire Regional de l'Est Parisien, France.

Bassett, R. H., and Last, M. C. [1978]. "Reinforcing Earth Below Footings and Embankments," *Proc. ASCE Symposium on Earth Reinforcement,* Pittsburgh, Apr. 27, 1978, pp. 202–231.

Brinch-Hansen, J. [1961]. "The Ultimate Resistance of Rigid Piles against Transversal Forces," *Bull.,* No. 12, Danish Geotechnical Institute.

Bustamente, H., et al. [1977]. "Comportement des Tirants Precontraints dans une Argile Plastique," Session Speciale No. 4, Congres Int. de Mecanique des Sols, Tokyo, 1977.

Cerciello [1977]. "Reinforcement of a Sliding Slope by Means of Reticulated Pali-Radice (Root-Piles) Structures," *Symposium Geotechnics of Structural Complex Formations,* Capri, Italy.

Colloque International sur le Renforcement des Sols: Terre Armee et Autres Techniques, Association Amicale des Ingenieurs Anciens Eleves de l'Ecole National des Ponts et Chaussees, Paris, Mar. 1979.

Gassler, G., and Gudehus, G. [1983]. "Soil Nailing, Statistical Design," *Proc. 8th European Conference on Soil Mechanics and Foundation Engineering,* Helsinki.

Guilloux A. and Schlosser, F. [1979]. "Etude du Frottement Sol-Armature en Laboratoire," *International Conference on Soil Reinforcement: Reinforced Earth and Other Techniques,* Paris, Mar. 1979, Vol. I.

Iwabuchi, S. [1979]. "Root-piles for Slope Stabilization," *International Conference on Soil Reinforcement: Reinforced Earth and Other Techniques,* Vol. II.

Juran, I., Schlosser, F. [1978]. "Theoretical Analysis of Failure in Reinforced Earth Structures," *Proc. ASCE Symposium on Earth Reinforcement,* Pittsburgh, Apr. 27, 1978, pp. 528–555.

Lizzi, F. [1982]. *Static Restoration of Monuments,* Sagep Publisher.

Rabcewicz, L. V. [1969]. "Stability of Tunnels under Rock Load," Water Power, June, July, and August.

Rabcewicz, L. V. [1971]. "Theorie et Pratique des Travaux Souterrains dans le Cas d'un Grand Projete," (en Allemand), *XX Colloque de Mecanique des Roches,* Salzbourg, October.

Rescher, O. J. [1968]. "Experience lors de la Construction de la Centrale Souterraine de Veytaux a l'aide de Beton Projete et Ancrages," (en Allemand), Felsmech. und Ingenieur Geologie, Supl. IV.

Schlosser, F. [1978]. "History, Current and Future Developments of Reinforced Earth," *Symposium on Soil Reinforcing and Stabilizing Techniques,* sponsored by New South Wales Institute of Technology and the University of New South Wales, Sydney, Australia, October.

Schlosser, F., and Guilloux, A. [1981]. "Le Frottement dans le Renforcement des Sols," *Revenue Francaise de Geotechnique,* No. 16.

Schlosser, F., Juran, I., and Jacobsen, H. M. [1983]. "Soil Reinforcement," General Report, *8th European Conference on Soil Mechanics and Foundation Engineering,* Helsinki.

Schlosser, F., and Segrestin, P. [1979]. "Dimensionnement des Ouvrage en Terre Armee par la Methode de l'Equilibre Local," *International Conference on Soil Reinforcement: Reinforced Earth and Other Techniques,* Paris, March, Vol. I.

Seed, H., Bolton and Idriss, I. M. [1969]. "Influence of Soil Conditions on Ground Motions During Earthquakes," *ASCE J. Soil Mechanics and Foundation Division,* Vol. 94, No. SM1, January.

Seventh European Conference on Soil Mechanics and Foundation Engineering, "Design Parameters in Geotechnical Engineering," Brighton, U.K., 1979.

Shen, C. K., Kim, Y. S., Bang, S., and Mitchell, J. F. [1979]. "Centrifuge Modelling of a Lateral Earth Support," *Proc. ASCE Symposium on Centrifuge Modelling of Geotechnical Problems,* October.

Symposium on Earth Reinforcement, *Proc.,* ASCE Annual Convention, Pittsburgh, April 1978.

Symposium on Soil Reinforcement: Reinforced Earth and Other Techniques, Paris, Mar. 1979.

Toudic, P. [1975]. "Desserte Ferroviaire de la Ville Nouvelle de St. Quentin-en-Yvelines," Revue Travaux.

SOIL NAILING IN SLOPE STABILIZATION

Baguelin, F., Jezequel, J. F., Lemee, E., and Le Mehaute, A. [1972]. "Expansion de Sondes Cylindriques dans les Sols Coherents," *Bull. de Liaison des Laboratoires des Ponts et Chaussees,* No. 61.

Baguelin, F., Frank, R., and Jezequel, J. F. [1975]. "Quelques Resultats Theoriques sur l'Essai d'Expansion dans les Sols et sur le Frottement Lateral des Pieux," *Bull. de Liaison,* No. 78.

Baguelin, F., Frank, R., and Said, Y. [1977]. "Theoretical Study of Lateral Reaction Mechanism of Piles," *Geotechnique,* Vol. 27, No. 3.

Baguelin, F., Jezequel, J. F., and Shields, D. H. [1978]. "The Pressuremeter and Foundation Engineering," Trans. Tech. Publications.

Baguelin, F. [1982]. "Rules for the Structural Design of Foundations Based on the Selfboring Pressuremeter Test," *Symposium on the Pressuremeter and Its Marine Applications,* Paris.

Broms, B. B. [1972]. "Stabilization of Slopes with Piles," Preprint of the *1st International Symposium on Landslides and National Committee on Counter Measures against Landslides* in Japan, pp. 115–123.

Broms, B. B., and Broman, P. [1976]. "Stabilization of Deep Cuts with Lime Columns," *Proc. 6th European Conference on Soil Mechanics and Foundation Engineering,* Vienna.

Cerciello [1977]. "Reinforcement of a Sliding Slope by Means of Reticulated Pali-Radice (Root-Piles) Structures," *Symposium, Geotechnics of Structural Complex Formations,* Capri, Italy.

Chiba-Ken [1973]. "Piles for Prevention of Landslides," (Fukuoka, M., Yoshida, Y., Nanbu, T.), *Preventive Measures of Natural Slope Collapse* (No. 1), Chiba-ken, pp. 1–23.

Fukumoto, Y. [1973]. "On the State of Collapse and Distribution of Reaction of Piles for Preventing Landslides," *Proc. 8th Symposium JSSMFE,* pp. 459–462.

Fukumoto, Y. [1974]. "On the Method of Piling for Preventing Landslides," *Journal of Landslides,* Vol. 11, No. 2., pp. 28–29.

Fukumoto, Y. [1975]. "Experiment Study on the Behavior of Lateral Resistance of Piles against a Land-Sliding (1)," *Journal of Landslides,* Vol. 12, No. 1, pp. 20–24.

Fukumoto, Y. [1975]. "Experiment Study on the Behavior of Lateral Resistance of Piles against a Land-Sliding (2)," *Journal of Landslides,* Vol. 12, No. 2, pp. 38–43.

Fukuoka, M., and Uto, K. [1959]. "Horizontal Subgrade Reaction Coefficient of a Pile by Using a Bore Hole (On K-Value)," *Proc. 15th Japanese Conference on Roads,* pp. 725–777.

Fukuoka, M., and Watari, M. [1960]. "Experiment on Resistance of Pile Against Landslides," Dokobu Gijyutsu Shiryo, Vol. 2, No. 5, pp. 20–23.

Fukuoka, M. [1972]. "Use Combined Steel Pipe Piles for Preventive Measures of Landslides," *Journal of Steel Pipe Piles Association (JASPP),* No. 3, pp. 12–15.

Fukuoka, M., Yoshida, Y., and Nanbu, T. [1973]. "Protection of Slopes Against Landslides by Using Piles," *Proc. 8th Symposium JSSMFE,* pp. 547–550.

Fukuoka, M. [1977a]. "Some New Methods of Protecting Natural Slope Without Disturbing Environment," *Proc., International Conference on Soil Mechanics and Foundation Engineering,* Specialty Session 11.

Fukuoka M. [1982]. "Fabric Retaining Walls," *2nd International Conference on Geotextiles,* Las Vegas.

Krynine, D. P. [1931]. "Landslide and Pile Action," *Engrg. News Record,* Vol. 107, No. 11, p. 860.

Lizzi, F. [1971]. "Special Patented Systems of Underpinning and Subsoil Strengthening by Means of Root Piles (Pali Radice)," Conference Donnee a l'MIT, Boston, Universite de L'Illinois; US Bureau de Reclamation, Denver, USA; Club of Civil Engineers, Vancouver, Canada.

Lizzi, F. [1977]. "Practical Engineering in Structurally Complex Formations (The In Situ Reinforced Earth)," *International Symposium on the Geotechnics of Structurally Complex Formations,* Capri, Italy.

Lizzi, F., and Carnavale, G. [1979]. "Networks of Root Piles for the Consolidation of Soils: Theoretical Aspects and Tests on Models," *International Conference on Soil Reinforcement: Reinforced Earth and Other Techniques,* Paris.

Lundgren, H., and Mortensen, K. [1953]. "Determination by the Theory of Plasticity of the Bearing Capacity of Continuous Footing in Sand," *Proc. 3rd International Conference on Soil Mechanics and Foundation Engineering,* Zurich.

Menard, L., and Rousseau, J. [1962]. "L'Evaluation des Tassements-Tendances Nouvelles," Sols–Soils 1, 1962.

Nakamura, H. [1968]. "Method of Designing Piles for Preventing Landslides," *Proc. 22nd Symposium on Engineering, Ministry of Construction,* pp. 791–795.

Nakamura, H. [1970]. "Earth Pressure Action on Piles for the Treatment of Landslides and Design," *Journal of Landslides,* Vol. 7, No. 2, pp. 8–12.

Nakamura, H. [1977]. "Three Roles of Piles for Landslide Control," *J. Jap. Soc. SMFE,* Vol. 17, No. 1, pp. 99–109.

Niigata-Ken [1977]. "Investigation of Piles for Preventing Landlsides," *Report on Landslide Investigation,* Chizan Section, Department of Agriculture and Forestry, Niigata-Ken, pp. 1–39.

Noo-Tsutsuichi [1880 to 1903].?

PWRI [1967]. "Report on Tests of Lines Plates for Preventing Landslides," Public Works Research Institute, Ministry of Construction.

Schlosser, F., and Juran, I. [1979]. "Design Parameters for Artificially Improved Soils," General Report, *Proc. 7th European Conference on Soil Mechanics and Foundation Engineering,* Brighton, U.K., Vol. 5.

Schlosser, F., Juran, I., and Jacobsen, H. M. [1983]. "Soil Reinforcement," General Report, *8th European Conference on Soil Mechanics and Foundation Engineering,* Helsinki.

Schlosser, F. [1983]. "Analogies et Differences dans le Comportement et le Calcul des Ouvrages de Soutenement en Terre Armee et par Clouage du Sol," *Annales de l'Institut Technique du Batiment et des Travaux Publics,* No. 418.

Tamada, B., and Tsuda, K. [1972]. "Effect of Piles for Stabilizing Landslope Slope," *Proc. 7th Symposium JSSMFE,* pp. 519–522.

Tamada, B., Tanizaki, A., and Kato, K. [1973]. "Measurement of Horizontal Resistance on Piles for Preventing Landslides," *Proc. 28th Symposium Japanese Society of Civil Eng.,* Part 3, pp. 182–184.

Tamada, B., Tanizaki, A., Hirao, K., and Kato, K. [1974]. "Earth Pressure on the Back of Piles for Preventing Landslides," *Proc. 9th Symposium JSSMFE,* pp. 609–612.

Tamada, B., Kudo, K., and Akimoto, N. [1976]. "Studies on the Stress Distribution of the Pile of Dowel Type and Movement of the Soil Around the Pile," *J. Landslides,* Vol. 13, No. 2, pp. 13–20.

Yamada, K., Naito, K., and Nakanishi, A. [1976]. "On the Behavior of Piles Preventing Landslides," J., Research Institute of Taisei Construction Company, pp. 163–169.

APPENDIX E

GLOSSARY OF TERMS AND DEFINITION OF SYMBOLS

GLOSSARY

Backfill is soil that is mechanically placed back into a space that has been excavated, such as against structures or behind the facing elements of an earth wall. Normally such backfill would be compacted to a minimum specified density. The backfill for an earth wall can be further divided into material that is within the zone of reinforcement and that which is outside the reinforced soil mass.

Composite Material in terms of soil reinforcement, is a material composed of soil (which normally has high strength in compression and shear) and reinforcements (which provide tensile strength). The composite material generally has high inherent strength.

Creep is the time dependent shear strain or volumetric strain under constant stress that develops at a rate controlled by the viscous resistance of the soil.

Deadmen are part of an anchoring system used in tie-back retaining walls. These blocks are connected to the retaining wall by tendons. The deadmen support the wall by the passive resistance achieved by pulling the deadmen through the soil.

Durability is the ability of a material to withstand degradation or loss of strength over time.

Earth Reinforcement/Soil Reinforcement is the process of increasing the strength of a soil mass by inserting tensile members into the soil mass. The composite material exhibits improved shear and compressive strength in comparison to the unreinforced material.

Extensible Reinforcement is an inclusion which has a rupture strain that is larger than the failure strain in the soil without inclusions under the same loading condition.

External Stability refers to the safety of a structure as a whole with respect to the reinforced soil sliding on its foundation, overturning about the toe of the wall, and bearing capacity failure.

Facing Element is a component of an earth wall used to prevent the soil from ravelling out between the rows of reinforcement. There are several types of facings available, including precast concrete panels, prefabricated metal sheets and plates, gabions, welded wire mesh, shotcrete (reinforced or not), inclusion of intermediate reinforcement layers between main reinforcement layers at the face, seeding of the exposed soil, and looping of geotextile reinforcements at the face.

Fiber Reinforcements are short flexible linear inclusions of high tensile strength. The fibers have the capacity to strengthen the soil mass in three dimensions.

Geotextile is a synthetic fabric used for geotechnical purposes such as soil reinforcement or as a filter material to prevent the movement of fines through the soil.

Grid/Mesh Reinforcement is geometrically composed of longitudinal members running perpendicular to the face of the wall, in horizontal planes, and transverse members which run parallel to the wall face. Both the longitudinal and transverse members are connected at their intersection points, thus giving the reinforcement its grid-like configuration.

Inextensible Reinforcement is an inclusion which has a rupture strain that is less than the failure strain in the soil without inclusions under the same stress conditions.

Internal Stability is the ability of the reinforced soil mass to act monolithically, without failure of its component parts through rupture, pullout, or corrosion.

Pullout Resistance is the ability of a reinforcing element to withstand movement within the reinforced soil mass when subjected to a tensile force.

Reinforcing Element refers to the inclusion within a reinforced soil mass. The reinforcing element commonly increases the tensile and shear strength of the composite material. The types of reinforcing elements include strips, grids, sheets, rods, and fibers.

Reinforced Zone is the section of the backfill that has reinforcing elements within its mass.

Rupture is the failure of a reinforcing element due to the development of tensile stress in excess of the strength of the reinforcement.

Sheet Reinforcement is a thin planar reinforcing element.

Soil Nails are round bar reinforcing elements either drilled or driven into the in-situ soil to improve its strength.

Strip Reinforcements are thin, narrow linear reinforcing elements commonly made of metal or plastic.

Tendon is usually associated with ground anchors, such as tie-backs, where the tendon is the prestressing steel or strand used between the wall face and the anchor.

SYMBOLS

Parenthetical notations in the following identify definitions unique to particular systems and methods.

a ..... transverse spacing of piles

a_h ..... horizontal component of earthquake acceleration

a_{si} ..... total structural cross-sectional area, parallel to the face of the wall, of the ith layer of reinforcement elements at the connection with the facing, per foot "run" of wall

A ..... cross-sectional area of reinforcement (soil nailing in excavation); also area of sliding surface (soil nailing in slope stabilization)

A_b ..... surface area of bearing member; also surface area of anchor on which bearing develops (Anchored Earth)
A_c ..... anchorage factor
A_{cr}, A_{CR} ..... cross-sectional area of the failure surface (soil nailing in excavation)
A_r ..... total grid surface area; i.e., length times width of the mat rather than just the grid members
$A_{reduced}$ ..... reduced cross-sectional area due to bolt hole
A_R ..... contributing area per reinforcement; also cross-sectional area of longitudinal wire at the end of the design life (Welded Wire Wall and Reinforced Soil Embankment)
A_s ..... surface area of reinforcement
A_{TR} ..... plan area of triangular region of anchor element
b ..... width of the reinforcement strip, or mesh, or unit; width of contact area of a horizontal load F_H or vertical load F_v at top of the earth wall (Anchored Earth); also transverse width of grid reinforcement mat (geogrid)
B ..... width of slab foundation on a bridge abutment (Reinforced Earth); length of horizontal facing element protruding into reinforced soil volume (Broms' Method) (geotextiles); also footing width (Welded Wire Wall and Reinforced Soil Embankment)
B' ..... reduced equivalent width of slab foundation on a bridge abutment
c ..... unit cohesion of soil
c_o ..... corrosion rate, in ounces/square foot/year
c_1 ..... residual cohesion along the sliding surface
c' ..... unit cohesion of soil under effective stress conditions; also mobilized cohesion, c/FS (soil nailing in excavation)
C_a ..... soil-to-reinforcement adhesion
C_a' ..... mobilized cohesion at soil-to-reinforcement interface $= C_a/FS_g$
C_u ..... coefficient of uniformity
C_R ..... corrosion rate of metal
C_R' ..... apparent cohesion
C^* ..... total apparent cohesion (soil nailing in excavation); also apparent anisotropic cohesion of nailed soil (soil nailing in slope stabilization)
C_o^* ..... additional shear resistance due to sum of shear forces in piles (soil nailing)
d ..... diameter of reinforcement (Welded Wire Wall, Reinforced Soil Embankment and bar mat systems); also distance behind wall face where a horizontal surface load F_H or vertical load F_v acts (Anchored Earth)
d_i ..... wire diameter at the start of year i, in inches
d_{100} ..... diameter of reinforcement bars after 100 years of corrosion
D ..... embedment depth of wall (Reinforced Earth); vertical depth of the failure surface below the slope face (geotextiles); diameter of bar (soil nailing in excavation); also transverse clear spacing of piles for Wang-Yen analysis (soil nailing in slope stabilization)
D_{crit} ..... critical transverse clear spacing between piles for arching to occur
D_f ..... overburden height
D_i ..... width over which line load is dispersed at depth Z_i
D_{50} ..... median soil grain diameter
e ..... eccentricity
e_1 ..... eccentricity of vertical strip load with respect to the center line of the contact area of the load on top of the wall
E ..... thickness of wall facings; also Young's modulus
E_s ..... spring coefficient for laterally loaded piles (soil nailing in excavation); also elastic spring coefficient, K_sD, for soil (soil nailing in slope stabilization)
f ..... friction along fabric (geotextiles); also skin friction developed on reinforcement (soil nailing)
f_a ..... allowable stress for the longitudinal wires; also allowable stress in steel (bar mats)
f_b ..... coefficient of pullout resistance for a reinforcement grid
$f_{bearing}$ ..... coefficient of bearing (passive resistance) for a grid reinforcement
f_c ..... compressive strength of concrete
f_{ds} ..... coefficient of resistance to direct sliding (geogrid)
f_m ..... tensile stress in longitudinal bars
f_{max} ..... limit skin friction developed on reinforcement
f_t ..... allowable working stress of reinforcement metal
f_y ..... yield stress of reinforcement metal (Reinforced Earth); yield strength of steel reinforcement (Welded Wire Wall); also yield strength of steel (bar mats)
F ..... pullout force per unit length of wall (Welded Wire Wall); force acting on a shear plane (Anchored Earth); also factor of safety (soil nailing in slope stabilization)
F_a ..... allowable tensile stress
F_{ad} ..... dynamic active force due to seismic event
F_{ds} ..... coefficient of resistance to direct sliding
F_E ..... a factor to account for dilation and other effects in anchor pullout resistance
FH ..... horizontal force per reinforcement
FH_{CONN} ..... horizontal force at connection
F_H ..... horizontal line load; also horizontal load to be resisted by a layer of reinforcement (bar mats)
F_i ..... initial factor of safety
F_p ..... available pullout resistance
F_R ..... factor of safety for tensile rupture
F_s ..... factor of safety of unreinforced soil
FS ..... factor of safety
FS_c ..... factor of safety with respect to cohesion
FS_g ..... factor of safety with respect to pullout resistance parameters
FS_p ..... required safety factor with respect to pullout resistance of reinforcement

FS_R ..... required safety factor with respect to tensile resistance of reinforcement material
$F.S.$ ..... factor of safety
$F.S._{rupture}$ ..... factor of safety against rupture
$F.S._{rupture\ 100\ years}$ .. factor of safety against rupture after reinforcement thickness is reduced by 100 years of corrosion
F_T ..... tensile force in reinforcement; also horizontal shear force (Welded Wire Wall)
F_{T100} ..... tensile stress in reinforcement after 100 years of corrosion
F_{TCONN} ..... tensile stress at connection
$F_{CONN100}$ ..... tensile stress in reinforcement at connection after 100 years of corrosion
F_{Tmax} ..... maximum tensile stress
F_v ..... vertical strip load
F^*_v ..... equivalent bridge abutment vertical line load (Reinforced Earth)
$F\gamma'$ ..... bearing factor
g ..... acceleration due to gravity
$g(z)$ ..... lateral displacement as a function of depth
h ..... overburden height (soil nailing in excavation); also effective length of pile; or depth of yielding or sliding plane (Wang-Yen Analysis) (soil nailing in slope stabilization)
H ..... height of wall; total height of wall for design calculations (Reinforced Earth); height of wall face (Welded Wire Wall); slope height (geogrid); also height of reinforced embankment or wall (soil nailing in excavation)
H_1 ..... total height of facing panels
H_2 ..... height of sloped portion of backfill
H_f ..... failure height of model wall
H_p ..... height of pavement layer
i ..... slope of backfill above horizontal
I_v ..... viscosity index
I_z ..... moment of inertia of structural member
K ..... coefficient of lateral earth pressure
K_{aH} ..... coefficient used to compute horizontal component of Rankine active earth force
K_b ..... coefficient of lateral earth pressure for Broms' Method
K_c ..... value of the coefficient of lateral earth pressure at failure caused by breakage of the reinforcement
K_D ..... coefficient of lateral earth pressure—design value used for Welded Wire Wall and RSE
K_o ..... coefficient of lateral earth pressure at rest
K_s ..... modulus of lateral soil reaction
K^* ..... nondimensional tensile force factor (Reinforced Earth)
L ..... length of reinforcement; also longitudinal, up and downslope, spacing of piles (soil nailing in excavation)
L_e ..... length of the reinforcement in the resisting zone
L_{ei} ..... required length of reinforcement in the resisting zone of the ith level of reinforcement
L_i ..... length of reinforcement at the ith level
L_n ..... length of fabric reinforcement beyond the failure zone for bottom layer of reinforcements, layer n (Broms' Method)
L_{n-i} ..... length of fabric reinforcement beyond the failure surface of the ith layer of reinforcement above the bottom layer (Broms' Method)
L_o ..... length of fabric overlap (geotextiles); transfer length of the reinforcement (soil nailing)
L_r ..... length of element of grid
L_T ..... length of entire failure surface (Shen method)
ΔL ..... displacement of reinforcing strip in pullout test
m ..... site-dependent corrosion factor
M ..... number of longitudinal wires; number of longitudinal bars in a bar mesh; bending moment
M_a ..... allowable bending moment
M_D ..... driving moment
M_i ..... bending moment about the center of the reinforcement at the ith level arising from external loads on the reinforced soil
M_1, M_p ..... limit bending moment (soil nailing)
M_R ..... resisting moment
n, N ..... number of transverse members in a grid or mesh; number of transverse bars behind assumed failure surface; number of reinforcement layers in a vertical section of the wall
N_c ..... bearing capacity factor due to cohesion
N_i ..... normal force on a failure surface
N_p ..... passive resistance anchorage factor
N_q ..... bearing capacity factor due to surcharge
N_y ..... number of years for design life
N_Z ..... number of layers of reinforcing elements in a vertical profile to depth Z
N_1 ..... number of spacings the failure surface is below the slope, the ratio of D to S_v
$N\gamma$ ..... bearing capacity factor due to friction
p ..... lateral earth pressure on pile, stress (soil nailing)
p_F ..... yield pressure from a pressuremeter test
P ..... pullout force or resistance; normal force in a shear box test (geotextiles); lateral earth thrust on the nail (soil nailing in excavation)
P_{at} ..... permissible axial tensile stress in the reinforcing elements (Anchored Earth)
P_B ..... pullout resistance per unit width developed by bearing on n grid members
P_c ..... collapse strip load per unit width
P_e ..... external horizontal force acting on reinforced mass
P_E ..... resultant horizontal force
P_f ..... pullout capacity developed from friction; shear force developed between the soil and a horizontal surface (geogrid); also limit pressure measured in a pressuremeter test (soil nailing in excavation)
P_l ..... limit earth pressure in a pressuremeter test
P_L ..... limit pressure from pressuremeter test
P_{max} ..... maximum pullout resistance; also maximum pullout force per unit width that can be maintained (geogrid)
P_n ..... normal earth force on a failure surface
P_P ..... pullout capacity developed by passive resistance

$P_{pullout}$ ..... the pullout resistance of anchors per lineal foot "run" of wall at the level considered
P_q ..... resultant horizontal force from surcharge loading
P_t ..... total pullout resistance (Welded Wire Wall); also tangential earth force on a failure surface (soil nailing in excavation)
P_T ..... total pullout capacity
P_{ult} ..... ultimate lateral force value from a p-y analysis
P_z ..... lateral earth thrust on the bars
P_Z ..... pullout resistance offered by a single reinforcing element at depth Z within the reinforced soil mass
q ..... surcharge load
Q ..... vertical depth below top of wall at which a horizontal surface load F_H is fully dispersed (Anchored Earth); spacing constant for reinforcements (geogrid); also total lateral earth force resisted by a nail (soil nailing in slope stabilization)
q_a ..... allowable bearing capacity
q_s ..... uniform surcharge on top of wall
Q_s ..... total lateral earth force acting on a single pile
q_{ult} ..... ultimate bearing capacity; also ultimate bearing capacity, stress per lineal foot (Welded Wire Wall)
Q_{ult} ..... ultimate bearing capacity, force per lineal foot
r_u ..... pore pressure ratio or coefficient
R ..... radius of slip circle; radius of logarithmic spiral
R_c ..... shearing resistance of reinforcement
R_f ..... final radius of logarithmic spiral defining the boundary slip field
R_n ..... tensile resistance of reinforcement
R_o ..... length of one side of the triangle defining an anchor element
R_s ..... restoring force due to soil (geotextiles)
R_T ..... tensile resistance of reinforcement; the maximum allowable tensile stress, or elastic limit, of the reinforcing material (Reinforced Earth); also restoring force due to reinforcement (geotextiles)
R_V ..... resultant vertical reaction
S_c ..... site-dependent corrosion factor
S_D ..... total driving force on failure surface (Shen method)
S_{eq} ..... equivalent surface of influence of inclusion
S_H ..... horizontal center-to-center spacing between longitudinal reinforcements
S_i ..... tangential force on failure surface, element i (Shen method)
S_{max} ..... maximum longitudinal spacing of transverse bearing members
S_M ..... horizontal mat spacing, center to center
S_{opt} ..... optimum spacing between transverse bearing members
S_R ..... total resisting force on failure surface (Shen method)
S_u ..... undrained shear strength
S_{ui} ..... initial undrained shear strength
$S_u\,(\dot{\epsilon}_c)$ ..... undrained shear strength for strain rate $\dot{\epsilon}_c$
$S_u\,(\dot{\epsilon}_o)$ ..... undrained shear strength for strain rate $\dot{\epsilon}_o$
S_v ..... vertical spacing between reinforcements
S_{vmin} ..... minimum vertical spacing of reinforcement
S_{vz} ..... vertical reinforcement spacing at depth z
S_x ..... horizontal spacing between transverse members
t ..... time; also thickness of reinforcement
T ..... tensile force in reinforcement; also pullout force in a pullout test
$\vec{T}$ ..... vector of total force in reinforcement
T_a ..... allowable tensile stress in fabric
T_f ..... tensile force at failure in reinforcement
T_{Fi} ..... tensile force in the reinforcement from a horizontal force applied to the top of the wall
T_H ..... total pullout resistance for an anchor at depth $Z = H$
T_i ..... tensile force in reinforcement layer i
T_m ..... mobilized pullout resistance
T_{max} ..... lesser of the pullout resistance or tensile strength of the reinforcement; maximum developed tensile force in reinforcement
ΔT_{max} ..... increment of tensile force in reinforcement due to external loading (Reinforced Earth)
T_{Mi} ..... tensile force in the reinforcement caused by external bending moments acting on the wall
T_N ..... normal component of axial tensile force in the reinforcing members (Shen method)
T_p ..... maximum pullout resistance that can be developed between a bar and soil
T_{p1} ..... limit pullout force
T_R ..... limit tensile force
T_{Si} ..... tensile force in the reinforcement derived from a vertical strip load applied to the top of the wall
T_T ..... tangential component of axial tensile force in the reinforcing members (Shen method)
T_u ..... ultimate tensile strength of fabric
T_{wi} ..... tensile force in the reinforcement derived from a uniform surcharge on top of the wall
T_Z ..... the total pullout resistance for the anchors at wall depth Z
T_{Zi} ..... tensile force in the reinforcement derived from the height of fill above a layer of reinforcement
V ..... shear force in reinforcement
V_f ..... shear force at failure in reinforcement
V_o ..... mobilized shear force in reinforcement at the failure surface
V_1 ..... corrosion loss rate during first several years of corrosion
V_2 ..... corrosion loss rate after first several years of corrosion
w ..... base width of triangular or z-type anchor element
W ..... weight; also mat width (Welded Wire Wall, Reinforced Soil Embankment)
W_i ..... weight of failure wedge, element i (Shen method)
W_s ..... uniformly distributed surcharge on top of the wall
W_1 ..... liquid limit of soil

x ..... horizontal distance from face of wall; ratio of the displacement of the upper box to the length of shear surface in a shear box test; also relative displacement of soil and reinforcement (soil nailing in excavation)
x_o ..... width of active zone at a given depth
x_1 ..... average loss of thickness for plain steel due to corrosion
x_H ..... nondimensional spacing factor (Reinforced Earth)
y ..... relative pile-to-soil displacement
$y(z)$ ..... lateral displacement of a bar at depth Z
z ..... the depth of embedment of a grid member (geogrid); also vertical depth from ground surface (soil nailing in slope stabilization)
z_1 ..... depth to interface of creeping and noncreeping soil zones
Z ..... depth below top of wall
Z_b ..... depth to bottom of layer
Z_f ..... depth to the top of a layer of reinforcement
Z_i ..... depth from the top of the wall to the ith layer of reinforcements
Z_{iy} ..... maximum depth to which reinforcements may be placed at a given vertical spacing
Z_m ..... depth to middle of layer
α ..... coefficient of soil reinforcement interaction; angle of tangent of logarithmic spiral failure surface (Reinforced Earth); angle between a line tangent to the slip circle and the horizontal (geotextiles); inclination of reinforcing elements from the horizontal (Anchored Earth); also inclination of the tangent to the failure surface with respect to the horizontal (soil nailing in excavation)
α_b ..... fraction of width b available for bearing (geogrid)
α_{ds} ..... ratio of grid plan area that resists direct shear with soil to total plan area at the level of reinforcement
α_i ..... inclination of failure surface relative to horizontal, element i (Shen method)
α_s ..... fraction of solid to the total surface area in a grid
α_1 ..... angle measured from the base of the isosceles triangle, defining the plan area of an anchor (Anchored Earth), to one of the equal side legs
β ..... slope angle
β_1 ..... ground slope in front of wall (Reinforced Earth); also inclination of failure plane relative to vertical (Anchored Earth)
γ ..... unit weight of soil
γ_{EF} ..... unit weight of an equivalent fluid
γ_m ..... partial factor used to derive service strength of Tensar
γ_R ..... unit weight of a pavement layer
γ' ..... effective unit weight of soil
δ ..... friction angle between soil and reinforcement surface; also lateral displacement of reinforcement required to generate shear force (soil nailing in slope stabilization)
$\vec{\delta}$ ..... vector of displacement of reinforcement at the failure surface
δ_c ..... tangential component of displacement of reinforcement at the failure surface
δ_n ..... normal component of displacement of reinforcement at the failure surface
Δ ..... lateral displacement; "difference in"
Δm ..... restoring moment (geotextiles)
ΔF ..... additional factor of safety due to reinforcement
ΔF_s ..... increase of overall factor of safety due to inclusions
$\Delta\sigma_v$ ..... increment of vertical stress due to external loading
$\Delta\tau$ ..... increase in overall shear resistance due to the reinforcement (soil nailing in excavation); also change in shear stress (in slope stabilization)
$\Delta\tau_{reinf}$ ..... contribution to soil shear strength due to additional normal stress generated by the component of the reinforcement force that acts across the failure surface
$tan\delta$ ..... coefficient of friction between soil and reinforcement
ϵ ..... strain or distortion
$\dot{\epsilon}$ ..... distortion rate in creeping zone of soil
$\dot{\epsilon}_c$ ..... current rate of distortion in creeping zone of soil
$\dot{\epsilon}_i$ ..... initial rate of distortion in creeping zone of soil
$\dot{\epsilon}_o$ ..... reference distortion rate in creeping zone of soil
η_p ..... plastic viscosity for a Bingham solid
θ ..... reinforcement orientation angle; subtended angle for slip field calculations (Anchored Earth); also angle between the reinforcement and the normal to the failure plane (soil nailing in excavation)
λ, η ..... dimensionless parameters, used in Brinch-Hansen analyses
μ ..... the coefficient of friction between soil and reinforcement
μ_o ..... value of apparent friction coefficient at top of the wall
μ^* ..... apparent or effective friction coefficient
υ ..... a factor used by Rowe and Davis (1982) to describe the tendency for soil to dilate during shear
σ ..... total stress; also normal stress on reinforcement
σ_a ..... average confining stress
σ_{adm} ..... allowable stress in steel
σ_b ..... passive resistance or bearing pressure on transverse members
σ'_b ..... effective horizontal stress on transverse members
σ_h ..... horizontal stress
σ_{hc} ..... horizontal pressure in middle of layer
σ_{hCONN} ..... horizontal stress at connection
σ_{h1} ..... horizontal stress due to external live loading
σ'_h ..... horizontal effective stress

σ'_{ho} ..... horizontal effective stress at the face of the wall
σ_H ..... total horizontal stress
σ_{HD} ..... horizontal dynamic active earth pressure
σ_{Hsup} ..... horizontal pressure from the horizontal component of a line load
σ_{HS} ..... horizontal static active earth pressure
σ_{HT} ..... total horizontal pressure at any depth
σ_n ..... normal stress
σ_{1R}, σ_{3R} ..... major, minor principal stress at failure
σ_{3C} ..... consolidation stress
σ_v ..... total vertical stress; overburden pressure; stress acting in normal direction, i.e., to reinforcing element, anchor element or slip plane (Anchored Earth)
σ'_v ..... vertical effective stress; also effective stress acting in normal direction (Anchored Earth)
σ_{vb} ..... vertical stress at bottom of a wall or layer using Meyerhof distribution
σ_{vline} ..... vertical pressure from the vertical component of a line load
σ_{vsoil} ..... vertical pressure from soil
σ'_{vo} ..... vertical effective stress at the face of the wall
$\sigma_v(x)$ ..... vertical stress on the soil-reinforcement interfaces at point x
$\sigma\ (\alpha)$ ..... normal stress acting on failure surface calculated using Koter's equation
$\sigma\ (\phi)$ ..... normal stress acting on the log-spiral failure surface
τ ..... shear stress
τ_i ..... initial shear stress
τ_s ..... shear stress mobilized in soil
τ_y ..... yield shear stress for a Bingham solid
$\tau\ (x)$ ..... mobilized shear stress at the soil-reinforcement interface at point x
ϕ ..... soil friction angle
ϕ' ..... effective soil friction angle
ϕ'_a ..... soil-to-reinforcement friction angle
ϕ_{ds} ..... angle of friction for soil in direct shear
ϕ'_i ..... developed friction angle for element i, ϕ_i/FS (Shen method)
ϕ'_r ..... residual effective friction angle of soil
ϕ_1 ..... internal friction angle of the soil retained by the wall; also residual angle of internal friction along sliding plane (soil nailing in slope stabilization)
ϕ^* ..... apparent soil friction angle